BULLETIN OF THE EARTHQUAKE RESEARCH INSTITUTE,
TOKYO UNIVERSITY. Vol. XXXI, Part 1. March, 1953.

東京大學
地震研究所彙報

第 31 號　第 1 册

昭和 28 年 3 月

目　次

論文及報告

			頁
1.	小さな異物を含む媒質内を伝はる彈性波の速さ (英文)	佐藤泰夫	1
2.	日本に於ける地磁気短周期変化の異常と地下構造 (第2報) (英文)	力武常次 横山泉 菱山よね子	19
3.	榛名山の地磁気異常とその浮石の逆熱残留磁気との関係 (英文)	横山泉	33
4.	地震動の振幅と周期との関係 (英文)	金井清 長田甲斐男 吉沢静代	45
5.	震害と地盤の性質との関係 (泥炭地にある木造家屋の場合) (英文)	金井清 田中貞二 鈴木富三郎	57
6.	高温に於ける火山岩の粘性及び彈性 第2報 (英文)	佐久間修三	63
7.	彈性波の発生機構に関する実験 (第2報) (英文)	笠原慶一	71

(The titles in occidental languages are given on the back cover.)

本彙報ハ年4回 (但シ第1號ヨリ第6號マデハ不定期ニ，第7號ハ3冊トシテ發行セリ)，彙報別冊ハ不定期ニ發行ス.

本彙報掲載ノ論文及ビ報告ノ內容ニ關シテハ著者ノミニ其責任アルモノトス.

本彙報ニ關スル照會通信ハ東京大學地震研究所長ヘ宛テラレタシ.

The Bulletin is published quarterly. (Vols. I–VI were published at irregular intervals and Vol. VII consisted of three parts.)
Supplementary Volume is published at irregular interval.

The authors of the papers alone are responsible for the statements and opinions contained in their respective papers.

All communications relating to this Bulletin should be addressed to the Director of the Earthquake Research Institute, Tokyo University.

1. *Velocity of Elastic Waves Propagated in Media with Small Obstacles.*

By Yasuo SATÔ,
Earthquake Research Institute.
(Read Oct. 21, 1952.—Received Dec. 20, 1952.)

1. Introduction.

In the previous paper entitled "Velocity of Elastic Waves Propagated in Media with Small Holes"[1] we have treated the substance with small holes which are filled up with some kind of liquid. As a natural sequel to this work, we will take up a substance with small solid obstacles, in this paper. Since it is very difficult to treat obstacles of irregular shape and magnitude, we are obliged to confine our attention to the case of small spherical bodies of the same size. We will also assume some postulates which are necessary to develop our theory.

Of course we must strictly examine the validity of our model when we apply the following theory to some actual problems, e. g. the velocity of elastic waves in gravel which is constituted by spherical pebbles and homogeneous matrix.

The calculations in this paper are performed under the following assumption:

1) We can replace any volume of actual material containing large number of obstacles by equivalent homogeneous continuum.

2) The obstacles are spherical bodies of the same size.

3) The proportion of the volume of obstcles is small compared with the whole medium, and its square terms can be neglected without causing fatal error.

4) The continuity of displacement and stress components strictly holds at the boundary surface.

5) When the velocity of wave propagation comes into question, the wave-length is assumed to be far larger than the distance or the diameter of the obstacles.

These conditions are the same as those of our previous paper, and so long as they are admitted, we believe that our theory can give a ready solution of first approximation.

1) Y. SATÔ, *Bull. Earthq. Res. Inst.*, **30** (1952), 179.

2. General type of the solution.[2]

Now, there are six independent solutions of the elastic equations which can be derived from solid harmonics of order n, that is[3]

$$\text{Type } \phi ; \quad \mathfrak{d}=\operatorname{grad}\phi_n$$

$$\text{Type } \omega ; \quad \mathfrak{d}=r^2\operatorname{grad}\omega_n+\alpha_n r\mathfrak{r}\omega_n \left(\alpha_n=-2\frac{n\lambda+(3n+1)\mu}{(n+3)\lambda+(n+5)\mu}\right) \tag{2.1}$$

$$\text{Type } \chi ; \quad \mathfrak{d}=[r\mathfrak{r}, \operatorname{grad}\chi_n]$$

where $\mathfrak{d}$ implies displacement, $\mathfrak{r}$ is a unit vector of radial direction and ϕ_n, ω_n, and χ_n are the spherical solid harmonics of order n. Therefore, using a spherical surface harmonics of order n, we can express as

$$\phi_n,\ \omega_n,\ \chi_n = r^nS_n,\ r^{-n-1}S_n \qquad \cdots\cdots\cdots\cdots\cdots\cdots\cdots\cdots (2.2)$$

Introducing these relations into the above expressions

$$\begin{aligned}
&\text{Type } \phi ; && \mathfrak{d}_{\phi n+}=\operatorname{grad}(r^nS_n)=\{n, 1\}_n r^{n-1}\\
&&& \mathfrak{d}_{\phi n-}=\operatorname{grad}(r^{-n-1}S_n)=\{-n-1, 1\}_n r^{-n-2}\\
&\text{Type } \omega ; && \mathfrak{d}_{\omega n+}=r^2\operatorname{grad}(r^nS_n)+\alpha_n\mathfrak{r}r^{n+1}S_n=\{n+\alpha_n, 1\}_n r^{n+1}\\
&&& \mathfrak{d}_{\omega n-}=r^2\operatorname{grad}(r^{-n-1}S_n)+\alpha_{-n-1}\mathfrak{r}r^{-n}S_n\\
&&&\qquad =\{-n-1+\alpha_{-n-1}, 1\}_n r^{-n} \qquad \cdots\cdots\cdots\cdots (2.3)\\
&\text{Type } \chi ; && \mathfrak{d}_{\chi n+}=[r\mathfrak{r}, \operatorname{grad}(r^nS_n)]=-r^nS_n'\mathfrak{s}\\
&&& \mathfrak{d}_{\chi n-}=[r\mathfrak{r}, \operatorname{grad}(r^{-n-1}S_n)]=-r^{-n-1}S_n'\mathfrak{s} \qquad (n\neq 0)
\end{aligned}$$

in which

$$\{p, q\}_n \equiv pS_n\mathfrak{r}+qS_n'\mathfrak{t}$$

$\mathfrak{s}$ and $\mathfrak{t}$ are unit vectors of azimuthal and colatitudinal direction.

Here, we must notice that when $n=0$, these expressions must be somewhat modified.

$$\left\{\begin{aligned}
&\mathfrak{d}_{\phi 0+}=0\\
&\mathfrak{d}_{\phi 0-}=\{-1, 0\}_0 r^{-2}\\
&\mathfrak{d}_{\omega 0+}=\{\alpha_0, 0\}_0 r\\
&\mathfrak{d}_{\omega 0-}=\{-1+\alpha_{-1}, 0\}_0 \qquad \cdots\cdots\cdots\cdots (2.3a)\\
&\qquad =0, \quad (\because\ \alpha_{-1}=1)\\
&\mathfrak{d}_{\chi 0+}=0\\
&\mathfrak{d}_{\chi 0-}=0
\end{aligned}\right.$$

2) Although we use the term "general", the following calculations are still restricted, for they employ only zonal harmonics and do not treat the type of solutions which involves tesseral harmonics. However, in view of the results obtained, the results will not be altered even if we use a solution containing tesseral harmonics.

3) LOVE, *Theory of Elasticity*. pp. 251, 252.

Corresponding to these fundamental types of displacement, we have the fundamental stresses which after some complicated calculations[4] turn to be

$$\begin{aligned}
&\text{Type } \phi: \quad \mathfrak{F}_{\phi n+} = \mu\, 2(n-1)\{n, 1\}_n r^{n-2} \\
&\qquad\qquad \mathfrak{F}_{\phi n-} = -\mu\, 2(n+2)\{-n-1, 1\}_n r^{-n-3} \\
&\text{Type } \omega: \quad \mathfrak{F}_{\omega n+} = \mu\{(n-3)\alpha_n + 2(n^2-2n-1), 2n+\alpha_n\}_n r^n \\
&\qquad\qquad \mathfrak{F}_{\omega n-} = \mu\{-(n+4)\alpha_{-n-1} + 2(n^2+4n+2), \\
&\qquad\qquad\qquad\qquad -2(n+1)+\alpha_{-n-1}\}_n r^{-n-1} \qquad \ldots\ldots(2.4) \\
&\text{Type } \chi: \quad \mathfrak{F}_{\chi n+} = -\mu(n-1) r^{n-1} S_n' \mathfrak{F} \\
&\qquad\qquad \mathfrak{F}_{\chi n-} = \mu(n+2) r^{-n-2} S_n' \mathfrak{F}
\end{aligned}$$

When $n=0$, these expressions must of course be modified as before.

$$\left\{\begin{aligned}
&\mathfrak{F}_{\phi 0+} = 0 \\
&\mathfrak{F}_{\phi 0-} = \mu\, 4\{1, 0\}_0 r^{-3} \\
&\mathfrak{F}_{\omega 0+} = \mu\{3\alpha_0 k/\mu, 0\}_0 \\
&\mathfrak{F}_{\omega 0-} = \mu\{-4\alpha_{-1}+4, 0\}_0 = 0 \\
&\mathfrak{F}_{\chi 0+} = 0 \\
&\mathfrak{F}_{\chi 0-} = 0
\end{aligned}\right. \qquad \ldots\ldots(2.4a)$$

If an arbitrary stress is applied to the surface of the equivalent homogeneous sphere (radius R), it can be expressed by

$$[K_n \mathfrak{F}_{\phi n+} + L_n \mathfrak{F}_{\omega n+} + M_n \mathfrak{F}_{\chi n+}]_{r=R} \qquad \ldots\ldots(2.5)$$

and the displacement at the same surface corresponding to this stress is

$$[K_n \mathfrak{d}_{\phi n+} + L_n \mathfrak{d}_{\omega n+} + M_n \mathfrak{d}_{\chi n+}]_{r=R} \qquad \ldots\ldots(2.6)$$

If we imply by the notation $\mathfrak{d}[\phi_n]$ the displacement in the part of the equivalent homogeneous continuum of the model in Fig. 1, when the stress $\mathfrak{F}_{\phi n+}$ is applied to the outer surface $r=R$, it can be expressed by the next formula

$$\begin{aligned}
\mathfrak{d}[\phi_n] = {} & A_n \mathfrak{d}_{\phi n+} + B_n \mathfrak{d}_{\phi n-} \\
& + C_n \mathfrak{d}_{\omega n+} + D_n \mathfrak{d}_{\omega n-}.
\end{aligned} \qquad \ldots\ldots(2.7)$$

Similarly, we have

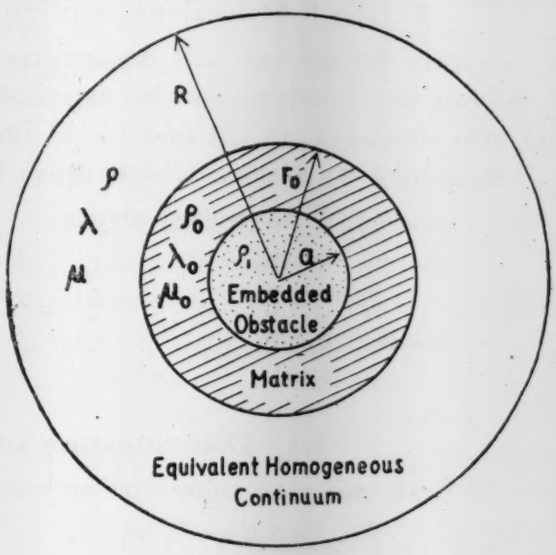

Fig. 1.

4) *cf.*, LOVE, *Elastisty.* p. 252.

$$\begin{aligned}\mathfrak{d}[\omega_n]&=E_n\mathfrak{d}_{\phi n+}+F_n\mathfrak{d}_{\phi n-}+G_n\mathfrak{d}_{\omega n+}+H_n\mathfrak{d}_{\omega n-}\\ \mathfrak{d}[\chi_n]&=I_n\mathfrak{d}_{\chi n+}+J_n\mathfrak{d}_{\chi n-}\end{aligned} \quad \cdots\cdots\cdots\cdots\cdots\cdots (2.8)$$

In the part of matrix, we have corresponding expressions;

$$\begin{cases}\mathfrak{d}_0[\phi_n]=A_{n0}\mathfrak{d}_{\phi n+}+B_{n0}\mathfrak{d}_{\phi n-}+C_{n0}\mathfrak{d}_{\omega n+}+D_{n0}\mathfrak{d}_{\chi n-}\\ \mathfrak{d}_0[\omega_n]=E_{n0}\mathfrak{d}_{\phi n+}+F_n\mathfrak{d}_{\phi n-}+G_{n0}\mathfrak{d}_{\omega n+}+H_{n0}\mathfrak{d}_{\omega n-}\\ \mathfrak{d}_0[\chi_n]=I_{n0}\mathfrak{d}_{\chi n+}+J_{n0}\mathfrak{d}_{\chi n-}\end{cases} \quad \cdots\cdots\cdots (2.9)$$

and in the part of obstacle,

$$\begin{cases}\mathfrak{d}_1[\phi_n]=A_{n1}\mathfrak{d}_{\phi n+}+C_{n1}\mathfrak{d}_{\omega n+}\\ \mathfrak{d}_1[\omega_n]=E_{n1}\mathfrak{d}_{\phi n+}+G_{n1}\mathfrak{d}_{\omega n+}\\ \mathfrak{d}_1[\chi_n]=I_{n0}\mathfrak{d}_{\chi n+}\end{cases} \quad \cdots\cdots\cdots\cdots\cdots\cdots (2.10)$$

If an arbitrary stress represented by the expression

$$\sum_n [K_n\mathfrak{F}_{\phi n+}+L_n\mathfrak{F}_{\omega n+}+M_n\mathfrak{F}_{\chi n+}]_{r=R} \quad \cdots\cdots\cdots\cdots\cdots (2.11)$$

is applied to the spherical surface $r=R$, then the displacements in the above model are as follows:

in the equivalent homogeneous continuum;

$$\mathfrak{d}=\sum_n K_n\mathfrak{d}[\phi_n]+\sum_n L_n\mathfrak{d}[\omega_n]+\sum_n M_n\mathfrak{d}[\chi_n]$$

in the matrix;

$$\mathfrak{d}_0=\sum_n K_n\mathfrak{d}_0[\phi_n]+\sum_n L_n\mathfrak{d}_0[\omega_n]+\sum_n M_n\mathfrak{d}_0[\chi_n] \quad \cdots\cdots\cdots (2.12)$$

in the obstacle;

$$\mathfrak{d}_1=\sum_n K_n\mathfrak{d}_1[\phi_n]+\sum_n L_n\mathfrak{d}_1[\omega_n]+\sum_n M_n\mathfrak{d}_1[\chi_n]$$

3. $\mathfrak{d}[\phi_n]$. Relevalent solution of A_n, B_n, C_n and D_n.

In this article we will determine the quantities such as A_n, B_n C_n D_n which are involved in the expressions (2.7), (2.8), (2.9) and (2.10), and also in (2.11), (2.12) and (2.13) implicitly.

Boundary conditions which must hold at the boundary surfaces are

$$\begin{aligned}&r=R\,;\ \mathfrak{F}=\text{external stress}\\ &r=r_0\,;\ \mathfrak{d}=\mathfrak{d}_0\\ &\qquad\ \mathfrak{F}=\mathfrak{F}_0\\ &r=a\,;\ \mathfrak{d}_0=\mathfrak{d}_1\\ &\qquad\ \mathfrak{F}_0=\mathfrak{F}_1\end{aligned} \quad \cdots\cdots\cdots\cdots\cdots\cdots (3.1)$$

3.1 Determination of A_n, B_n, C_n, D_n.

At first, we will take up the case when the external stress

$$\mathfrak{F}_{\phi n+}=\mu 2(n-1)\{n,1\}_n \quad \cdots\cdots\cdots\cdots\cdots\cdots (3.2)$$

is applied at the spherical surface

$$r=R,$$

A_n, B_n, C_n, D_n; A_{n0}, B_{n0}, C_{n0}, D_{n0}; A_{n1}, C_{n1} are determined by the next equations which are obtained from the boundary conditions.

$$\mathfrak{M}\mathfrak{A}=\mathfrak{S}_\phi \qquad \cdots\cdots(3.3)$$

or

$$\begin{pmatrix}
f_1R^{n-2} & f_2R^{-n-3} & f_3R^n & f_4R^{-n-1} & 0 & 0 \\
g_1R^{n-2} & g_2R^{-n-3} & g_3R^n & g_4R^{-n-1} & 0 & 0 \\
d_1r_0^{n-1} & d_2r_0^{-n-2} & d_3r_0^{n+1} & d_4r_0^{-n} & -d_{10}r_0^{n-1} & -d_{20}r_0^{-n-2} \\
r_0^{n-1} & r_0^{-n-2} & r_0^{n+1} & r_0^{-n} & -r_0^{n-1} & -r_0^{-n-2} \\
\chi f_1r_0^{-n-2} & \chi f_2r_0^{-n-3} & f_3r_0^n & f_4r_0^{-n-1} & f_{10}r_0^{n-2} & -f_{20}r_0^{-n-3} \\
\chi g_1r_0^n & \chi g_2r_0^{-n-3} & g_3r_0^n & g_4r_0^{-n-1} & g_{10}r_0^{n-2} & -g_{20}r_0^{-n-3} \\
0 & 0 & 0 & 0 & d_{10}r_0^{n-1} & d_{20}a^{-n-2} \\
0 & 0 & 0 & 0 & a^{n-1} & a^{-n-2} \\
0 & 0 & 0 & 0 & f_{10}a^{n-2} & f_{20}a^{-n-3} \\
0 & 0 & 0 & 0 & g_{10}a^{n-2} & g_{20}a^{-n-3}
\end{pmatrix}$$

$$\begin{pmatrix}
0 & 0 & 0 & 0 \\
0 & 0 & 0 & 0 \\
-d_{30}r_0^{n+1} & -d_{40}r_0^{-n} & 0 & 0 \\
-r_0^{n+1} & -r_0^{-n} & 0 & 0 \\
-f_{30}r_0^n & -f_{40}r_0^{-n-1} & 0 & 0 \\
-g_{30}r_0^n & -g_{40}r_0^{-n-1} & 0 & 0 \\
d_{30}a^{n-1} & d_{40}a^{-n} & -d_{11}a^{n-1} & -d_{11}a^{n-1} \\
a^{n+1} & a^{-n} & -a^{n-1} & -a^{n+1} \\
f_{30}a^n & f_{40}a^{-n-1} & -\chi_1f_{11}a^{n-2} & -\chi_1f_{31}a^n \\
g_{30}a^n & g_{40}a^{-n-1} & -\chi_1g_{11}a^{n-2} & -\chi_1g_{31}a^n
\end{pmatrix}
\cdot
\begin{pmatrix} A_n \\ B_n \\ C_n \\ D_n \\ A_{n0} \\ B_{n0} \\ C_{n0} \\ D_{n0} \\ A_{n1} \\ C_{n1} \end{pmatrix}
=
\begin{pmatrix} f_1 \\ g_1 \\ 0 \\ 0 \\ 0 \\ 0 \\ 0 \\ 0 \\ 0 \\ 0 \end{pmatrix}$$

$$\cdots\cdots(3.4) \qquad (n \gtrless 0)$$

in which

$$\begin{cases}
\chi=\mu/\mu_0, \quad \chi_1=\mu_1/\mu_0 \\
\mathfrak{d}_{\phi n+}=\{d_1, 1\}_n r^{n-1}, & \mathfrak{F}_{\phi n+}/\mu=\{f_1, g_1\}_n r^{n-2} \\
\mathfrak{d}_{\phi n-}=\{d_2, 1\}_n r^{-n-2}, & \mathfrak{F}_{\phi n-}/\mu=\{f_2, g_2\}_n r^{-n-3} \qquad \cdots\cdots(3.5) \\
\mathfrak{d}_{\omega n+}=\{d_3, 1\}_n r^{n+1}, & \mathfrak{F}_{\omega n+}/\mu=\{f_3, g_3\}_n r^n \\
\mathfrak{d}_{\omega n-}=\{d_4, 1\}_n r^{-n}, & \mathfrak{F}_{\omega n-}/\mu=\{f_4, g_4\}_n r^{-n-1} \quad \text{etc.}
\end{cases}$$

Solving these equations we have

$$\begin{cases}
A_n=\Delta_{An}/\Delta_n \\
B_n=\Delta_{Bn}/\Delta_n \\
C_n=\Delta_{Cn}/\Delta_n \\
D_n=\Delta_{Dn}/\Delta_n
\end{cases} \qquad \cdots\cdots(3.6)$$

$$(n \gtrless 0)$$

$$\Delta_n=\det(\mathfrak{M})=-R^{2n-2}(f_1g_3-g_1f_3)\Delta_n\begin{pmatrix}1,2\\1,3\end{pmatrix}$$
$$\cdot\left\{1-R^{-2n+1}\frac{f_3g_4-g_3f_4}{f_1g_3-g_1f_3}\Delta_n\begin{pmatrix}1,2\\3,4\end{pmatrix}\Big/\Delta_n\begin{pmatrix}1,2\\1,3\end{pmatrix}\right\}$$

$$\begin{cases}\Delta_{An}=-R^n(f_1g_3-g_1f_3)\Delta_n\begin{pmatrix}1,2\\1,3\end{pmatrix}+O(R^{-n-1})\\ \Delta_{Bn}=\ R^n(f_1g_3-g_1f_3)\Delta_n\begin{pmatrix}1,2\\2,3\end{pmatrix}+O(R^{-n-1})\\ \Delta_{Cn}=\ R^{-n-1}(f_1g_4-g_1f_4)\Delta_n\begin{pmatrix}1,2\\3,4\end{pmatrix}+O(R^{-n-3})\\ \Delta_{Dn}=-R^n(f_1g_3-g_1f_3)\Delta_n\begin{pmatrix}1,2\\3,4\end{pmatrix}+O(R^{-n-3})\quad(n\neq 0)\end{cases}\quad\cdots\cdots\cdots(3.7)$$

where $\Delta_n\begin{pmatrix}i,j\\p,q\end{pmatrix}$ means a minor determinant of the $(n-2)$-th degree which is obtained from the original Δ_n erasing the i-th and j-th rows and the p-th and q-th columns.

Introducing these expressions into (2.7), we have

$$\mathfrak{d}[\phi_n]=R\{n,1\}_n+R^{-2n+2}\Delta_n\begin{pmatrix}1,2\\3,4\end{pmatrix}\Big/\Delta_n\begin{pmatrix}1,2\\1,3\end{pmatrix}$$
$$\cdot\left[\{n,1\}_n\frac{f_3g_4-g_3f_4}{f_1g_3-g_1f_3}-\{n+\alpha_n,1\}_n\frac{f_1g_4-g_1f_4}{f_1g_3-g_1f_3}\right.$$
$$\left.+\{-n-1+\alpha_{-n-1},1\}_n+O(R^{-2})\right](n\neq 0)\quad\cdots\cdots(3.8)$$

On the other hand, from (2.3a) and (2.4a)

$$\mathfrak{d}[\phi_0]=0\qquad\cdots\cdots(3.8a)$$

4. $\mathfrak{d}[\omega_n]$. Relevant solution of E_n, F_n, G_n, H_n.

By a similar treatment, we can obtain E_n, F_n, G_n, H_n; E_{n0},..... although, in this case, the external stress takes the form

$$\mathfrak{F}_{\omega n+}=\mu\{(n-3)\alpha_n+2(n^2-2n-1),2n+\alpha_n\}_n\qquad\cdots\cdots(4.1)$$
$$\equiv\mu\{f_3,g_3\}$$

Simultaneous equations to determine E_n, F_n, and so forth are expressed by the following form;

$$\mathfrak{M}\cdot\mathfrak{E}=\mathfrak{S}_\omega\qquad\cdots\cdots(4.2)$$

in which

$$\mathfrak{E}=\begin{pmatrix} E_n \\ F_n \\ G_n \\ H_n \\ E_{n0} \\ F_{n0} \\ G_{n0} \\ H_{n0} \\ E_{n1} \\ G_{n1} \end{pmatrix}, \qquad \mathfrak{S}_\omega=\begin{pmatrix} f_3 \\ g_3 \\ 0 \\ 0 \\ 0 \\ 0 \\ 0 \\ 0 \\ 0 \\ 0 \end{pmatrix}$$

and $\mathfrak{M}$ is same with the previous one.

.....(4.3)

Solving these equations we obtain

$$\begin{cases} E_n=\Delta_{En}/\Delta_n \\ F_n=\Delta_{Fn}/\Delta_n \\ G_n=\Delta_{Gn}/\Delta_n \\ H_n=\Delta_{Hn}/\Delta_n \qquad (n\neq 0) \end{cases} \qquad \text{.....(4.4)}$$

in which

$$\begin{cases} \Delta_{En}= R^{-n-1}(f_3g_4-g_3f_4)\Delta_n\begin{pmatrix}1,2\\1,4\end{pmatrix}+O(R^{-n-3}) \\ \Delta_{Fn}= R^{n-2}(f_1g_3-g_1f_3)\Delta_n\begin{pmatrix}1,2\\1,2\end{pmatrix}O(R^{-n-1}) \\ \Delta_{Gn}=-R^{n-2}(f_1g_3-g_1f_3)\Delta_n\begin{pmatrix}1,2\\1,3\end{pmatrix} \\ \qquad\qquad +(f_3g_4-g_3f_4)R^{-n-1}\Delta_n\begin{pmatrix}1,2\\3,4\end{pmatrix}+O(R^{-n-3}) \\ \Delta_{Hn}= R^{n-2}(f_1g_3-g_1f_3)\Delta_n\begin{pmatrix}1,2\\1,4\end{pmatrix}+O(R^{-n-3}) \end{cases}$$

and Δ_n has already appeared in the previous section.

Introducing these expressions into (2.8), we have

$$\begin{aligned} \mathfrak{d}[\omega_n]=&R\{n+\alpha_n,1\} \\ &-R^{-2n}\frac{\Delta_n\begin{pmatrix}1,2\\1,4\end{pmatrix}}{\Delta_n\begin{pmatrix}1,2\\1,3\end{pmatrix}}\left[\frac{f_3g_4-g_3f_4}{f_1g_3-g_1f_3}\{n,1\}+\{-n-1+\alpha_{-n-1},1\}^*\right] \\ &+O(R^{-2n-2}) \qquad (n\neq 0) \qquad \text{.....(4.5)} \end{aligned}$$

When $n=0$, the solution must be obtained in another way. Introducing the expressions (2.3a) and (2.4a) into the boundary conditions, we have

$$\begin{pmatrix} 4\mu R^{-3} & 3\alpha_0 k & 0 & 0 & 0 \\ -r_0^{\,2} & \alpha_0 r_0 & r_0^{-2} & -\alpha_{00} r_0 & 0 \\ 4\mu r_0^{-3} & 3\alpha_0 k & -4\mu_0 r_0^{-3} & -3\alpha_{00} k_0 & 0 \\ 0 & 0 & -a^{-2} & \alpha_{00} a & -\alpha_{01} a \\ 0 & 0 & 4\mu_0 a^{-3} & 3\alpha_{00} k_0 & -3\alpha_{01} k_1 \end{pmatrix} \begin{pmatrix} F \\ G \\ F_0 \\ G_0 \\ G_1 \end{pmatrix} = \begin{pmatrix} 3\alpha_0 k \\ 0 \\ 0 \\ 0 \\ 0 \end{pmatrix} \quad \cdots\cdots(4.6)$$

from which we arrive at the following solution

$$\mathfrak{d}[\omega_0] = \alpha_0 R + \left\{1 + \frac{4\mu}{3k}\right\} R^{-2} \frac{\Delta_0\binom{1}{1}}{\Delta_0\binom{1}{2}} \quad \cdots\cdots(4.7)$$

in which $\Delta_0\binom{i}{p}$ is a minor of the (i, p)-element of the determinant of degree 5 obtained from (4.6).

5. $\mathfrak{d}[\chi_n]$. Relevant solution of I_n, J_n.

In the former sections we have obtained A_n, B_n, C_n, D_n and E_n, F_n, G_n, H_n, which give the relevalent solution of the cases of type ϕ_n and ω_n. Now here, we will get the solution of I_n and J_n which are necessary to express the displacement of the type χ_n.

External stress in this case, applied to the outer spherical surface is

$$\mathfrak{F}_{\chi n+} = -\mu(n-1) S_n' \mathfrak{s} \quad \cdots\cdots(5.1)$$

Boundary conditions are

$$\begin{aligned} r=R: \quad & \mathfrak{F}[\chi_n] = -\mu(n-1) S_n' \mathfrak{s} \\ r=r_0; \quad & \mathfrak{d}[\chi_n] = \mathfrak{d}_0[\chi_n] \\ & \mathfrak{F}[\chi_n] = \mathfrak{F}_0[\chi_n] \quad \cdots\cdots(5.2) \\ r=a; \quad & \mathfrak{d}_0[\chi_n] = \mathfrak{d}_1[\chi_n] \qquad (n \neq 0) \\ & \mathfrak{F}_0[\chi_n] = \mathfrak{F}_1[\chi_n] \end{aligned}$$

in which $\mathfrak{d}[\chi_n]$, $\mathfrak{d}_0[\chi_n]$ etc. are given in (2.8) and so on.

Simultaneous equations to determine I_n, J_n; I_{n0}, J_{n0}; and I_{n1} which are involved in (5.2) take the next form by the matrix expression.

$$\mathfrak{M}\dagger \cdot \mathfrak{J} = \mathfrak{S}_\chi \quad \cdots\cdots(5.3)$$

or

$$\mathfrak{M}\dagger = \begin{pmatrix} (n-1)R^{n-1} & -(n+2)R^{-n-2} & 0 & 0 & 0 \\ -r_0^{\,n} & -r_0^{-n-1} & r_0^{\,n} & r_0^{-n-1} & 0 \\ -\chi(n-1)r_0^{\,n-1} & \chi(n+2)r_0^{-n-2} & (n-1)r_0^{-n-2} & -(n+2)r_0^{-n-2} & 0 \\ 0 & 0 & a^n & a^{n-1} & -a^n \\ 0 & 0 & -(n-1)a^{n-1} & (n+2)a^{-n-2} & \chi_1(n-1)a^{n-1} \end{pmatrix}$$

and

$$\mathfrak{I}=\begin{pmatrix} I_n \\ J_n \\ I_{n0} \\ J_{n0} \\ I_{n1} \end{pmatrix}, \qquad \mathfrak{S}_\chi=\begin{pmatrix} n-1 \\ 0 \\ 0 \\ 0 \\ 0 \end{pmatrix} \qquad \cdots\cdots(5.4)$$

The solution is easily obtained in the following form

$$\begin{aligned} I_n&=\Delta_n^\dagger\begin{pmatrix}1\\1\end{pmatrix}\Big/\Delta_n^\dagger \\ J_n&=-\Delta_n^\dagger\begin{pmatrix}1\\2\end{pmatrix}\Big/\Delta^\dagger \qquad \cdots\cdots(5.5) \\ \Delta_n^\dagger&=\det(\mathfrak{M}\dagger) \end{aligned}$$

$\Delta_n^\dagger\begin{pmatrix}p\\q\end{pmatrix}$ is a minor determinant of the (p,q)-element of $\Delta_n^\dagger$.

Hence, at $r=R$

$$\begin{aligned} \mathfrak{d}[\chi_n]&=I_n(-R^nS_n'\hat{\mathfrak{s}})+J_n(-R^{-n-1}S_n'\hat{\mathfrak{s}}) \\ &=\left[-R+R^{-2n}\frac{\Delta_n^\dagger\begin{pmatrix}1\\2\end{pmatrix}}{\Delta_n^\dagger\begin{pmatrix}1\\1\end{pmatrix}}\left\{1+\frac{n+2}{n-1}\right\}\right]\cdot(S_n'\hat{\mathfrak{s}}) \quad (n\neq 0) \quad \cdots(5.6) \end{aligned}$$

When $n=0$

$$\mathfrak{d}[\chi_0]=0 \qquad \cdots\cdots(5.6a)$$

6. General form of displacement in the equivalent homogeneous shell corresponding to the general type of stress.

When a general type of stress

$$\mathfrak{F}=\sum_n[K_n\mathfrak{F}_{\phi n+}+L_n\mathfrak{F}_{\omega n+}+M_n\mathfrak{F}_{\chi n+}]_{r=R} \qquad \cdots\cdots(6.1)$$

is given at the outer spherical surface $r=R$, the corresponding displacement is

$$\mathfrak{d}=\sum_n[K_n\mathfrak{d}[\phi_n]+L_n\mathfrak{d}[\omega_n]+M_n\mathfrak{d}[\chi_n]] \qquad \cdots\cdots(6.2)$$

which is now explicity written down by means of the above preparations.

Introducing $\mathfrak{d}[\phi_n]$, $\mathfrak{d}[\omega_n]$ and $\mathfrak{d}[\chi_n]$ given in (3.8), (3.8a), (4.5), (4.7) (5.6) and (5.6a) we have

$$\begin{aligned} \mathfrak{d}=&L_0\cdot R\alpha_0 \\ &+\sum_{n=1}[K_n\cdot R\{n,1\}_n+L_n\cdot R\{n+\alpha_n,1\}_n+M_n\cdot(-)R] \\ &+L_0\cdot R^{-2}\left\{1+\frac{4\mu}{3k}\right\}\Delta\begin{pmatrix}1\\1\end{pmatrix}\Big/\Delta\begin{pmatrix}1\\2\end{pmatrix} \end{aligned}$$

$$+\sum_{n=1}\Big[K_n\cdot R^{-2n+2}\Big\{\Delta_n\begin{pmatrix}1,2\\3,4\end{pmatrix}\Big/\Delta_n\begin{pmatrix}1,2\\1,3\end{pmatrix}\Big\}\cdot\Big[\{n,1\}_n\frac{f_3g_4-g_3f_4}{f_1g_3-g_1f_3}-\cdots\Big]$$

$$+L_n\cdot R^{-2n}(-)\Big\{\Delta_n\begin{pmatrix}1,2\\1,4\end{pmatrix}\Big/\Delta_n\begin{pmatrix}1,2\\1,3\end{pmatrix}\Big\}\cdot\Big[\{n,1\}_n\frac{f_3g_4-g_3f_4}{{}_1fg_3-g_1f_3}-\cdots\Big]$$

$$+M_n\cdot R^{-2n}\Big\{\Delta_n^{\dagger}\begin{pmatrix}1\\2\end{pmatrix}\Big/\Delta_n^{\dagger}\begin{pmatrix}1\\1\end{pmatrix}\Big\}\cdot\Big[\Big\{1+\frac{n+2}{n-1}\Big\}\cdot S_n'\mathfrak{s}\Big]\Big] \quad \ldots(6.3)$$

On the other hand, the displacement at the same surface $r=R$ of the equivalent homogeneous sphere under the same external stress is

$$\sum_{n=0}[K_n\mathfrak{d}_{\phi n+}+L_n\mathfrak{d}_{\omega n+}+M_n\mathfrak{d}_{\chi n+}]_{r=R}$$

$$=L_0R\alpha_0+\sum[K_n\cdot R\{n,1\}_n+L_n\cdot R\{n+\alpha_n,1\}_n+M_n\cdot(-)R] \quad \ldots(6.4)$$

which is exactly equal to the first and second lines of (6.3). Therefore the right hand member of the expression (6.3), excluding these two lines, must vanish. Thus

$$L_0R^{-2}\Big\{1+\frac{4\mu}{3k}\Big\}\Delta\begin{pmatrix}1\\1\end{pmatrix}\Big/\Delta\begin{pmatrix}1\\2\end{pmatrix}$$

$$+\sum_{n=1}\Big[K_n\cdot R^{-2n+2}\Big\{\Delta_n\begin{pmatrix}1,2\\3,4\end{pmatrix}\Big/\Delta_n\begin{pmatrix}1,2\\1,3\end{pmatrix}\Big\}\cdot\Big[\cdots\cdot\Big]$$

$$+L_nR^{-2n}(-)\Big\{\Delta_n\begin{pmatrix}1,2\\1,4\end{pmatrix}\Big/\Delta_n\begin{pmatrix}1,2\\1,3\end{pmatrix}\cdot\Big[\cdots\cdot\Big]$$

$$+M_n\cdot R^{-2n}\Big\{\Delta_n^{\dagger}\begin{pmatrix}1\\2\end{pmatrix}\Big/\Delta_n^{\dagger}\begin{pmatrix}1\\1\end{pmatrix}\Big\}\cdot\Big[\cdots\cdot\Big]\Big]=0 \quad \ldots\ldots(6.5)$$

or

$$K_1\cdot\Big\{\Delta_1\begin{pmatrix}1,2\\3,4\end{pmatrix}\Big/\Delta_1\begin{pmatrix}1,2\\1,3\end{pmatrix}\Big\}\cdot[\{1,1\}_1\ \ldots.]$$

$$+R^{-2}\cdot\Big[L_0\Big\{1+\frac{4\mu}{3k}\Big\}\Delta\begin{pmatrix}1\\1\end{pmatrix}\Big/\Delta\begin{pmatrix}1\\2\end{pmatrix}$$

$$+K_2\Big\{\Delta_2\begin{pmatrix}1,2\\3,4\end{pmatrix}\Big/\Delta_2\begin{pmatrix}1,2\\1.3\end{pmatrix}\Big\}\cdot[\{2,1\}_2\ \ldots.]$$

$$+L_1(-)\Big\{\Delta_1\begin{pmatrix}1,2\\1,4\end{pmatrix}\Big/\Delta_1\begin{pmatrix}1,2\\1,3\end{pmatrix}\Big\}\cdot[\{1,1\}_1\ \ldots.]$$

$$+M_1\Big\{\Delta_1^{\dagger}\begin{pmatrix}1\\2\end{pmatrix}\Big/\Delta_1^{\dagger}\begin{pmatrix}1\\1\end{pmatrix}\Big\}\cdot[\ \ldots\ldots]\Big]$$

$$+O(R^{-4}) \qquad =0 \qquad \ldots\ldots\ldots\ldots(6.5)$$

Since this expression is arranged according to the descending power of R, an upper term is larger than the lower one. Therefore we will equate every term to zero from above one by one.

Fortunately the first line involving K_1 vanishes, for the determinant

$\Delta_1\begin{pmatrix}1,2\\3,4\end{pmatrix}$ is identically zero. (This terms denotes a mere translation of a sphere to the direction of z-axis as a rigid body.)

Among the remaining terms, the fourth line involving L_1 also vanishes, for

$$\Delta_1\begin{pmatrix}1,2\\1,4\end{pmatrix}=0$$

The fifth line involving M_1 is a term derived from χ_1. Now, this solution implies the mere rotation of a sphere as a rigid body. Therefore it has nothing to do with the stress distribution.

Now, we must equate the remaining terms to zero. Since L_0 and K_2 take independent values both terms must vanish independently.

$$\Delta\begin{pmatrix}1\\1\end{pmatrix}=0 \qquad \ldots\ldots\ldots\ldots\ldots\ldots\ldots\ldots\ldots\ldots(6.7)$$

$$\Delta_2\begin{pmatrix}1,2\\3,4\end{pmatrix}=0 \qquad \ldots\ldots\ldots\ldots\ldots\ldots\ldots\ldots\ldots\ldots(6.8)$$

7. Bulk modulus.

Solving the equation (6.7), we have the following solution;

$$k=k_0-(k_0-k_1)\frac{3k_0+4\mu_0}{3k_1+4\mu_0}(1-\rho) \qquad \ldots\ldots\ldots\ldots\ldots\ldots(7.1)^{5)}$$

which is equivalent to the formula of bulk modulus obtained in our former paper. ($1-\rho$ is the proportion of the volume occupied by the obstacle.)

7.1 Weighted mean of the compressibility.

Some thirty years ago, Adams[6] made a comprehensive investigation upon the compressibility of heterogeneous medium. He concludes that at a high pressure (above about 3000 bars) the compressibility of a rock is the average (according to volumes) of those of constituent minerals.

At a sight this conclusion seems very natural, but the weighted mean (according to volumes) of the compressibilities $1/k_0$ and $1/k_1$ of two materials is (σ_0 implies Poisson's ratio.)

$$\rho\frac{1}{k_0}+(1-\rho)\frac{1}{k_1}=\frac{1}{k_0}\left\{1+(1-\rho)\frac{1-K}{K}\right\} \qquad \ldots\ldots\ldots\ldots(7.2)$$

5) *loc. cit.*, 1) Expressions (4.8), (4.9).

6) L. H. ADAMS, *Beitr. z. Geophys.*, **31** (1931), 315. Afterwards he modified his theory a little. *cf. Journ. Franclin Inst.*, **208** (1929).

while the corresponding value calculated by means of (7.1) is

$$\frac{1}{k}=\frac{1}{k_0}\left[1+(1-\rho)\frac{3(1-K)(1-\sigma_0)}{2(1-2\sigma_0)+K(1+\sigma_0)}\right],\quad (K=k_1/k_0) \qquad \cdots\cdots(7.3)$$

and these two expressions are generally not equal.

Equating the right hand members of (7.2) and (7.3) we can easily find the condition when Adams' simple theory strictly holds. This gives

$$(1-2\sigma_0)(1-K)^2=0 \qquad \cdots\cdots(7.4)$$

which is statisfied by

$$\sigma_0=1/2 \quad \text{or} \quad K=1 \qquad \cdots\cdots(7.5)$$

The former condition implies that the material of the matrix is incompressible, while the latter gives $k_0=k_1$, or the condition that the compressibilities of the pebble and the matrix are altogether equal.

8. Rigidity.

The equation $\Delta_2\binom{1,2}{3,4}=0$ gives the rigidity.

In Mackenzie's paper[7], when he calculates the bulk modulus, he arbitrarily applies the hydrostatic pressure, and when he aims at the rigidity, he uses the spherical solid harmonics of degree two, but without sufficient proof. Therefore one fears that another way of calculation using other types of stress distribution may give another result.

However, in this paper, we have employd a general type of solution, and arrived at the same result with the former paper in regard to the bulk modulus. Also with respect to the rigidity, we arrived at a similar conclusion, which means the method of applying the stress given by the spherical solid harmonics of degree two was justified.

We will now proceed to the solution of (6.8).

$$\Delta_2\binom{1,2}{3,4}=0 \qquad \cdots\cdots(6.8\text{ bis})$$

After some complicated calculations the above equation assumes the following form:

7) J. K. MACKENZIE, "The Elastic Constants of a Solid Containing spherical Holes," *Proc. Phys. Soc.*, **B63** (1950), 2.

$$\Delta_2\begin{pmatrix}1,2\\3,4\end{pmatrix}=\mu_0^4\cdot 50a^{-4}r_0^{-1}(-\alpha_{20}+2)\{-8\alpha_{21}+(3\alpha_{21}+10\chi_1)\}$$
$$\cdot\Big[-(\chi-1)\{(2\chi_1+3)(\alpha_{-30}-5)+5(2\chi_1+1)\}$$
$$+(\chi_1-1)\frac{a^3}{r_0^3}5(\alpha_{-30}-2)$$
$$+0(a^5/r_0^5)\Big]$$
$$=0 \qquad \cdots\cdots\cdots\cdots\cdots\cdots\cdots\cdots(8.1)$$

in which

$$\alpha_{n0}=\frac{4(2n+1)\sigma_0-2(3n+1)}{-4\sigma_0+n+5}$$
$$\chi=\mu/\mu_0$$
$$\chi_1=\mu_1/\mu_0$$

σ_0 is Poisson's ratio of the matrix.

Since the first line of the expression (8.1) does not vanish, terms in [ ] must be equal to zero.

Therefore we have, as the first approximation, the following formula

$$(\chi-1)\{(2\chi_1+3)(\alpha_{-30}-5)+5(2\chi_1+1)\}=(\chi_1-1)\frac{a^3}{r_0^3}5(\alpha_{-30}-2)$$

or

$$\mu=\mu_0\Big[1+(1-\rho)\frac{15(\chi_1-1)(1-\sigma_0)}{2\chi_1(4-5\sigma_0)+(7-5\sigma_0)}\Big] \qquad \cdots\cdots\cdots\cdots(8.2)$$

If we put $\chi_1=0$ (, or $\mu_1=0$) into the above expression, we have

$$\mu=\mu_0\Big[1+(1-\rho)\frac{-15(1-\sigma_0)}{7-5\sigma_0}\Big] \qquad \cdots\cdots\cdots\cdots\cdots\cdots(8.3)$$

This is equivalent to the formula introduced by Mackenzie[8] and the author[9], and applicable to the case of hollow or liquid sphere.

9. Other elastic constants.

We have obtained two independent elastic constants; i.e. k (cf. (7.1) or (7.3)) and μ (cf. (8.3)), from which we are able to deduce other elastic constants and the velocity of prepagation of waves with long wave-lengths.

The principle of calculation is very simple in each case. We will only show the results here.

8) *loc. cit.*, 7). Expression (19).
9) *loc. cit.*, 1). Expression (3.2).

$$\begin{cases} \lambda=\lambda_0\left[1+(1-\rho)\left(-\dfrac{1-\sigma_0}{\sigma_0}\right)\right. \\ \qquad \left.\cdot\left\{\dfrac{(1-K)(1+\sigma_0)}{2(1-2\sigma_0)+K(1+\sigma_0)}+\dfrac{5(\chi_1-1)(1-2\sigma)}{2\chi_1(4-5\sigma_0)+(7-5\sigma_0)}\right\}\right] \quad \ldots(9.1) \\ \sigma=\sigma_0\left[1+(1-\rho)\left(-\dfrac{(1-2\sigma_0)(1-\sigma_0^2)}{\sigma_0}\right)\right. \\ \qquad \left.\cdot\left\{\dfrac{1-K}{2(1-2\sigma_0)+K(1+\sigma_0)}+\dfrac{5(\chi_1-1)}{2\chi_1(4-5\sigma_0)+(7-5\sigma_0)}\right\}\right] \quad \ldots(9.2) \end{cases}$$

On the other hand, density δ is

$$\delta=\delta_0[1-(1-\rho)(1-D)] \quad \ldots\ldots\ldots\ldots\ldots(9.3)$$

in which δ_0 and $\delta_1\equiv D\delta_0$ are the density of the matrix and the obstacle respectively.

From (8.2), (9.1) and (9.3) we have

$$V_p=V_{p0}\left[1+(1-\rho)\frac{1}{2}\left\{(1-D)\right.\right. \\ \left.\left.+\frac{-(1-K)(1+\sigma_0)}{2(1-2\sigma_0)+K(1+\sigma_0)}+\frac{10(\chi_1-1)(1-2\sigma_0)}{2\chi_1(4-5\sigma_0)+(7-5\sigma_0)}\right\}\right] \quad \ldots.(9.4)$$

$$V_s=V_{s0}\left[1+(1-\rho)\frac{1}{2}\left\{(1-D)+\frac{15(\chi_1-1)(1-\sigma_0)}{2\chi_1(4-5\sigma_0)+(7-5\sigma_0)}\right\}\right] \quad \ldots(9.5)$$

as the propagation velocity of longitudinal and transverse waves in this composite medium.

10. Numerical examples.

10.1 When the obstacle is rigid.

When the embedded spherical body is rigid we must take

$$K=\infty, \qquad \chi_1=\infty. \quad \ldots\ldots\ldots\ldots\ldots\ldots(10.1)$$

Therefore, we have from (7.3), (8.2), (9.1), (9.2) and (9.4).

$$\begin{cases} k=k_0\left[1+(1-\rho)\dfrac{3(1-\sigma_0)}{1+\sigma_0}\right], \\ \mu=\mu_0\left[1+(1-\rho)\dfrac{15(1-\sigma_0)}{2(4-5\sigma_0)}\right], \\ \lambda=\lambda_0\left[1+(1-\rho)\dfrac{3(1-\sigma_0)}{2\sigma_0(4-5\sigma_0)}\right], \quad \ldots(10.2) \\ \sigma=\sigma_0\left[1+(1-\rho)\dfrac{(1-\sigma_0^2)(1-2\sigma_0)}{\sigma_0}\left\{\dfrac{1}{1+\sigma_0}-\dfrac{5}{2(4-5\sigma_0)}\right\}\right], \\ V_p=V_{p0}\left[1+(1-\rho)\dfrac{1}{2}\left\{\dfrac{3(3-5\sigma_0)}{4-5\sigma_0}+(1-D)\right\}\right], \end{cases}$$

$$V_s = V_{s0}\left[1+(1-\rho)\frac{1}{2}\left\{\frac{15(1-\sigma_0)}{2(4-5\sigma_0)}+(1-D)\right\}\right].$$

These formulae will be applied when the bulk modules and the rigidity of the embedded obstacles are far larger than those of the matrix. It will be interesting to compare them with the formulae which are applicable to the case of vacant spherical holes[10].

Figs. 2a, b, c and d show the variation of k/k_0, μ/μ_0, λ/λ_0 and σ/σ_0 as functions of $(1-\rho)$. The parameter in the figures is Poisson's ratio σ_0 of the matrix.

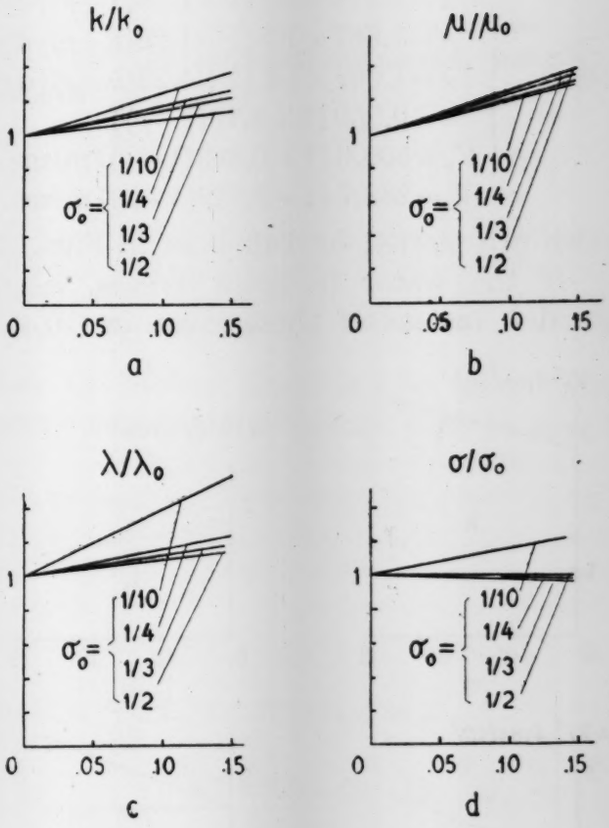

Fig. 2. Variation of k/k_0, μ/μ_0 and σ/σ_0 when the embedded obstacle is rigid. Abscissa is $1-\rho$, or the proportion of volume occupied by the obstacle.

10.2 When the holes are filled with water or ice.

Suppose a soft material with a sound velocity as small as

$$V_{p0}=500\ \text{m/sec},$$

and

$$\delta_0=2.0\ \text{gr/cm}^3, \qquad \sigma_0=1/4. \qquad \text{.....(10.3)}$$

Then

$$\lambda_0=\mu_0=1.667\times10^9\ \text{dyne/cm}^2.$$

If water is contained in the holes of this material, we have

$$k_1=2.1\times10^{10}\ \text{dyne/cm}^2, \qquad \delta_1=1\ \text{gr/cm}^3, \qquad \text{.....(10.4)}$$

or combining with the above values we can easily obtain

$$K=k_1/k_0=75.6 \qquad D=\delta_1/\delta_0=0.5 \qquad \text{.....(10.5)}$$

10) *loc. cit.*, 1). Expression (3.2).

Putting these numerical values into the expressions (7.1), (8.2), (9.1), (9.2), (9.4) and (9.5) we get

$$\begin{cases} k=2.778\times10^{9}\,[1+1.76(1-\rho)]\ \text{dyne/cm}^2, \\ \mu=1.667\times10^{9}\,[1-1.96(1-\rho)]\ \text{dyne/cm}^2, \\ \lambda=1.667\times10^{9}\,[1+4.23(1-\rho)]\ \text{dyne/cm}^2, \\ \sigma=0.250\,[1+3.10(1-\rho)] \\ V_p=500.0\,[1+0.303(1-\rho)]\ \text{m/sec}, \\ V_s=288.7\,[1-0.729(1-\rho)]\ \text{m/sec}. \end{cases} \quad \ldots\ldots\ldots(10.6)$$

which are plotted by full lines in Figs. 3a, b, c, d, e and f.

If the water in holes freezes, we must introduce other values of k_1 and δ_1 instead of those given in (10,4). In this case we assume[11]

$$\begin{cases} V_{p1}=3480\ \text{m/sec}, \\ \delta_1=1/1.09\ \text{gr/cm}^3, \\ \sigma_1=1/3 \end{cases} \quad \ldots(10.7)$$

Then we have

$$\begin{cases} \lambda_1=5.56\times10^{11}\ \text{dyne/cm}^2, \\ \mu_1=2.78\times10^{11}\ \text{dyne/cm}^2. \end{cases}$$

Consequently

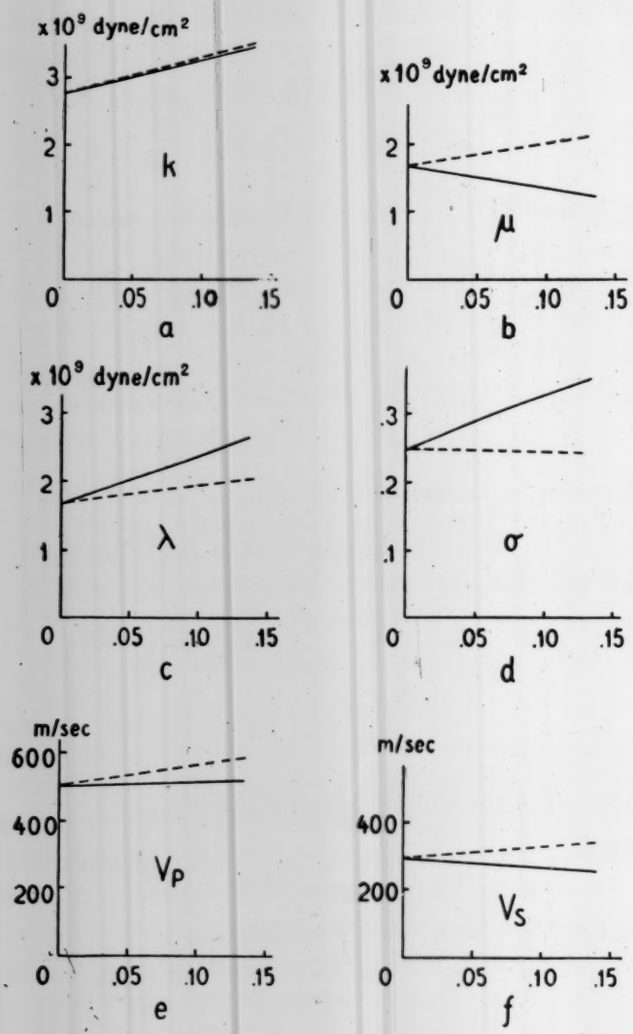

Fig. 3. Numerical values of the elastic constants k, μ, λ, σ and the propagation velocity V_p and V_s, assuming the material constants

$V_{p0}=500$ m/sec, $\delta_0=2.0$ gr/cm³, $\sigma_0=1/4$.,

($\lambda_0=\mu_0=1.667\times10^9$ dyne/cm²)

Full line shows the case when the holes are filled with water

($k=2.1\times10^{10}$ dyne/cm², $\rho_1=1.000$ gr/cm³),

while the broken line shows the case when the water was frozen.

$V_{p1}=3480$ m/sec,
$\delta_1=1/1.09$ gr/cm³,
$\sigma_1=1/3$.
($\lambda_1=5.56\times10^{11}$ dyne/cm²,
$\mu_1=2.78\times10^{11}$ dyne/cm²)

11) Y. SATÔ, *Bull. Earthq. Res. Inst.*, **29** (1951), 223. See foot-note 17).

$$\begin{cases} \chi_1=\mu_1/\mu_0=167 \\ K=k_1/k_0=267 \\ D=\delta_1/\delta_0=0.459 \end{cases} \qquad \cdots\cdots\cdots\cdots\cdots\cdots (10.8)$$

Introducing (10.7) and (10.8) into the previous formulae, we obtain the following numerical expressions:

$$\begin{cases} k=k_0\ [1+1.79\ (1-\rho)] \\ \mu=\mu_0\ [1+2.02\ (1-\rho)] \\ \lambda=\lambda_0\ [1+1.60\ (1-\rho)] \\ \sigma=\sigma_0\ [1-0.218(1-\rho)] \\ V_p=V_{p0}[1+1.211(1-\rho)] \\ V_s=V_{s0}[1+1.281(1-\rho)] \end{cases} \qquad \cdots\cdots\cdots\cdots\cdots\cdots (10.9)$$

the values of which are plotted by broken lines in the same figure with the former case. The most remarkable difference is to be seen in Figs. 3b and 3d.

---

1. 小さな異物を含む媒質内を伝はる彈性波の速さ

地震研究所 佐 藤 泰 夫

前の論文においては,[1] 小さな球形の穴を持つ媒質の彈性常数を, Mackenzie[8] の結果を用ゐて求め, あはせて十分に長い波長の彈性波がつたはる場合の速さを近似的に出したのであった. なほ, 穴の中に流体がつまってゐる場合にも公式を拡張したが, 本論文では, この穴をうづめてゐる物質が, 固体の時にはどのやうな式が得られるかといふ問題を扱った. Mackenzie の論文では, 適当なモデルを考へた上で, 体積彈性率を求める場合には外力として靜水圧を, 剛性率を求める時には 2 次の球函数で与へられるやうな応力を仮定して来た. しかし, 勝手にこのやうな函数形を採用してその結果えられた式が, 果してどのやうな外力を加へた場合にも通用する, 一般的な公式を与へ得るか否か, といふ事は必ずしも自明のことではない.

そこで, この論文では, まづ n 次の球函数で与へられる外力を仮定して, これに対する解を求め, 次に, 任意の外力を[2] 球函数に展開する事によって, 一般の解をさきに得られた解の線型結合としてあらはした. その上で境界條件をあはせ (第1図参照), equivalent homogeneous continuum の考へに従って彈性常数を求めた. すると, 体積彈性率を求める場合には結局靜水圧に対する項が, 剛性率については 2 次の球函数の項が, ものをいってくる事がわかる. 従って, 先に Mackenzie が採用し, 又我々が従って来た方法は正しいものであることが証明される (§ 8).

かくして得られる結果は, 体積彈性率については, 穴の中が流体の場合と同じである. ((7.1), (7.3) 参照.) 剛性率について, 2 次の球函数を用ゐて計算を行へば, 途中は複雑であるが, 最後には簡単な結果 (8.2) に到達する. この式で, 内部の剛性を 0 とおけばさきに得られた公式と一致する[8], [9]. 他の彈性常数は, k と μ とから容易に求められる. ((9.1)~(9.5)参照)

混合物質の圧縮率は, それを構成する物質の圧縮率を体積の割合で平均すれば得られることの考へがあり,[7] 一応もっともものやうであるが, 嚴密にはなりたたないもののやうである, (§ 7.1)

数値計算の例として，異物が剛体の場合 (§ 5.1)，水の場合，それが氷で置きかへられた場合 (§ 5.2) を行った。結果は式 (10.2)，第2図 a, b, c, d，および式 (10.6)，(10.9) と第3図 a, b, c, d, e, f に示してある．(§ 10)

以上の計算を行ふにあたって我我の採用した前提は前と同様で (§ 1)，

1) 多数の異物を含む相当の体積をもった媒質は全体として一様な連続した媒質と同等であること，

2) 異物は同じ大きさの球であること，

3) 異物が全媒質内でしめる体積の割合は十分に小さく，その二次の項を省略してもさしつかへないこと，

4) 境界面では変位と応力が連続であること，

5) 彈性波の速さを考へる時には，波長が異物相互間の距離や直徑にくらべて十分に大きく，準靜的な取扱ひが許されること，

などである．

2. *The Anomalous Behavior of Geomagnetic Variations of Short Period in Japan and Its Relation to the Subterranean Structure. The 2nd report.*

By Tsuneji RIKITAKE, Izumi YOKOYAMA
and Yoneko HISHIYAMA,

Earthquake Research Institute.

(Read Nov. 18, 1952.—Received Dec. 20, 1952.)

1. Introduction.

In the previous paper[1], the writers pointed out the anomalously large amplitude of changes in the vertical component of the earth's magnetic field of short period in the central part of Japan. And according to the results of some simple analyses, the anomalous behavior is preliminarily ascribed to a peculiar distribution of electrical property under Japan. Those analyses, however, were done on the basis of geomagnetic data obtained only from the stations in Japan and her neighborhood.

In order to make a more complete analysis, the writers intended to collect copies of magnetograms of the magnetic storm on June 18, 19 and 20, 1936 from various observatories all over the world. And we have now some 30 copies kindly sent from foreign observatories at the writers' request. The writers are very much obliged to these observatories and it is the writers' duty to report the results of the new analysis as soon as they can. The copies of magnetograms thus collected are so useful that we can analyse them from various viewpoints. But, first of all, the writers would here like to report the study concerning the sudden commencement (SC) observed at $9h$ $41m$ GMT on June 18, 1936.

2. Data used in the analysis.

A magnetic storm occurred with a SC at $9h$ $41m$ GMT on June 18, 1936, an example of the magnetograms obtained at Toyohara Magnetic

1) T. RIKITAKE, I. YOKOYAMA and Y. HISHIYAMA, *Bull. Earthq. Res. Inst.*, **30** (1952), 207.

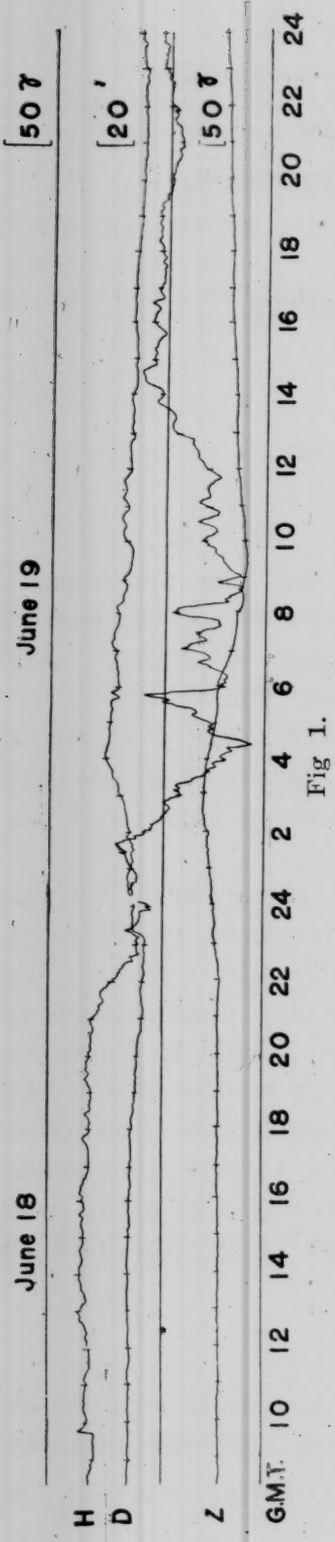

Fig. 1.

Observatory being reproduced in Fig. 1.

The writers read off the amplitude of the changes in the three components (ΔH, ΔD and ΔZ) on the magnetograms and then calculated the geomagnetic north (ΔX_m) and east (ΔY_m) components. The results are given in Table I together with the abbreviations and positions of the observatories. The distribution of the observatories is also shown in Fig. 2.

3. Magnetic potential for SC.

In the first place, the writers constructed a chart for showing the distribution of the overhead equivalent current-arrows as shown in Fig. 3 in geomagnetic coordinates. As may be seen in the figure, the arrows seem to be fairly parallel each other in the respective regions such as Europe, Asia and America. And we also find that the arrows are roughly parallel to the latitude circles excepting both sides of the Atlantic Ocean. To bring out the distribution more clearly, we plotted ΔX_m against the geomagnetic latitude as shown in Fig. 4, ΔZ being also plotted in the figure.

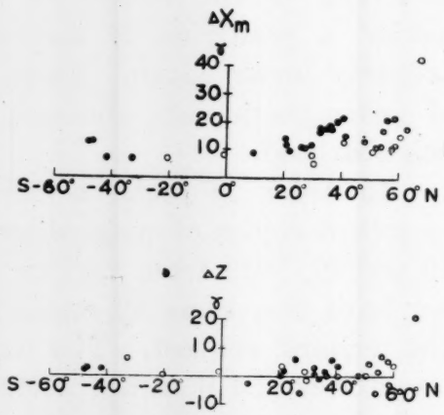

Fig. 4. The distribution of ΔX_m and ΔZ with respect to the geomagnetic latitude.
●: Asia and Australia
○: America
◎: Europe and Africa.

As will be seen in Fig. 4, ΔX_m takes a nearly constant value near the equator and it increases towards the north and south reaching

Fig. 1. The magnetic storm observed at Toyohara Magnetic Observatory on June 18 and 19, 1936.

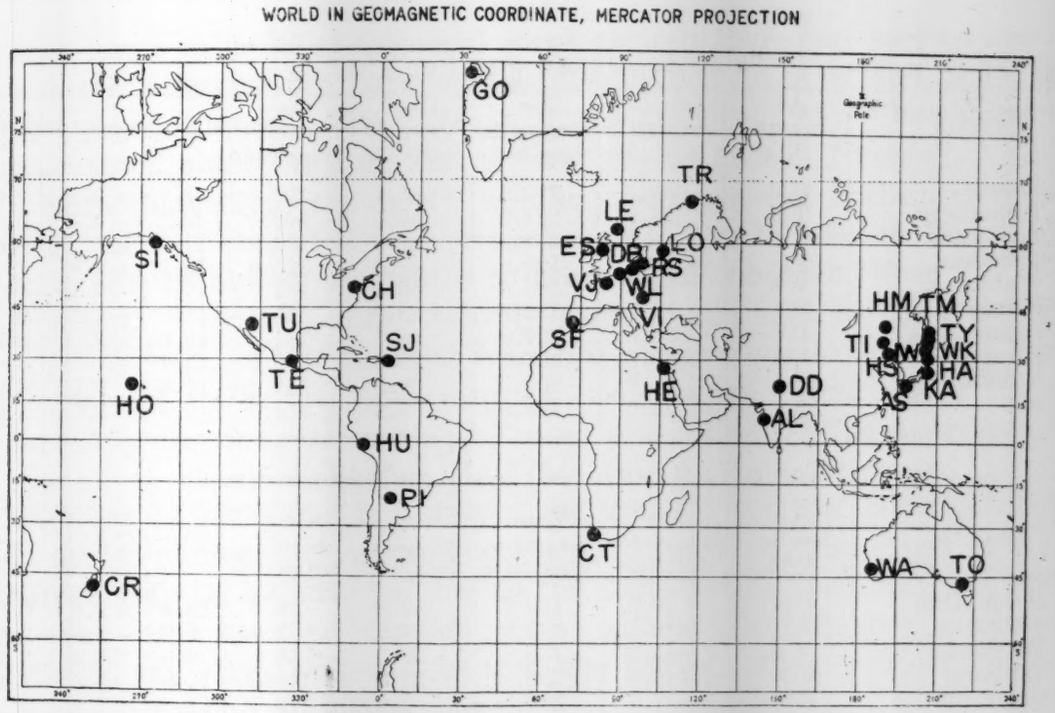

Fig. 2. The distribution of the magnetic observatories.

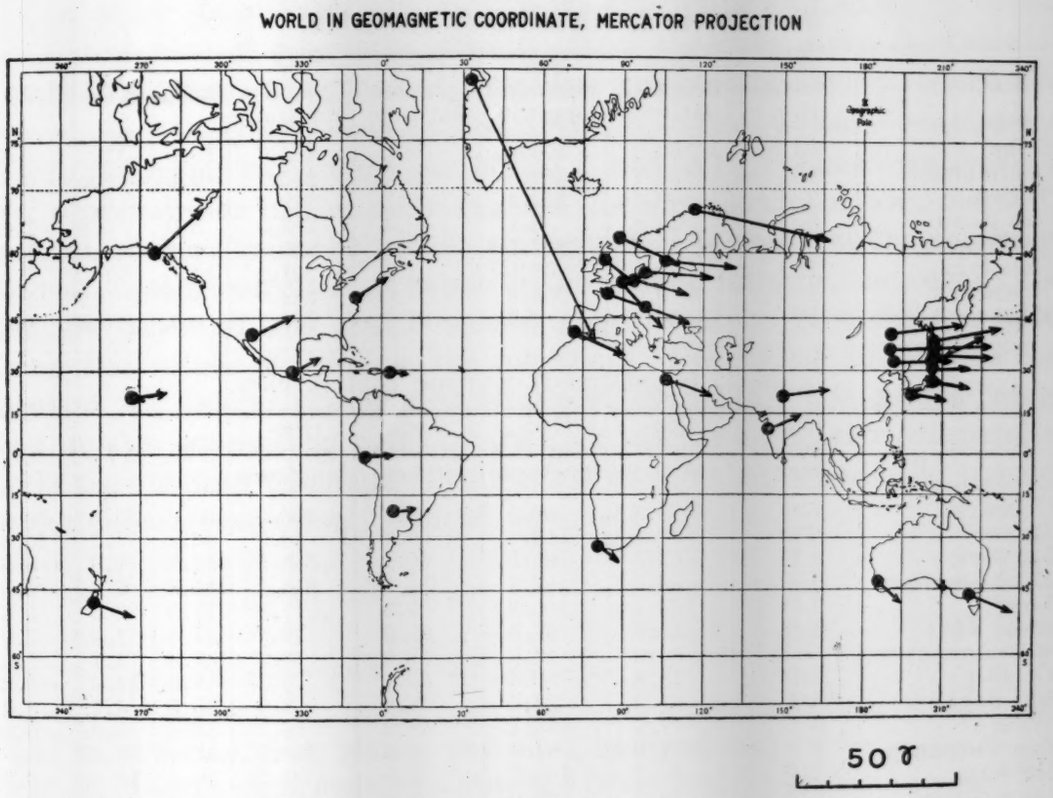

Fig. 3. The distribution of the overhead equivalent current-arrows of the SC at $9h\ 41m$ on June 18, 1936.

Table I. Japan and her vicinity.

Station	Abbreviation	Geomagnetic latitude	Geomagnetic longitude	Geographic latitude	Geographic longitude	ΔX_m	ΔY_m	ΔZ
Huma	HM	40°.6	192°.7	51°.7	126°.7	21γ.7	−3γ.4	3γ.7
Tomarigishi	TM	38.6	203.5	49.0	142.9	20.2	−4.4	5.8
Toyohara	TY	36.9	203.5	47.0	142.8	17.4	−1.2	0.0
Tsitsihar	TI	36.1	191.9	47.3	123.9	18.5	−1.9	1.4
Wakkanai	WK	34.4	203.4	45.4	141.7	17.6	−0.1	−1.0
Hsinking	HS	32.7	193.3	43.9	125.3	17.8	−1.7	0.9
Iwamizawa	IW	32.5	207.8	43.2	141.8	16.3	−8.0	3.1
Hirosaki	HA	29.5	206.2	40.6	140.5	11.7	−1.1	—
Kakioka	KA	26.0	206.0	36.2	140.2	10.8	2.3	6.0
Aso	AS	22.0	198.0	32.9	131.0	9.7	1.7	1.8

Table I. (Continued) Asia and Australia.

Station	Abbreviation	Geomagnetic latitude	Geomagnetic longitude	Geographic latitude	Geographic longitude	ΔX_m	ΔY_m	ΔZ
Dehra Dun	DD	20°.5	149°.9	30°.3	78°.0	13γ.9	−1γ.9	0γ.0
Alibag	AL	9.5	143.6	18.6	72.9	8.9	−3.3	−2.7
Watheroo	WA	−41.8	185.6	−30.3	115.9	6.6	6.3	2.7
Toolangi	TO	−46.7	220.8	−37.5	145.5	12.8	5.2	3.1
Christchurch	CR	−47.7	252.5	−43.5	172.7	12.4	4.4	2.2

Table I. (Continued) America.

Station	Abbreviation	Geomagnetic latitude	Geomagnetic longitude	Geographic latitude	Geographic longitude	ΔX_m	ΔY_m	ΔZ
Sitka	SI	60°.0	275°.4	57°.0	224°.7	15γ.0	−12γ.7	3γ.8
Cheltenham	CH	50.1	350.5	38.7	283.2	9.5	− 5.5	0.3
Tucson	TU	40.4	312.2	32.2	249.2	12.6	− 6.3	0.0
San Juan	SJ	29.9	3.2	18.4	293.9	5.0	0.4	−1.6
Teoloyucan	TE	29.6	327.1	19.7	260.8	7.8	− 4.7	1.8
Honolulu	HO	21.1	266.5	21.3	201.9	11.6	− 1.3	3.3
Huancayo	HU	− 0.6	353.8	−12.0	284.7	8.2	− 0.9	1.5
Pilar	PI	−20.2	4.6	−31.7	296.1	6.1	− 0.8	0.0

Table I. (Continued) Europe and Africa.

Station	Abbreviation	Geomagnetic latitude	Geomagnetic longitude	Geographic latitude	Geographic longitude	ΔX_m	ΔY_m	ΔZ
Godhavn	GO	79°.8	32°.5	69°.2	306°.5	36γ.8	80γ.8	98γ.0
Tromsö	TR	67.1	116.7	69.7	18.9	42.2	9.2	20.4
Lerwick	LE	62.5	88.6	60.1	358.8	17.9	8.0	−5.5
Eskdalemuir	ES	58.5	82.9	55.3	356.8	11.8	7.3	−3.5
Lovö	LO	58.1	105.8	59.4	17.8	21.9	2.0	5.5
Rude Skov	RS	55.8	98.5	55.8	12.4	21.4	1.5	7.0
Wilhelmshaven	WL	54.5	92.9	53.5	8.2	17.4	4.1	1.4
De Bilt	DB	53.8	89.6	52.1	5.2	11.5	14.4	−6.2
Val Joyeux	VJ	51.3	84.5	48.8	2.0	10.5	4.1	4.4
Wien	VI	47.9	98.1	48.2	16.2	13.4	5.0	0.0
San Fernando	SF	41.0	71.3	36.5	353.8	15.0	6.9	—
Helwan	HE	27.2	106.4	29.9	31.3	10.2	10.5	−6.3
Cape Town	CT	−32.7	79.9	−33.9	18.5	6.2	4.8	6.4

a very large value at the auroral zones though there may be seen some systematic discrepancies between the distribution in Asia and that in America and Europe. The increase of the amplitude of SC has already been pointed out by one of the writers[2] (T. R.) and T. Nagata[3].

Notwithstanding the fairly regular distribution of horizontal component, ΔZ is distributed very irregularly as is to be seen in Fig. 4, so that it will be almost impossible to draw equal variation lines for Z-component. Even in a comparatively narrow area such as the Western Europe, the sign of ΔZ changes from one observatory to another. For example, ΔZ in British observatories takes minus signs, while those observed in Sweden, Denmark or France are positive. The distribution in Japan is also complicated. ΔZ at Kakioka is positive and large, while that at Wakkanai is negative and small. As has been pointed out by a number of geomagneticians, a part of the cause of the heterogeneity in ΔZ may be due to the influence of the form of land and sea. However, no detailed study on the said influence has been conducted yet. The writers hope that the present study will contribute to the clarification of this problem.

In order to discuss quantitatively, the writers intended to obtain the distribution of magnetic potential from the data given in Table I. For that purpose, a method of graphical integration devised by M. Hasegawa and M. Ôta[4] seems to be adequate. The writers constructed charts for equal variation lines of ΔX_m and ΔY_m. Since we have a few observatories in the polar regions, the distribution of ΔX_m and ΔY_m determined here must be rather ambiguous. As concerns the neighborhood of Japan which is situated in the middle latitude, however, the analysis based on the charts should approximately give right results. Using the values of ΔX_m on the meridians of every 30° in latitude and those of ΔY_m along the parallel circles of every 15°, the pseudo-potentials at the intersection point of the i-th meridian and the j-th parallel circle are obtained by means of numerical integration, where the pseudo-potentials are respectively defined by

$$\left.\begin{aligned} W_{x,ij} &= a\int_0^{\theta} \Delta X_m d\theta \,, \\ W_{y,ij} &= -a\sin\theta\int_0^{\phi} \Delta Y_m d\phi \,. \end{aligned}\right\} \qquad (1)$$

2) T. RIKITAKE, *Bull. Earthq. Res. Inst.*, **28** (1950), 219.
3) T. NAGATA, *Rep. Ionos. Res. Japan*, **5** (1951), 134.
4) M. HASEGAWA and M. ÔTA, *Trans. Oslo Meeting, I.A.T.M.E.I.U.G.G.*, (1950), 431.

In (1), θ and ϕ denote respectively the co-latitude and longitude, while a is the radius of the earth. Since the integration constants are not known, the true value of magnetic potential should be obtained by the following means. If we denote the true value of potential at the point (i,j) by W_{ij}, we have the relations

$$\left.\begin{aligned} W_{x,ij} &= W_{ij} + C_{x,i}\,, \\ W_{y,ij} &= W_{ij} + C_{y,j}\,, \end{aligned}\right\} \qquad (2)$$

where $C_{x,i}$ is the constant on the i-th meridian, while $C_{y,i}$ is that along the j-th parallel circle. Hence, we have the next relations on the i-th and $i+1$-th meridians.

$$\left.\begin{aligned} W_{x,ij} - W_{y,ij} &= C_{x,i} - C_{y,j}\,, \\ W_{x,i+1j} - W_{y,i+1j} &= C_{x,i+1} - C_{y,j}\,. \end{aligned}\right\} \qquad (3)$$

And making the difference of the above two expressions, it follows that

$$(W_{x,ij} - W_{y,ij}) - (W_{x,i+1j} - W_{y,i+1j}) = C_{x,i} - C_{x,i+1}\,. \qquad (4)$$

After the same calculation along the j-th parallel circle, we can estimate $C_{x,0} - C_{x,1}$, $C_{x,0} - C_{x,2}$, ..., $C_{x,0} - C_{x,11}$. Thus all constants except $C_{x,0}$ are determined. The same calculation should be made along the other parallel circles. After all, the mean value $\bar{C}_{x,i}$ of all can be taken as the most probable value if all errors are considered to be accidental.

Thus we can obtain the true potential W_{ij} from (2) apart from a constant $C_{x,0}$ which is determined so as to make the sum of all values of $W_{x,ij}$, corrected by $C_{x,i}$, vanish. That is to say, the constant should be determined so as to satisfy the relation

$$\int_{\theta=0}^{\pi}\int_{\phi=0}^{2\pi} W \sin\theta d\theta d\phi = 0\,,$$

where the integral must cover the whole surface of the earth. Since the potential satisfies

$$\nabla^2 W = 0\,,$$

the integral becomes equal to $4\pi C$ where C denotes the constant part of potential. The constant part of the potential for geomagnetic variation has no meaning. Hence, C may be taken to be zero. But in actual analysis, the accuracy of the procedure for obtaining $C_{x,0}$ may not be satisfactory. We are going to discuss this error later.

The distribution of potential determined after the graphical method mentioned above is shown in Fig. 5 in which we see that the contours are fairly parallel to the direction of the equivalent current arrows shown in Fig. 3. It seems remarkable that the distribution of the potential is nearly zonal.

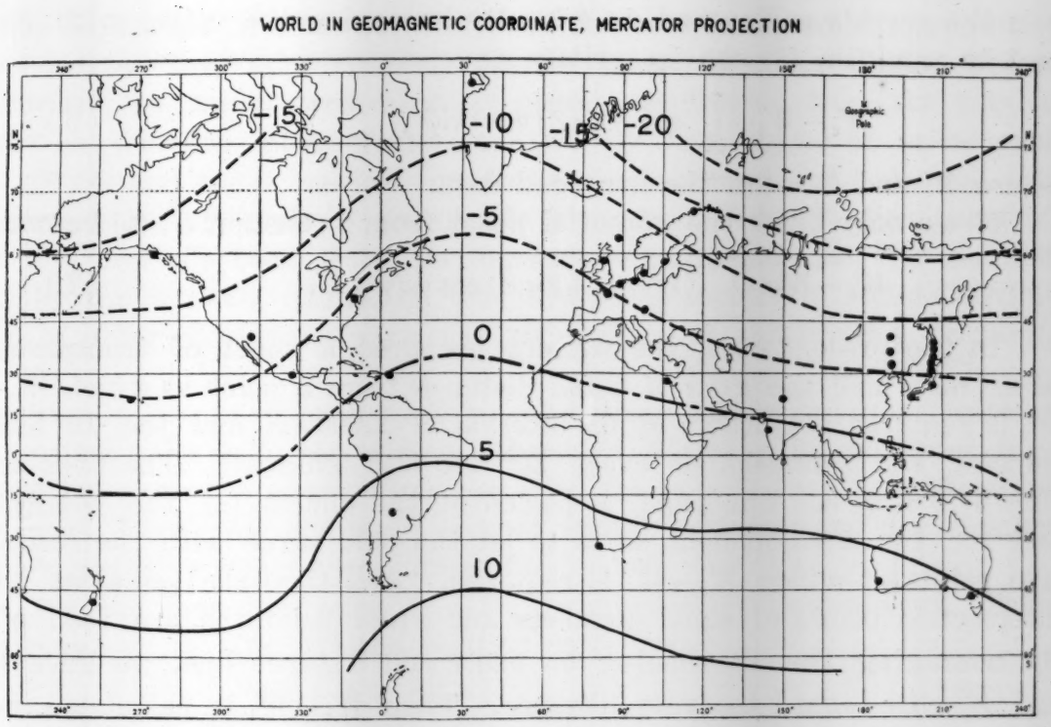

Fig. 5. The distribution of magnetic potential as obtained by means of the graphical method. The figures should be read in *gamma* multiplied by the earth's radius.

4. Separation of the potential into external and internal origin parts.

Combining the distribution of the potential with that of Z-component the writers wish to separate the parts originated out- and inside the earth. For that purpose, a method of surface integral due to E. H. Vestine[5] can be used. In case of a complicated distribution of magnetic field, the surface integral method seems to be easier than the usual spherical surface harmonic method as stated by Vestine himself. And one of the writers (T. R.)[6] applied the method to the field of geomagnetic daily variation with success.

According to Vestine, the difference of the potential of external origin W_e and internal one W_i satisfies the relation

$$W_e - W_i = (1/2\pi)\int_0^{2\pi}\int_0^{\pi/2} (W + 2aZ)\cos\psi d\psi d\phi \ , \qquad (5)$$

which is derived from the theory of potential, where the pole of polar coordinates (a, θ, ϕ) is taken at the point at which $W_e - W_i$ is required.

5) E. H. VESTINE, *Terr. Mag.*, **46** (1941), 27.

6) T. RIKITAKE, *Coll. Paper Ionos. Res. Comm. N.R.C. Japan*, **4** (1948), 61.

a is the earth's radius and $\psi=\theta/2$. By averaging the values with respect to azimuth, (5) can be written as

$$W_e-W_i=\int_0^{\pi/2}(\overline{W}+2a\overline{Z})\cos\psi d\psi\ , \qquad (6)$$

where $\overline{W}$ and $\overline{Z}$ mean the averaged data.

If we only know the potential apart from a constant U, (6) becomes

$$W_e-W_i=\int_0^{\pi/2}(\overline{W}-U+2a\overline{Z})\cos\psi d\psi+U. \qquad (7)$$

In the present case, the writers prepared a sheet of transparent paper on which the lines of equal distance from a point at which W_e-W_i is required are drawn at an interval of 1,000 km and the 12 lines showing the azimuths of every 30° are also indicated. The lines are shown in Fig. 6. The paper is placed on the charts for the potential and for the Z-component so as to let the pole agree with the respective points at which W_e-W_i is required. And then the values at the intersection points of equal distances and equal azimuths are read off. By averaging the 12 reading on one equal distance line, we have $\overline{W}$ and $\overline{Z}$ with regard to every distance. Then W_e-W_i is calculated according to (6) or (7) by means of the numerical integration method. The transparent paper is prepared for 35° in latitude. In order to

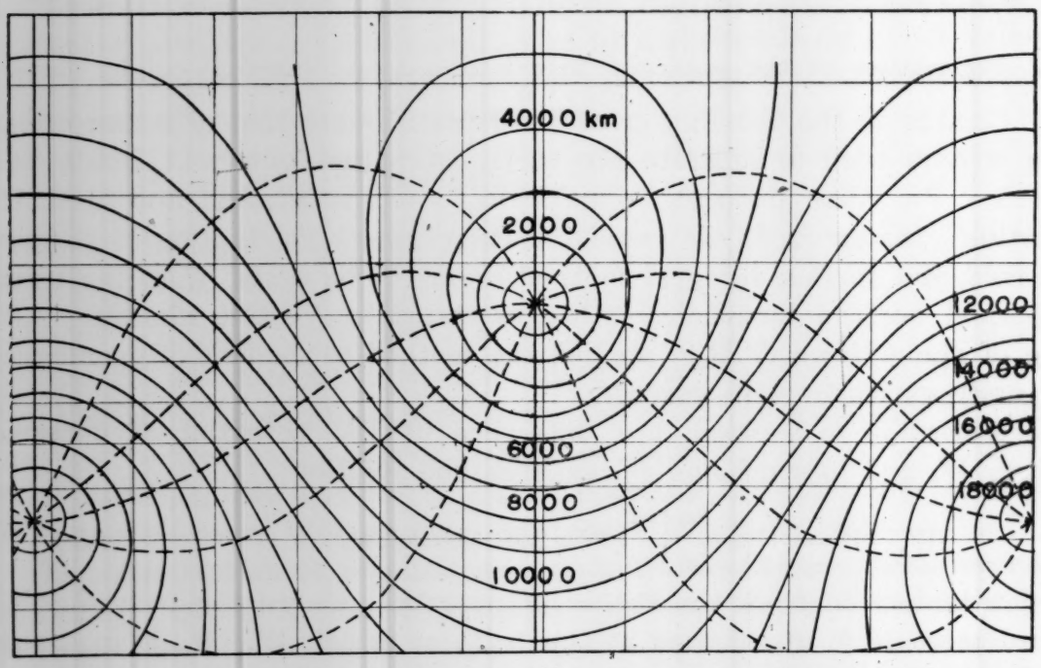

Fig. 6. The lines of equal distance written at an interval of 1,000 km and of showing the azimuths of every 30° from a point whose latitude is 35°.

make separation of both parts of potential only in Japan and her neighborhood, we may approximately use the same paper for all the observatories. In actual treatment, however, the region from the pole to 1,000 km which is most effective for $W_e - W_i$ are divided at an interval of 100 km and the numerical integrations are carried out. As for the Z-component, it is almost impossible to make the distribution chart of world-wide scale because of its irregular distribution as was pointed out by the writers. However, we have a comparatively dense distribution of observatories in Japan and her vicinity at the present occasion, so that we might tentatively draw equal variation lines near Japan. Meanwhile, we have to get ΔZ on the basis of ambiguous interploations for points such as in the oceans, Siberia or Africa. Roughly speaking, however, since the distribution nearer to the pole is the most effective, we may have approximately correct results in Japan and her vicinity where we have many observations.

We can thus determine $W_e - W_i$ for respective observatories. Then we may write after (7) the relation as follows:

$$W_e - W_i = W' + U\,, \tag{8}$$

where U is the same constant for the potential. Combining (8) with the relation

$$W_e + W_i = W + U\,, \tag{9}$$

we get

$$\left.\begin{aligned} W_e &= \tfrac{1}{2}(W + W') + U\,, \\ W_i &= \tfrac{1}{2}(W - W')\,. \end{aligned}\right\} \tag{10}$$

As was stated at the end of the last section, the constant part of

Table II.

The external and internal parts for SC. (The values are divided by the radius of the earth.)

Station	W_e	W_i
HM	-3.6^{γ}	-4.3^{γ}
TM	-2.7	-4.8
TY	-2.5	-4.5
TI	-2.5	-3.9
WK	-2.0	-4.4
HS	-1.7	-3.8
IW	-1.7	-4.2
KA	-0.5	-4.0
AS	$+0.2$	-3.5

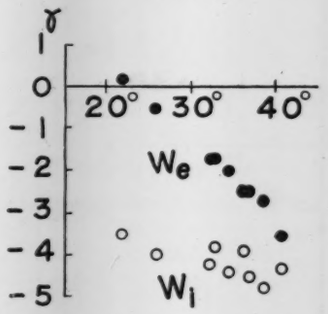

Fig. 7. The external and internal parts of the potential are arranged according to the geomagnetic latitude of the stations which are situated in Japan and her vicinity.

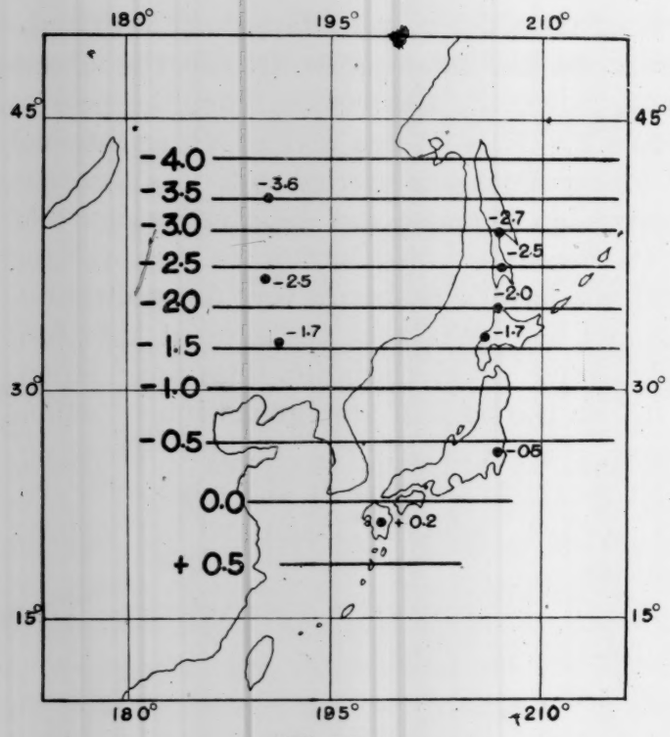

Fig. 8.

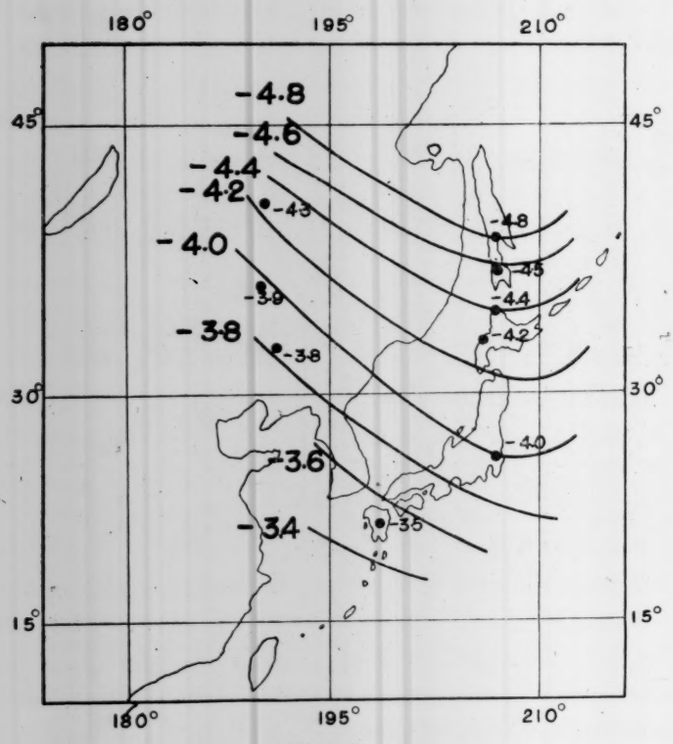

Fig. 9.

potential was considered to be zero. In determining actually, however, the writers are afraid that the constant part may not vanish wholly on account of errors. In that case, the comparison of the magnitude of the external part with the internal one may be somewhat dangerous.

W_e and W_i thus determined are given in Table II for respective stations.

The distributions of W_e and W_i are graphically shown in Fig. 7 in which we see that the values of W_i are large compared with those of W_e. Although W_e seems to be distributed fairly zonally, the distribution of W_i is somewhat complicated. The equi-potential lines for the external and internal origin parts are tentatively shown in Figs. 8 and 9.

Fig. 8. The equi-potential lines for the external origin part of the magnetic potential. The unit is *gamma* multiplied by the earth's radius.

Fig. 9. The equi-potential lines for the internal origin part of the magnetic potential. The unit is *gamma* multiplied by the earth's radius.

5. Discussions.

In the last section, it has been proved that the peculiar distribution of W_i occurs at the time of SC, while W_e is distributed almost zonally. As is well known, the relation between the external and internal origin parts of various geomagnetic variations can be explained by the electromagnetic induction theory within the conducting earth so far as the averaged state such as deduced from a spherical harmonic analysis is concerned. From the standpoint of that theory, it is impossible to explain the anomalous distribution of the internal part which is obtained here. And, as the writers have briefly dealt with in their preliminary study, we naturally suppose that some heterogeneous distribution of electrical conductivity might exist beneath the area.

If W_i is supposed to be caused by electric currents flowing near the earth's surface, the stream lines are almost the same as shown in Fig. 9 and currents of 2,000 *amperes* flow between the consecutive lines from east to west. The loops of the stream lines in the neighborhood of Japan seems to be the most remarkable, the fact corresponding to the anomalously large amplitude of ΔZ in that locality.[7]

A noticeable result obtained in the present study is that the values of internal parts are large compared with those of external parts. One of the writers (T.R.)[2] found out in his previous analysis of SC in the middle and low latitude that the ratio of the coefficients of internal part to external one for the first harmonic amounts to about 0.25 on the whole. As already mentioned in the last section, the elimination of the constant part of potential might not have been perfectly done,

7) According to Vestine's method, we can obtain the external and internal origin parts of Z from the following relations;

$$Z_e + Z_i = Z\,,$$

$$Z_e - Z_i = W_i - \frac{1}{2a}\int_0^{\pi/2} (\overline{W} - \overline{U}) \operatorname{cosec}^2\psi \cos\psi\, d\psi\,.$$

The writers calculated ΔZ_e and ΔZ_i with these relations as shown in the following table.

However, the accuracy of the numerical integration of the above expression is not good because the integrand becomes enormously large for small value of ψ owing to the factor $\operatorname{cosec}^2\psi$. Notwithstanding the bad accuracy of integration, we can clearly see the large amplitude of ΔZ_i at Kakioka in the table.

Station	ΔZ_e	ΔZ_i
HM	-2γ	5γ
TM	-2	7
TY	-4	4
TI	-2	4
WK	-5	4
HS	-4	4
IW	-3	5
KA	-2	8
AS	-2	4

so that it will be meaningless to compare the magnitude of W_i with that of W_e. However, we obtain $\Delta X_{m,e}=12\gamma$ from the distribution of W_e which is shown in Fig. 8 and $\Delta X_{m,i}=3.5\gamma$ from that of W_i in Fig. 9 for Japan. Hence the internal part of the horizontal force amounts to about 30 percent of the external part, the result being roughly compatible with the aforementioned study.

6. Conclusion and Acknowledgement.

On the basis of world-wide geomagnetic data, the SC at $9h\ 41m$ GMT on June 18, 1936 is analysed especially with regard to the peculiar distribution of changes in geomagnetic field in Japan and her neighborhood where we have many temporary stations. The internal origin parts of the potential of SC is separated from the external ones with the aid of the surface integral method. It is made clear that the distribution of the internal part near Japan is anomalous. If it is supposed that the distribution is caused by the electric currents beneath the earth's surface, we find circular flows around Japan. That seems why we notice an anomalously great amplitude in Z-component there.

The writers are now carrying on the same analysis with respect to the other marked changes during the same storm. The results will be published in this Bulletin as soon as possible.

In conclusion, the writers are very much obliged to many geomagneticians who kindly cooperate with them by sending them geomagnetic data. The writers wish to express their hearty thanks to the following persons:

Dr. M. ÔTA, Kyoto University, Japan.
Dr. S. IMAMITI, Kakioka Magnetic Observatory, Japan.
Prof. E. SELZER, Institut de Physique du Globe, Université de Paris, France.
Dr. A. M. VAN WIJK, Hermanus Magnetic Observatory, S. A.
Dr. E. TÖNSBERG, Nordlyobservatoriet, Tromsö, Norway.
Mr. L. S. PRIOR, Watheroo Magnetic Observatory, Western Australia.
Dr. J. C. MORAIS, Instituto Geofisico da Universidade de Coimbra, Portugal.
Dr. NILS AMBOLT, Kungl. Sjökarteverket, Stockholm, Sweden.
Dr. ROBERT WILKOX, U. S. Coast and Geodetic Survey, U. S. A.
Dr. PAUL G. LEDIG, San Juan Magnetic Observatory, Puerto Rico.
Der DIREKTOR, Zentralanstalt für Meteorologie und Geodynamik, Wien, Austria.
Dr. OLAF LITZOW-HOLM, Observatorio Geofísico, Pilar, Argentina.
Dr. HELGE PETERSEN, Det Danske Meteorologiske Institut, Köbenhavn, Denmark.
Dr. M. DOPORTO, Meteorological Service, Dublin, Ireland.
Prof. Dr. J. J. M. REESINCK, Meteorological and Geophysical Service, Djakarta, Indonesia.
Dr. J. VELDKAMP, Koninklijk Nederlands Meteorologisch Institut, De Bilt, Netherlands.

Dr. S. L. MALURKAR, Colaba and Alibag Observatories, India.
Dr. ROSENDO OCTAVIO SANDOVAL, Instituto de Geofisica, Mexico.
Dr. RICARDO MONGES LÓPEZ, Instituto de Geofisica, Mexico.
The SUPERINTENDENT, Eskdalemuir Magnetic Observatory, Scotland.
Dr. J. ORIOL CARDÚS, Observatorio del Ebro, Spain.
Dr. WENCESLAO BENÍTEZ, Instituto y Observatorio de Marina, San Fernando, Spain.
Dr. R. F. THYER, Bureau of Mineral Resources, Melbourne, Australia.
Prof. H. AMORIM FERREIA, Servico Meteorológico Nacional, Portugal.
Dr. H. F. BAIRD, Amberley Magnetic Observatory, New Zealand.
The DIRECTOR GENERAL, Royal Observatory, Helwan, Egypt.
Dr. M. M. GILL, Apia Magnetic Observatory, Western Samoa.
Dr. JOHANNES OLSEN, Det. Danske Meteorologiske Institut, Köbenhavn, Denmark.
Mr. B. L. GULATEE, Geodetic and Training Circle, Dehra Dun, India.
Mr. A. A. GIESECKE, Jr., Instituto Geofísico de Huncayo, Peru.

The writers are also grateful to Professor T. Nagata for his helpful discussions in the course of the study.

Note added in the proof: After the preparation of the manuscript, the observation at Apia (geomagnetic latitude: $-16°.0$, geomagnetic longitude: $260°.2$, geographic latitude: $-13°.8$, geographic longitude: $188°.2$) became available. The writers would here like to note that $\Delta X_m = 5.8\gamma$, $\Delta Y_m = 0.1\gamma$, and $\Delta Z = -1.6\gamma$ at Apia.

---

2. 日本に於ける地磁気短周期変化の異常と地下構造 (第2報)

地震研究所 { 力武常次 / 横山泉 / 菱山よね子 }

序報に於て日本に於ける地磁気短周期変化の異常を指摘したが，本報文に於ては世界各地の観測結果をもとゝして検討を加えた．

1936年6月18日9時41分 GMT の磁気嵐急始を解析して，ポテンシヤルと鉛直分力より，日本附近の変化磁場を地球外および地球内に原因を有する2部分に分離した．その結果地球内に起因する部分は第9図のような分布を示し，これが地表近くを流れる電流によって起ると考える時は，日本附近に渦状の電流系があることゝなり，通常の電磁感応の理論によっては，その分布を説明できず，地下に特殊の電気伝導度分布を考えねばならない．

---

3. *Geomagnetic Anomaly on Mt. Haruna and Its Relation to the Reverse Thermo-Remanent Magnetism of the Pumice Covering the Place.*

By Izumi YOKOYAMA,

Earthquake Research Institute.

(Read Nov. 18, 1952.—Received Dec. 20, 1952)

1. Introduction.

Mt. Haruna is one of the extinct volcanoes standing at the north-western edge of Kwanto-plain, Central Japan. It consists of an older, dissected cone and four younger lava domes. Its topographical map is shown in Fig. 1. The history of the volcanic activity was summarized by S. Taneda[1] as follows: The older cone was built up by alternate eruption of lavas and pyroclastics largely of pyroxene andesite. The cone was then subjected to intense erosion during the succeeding period of quiescence. During the next period of activity, the domes of horn-blende dacite, Mts. Sōma, Mizusawa-yama, Haruna-Fuji and Futatsu-dake, were erupted in the order just mentioned. It seems likely that tuff-breccia and pumice were erupted from a crater which was later filled up by the dome of Futatsu-dake. The pumice layer covers widely the eastern slope of the volcano, its eastern extension being found even beyond the Tone River. A geologic sketch map is shown in Fig. 2.

In October and November, 1952, a magnetic dip survey was carried out at Mt. Haruna by the writer with a miniature earth-inductor.[2] The purpose of the survey is to study the relation between geomagnetic anomaly and the reverse thermo-remanent magnetism of the pumice covering the eastern part of the volcano. The number of surveyed sites reached 25, while the error of each measurment was about 1 *minute* of arc. The observed values are shown in Table I and plotted in Fig. 3 with an altitude abscissa where the corrections for diurnal variations are made with reference to the magnetograms of the Aburatsubo base-station which is about 150 *km* distant from Mt. Haruna. The normal value for this district is 49°50′.

1) S. TANEDA, *Mem. Fac. Sci. Kyūsyū Imp. Univ. D*, **1** (1941), 44.
2) T. RIKITAKE, *Bull. Earthq. Res. Inst.*, **29** (1951), 147.

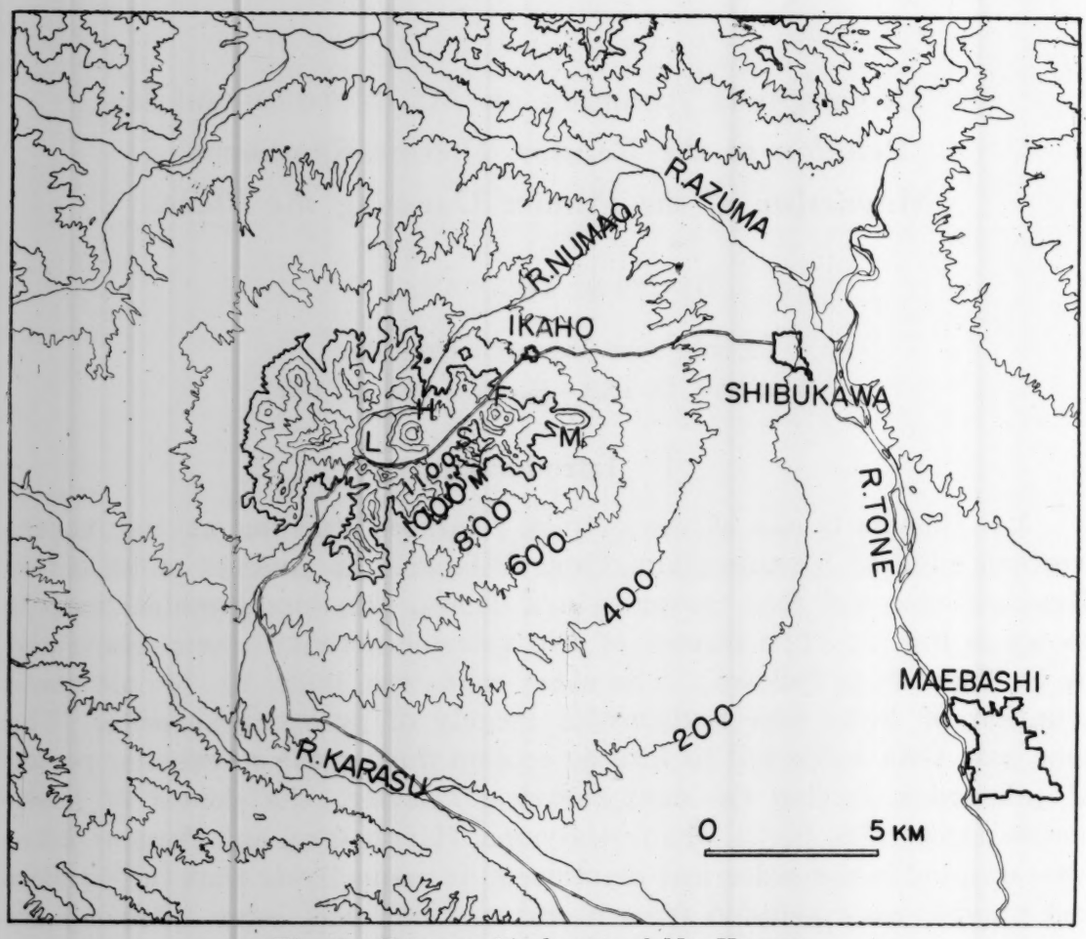

Fig. 1. Topographical map of Mt. Haruna.
H: Mt. Haruna-Fuji S: Mt. Sōma F: Mt. Futatsu-dake
M: Mt. Mizusawa L: the Haruna Lake.

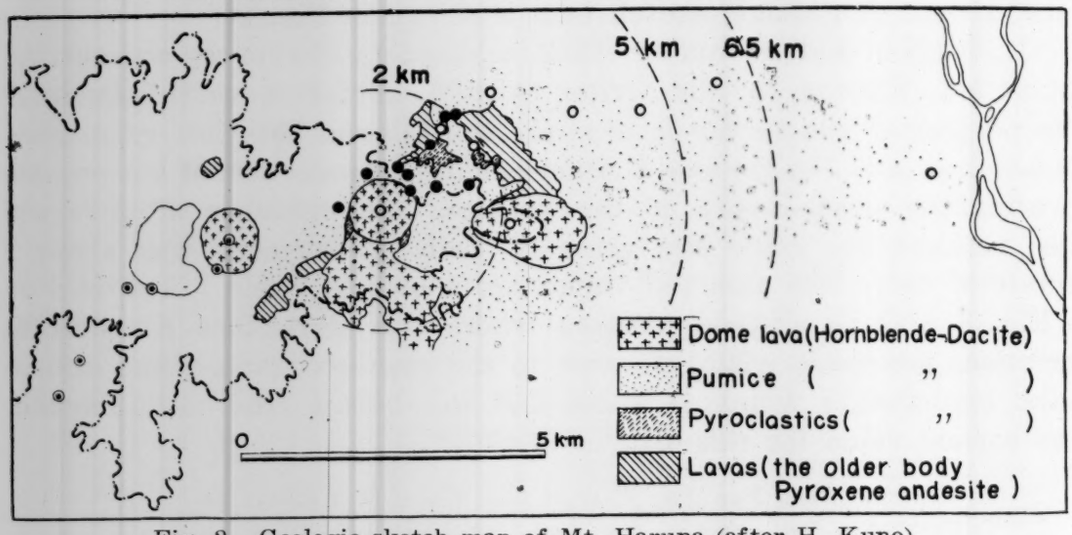

Fig. 2. Geologic sketch map of Mt. Haruna (after H. Kuno).

Table I.

The observed values of magnetic dip.

Time		Locality		Approximate Altitude	Dip
Oct. 29	13h48m	榛名湖畔	Side of Lake Haruna	1100m	49°32′
	14 22	榛名富士山麓	Foot of Mt. Haruna-Fuji	1120	49 02
	15 17	富士山頂三角点	Summit of Mt. Haruna-Fuji	1391	54 56
	16 36	ヤセオネ峠	Pass Yaseone	1179	50 48
	17 00	ケーブルと旧道との交叉点	Cross-point of cable-way and road	1060	50 34
	17 40	橋本ホテル前	Near Hotel Hashimoto	900	50 42
	18 02	天溪園玄関	Tenkeien	840	47 55
Oct. 30	08 24	伊香保神社上	Ikaho Shrine	510	51 10
	08 52	見晴台三角点	Summit of Miharashidai	976	51 42
	09 22	水沢山の麓	Foot of Mt. Mizusawa	1020	51 24
	09 45	水沢山と二ツ嶽の間の沢	Between Mts. Mizusawa and Futatsu-dake	1000	50 00
	10 16	二ツ嶽の麓	Foot of Mt. Futatsu-dake	1010	49 37
	10 36	わしの巣附近	Near Washinosu	960	49 55
	10 49	わしの巣	Washinosu	970	49 37
	12 34	伊香保ホテル附近	Near Hotel Ikaho	670	50 22
	13 13	大日向驛前	Ohinata-station	560	50 13
	13 40	六本松	Ropponmatsu	460	49 56
	14 14	御蔭松	Okagenomatsu	390	49 50
	14 50	渋川驛前	Shibukawa-station	190	49 36
Nov. 8	06 28	スケート・リンク	Skating-rink	840	49 52
	10 02	水沢山三角点	Summit of Mt. Mizusawa	1194	54 02
	12 34	二ツ嶽頂上	Summit of Mt. Futatsu-dake	1342	56 01
	15 07	天神峠	Pass Tenzin	1121	50 30
	15 49	榛名神社	Haruna Shrine	870	48 45
	16 11	榛名山町	Harunasan Town	800	47 44

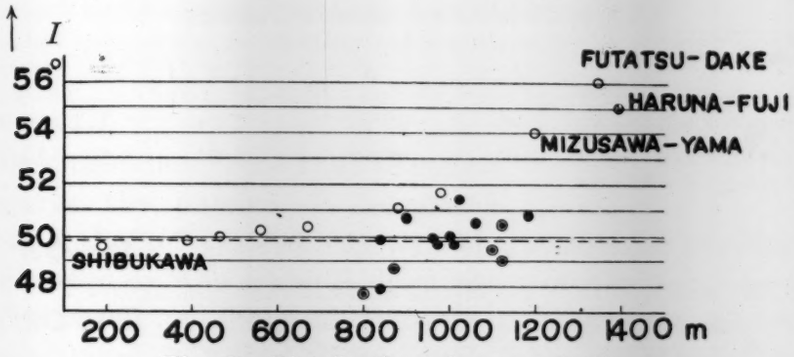

Fig. 3. Distribution of magnetic dip.

Looking at the general aspect of the distribution, the dip values observed in the region east of Mt. Haruna-Fuji (shown by double circles in Fig. 3) seem to form different series from those in the region to the west of it. Here the discussion will be confined to the eastern region where the geology is well known. Taking into consideration the fact that the dip-angle usually increases with the increase in height on an

ordinary volcano, the low values observed at the foot of Mt. Futatsu-dake (shown by black circles in Fig. 3) look very anomalous.

2. The magnetization of the pumices.

After T. Rikitake's method,[3] it is possible to calculate the intensity of magnetization J of a uniformly magnetized circular cone if the shape of the cone and the dip anomaly on the central axis due to the cone are known. Corresponding to dip anomaly ΔI, if ΔI is small and the cone is magnetized in a direction in xz-plane with inclination θ, the following relation is obtained

$$\begin{aligned} f(\Delta I) &= \{\tan(I_0+\Delta I)-\tan I_0\}/\tan I_0 \\ &= \Delta Z/Z_0-\Delta X/X_0 \\ &= \pi JG(2\sin\theta/Z_0+\cos\theta/X_0)\ , \end{aligned}$$

where I_0, Z_0 and X_0 denote respectively the normal value of I, Z and X there and G is theoretically determined depending on the shape of the cone. Applying this relation to the cases of Mts. Haruna-Fuji and Futatsu-dake, the specific intensities of magnetizations of the rocks composing the mountain-bodies are surmised as shown in Table II.

The results of the observation in the region east of Mt. Futatsu-dake are shown in Fig. 4 with the altitude from the bottom plane of Mt. Haruna as abscissa, where a mean profile curve of the mountain

Table II.

Dip anomaly and magnetization.

	G	I	ΔI	J
Mt. Haruna-Fuji	1.08	49°02′	5°54′	1.1×10^{-2} *emu*
Mt. Futatsu-dake	2.10	49 37	6 24	5×10^{-3}

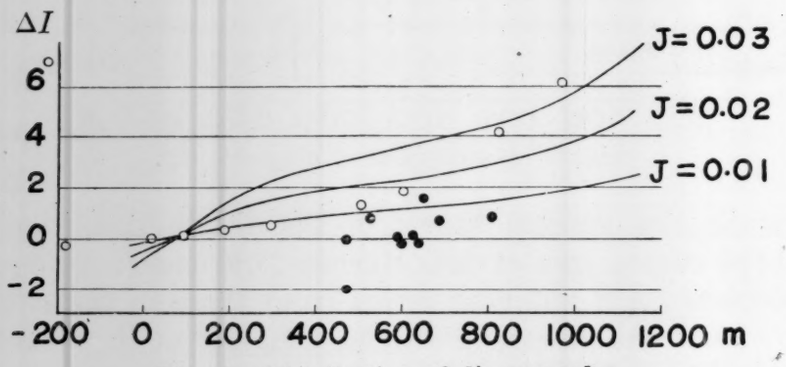

Fig. 4. Distribution of dip-anomaly.

3) T. RIKITAKE, *Bull. Earthq. Res. Inst.*, **30** (1952), 71.

is determined after T. Terada's method.[4] As already studied by T. Rikitake,[5] the distribution of the components of the magnetic field over a circular cone due to the magnetization of this cone are obtainable if the intensity of magnetization and the shape of the cone are known. On the assumption that Mt. Haruna is a circular cone with the radius 8 *km* at the bottom and the height 1270 *m* and uniformly magnetized northward with inclination 49°50′ (the normal dip-angle in this district), the increase in the dip-anomaly along the eastward slope of the mountain is obtained for each respective magnetization as shown in Fig. 4. Comparing the calculated anomaly with the observed one, we may presume that the mean intensity of magnetization amounts to about 0.01 *emu*. Taking into account the values obtained from both Mts. Haruna-Fuji and Futatsu-dake, the figure seems to be reasonable. As mentioned before, one noticed the conspicuous lower values deviating from this curve at the foot of Mt. Futatsu-dake, where hornblende dacite pumice covers the slope for a thickness more than 10 *meters*.

Table III.

Chemical composition (HK 51070801 b).

Fe_2O_3	FeO	TiO_2	MnO	V_2O_3
53.15	31.93	6.82	0.69	0.49%

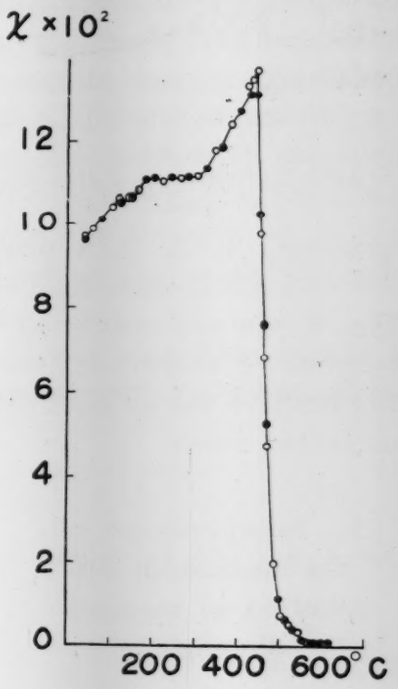

Fig. 5.
○ cooling ● heating.
(After T. Nagata, S. Uyeda and S. Akimoto)

As regards the pumice, T. Nagata, S. Uyeda and S. Akimoto[6] studied magnetic characteristics in detail. Referring to their studies, the general description of the rock samples is as follows. The result of chemical analysis of magnetite separated from the pumice is given in Table III and their intensity of natural remanent magnetism is 4.3×10^{-3} *emu* in average and the direction is almost opposite to that of the present geomagnetic field. The change of magnetic susceptibility of the ferromagnetic mineral in a weak magnetic field with temperature is illustrated in Fig 5. Its singularity is a stepwise

4) T. Terada, *Bull. Earthq. Res. Inst.*, **7** (1929), 207.
5) T. Rikitake, *Bull. Earthq. Res. Inst.*, **29** (1951), 170.
6) T. Nagata, S. Uyeda and S. Akimoto, *Journ. Geomag. Geoelectr.*, **4** (1952), 22.

change, having apparently two Curie points i. e. 540°C and about 280°C. The thermo-remanent magnetizations (T. R. M. s) produced by cooling down the rock sample to the room temperature (10°C) from various temperatures from 200°C to 600°C in a magnetic field of 0.5 *Oe* are shown in Fig. 6. As shown in this figure, the direction of T. R. M. thus produced are opposite to that of applied magnetic field (Reverse T. R. M.). In the ordinary rock samples, T. R. M. is always "positive" i. e. the direction of T. R. M. is parallel to that of applied magnetic field. In the case of the pumice from Mt. Haruna, however, T. R. M. s produced by cooling from a temperature above 300°C in a magnetic field of 0.5 *Oe* are always Reverse T. R. M. Seeing Fig. 6, we are convinced of the existence of the phenomenon of self-reversal of thermo-remanent magnetism of the pumice notwithstanding the positive values obtained for the mountain-body of Mt. Futatsu-dake as stated above.

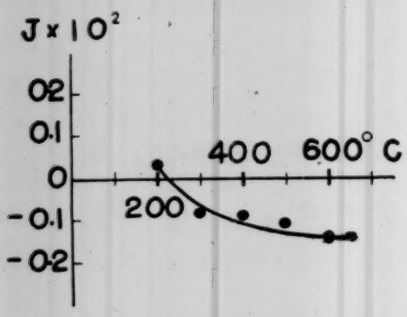

Fig. 6.
(After T. Nagata, S. Uyeda and S. Akimoto)

3. Interpretation of the anomalous distribution of magnetic dip-angle.

Taking into account both the anomalous distribution of dip-angle at the foot of Mt. Futatsu-dake and the above-mentioned phenomenon of self-reversal of thermo-remanent magnetism of the pumices, there seems to be a causal relation between them. Next it comes into question whether the ejected pumice from Mt. Futatsu-dake cools

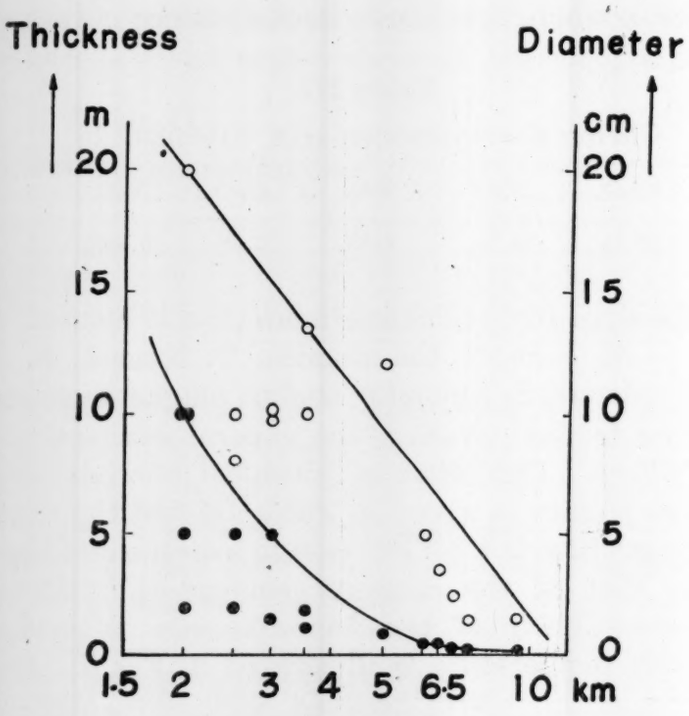

Fig. 7.
● Thickness of pumice layer
○ Mean diameter of pumice particle.

down below Curie point before landing in the present position.

The variations in the thickness of the pumice layer with the distance from Mt. Futatsu-dake is shown in Fig. 7, where the thickness is probably underestimated since the pumice layer cannot be seen in its original state. The distribution of the mean diameter of the five largest particles of each outcrop of the pumice layer gives mean diameters at distances of $2\,km$, $5\,km$ and $6.5\,km$ of $20\,cm$, $10\,cm$ and $5\,cm$ respectively (see Fig. 7). According to T. Minakami's investigation[7] made on Mt. Asama, as soon as the vertical velocity of the small fragments shot upward by the explosion diminishes at a certain height after about $120\,sec$ for instance, the column is diffused in all directions assuming a cauliflower shape. At the same time, the smoke drifts with the wind, the larger fragments falling more rapidly on the lee side of the mountain. Therefore, the pumices from Mt. Futatsu-dake are thought to be distributed on the lee side of the volcano following the prevailing wind direction of the upper atomosphere.

Taking the origin of the co-ordinate at the maximum height to which the pumice was ejected from the crater, the equations of its motion are given by

$$\ddot{x}-\lambda(v_0-\dot{x})^2=0\,,$$
$$\ddot{z}+\lambda\dot{z}-g=0\,,$$

where the x axis is taken in the direction of the wind and the z axis downward and

$$\lambda=\frac{3k\rho'}{4\rho d}\,,$$

and ρ', ρ, d and k denote the mean density of air, bulk density of pumice, diameter of pumice and coefficient of resistance respectively. The initial conditions are

$$t=0: \qquad x=z=0\,,$$
$$\dot{x}=\dot{z}=0\,.$$

Solving one of the above equations, we have

$$x=v_0 t-\frac{1}{\lambda}\log(\lambda v_0 t+1)\,.$$

Here k is taken to be 1.35 after Minakami and v_0 is assumed to be $30\,m/sec$ as a rather high value. Then, the time of flight is calculated with the aid of the relation between the diameters of the pumice particles and the distance to which they were sent, the results being shown in Table IV.

7) T. MINAKAMI, *Bull. Earthq. Res. Inst.*, **20** (1942), 93.

Thus the total time of flight obtained for pumice particles of diameter of 20 *cm*, 10 *cm* and 5 *cm* become roughly 200 *sec*, 300 *sec* and 400 *sec* respectively in rather an overestimate. Concerning the heat conduction of the pumice particle, it is assumed for brevity that the particle is a sphere with radius a and it flies through air of which the temperature is constant, i.e. θ_0. The equations of heat conduction are given by

Table IV.

d	x	t
20 *cm*	2000 *m*	80 *sec*
10	5000	175
5	6500	220

d: diameter of pumice particle (observed)
x: horizontal distance from Mt. Futatsu-dake (observed)
t: time of flight from the maximum height (calculated).

$$\frac{\partial(r\theta)}{\partial t}=\kappa\frac{\partial^2(r\theta)}{\partial r^2}\ ,$$

$$\theta=\theta_1 \quad \text{when} \quad t=0\ ,$$

$$\frac{\partial\theta}{\partial r}+h(\theta-\theta_0)=0 \quad \text{when} \quad r=a\ ,$$

where h is an experimental constant depending upon what is called the surface conductivity of the sphere. In solving these equations, let $r(\theta-\theta_0)=u$, then a particular solution is given by

$$u=e^{-\kappa\frac{\mu_s^2}{a^2}t}\sin\frac{\mu_s}{a}r\ ,$$

where μ_s is a value of μ which is a root of the next transcendental equation:

$$\mu\cos\mu+(ah-1)\sin\mu=0\ .$$

The general solution is given by

$$u=\sum_{s=1}^{\infty}A_s\,e^{-\kappa\frac{\mu_s^2}{a^2}t}\sin\frac{\mu_s}{a}r\ .$$

Using the initial condition $r(\theta_1-\theta_0)=\sum_{s=1}^{\infty}A_s\sin\frac{\mu_s}{a}r$, we have

$$A_s=\frac{2}{a}\,\frac{\mu_s^2+(ah-1)^2}{\mu_s^2+ah(ah-1)}\times\frac{a^3h(\theta_1-\theta_0)}{\mu_s^2}\times\sin\mu_s\ .$$

Therefore

$$\theta-\theta_0=\frac{2a^2h(\theta_1-\theta_0)}{r}\sum_{s=1}^{\infty}\frac{\mu_s^2+(ah-1)^2}{\mu_s^2\{\mu_s^2+ah(ah-1)\}}e^{-\kappa\frac{\mu_s^2}{a^2}t}\times\sin\mu_s\times\sin\frac{\mu_s}{a}r\ .$$

At the centre of the sphere, we have

$$\theta-\theta_0=2ah(\theta_1-\theta_0)\sum_{s=1}^{\infty}\frac{\mu_s^2+(ah-1)^2}{\mu_s^2\{\mu_s^2+ah(ah-1)\}}e^{-\kappa\frac{\mu_s^2}{a^2}t}\times\sin\mu_s\times\mu_s\,.$$

For the particle of the pumice concerned here, various constants are taken as follows :

K: thermal conductivity	0.44×10^{-3} *cal/cm. sec.* °*C*
$\kappa=K/C\rho$: diffusivity (C : specific heat, ρ : density)	3.1×10^{-3} *cm²/sec*
α : emissivity	1.1×10^{-2} *cal/cm². sec.* °*C*
$h=\alpha/K$	25/*cm*

Taking $\theta_0=50$°C and $\theta_1=1000$°C for simplicity's sake, the changes in temperature numerically calculated at the centre of the pumice particle of various diameter are shown in Fig. 8 respectively. As seen in the figure, the particles of 20 *cm* and 10 *cm* diameter are considered to cool down below Curie point (about 300°C) certainly after landing in

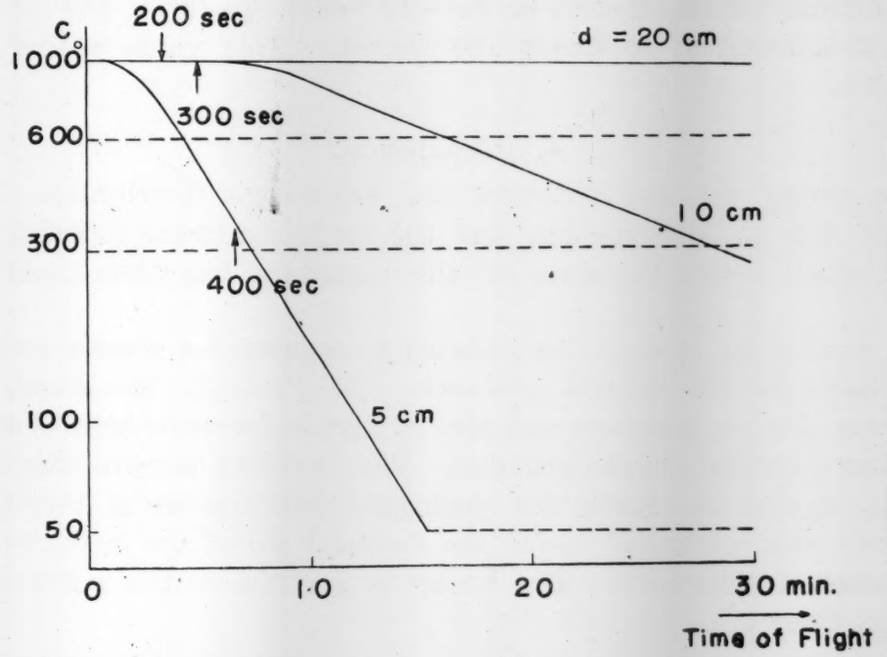

Fig. 8. The changes in temperature at the centre of the pumice particle.

the present position. Therefore they are to be magnetized opposite to the applied geomagnetic field at that time unless they have been moved. Anomalous distribution of dip-angle about the basin covered with the pumice layer between Mts. Futatsu-dake and Mizusawa-yama seems to

be due to the reversal of thermo-remanent magnetism of the pumice there.

In order to fathom the depth of the pumice layer so as to show the anomalies, we assume a magnetized disk with the same diameter as that of the basin. At a point on the central axis of the disk with radius R and depth d, the magnetic anomaly is given by

$$\Delta Z=\frac{\gamma}{G\sigma}\frac{\partial^2 U}{\partial z^2}=2\pi d\gamma\frac{R^2}{(z^2+R^2)^{3/2}},$$

where γ, G, σ and U denote the vertical component of the magnetization, gravitational constant, density and gravitational potential respectively. Taking $R\gg z$

$$\Delta Z=2\pi d\gamma\frac{1}{R}.$$

Thus we have

$$\Delta I=\sin I_0\times\cos I_0\times\frac{\Delta Z}{Z}=\sin I_0\times\cos I_0\times\frac{2\pi d\gamma}{RZ}.$$

Approximately taking $R=500\ m$, $\gamma=-10^{-2}\ emu$, $I_0=49°50'$ and $\Delta I=-1°$, the depth d amounts to about 100 *meters*. This value seems to be reasonable.

4. Conclusion.

The causal relation between the anomalous distribution of the magnetic dip at Mt. Haruna and the magnetic characteristics of the pumice which covers the slope of the mountain has thus been made clear.

In concluding, the writer wishes to express his sincere thanks to Dr. Rikitake for his helpful guidance. To Prof. T. Minakami, Prof. T. Nagata, Mr. S. Akimoto and Mr. S. Uyeda for their helpful advices, the writer's cordial thanks are due. The writer's sincere thanks are also due to Dr. H. Kuno for geological informations of the volcano. This study was conducted under the financial aid of the grant from the Department of Education. The writer is grateful to the authorities of the Department.

3. 榛名山の地磁気異常とその浮石の逆熱残留磁気との関係

地震研究所 横山 泉

1952年10月，11月にわたり，小型地磁気感応儀を用いて，榛名山の地磁気伏角を測定した。その目的は，既に，地球物理学教室の永田研究室により発見されたところの榛名山一帯に分布する浮石の逆熱残留磁気と，地磁気異常との関連を調べることである。二ッ嶽と水沢山との間の，浮石層に厚く蔽われていると思われる地域一帯に於ては，伏角分布の異常が明かに認められる。この異常は，二ッ嶽より噴出された浮石の逆帯磁に因るものであることが略々結論された。然るに，榛名富士，二ッ嶽を夫々独立した円錐と見做して，その山体の帯磁を求めると，正常な帯磁を得た。榛名山全体に就ても同じである。即ち噴出された浮石は逆熱残留磁気的であるが，これを噴出した山体は正常に帯磁しているという事が明かになった。

4. *The Relation between the Amplitude and the Period of Earthquake Motion.*

By Kiyoshi KANAI, Kaio OSADA
and Shizuyo YOSHIZAWA,

Earthquake Research Institute.

(Read Oct. 21, 1952.—Received Dec. 20, 1952.)

1. Introduction.

Needless to say, the amplitude of earthquake motion becomes larger in a great earthquake, and it is also a well-known fact that the period becomes longer as the earthquake becomes greater. Several articles concerning the relation between the magnitude of earthquake and the amplitude of earthquake motion[1] have been published till now, but concerning the relation between these two and the period of earthquake motion we can give only a few studies[2], and naturally there are many problems yet unsolved.

In order to study analytically the mechanism of earthquake origin from the property of earthquake motion, it is desired to use the waves of unchanged wave-form on their way from the earthquake origin to the observing station.

The waves starting from the earthquake origin change their forms on their way of propagation and the degree of change is the smallest in the initial motion of P-waves.

Naturally the regional distribution of "push" and "pull" in the initial motion of P-waves has served greatly for the study on the mechanism of earthquake origin.

In ordinary districts, the wave form of seismic waves is changed to a great degree because of the complicated geological conditions of the

1) C. F. RICHTER, "An Instrumental Earthquake Magnitude Scale", *Bull. Seism. Soc. Amer.*, **25** (1935), 1.

B. GUTENBERG and C. F. RICHTER, "Earthquake Magnitude, Intensity, Energy and Acceleration", *Bull. Seism. Soc. Amer.*, **32** (1942), 163.

H. KAWASUMI, "Measures of Earthquake Danger and Expectancy of Maximum Intensity throughout Japan as Inferred from the Seismic Activity in Historical Times", *Bull. Earthq. Res. Inst.*, **29** (1951), 469.

C. TSUBOI, "Determination of the Richter-Gutenberg's Instrumental Magnitudes of Earthquakes Occurring in and near Japan", *Geophys. Notes, Geophys. Inst., Tokyo Univ.*, **4** (1951), No. 5.

2) H. HONDA and H. ITO, "On the Period of the P-waves and the Magnitude of the Earthquake", *Geophys. Mag.*, **13** (1939), 155.

R. YOSHIYAMA, Monthly Coll. Earthq. Res. Inst., Tokyo Univ., Nov. 18, 1947.

ground near the surface. But Hitachi Mine (Ibaraki prefecture), where we have been making observations for these several years, has a very good condition[3] in this sense. There, the difference between the wave forms near the ground surface and those at a depth of several hundred meters can be easily explained analytically.

In this paper, we are going to examine the relation between the amplitude and the period of earthquake motion using the initial motion of P-waves shown in the seismograms obtained at Hitachi Mine, and from the results we will enter into the discussion of the mechanism of seismic wave generation.

Table I.

Earthq. No.	Date	Hypocenter (Central Meteor. Observ.) Epicenter N	Epicenter E	Depth (km)	Duration of prelim. tremor at Hitachi Mine (sec)
170	Jan. 26, 1951	37.2	140.1	shallow	12.0
171	Jan. 28, 1951	36.6	141.2	40	7.0
181	Feb. 20, 1952	36.1	139.9	55	10.3
200	Mar. 10, 1952	36.7	141.1	40	7.0
252	June 12, 1952	36.2	140.1	55	8.7

Table II. Instrumental constants of the seismographs.

Earthq. No.	Direction	Natural period (sec)	Magnification	Damping ratio
170	EW	1.0	250	13:1
	UD	0.25	210	〃
171	EW	1.0	250	〃
	UD	0.25	210	〃
181	EW	1.0	215	〃
	NS	〃	288	〃
	UD	0.10	220	〃
200	EW	1.0	215	〃
	NS	〃	288	〃
	UD	0.10	260	〃
252	NS	1.0	250	〃
	UD	0.26	120	〃

2. Correction of Seismograms.

Table I shows the positions of the origin of the earthquakes treated herein which were determined by the Central Meteorological Obser-

3) K. KANAI and T. TANAKA, "Observations of the Earthquake-motion at the Different Depths of Earth. I", *Bull. Earthq. Res. Inst.*, **29** (1951), 107.
K. KANAI, "The Results of Observation of Wave Velocity in the Ground", *Bull. Earthq. Res. Inst.*, **29** (1951), 503.

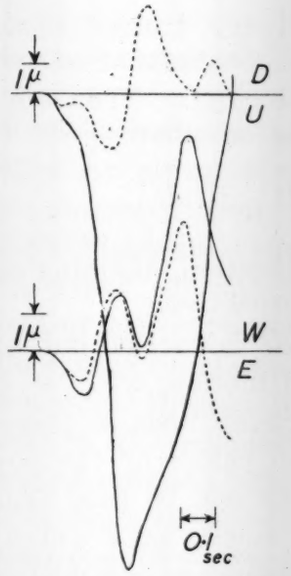

Fig. 1. Earthq. No. 170: Jan. 26, 1951: Δ=82 km, D=76 km. Full and broken lines represent the actual ground motions and the records of seismograms respectively.

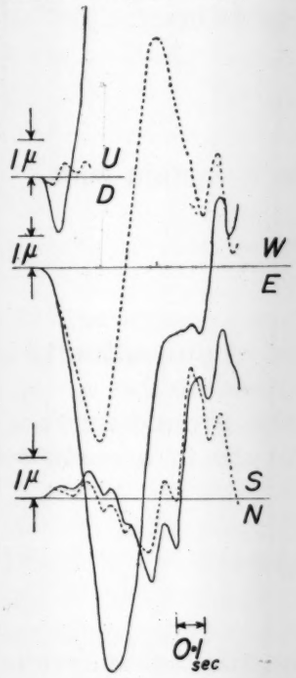

Fig. 4. Earthq. No. 200: Mar. 10, 1952: Δ=42 km, D=46 km. Full and broken lines represent the actual ground motions and the records of seismograms respectively.

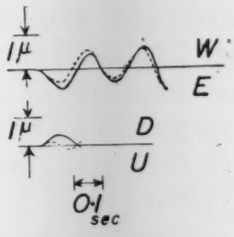

Fig. 2. Earthq. No. 171: Jan. 28, 1951: Δ=55 km, D=29 km. Full and broken lines represent the actual ground motions and the records of seismograms respectively.

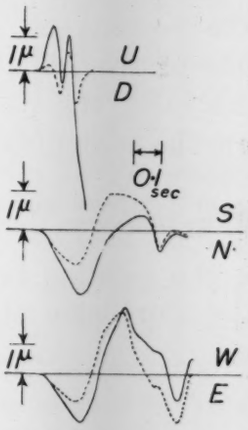

Fig. 3. Earthq. No. 181: Feb. 20, 1952: Δ=82 km, D=44 km. Full and broken lines represent the actual ground motions and the records of seismograms respectively.

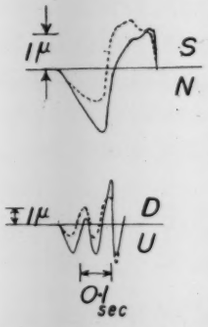

Fig. 5. Earthq. No. 252: June 12, 1952: Δ=67 km, D=40 km. Full and broken lines represent the actual ground motions and the records of seismograms respectively.

vatory, Tokyo, and the duration of preliminary tremor observed at Hitachi Mine. Table II shows the intrumental constants of seismographs.

Let the wave form of seismograms be $f(t)$. Then we get the actual ground motion $F(t)$ from the following equation:

$$F(t)=\frac{-1}{V}\left[f(t)+2\varepsilon\int_0^t f(t)dt+n^2\int_0^t dt\int_0^t f(t)dt\right], \qquad (1)$$

where V, ε and n are the geometrical magnification, damping coefficient and natural frequency of the seismograph respectively.

From equation (1), the graphical calculation is carried out by applying the seismograms, then the actual ground motion will be given as shown in Figs. 1—5 by full lines. The broken lines in these figures represent the records of seismograms. The values of the period and the amplitude of the initial motion of P-waves can be read from Figs. 1—5. In this case, the period of the initial motion of P-waves is twice the time from the beginning of motion to the moment to cross the zero-line.

3. Relation between the period and the amplitude of seismic waves.

Suppose the relation between the viscosity of the material of earth crust and the amplitude at a certain spot is as follows:

$$A\propto e^{-\frac{kx}{T^2}}, \qquad (2)$$

where

x=distance from the earthquake origin to a certain spot,
$k=(2\pi)^2\xi/2\rho v^3$,
ξ=coefficient of solid viscosity,
ρ=density,
v=velocity.

If the penetrating power of seismic waves at discontinuity surfaces of the material within the earth crust is assumed to be τ_1, τ_2, ..., τ_n, and the ratio of the actual amplitude at the ground surface to that of the incident wave to be κ_0, A_0, the amplitude at a certain spot on ground surface may be

$$A_0=\frac{\mathfrak{A}}{\sum_{i=1}^{n} x_i}\times e^{-\frac{1}{T^2}\sum_{i=1}^{n} k_i x_i}\times(\tau_1\tau_2\ldots\ldots\tau_n)\times\kappa_0 \qquad (3)$$

where $\mathfrak{A}$ indicates the constant determined from the mechanism of earthquake origin.

Then, suppose the seismic wave reaches a spot 100 km from the earthquake origin, through a non-viscous homogeneous material. The amplitude, A, at this spot may be written, based on equation (3), as follows:

$$A=\frac{A_0 e^{\frac{1}{T^2}\sum_{i=1}^{n} k_i x_i}}{(\tau_1\tau_2\ldots\ldots\tau_n)\times\kappa_0}\times\frac{\sum_{i=1}^{n} x_i}{10^7}\ . \qquad (4)$$

Then let us compare the amplitudes of several earthquakes by using the value of amplitude, A, at this supposed spot.

Fig. 6[4] illustrates the structure model of the earth crust adopted by us, Fig. 7 shows the origins of the earthquakes determined from the incident angle and the duration of preliminary tremor at Hitachi Mine, both of which were given by the calculated results of reflection phenomena at ground surface[5] and the analytical results of seismograms. (The origins thus determined approximately coincide with those determined by the Central Meteorological Observatory, Tokyo, using many data obtained by the various meteorological stations,)

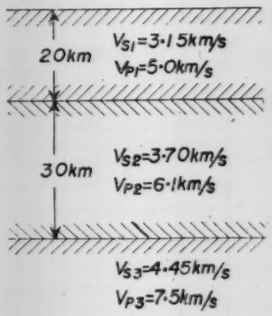

Fig. 6. The structure model of the earth crust.

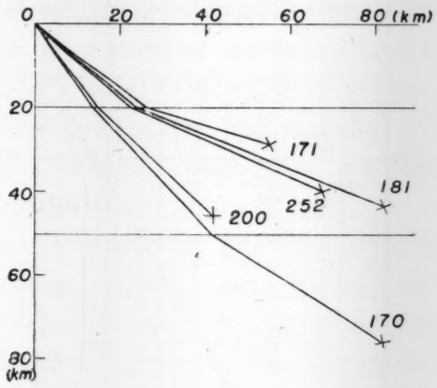

Fig. 7. The origins of the earthquake.

τ_1 and τ_2 are given by the path shown in Fig. 7[6] and κ_0 by the calculation of reflection at ground surface[7], and they are shown in Table III. (As seen in Table III, all the values of τ_1 and τ_2 are approximate to 1 and those of κ_0 approximate to 2. Therefore, some changes in the structure model of earth crust may have no influence upon the results stated in this paper.)

Table III.

Earthq. No.	τ_1	τ_2	κ_0	Incident angle
170	1.07	0.97	2.03	34°02′
171	0.75	—	2.04	52°18′
181	0.83	—	2.03	49°39′
200	1.01	—	2.03	36°16′
252	0.87	—	2.04	48°25′

4) T. MATUZAWA, K. YAMADA and T. SUZUKI, "On the Forerunners of Earthquake-motions (The Second Paper)", *Bull. Earthq. Res. Inst.*, **7** (1929), 241.

5) T. MATUZAWA, *Zisin* (*Jour. Seism. Soc., Japan*), **4** (1932), 125 (in Japanese).

6) H. KAWASUMI and T. SUZUKI, *Zisin* (*Jour. Seism. Soc., Japan*), **4** (1932), 277 (in Japanese).

7) *loc. cit.*, 5).

The values of A are determined by introducing the values shown in Table III into equation (4), and in Fig. 8 the relation between the amplitude, A, and the period, T, of the initial motion of P-waves is shown. In this case the viscosity coefficient of materials from the earthquake origin to the ground surface, is assumed to be constant. In Fig. 8, the marks ● show the values, reduced to the spot 100 km from earthquake origin, which were obtained by H. Honda and H. Ito[8] from the results of conspicuous deep earthquakes.

Fig. 8 shows that general earthquakes adopted by us and conspicuous deep earthquakes adopted by H. Honda and H. Ito form nearly a straight line. This fact seems to prove that the relationship

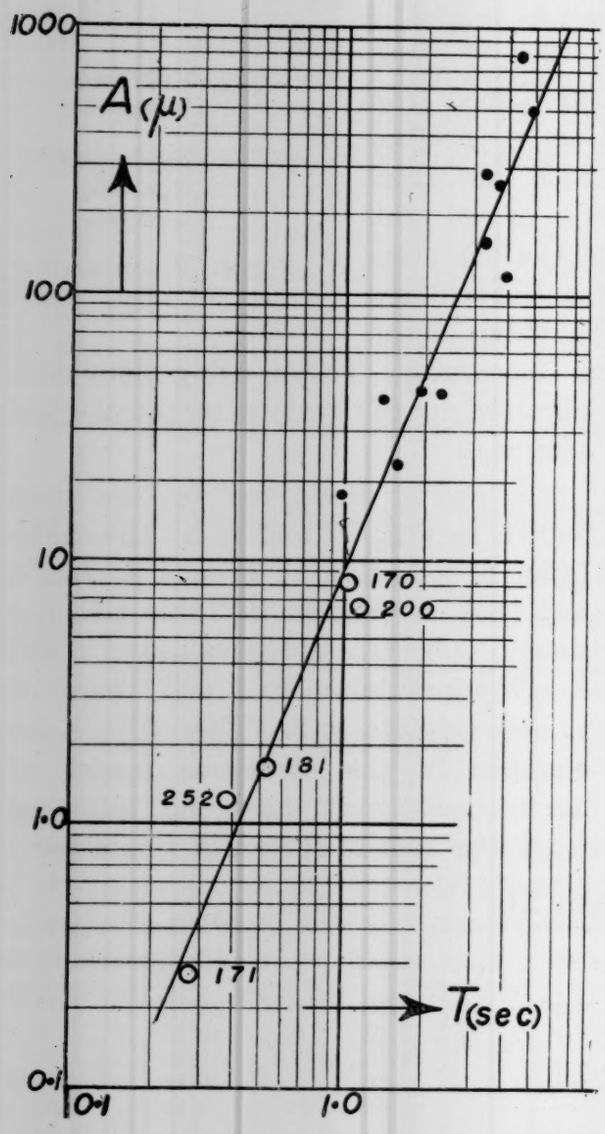

Fig. 8a. The relation between the amplitude, A, and the period, T, of the initial motion of P-waves. The case in which damping factor k is 0. (Marks ● show the values of conspicuous deep earthquakes).

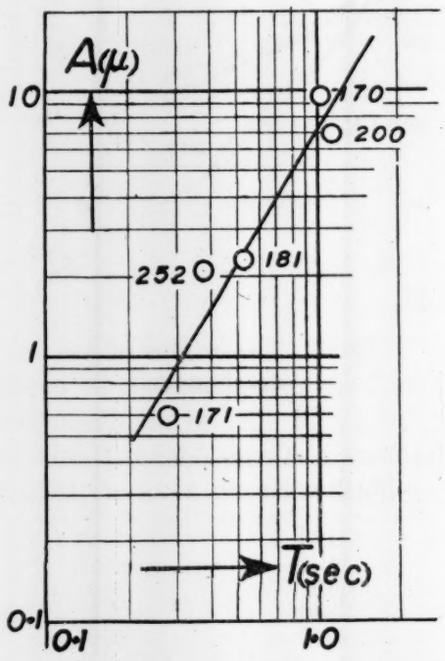

Fig. 8 b. The relation between the amplitude, A, and the period, T, of the initial motion of P-waves. The case in which damping factor k is 10^{-8} C.G.S.

8) H. HONDA and H. ITO, *loc. cit.*, 2), 159.

between the amplitude and the period of seismic waves has a considerable generality.

Then the relation between the period and amplitude of the initial motion of S-waves is presented for reference in Fig. 9. The case of S-waves is very complicated because the influence of the preliminary tremor upon the initial motion cannot be wholly removed. Therefore, the correction of amplitude is carried out with regards to only the relation that the amplitude decreases in inverse proportion to the distance from the earthquake origin.

From Figs. 8 and 9, it is found that with the initial motion of seismic wave the amplitude is approximately in proportion to the square of the period. As stated before, of all the seismic waves observed on the ground surface, the initial motion (particularly of P-wave) is the best in communicating the characteristics of seismic waves generated at the earthquake origin.

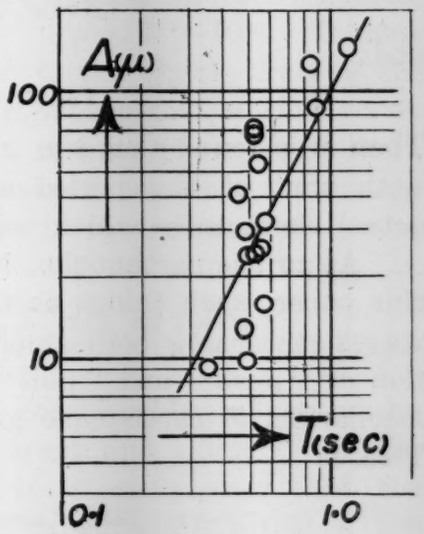

Fig. 9. The relation between the amplitude and the period of the initial motion of S-waves. The case in which damping factor k is 4.5×10^{-8} C.G.S.

Therefore, the characteristics of the initial motion of earthquake motion is supposed to be the first approximation of the characteristics of the seismic waves generated at the earthquake origin. Then the relation between the amplitude and the period of seismic wave may be expressed as

$$\text{Amplitude} \propto (\text{Period})^2. \qquad (5)$$

4. Presumption of the mechanism of seismic wave generation.

When pressure change or shearing force suddenly acts at a spherical origin, the amplitude of the generated seismic waves at a fairly far-off spot from the origin may be written for both P-waves and S-waves as follows:

$$A \propto a^2 p_0 \sin\frac{\alpha t}{a}\ ^{9)}, \qquad (6)$$

where p_0: pressure or shearing force which acts on spherical surface,

9) K. SEZAWA and K. KANAI, "Transmission of Arbitrary Elastic Waves from a Spherical Source, Solved with Operational Calculus, I, II, III," *Bull. Earthq. Res. Inst.*, **19** (1941), 151, 417, **20** (1942), 1.

a: radius of spherical origin, t: time, α: constant determined from the property of the material existing near the spherical origin.

If the pressure or shearing force p_0 acting upon the spherical surface is constant in every earthquake, from equation (6) it becomes

$$A \propto a^2, \quad T \propto a, \tag{7}$$

and

$$A \propto T^2. \tag{8}$$

Then it is found that the relation expressed in equation (8) coincides with that of the period and the amplitude of the initial motion of actual earthquake which was obtained from the seismograms.

As to the earthquake, No. 170, one of the earthquakes we used in this paper, such things as the relation between the P-waves and the S-waves concerning both amplitude and period, and the regional distribution of "push" and "pull" of initial motion were explained from the mechanism of earthquake generation in the author's previous paper[10], That is

$$\left.\begin{aligned} \widehat{rr}_{r=a} &= p_0 P_2(\cos\theta), & t>0, \\ &= 0 & t<0, \end{aligned}\right\} \tag{9}$$

Considering the mechanism of earthquake generation expressed in equation (9), the radius of spherical origin a is given by

$$a = \frac{T}{2.6\,C_2} = \frac{T}{2.6}\sqrt{\frac{\mu}{\rho}}\ ^{11)} \tag{10}$$

When the radius a of spherical origin is determined from equation (10), strain, p_0/μ, will be given by

$$\frac{p_0}{\mu} = \frac{u_{f1} r}{0.06 a^2}\ ^{12)} \tag{11}$$

Now, we calculate p_0/μ by applying equation (10) and (11) to the results obtained from the observation of the earthquake No. 170 as an example. In this case, as $t=0.53$ sec, if it is assumed to be $\sqrt{\mu/\rho}=4.45$ km/sec, the radius of spherical origin becomes from equation (10) $a \fallingdotseq 1$ km. In the earthquake concerned, since $u_{f1}=9$ micron, with such numerical data as $r=100$ km and $a=1$ km as already known, equation (11) becomes p_0/μ

10) K. KANAI, "Examinations of the Assumption concerning Mechanism of Earthquake Origin through Seismograms", *Bull. Earthq. Res. Inst.*, **30** (1952), 39.

11) K. KANAI, "Possibility of the Period of P-waves becoming smaller than those of S-waves", *Bull. Earthq. Res. Inst.*, **29** (1951), p. 533, Fig. 3. (−0.5 on the ordinate scale of Fig. 3 should be read −0.05.)

12) *ibid.*, 11)

(strain of spherical surface)$\fallingdotseq 10^{-4}$.

From the results of calculation about various earthquakes, it is found that, when the mechanism of earthquake generation is assumed thus, the strain at the spherical surface where seismic waves are generated is expressed in the following equation. $p_0/\mu = 10^{-4} \sim 10^{-3}$. It may be considered that this value is nearly equal to the elastic limit of the material which constitutes the earth crust. It means that seismic waves are generated near the zone where the strain reaches the rupture limit.

In case of such a mechanism of earthquake generation, the energy of earthquake, E, and the amplitude, A, are in the relation of

$$E \propto A^{1.5} (\equiv a^3), \tag{12}$$

and the relation between E and the period, T, are as follows

$$E \propto T^3. \tag{13}$$

The amplitude of earthquake motion is considerably influenced by direction, damping, construction of earth crust and property of the ground near the observation point. Then it is easily seen that the relationship between the amplitudes at earthquake origin and at the observation point is not so simple. Therefore, in general, there will be a considerable inaccuracy in determining the energy or magnitude of earthquake by using the amplitude of earthquake motion even if we adopt the initial motion of P-waves which is considered to communicate the characteristics of seismic waves generated at the earthquake origin comparatively well.

On the contrary, the period of seismic waves, particularly that of the initial motion of P-waves, can be considered to keep the characteristics of the waves unchanged from the earthquake origin to the observation point. Consequently, if the relation between the period and the energy can be clarified, the energy or the magnitude of earthquake will be given more accurately by using the period of seismograms than by using the amplitude. In this sense, we can say that equation (13) is more important than equation (12).

5. Concluding remarks.

It was found from the initial motion of seismograms obtained at Hitachi Mine that there is such a relation between the amplitude, A and the period T of seismic waves as $A \propto T^2$.

This coincides with the mathematical results in case the pressure or shearing force at a spherical origin is assumed to be constant in every earthquake and the factor to determine the amplitude to be the

radius of a spherical origin.

Then by calculating the strain at the spherical surface where seismic waves are generated with numerical data obtained from observations, it was found to be $10^{-4}\sim10^{-3}$.

As the results of these studies, it is considered that seismic waves are generated at the spherical surface where a pressure causes strain near the elastic limit of the material constituting the earth crust. In such a mechanism of earthquake generation, the energy of earthquake E and the amplitude A are in the relation of $E\propto A^{1.5}$ and the relation between E and the period T are $E\propto T^3$.

The author would like to take this opportunity to thank the members of Motoyama Office, Hitachi Mine for their contributions and also Messrs. T. Tanaka and T. Suzuki for carrying out the observations.

Added Note:

The comparison is made between the seismogram and the actual ground motion concerning the initial motion. By the definition of an initial motion, it is found that $f(t)$ in equation (1) is always larger than zero within the range of the initial motion. Consequently, the second

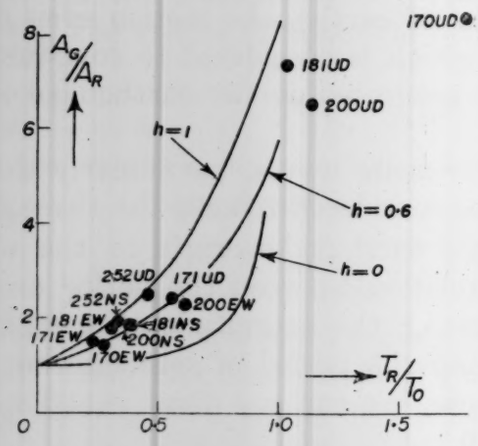

Fig. 10. T_R and T_0 represent the period of the initial motion of record and the period of seismograph. A_G and A_R represent the amplitude of the initial motion of actual ground motion and of record. The curves illustrate the calculated results of the first motion in a sudden occurrence of sinusoidal wave form.

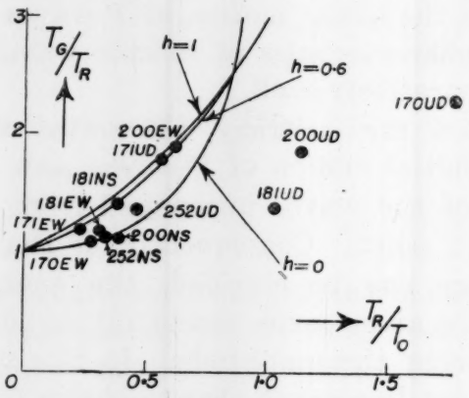

Fig. 11. T_G, T_R and T_0 represent the period of initial motion of actual ground motion, of record and the period of seismograph. The curves illustrate the calculated results of the first motion in a sudden occurrence of sinusoidal wave form.

and the third term of equation (1) are also larger than zero within the range of the initial motion. In other words, $f(t)$ is always smaller than $F(t)$ from the moment when $f(t)$ begins to move to the moment when it crosses the zero line (that is within the range of the initial motion of $f(t)$).

It means that, whatever kind of seismographs we may use or whatever form the seismic waves may assume, so far as it concerns the initial motion, the amplitude of seismogram is always smaller than that of the actual ground motion.

Similarily, as far as concerns the initial motion, the period given by the record is in every case shorter than that of the actual ground motion.

Figs. 10, 11 show the above mentioned relations of the actual earthquakes which can be found from Figs. 1～5. If the period of earthquake motion is approximately equal or smaller than that of the seismographs, by using Figs. 10, 11, the amplitude and period of actual ground motion can be easily found out from the seismograms within only a few per cent error.

---

4. 地震動の振幅と周期との関係

地震研究所 { 金井　清 / 長田甲斐男 / 吉沢　静代 }

日立鉱山で観測した地震記象の初動を解析して，$A \propto T^2$ の関係が得られた．

地震波の振幅は，たとえP波の初動でも，伝播中に反射，屈折，吸収，拡散などの現象があり，又，方向性の問題もあるから，観測値から震源附近での大きさを推定することは容易ではない．特に，普通の観測場所では，地表面附近の複雑な地層の影響が地震波の振幅には大きくひゞくから，問題は益々やっかいになる．

その意味では，P波の初動の周期は，震源附近の性質を観測場所まで保持する度合が最も大きい筈である．

従って，地震のエネルギーと初動の周期との関係を，なにらかの方法で求めることができれば，任意の観測所の地震記象から，地震のエネルギーをたやすく，しかも比較的に精度をよく，きめることができるであろう．

1つの試みとして，簡単な発震機構の仮定のもとに，この関係を求めてみたら，$E \propto T^3$ ということになった．

5. *Relation between the Earthquake Damage and the Nature of the Ground.* (*Case of Wooden Houses and Peat Bed.*)

By Kiyoshi KANAI, Teiji TANAKA
and Tomisaburo SUZUKI,

Earthquake Research Institute.

(Read Dec. 16, 1952.—Received Dec. 20, 1952.)

1. Introduction.

The magnitude, M, of Tokachi-oki Earthquake, March 4, 1952, was 8.1 and the numbers of totally-destructed, semi-destructed and slightly damaged houses in the southern and eastern parts of Hokkaido were about 1,400, 5,400 and 15,000 respectively.

The peculiarity of this earthquake concerning the damage to buildings is that such main buildings as public offices were damaged more seriously than ordinary houses. The reason is that the wooden ordinary houses in Hokkaido have small beams and the roofs are made of light stuff. In short, the upper-construction is very light in those houses.

The district which suffered from this earthquake includes a peat region of considerable area, which is an unprecedented case.

In the present paper, first, the results of the seismic prospecting made at two places within the peat region where the shock was "very strong" are stated. Then, as these two places were extremely different from each other in the degree of

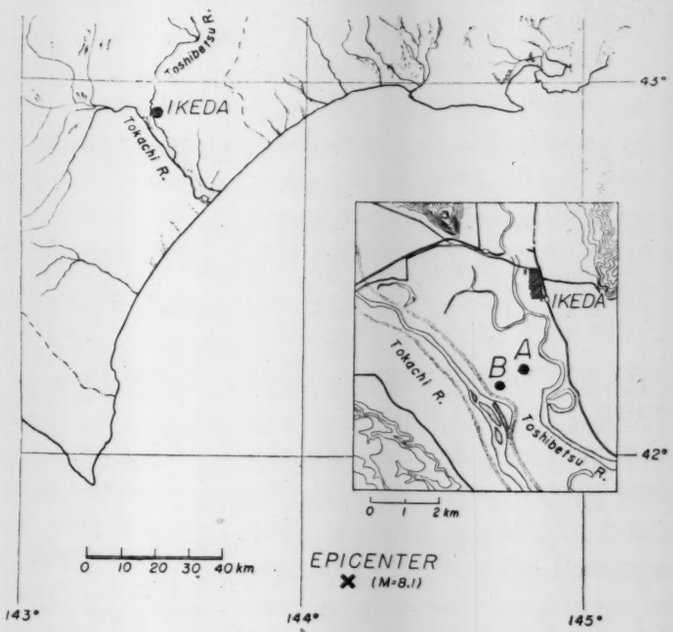

Fig. 1. Map of the examination places.

the damage done by the earthquake, the causes for this fact is searched by using the data obtained from the seismic prospecting.

2. Results of seismic prospecting.

(i) Date of prospecting: July 17 and 18, 1952.

(ii) Places of prospecting: The cultivated land hemmed in by the Tokachi River and the Toshibetsu River. The surface is of clay bed associated with peat-soil.

Place "A": Kawai, Tokachi-Ikeda-machi (about 2.2 km SSW of Ikeda Station).

Place "B": " (about 2.9 km SW of Ikeda Station).

The places of seismic prospecting are shown in the map of Fig. 1.

(iii) Results of prospecting: Figs. 2 and 3 show the travel time curves of the initial motion at place "A" and "B" respectively. The velocities of two media and thickness of the surface layer obtained from Figs. 2 and 3 are shown in Table I.

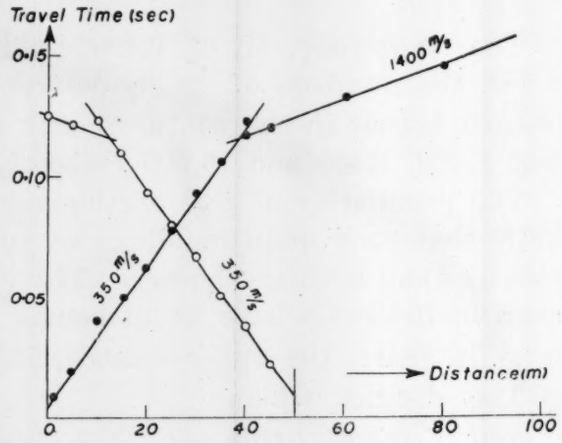

Fig. 2. Travel-time curves at the examination place "A".

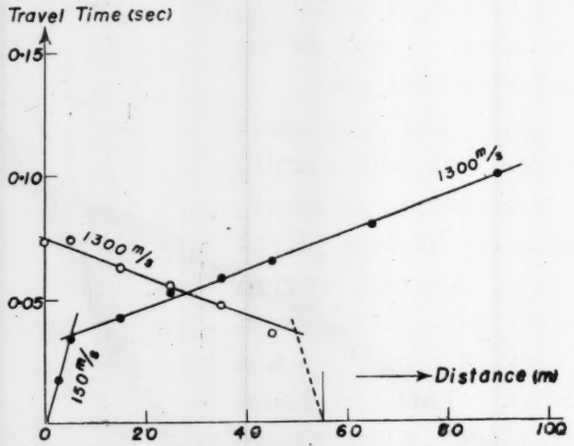

Fig. 3. Travel-time curves at the examination place "B".

It is found from Table I that the velocity of P-waves in the peat bed is not of a particular value compared with that in ordinary regolith bed. This must be due to much quantity of clay contained in the peat-soil. (Another seismic prospecting[1]) was performed in crossing the Toshibetsu River which is at the distance of 5 km from the places mentioned above. The results were as follows: v_1= 300 m/s, v_2=1,600 m/s, thickness=several meters, and the second layer = gravel bed associated with clay. Though the measured line was about

1) K. WATANABE, "Geophysical Prospecting", 1937, Appendix A), 10), d).

200 m in length in this case, no data about the third layer are seen.)

Table I.

Examination place	Velocity of P-waves (m/sec)		Thickness of 1st layer (m)
	1st layer	2nd layer	
A	350	1,400	15
B	150	1,300	2

3. The examination of the results obtained from the seismic prospecting.

The farm houses in the district within which the place of prospecting "A" is, were damaged only slightly. On the contrary, the farm houses in the district of place "B" were so heavily damaged that almost all houses had to be rebuilt. Also in the latter district, many horses working in the fields stumbled during the earthquake, while in the former district such things never happened.

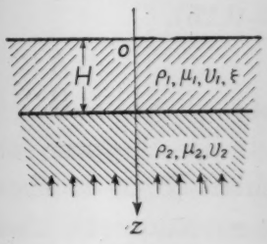

Fig. 4.

These facts show that the earthquake motion was larger in "B" district than in "A" district.

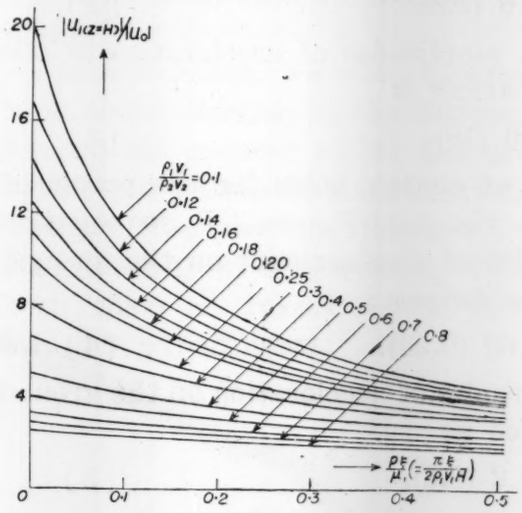

Fig. 5. $u_{1(z=H)}$ and u_0 represent the amplitude of surface motion and of incident wave at lower boundary respectively. ξ, μ_1, ρ_1. v_1, H and p represent viscosity coefficient, rigidity, density, velocity, thickness of surface layer and frequency respectively.

Now the authors will try to explain the above-mentioned facts using the results of seismic prospecting.

Let us assume that seismic waves is the superposition of waves of various period and the largest amplitude at the free surface is caused by the wave of which the period is equal to the synchronized one of the surface layer.

The theoretical investigation[2] in case a semi-infinite elastic body is beneath a surface layer with solid viscosity and S-waves propagate perpendicularly across them gives the result shown in Fig. 5.

2) K. KANAI, "Relation between the Nature of Surface Layer and the Amplitudes of Earthquake Motions", *Bull. Earthq. Res. Inst.*, **30** (1952), 35, Fig. 5.

(To simplify the problem, the solid viscosity in lower layer is neglected, because it is without influence upon the final results.)

As values of ξ/v^3 concerning various materials in the earth crust are always of same order[3], it is supposed, for the present, that $\xi/v^3=10^{-7}$ C.G.S. Poisson's ratio of the materials of the first and the second layers at the observing points, "A" and "B", is assumed to be $\sigma=0.48$[4]. The densities of the materials are assumed to be $\rho_1=1.5$ and $\rho_2=2.0$.

Under such assumptions, introducing the results obtained from the seismic prospecting at "A" and "B" districts into Fig. 5, we get the following results. (The values in the parenthesis are when Poisson's ratio $\sigma=0.25$).

$$\begin{aligned} &\text{"A" district ; } |u_{1A(z=H)}|/|u_{0A}|=7.6 \ (7.3), \\ &\text{"B" district ; } |u_{1B(z=H)}|/|u_{0B}|=15.2 \ (13.5). \end{aligned} \tag{1}$$

(I) Suppose the amplitude in any period of the incident waves which come to the boundary to be constant, that is to say, $|u_{0A}|=|u_{0B}|$ in equation (1), then the ratio between the amplitudes of displacement at the ground surface of "A" and "B" districts becomes

$$|u_{1B(z=H)}|/|u_{1A(z=H)}|=2.0 \ (1.8). \tag{2}$$

In this case the ratio between the amplitudes of acceleration at the ground surface of "A" and "B" districts is

$$|\alpha_{1B(z=H)}|/|\alpha_{1A(z=H)}|=20 \ (18). \tag{3}$$

(II) Assuming that equipartition of energy holds for the waves of various periods in the incident waves, viz. $|u_{0A}|/T_A=|u_{0B}|/T_B$ in equation (1), the ratio between the amplitudes of displacement on the ground surface of "A" and "B" is given as follows :

$$|u_{1B(z=H)}|/|u_{1A(z=H)}|=0.62 \ (0.58). \tag{4}$$

In this case the ratio of the amplitudes of acceleration on the ground surface of "A" and "B" is expressed as

$$|\alpha_{1B(z=H)}|/|\alpha_{1A(z=H)}|=6.2 \ (5.8). \tag{5}$$

(III) Though nothing definite can be said before finding the correct

3) K. KANAI and K. OSADA, "The Result of Observation concerning the Waves Caused in the Ground by Building Vibration", *Bull. Earthq. Res. Inst.*, **29** (1951), 514, Table II.

4) Reference data:

K. MANAI, *Bull. Faculty Eng., Hokkaido Univ.*, **6** (1952), 77, Table 2.

H. KAWASUMI and others, *Monthly Colloquium, Earthq. Res. Inst., Tokyo Univ.*, Sept. 16, 1952.

Bull. Disast. Prevent. Res. Inst., Kyoto Univ., **2** (1949), 6, 17; **3** (1950), 1, 3, 7.

value of Poisson's ratio, the periods of the waves at "A" and "B" which have predominant amplitudes become $4H/v_s=0.9$ sec ($\equiv T_A$) and 0.3 sec ($\equiv T_B$), using the foregoing assumption $\sigma=0.48$ and the values of Table I. The natural period of top-light farm houses which are peculiar to Hokkaido seems to be approximate to the period of predominant amplitude at "B" district, viz. $T_B=0.3$ sec.

In summarizing the calculated results in case of (I), (II) and (III), it is found that in case of a great earthquake the houses in "B" district will be under worse vibrational condition than those in "A" district. Therefore, why the damage differs extremely in two district so close to each other may be explained from the present investigation.

4. Concluding remarks.

In applying the data obtained from the seismic prospecting to the results of vibration problems concerning the surface layer with the consideration of solid viscosity, numerical calculations were carried out. In Tokachi-oki Earthquake of March 4, 1952, there was much difference in the damage at two districts very close to each other. The cause for that is to some extent explained from the results of the present investigation.

In conclusion, we wish to express our thanks to the officials of the Construction Section in the Bureau of Development, Hokkaido, for the financial aid granted us for the present investigations. We also wish to express our thanks to Assistant Professor Y. Sakai and other staffs of the Faculty of Engineering, Hokkaido University, Assistant Professor T. Shiga of the Faculty of Engineering, Tohoku University and the staffs of the Town office of Tokachi-Ikeda, Hokkaido, who cooperated heartily with us in our experiments.

5. 震害と地盤の性質との関係（泥炭地にある木造家屋の場合）

地震研究所 { 金井　清
田中貞二
鈴木富三郎

1952年3月4日の十勝沖地震の震害地である十勝平野の泥炭地で彈性波試験を行い，その結果を使って地震時の地盤の振動的性質を研究した。

卽ち，彈性波試験の場所は震害程度に大きな差違のある2ケ所をえらんだ。次に，固体粘性を入れた表面層の振動問題の解に，彈性波試験で得た数値を代入して計算を行った。

その結果として，震害の大きかった地域は，地震動の変位振幅，加速度振幅のいづれについても，震害の少かった地域よりも大きいことになり，震害程度の差違の一つの説明になる。

又，大震害のあった土地の卓越周期は約 0.3 sec，小震害の土地のそれは 0.9 sec 位となり，この地方の農家の固有周期は 0.3 sec 前後と考えられるから，この意味でも，震害程度に差違が生じ得ることになる。

6. *Elastic and Viscous Properties of Volcanic Rocks at Elevated Temperatures. Part 2.*

By Shūzō SAKUMA,

Earthquake Research Institute.

(Read Dec. 16, 1952.—Received Dec. 20. 1952.)

1. Introduction.

In the previous report[1], the writer described the mechanical properties of lava-specimens from the Oo-sima volcano. The newly ejected tholeiitic basalt showed quite extraordinary behaviours when its temperature was changed within the range of 20°–1100°C. Young's modulus for it increased at first at low temperature, then it showed a rapid decrease at 700–800°C and viscous flow could be seen beyond that temperature. Elasticity and viscosity were influenced by the time spent in heating as well as the frequency of heat-treatments in the laboratory. The properties were so extraordinary that the writer failed to explain them on the basis of our knowledges concerning metals, artificial glass and other materials. Subsequently, the writer thought it more appropriate at present to study other rocks of simpler structures. From the standpoint just mentioned, the following experiments on vitreous silica, obsidian and Sanukite were carried out.

2. Method.

The same method of bending and sagging thin plates of specimens (ca. 8 cm × 1 cm × 0.3 cm) was adopted as in the previous studies. The specimens acted more or less visco-elastically at high temperatures without exception. Fig. 1 shows the trend of deformation when constant load is applied and then removed. The method of analysis for such visco-elastic bodies, which was adopted in the previous report, was revised a little as follows. By assuming the condition of constant stress,

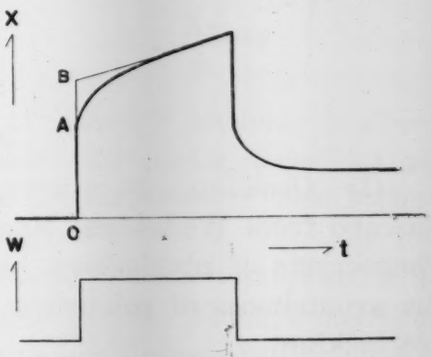

Fig. 1. Deformation (x) of a visco-elastic body under constant load (W).

1) S. SAKUMA, *Bull. Earthq. Res. Inst.*, **30** (1952), 269.

$$\frac{P_{xx}}{\tau}=E(\dot{e}_{xx}+\tau'\ddot{e}_{xx}) , \qquad (1)$$

where E is Young's modulus, and τ and τ' are relaxation times. Then by integration,

$$e_{xx}=\frac{P_{xx}}{E\tau}t+\left(C_1-\frac{P_{xx}}{E\tau}\right)\tau'+C_2e^{-\frac{t}{\tau'}} . \qquad (2)$$

Put $e_{xx}=\frac{P_{xx}}{E}$ at $t=0$, we obtain

$$e_{xx}=\frac{P_{xx}}{E}+\frac{P_{xx}}{E\tau}t-C_2\left(1-e^{-\frac{t}{\tau'}}\right) . \qquad (3)$$

In the previous paper[2], the whole recoverable part (OB in Fig. 1), including the delayed elastic deformation (AB in Fig. 1, elastic fore-effect or fore-creep in other words), was regarded as the elastic deformation, and Young's modulus was calculated on the basis of the deformation OB. In the present analysis Young's modulus E corresponds to the instantaneous deformation (OA), and the delayed elastic effect can be discussed separately.

At any rate, the amount (x) of deformation actually observed through the apparatus is connected with the coefficients of elasticity E and viscosity η by the following formulae[2].

$$\begin{cases} x=\left(\frac{Wl^3g}{48I}+\frac{5wl^4g}{384I}\right)\left\{\frac{1}{E}\left(1+\frac{t}{\tau}\right)+C\left(1-e^{-\frac{t}{\tau'}}\right)\right\} & (4) \\ \text{where } I=\frac{1}{12}bd^3 . & \\ \eta\fallingdotseq\frac{\tau E}{3} . & (5) \end{cases}$$

3. Specimens.

(1) Obsidian. It is a typical natural glass, collected by Dr. Y Kawano from Wadatōge, Nagano Pref. The rock[3] is of blackish colour. Phenocrysts of plagioclase, biotite and augite are scattered sparsely in the groundmass of colourless glass, and microlites as well as crystallites are lacking.

(2) Sanukite. Collected by Dr. R. Morimoto from Kasuga-yama,

2) S. SAKUMA, *loc. cit.*, 1).

3) Y. KAWANO, Report No. 134, *Geol. Surv. Japan.* (in Japanese)

Nijō-san, Osaka Pref. The aphanitic andesite[4] contains phenocrysts of plagioclase and hypersthene sparsely in the glassy groundmass. The compact and uniform groundmass consists of glass and equigranular minute crystals of plagioclase, hypersthene, magnetite and of biotite. The rock is hard and of blackish colour as a whole.

(3) Vitreous silica. Specimens of vitreous silica were furnished by the Nihon Quartz Co. Though it was annealed at about 1500°C, a slight heterogeneity was seen even with naked eye.

Dr. Y. Kawano and Dr. R. Morimoto kindly placed at the writer's disposal their rock specimens. To them the writer's cordial thanks are due. The results of chemical analysis are also cited in Table 1.

Table I. Chemical Composition of Specimens.

	Obsidian[3]	Sanukite[4]
SiO_2	76.24	61.72
Al_2O_3	12.56	19.18
Fe_2O_3	0.68	0.53
FeO	0.58	4.11
MgO	0.23	2.12
CaO	0.96	5.59
Na_2O	2.84	2.65
K_2O	4.20	1.99
H_2O_+	0.69	0.45
H_2O_-	0.17	0.23
TiO_2	0.38	0.62
MnO	0.05	0.10
P_2O_5	0.25	0.18
Total	99.83	99.47
Analyst	Y. Kawano	T. Kushida
Location	Wadatōge	Kasugayama

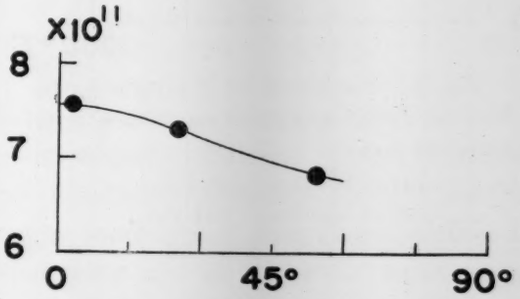

Fig. 2. Young's modulus of obsidian at room temperature (in dyne/cm²) versus the angle of stress to the direction of flow structure in the specimen.

4. Results.

(1) The obsidian. The absolute value of Young's modulus is affected slightly by the flow structure in the rock. It varies according to the angle between the principal stress and the direction of flow structure in the specimen, as is shown in Fig. 2.

The general trend of variation of elasticity versus temperature is quite similar among three examined obsidian specimens. Young's modulus hardly decreases with the rise of temperature until above 600°C, where the rapid augmentation of delayed elastic effect and decrease of elasticity take place. (Figs. 3 & 4). Viscous flow also develops so much

4) R. MORIMOTO, unpublished data, oral communications.

within the range from 650° to 760°C that the present method of experiment failed beyond that temperature. (Fig. 7)

Repeated heating and cooling resulted in a slight decrease of elasticity as well as viscosity.

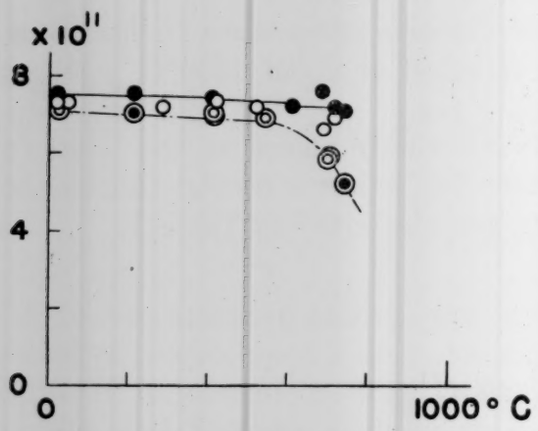

Fig. 3. Variation of Young's modulus of obsidian specimen No. 4 with temperature.
single circles: 1st run;
double circles: 2nd run;
filled circles: heating.

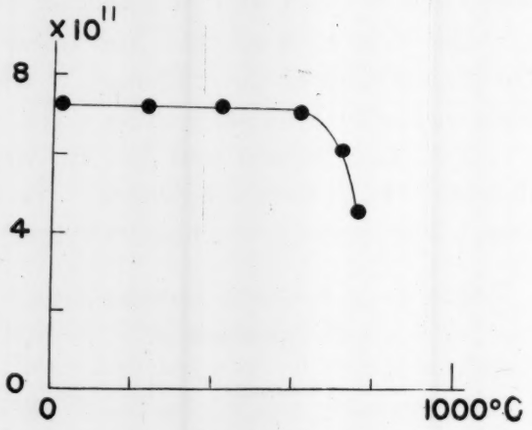

Fig. 4. Variation of Young's modulus of obsidian specimen No. 3 with rise of temperature.

(2) The Sanukite. Only one specimen was examined to this date. With the rise of temperature, elasticity shows no remarkable change till above 650°C, then both the delayed elasticity and viscous flow become noticeable. However, the rate of decrease of viscosity with rising temperature around 700°–800°C is far less than that of the obsidian, and the rate comes to increase remarkably again at above 1000°C. (Figs. 7(a) & 7(b)). Young's modulus for the instantaneous part of deformation also decreases greatly at high temperature as will be seen in Fig. 5. In detail, however, we can notice that the delayed elastic deformation does not change in accordance with the variation of Young's modulus with temperature. Really, Young's modulus begins to decrease significantly from above 800°C, about 150°C higher than the temperature (650°C) at which anelasticity becomes measurable. As a result, the ratio of the delayed elastic part to the instantaneous part of deformation does not change monotonously with temperature. (Fig. 8)

Young's modulus in the cooling process is same as in the heating stage. Lower viscosity in cooling is also worthy of notice.

(3) Vitreous silica. Two specimens were tested up to 1100°C. As

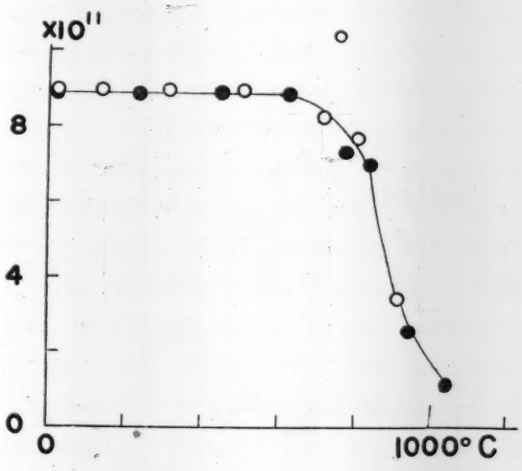

Fig. 5. Variation of Young's modulus of Sanukite.
filled circles: heating;
open circles: cooling.

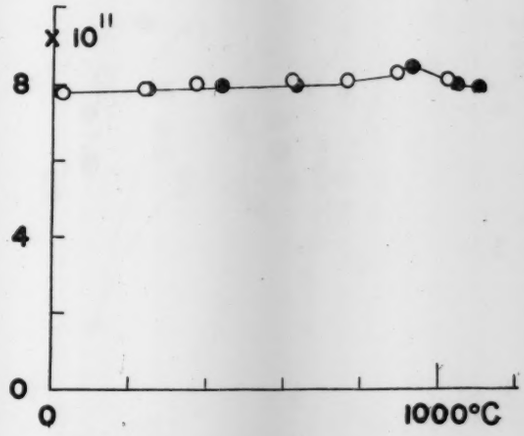

Fig. 6. Variation of Young's modulus of vitreous silica with temperature.
filled circles: heating;
open circles: cooling.

will be seen in Fig. 6, Young's modulus increases slightly with the rise of temperature and tends to decrease at about 1000°C. Only a small amount of viscous flow and delayed elasticity appears beyond 900°C. The whole trend of variation of Young's modulus is nearly reversible in the cooling stage. The increase of elasticity up to 1000°C, amounting to several per cents, was already revealed[5] by many authors in the experiments concerning rigidity of silica. The tendency of increasing elasticity with temperature is somewhat similar to that observed in the case of the Oo-sima lava, although to larger extent in the latter case. It seems not improbable that the growth of microcrystals, if any in super-cooled vitreous materials, would cause an anomalous increase of elasticity.

It is a particular feature of the vitreous silica that, when compared with the obsidian and the Sanukite, no anelasticity can be observed at such temperature as 650°–800°C.

5. Discussion.

When the behaviours of the three typical specimens are compared with one another, they can be distinguished unmistakably. The variations of Young's moduli of the obsidian and the Sanukite are rather ordinary and resemble that of artificial glass. In contrast to them, that

5) R. Sosman, "The Properties of Silica," U.S.A. (1927).
K. Iida. *Bull. Earthq. Res. Inst.*, **13** (1935), 665.

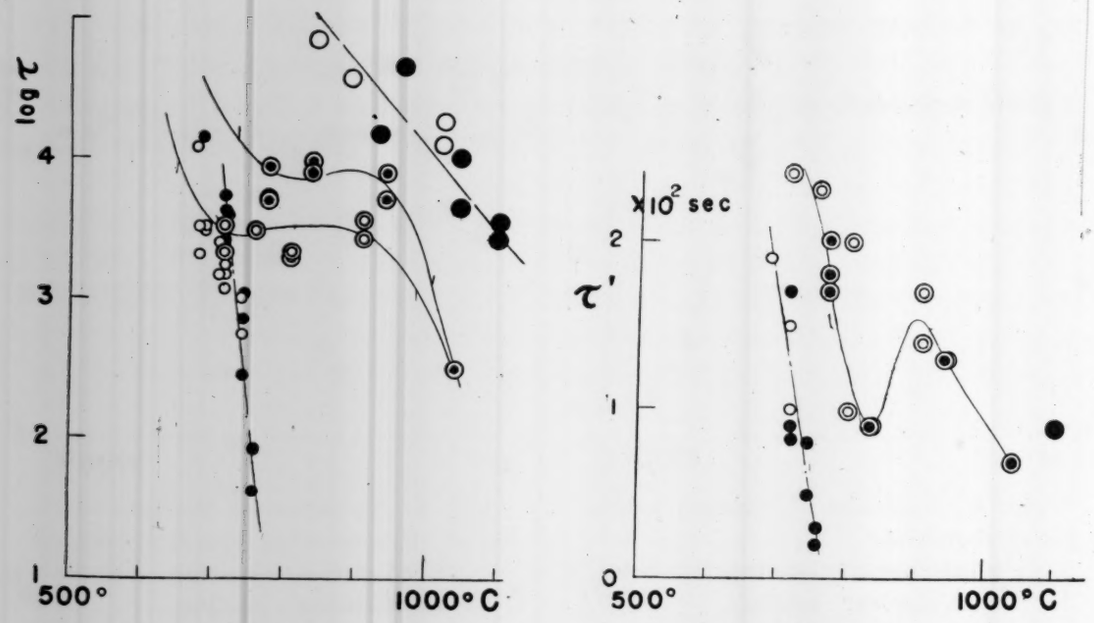

(a) τ versus temperature. (b) τ' versus temperature.

Fig. 7. Variation of relaxation times with temperature.
larger circles: vitreous silica; smaller circles: obsidian;
double circles: Sanukite; filled circles: heating; open circles: cooling.

of vitreous silica is extraordinary. Distinct difference may be noticed also in their softening temperatures. The obsidian can be regarded as vitreous, because very sparse phenocrysts only can be found in the glassy base by microscopic studies. The differences in elasticity as well as in anelasticity existing between the two vitreous materials must be ascribed to the difference in their chemical compositions. Consequently, we are inclined to conclude that the interstitial glass itself does influence very much the dynamical properties of glassy rocks at least at elevated temperatures. It is not unreasonable to imagine that the conclusion may hold even in the case of volcanic rocks of higher crystallinity.

The aphanitic andesite (Sanukite), with minute minerals scattered in hard glass, softens at only a little higher temperature than the obsidian, but its viscosity does not decrease so rapidly as the latter. We cannot tell at present whether it is due to their differences in the chemical composition in their glassy parts, or to the existence of the microlites in the glassy base of the Sanukite.

Quantities concerning the delayed elasticity are also illustrated in Figs. 7(b) & 8. There also will be seen obvious differences between the two kinds of glass, and somewhat intermediate characteristics of the Sanukite.

Some more words have to be added here about the coefficients E, τ,τ' and the constant C in the equation (4). In the previous paper, the coefficients were regarded simply to be concerned with the rock specimen as a whole. However, what part of the rock deforms instantaneously and what part behaves anelastically in process of time? This problem is too much complicated to be solved at once. When we attempt to summarize the results with the aid of the rheological methods, a puzzling fact turns up. Various rheological models can yield quite the same curve of deformation versus time under constant load. It is highly confusing that not one but several models behave in a similar way. Two of them are illustrated in Fig. 9. One of them (A), i. e. Burger's model, which is the Maxwell body coupled with the Kelvin body in series, is frequently used in chemistry. The equation (1) was derived from the model after some procedures of approximations[6]. Our coefficients E, τ, τ' correspond to E_1, τ_1, τ_2 respectively in this Burger's model. The other model (B) of pararell Maxwell bodies is adopted widely in the research field of artifical glass[7], in which our E corresponds to $E_1 + E_2$ and other coefficients can be replaced by functions of E_1, E_2, τ_1 and τ_2. Both of the models give solutions of the same form under the condition of constant load. Accordingly, it is not easy at present to build up a single definite rheological model for the observed

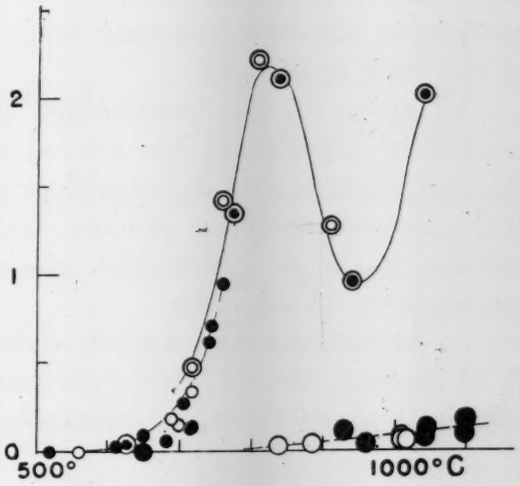

Fig. 8. Ratio of delayed elastic part (AB) to instantaneous part (OA) of deformation under constant load.
larger circles: vitreous silica;
smaller circles: obsidian;
double circles: Sanukite;
filled circles: heating;
open circles: cooling.

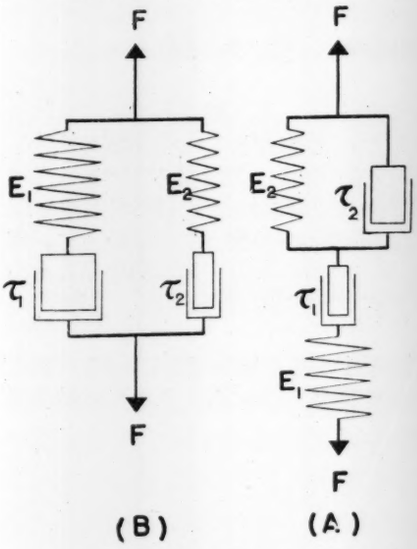

Fig. 9. Rheological models for the behaviours of rocks at high temperature.

6) M. REINER, "Deformation and Flow," *London* (1949). p. 279.
7) T. SATÔ. read at the annual meeting of Physical Society of Japan, 1951.

visco-elastic deformation of the rocks, much less to correlate the obtained coefficients directly and duly with the actual petrographical constituents in the rock specimens.

In spite of the restrictions just mentioned, however, the present method of experiment has proved itself useful and reliable enough for the investigations of dynamical properties of rocks. The writer believes that more systematic studies are desirable concerning the rocks of various kinds of interstitial glass as well as those of various mode of aggregation of minerals.

In concluding, the writer wishes to express his hearty thanks to Dr. T. Minakami, Dr. R. Morimoto and Mr. J. Ossaka for their advices and criticisms given from the volcanological and petrological viewpoints.

---

6. 高溫に於ける火山岩の粘性及び彈性

第2報

地震研究所　佐久間修三

第1報と同じ撓み法によって，和田峠産の黒曜岩，二上火山の讃岐岩，人工熔融石英の三者について，その粘彈性的性質を室溫から1100°Cまでの範囲で測定した．前に報告した大島熔岩に比して，これらの物質はより簡単な変化形式をもっていることが判った．即ち，天然ガラスである黒曜石では，650°C 附近から急に粘性が減り，ヤング率も亦減少する．これに対して，同じくガラス状物質であり乍ら熔融石英では，粘性は前者よりはるかに大きく，その減少の割合も小さい上に，彈性率は 1000°C 附近までは溫度と共にむしろ增加する．一方，ガラス質の石基中に微細な結晶を均一にまじえた讃岐岩では，溫度上昇に伴う粘性の減り方は前2者の中間的な性質を示し，彈性率の変化はむしろ黒曜岩のそれに類似している．

これらの粘彈性現象を，微視的な過程に直ちにむすびつけて說明することはむづかしいが，岩石の粘性のみならず彈性も或せまい溫度領域で急減することは著しい事実であって，これらは結晶粒間を埋めるガラス質部分の性質に多く関係していると思われる．

---

7. *Experimental Studies on the Mechanism of Generation of Elastic Waves II.*

By Keichi KASAHARA,

Earthquake Research Institute.

(Read Oct. 21, 1952.—Received Dec. 20, 1952.)

1. Introduction.

In the previous paper[1], the author gave a report of a noticeable phenomenon which can be seen in the vicinity of a wave source. When an impulsive vertical force acts downwards on the surface of an elastic medium, a part of the surface within a certain region begins in upward motion. The disturbance which occurs in such a way is propagated as time passes on, forming gradually a perfect type of the surface wave and other kind of waves. Such phenomenon seems rather curious from the standpoint of the theory of the statical deformation of elastic bodies. Because, as Boussinesq has studied[2], every part of the surface of a semi-infinite elastic body subjected to an external vertical force acting downwards at a point, is displaced downwards and no part showing upward displacements can exist on the surface. In fact, a statical experiment carried out on the same medium produces such results.

These facts can be considered to indicate that such phenomenon as mentioned above occurs only in the transient case of elastic deformation of the surface. Inouye has formerly pointed out that the surface of the ground subject to the shock of a falling body showed a peculiar distribution of initial motion[3].

Wave phenomena which would take place on the surface of a semi-infinite elastic body subjected to an external impulsive force have been investigated theoretically by H. Lamb[4]. His consideration, however, has been limited mainly to the problem on the phenomena which can be observed at a place on the surface distant enough from the origin. We have, to the present, scarcely any theoretical basis, to which we may refer when we undertake experimental investigations on the phe-

1) K. KASAHARA, *Bull. Earthq. Res. Inst.*, **30** (1952), 267.
2) A. E. H. LOVE, The Mathematical Theory of Elasticity, (1927), 185.
3) W. INOUYE, *Bull. Earthq. Res. Inst.*, **13** (1935), 194.
4) H. LAMB, *Phil. Trans. Roy. Soc.*, **A, 203** (1904), 1.

nomena in the vicinity of the origin. These circumstances led the author into the present study, which is considered to be of use in checking the reliability of the model experiment as well as in obtaining a practical way to study the theoretical basis of related phenomena.

2. Fundamental Considerations.

The two-dimensional problem is treated in the present paper, because it is rather easy to study and may be readily compared with the results obtained in the previous experiments. Wave equations in two-dimensions are

$$\left.\begin{aligned}\partial^2\phi/\partial t^2 &= \{(\lambda+2\mu)/\rho\}\nabla^2\phi,\\ \partial^2\psi/\partial t^2 &= (\mu/\rho)\nabla^2\psi,\end{aligned}\right\} \tag{1}$$

where ρ, λ and μ represent density and Lamé's constants, respectively, and ϕ and ψ are the wave functions which have the following relations with two components of displacements u and v.

$$\left.\begin{aligned}u &= (\partial\phi/\partial x)+(\partial\psi/\partial y),\\ v &= (\partial\phi/\partial y)-(\partial\psi/\partial x).\end{aligned}\right\} \tag{2}$$

Stress components become, then,

$$\left.\begin{aligned}P_{xy} &= \mu\{(\partial u/\partial x)+(\partial v/\partial y)\} = \text{func. } (\phi,\ \psi),\\ P_{yy} &= \lambda\Delta+2\mu(\partial v/\partial y) \quad = \text{func. } (\phi,\ \psi).\end{aligned}\right\} \tag{3}$$

Let us consider, now, the case of a semi-infinite elastic body, bounded by the plane $y=0$ (Fig. 1), which is subjected to a vertical force as follows,

$$\left.\begin{aligned}&[P_{xy}]_{y=0}=0,\\ &[P_{yy}]_{y=0}=Y\exp(i\xi x)\cdot\mathbf{1},\end{aligned}\right\} \tag{4}$$

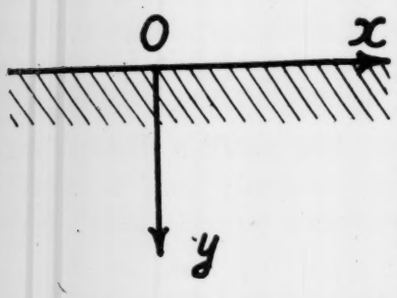

Fig. 1. Two-dimensional coordinates employed in the present study.

where **1** is the unit function, employed in operational calculus. Then the equation (1) can be written in the operational form, viz.:

$$\left.\begin{aligned} a^2p^2\phi-\nabla^2\phi&=0,\\ b^2p^2\psi-\nabla^2\psi&=0,\end{aligned}\right\} \tag{5}$$

where $$a^2=\rho/(\lambda+2\mu),\quad b^2=\rho/\mu, \tag{6}$$

and we may consider as the solutions for (5)

$$\left.\begin{aligned} \phi&=A\exp(-\alpha y)\exp(i\xi x)\cdot\mathbf{1},\\ \psi&=B\exp(-\beta y)\exp(i\xi x)\cdot\mathbf{1}.\end{aligned}\right\} \tag{7}$$

In this case, we obtain from (5) the following relations,

$$\left.\begin{aligned} \{\alpha^2-(\xi^2+h^2)\}\cdot\mathbf{1}&=0,\\ \{\beta^2-(\xi^2+k^2)\}\cdot\mathbf{1}&=0,\end{aligned}\right\} \tag{8}$$

where

$$\left.\begin{aligned} h^2&=a^2p^2,\\ k^2&=b^2p^2.\end{aligned}\right\} \tag{9}$$

Surface displacements become, then,

$$\left.\begin{aligned} u_0&=(i\xi A-\beta B)\cdot\exp(i\xi x)\cdot\mathbf{1},\\ v_0&=(-\alpha A-i\xi B)\cdot\exp(i\xi x)\cdot\mathbf{1},\end{aligned}\right\} \tag{10}$$

and stress components on the surface are

$$\left.\begin{aligned} [P_{xy}]_0&=\mu\{-2i\xi\alpha A+(\xi^2+\beta^2)B\}\exp(i\xi x)\cdot\mathbf{1},\\ [P_{yy}]_0&=\mu\{(\xi^2+\beta^2)A+2i\xi\beta B\}\exp(i\xi x)\cdot\mathbf{1}.\end{aligned}\right\} \tag{11}$$

To satisfy the initial conditions (4) given for surface stresses, constants A and B in the above relations should be

$$\left.\begin{aligned} A&=\{(2\xi^2+k^2)/F(\xi)\}(Y/\mu),\\ B&=\{2i\xi\alpha/F(\xi)\}(Y/\mu),\end{aligned}\right\} \tag{12}$$

where $$F(\xi)=(2\xi^2+k^2)^2-4\xi^2\alpha\beta. \tag{13}$$

Therefore, both components for surface displacements can be written as follows,

$$\left.\begin{aligned} u_0&=[i\xi\{(2\xi^2+k^2)-2\alpha\beta\}/F(\xi)](Y/\mu)\exp(i\xi x)\cdot\mathbf{1},\\ v_0&=[\quad -\alpha k^2/F(\xi)\quad](Y/\mu)\exp(i\xi x)\cdot\mathbf{1}.\end{aligned}\right\} \tag{14}$$

3. Numerical Considerations.

Let us extend our numerical considerations to the case of external force acting in the following form,

$$\left.\begin{array}{ll} 0 & \text{when } t<0 \\ Q\,H_{2m}(x)\exp(-x^2/2) & \text{when } t>0\,, \end{array}\right\} \tag{15}$$

where $H_{2m}(x)$ represents Hermite's functions of $2m$ mode. The above form may be written as

$$Q(-1)^m(2/\pi)^{1/2}\int_0^\infty H_{2m}(\xi)\cdot\exp(-\xi^2/2)\cos\xi x d\xi, \tag{16}$$

then equation (14) becomes

$$\left.\begin{aligned} u_0=\boldsymbol{R}(Q/\mu)(-1)^m(2/\pi)^{1/2}\int_0^\infty &\{i\xi(2\xi^2+k^2-\alpha\beta)/F(\xi)\}H_{2m}(\xi) \\ &\times\exp\{(-\xi^2/2)+i\xi x\}d\xi\cdot\mathbf{1}, \\ v_0=\boldsymbol{R}(Q/\mu)(1-1)^m(2/\pi)^{1/2}\int_0^\infty &\{-k^2\alpha/F(\xi)\}H_{2m}(\xi) \\ &\times\exp\{(-\xi^2/2)+i\xi x\}d\xi\cdot\mathbf{1}, \end{aligned}\right\} \tag{17}$$

where $\boldsymbol{R}$ represents the real part of the complex.

When $m=0$,

$$\begin{aligned} v_0&=\boldsymbol{R}(Q/\mu)(2/\pi)^{1/2}\int_0^\infty\{-k^2\alpha/F(\xi)\}\exp\{(-\xi^2/2)+i\xi x\}d\xi\cdot\mathbf{1} \\ &=-(Q/\mu)(2/\pi)^{1/2}\int_0^\infty\{k^2\alpha/F(\xi)\}\exp(-\xi^2/2)\cos\xi x d\xi\cdot\mathbf{1}. \end{aligned} \tag{18}$$

For the numerical evaluation of the surface displacement, the above expression is expanded in series of p^{-n}, viz.,

$$\begin{aligned} v_0=-(Q/\mu)(2/\pi)^{1/2}(a/b^2)[&p^{-1}\int_0^\infty\exp(-\xi^2/2)\cos\xi x d\xi \\ &+A'p^{-3}\int_0^\infty\xi^2\exp(-\xi^2/2)\cos\xi x d\xi \\ &-B'p^{-5}\int_0^\infty\xi^4\exp(-\xi^2/2)\cos\xi x d\xi \\ &+C'p^{-7}\int_0^\infty\xi^6\exp(-\xi^2/2)\cos\xi x d\xi \\ &-D'p^{-9}\int\xi^8\exp(-\xi^2/2)\cos\xi x d\xi+\ldots]\cdot\mathbf{1}. \end{aligned} \tag{19}$$

Then we can replace operators p^{-1}, p^{-3},... by t, t^3,... in the following way,

$$p^{-n}\cdot\mathbf{1}=t^n/n!\,, \tag{20}$$

and finally, the surface displacement can be expressed in finite series of t when t does not assume a large value, viz.,

$$\begin{aligned} v_0 = &-(Q/\mu)(c_2^2/c_1)[t\phi_0(x)-(1/3!\cdot 2)\{A+(c_1^2/2)\}t^3\phi_2(x) \\ &+(1/5!\cdot 4)\{B+(c_1^2A/2)-(c_1^4/8)\}t^5\phi_4(x) \\ &-(1/7!\cdot 8)\{C+(c_1^2B/2)-(c_1^4A/8)+(c_1^6/16)\}t^7\phi_6(x) \\ &+(1/9!\cdot 16)\{D+(c_1^2C/2)-(c_1^4B/8)+(c_1^6A/16)-(5c_1^8/128)\}t^9\phi_8(x)+\ldots] \end{aligned} \quad (21)$$

where each constant in the above expression means,

$$\left.\begin{aligned} A &= -4c_2^2\{1+(c_2/c_1)\}, \\ B &= 2c_2^3\{1-(c_2/c_1)\}^2(-c_1+8c_2), \\ C &= (c_2^3/2)\{1-(c_2/c_1)\}^2[-c_1^3\{1+(c_2/c_1)\}^2+32c_1c_2^2\{1-(c_2/c_1)\} \\ &\qquad -128c_2^3\{1-(c_2/c_1)\}], \\ D &= (c_2^3/4)\{1-(c_2/c_1)\}^2[c_1^5\{1+(c_2^2/c_1^2)\}\{1+(c_2/c_1)\}^2 \\ &\qquad +16c_1^2c_2^3\{1+(c_2/c_1)\}^4\{1-(c_2/c_1)\}^2 \\ &\qquad -384c_1c_2^4\{1+(c_2/c_1)\}^4\{1-(c_2/c_1)\}^2 \\ &\qquad +1024c_2^5\{1+(c_2/c_1)\}^4\{1-(c_2/c_1)\}^2], \\ c_1 &= 1/a, \quad c_2 = 1/b, \end{aligned}\right\} \quad (22)$$

and

$$\phi_n(x) = H_n(x/\sqrt{2})\cdot\exp(-x^2/2).^{5)}$$

Equation (21) is one of the fundamental results which clarifies the transient deformation of the surface subjected to the external force expressed by (4) and (15). When we expand (18) in series of p^n and take $t=\infty$, we can obtain the surface deformation in statical case. Equation (23) is the result which shows no upward displacement of the surface when the external force acts downwards,

$$v_0 = (-Q/2\mu)\{(\lambda+2\mu)/(\lambda+\mu)\}\cdot\exp(-x^2/2). \quad (23)$$

The present problem may be advanced by replacing the time factor of the vertical force (15) with the impulsive one, viz.,

$$\left.\begin{aligned} &0 && \text{when} \quad t<0 \text{ and } t>(\pi/a), \\ &QH_{2m}(x)\exp(-x^2/2)\sin at && \text{when} \quad 0\leqq t\leqq(\pi/a). \end{aligned}\right\} \quad (24)$$

It this case, the fundamental relation (25) in the operational calculus can be applied to obtain the expression for the vertical displacement of the surface

$$g_2(p)f_1(t) = \frac{d}{dt}\int_0^t f_2(t-\tau)f_1(\tau)d\tau, \quad (25)$$

and the following expression is obtained as the result:

5) T. RIKITAKE, *Bull. Earthq. Res. Inst.*, **30** (1952), 293.

$$v_0=(-Q/\mu)(c_2^2/c_1)[(1/a^2)\{2-\cos at-\cos(at-\pi)\}\phi_0(x)$$
$$-(1/3!\cdot 2)\{A+(c_1^2/2)\}(1/a^4)\{2(3a^2t^2-6)+6\cos at+6\cos(at-\pi)\}\phi_2(x)$$
$$+(1/5!\cdot 4)\{B+(c_1^2A/2)-(c_1^4/8)\}(1/a^6)\{2(5a^4t^4-60a^2t^2+120)$$
$$-120\cos at-120\cos(at-\pi)\}\phi_4(x)$$
$$-(1/7!\cdot 8)\{C+(c_1^2B/2)-(c_1^4A/8)+(c_1^6/16)\}(1/a^8)$$
$$\times\{2(7a^6t^6-210a^4t^4+2250a^2t^2-5040)-5040\cos at+5040\cos(at-\pi)\}\phi_6(x)$$
$$+(1/9!\cdot 16)\{D+(c_1^2C/2)-(c_1^4B/8)+(c_1^6A/16)-(5c_1^8/128)\}(1/a^{10})$$
$$\times\{2(9a^8t^8-504a^6t^6+15120a^4t^4-181440a^2t^2+362880)$$
$$-362880\cos at-362880\cos(at-\pi)\}\phi_8(x), \qquad (26)$$

where $A, B, C, \ldots$ have the identical meaning with those employed in the former case.

When we undertake numerical calculation for (21) and (26), it is desirable to adopt suitable values for constants and parameters in the expression so that they may fit the conditions, under which the previous experiment had been undertaken. Values thus determined are listed in Table I, in comparison with those employed in the experiment[6].

Table I.

	Calculation	Experiment
Velocity of longitudinal wave	$3c$	610 cm/sec
Velocity of transversal wave	c	240 cm/sec
Poisson's ratio	0.48	0.41
Unit distance	x	5 cm
Unit time	$\tau=(x/c)$	20 m sec
Time interval between each observation	$\frac{1}{8}$ or $\frac{1}{4}\tau$	5 m sec
Duration time of the impulsive force	$\frac{1}{2}\tau$[7]	10 m sec
Width of the impulsive force	$5x$[8]	0.6 cm

To keep the accuracy of the calculation as high as possible the value of t in (21) and (26) should not exceed a certain limit and the final results thus obtained are illustrated in Figs. 2 and 3.

Fig. 4 is the result of the previous experiment drawn for the purpose of comparison.

6) *loc. cit.*

7) This indicates the duration time of force acting like (24).

8) This indicates the dimension of the region, in which the force can be considered acting effectively.

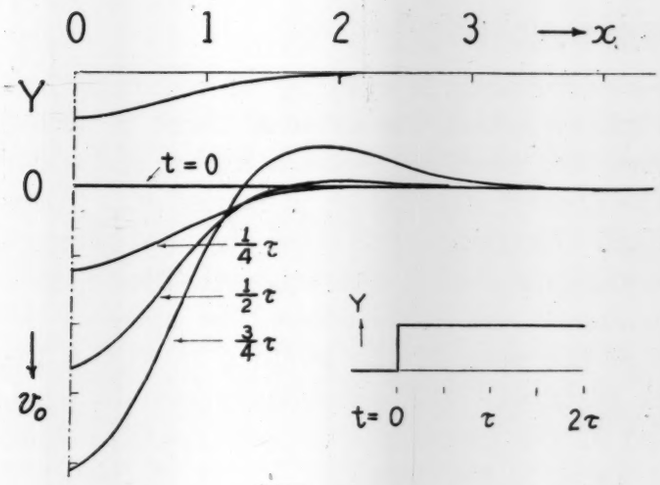

Fig. 2. Results of the numerical calculations. (1).
From top: spatial distribution of the external force, displacements of the surface at each instant, and time characteristics of the force.

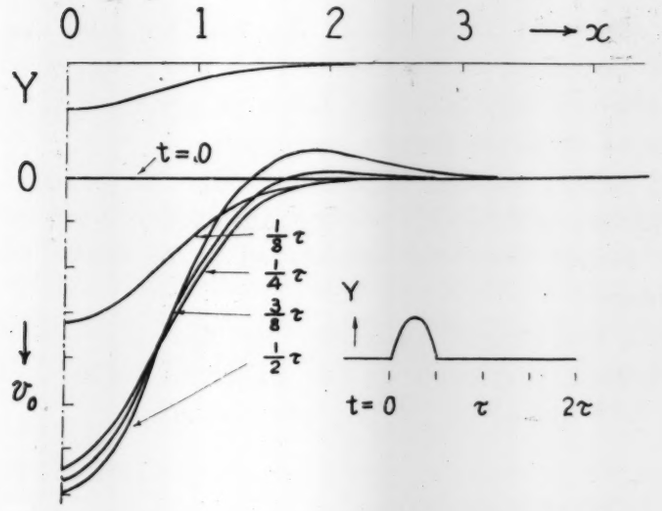

Fig. 3. Results of the numerical calculations (2).
Curves are drawn similarly with Fig. 2.

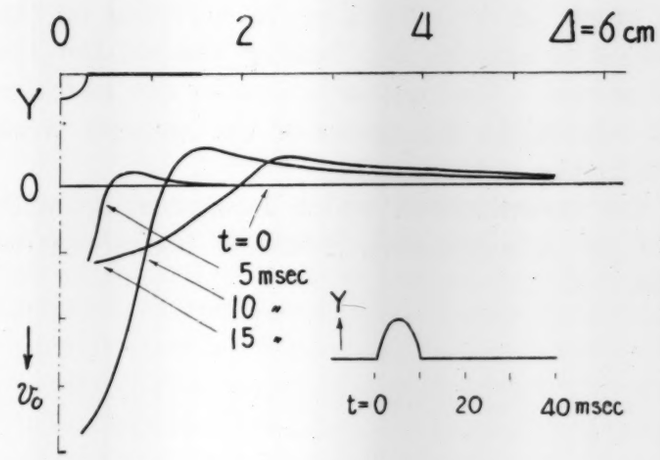

Fig. 4. Results of the previous experiments.
Curves are drawn similarly with Fig. 2.

4. Discussions and Conclusions.

In Figs. 2 and 3 we observe remarkable swelling up occurring in a certain region near to the origin on which the external force is acting downwards. As time passes on, the swelling becomes higher and wider within the period in which the present calculation is carried on. These features are quite similar in their characters with those observed through experiments. We cannot, however, overlook a characteristic discrepancy seen between results of experiments and calculations. In spite of the extinguished travelling away of the peak of the swelling in Fig. 4, the former two do not show such features. The discrepancy results possibly from the wide distribution of the external force expressed by (15), that is, as can be seen from Table I, the effective width of the force amounts to more than several ten times of that employed in the experiments and this condition seems to have caused the above-stated discrepancy. The speculation is expected to be checked by the progressed calculation employing more sharply concentrated force in place of (15), but the study will be postponed to some future occassion.

We have, in the present paper, studied mathematically the possibility of swelling up of the surface subjected to the impulsive vertical force. The method and the result may be considered to be useful to study related problems in future.

These kinds of phenomena are caused probably by the concentration and releasing of local stresses produced by the external force, but their physical mechanism is left unknown, in the present step.

5. Acknowledgements.

The author owes very much to Dr. Rikitake in carrying on the study here described and wishes to express his hearty thanks for the guidance and encouragement given. The author's thanks are also due to Prof. Hagiwara, who has interest in the series of the present work and gives his cordial support to the author.

This study is a part of the investigation which is carried on with the help of the Grant in Aid for Miscellaneous Scientific Researches of the Department of Education.

7. 彈性波の発生機構に関する実験
(第2報)

地震研究所 笠 原 慶 一

半無限彈性体の表面に垂直衝撃力を下向きに作用させると，ある範囲内の表面は上向きに動き始めることが，第1報の模型実験において観察された．半無限体の波動現象のうち，原点附近の問題は理論的にも従来殆んど取扱われていないが，近似的にせよ之を取扱う方法を見出す事は今後の研究をすゝめる上にも無意味であるまい．

本報においては H. LAMB の展開した方法に沿いつゝ，之を演算子法的に取扱っている．二次元の半無限体において原点を中心に垂直衝撃力が作用した時の表面の垂直変位が主な対象であり，実例として，ごく簡単な條件の下で解いた数値計算の結果を図示してある．それによると原点近傍ある範囲の表面は明らかに盛上りの傾向を示す．時と共に，この範囲は遠方に及ぶが，模型実験の際観られたような“ピーク”の移動は明瞭でない．この差異は，計算の際仮定した外力の空間的分布が実験條件に比べて余りに広すぎた爲ではないかと思われる．

昭和28年4月20日印刷
昭和28年4月25日發行

東京都文京區本富士町一番地
東京大學構内
編纂兼發行者 東京大學地震研究所

東京都千代田區富士見町一丁目十番地
印刷者 笠井康賴

東京都千代田區富士見町一丁目十番地
印刷所 株式會社 國際文献印刷社

賣捌所 東京都千代田區神田一ツ橋通
岩波書店

東京都中央區日本橋通二丁目六番地
丸善株式會社

Sold by

Iwanami Shoten,

Hitotsubashi dôri, Chiyoda-ku, Tôkyô,

and

Maruzen Co., Ltd.,

Nihonbashi dôri, Chûô-ku, Tôkyô.

Price of this copy: 276 Yen. (Postage exclusive.)

BULLETIN OF

THE EARTHQUAKE RESEARCH INSTITUTE

TOKYO UNIVERSITY

Vol. XXXI, Part 1. March, 1953.

Contents.

Papers and Reports.

Page

1. Y. SATÔ, Velocity of Elastic Waves Propagated in Media with Small Obstacles. (in English) 1
2. T. RIKITAKE, I. YOKOYAMA and Y. HISHIYAMA, The Anomalous Behavior of Geomagnetic Variations of Short Period in Japan and Its Relation to the Subterranean Structure. The 2nd report. (in English) 19
3. I. YOKOYAMA, Geomagnetic Anomaly on Mt. Haruna and Its Relation to the Reverse Thermo-Remanent Magnetism of the Pumice Covering the Place. (in English) 33
4. K. KANAI, K. OSADA and S. YOSHIZAWA, The Relation between the Amplitude and the Period of Earthquake Motion. (in English) 45
5. K. KANAI, T. TANAKA and T. SUZUKI, Relation between the Earthquake Damage and the Nature of the Ground. (Case of Wooden Houses and Peat Bed.) (in English) 57
6. S. SAKUMA, Elastic and Viscous Properties of Volcanic Rocks at Elevated Temperatures. Part 2. (in English) 63
7. K. KASAHARA, Experimental Studies on the Mechanism of Generation of Elastic Waves II. (in English) 71

(For the papers written in Japanese or in occidental languages, the abstracts are given in occidental languages or in Japanese respectively.)

BULLETIN

OF THE

EARTHQUAKE RESEARCH INSTITUTE

TOKYO UNIVERSITY

VOL. XXXI

1953

東京大學

地震研究所彙報

第 31 号

昭和 28 年

CONTENTS.

Vol. XXXI.

Part 1. March, 1953.

Papers and Reports.

Page

1. Y. SATÔ, Velocity of Elastic Waves Propagated in Media with Small Obstacles. (in English) 1
2. T. RIKITAKE, I. YOKOYAMA and Y. HISHIYAMA, The Anomalous Behavior of Geomagnetic Variations of Short Period in Japan and Its Relation to the Subterranean Structure. The 2nd report. (in English) 19
3. I. YOKOYAMA, Geomagnetic Anomaly on Mt. Haruna and Its Relation to the Reverse Thermo-Remanent Magnetism of the Pumice Covering the Place. (in English) 33
4. K. KANAI, K. OSADA and S. YOSHIZAWA, The Relation between the Amplitude and the Period of Earthquake Motion. (in English) 45
5. K. KANAI, T. TANAKA and T. SUZUKI, Relation between the Earthquake Damage and the Nature of the Ground. (Case of Wooden Houses and Peat Bed.) (in English) 57
6. S. SAKUMA, Elastic and Viscous Properties of Volcanic Rocks at Elevated Temperatures. Part 2. (in English)..... 63
7. K. KASAHARA, Experimental Studies on the Mechanism of Generation of Elastic Waves II. (in English) 71

Part 2. June, 1953.

8. Y. SATÔ, Study on Surface Waves VIII. Nomogram for the Phase Velocity of Love-Waves and Maximum Thickness of the Surface Layer. (in English)..... 81
9. T. RIKITAKE, I. YOKOYAMA and Y. HISHIYAMA, The Anomalous Behavior of Geomagnetic Variations of Short Period in Japan and Its Relation to the Subterranean Structure. The 3rd report. (in English) 89
10. T. RIKITAKE, I. YOKOYAMA and Y. HISHIYAMA, The Anomalous Behavior of Geomagnetic Variations of Short Period in Japan

and Its Relation to the Subterranean Structure. The 4th report. (in English) 101
11. T. RIKITAKE, I. YOKOYAMA and Y. HISHIYAMA, The Anomalous Behavior of Geomagnetic Variations of Short Period in Japan and Its Relation to the Subterranean Structure. The 5th report. (in English) 119
12. T. ICHIMURA, Geological Investigations on the Zaō Volcanoes. II. Aoso Volcano. (in English)..... 129
13. T. ICHIMURA, H. TSUYA and H. MINATO, Sulphur Crystals from the Yakeyama Volcano. (in English)..... 151
14. T. ICHIMURA and H. MATSUBAYASHI, Igneous Activities prior to the Deposition of the Chichibu System. (in English) 155
15. A. OKADA and T. NAGATA, Land Deformation of the Neighbourhood of Muroto Point after the Nankaido Great Earthquake in 1946. (in English) 169

Part 3. September, 1953.

16. T. MATUZAWA, Feldtheorie der Erdbeben. (im Deutschen)..... 179
17. Y. SATÔ, Transformation of Spherical Solid Harmonics Related to the Translation of Coordinates System. (in English)..... 203
18. I. YOKOYAMA, A New Method for Regulating Electric Currents and its Application to Measurements of Geomagnetic Field. (in English)..... 211
19. K. KANAI, Relation between the Nature of Surface Layer and the Amplitude of Earthquake Motions. II. (in English) ... 219
20. K. KANAI, K. OSADA and S. YOSHIZAWA, Observational Study of Earthquake Motion in the Depth of the Ground. IV. (Relation between the Amplitude at Ground Surface and the Period.) (in English)..... 227
21. K. KASAHARA, Experimental Studies on the Mechanism of Generation of Elastic Waves III. (in English) 235
22. K. KANAI, Examination of the Assumption of the Concentrated Mass in the Vibration of Framed Structure (Rahmen). (in English) 245

Part 4. December, 1953.

23. T. MATUZAWA, Feldtheorie der Erdbeben: Vergleichung Grossbeben vom 21. Dez. 1946 mit dem Nachbeben vom 18. April

1948. (im Deutschen) 249
24. Y. SATÔ, Study on Surface Waves IX. Nomogram for the Group Velocity of Love-Waves. (in English) 255
25. T. MATUMOTO, Transmission and Reflection of Seismic Waves through Multilayered Elastic Medium. (in English) 261
26. K. KANAI and S. YOSHIZAWA, Relation between the Amplitude of Earthquake Motions and the Nature of Surface Layer. III. (in English) 275
27. The Research Group for Explosion Seismology, The Third Explosion Seismic Observations in North-Eastern Japan. (in English) 281
28. S. SAKUMA, Elastic and Viscous Properties of Volcanic Rocks at High Temperatures. Part 3. Oosima lava. (in English). 291
29. K. KANAI and T. SUZUKI, Relation between the Property of Building Vibration and the Nature of Ground. (Observation of Earthquake Motion at Actual Buildings.) (in English)... 305
30. G. NISHIMURA, M. SUZUKI, E. FURUKAWA, T. KOTAKI and K. TAKAHASHI, A New-Designed Prospecting Apparatus. (in English) 317
31. N. NASU, F. KISHINOUYE and A. OKADA, Levellings of the Subsiding Area in the South-eastern Part of Tokyo. (in Japanese) 335

8. *Study on Surface Waves VIII. Nomogram for the Phase Velocity of Love-Waves and Maximum Thickness of the Surface Layer.*

By Yasuo SATÔ,

Earthquake Research Institute.

(Read Jan. 22, 1952 and Feb. 17, 1953.—Received March 20, 1953.)

1. Introduction.

In the theoretical and observational study of seismic waves, we always pay attention to their velocity, especially when the waves have the property of dispersing. Consequently our study on Love-waves necessarily leads us to the examination of their velocity and we have published papers concerning this subject[1].

Hitherto, we chose some typical distribution of material and performed numerical calculations. Such a way of investigation, however, is not perfect for our practical purposes, for the variety of material constants and their distribution are not few, and we cannot calculate all the possible combinations of them. Thus it becomes desirable to make a nomogram by which we can obtain the velocity of Love-waves corresponding to any given state of media, or to get a material constant by means of the data of velocity and period[2].

2. Formula.

We adopted the following formula[3] which seems to be the most convenient for the present.

$$\omega_n = \sec\theta \cdot [\operatorname{Arctan}\{\chi \sec\theta \sqrt{(\sin^2\theta - \sin^2\theta_0)}\} + n\pi] \quad \ldots\ldots (2.1)^{4)}$$

where, ω_n: frequency of waves belonging to the n-th branch of Love-waves,

1) Y. SATÔ, "Study on Surface Waves," I, *Bull. Earthq. Res. Inst.*, **29** (1951), 1. III, *ibid.*, 435. IV, *ibid.*, 519. V, *ibid.*, **30** (1952), 1.

2) This nomogram will be of use in another case, too. Cf. K. SEZAWA and K. KANAI, *Bull. Earthq. Res. Inst.*, **17** (1939), 685.

3) Y. SATÔ, "Study on Surface Waves, I. Velocity of Love-Waves," *Bull. Earthq. Res. Inst.*, **29** (1951), 1. Expression (4.2).

4) In this paper we assume n to be zero or one.

χ $=\mu'/\mu$ (μ' and μ the rigidity of the lower and upper medium respectively),

$\operatorname{cosec}\theta_0 = V_s'/V_s$ (V_s' and V_s the velocity of S-waves in the lower and upper medium respectively),

$\operatorname{cosec}\theta$: phase velocity of Love-waves measured by the unit V_s, and throughout this paper, the unit length is the thickness of the layer H, and that of time H/V_s, the physical meaning of which is quite evident.

By somewhat modifying the above expression we obtained the following form,

T(=period measured by the unit H/V_s)

$$=2\pi \div \left[\frac{\frac{V}{V_s}}{\sqrt{\frac{V^2}{V_s^2}-1}} \operatorname{Arctan} \left\{ \frac{\frac{V}{V_s}}{\sqrt{\frac{V^2}{V_s^2}-1}} \cdot \chi \sqrt{\frac{V_s^2}{V^2}-\frac{V_s^2}{V_s'^2}} \right\} + n\pi \frac{\frac{V}{V_s}}{\sqrt{\frac{V^2}{V_s^2}-1}} \right] \quad \cdots\cdots\cdots\cdots\cdots\cdots (2.2)$$

and calculated the values of T corresponding to the given values of V/V_s.

3. Explanation of the figure and direction for use.

At first we will explain the nomogram for the computation of the fundamental branch.

In Fig. 1, [1] is the axis of V_s/V_s'. When some value of V_s/V_s' is given, we take a point A on this axis corresponding to this assigned value.

Next, α is the curve of $1\Big/\sqrt{\frac{V_s^2}{V^2}-\frac{V_s^2}{V_s'^2}}$. At first we chose some value of V/V_s and determine a point B on [2]-axis, and then we take a curve α which begins from the very point. The point C on [2]-axis

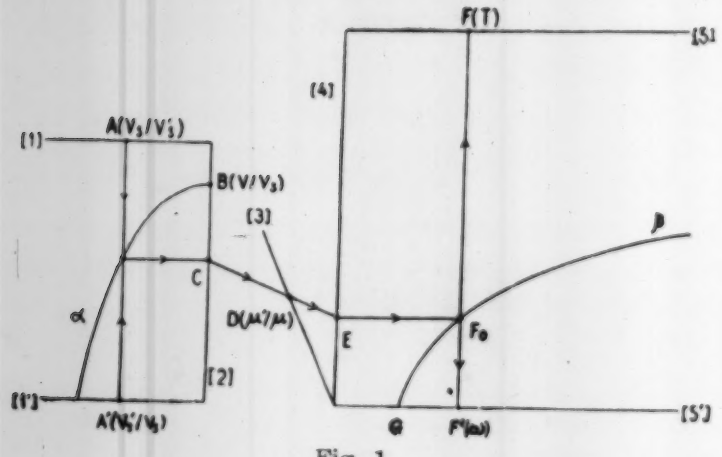

Fig. 1.

shows the value $1\Big/\sqrt{\frac{V_s^2}{V^2}-\frac{V_s^2}{V_s'^2}}$.

[3] is the axis of $\chi\equiv\mu'/\mu$. When the distribution of matter is determined, the value of χ is naturally given, therefore we can take a point D on [3]-axis.

Making a straight line passing the points C and D, we obtain a point E on [4]-axis, which is equal to [2]+[3], or $1\Big/\chi\sqrt{\frac{V_s^2}{V^2}-\frac{V_s^2}{V_s'^2}}$,

Finally, the curve β gives

$$2\pi:\left[\frac{\frac{V}{V_s}}{\sqrt{\frac{V^2}{V_s^2}-1}}\cdot\mathrm{Arctan}\left\{\frac{\frac{V}{V_s}}{\sqrt{\frac{V^2}{V_s^2}-1}}\cdot\frac{1}{[4]}\right\}\right] \qquad \cdots\cdots\cdots(3.1)$$

or the value of the right hand member of the expression (2.2). (Point F on [5]-axis). V/V_s, the parameter of the curve β, must of course be same with that of α.

The value of $\omega=2\pi/T$ can be found on the lower side of the figure ([5']-axis).

Axis [1'] gives V_s'/V_s, or the reciprocal of the [1]-axis.

The second nomogram which gives the first higher branch of waves shall be used without further explanation.

When we intend to get $\chi=\mu'/\mu$ by means of the data of the velocity and period, we can of course utilize this nomogram. However the procedure is very easy and it does not seem necessary to state the precise way of usage here.

4. Numerical example.

Let us give some numerical example in this section.

We assume

$$\begin{cases} \chi\equiv\mu'/\mu=5.0\,, & \rho'/\rho=1.25\,, \\ \sin\theta_0\equiv V_s/V_s'=0.50\,, \end{cases} \qquad \cdots\cdots\cdots(4.1)$$

and obtain the period corresponding to

$$V/V_s=\mathrm{cosec}\,\theta=1.05,\ 1.1,\ 1.2,\ 1.3,\ 1.4,\ 1.5,\ 1.6,\ 1.7,\ 1.8,\ 1.9 \quad \ldots(4.2)$$

The results obtained by strict calculation and those by the nomogram are given in the following table. The coincidence seems to be satisfactory.

Table I.

V/V_s	T (numerical calculation)	T (nomogram)	V/V_s	T (numerical calculation)	T (nomogram)
1.05	1.281	1.28	1.5	3.762	3.75
1.1	1.791	1.79	1.6	4.169	4.16
1.2	2.469	2.47	1.7	4.663	4.65
1.3	2.962	2.96	1.8	5.391	5.38
1.4	3.375	3.37	1.9	6.954	6.97

5. Maximum thickness of the surface layer.

If the velocity of S-waves and the rigidity of both media are given, and the period and the phase velocity of Love-waves are observed, we can determine the thickness of the surface layer from this nomogram easily. However, even if the complete data are not given, we can give a maximum value of thickness only from the data V_s, V and T'' (period of Love-waves in second).

A glance at the Plate I or the curve β in Fig. 1 shows that T has a minimum value corresponding to a given value of V/V_s (point G in Fig. 1). This is a somewhat interesting and peculiar phenomenon, for by means of these data only we can calculate the upper limit or the maximum value of H, the thickness of the layer. Whatever data we may add to those given above, the estimated thickness of the layer can not exceed this maximum value H_{max}.

Employing a set of numerical data, we will explain the procedure of getting this thickness.

If we give

$$V_s=3.40\ \text{km/sec},$$

when the observed data of Love-waves are

$$V=4.01\ \text{km/sec},$$

and

$$T''=45\ \text{sec},$$

then we find from Plate I

$$T_{min}=2.12, \qquad \cdots\cdots\cdots\cdots(5.1)$$

this same value is expressed by

$$T''\Big/\left(\frac{H_{max}}{V_s}\right)=153/H_{max}. \qquad \cdots\cdots\cdots\cdots(5.2)$$

Therefore, combining (5.1) and (5.2), we obtain at once

$$H_{max}=72\,\text{km}\,.$$

In order to get the value of H_{max} alone, however, it is neither necessary nor convenient to use Plate I. We will here make another nomogram useful for computing the upper limit of thickness of the surface layer.

Getting back to the first

$$\omega_0=\sec\theta\cdot[\text{Arctan}\{\chi\sec\theta\sqrt{(\sin^2\theta-\sin^2\theta_0)}\}+n\pi]\,. \quad \ldots\ldots(5.3)$$

Therefore, the maximum value of ω_0 is

$$\omega_{max}=\frac{\pi}{2}\sec\theta=\frac{\pi}{2}\frac{V}{V_s}\Big/\sqrt{\frac{V^2}{V_s^2}-1} \quad \ldots\ldots\ldots(5.4)$$

and this expression is equal to $2\pi\Big/\Big(\frac{T''}{H/V_s}\Big)$; thus

$$H_{max}=L\Big/4\sqrt{\frac{V^2}{V_s^2}-1} \quad \ldots\ldots\ldots\ldots\ldots(5.5)$$

in which $L(=T''V)$ implies the wave-length of Love-waves.

We give the numerical relation V/V_s versus H_{max}/L in Table II and Fig. 2.

Table II.

V/V_s	H_{max}/L	V/V_s	H_{max}/L	V/V_s	H_{max}/L
1.05	0.7808	1.6	0.2002	4.5	0.0645
1.10	0.5455	1.8	0.1670	5.0	0.0510
1.15	0.4402	2.0	0.1444	5.5	0.0462
1.20	0.3770	2.2	0.1276	6.0	0.0423
1.25	0.3333	2.4	0.1146	6.5	0.0389
1.30	0.3010	2.6	0.1042	7.0	0.0361
1.35	0.2756	2.8	0.0956	7.5	0.0336
1.40	0.2552	3.0	0.0884	8.0	0.0315
1.45	0.2381	3.5	0.0745	9.0	0.0280
1.50	0.2236	4.0	0.0645	10.0	0.0251

Using the same data again, we will calculate H_{max}.

Since $V/V_s=1.18$, we get from Fig. 2

$$H_{max}/L=0.400\,,$$

while

$$L=T''V=180\,\text{km}\,,$$

therefore

$$H_{max}=72\,\text{km.}^{5)}$$

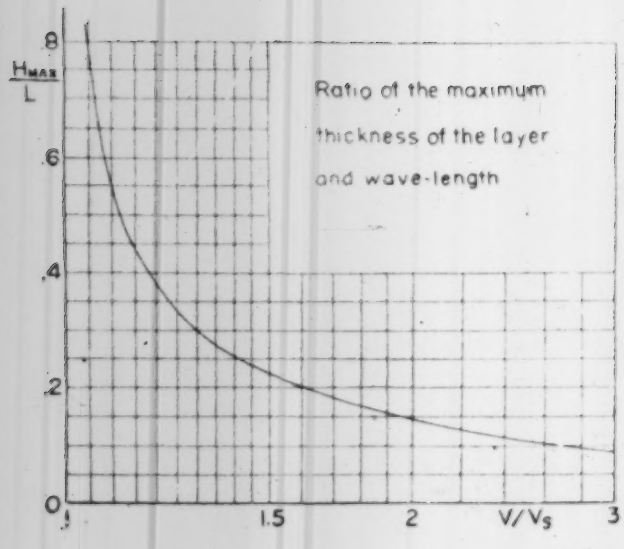

Fig. 2.

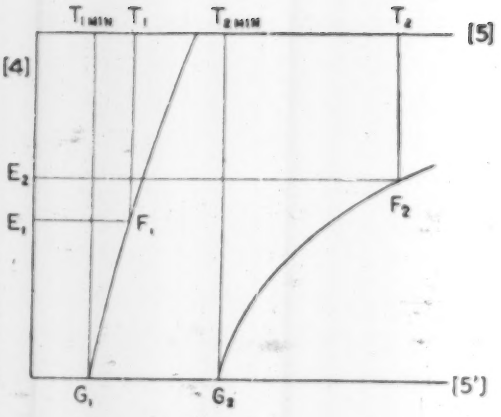

Fig. 3.

5.1 Precision of this method.

Although we can determine H_{max}, this method would be useless if this estimated value is much more larger than the real thickness of layer. We will examine, in this section, the condition wherein the estimated H_{max} does not differ so much from the real one and may be used effectively.

For the determination of this value we used the left terminal point G of the curve β in Fig. 1 or Fig. 3 and obtained T_{min}. However, the real thickness of the layer should be determined by means of T (cf. Fig. 2, [5]-axis). Therefore, if the difference $T\sim T_{min}$ is small, or $|\Delta T/\Delta[E]|_\beta$ is small, the estimation of T_{min} will be fairly accurate.

---

5) If we have the complete data with regard to the media, i.e. μ'/μ and ρ'/ρ, we can strictly determine the thickness of the layer. For example, if

$$\mu'/\mu=2.00, \qquad \rho'/\rho=1.22,$$

taking on [1]-axis $V_s/V_s'=0.782$ [2]-axis $V/V_s=1.18$ [3]-axis $\mu'/\mu=2.00$, and the curve with a parameter $V/V_s=1.18$,
we can determine the points B_0, C, E, F_0 and finally F. In this case $F(=T)=3.72$.

Now, T implies $T=T''/\left(\frac{H}{V_s}\right)$,

therefore, introducing $T''=45$ sec. $V_s=3.40$ km/sec.
we obtain $H=41$ km.

On the other hand, the smaller the velocity of Love-waves is, the steeper the slope of the curve β will become. Thus we can employ slow, or short Love-waves more effectively than the fast, or long ones. (cf. Fig. 2.)

However, if we compare Plate I and II, we can notice by a glance that the curve β is much steeper in Plate II than in Plate I. Therefore, if we can observe Love-waves with a node in the layer, they will be of more use than those without a node.

---

8. 表面波の研究 VIII

ラブ波の位相速度を求める図表と表面層の厚さの極大値

地震研究所　佐藤泰夫

1. ラブ波の伝播を研究する場合に，その速度は忘れる事のできない重要なものであるが，物質常数の分布に関するあらゆる組合せを与へて，これを計算し盡すといふ事は到底できない．

そこで，上下二つの物質内でのS波の速度比及び剛性率の比を与へた時に，ラブ波の速度と周期（もしくは周回振動数）との関係を与へる計算図表を作った．層内に一つも節のない場合を図版Iに，一つある場合を図版IIに示す．使用法は第3節と第1図から明らかであらう．

正しい計算値と比べた時，精度はこの種のものとしてはほぼ満足しうるものと思ふ．

2. ラブ波の周期，速度及び上下の媒質内でのS波の速さ，剛性率の比を与へれば，表面層の厚さはもとより決定する．しかし，図表をみて気づく事であるが，ラブ波の周期と速度，それに加へて表面層内でのS波の速さだけをしれば，層の厚さがとりうる最大値は他の物質常数の如何にかかはらず決定する．この事は興味ある事と思ひ，そのための一二の計算とグラフとを用意した．

---

9. *The Anomalous Behavior of Geomagnetic Variations of Short Period in Japan and Its Relation to the Subterranean Structure. The 3rd report.*

By Tsuneji RIKITAKE, Izumi YOKOYAMA and Yoneko HISHIYAMA,

Earthquake Research Institute.

(Read March 17, 1953.—Received March 20, 1953.)

1. Introduction.

As has been already reported[1], a continuous observation of three geomagnetic components has been carried on at Aburatsubo (35°09′ N, 139°37′ E) near the southern extremity of the Miura Peninsula, Kanagawa Prefecture by the Earthquake Research Institute. Since September, 1952, a similar observation has been carried on also at Maze (37°44′N, 138°48′E), Niigata Prefecture, facing the Japan Sea.

The writers found out that the magnetograms obtained at Maze do not always show parallelism between short-period changes in horizontal (H) and vertical (Z) components. In general, the changes in Z-component (ΔZ) corresponding to those in H-component (ΔH) are small and signs of ΔZ fluctuate from plus to minus on different occasions. The above-mentioned facts are both contrary to the characteristics at Aburatsubo. Taking into consideration the fact that the distance between both stations amounts to only 300 *km*, it is notable that such a great difference in geomagnetic changes should be observed.

In order to study the peculiarity, the writers analyzed the geomegnetic data from Maze comparing them with those from Aburatsubo. For the purpose of showing a general aspect of the behavior of geomagnetic variations in Japan, the writers constructed a chart showing the distribution of $\Delta Z/\Delta H$ for short-period variations.

2. Outline of the observation at Maze.

The magnetometer-room was built in a corner of a geophysical station for observing the deformation of the earth's surface. Its purpose

1) T. RIKITAKE, I. YOKOYAMA and Y. HISHIYAMA, *Bull. Earthq. Res. Inst.*, **30** (1952), 207.

is to find out changes in the earth's magnetic field that might accompany with an earthquake and also to record geomagnetic variations of short period.

The magnetic variometers are set up in a wooden house built in a cave excavated in the Tertiary tuff, adjacent to the room for the observation of crustal deformation. The topography near the magneto-

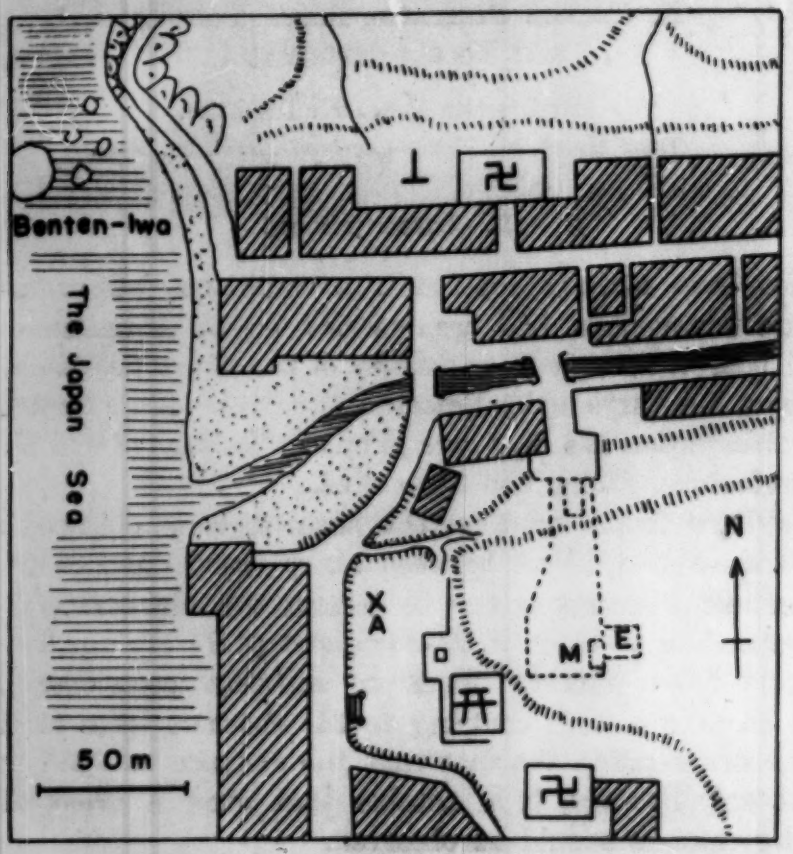

Fig. 1. The sketch map near the magnetometer-room. M: Magnetometer-room, E: The room for the observation of crustal deformation, A: The place on which the absolute measurements were made.

meter-room is shown in Fig. 1. The sensibility of the D (declination)-variometer is $0.575'/mm$ with $3\,m$ optical lever, a M.K. magnet being suspended with a quartz fibre of 10μ. The H (horizontal intensity)-variometer has a suspending quartz fibre of 60μ, the sensibility being usually $1.4\gamma/mm$. The Z (vertical intensity)-variometer is one of the Watson type with the sensibility of $1.5\gamma/mm$ as a rule. An example of the record is shown in Fig. 2.

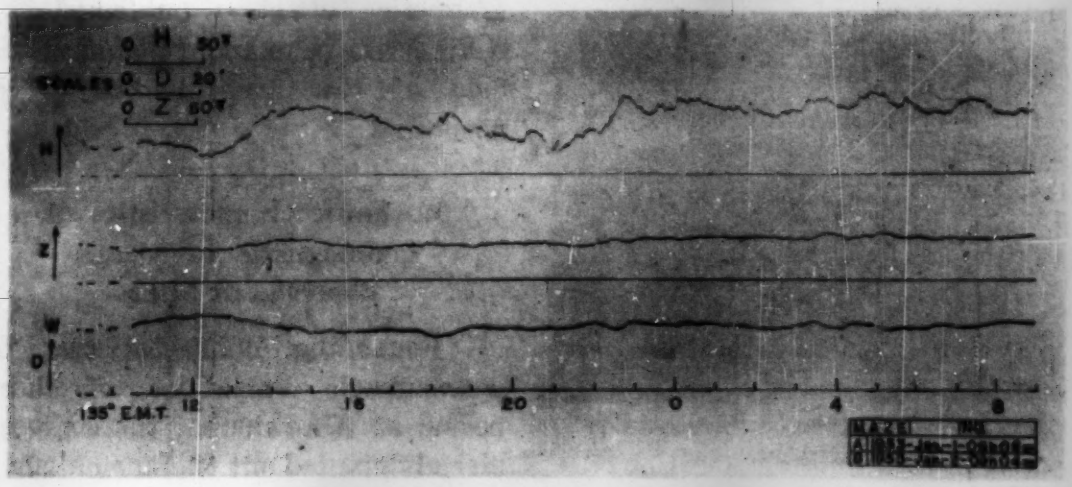

Fig. 2. An example of the record. (Jan. 1 and 2, 1953)

Absolute measurements of the three components were carried out with a G.S.I. (Geographical Survey Institute) second order magnetometer on Sept. 9 and 10, 1952 in the vicinity of the station, and the place where the measurements were made is shown in Figs. 1 and 3. The results are given in the footnote[2] for future use. Referring to the

2) The results of the absolute measurements are as follows:

Declination and Dip

Time (J.S.T.)	*D*	*I*
Sept. 9th		
18*h* 18*m*	7° 8′.4 W	51°46′.3
21 50	8.5	47.2
23 10	10.4	45.4
10th		
00 42	12.0	45.3
01 54	9.8	45.5
02 54	8.9	45.5
05 15	9.8	45.2
07 17	8.3	42.9
08 38	13.2	44.3
09 53	15.2	43.7
11 18	12.9	44.4
12 47	14.1	44.1
15 03	13.3	46.3
16 00	10.3	46.6

Horizontal Intensity

Time (J.S.T.)	*H*
Sept. 9th	
18*h* 37*m*	29644γ
22 02	626
23 22	648
10th	
00 52	653
02 01	650
02 58	646
05 21	646
07 22	659
08 42	652
09 56	654
11 21	661
12 54	675
14 04	671
15 08	642
16 04	650

Fig. 3. The scene of the absolute measurement.

magnetic charts[3] published by G.S.I., the permanent geomagnetic field of this area seemed to be normal.

3. Some characteristics of geomagnetic variations observed at Maze.

Regarding characteristics of geomagnetic variations of short period at Aburatsubo, the writers[1] already pointed out the anomalously large amplitude of ΔZ and the marked parallelism between ΔH and ΔZ. As for the observation at Maze the amplitude of ΔZ is usually not so large and such parallelism is not to be seen on the magnetograms.

By way of an example we will discuss the behavior of geomagnetic field at the time of a bay-type disturbance on Sept. 11, 1952, when the 36th cooperative observation of the Ionosphere Research Committee was under way. Fortunately the writers could collect the copies of magnetograms on that date from Wakkanai (45.4° N. 141,7° E), Memanbetsu

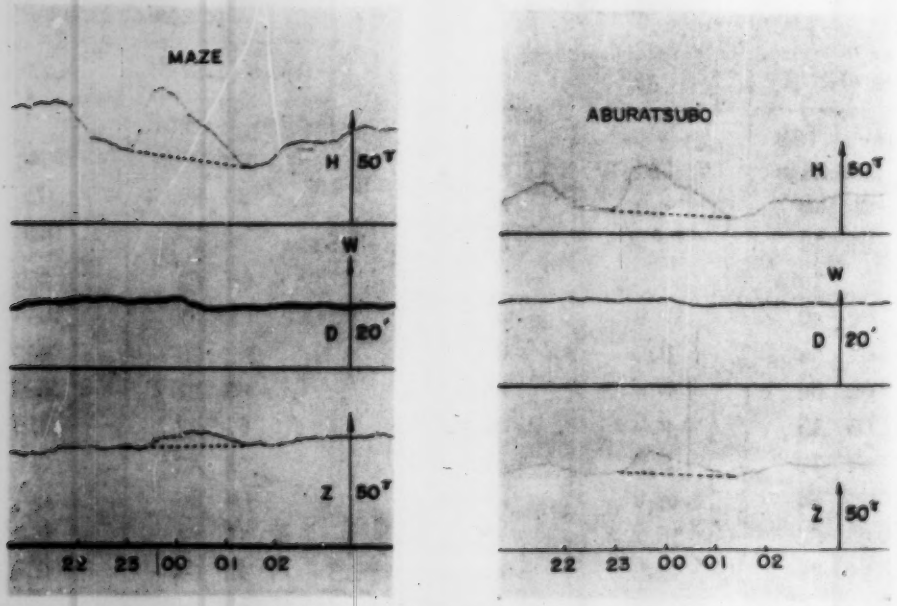

Fig. 4. The records of the bay that occurred at 23*h*, Sept. 11 and ended at 1*h*, Sept. 12, 1952 (J.S.T.).

3) I. TSUBOKAWA, *Bull. Geograp. Surv. Inst.*, **3** (1952), 29.

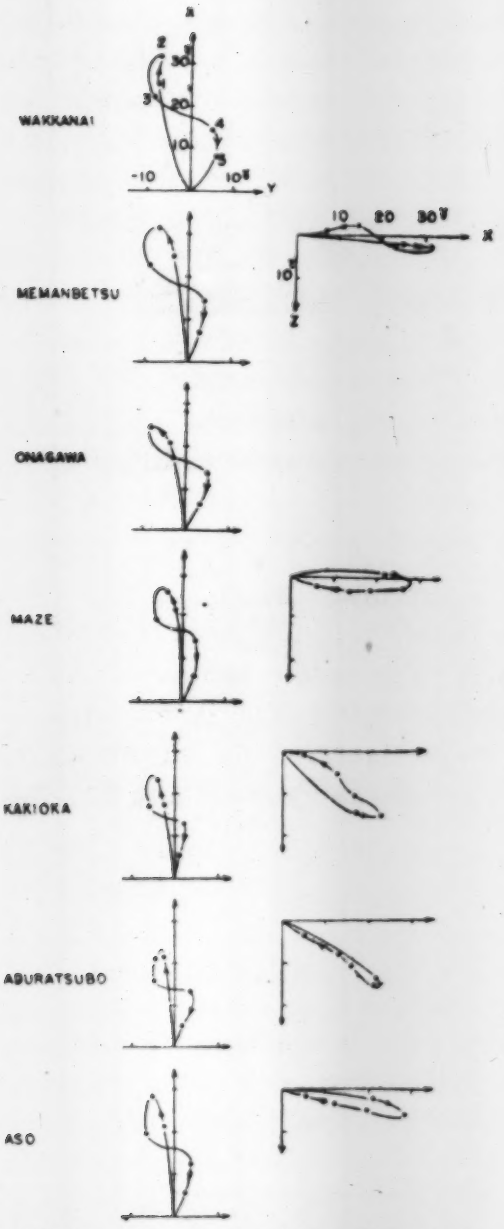

Fig. 5. The horizontal and vertical vector-diagrams for the bay from 23*h*, Sept. 11 to 1*h*, Sept. 12, 1952.

(43.9°N, 144.4°E). Onagawa (38.4°N, 141.5° E), Kakioka (36.2° N, 140.2° E) and Aso (32.9° N, 131.0° E) Observatories together with those from Maze and Aburatsubo. The records of this bay from both of our stations are shown in Fig. 4.

Here, the normal curves are assumed to be straight lines for convenience's sake. The equivalent overhead current arrows which represent the direction and intensity of the overhead electric currents corresponding to the magnetic disturbance seem to agree with those of typical bay-disturbance.[4] Their horizontal and vertical vector-diagrams are shown in Fig. 5 for respective stations where the time interval between the beginning and ending of the disturbance was divided into six parts and the deviation of each component from the normal line was read and plotted. As will be seen in the figures, the changing part of the geomagnetic field behaves almost uniformly in the horizontal plane at each station, but differently in its direction in the vertical plane. The ratio of ΔZ to ΔH at Kakioka and Aburatsubo is conspicuously larger than that of the other stations and the amount of the ratio is almost always constant as stated in the preliminary study.

To find a clue for the cause of the heterogeneity of geomagnetic variations, especially in Z-component, the data from Maze and Aburatsubo will be statistically examined in detail. In Fig. 6, ΔZ is plotted against ΔH at their maximum amplitudes for variations having duration-

4) H. HATAKEYAMA, *Geophys. Mag.*, **12** (1938), 15.

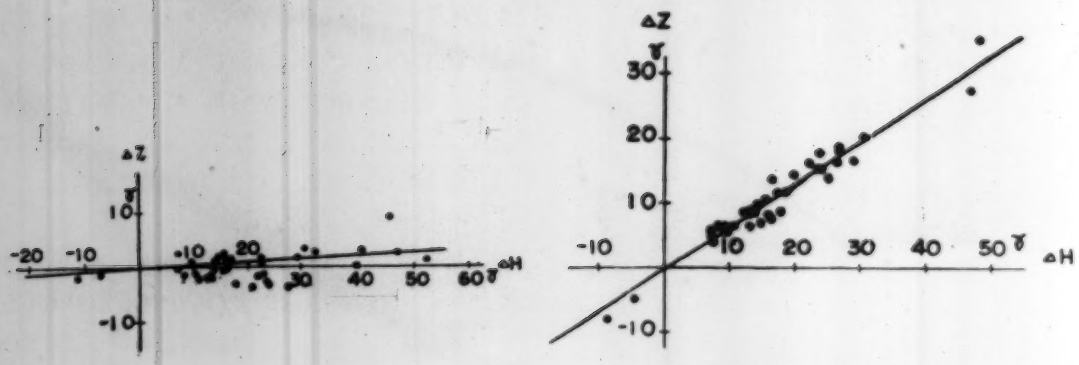

(a) Maze (b) Aburatsubo

Fig. 6. The relation between ΔH and ΔZ for short-period variations in September, 1952 and January, 1953.

time of scores of minutes in September, 1952 and January, 1953. Almost the same variations were used for both stations. At Maze, the values of ΔZ at the instant of the maximum variation of ΔH were read though ΔZ is not always exactly similar to ΔH. The mean values of $\Delta Z/\Delta H$ for Maze and Aburatsubo are estimated at 0.055 and 0.655 with the standard deviations 0.145 and 0.106 respectively. As shown in the figures, the value of $\Delta Z/\Delta H$ at Maze is remarkably small and fluctuates on both sides of the zero-line.

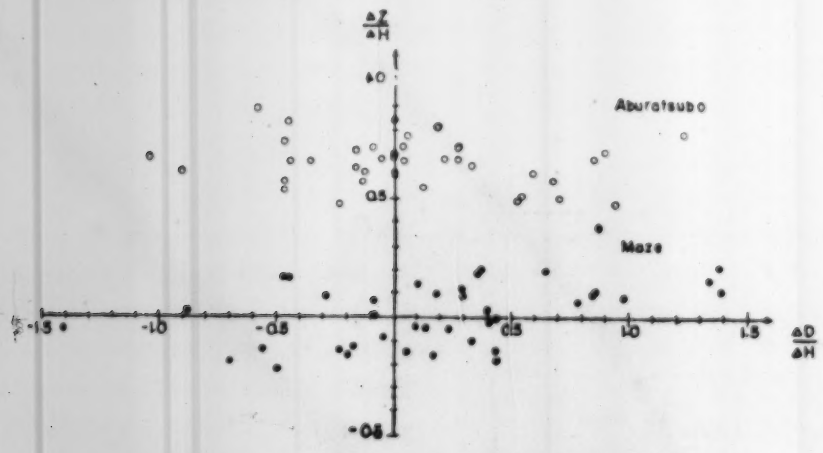

Fig. 7. The dependency of $\Delta Z/\Delta H$ on $\Delta D/\Delta H$.

In order to find the dependency of $\Delta Z/\Delta H$ on the overhead disturbing current-system, $\Delta Z/\Delta H$ is plotted against $\Delta D/\Delta H$ in Fig. 7, where ΔD is counted in γ and as positive eastward. The fact that ΔH is usually larger than ΔD at these stations should be understood by taking into consideration the fact that the current-system of bay-type disturbances observed here

might be of almost the same character as bay. As may be seen in the figure, no distinct tendency is found for both stations but the next characteristics would be noteworthy; the values of $\Delta Z/\Delta H$ at Maze for the case of $\Delta D/\Delta H>0.6$ are always positive. These nine points are plotted in $\Delta Z-\Delta H$ diagram as shown in Fig. 8, where the mean value

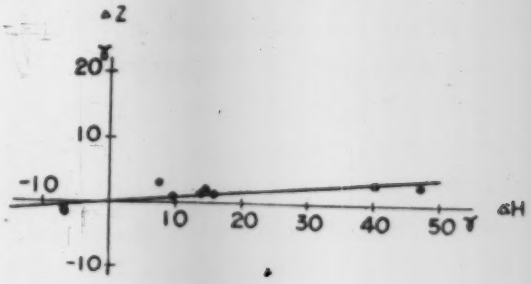

Fig. 8. $\Delta Z-\Delta H$ diagram for the nine points of which $\Delta D/\Delta H>0.6$ at Maze.

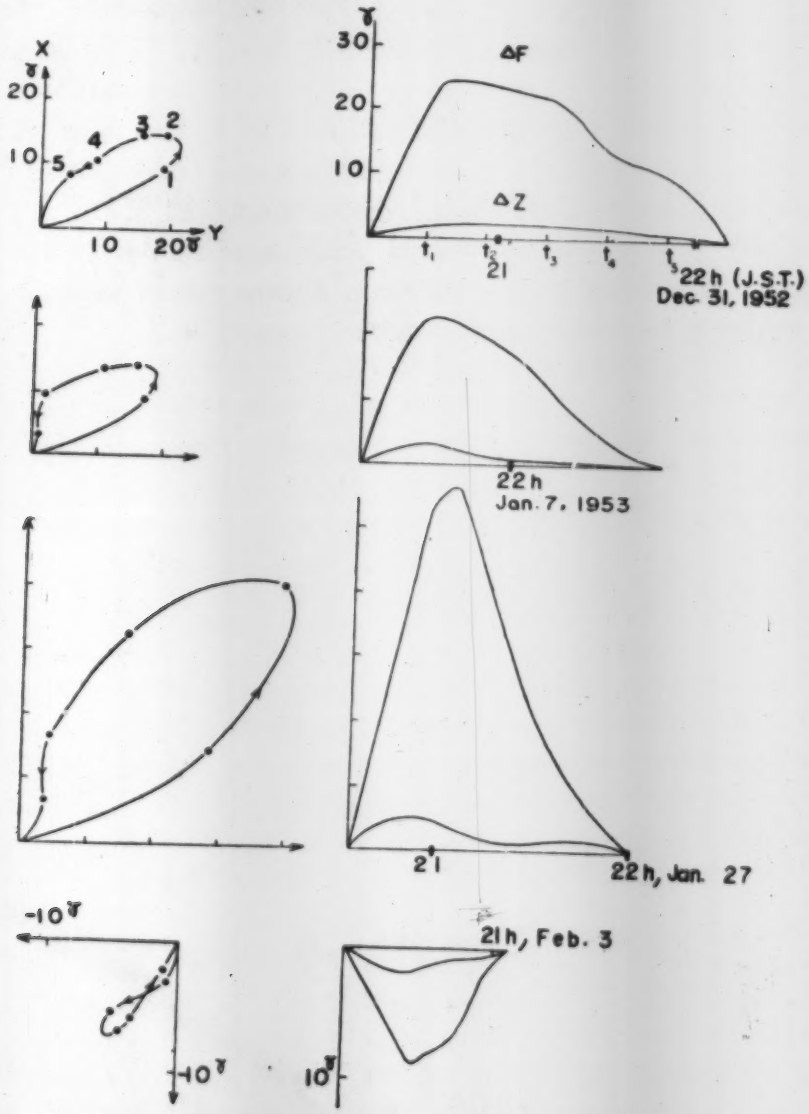

Fig. 9. The horizontal vector-diagrams and corresponding variations of ΔF and ΔZ at Maze.

of $\Delta Z/\Delta H$ is estimated at 0.081 with the standard deviation 0.123.

If we plot ΔZ against ΔF (changes in horizontal total force) in place of ΔH with regard to the above-mentioned nine points, the mean value of $\Delta Z/\Delta H$ is obtained at 0.061 with the standard deviation 0.091 which is smaller than the former. It may thus be said that ΔZ varies similarly with ΔF in shape, though the amplitude of it is rather small, when the horizontal vector-diagram of disturbing field lies approximately in a north-easterly direction. At Aburatsubo, on the other hand, the anomalously large amplitude of ΔZ and the marked parallelism between ΔZ and ΔH do not depend on the direction of the disturbing field as can be seen in Fig. 7. The mean value of $\Delta Z/\Delta F$ for all points at Aburatsubo is 0.549 with the standard deviation 0.065 which is smaller than that of $\Delta Z/\Delta H$ as is the case at Maze.

Illustrations of horizontal vector-diagram and corresponding variation of ΔF and ΔZ in the course of the disturbances at Maze are shown in Fig. 9, where the horizontal vectors point approximately to the northeast. In Fig. 10, a comparison between geomagnetic variations at Maze and Aburatsubo is made regarding a few examples.

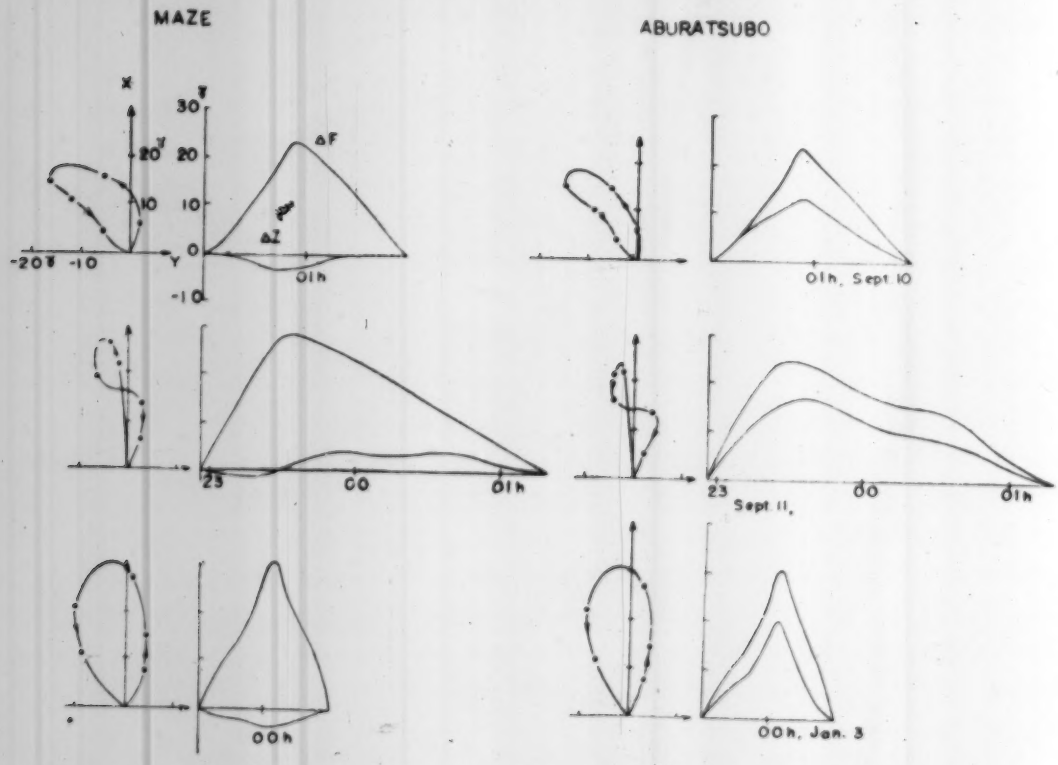

Fig. 10. Comparison between geomagnetic variations at Maze and Aburatsubo.

4. The distribution of $\Delta Z/\Delta H$ for short-period variations in Japan.

As stated above, the remarkable difference between the values of $\Delta Z/\Delta H$ at Maze and those at Aburatsubo which is only 300 *km* distant from the former is striking. The writers have not heard of such a peculiarity in foreign countries. To study the distribution of $\Delta Z/\Delta H$ for short-period variations in Japan more widely, the writers have collected as many copies of magnetograms as possible from permanent and temporary stations. The values of $\Delta Z/\Delta H$ thus calculated are tabulated in Table I while the period of observations for these stations differs from one another.

Furthermore, the results[5] of magnetic survey during 1948–1951 published by the Geographical Survey Institute are sometimes available for the study. The observation for one place of the survey have been carried out through a day usually with an hour interval. We could, fortunately, estimate the approximate values of $\Delta Z/\Delta H$ when favourable short-period variations occurred during the

Table I.

Station	$\Delta Z/\Delta H$
Toyohara	0.02
Wakkanai	−0.15
Memanbetsu	0.065
Iwamizawa	−0.018
Zenigamezawa	−0.008
Maze	0.055
Kakioka	0.56
Aburatsubo	0.62
Shimoda	1.07
Beppu	0.18
Aso	0.20

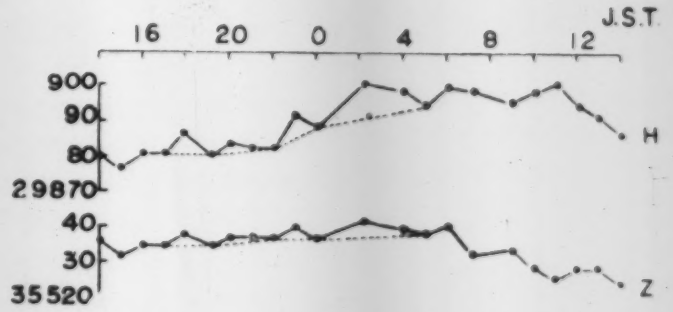

(a) Utsunomiya (36.5° N, 139.9° E), Dec. 1-2, 1950.

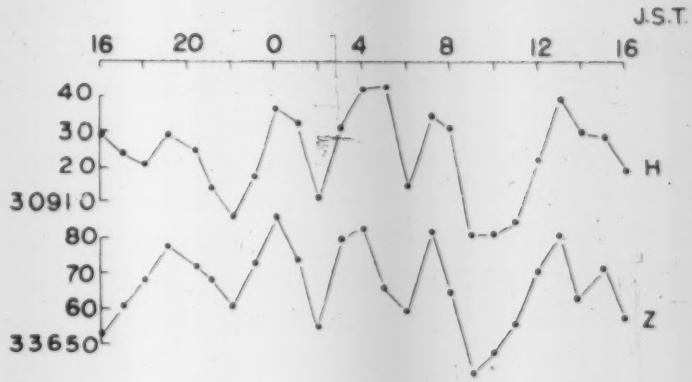

(b) Shimoda (34.7°N, 139.0°E), Feb. 9-10, 1951.

Fig. 11. The results of magnetic survey by G.S.I. at Utsunomiya and Shimoda (unit in γ).

5) Geographical Survey Institute, *Bull. Geograp. Surv. Inst.*, **2** (1951), 121.

observation. For example the results of magnetic surveys at Utsunomiya, Tochigi Prefecture and Shimoda, the southern extremity of the Izu Peninsula, are graphically shown in Fig. 11. In regard to Shimoda, the anomalously large value of $\Delta Z/\Delta H$ obtained from the magnetograms conforms exactly to the value obtained by absolute measurement. But, generally speaking, the values of $\Delta Z/\Delta H$ thus obtained from the results of the survey are not accurate owing to a small number of variations. These values serve therefore as auxiliary aids.

The distribution of $\Delta Z/\Delta H$ for short-period variations in Japan thus obtained is shown in Fig. 12. As may be seen, the large values of $\Delta Z/\Delta H$ are expressed by the roughly circular contours centred at Shimoda district, while no special condition in the permanent geomagnetic field is to be seen there. In the region where the value is small, $\Delta Z/\Delta H$ fluctuates from time to time as was observed at Maze. We should pay attention to the anomalous distribution of $\Delta Z/\Delta H$ observed in a narrow area such as in Japan. A phenomenological explanation of the distribution will be attempted in the forthcoming paper.

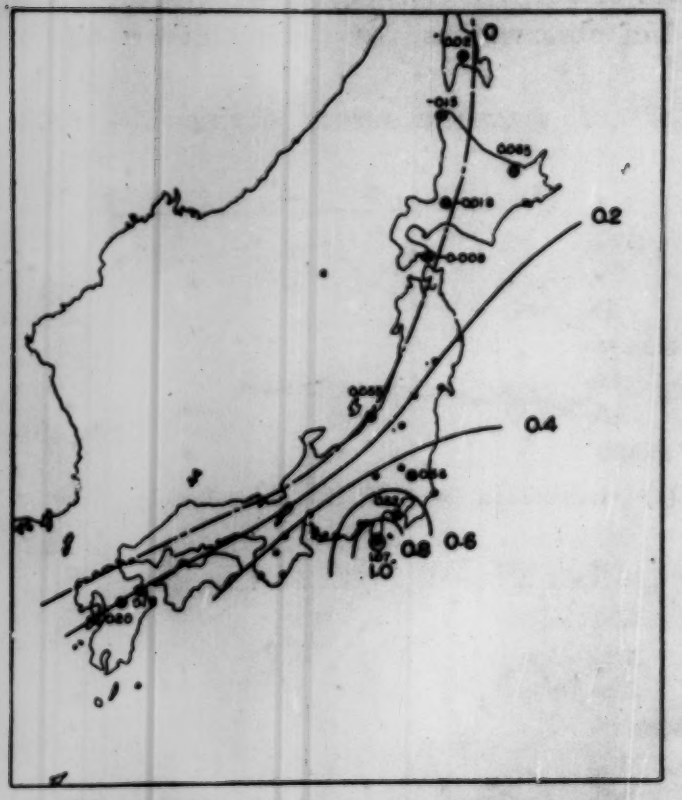

Fig. 12. The distribution of $\Delta Z/\Delta H$ for short-period variations in Japan. Black circles show the stations of continuous observation, while small circles correspond to the results of surveys.

Since the anomalous behavior of short-period geomagnetic variations become clear, the reduction of the results of a magnetic survey to the standard point, for example to Kakioka, should be carefully made by taking into account the distribution of $\Delta Z/\Delta H$. Though it seems difficult to make an accurate reduction, we shall be able to get approximately correct results if we have some more magnetic observatories in various districts in Japan.

5. Conclusions.

An outline of geomagnetic observation at Maze is described. The relation between ΔZ and ΔH is statistically studied in comparison with Aburatsubo. Geomagnetic heterogeneity in the short-period variation is certified at Maze where the mean value of $\Delta Z/\Delta H$ is very small and the parallelism between ΔZ and ΔH is not always found. The behavior of ΔZ at Maze has the same tendency as that at Aburatsubo only when the horizontal vector of the disturbing field points approximately to the north-east direction. A chart showing the distribution of $\Delta Z/\Delta H$ for short-period variations in Japan was constructed with the aids of continuous observations and magnetic surveys.

Although the writers have arrived at no decisive conclusion concerning the origin of the anomalous behavior of geomagnetic variation in Japan, the writers think it is of some use to report the results of the analysis. The writers are going to study the anomalous behavior further with world-wide data in the next report.

In the end, the writers would like to express their thanks to the Ionosphere Research Committee of Japan who provided them with data for a part of the present study. The writers' hearty thanks are also due to Mr. K. Wakô of the Aburatsubo Station and Messers S. Ishizuka, T. Hayakawa and S. Hirota of the Maze Station for their helpful cooperations. Some informations concerning the values of $\Delta Z/\Delta H$ at Beppu and Yamagawa in Kyusyu district were kindly given by Dr. M. Ôta to whom the writers' sincere thanks are also due.

9. 日本における地磁気短周期変化の異常と地下構造

第 3 報

地震研究所 力武常次
横山泉
菱山よね子

神奈川県油壺に加えて，1952年9月より，新たに新潟県間瀬で地磁気三成分の連続観測が開始された．間瀬においては，油壺で見出されたような，短周期変化の水平分力と鉛直分力との平行性は必ずしも見出されず，又，鉛直分力の変化量そのものも，油壺のそれの殆ど10分の1程度である．統計的に調べると，間瀬においても，擾乱磁場の水平成分が大体北東に向くと，量的には小さいが，油壺の場合と同じような平行性を呈することを知った．

油壺と間瀬と，僅か 300 *km* の距離で，鉛直成分がこのような相異を示すことは注目すべきことがらである．各観測所の連続記録及び地理調査所の各地における 24 時間絶対測定の成果を利用して，日本における $\Delta Z/\Delta H$ の分布を求めた．

10. *The Anomalous Behavior of Geomagnetic Variations of Short Period in Japan and Its Relation to the Subterranean Structure. The 4th report.*

By Tsuneji RIKITAKE, Izumi YOKOYAMA and Yoneko HISHIYAMA,

Earthquake Research Institute.

(Read March 17, 1953.—Received March 20, 1953.)

1. Introduction.

As has been investigated in a series of the writers' papers[1),2),3)], geomagnetic variations of short period show anomalous behavior in Japan, especially in vertical component. That behavior is most clearly expressed in a chart[4)] showing the distribution of the ratio of the amplitude in ΔZ (vertical component) to that in ΔH (horizontal component). Although the chart was constructed on the basis of observations obtained at observatories not quite adequately distributed, it should be noted that $\Delta Z/\Delta H$ covers a range from 1 to -0.2 in such a narrow area as Japan. The writers have never heard of such a curious anomaly except the reversal of sign of ΔZ in British Isles on the occasions of SC's.

In order to study the anomalous behavior more clearly, the writers analyzed a remarkable magnetic change that occurred at $5h\,50m$ GMT, June 19, 1936, the same change as treated in the preliminary report[1)]. As the writers had already done in an analysis of SC that occurred at the beginning of the same storm, the writers constructed the world chart of magnetic potential for the said variation and separated the internal origin part from the external origin part in the neighborhood of Japan. Some discussions will be made in this paper on the basis of the distribution of both parts thus obtained.

2. Data used in the analysis.

The values of H, D, and Z are read on the copies of magnetograms

1) T. RIKITAKE, I. YOKOYAMA and Y. HISHIYAMA, *Bull. Earthq. Res. Inst.*, **30** (1952), 207.

2) T. RIKITAKE, I. YOKOYAMA and Y. HISHIYAMA, *Bull. Earthq. Res. Inst.*, **31** (1953), 19.

3) T. RIKITAKE, I. YOKOYAMA and Y. HISHIYAMA, *Bull. Earthq. Res. Inst.*, **31** (1953), 89.

4) See Fig. 12 of 3).

kindly sent to the writers from various observatories all over the earth. The changes from 4*h* to 8*h* are shown in Figs. 1, 2, 3 and 4 respectively

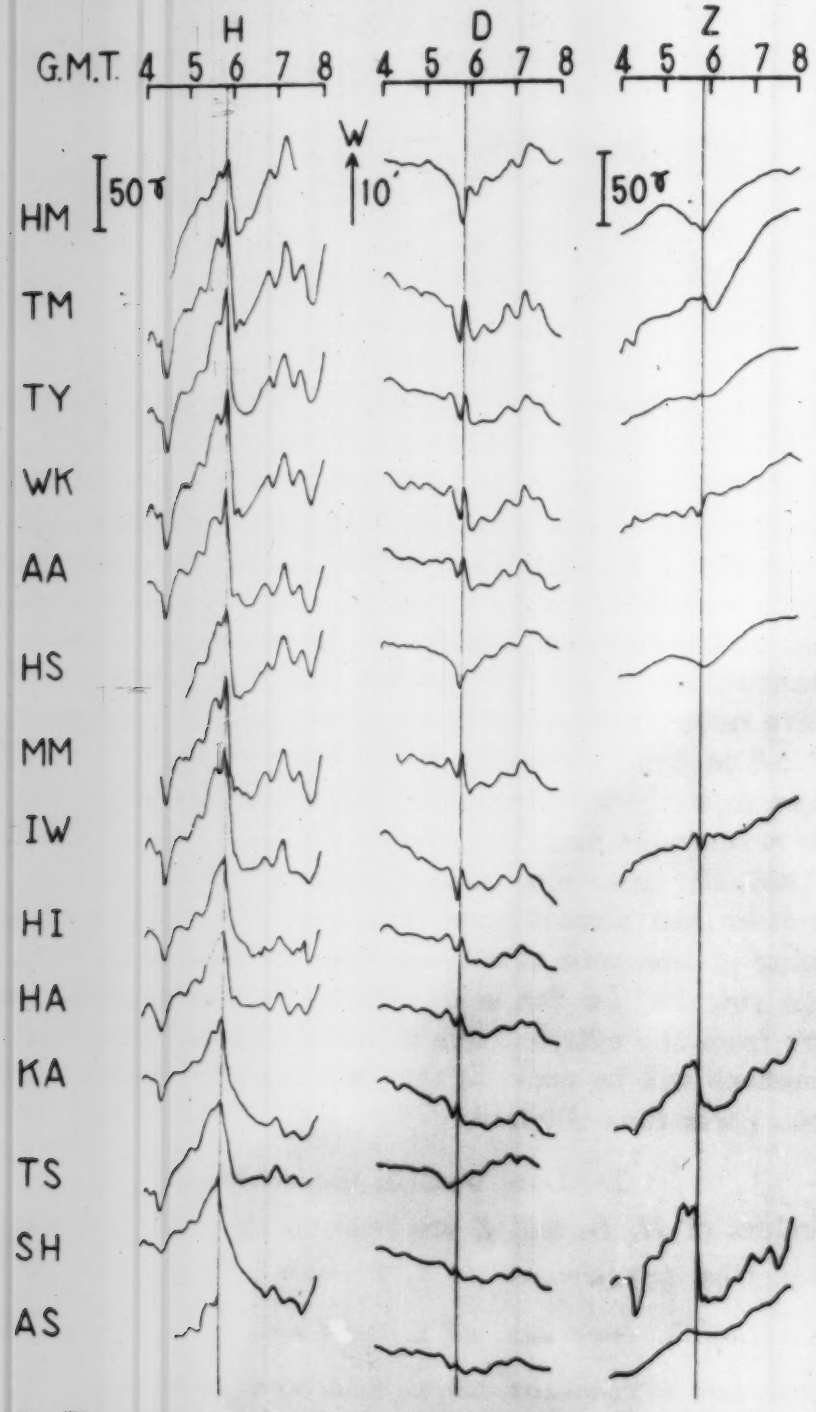

Fig. 1. The magnetograms for the observatories in Japan and her vicinity from 4*h* to 8*h* GMT on June 19, 1936.

for the observatories situated in Japan and her vicinity, Asia and Australia, Europe and Africa. Meanwhile the distribution of the observatories are shown in Fig. 5 together with their abbreviations. In order to pick up a remarkable change at about $5h\ 50m$, the writers made running averages by averaging 13 readings of every 5 *minutes*. After subtracting the running averages from the original values, we tentatively got the values of ΔH, ΔD and ΔZ at $5h\ 50m$ from which the influence of long period variation is approximately eliminated. On the basis of these values, ΔX_m (geomagnetic north component) and ΔY_m (geomagnetic east component)

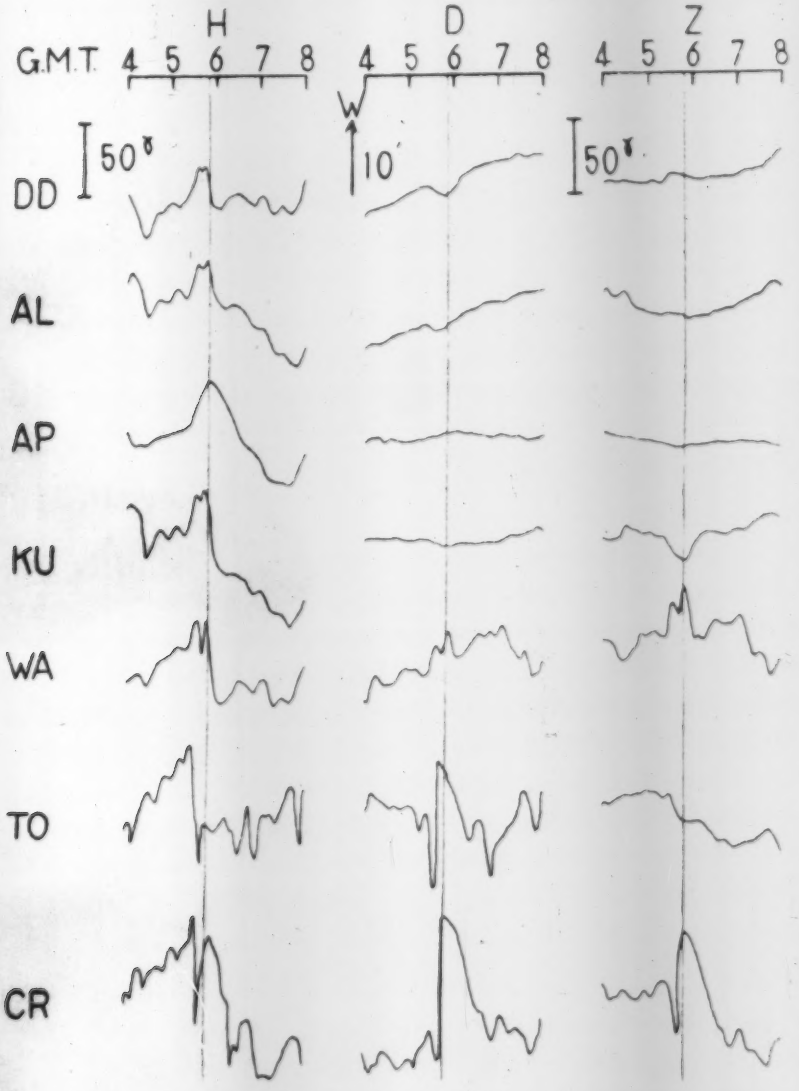

Fig. 2. The magnetograms for the observatories in Asia and Australia from 4h to 8h GMT on June 19, 1936.

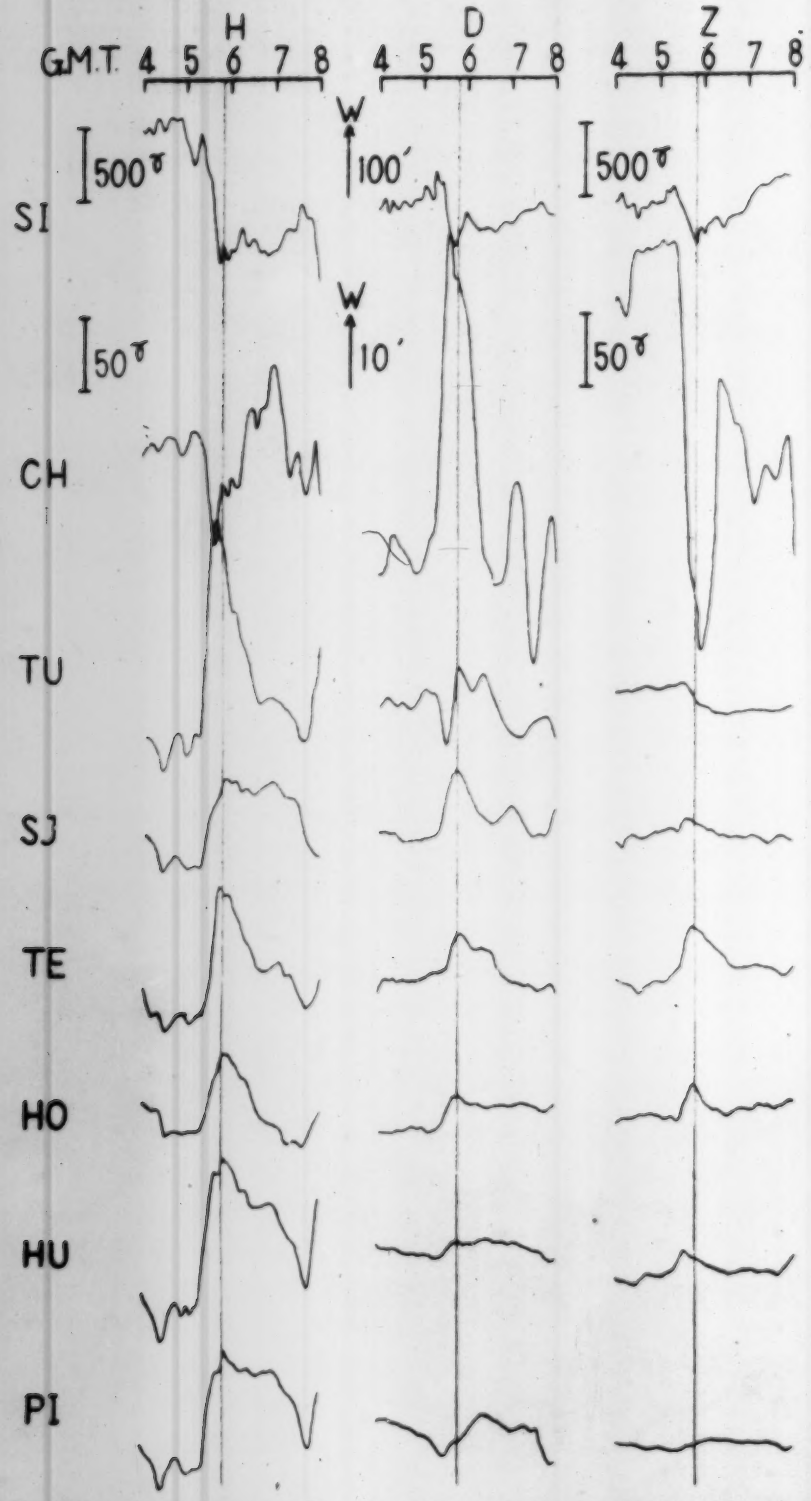

Fig. 3. The magnetograms for the observatories in America from 4h to 8h GMT on June 19, 1936.

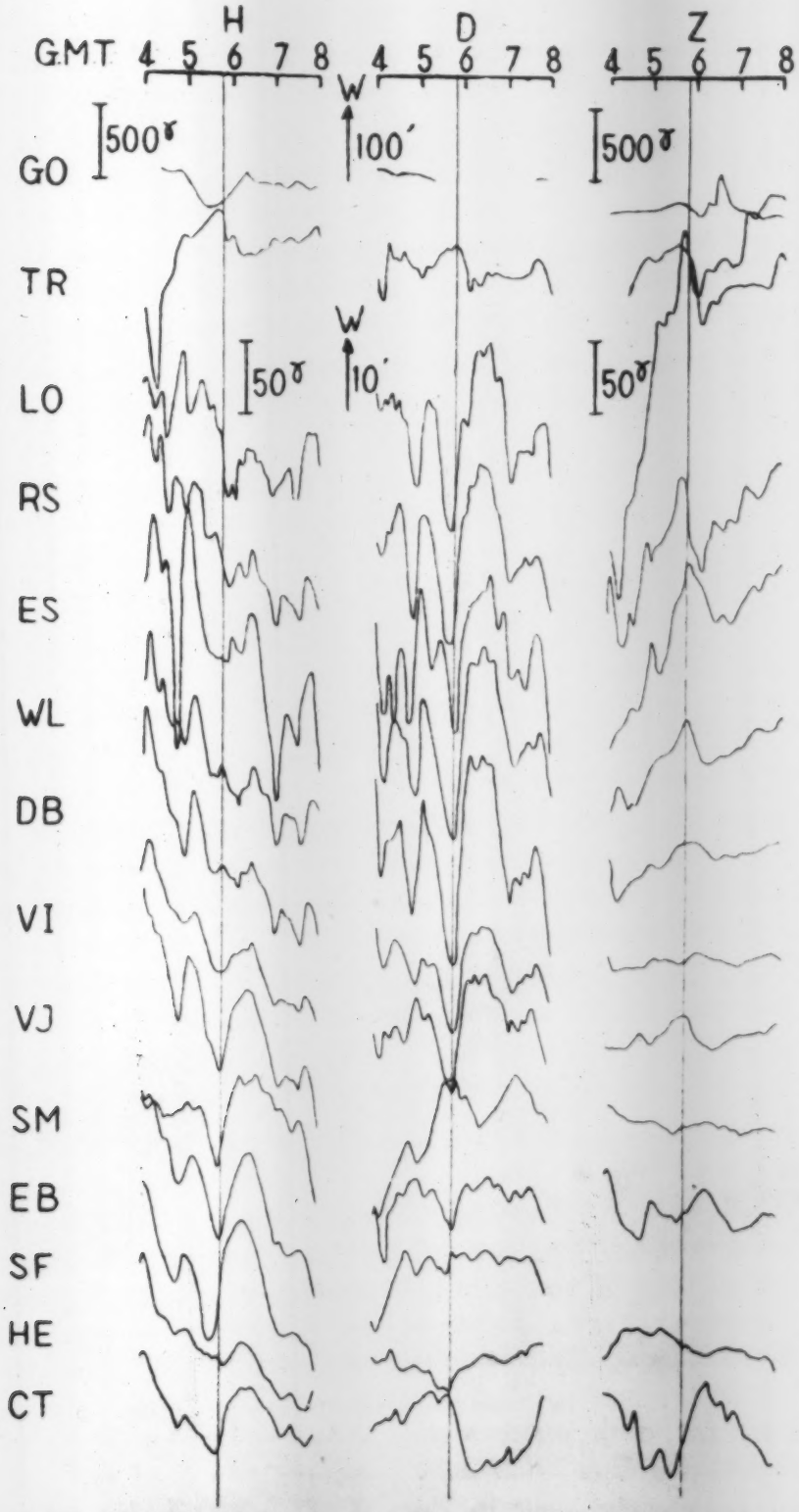

Fig. 4. The magnetograms for the observatories in Europe and Africa from 4*h* to 8*h* GMT on June 19, 1936.

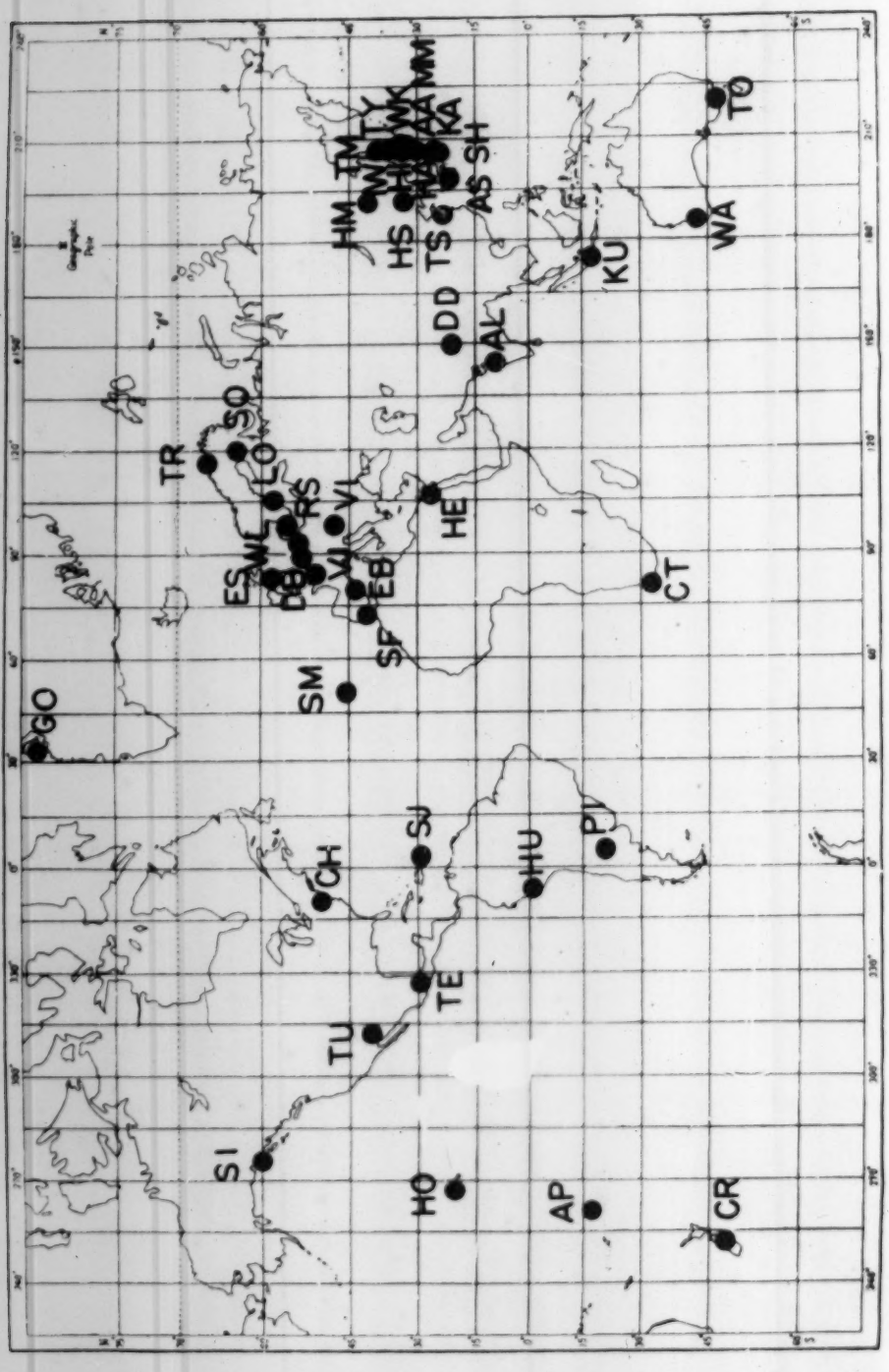

Fig. 5. The distribution of the observatories.

are calculated for each observatory. ΔX_m and ΔY_m thus obtained are given in Table I together with ΔZ.

As will be clearly seen in Figs. 1, 2, 3 and 4, the changes in the three components are fairly systematic. And it would be of much interest

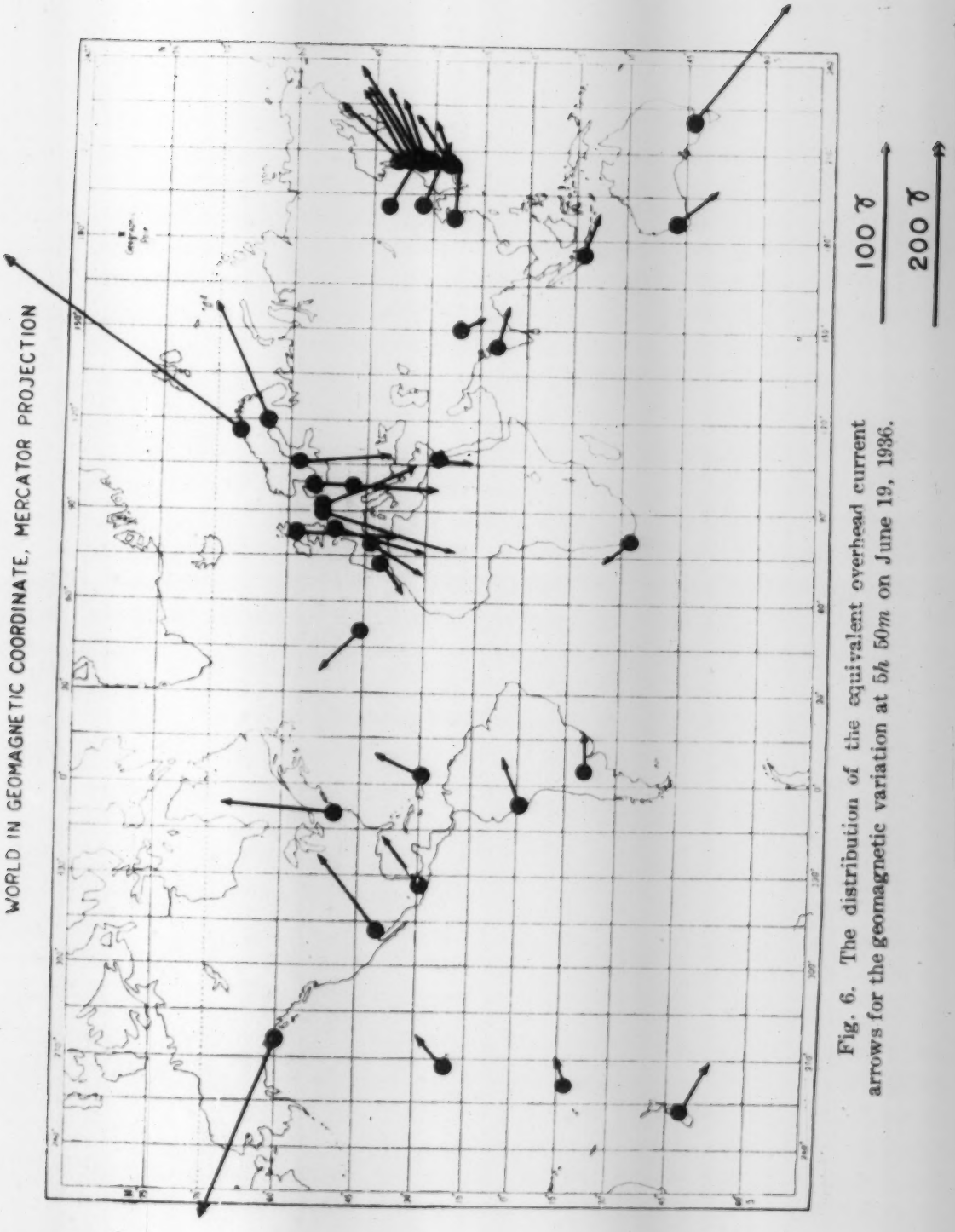

Fig. 6. The distribution of the equivalent overhead current arrows for the geomagnetic variation at 5*h* 50*m* on June 19, 1936.

to study the disturbance field itself. As a matter of fact, the distribution of the equivalent overhead current arrows which is obtained from the data in Table I and is shown in Fig. 6 seems to be fairly regular. The mode of the distribution is the same as those of a polar magnetic

Table I. Japan and her vicinity.

Station	Abbreviation	Geomagnetic latitude	Geomagnetic longitude	Geographic latitude	Geographic longitude	ΔX_m	ΔY_m	ΔZ
		°	°	°	°	γ	γ	γ
Huma	HM	40.6	192.7	51.7	126.7	32.2	16.3	− 9.1
Tomarigishi	TM	38.6	203.5	49.0	142.9	29.1	−32.6	4.9
Toyohara	TY	36.9	203.5	47.0	142.8	36.2	−25.0	0.6
Wakkanai	WK	34.4	203.4	45.4	141.7	38.1	−28.0	− 1.3
Abashiri	AA	34.2	209.2	44.0	144.3	26.9	−25.8	—
Hsinking	HS	32.7	193.3	43.9	125.3	34.3	11.6	− 4.8
Memanbetsu	MM	34.1	209.2	43.9	144.4	45.5	−35.6	—
Iwamizawa	IW	32.5	207.8	43.2	141.8	40.0	−21.5	− 5.3
Hiroo	HI	31.0	208.5	42.3	143.3	27.2	−13.0	—
Hirosaki	HA	29.5	206.2	40.6	140.5	18.0	−17.1	—
Kakioka	KA	26.0	206.0	36.2	140.2	22.6	−17.2	15.7
Tsingtau	TS	24.7	188.3	36.1	120.3	27.8	2.1	—
Shimoda	SH	24.4	205.0	34.7	138.9	20.5	−10.3	31.3
Aso	AS	22.0	198.0	32.9	131.0	—	—	2.9

Table I. (Continued) Asia and Australia.

Station	Abbreviation	Geomagnetic latitude	Geomagnetic longitude	Geographic latitude	Geographic longitude	ΔX_m	ΔY_m	ΔZ
		°	°	°	°	γ	γ	γ
Dehra Dun	DD	20.5	149.9	30.3	78.0	5.2	10.9	2.0
Alibag	AL	9.5	143.6	18.6	72.9	19.9	5.5	0.0
Apia	AP	−16.0	260.2	−13.8	188.2	11.9	− 3.1	− 1.1
Kuyper	KU	−17.5	175.5	− 6.0	106.7	24.4	8.3	−10.2
Watheroo	WA	−41.8	185.6	−30.3	115.9	22.8	22.8	24.4
Toolangi	TO	−46.7	220.8	−37.5	145.5	68.4	51.0	9·2
Christchurch	CR	−47.7	252.5	−43.5	172.7	27.2	14.5	− 7.5

Table I. (Continued) America.

Station	Abbreviation	Geomagnetic latitude	Geomagnetic longitude	Geographic latitude	Geographic longitude	ΔX_m	ΔY_m	ΔZ
		°	°	°	°	γ	γ	γ
Sitka	SI	60.0	275.4	57.0	224.7	−193.6	−76.3	−179.7
Cheltenham	CH	50.1	350.5	38.7	283.2	5.3	−60.5	− 97.9
Tucson	TU	40.4	312.2	32.2	249.2	38.6	−33.0	− 2.5
San Juan	SJ	29.9	3.2	18.4	293.9	11.1	−27.4	2.5
Teoloyucan	TE	29.6	327.1	19.7	260.8	25.2	−24.8	11.0
Honolulu	HO	21.1	266.5	21.3	201.9	16.5	−13.6	11.0
Huancayo	HU	− 0.6	353.8	−12.0	284.7	24.3	−10.1	2.5
Pilar	PI	−20.2	4.6	−31.7	296.1	21.2	− 1.1	− 0.4

Table I. (Continued) Europe and Africa.

Station	Abbreviation	Geomagnetic latitude	Geomagnetic longitude	Geographic latitude	Geographic longitude	ΔX_m	ΔY_m	ΔZ
		°	°	°	°	γ	γ	γ
Godhavn	GO	79.8	32.5	69.2	306.5	—	—	4.2
Tromsö	TR	67.1	116.7	69.7	18.9	− 93.2	−128.9	125.0
Sodankylä	SO	63.8	120.0	67.4	26.6	59.8	− 32.8	128.6
Eskdalemuir	ES	58.5	82.9	55.3	356.8	− 0.5	54.0	25.2
Lovö	LO	58.1	105.8	59.4	17.8	6.1	48.9	13.2
Rude Skov	RS	55.8	98.5	55.8	12.4	0.2	39.1	14.0
Wilhelmshaven	WL	54.5	92.9	53.5	8.2	17.4	53.1	17.8
De Bilt	DB	53.8	89.6	52.1	5.2	− 21.9	69.5	3.4
Val Joyeux	VJ	51.3	84.5	48.8	2.0	− 13.2	49.8	8.7
Wien	VI	47.9	98.1	48.2	16.2	− 1.1	44.7	− 1.8
San Miguel	SM	45.6	334.4	36.6	101.4	− 20.1	— 22.8	1.4
Ebro	EB	43.9	79.7	40.8	0.5	− 15.4	27.9	− 1.4
San Fernando	SF	41.0	71.3	36.5	353.8	− 13.7	9.2	—
Helwan	HE	27.2	106.4	29.9	31.3	0.0	17.4	− 2.3
Cape Town	CT	−32.7	79.9	−33.9	18.5	− 12.3	− 13.7	− 7.5

storm which were recently examined by T. Nagata and N. Fukushima[5),6)]. Though it is beyond the scope of this paper to examine the cause or origin of the disturbance, the origin of the change could be ascribed to a high ionization at somewhere near the auroral zones which would cause intense electric currents flowing in the ionosphere owing to the dynamo-action there.

3. The magnetic potential and the separation of it into the external and internal parts.

As fully studied in the writers' previous paper[2)], the magnetic potential for the change at $5h\ 50m$ is calculated with the aid of the graphical method. The detail of the procedure will not be described here because it is just the same as that carried out in the former paper. After integrating ΔX_m along meridians and ΔY_m along parallel circles, we got the distribution of the magnetic potential as shown in Fig. 7 where the integration constants are suitably adjusted so as to keep the constant part of potential at zero.

Combining the distribution of potential with that of ΔZ, the writers calculated the external and internal parts of potential and ΔZ by means of the surface integral method the application of which was also stated in the former paper. Since we do not have many observatories in the polar regions, oceans and some continents, the accuracy of the calculation

5) T. Nagata and N. Fukushima, *Rep. Ionos. Res. Japan*, **6** (1952), 85.
6) N. Fukushima, *Rep. Ionos. Res. Japan*, **6** (1952), 185.

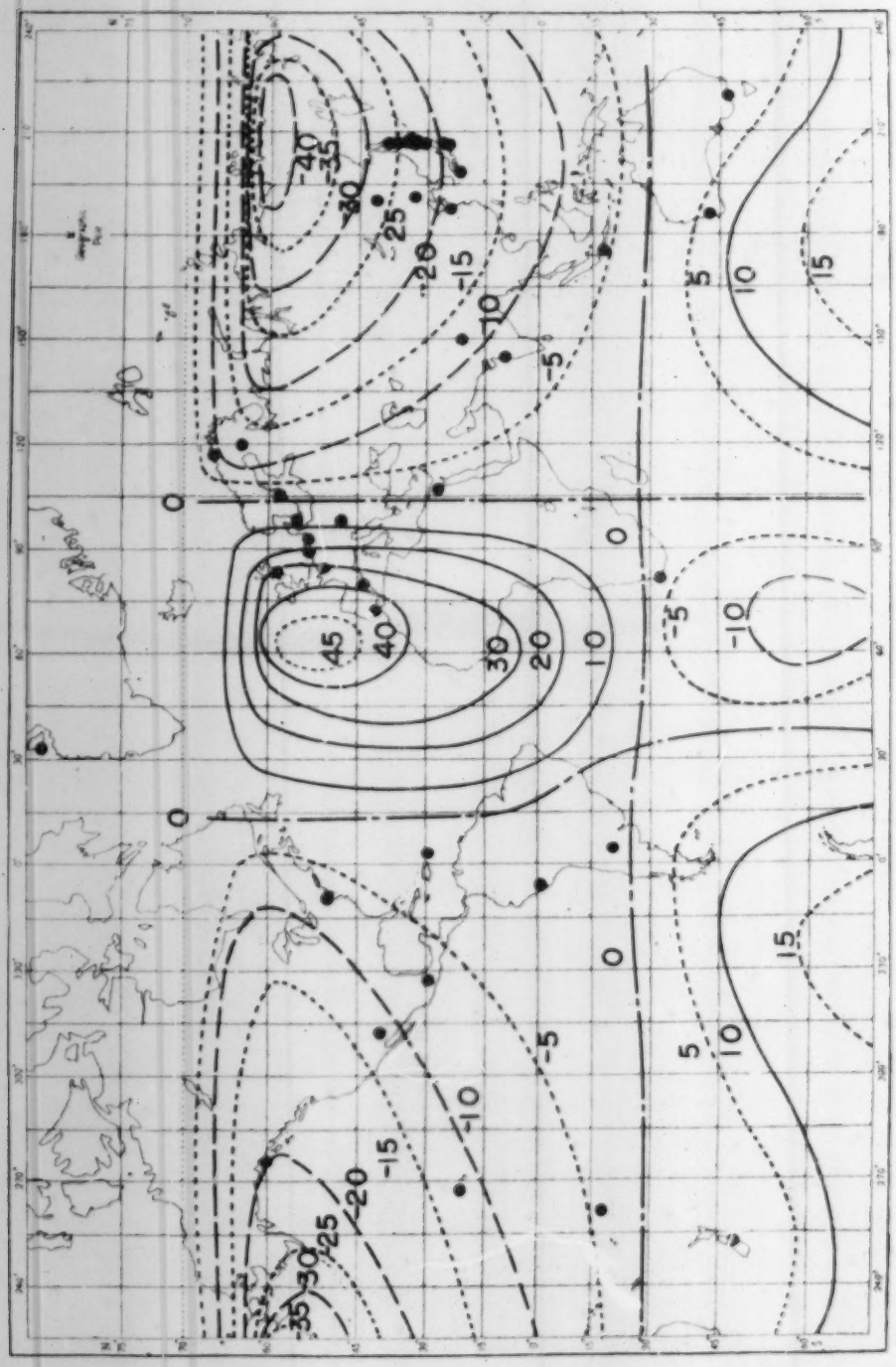

Fig. 7. The distribution of the magnetic potential which is calculated by the graphical integration method. The unit is *gamma* multiplied by the earth's radius.

is not so reliable in general. However, as regards the observatories in and around Japan, the results should be approximately right because the values near a point are much more effective than those of distant places in obtaining the values of potential and ΔZ of both parts at that point.

The external and internal parts at each observatory are tabulated in Table II for the potential and ΔZ while the suffices e and i denote respectively the parts originated out- and inside the earth.

Table II. The magnetic potential and ΔZ. The values of potential should be multiplied by the earth's radius.

Station	W_e	W_i	ΔZ_e	ΔZ_i
HM	-17.1γ	-9.9γ	-23γ	$+14\gamma$
TM	-16.9	-10.1	-19	$+24$
TY	-16.0	-9.0	-19	$+19$
WK	-15.0	-8.7	-17	$+16$
HS	-14.9	-7.3	-19	$+14$
IW	-15.5	-7.4	-17	$+12$
KA	-14.3	-5.8	-12	$+28$
SH	-11.7	-7.1	-11	$+42$
AS	-12.8	-5.6	-10	$+13$

Meanwhile the distribution of the quantities in Table II are shown in Figs. 8, 9, 10 and 11. As will be seen in the figures, the part originating outside the earth is distributed fairly regularly. If the origin is attributed to the electric currents flowing in the ionosphere, the electric current systems should be of almost the same distribution as that of W_e where currents of 10,000 *amperes* flow eastward between consecutive lines. On the contrary, the distributions of W_i and ΔZ_i are complicated. First of all, we should pay attention to the fact that there is a zone along Japan where W_i takes almost a constant value and, to the south of the zone, we find an anomalous distribution

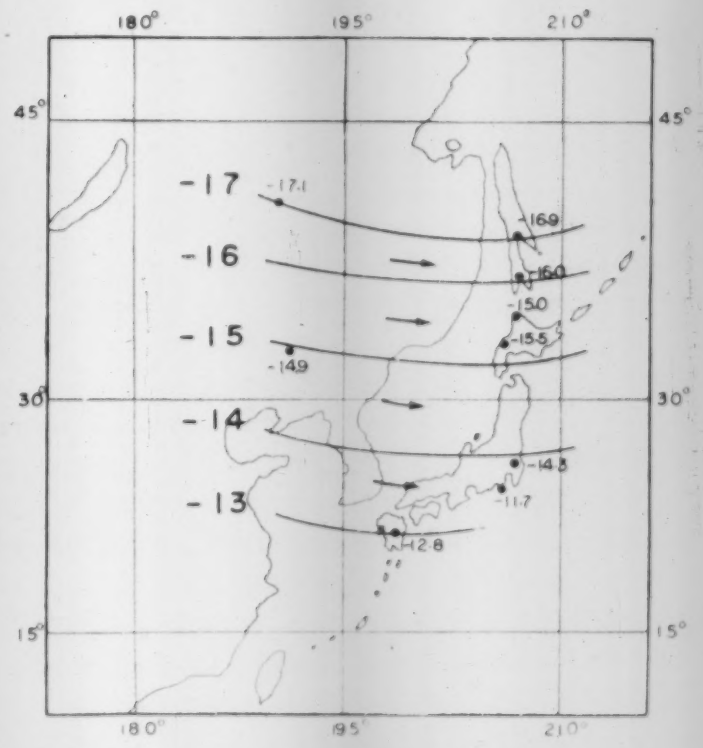

Fig. 8. The distribution of the external part of the magnetic potential. The unit is *gamma* multiplied by the earth's radius.

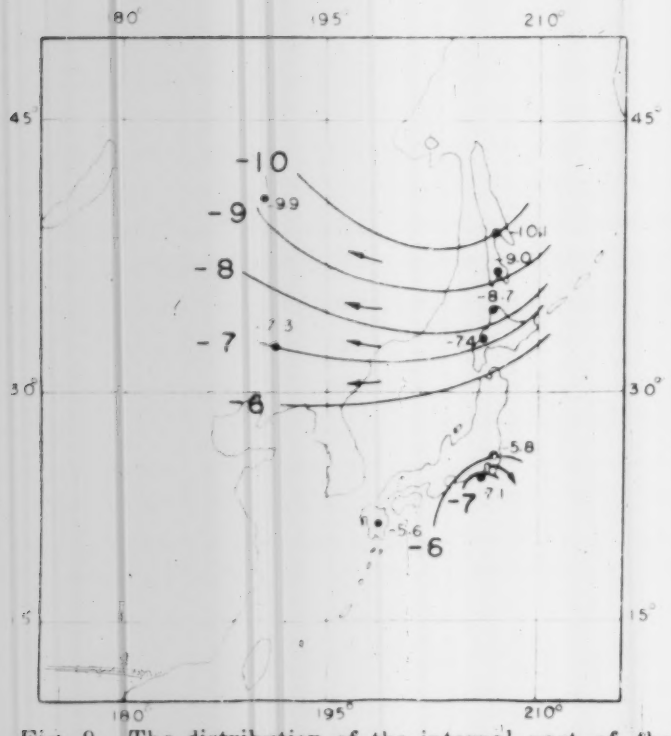

Fig. 9. The distribution of the internal part of the magnetic potential. The unit is *gamma* multiplied by the earth's radius.

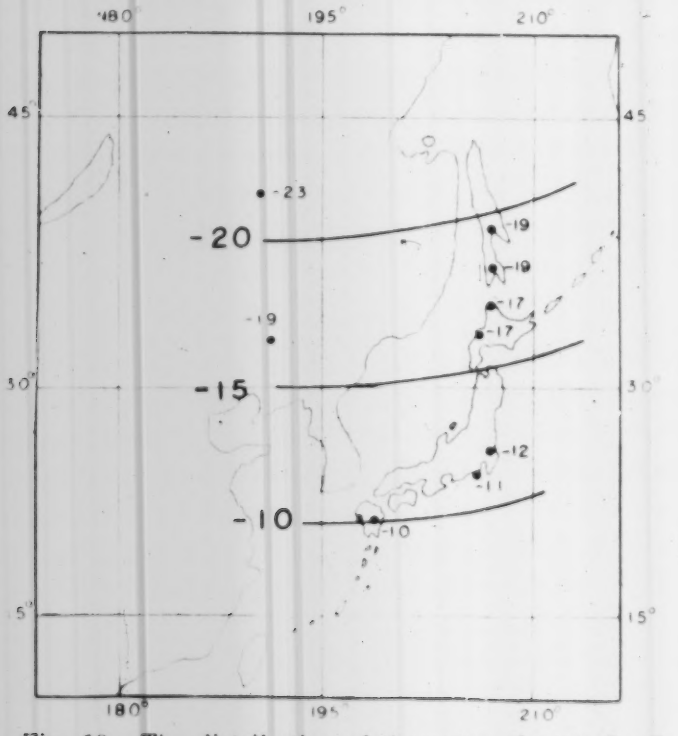

Fig. 10. The distribution of the external part of ΔZ. The unit is *gamma*.

of W_i expressed by circular equi-potential lines. The latter corresponds to the area in which we find large ΔZ as is obtained at both Kakioka and Shimoda. The distribution of W_i in the northern part of the chart looks approximately the same as that obtained in the previous analysis of SC. If we assume that the internal part of the change is caused by electric currents flowing just under the earth's surface, we have currents of 10,000 *amperes* flowing to the direction which is shown by the arrows in Fig. 9. Following the usual theory, if we interpret the internal field as one caused by electric currents electromagnetically induced within the earth by the external inducing field, it would be difficult to realize the currents under the earth's surface flowing to the same direction as that of the overhead currents. Hence it is impossible to explain the curious distribution of magnetic variation by the electromagnetic induction theory within a homogeneous earth. An alternative explanation would be pos-

sible only in case of heterogeneous or anisotropic distribution of electrical conductivity under Japan.

4. Phenomenological explanation of the distribution of $\Delta Z/\Delta H$ in Japan.

According to the statistical examination[1] of short-period geomagnetic variations in Japan, ΔZ amount to as much as 50 *per cent* or more of ΔH at Kakioka, Aburatsubo and Shimoda while, as has been recently clarified by the observation at Maze in Niigata Prefecture, ΔZ is very small along the coast of Japan Sea, the line for $\Delta Z=0$ seeming to run along that coast and across the central part of Hokkaido. The behavior of this anomalous distribution is best manifested in Fig. 12 of the 3rd report of this study. And we are now going to explain this characteristics of geomagnetic variation on the basis of the analysis carried out in this paper.

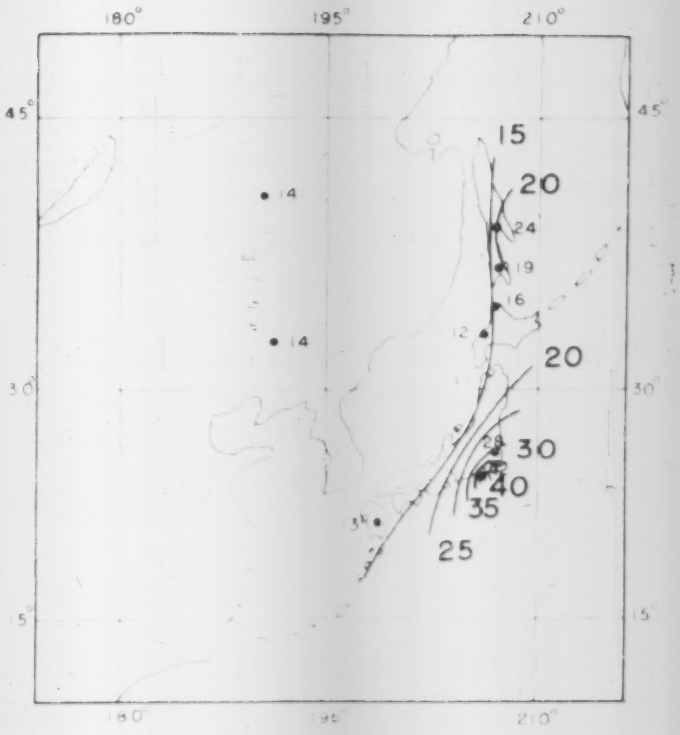

Fig. 11. The distribution of the internal part of ΔZ. The unit is *gamma*.

In the first place, we can readily see in Fig. 11 that ΔZ_e and ΔZ_i both amount to about 15 *gammas* in the northern part of Honshu (Main Island) and Hokkaido. Hence $\Delta Z(\Delta Z_e+\Delta Z_i)$ will be nearly zero in these districts, which fact is consistent with the aforementioned tendency if we assume the same overhead electric current systems for all variations. We may expect some shift of the line on which $\Delta Z=0$ in cases of slightly different current systems. That seems to be the reason why the value of $\Delta Z/\Delta H$ fluctuates at the observatories situated in the districts. Meanwhile, in the central part of Japan, ΔZ_i is decisively large and positive. And consequently, it overcomes ΔZ_e whence we have large ΔZ there. Of course, the above-mentioned discussion would not hold if the variations in question were of different types. But since the variations treated in

the statistical examination are mainly composed of bay-type disturbances or polar magnetic storms whose original current systems are expected to be almost the same as that analyzed here, it would be safe to offer the above-mentioned explanation.

Turning to ΔH, however, the external part of ΔX_m which occupies the main part of ΔH will be of almost the same magnitude in and around Japan as may be directly assumed from the regular distribution of W_e, while the internal part of ΔX_m will be positive in Manchuria, Saghalien and Hakkaido, nearly zero in the nothern part of Honshu, and negative in the neighborhood of Kakioka as may be expected from the distribution of W_i in Fig. 9. But since the magnitude of the internal part of ΔX_m are generally small compared with that of the external part, detailed distribution of ΔX_m would not seriously influence the distribution of $\Delta Z/\Delta H$.

Thus the statistical aspect of $\Delta Z/\Delta H$ could, to a fair degree of approximation, be explained by taking into account the peculiar characteristics of the distribution of W_i and ΔZ_i in the neighborhood of Japan.

5. Two types of anomalous-behavior of ΔZ.

As is well known, the opposition of sign of ΔZ in case of SC has been observable at relatively near observatories, for example Greenwich and Paris[7]. According to N. F. Barber[8], some electric currents flowing through the English channel could be observed on the occasion of SC, the currents being so intense that the reversal of sign of ΔZ on both sides of the channel may be explained by the magnetic field produced by these currents. Hence the distribution of land and sea would sometimes play an important role for changes in geomagnetic field, especially in its Z-component.

In the 2nd report of this study, the writers also found out that the sign of ΔZ at the British observatories such as Lerwick and Eskdalemuir were negative while those at other observatories in Western Europe were generally positive. At the time of the change at $5h$ $50m$, however, ΔZ shows the same sign in both regions as may be seen in Fig. 12 in which ΔZ observed at observatories in Europe is plotted according to the geomagnetic latitude except at those situated in high latitude, ΔZ of SC being also shown there in the same manner.

Looking at the figures, we can see that ΔZ for the $5h$ $50m$ change

7) S. CHAPMAN and J. BARTELS, *Geomagnetism* Vol. I, p. 297.
8) N. F. BARBER, *M. N. R. A. S. Geophys. Suppl.*, **5** (1948), 258.

increases fairly regularly to the north while ΔZ for the SC is scattered widely around zero line. Taking into consideration the fact that SC changes much faster than another ones, we suspect some local characteristics which are sensitive to rapid changes in the earth's magnetic field. However, the characteristics do not seem to be observable in case of magnetic change with a duration time of an hour or so.

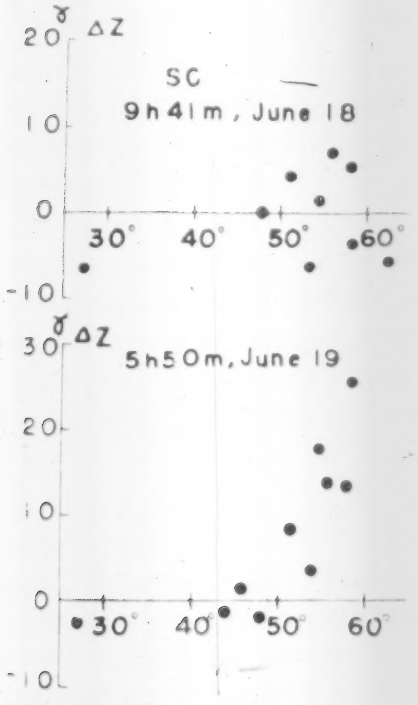

Fig. 12. The distribution of ΔZ arranged according to geomagnetic latitude in Europe. The upper figure corresponds to the SC at $9h\ 41m$, June 18 and the lower one to the variation at $5h\ 50m$ GMT, June 19, 1936.

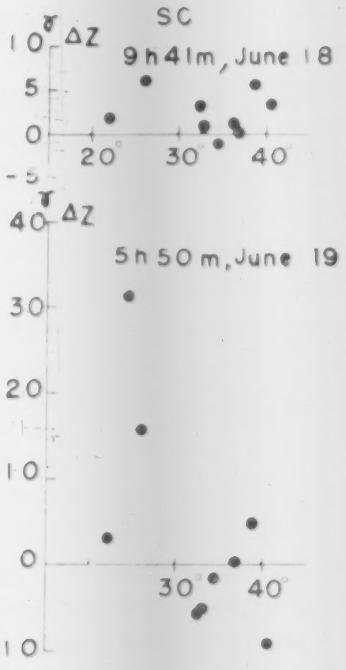

Fig. 13. The distribution of ΔZ arranged according to geomagnetic latitude in Japan and her vicinity. The upper figure corresponds to the SC at $9h\ 41m$, June 18 and the lower one to the variation at $5h\ 50m$, GMT, June 19, 1936.

Turning now to ΔZ in Japan and her vicinity, the distribution is shown in Fig. 13 for both changes. Although it will be rather difficult to deduce a clear conclusion from the figure because of the smallness of amplitude in the northern part, we can see large amplitude of ΔZ at Kakioka and the reverse of sign at Wakkanai for both variations. In addition to this fact, it has been clarified by the statistical examinations that $\Delta Z/\Delta H$ at these observatories generally show an almost constant value whatever the observed changes may be. Hence we may roughly conclude that the local characteristics for ΔZ in Japan and her vicinity will be the same for any changes so far as the geomagnetic variations

having period or duration time shorter than 2 or 3 *hours* are concerned.

Thus we may classify the local characteristics of geomagnetic changes into the next two types.

i) Sensitive to only rapid changes such as SC, but not observable in case of bay or polar magnetic storm. Examples found in Western Europe.

ii) Observable in all changes, rapid or slow. Examples found in Japan and her vicinity.

6. Conclusions.

By analyzing the remarkable geomagnetic change that occurred at $5h\ 50m$ GMT, June 19, 1936 on the basis of the observations at 44 observatories all over the earth, the writers can abstract the anomalous distribution of magnetic potential for that change as well as that of Z-component, both originating within the earth, in Japan. And it is made clear that this anomaly can not be explained by the usual theory of electromagnetic induction within a homogeneous earth. In the writers' previous analysis of the SC with which the magnetic storm treated here commenced, the anomalous behavior was not so clear partly because of its smallness in amplitude. Since the anomaly seems to be caused by the internal origin part of the change, we suspect some peculiar conditions or distributions of electric property under Japan. The writers are going to study those conditions in the forthcoming papers.

Although we can not yet explain the cause or origin of the characteristics of short-period geomagnetic variations in Japan, a phenomenological explanation is successfully made concerning the statistical behavior of $\Delta Z/\Delta H$ which was examined in the 3rd report. It is also found out that the well known opposition of sign of ΔZ at British observatories and at others in Western Europe can be observed only in case of SC, while the distribution of ΔZ in Europe appear to be fairly regular for slower variations. Meanwhile the anomalous behavior in Japan shows the same tendency in all variations. With these facts in mind, the writers imagine that there are at least two types in anomalous behavior in geomagnetic variations, the first which is sensitive to rapid changes may be due to some superficial effects such as the influence of sea while the second which responds to all variations may be rather intrinsic related with the underground structure.

7. Acknowledgement.

The present study was done with many copies of magnetograms which were sent to the writers from many observatories at the writers' request. The writers are very much grateful to the next persons who cooperated kindly with them :

Dr. M. Ôta, Kyoto University, Japan.
Dr. S. Imamiti, Kakioka Magnetic Observatory, Japan.
Prof. E. Selzer, Institut de Physique du Globe, Université de Paris, France.
Dr. A. M. van Wijk, Hermanus Magnetic Observatory, S. A.
Dr. E. Tönsberg, Nordlyobservatoriet, Tromsö, Norway.
Mr. L. S. Prior, Watheroo Magnetic Observatory, Western Australia.
Dr. J. C. Morais, Instituto Geofisico da Universidade de Coimbra, Portugal.
Dr. Nils Ambolt, Kungl. Sjökarteverket, Stockholm, Sweden.
Dr. Robert Wilkox, U. S. Coast and Geodetic Survey, U. S. A.
Dr. Paul G. Ledig, San Juan Magnetic Observatory, Puerto Rico.
Der Direktor, Zentralanstalt für Meteorologie und Geodynamik, Wien, Austria.
Dr. Olaf Litzow-Holm, Observatorio Geofisico, Pilar, Argentina.
Dr. Helge Petersen, Det Danske Meteorologiske Institut, Köbenhavn Denmark.
Dr. M. Doporto, Meteorological Service, Dublin, Ireland.
Prof. Dr. J. J. M. Reesinck, Meteorological and Geophysical Service, Djakarta, Indonesia.
Dr. J. Veldkamp, Koninklijk Nederlands Meteorologisch Institut, De Bilt, Netherlands.
Dr. S. L. Malurkar, Colaba and Alibag Observatories, India.
Dr. Rosendo Octavio Sandoval, Instituto de Geofisica, Mexico.
Dr. Ricard Monges López, Instituto de Geofisica, Mexico.
The Superintendent, Eskdalemuir Magnetic Observatory, Scotland.
Dr. J. Oriol Cardús, Observatorio del Ebro, Spain.
Dr. Wenceslao Benítez, Instituto y Observatorio de Marina, San Fernando, Spain
Dr. R. F. Thyer, Bureau of Mineral Resources, Melbourne, Australia.
Prof. H. Amorim Ferreia, Servico Meteorológico Nacional, Portugal.
Dr. H. F. Baird, Amberley Magnetic Observotory, New Zealand.
The Director General, Royal Observatory, Helwan, Egypt.
Dr. M. M. Gill, Apia Magnetic Observatory, Western Samoa.
Dr. Johannes Olsen, Det Danske Meteorologiske Institut, Köbenhavn, Denmark.
Mr. B. L. Gulatee, Geodetic and Training Circle, Dehra Dun, India.
Mr. A. A. Giesecke, Jr., Instituto Geofisico de Huancayo, Peru.
Dr. Eero Kataja, Sodankylä Magnetic Observatory, Finland.

The writers are also grateful to Professor T. Nagata for his helpful discussions in the course of the study.

Note added on April 20 : The data from Sodankylä Magnetic Observatory became available after the preparation of the manuscript. Though the current arrow or the values of the three components were added in the figure or table, the aspect of the variation observed there will be

shown in figure 14.

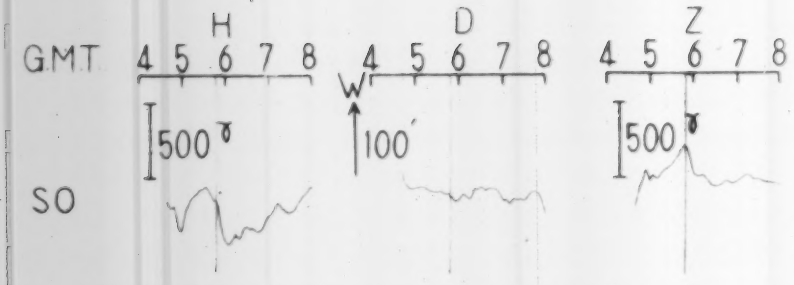

Fig. 14. The changes observed at Sodankyla.

10. 日本に於ける地磁気短周期変化の異常と地下構造 第4報

地震研究所 { 力武常次 / 横山泉 / 菱山よね子 }

1936年6月19日5時50分 GMT に起ったいちじるしい地磁気変化の世界的観測結果を解析した．その方法は第2報の SC の解析と同様である．その結果地球内部に原因をもつ部分は日本中部に於いて異常な分布を示すことがわかった．この分布は通常の電磁感応の考によっては説明が困難である．

またこの結果を利用して，第3報に統計的に示した地磁気変化の際の $\Delta Z/\Delta H$ の日本に於ける異常分布を都合よく説明出来る．これは現象論的解釈に過ぎないが，本州の日本海沿岸および北海道に於ては ΔZ の外部磁場と内部磁場の大きさがほゞ匹敵するので ΔZ の値は結局に於て小さい．

ところが関東地方，中部地方に於いては内部磁場はいちじるしく大きい正の値をとるので，外部磁場を打消してさらに全体の ΔZ が正の大きい値をとることになる．このような傾向がいつでもほゞ成立つとすると，第3報で述べた $\Delta Z/\Delta H$ の分布が解釈出来る．

この時の変化の ΔZ がイギリスをも含めて西部ヨーロッパできわめて規則的な分布をしていることは注目しなければならない．第2報の SC の ΔZ はこの地方に於てはいちじるしくばらついていて，イギリスと大陸とでは符号が相反している．一方日本に於てはどちらの変化も柿岡に於ては大きな ΔZ を示し，雅内に於ける符号の反転も共通である．これらのことから地磁気変化の異常に2種が考えられ，その一つはヨーロッパに見られるように SC のようにはやい変化に対して敏感であって，おそらく海陸分布のような比較的地球表面の事情によるのではないかと思われる．これに反して日本に見られる異常は両方の変化に見られ，むしろ SC よりもおそい変化によくあらわれるから，地下構造に関連したより本質的なものであろうと推察される．

いずれにしても，このような異常が地磁気変化に伴つて起る原因については未だ全く不明である．

11. *The Anomalous Behavior of Geomagnetic Variations of Short Period in Japan and Its Relation to the Subterranean Structure. The 5th report.*

By Tsuneji RIKITAKE, Izumi YOKOYAMA and Yoneko HISHIYAMA,

Earthquake Research Institute.

(Read March 17, 1953.—Received March 20, 1953.)

1. Introduction.

The writers have investigated the anomalous behavior of short-period geomagnetic variations in Japan through geomagnetic observations carried out by the writers themselves and with the aid of world-wide geomagnetic data. According to the detailed examination based on the theory of potential which were already published in this Bulltein[1),2),3),4)], it became clear that the anomalous behavior of geomagnetic variations could be ascribed to the magnetic field originating within the earth and that the distributions of the magnetic field which originated outside the earth were fairly regular in all variations already analyzed. The curious mode of distribution of the internal origin part seems to be concentrated near the central part of Japan. Though geomagnetic data necessary for a more detailed analysis seem to be still insufficient, the writers intend to study the cause or origin of the abnormal internal origin part as minutely as they can.

2. Abstraction of the anomaly.

The geomagnetic variation that occurred at $5^h\ 50^m$ GMT, June 19, 1936 is the most appropriate for studying the anomalous behavior because of the well-distributed observatories as mentioned in the preliminary[1)] and 4th[1)] reports. The external and internal parts of magnetic potential

1) T. RIKITAKE, I. YOKOYAMA and Y. HISHIYAMA, *Bull. Earthq. Res. Inst.*, **30** (1952), 207.
2) T. RIKITAKE, I. YOKOYAMA and Y. HISHIYAMA, *Bull. Earthq. Res. Inst.*, **31** (1953), 19.
3) T. RIKITAKE, I. YOKOYAMA and Y. HISHIYAMA, *Bull. Earthq. Res. Inst.*, **31** (1953), 89.
4) T. RIKITAKE, I. YOKOYAMA and Y. HISHIYAMA, *Bull. Earthq. Res. Inst.*, **31** (1953), 101.

and Z-component were given in Table II and Figs. 8, 9, 10 and 11 of the 4th report. As is well known, however, a geomagnetic variation ordinarily contains the part caused by the electric currents mainly flowing in the conducting core, the depth of its upper surface being estimated at about 400 km. The existence of such a core is well confirmed through the electromagnetic induction theory studied by S. Chapman[5], A. T. Price[6], B. N. Lahiri[7] and one of the present writers (T. R.)[8),9),10),11),12),13)]. Those studies dealt with the analyses of geomagnetic variation of a world-wide scale. In order to examine the anomalous behavior which is confined within such a narrow area as Japan, the internal origin part due to the general field which originated in the said conducting region should be eliminated. Strictly speaking, such elimination is not possible because of the electromagnetic coupling between the fields in the conducting core and in the anomalous region. But the writers will neglect the coupling for the first approximation.

As has been studied by one of the writers[9], the distribution of the potential of the disturbance field in low and middle latitude may be expressed approximately by $Q_i^1(\cos\theta)\frac{\cos}{\sin}\phi$ for bay-type disturbances and polar magnetic storms, θ and ϕ denoting respectively the geomagnetic co-latitude and longitude. From the distribution of the potential and Z-component this expression seems to be adequate for the present variation. By means of the least square method the coefficient of the potential of the external origin part is computed at $14a$ γcm (a : earth's radius) which fits both W_e and ΔZ_e. Adopting this value, the normal internal part of both potential ($W_{i,n}$) and Z-component ($\Delta Z_{i,n}$) are calculated by the relation

$$W_{i,n}=\frac{q^3}{2}W_e \qquad (q=0.94)$$

which is derived from the theory of electromagnetic induction within the uniform core model of the earth described above, the phase difference

5) S. CHAPMAN, *Phil. Trans. Roy. Soc. London A*, **218** (1919), 1.
6) S. CHAPMAN and A. T. PRICE, *Phil. Trans. Roy. Soc. London A*, **229** (1930), 427.
7) B. N. LAHIRI and A. T. PRICE, *Phil. Trans. Roy. Soc. London A*, **237** (1939), 509.
8) T. RIKITAKE, *Trans. Oslo Meeting I. U. G. G. A. T. M. E.*, (1950), 435.
9) T. RIKITAKE, *Bull. Earthq. Res. Inst.*, **28** (1950), 45.
10) T. RIKITAKE, *Bull. Earthq. Res. Inst.*, **28** (1950), 219.
11) T. RIKITAKE, *Bull. Earthq. Res. Inst.*, **28** (1950), 263.
12) T. RIKITAKE, *Bull. Earthq. Res. Inst.*, **29** (1951), 61.
13) T. RIKITAKE, *Bull. Earthq. Res. Inst.*, **29** (1951), 539.

between both parts being neglected for short-period variation. The results are given in Table I for respective stations together with the differences $\delta W_i = W_i - W_{i,n}$ and $\delta Z_i = \Delta Z_i - \Delta Z_{i,n}$ which are considered to correspond to the anomaly in question.

Table I.

Station	$W_{i,n}$	δW_i	$\Delta Z_{i,n}$	δZ_i
HM	-8.4γ	-1.0γ	17γ	-3γ
TM	−7.9	−2.2	16	8
TY	−7.6	−1.4	15	4
WK	−7.0	−1.7	14	2
HS	−6.7	−0.4	13	1
IW	−6.6	−0.8	13	−1
KA	−5.5	−0.3	11	17
SH	−5.0	−2.1	10	32
AS	−4.5	−1.1	9	4

(The values of potential should be multiplied by a.)

δW_i and δZ_i are also shown in Figs. 1 and 2 in which we can see that the distribution on a large scale vanishes and the anomalous circular contours around the central part of Japan become very remarkable. Though the normal internal part is eliminated for convenience's sake, we may discuss the origin of the anomalous behavior on the basis of the distribution obtained here. The geomagnetic north ($\delta X_{m,i}$) and east ($\delta Y_{m,i}$) components are also obtained by differentiating δW_i to the respec-

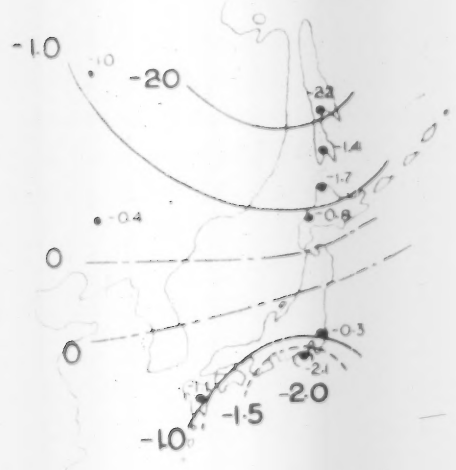

Fig. 1. The distribution of the internal part of the magnetic potential which corresponds to the anomaly in Japan. The unit is *gamma* multiplied by the earth's radius.

Fig. 2. The distribution of the internal part of ΔZ which corresponds to the anomaly in Japan. The unit is *gamma*.

tive directions. They are shown in Figs. 3 and 4.

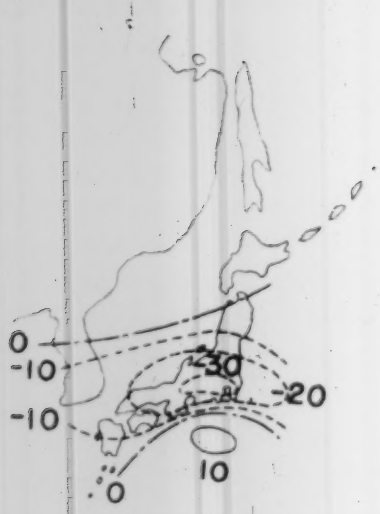

Fig. 3. The distribution of $\delta X_{m,i}$. The unit is *gamma*.

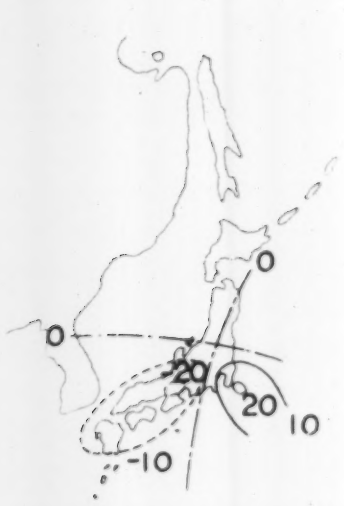

Fig. 4. The distribution of $\delta Y_{m,i}$. The unit is *gamma*.

3. Magnetic dipole corresponding to the anomaly.

Looking at the figures of the anomalous field thus abstracted, it will be easily imagined that an apparent magnetization of particular distribution occurs beneath Japan. The main part of the apparent magnetization seems capable of explanation by assuming a hypothetical magnetic dipole in the earth as one can see from the distribution of the magnetic field which is shown in Figs. 2, 3 and 4.

The writers would here like to determine the position, direction and intensity of that dipole following the method introduced by one of the writers[14),15)]. According to this method, we can obtain the position, direction and intensity of an underground dipole directly from the corresponding magnetic anomaly on the earth's surface. The method has dealt with the anomaly in Z-component and inclination. If we know the anomaly in all the three components of geomagnetic field, the method can be written in a more convenient form. The writers will give the revised method based on the knowledge of three components in the following.

Let us consider a sphere which is large enough to contain the entire magnetic matter in question. Denoting the radius of the sphere by R

14) T. RIKITAKE, *Journ. Geomag. Geoelectr.*, **2** (1950), 20.
15) T. RIKITAKE, *Journ. Geomag. Geoelectr.*, **2** (1950), 25.

the magnetic potential can be expressed as

$$W=R\sum_n\sum_m(R/r)^{n+1}P_{nm}(\cos\theta)(a_n^m\cos m\phi+b_n^m\sin m\phi)(r>R)\,, \quad (1)$$

where P_{nm} denotes Neumann's spherical surface harmonics. Taking the Cartesian coordinates of which the origin coincides with the centre of the sphere, $\theta=0$ axis agreeing with z axis, and using the relations

$$\left.\begin{aligned} r^{-n-1}P_{nm}\cos m\phi&=\frac{(-i)^m n!}{2\pi(n-m)!}\int_{-\pi}^{\pi}(z+ix\cos u+iy\sin u)^{-n-1}\cos mu\,du\,,\\ r^{-n-1}P_{nm}\sin m\phi&=\frac{(-i)^m n!}{2\pi(n-m)!}\int_{-\pi}^{\pi}(z+ix\cos u+iy\sin u)^{-n-1}\sin mu\,du\,, \end{aligned}\right\} \quad \ldots\ldots(2)$$

the typical term of (1) can be written as

$$W_n^m=\frac{(-i)^m}{2\pi}\frac{n!}{(n-m)!}R^{n+2}\int_{-\pi}^{\pi}(z+ix\cos u+iy\sin u)^{-n-1}(a_n^m\cos mu+b_n^m\sin mu)du\,. \quad \ldots\ldots(3)$$

By differentiating repeatedly with respect to x, y and z, the partial derivatives of X, Y and Z (downward positive) components of the magnetic field at $x=y=0$ are expressed as

$$\left.\begin{aligned} \frac{\partial^j X_{00}}{\partial x^{j-k}\partial y^k}&=\frac{1}{2\pi}\sum\sum(-i)^{m+j-1}\frac{(n+j+1)!}{(n-m)!}R^{n+2}Z^{-n-j-2}(a_n^m p_{jk}^m+b_n^m q_{jk}^m)\,,\\ \frac{\partial^j Y_{00}}{\partial x^{j-k}\partial y^k}&=\frac{1}{2\pi}\sum\sum(-i)^{m+j+1}\frac{(n+j+1)!}{(n-m)!}R^{n+2}Z^{-n-j-2}(a_n^m r_{jk}^m+b_n^m s_{jk}^m)\,,\\ \frac{\partial^j Z_{00}}{\partial x^{j-k}\partial y^k}&=\frac{1}{2\pi}\sum\sum(-i)^{m+j}\frac{(n+j+1)!}{(n-m)!}R^{n+2}Z^{-n-j-2}(a_n^m f_{jk}^m+b_n^m g_{jk}^m)\,, \end{aligned}\right\} \quad \ldots\ldots(4)$$

where

$$\left.\begin{aligned} \left.\begin{matrix} f_{jk}^m\\ g_{jk}^m \end{matrix}\right\}&=\int_{-\pi}^{\pi}\cos^{j-k}u\sin^k u\left.\begin{matrix}\cos\\ \sin\end{matrix}\right.mu\,du\,,\\ \left.\begin{matrix} p_{jk}^m\\ q_{jk}^m \end{matrix}\right\}&=\int_{-\pi}^{\pi}\cos^{j-k+1}u\sin^k u\left.\begin{matrix}\cos\\ \sin\end{matrix}\right.mu\,du\,,\\ \left.\begin{matrix} r_{jk}^m\\ s_{jk}^m \end{matrix}\right\}&=\int_{-\pi}^{\pi}\cos^{j-k}u\sin^{k+1}u\left.\begin{matrix}\cos\\ \sin\end{matrix}\right.mu\,du\,. \end{aligned}\right\} \quad \ldots\ldots(5)$$

f, g, p, q, r and s for $m\leqq 3$ and j, $k\leqq 2$ are calculated as given in Table II.

On the other hand, we can obtain $\dfrac{\partial^j X_{00}}{\partial x^{j-k}\partial y^k}$, $\dfrac{\partial^j Y_{00}}{\partial x^{j-k}\partial y^k}$ and

Table II.

f \ m	0	1	2	3
$f_{00}{}^m$	2π	0	0	0
$f_{10}{}^m$	0	π	0	0
$f_{11}{}^m$	0	0	0	0
$f_{20}{}^m$	π	0	$\frac{\pi}{2}$	0
$f_{21}{}^m$	0	0	0	0
$f_{22}{}^m$	π	0	$-\frac{\pi}{2}$	0

g \ m	0	1	2	3
$g_{00}{}^m$	0	0	0	0
$g_{10}{}^m$	0	0	0	0
$g_{11}{}^m$	0	π	0	0
$g_{20}{}^m$	0	0	0	0
$g_{21}{}^m$	0	0	$\frac{\pi}{2}$	0
$g_{22}{}^m$	0	0	0	0

p \ m	0	1	2	3
$p_{00}{}^m$	0	π	0	0
$p_{10}{}^m$	π	0	$\frac{\pi}{2}$	0
$p_{11}{}^m$	0	0	0	0
$p_{20}{}^m$	0	$\frac{3}{4}\pi$	0	$\frac{\pi}{4}$
$p_{21}{}^m$	0	0	0	0
$p_{22}{}^m$	0	$\frac{\pi}{4}$	0	$-\frac{\pi}{4}$

q \ m	0	1	2	3
$q_{00}{}^m$	0	0	0	0
$q_{10}{}^m$	0	0	0	0
$q_{11}{}^m$	0	0	$\frac{\pi}{2}$	0
$q_{20}{}^m$	0	0	0	0
$q_{21}{}^m$	0	$\frac{\pi}{4}$	0	$\frac{\pi}{4}$
$q_{22}{}^m$	0	0	0	0

r \ m	0	1	2	3
$r_{00}{}^m$	0	0	0	0
$r_{10}{}^m$	0	0	0	0
$r_{11}{}^m$	π	0	$-\frac{\pi}{2}$	0
$r_{20}{}^m$	0	0	0	0
$r_{21}{}^m$	0	$\frac{\pi}{4}$	0	$-\frac{\pi}{4}$
$r_{22}{}^m$	0	0	0	0

s \ m	0	1	2	3
$s_{00}{}^m$	0	π	0	0
$s_{10}{}^m$	0	0	$\frac{\pi}{2}$	0
$s_{11}{}^m$	0	0	0	0
$s_{20}{}^m$	0	$\frac{\pi}{4}$	0	$\frac{\pi}{4}$
$s_{21}{}^m$	0	0	0	0
$s_{22}{}^m$	0	$\frac{3}{4}\pi$	0	$-\frac{\pi}{4}$

$\frac{\partial^j Z_{00}}{\partial x^{j-k}\partial y^k}$ from the observation, *i.e.* the observed distribution of the anomaly can be expressed as

$$\left.\begin{aligned} X &= \sum_j \sum_k \binom{j}{k} \frac{\partial^j X_{00}}{\partial x^{j-k}\partial y^k} x^{j-k} y^k , \\ Y &= \sum_j \sum_k \binom{j}{k} \frac{\partial^j Y_{00}}{\partial x^{j-k}\partial y^k} x^{j-k} y^k , \\ Z &= \sum_j \sum_k \binom{j}{k} \frac{\partial^j Z_{00}}{\partial x^{j-k}\partial y^k} x^{j-k} y^k . \end{aligned}\right\} \quad \cdots\cdots(6)$$

In case of j, $k \leqq 2$ and $n \leqq 3$, (4) gives the next relations :

$$
\left.\begin{aligned}
&2a_2^0+3a_2^0+4a_3^0=Z_{00}\ ,\\
&3a_1^1+4\sqrt{3}\,a_2^1+5\sqrt{6}\,a_3^1=R\partial Z_{00}/\partial x\ ,\\
&3b_1^1+4\sqrt{3}\,b_2^1+5\sqrt{6}\,b_3^1=R\partial Z_{00}/\partial y\ ,\\
&12a_1^0+30a_2^0-5\sqrt{3}\,a_2^2+60a_3^0-6\sqrt{15}a_3^2=-R^2\partial^2 Z_{00}/\partial x^2\ ,\\
&-5\sqrt{3}\,b_2^2-6\sqrt{15}b_3^2=-R^2\partial^2 Z_{00}/\partial x\partial y\ ,\\
&12a_1^0+30a_2^0+5\sqrt{3}\,a_2^2+60a_3^0+6\sqrt{15}a_3^2=-R^2\partial^2 Z_{00}/\partial y^2\ ,\\
&-a_1^1-\sqrt{3}\,a_2^1-\sqrt{6}\,a_3^1=X_{00}\ ,\\
&-3a_1^0-6a_2^0+\sqrt{3}\,a_2^2-10a_3^0+\sqrt{15}a_3^2=-R\partial X_{00}/\partial x\ ,\\
&\sqrt{3}\,b_2^2+\sqrt{15}b_3^2=-R\partial X_{00}/\partial y\ ,\\
&9a_1^1+15\sqrt{3}\,a_2^1-45/2\cdot\sqrt{6}\,a_3^1-3/2\cdot\sqrt{10}a_3^3=R^2\partial^2 X_{00}/\partial x^2\ ,\\
&3b_1^1+5\sqrt{3}\,b_2^1+15/2\cdot\sqrt{6}\,b_3^1-3/2\cdot\sqrt{10}b_3^3=R^2\partial^2 X_{00}/\partial x\partial y\ ,\\
&3a_1^1+5\sqrt{3}\,a_2^1+15/2\cdot\sqrt{6}\,a_3^1+3/2\cdot\sqrt{10}a_3^3=R^2\partial^2 X_{00}/\partial y^2\ ,\\
&-b_1^1-\sqrt{3}\,b_2^1-\sqrt{6}\,b_3^1=Y_{00}\ ,\\
&-3a_1^0-6a_2^0-\sqrt{3}\,a_2^2-10a_3^0-\sqrt{15}a_3^2=-R\partial Y_{00}/\partial y\ ,\\
&9b_1^1+15\sqrt{3}\,b_2^1+45/2\cdot\sqrt{6}\,b_3^1+3/2\cdot\sqrt{10}b_3^3=R^2\partial^2 Y_{00}/\partial y^2\ ,
\end{aligned}\right\}\qquad(7)
$$

where the identities

$$\partial Y_{00}/\partial x=\partial X_{00}/\partial y\ ,\qquad \partial^2 Y_{00}/\partial x^2=\partial^2 X_{00}/\partial x\partial y\ ,\qquad \partial^2 Y_{00}/\partial x\partial y=\partial^2 X_{00}/\partial y^2$$

are taken into consideration.

In obtaining (7), it is assumed that $z=-R$. a_1^0, a_1^1, b_1^1, ... are taken so as to correspond to Schmidt's spherical surface harmonics instead of Neumann's.

Solving the simultaneous equations which are composed of 15 equations containing unknown coefficients of the same number, we have the coefficients a_1^0, a_1^1, b_1^1, ... in terms of quadratic expressions of R. Then R is determined so as to minimize $(a_2^0)^2+(a_2^1)^2+(b_2^1)^2+(a_2^2)^2+(b_2^2)^2+(a_3^0)^2+\cdots\cdots$. After that the position of the magnetic centre or of the dipole is determined according to the well-known procedure followed with respect to the eccentric dipole for the earth's main magnetic field[16),17)]. As will be

16) Ad. Schmidt, *Gerl. Beitr. z. Geophys.*, **41** (1934), 346.

17) J. Bartels, *Terr. Mag.*, **41** (1936), 225.

Fig. 5. The position and the direction of the hypothetical magnetic dipole that corresponds to the anomaly of geomagnetic variation in Japan.

shown in a simple test[18], the method is applicable to an actual analysis.

In order to apply the above-mentioned method to the present problem, ΔX_m, ΔY_m, and ΔZ as shown in Figs. 3, 4 and 2 are respectively expressed with expressions such as $\Delta X_m = A + Bx + Cy + Dx^2 + Exy + Fy^2$ by means of the least square method where the origin was suitably chosen near the centre of the anomaly.

The determined depth of the apparent dipole amounts to 150 km and its position and direction are shown in Fig. 5, while its dip is computed at 20° and the magnetic moment becomes 8.6×10^{25} emu. As for the second and third degree coefficients, their numerical values can be easily calculated. However, when the degree of accuracy of the distribution of the magnetic field is taken into account, it would be of little worth to discuss the higher terms.

4. Discussions and conclusions.

It is made clear that a particular distribution of geomagnetic field occurs in Japan accompanying the disturbance in the earth's magnetic field, the character of that anomaly being plausibly interpreted by assuming a hypothetical dipole situated under the central part of Japan. It must be noted that the anomalous behavior in the geomagnetic variation

18) If we consider a dipole of unit intensity which is buried at a depth of D and has a downward direction, we have

$$Z_{00} = \frac{2}{D^3}, \quad \partial^2 Z_{00}/\partial x^2 = -\frac{12}{D^5}, \quad \partial^2 Z_{00}/\partial y^2 = -\frac{12}{D^5}, \quad \partial X_{00}/\partial x = \frac{3}{D^4}, \quad \partial Y_{00}/\partial y = \frac{3}{D^4},$$

while all of the other derivatives are zero. In that case, it becomes

$$a_1^0 = \frac{1}{D^3}\left(6\frac{R^2}{D^2} - 15\frac{R}{D} + 10\right),$$

$$a_2^0 = -\frac{2}{D^3}\left(4\frac{R^2}{D^2} - 9\frac{R}{D} + 5\right),$$

$$a_3^0 = \frac{3}{D^3}\left(\frac{R^2}{D^2} - 2\frac{R}{D} + 1\right).$$

Hence we should take $R = D$ in order to minimize the second and third degree constituents of the potential. For $R = D$, we get $a_1^0 = 1/D^3$, $a_2^0 = a_3^0 = 0$, from these coefficients we know that the dipole has unit intensity and a downward direction.

in Japan can be explained fairly well from this assumption of a localized source. However, we can say nothing about the mechanism of generation of such an apparent dipole. It will be impossible to explain the direction of the apparent magnetization by usual theory, for instance by electromagnetic induction within a conducting sphere.

Though the writers can not clarify the phenomena at the present stage of investigation, they think that the anomalous behavior in geomagnetic variations in Japan should be investigated in more detail in the future. It seems to be not only an interesting problem in the study of geomagnetism but also to be connected with the underground structure of Japan which is one of the most seismically active countries in the world.

11. 日本に於ける地磁気短周期変化の異常と地下構造
第 5 報

地震研究所　力武常次・横山泉・菱山よね子

第1～4報に於て，日本に於ける地磁気短周期変化の異常が，主として日本中部に集中した地球内部に起因する磁場によることが明らかになった。この内部磁場をより詳細に調べるために，第4報の解析結果にさらに吟味を加えた．従来の研究によって確立されている地球内部の電気的性質を考慮することによって，内部磁場から地下 400 *km* 以下の導電的部分内の感応電流に起因する磁場を差引くことが出来る．その残りが一応日本の地下に存在する異常によるものと考えることが許されるであろう．このようにして取出された残留内部磁場は極めて簡単な分布様式をとし，地下の適当な処に磁気双極子を考えることにより説明が出来るように思われる．地表に於ける磁場分布より地下の磁気中心を直接求める力武の方法を改良して，地磁気三成分の分布が与えられている場合の方法を新しく考案し，現在の問題に応用したところ，日本中部の地下 150 *km* にほゞ北向きの双極子を考えればよいことになった．この双極子の偏向は 20° ということになる．

しかし何故このような双極子で表現されるような異常磁場が地磁気変化に伴って発生するかは明らかでない．その見かけの帯磁方向は通常の電磁感応の理論をもってしては理解に苦しむ．ともあれ，日本に於ける地磁気変化の異常がこのような集中的モデルによってあらわされることは注目すべきことであろう．

この電磁気学的研究によって明らかにされた地下の特殊条件と他の地球物理学的現象との関連を究明することは，日本の地下構造を論ずる上に極めて重要なことゝ思われる．

12. *Geological Investigations on the Zaō Volcanoes.* *II Aoso Volcano.*

By Takeshi ICHIMURA,

Earthquake Research Institute.

(Read December 16, 1952.—Received January 20, 1953.)

Introduction.

The Aoso volcano[1] is included in the Zaō volcanic group and rises at the eastern end of the South Zaō. It is a small composite volcano isolated from the main part of the Zaō volcanoes, being bordered by the Akiyama-zawa, Matsu-kawa and Kosute-gawa. This volcano rests upon the Tertiary formation and is composed of Aoso-yama (799.9 m.),[2] Ōmori-yama (800 m.), Takokura-yama (666.1 m.), Tōmori-yama (564 m.), etc. It is now dissected deeply by Akamatsu-zawa, Dō-zawa, Onashi-zawa, Namin-zawa, Taiko-zawa and Itahashi-zawa. The structure of the Aoso volcano is greatly complicated by its successive eruption, as can be seen along these valleys.

One of the remarkable features observed here is the occurrence of dacite flow[3] which is entirely lacking in other parts of the Zaō volcanoes. It forms central cones represented by Aoso-yama and Ōmori-yama, and its eruption seems to have been investigated by the writer since the autumn of 1947. They are summarized in this paper, with a brief description of lavas and ejecta.

Location.

The Aoso volcano (Figs. 1, 2, 3) is situated near the northern corner of Katta-gun, Miyagi Prefecture. It is easy of access from Shiroishi or Ōgawara of the Tōhoku Railway Line, since there is a bus road between these towns and Aone, going round the eastern or northern periphery of this volcano. The summit of Aoso-yama is accessible from such villages Miya, Teppō-chō, Magatake, Nagano, Kotsumazaka, Tōgatta and Kitahara.

1) The Aoso volcano was formerly named "Ōgatta volcano" (A. TAKADA, The Zaō Volcanoes, *M. S.*, 1922).

2) Aoso-yama was once called "Ōgatta-dake" (B. KOTŌ, *Jour. Geol. Soc. Japan*, **23** (1926), 34).

3) The eruption of dacite flows is also known in the final activity of the Kurikoma volcanoes and Osore-yama volcanoes which belong to the Nasu volcanic zone.

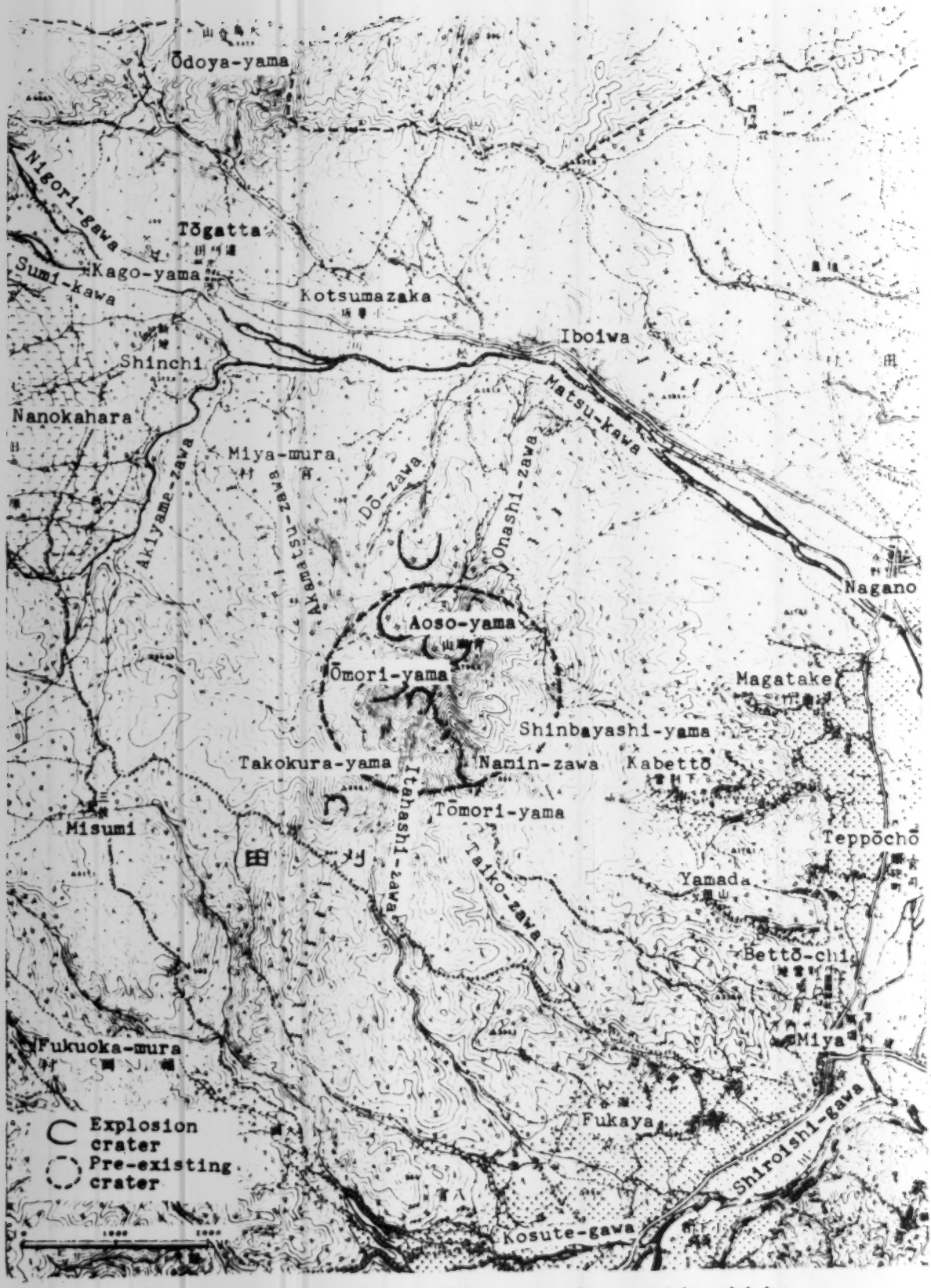

Fig. 1. Topographical map of the Aoso volcano and its vicinity.

Geological Features of Aoso Volcano and Its Adjacent Area.

Besides lavas and ejecta of the Aoso volcano, the area under consideration is composed of Tertiary sediments, agglomerate, andesite, felsite (?) and basalt as well as of Quaternary fluviatile deposits. There is, however, no exposure of granite which can commonly be seen in other parts of the Zaō volcanoes. The Tertiary formation exposed here consists mostly of shale, sandstone and green tuff, but it is represented by alternate beds of sand, clay and gravel in some places. The Aoso volcano rests upon the eroded surface of these Tertiary sediments (Figs. 2, 3).

(1) Shale, sandstone and green tuff beds: In Aoso volcanic area, important base rock are shale, sandstone and green tuff. They are extensively exposed on the hills extending northwards or eastwards from this volcano.

Characteristic exposures of shale and sandstone beds can be seen near Miya and Magatake as well as Tōgatta. In the former case, the eastern extension of shale and sandstone beds disappears beneath the accumulation of volcanic detritus. These beds change their strike and dip from place to place. The shale bed of Tōgatta has a strike of N 70° E to N 80° E and a dip of 5° to 10° N, whereas the shale and sandstone bed exposed near Magatake and Miya indicate respectively a strike of N 20° E or N 10° W to N 45° W and a dip of 70° to 80° ESE or 13° WSW and 10° to 40° NE.

Green tuff is the commonest rock in the area including Tōgatta and Kotsumazaka. Generally, it has a light green color which grades into greyish white in weathered specimens.

The writer has not yet found any fossil in these shale, sandstone and green tuff beds, but they have some lithological similarities to those which has been assigned hitherto to the Miocene in the neighboring districts.

(2) Clay, sand and gravel beds: The horizontal beds of clay, sand and gravel are exposed on the cliff which extends from east to west along the southern side of the Akiyama-zawa and Matsu-kawa. Of these, the gravel bed contains such pebbles as granite, propylite, andesite, etc. The almost flat surface of these beds is covered by mud flows, pumice layers and lava flows. The field evidence suggests that they have not been subjected to any strong disturbance since their deposition, and the distribution is restricted to a small extent. Most of them are, furthermore, represented by very loose sediments without any fossil. They are probably Pliocene sediments (Fig. 4).

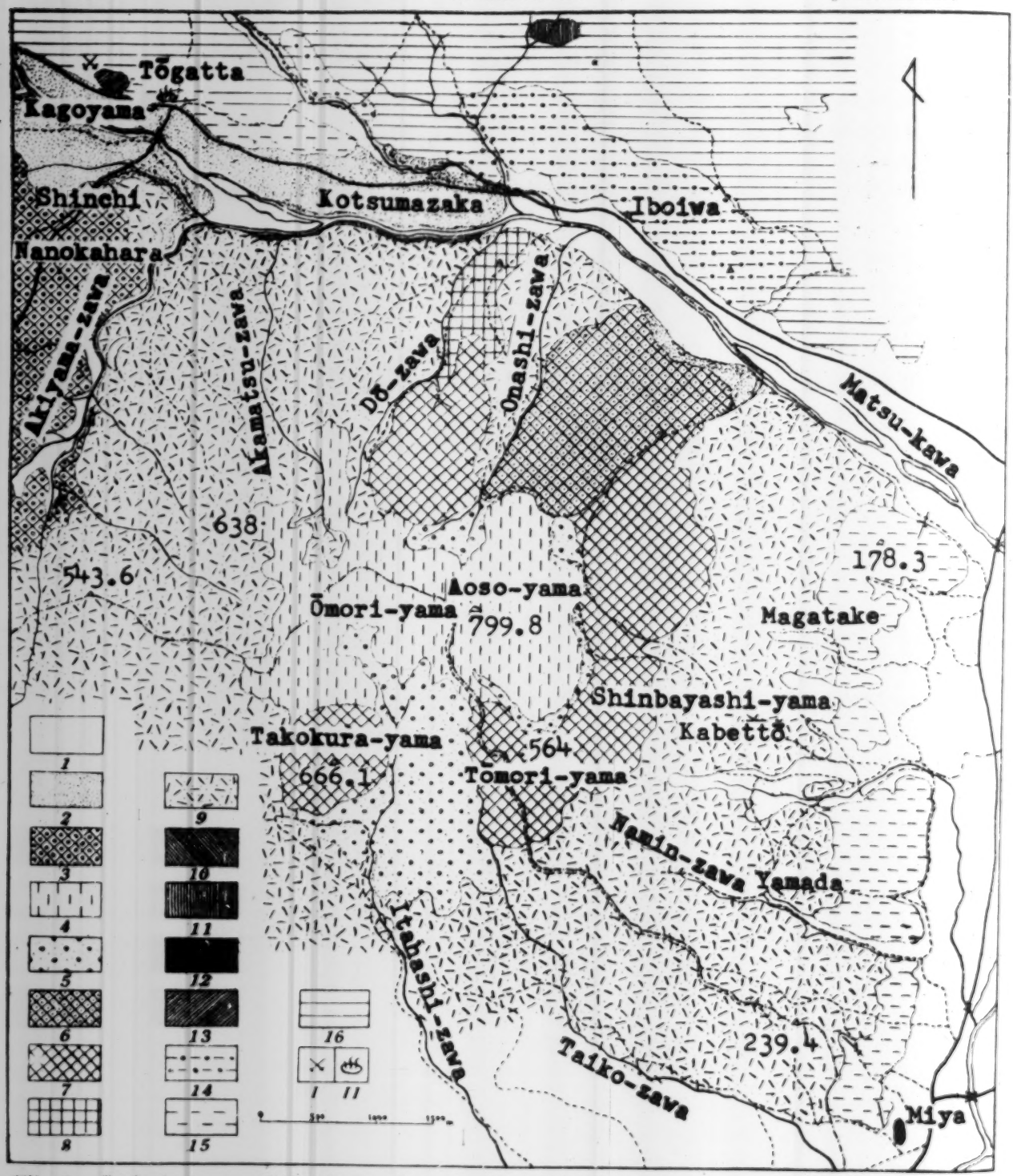

Fig. 2. Geological map of the Aoso volcano and its vicinity. 1. Recent fluviatile deposits, 2. Older fluviatile deposits, 3. Nanokahara mud flow, 4. Ōmori-yama lava (hornb. -bearing two-pyrox. andesite), 5. Itahashi-zawa agglomerate, 6. Onashi-zawa lava (01.-bearing two-pyrox. andesite or two-pyrox. andesite), 7. Tōmori-yama lava (01.-bearing two-pyrox. andesite or 01. two-pyrox. andesite), 8. Dō-zawa lava (two-pyrox. andesite) and agglomerate, 9. Matsu-kawa mud flow covered partly by talus deposits, 10. Clay, sand & gravel (Pliocene?), 11. Two-pyrox. basalt, 12. Aug. andesite, 13. Felsite, 14. Agglomerate, 15. Shale & sandstone, 16. Green tuff, I. Mine abandoned, II. Hot spring.

(3) Agglomerate and some effusive independent of the activities of the Aoso volcano: In association with the green tuff mentioned above, the occurrence of andesitic agglomerate and basalt is a characteristic feature of this district.

The andesitic agglomerate can be seen on the hill behind Kotsumazaka and Iboiwa. In the latter case, it is remarkably exposed along the bus road between Nagano and Tōgatta. The agglomerate here is intercalated with tuff beds, showing a strike of N 45° E to N 60° E and a dip of 30° to 40° NW or NNW. The fragments in agglomerate usually have an angular or subangular form and range mostly from 5 cm. to 20 cm. in diameter. They are olivine two-pyroxene andesite with a dark grey color and porphyritic texture. The similar condition is seen in the agglomerate of Kotsumazaka which contains fragments of two pyroxene andesite or olivine-bearing two-pyroxene andesite and extends from northwest to southeast.

Moreover, the occurrence of basalt in the area of green tuff is to be seen on a hill about 1500 m. north from the bus road near Iboiwa. The exposure of this rock has a nearly circular outline about 400 m. across. It is two-pyroxene olivine basalt which has a black color and is porphyritic in its texture. Under the microscope, the rock consists of plagioclase, olivine, augite, hypersthene, magnetite, goethite, serpentine and brown glass. Of these, phenocrystic minerals are plagioclase, augite, hypersthene and olivine.

It is also noteworthy that the felsitic rock is found together with shale or green tuff bed. An example is shown at the Miya Mine where it projects out as a cliff called "Kago-yama" along the bus road. The felsitic rock here has a white or greyish white color and it frequently stained by iron oxide derived from pyrite. It strongly resembles the silicified shale in its appearance, being composed of fine aggregates of quartz, feldspar and sericite under the microscope.

The small isolated hill behind Miya is an erosion remnant of augite andesite. The fresh specimen has a black color and is indistinctly porphyritic to the naked eye. When it is intensely subjected to weathering, an onion structure is to be seen on the surface. The phenocrystic mineral of this rock are plagioclase and augite. They are embedded in the groundmass consisting of minute crystals of lath-shaped plagioclase, augite and magnetite.

(4) Lavas and ejecta erupted from the Aoso volcano: The Aoso volcano is composed of lava flows and various kinds of ejecta which rest

upon the Tertiary formation. They are the Matsu-kawa mud flow, Dō-zawa lava and agglomerate, Tōmori-yama lava, Onashi-zawa lava, Itahashi-zawa agglomerate and Ōmori-yama lava in the order of eruption.

(i) Matsu-kawa mud flow. The Aoso volcano is skirted with the exposures of the Matsu-kawa mud flow which is supposed to have poured out from its pre-existing crater or its neighboring Byōbu volcano[4] at the earliest stage of activity. The northern end of this mud flow is highly cliffed along the Matsu-kawa and the lower course of the Akiyama-zawa where it is underlain by nearly horizontal beds of clay, sand and gravel (Fig. 4).

The mud flow exposed here is intercalated with several ash beds, pumice layers and thin lava flows. Such a mud flow is also seen along the Akamatsu-zawa, Dō-zawa and Itahashi-zawa, but it has some different appearance in the area including the lower course of the Taiko-zawa, Yamada, Kabettō, etc. In the latter case, it is extensively covered by talus deposits and is underlain by shale and sandstone beds.

The repeated occurrence of pumice layer is also found in this place. It is generally 30 cm. to 1 m. and consists of pumice fragments with a grey or light grey color. Lava flows associated with this mud flow are seen on the cliff of the Akiyama-zawa. They are mostly two-pyroxene andesite.

(ii) Dō-zawa lava (olivine-bearing two-pyroxene andesite) and agglomerate: The Matsu-kawa mud flow was followed by the eruption of the Dō-zawa lava and agglomerate. They extend from south to north, forming a narrow ridge between the Dō-zawa and Onashi-zawa. The northern end of this lava flow and agglomerate is highly cliffed along the Matsu-kawa, but they disappear beneath the Tōmori-yama lava southwards and are supposed to have been supplied from the pre-existing crater.

(iii) Tōmori-yama lava (olivine two-pyroxene andesite or olivine-bearing two-pyroxene andesite): It is widely exposed around the central cones of the Aoso volcano and forms a part of somma which is now dissected deeply by the Akamatsu-zawa, Dō-zawa, Onashi-zawa, Namin-zawa, Taiko-zawa, Itahashi-zawa, etc. The lava is amply exposed on Tōmori-yama, Takokura-yama and Shinbayashi-yama. Of these, Tōmori-yama rises as a small but characteristic cone which is easily distinguishable from other parts of the Aoso volcano. The Tōmori-yama lava is partly covered by the Onashi-zawa lava, Itahashi-zawa agglomerate, Ōmori-yama lava and talus deposits, but is underlain by the Matsu-kawa mud flow.

4) The Byōbu volcano belongs to the South Zaō.

(iv) Onashi-zawa lava (olivine-bearing two-pyroxene andesite or two-pyroxene andesite): The lava flow poured out from the same crater as mentioned above. It is underlain by the Tōmori-yama, but is covered by the Ōmori-yama lava. The lava exposed here seems to have run down northeastwards, and its terminal is now cut off by the Matsu-kawa.

(v) Itahashi-zawa agglomerate: It is amply exposed along the Itahashi-zawa and at the uppermost course of the Onashi-zawa in close association with the Ōmori-yama lava. It contains abundant fragments, large or small, of hornblende-bearing two-pyroxene dacite. In this case, this agglomerate is covered by the Ōmori-yama lava and seems to have been the forerunner of the lava which formed the central cones.

(vi) Ōmori-yama lava (hornblende-bearing two-pyroxene dacite): A different type of lava can be observed on Ōmori-yama and Aoso-yama which were deformed by the presence of explosion craters. It rests directly upon the Itahashi-zawa agglomerate and Tōmori-yama lava. The relationship between this and the Itahashi-zawa agglomerate can be seen on the northern cliff of Ōmori-yama and the uppermost course of the Itahashi-zawa and Taiko-zawa. In this case, the lava eruption took place within the crater surrounded by the Tōmori-yama lava.

(5) Quaternary fluviatile deposits: Younger or older fluviatile deposits are found along the present river course where they are composed of clay, sand and gravel.

(6) Talus deposits: The eastern or western flank and foot of the Aoso volcano is widely covered by talus deposits supplied from various kinds of lava flow and agglomerate. In such a case, the andesite fragments derived from the Tōmori-yama lava are more predominant than others.

Structure of the Aoso Volcano and Its Pre-existing Crater.

The present Aoso volcano is composed of somma and central cones, but it seems to have been a characteristic homate in the earlier stage of its activity. Such cones as Takokura-yama (Figs. 6, 7), Tōmori-yama (Figs. 5, 6), Shinbayashi-yama, etc. seem to have been formed on the peripheral part of the crater which is supposed to be 2.5 km. or thereabouts in diameter. The original form of this crater was subsequently destructed by the eruption of the Onashi-zawa lava, Itahashi-zawa agglomerate and Ōmori-yama lava.

As has already been stated, the Aoso volcano is constructed by mud flow, two-pyroxene andesite, olivine-bearing two-pyroxene andesite,

olivine two-pyroxene andesite, hornblende-bearing two-pyroxene dacite and agglomerate. It rests upon the Tertiary formation, and there is an evidence that the mud flow directly covers the flat surface of horizontal beds composed of sand, clay and gravel assigned to Pliocene (?). Of these, the Tōmori-yama lava is most extensively distributed and almost surrounds the Ōmori-yama lava, although it partly disappears beneath the Ōmori-yama lava, Onashi-zawa lava and Itahashi-zawa agglomerate. The structure of this volcano can be confirmed along several valleys to some extent, but lavas and ejecta are poorly exposed within the crater where it is thickly forested. The crater here is almost filled up with the Itahashi-zawa agglomerate and Ōmori-yama lava.

Central Cones.

There are two central cones called Ōmori-yama and Aoso-yama in the crater mentioned above (Figs. 3. 5). These central cones stand side by side with a narrow watershed of the Onashi-zawa and Itahashi-zawa between them. They are composed of the Ōmori-yama lava underlain by the Itahashi-zawa agglomerate. Such a feature can be observed at the uppermost course of the Onashi-zawa, Taiko-zawa and Itahashi-zawa, where the Ōmori-yama lava directly covers the Itahashi-zawa agglomerate. Ōmori-yama and Aoso-yama seem to have been formed almost simultaneously on the fissure running from east to west. The present topographical features of these cones are much affected subsequently by the formation of explosion craters here and there.

Explosion Craters.

The presence of 6 explosion craters have been hitherto known on the Aoso volcano. They are respectively found on the northern or southern side of central cones and the southern flank of Takokura-yama as well as on the northern side of a cone situated about 1 km. northwest from the summit of Aoso-yama. Of these, two are characteristic explosion craters opened semicircularly northwards and northeastwards at the source of the Onashi-zawa and its branch. They are highly cliffed and are walled by a thick accumlation of the Ōmori-yama lava and Itahashi-zawa agglomerate.

Other explosion craters of these central cones can be seen at the opposite side, but are of a small scale as compared with those of the northern flank. They open westwards or southwards, passing downwards into the valleys of the Itahashi-zawa and Taiko-zawa.

The explosion craters of Takokura-yama and the cone 1 km. northwest from the summit of Aoso-yama are smaller and older than those of the central cones. The former exploded southwards on the southern flank of Takokura-yama, but it has been more or less obscured by the subsequent erosion. The latter is, on the other hand, still preserved as a horse-shoe-shaped hollow on the northern slope of the cone. This topographical feature can be observed fully from the opposite side near Kotsumazaka.

Mineral Composition of Lavas and Ejecta.

(1) Andesite fragments of the Matsu-kawa mud flow: Andesite fragments, large or small, are abundantly contained in the Matsu-kawa mud flow. Most of these are two-pyroxene andesite, but they are sometimes represented by olivine-bearing two-pyroxene andesite. The writer collected such specimens along the Matsu-kawa, Akamatsu-zawa, Akiyama-zawa, etc., where this mud flow is well exposed. The specimens thus obtained show features differing from place to place. They, however, have a porphyritic texture and black or dark grey color, being composed of such ingredients as plagioclase, augite, hypersthene, olivine, magnetite, tridymite, apatite and brown or colorless glass. Of these, the occurrence of olivine is restricted to some specimens obtained from the middle course of the Akamatsu-zawa.

Plagioclase is the most predominant mineral as phenocryst and also in the groundmass. The phenocryst of this mineral has a tabular or rectangular form and is 2.04 mm. × 1.16 mm. in its maximum size. It ranges from labradorite to bytownite with a composition between An_{65} and An_{80}. Moreover, the crystal is always characterized by the frequency of zonal structure and turbid zone. In such a case, the turbid zone is generally found in the central part or periphery of the crystal. It sometimes contains augite, hypersthene, magnetite and brown glass.

The minute crystals of lath-shaped or rectangular labradorite are abundantly found in the groundmass together with augite and magnetite as well as glass. Such crystals are mostly 0.03 mm.~0.2 mm. in length.

In several specimens collected along the Akiyama-zawa, Matsu-kawa and Akamatsu-zawa, augite is always an important ingredient. It takes an euhedral or suhhedral form, being 2.04 mm. × 0.68 mm. in its maximum size. It sometimes shows that the extinction angle, $Z \wedge c$, is 38°~40° and twins on (100) or (101). The crystal is closely associated with hypersthene in parallel intergrowth or granular aggregation. It contains magnetite as an enclosure. Small prismatic or granular augite crystals are commonly

seen in the groundmass where they are 0.01 mm.~0.03 mm. in length or longer diameter.

The occurrence of hypersthene is known in all specimens. It is frequently more abundant than the phenocrystic augite. This mineral usually occurs as subhedral or anhedral phenocrysts, but well-defined crystals are not rare in the specimens of the Akamatsu-zawa. The largest one is 2.14 mm. × 0.81 mm. in size. Such crystals often include magnetite, apatite and plagioclase. When hypersthene and augite occur together in parallel intergrowth, the former is always fringed by the latter.

Olivine is rarely present as a phenocrystic mineral, and its occurrence is only known in the andesite fragments from the Akamatsu-zawa. It has a granular form. Octahedral or granular magnetite is a common accessory mineral in the groundmass. In most cases. it is shorter than 0.01 mm. in diameter, although there are some large crystals whose diameter is more than 0.5 mm.

Besides the ingredients mentioned above, chlorite is an alteration product derived from hypersthene. Tridymite and brown or colorless glass are sometimes found in the groundmass where they fill up the interstices of other ingredients. Moreover, some xenoliths of basaltic or noritic character are contained in the specimens obtained from the mud flow exposed along the Matsu-kawa, the lower course of the Akiyama-zawa and the middle course of the Akamatsu-zawa.

(2) Dō-zawa lava and agglomerate: The Dō-zawa lava and the fragments of its agglomerate have similar characters megascopically and microscopically. They are olivine-bearing two-pyroxene andesite with a black color and porphyritic texture. The andesite specimens collected by the writer on the cliff of the Matsu-kawa is a compact and hard rock composed of plagioclase, augite, hypersthene, olivine, magnetite and brown glass. Of these, plagioclase, augite, hypersthene and olivine are found as phenocrysts and ingredients of groundmass.

The phenocrystic plagioclase is usually euhedral or subhedral and takes a tabular or rectangular form. The largest crystal is 7 mm. in longer diameter. Some of it is well zoned and remarkably turbid, containing small grains of augite and magnetite as well as irregular patches of brown glass. The indices of refraction measured on (010) indicate that this plagioclase ranges from labradorite to bytownite and is An_{72}~An_{81} in composition.

The plagioclase in the groundmass mostly occur as minute lath-shaped crystals, 0.03 mm.~0.2 mm. in length, and is more acidic than the pheno-

crystic one. In some specimens, the parallel arrangement of this mineral in the brown glass gives a hyalopilitic texture to the groundmass.

Augite is one of remarkable ingredients, and most of phenocrysts have a subhedral or anhedral form. Among them, the largest one is 2.5 mm. long and 1.05 mm. across. Such phenocrysts are occasionally twinned on (100) or (101), and the maximum extinction angle, $Z \wedge c$, is 40°. In these crystals, hypersthene and magnetite are always contained. Moreover, small prismatic or granular augite is abundantly found in the groundmass together with plagioclase, magnetite and brown glass. In this case, the length of prismatic crystals is less than 0.05 mm.

Hypersthene is also an important mineral as augite in all of the specimens collected by the writer. The amount of this mineral is, however, variable in different specimens. Thus, andesite fragments of Dō-zawa agglomerate contain hypersthene less abundantly than augite. The large phenocryst is 1.2 mm. or more in length, and it is sometimes associated with augite in parallel intergrowth, the former passing suddenly outwards into the latter.

The composition of phenocrystic plagioclase and the optical characters of phenocrystic augite and hypersthene are summarized in the following table.

	No. 1 (T.I. 47110101)	No. 2 (T.I. 47110102)
Plagioclase	Core $(-)2V=86°$ An_{78} Margin $(-)2V=88°$ An_{72}	An_{72-81}
Augite	$\alpha=1.685\pm0.002$ $\beta=1.694\pm0.002$ $\gamma=1.711\pm0.002$ $\gamma-\alpha=0.028$ $(+)2V=50°$	$\alpha=1.681\pm0.002$ $\beta=1.692\pm0.002$ $\gamma=1.709\pm0.002$ $\gamma-\alpha=0.028$ $(+)2V=52°$
Hypersthene	$\alpha=1.693\pm0.002$ $\beta=1.700\pm0.002$ $\gamma=1.705\pm0.002$ $\gamma-\alpha=0.012$ $(-)2V=64°$ $\rho>v$	$\alpha=1.696\pm0.002$ $\beta=1.705\pm0.002$ $\gamma=1.709\pm0.002$ $\gamma-\alpha=0.013$ $(-)2V=62°$ $\rho>v$

No. 1. = Andesite frgment in the Dō-zawa agglomerate.
No. 2. = The Dō-zawa lava. (Measured by F. Hori)

Olivine is an important phenocrystic mineral, 2.12 mm. × 1.11 mm. in its maximum size. It is subhedral or anhedral and partly or entirely alters

into serpentine. The crystal encloses magnetite like other phenocrysts.

Magnetite is either octahedral, granular or skeletal in form. The crystal contained in plagioclase, augite. hypersthene and olivine are larger than those in the groundmass. It is 0.51 mm. by 0.34 mm. in the biggest crystal, but its diameter is mostly shorter than 0.02 mm. in the latter case.

Brown glass fills up the interstices of all other ingredients. It is less abundant in the Dō-zawa lava.

(3) Tōmori-yama lava: Of various lavas and agglomerates exposed on the Aoso volcano, the most remarkable one is the Tōmori-yama lava, which has a wide area of distribution including Tōmori-yama, Takokura-yama, Shinbayashi-yama and others. It is a compact and porphyritic rock with a grey color. In weathered specimens, the porphyritic texture is shown more distinctly than in fresh ones. The mineral ingredients of this lava is represented by plagioclase, augite, hypersthene, olivine, magnetite, tridymite, apatite, hematite and brown glass. Of these, phenocrystic minerals are plagioclase, augite, hypersthene and olivine. There are, however, some mineralogical differences even in the same lava. In certain specimens, olivine is abundantly present, but it is lacking in others, although the lava has a quite similar texture in the groundmass. Hence, the lavas from Tōmori-yama and Shinbayashi-yama are olivine two-pyroxene andesite or olivine-bearing two-pyroxene andesite, whereas those of Takokura-yama or elsewhere are composed of two-pyroxene andesite.

In such cases, various features are indicated by plagioclase, which takes an euhedral or subhedral form. It is well zoned and turbid in the inner or outer part, althougn each shows a fresh appearance. The largest phenocryst is 3.14 mm. × 2.38 mm. in size. Some of its crystal has a worm-eaten structure due to the abundance of irregular patches of brown glass. Besides brown glass, it encloses augite, hypersthene, magnetite, actinolite (?) needles and biotite which are often found in the turbid zone. Some of these are often arranged parallel to the periphery of plagioclase phenocrysts. Indices of refraction measured on (010) suggest that this plagioclase belongs to labradorite or bytownite with a composition ranging from An_{68} to An_{78}.

In the gronndmass, abundant lath-shaped crystals, mostly 0.025 mm.~ 0.2 mm. in length, generally takes a fluidal arrangement between phenocrystic minerals.

Augite and hypersthene are common ingredients of this rock. Hypersthene is sometimes more abundant than augite or *vice versa*. The augite phenocryst is generally subhedral or anhedral, but it is euhedral in some specimens. The largest phenocryst is 1.78 mm. × 1.07 mm. When the

crystal is euhedral or subhedral, it has a stout prismatic form. It is sometimes found in parallel intergrowth with hypersthene. In this case, the latter is always fringed by the former. In zoned crystals, the inner part has a large extinction angle as compared with the periphery. It twins on (100) or (101), and its maximum extinction angle, $Z \wedge c$, is 41°. In the groundmass, augite is abundant and occurs as a prismatic or irregular form.

Hypersthene is a characteristic mineral with a distinctly pleochroic scheme. It is frequently found as an euhedral or subhedral crystal with a long prismatic form, 4.59 mm. × 0.93 mm. in its maximum size. This mineral contains mostly magnetite as enclosure.

The composition of phenocrystic plagioclase and the optical characters of phenocrystic augite and hypersthene are summarized in the following table.

	No. 1 (T.I. 47110201)	No. 2 (T.I. 51040101)	No. 3 (T.I. 51040106)	No. 4 (T.I. 51040201)	No. 5 (T.I. 51033106)
Plagioclase		$An_{60\sim74}$	$An_{70\sim78}$	$An_{58\sim75}$	
Augite	$\alpha=1.683 \pm 0.002$	$\alpha=1.686 \pm 0.002$	$\alpha=1.690 \pm 0.002$	$\alpha=1.683 \pm 0.002$	$\alpha=1.686 \pm 0.002$
	$\beta=1.695 \pm 0.002$	$\beta=1.693 \pm 0.002$	$\beta=1.695 \pm 0.002$	$\beta=1.690 \pm 0.002$	$\beta=1.692 \pm 0.002$
	$\gamma=1.711 \pm 0.002$	$\gamma=1.708 \pm 0.002$	$\gamma=1.710$	$\gamma=1.710 \pm 0.002$	$\gamma=1.712 \pm 0.002$
	$\gamma\sim\alpha=0.028$	$\gamma\sim\alpha=0.028$	?	$\gamma\sim\alpha=0.027$	$\gamma\sim\alpha=0.026$
	$(+)2V=50°$	$(+)2V=51°$	$(+)2V=49°$	$(+)2V=50°$	$(+)2V=49°$
Hypersthene	$\alpha=1.700 \pm 0.002$	$\alpha=1.691 \pm 0.002$	$\alpha=1.689 \pm 0.002$	$\alpha=1.689 \pm 0.002$	$\alpha=1.693 \pm 0.002$
	$\beta=1.708 \pm 0.002$	$\beta=1.700 \pm 0.002$	$\beta=1.699 \pm 0.002$	$\beta=1.700 \pm 0.002$	$\beta=1.699 \pm 0.002$
	$\gamma=1.713 \pm 0.002$	$\gamma=1.704 \pm 0.002$	$\gamma=1.704 \pm 0.002$	$\gamma=1.703 \pm 0.002$	$\gamma=1.705 \pm 0.002$
	$\gamma\sim\alpha=0.013$	$\gamma\sim\alpha=0.013$	$\gamma\sim\alpha=0.015$	$\gamma\sim\alpha=0.014$	$\gamma\sim\alpha=0.012$
	$(-)2V=59°$	$(-)2V=59°$	$(-)2V=60°$	$(-)2V=60°$	$(-)2V=58°$

No. 1. = The Tōmori-yama lava from the upper course of the Dō-zawa.
No. 2. = The Tōmori-yama lava from the Namin-zawa.
No. 3. = The Tōmori-yama lava from the hill at the north of Shinbayashi-yama.
No. 4. = The Tōmori-yama lava from the hill at the north of Shinbayashi-yama.
No. 5. = The Tōmori-yama lava from Takokura-yama. (Measured by F. Hori)

The occurrence of olivine is not so important when compared with other phenocrystic minerals, although it is frequently seen in the specimens collected from the lower course of the Akamatsu-zawa. The crystal of this mineral usually takes a subhedral or anhedral form, and its maximum

size is 0.88 mm. × 0.59 mm. Part of it changes into bowlingite along the peripheries and cracks. Commonly, it contains magnetite.

One of characteristic features of this rock is the abundance of small magnetite crystals or grains in the groundmass together with minute lath-shaped plagioclase and augite. They are frequently represented by octahedral crystals. In some cases, these crystals are contained in the aggregate of granular augite. The crystal is 0.06 mm. in its maximum diameter, but it is mostly 0.01 mm.–0.05 mm. across.

There are rarely apatite crystals which have a dark brown color due to decomposition, being 0.39 mm. × 0.05 mm. in the maximum size. Tridymite fills up the interstices of various ingredients of the groundmass. It is not a rare mineral in the specimens from the Namin-zawa and the east flank of Takokura-yama. Long prismatic actinolite (?) occurs as an enclosure of plagioclase phenocrysts. The mineral shows a weak pleochroism and a small extinction angle, $Z \wedge c$, of 16° or thereabouts.

Besides these, doleritic, noritic or gabboic inclusions are found in most specimens. They are composed of plagioclase, augite, hypersthene and magnetite.

(4) Onashi-zawa lava: The ridge extending northeastwards along the eastern side of the Onashi-zawa is formed of two-pyroxene andesite or olivine-bearing two-pyroxene andesite with a remarkable porphyritic texture. The lava exposed here has a dark grey color, but it usually assumes a grey or reddish color by alteration.

The specimens collected by the writer are composed of plagioclase, augite, hypersthene, olivine, magnetite, hematite, tridymite, apatite, brown glass and actinolitic mineral.

Under the microscope, the phenocrystic plagioclase mostly has an euhedral or subhedral form, being 3.16 mm. × 2.15 mm. at its maximum size. It is well-zoned and occasionally turbid. It is sometimes characterized by a worm-eaten structure and includes such minerals as augite, magnetite and brown glass which occur as irregular patches. The indices of refraction on (010) suggest that the phenocrystic plagioclase ranges from labradorite to bytownite with a composition between An_{65} and An_{70}.

In the groundmass, lath-shaped or rectangular crystals are abundantly present. The former is 0.02 mm.~0.05 mm. long and occasionally shows a fluidal arrangement around phenocrystic minerals. It belongs to labradorite.

Augite is found as phenocryst and is an important ingredient in the groundmass. The phenocrystic augite is, however, less abundant than hypersthene and commonly takes a subhedral or anhedral form, twinning

on (100) or (101). In this case, the largest crystal is 1.75 mm. × 0.49 mm. in size, and the maximum extinction angle, Z∧c, 14°. Moreover, most phenocrysts contain magnetite as enclosure. The augite crystals of the groundmass have a granular or stout prismatic form, being 0.03 mm.~0.08 mm. in the latter case.

Hypersthene with an euhedral or subhedral form is usually characterized by a long prismatic habit. The crystal is 2.75 mm. in its maximum lengh and includes magnetite. It is sometimes intergrown with augite in parallel position, the former passing outwards into the latter. In the andesite with a reddish color, it is intensely affected and segregates hematite.

The composition of phenocrystic plagioclase and the optical characters of phenocrystic augite and hypersthene are shown in the following table.

	(T.I. 51040301)*
Plagioclase	$An_{63\sim70}$
Augite	$\alpha = 1.684 \pm 0.002$ $\beta = 1.693 \pm 0.002$ $\gamma = 1.709 \pm 0.002$ $\gamma - \alpha = 0.025$ $(+)2V = 51°$
Hypersthene	$\alpha = 1.690$ $\beta = 1.699$ $\gamma = 1.703$ $\gamma - \alpha = 0.013$ $(\mp)2V = 60°$

* The Onashi-zawa lava from the Onashi-zawa. (Measured by F. Hori)

Olivine is a rare ingredient in the Onashi-zawa lava as compared with hypersthene and augite. The occurrence of this mineral is only known in several specimens. It has a very irregular form and partly changes into bowlingite along its periphery and crack.

Magnetite is always a very common mineral in the groundmass where it abundantly occurs in a granular or octahedral form. Most of magnetite crystals have a diameter ranging from 0.01 mm. to 0.05 mm., although there are some large crystals more than 0.4 mm. across. It passes into hematite in the specimens subjected to reheating.

The interstices of the minute ingredients in the groundmass is occasionally filled up by tridymite which is characterized by its irregular form and exceedingly low birefringence.

The occurrence of apatite is very rare. Its prismatic crystal is usually traversed by cracks and is somewhat decomposed in its inner part and obtains a dark brown color. Actinolitic mineral is only found as an enclosure of phenocrystic plagioclase. This mineral occurs as minute prismatic or acicular crystal traversed by cracks. It is always colorless and has a small extinction angle. The frequent occurrence of brown

glass is noticed in the phenocrystic plagioclase and also in the groundmass of almost all specimens.

The groundmass consists of plagioclase, augite, magnetite, apatite and brown glass and reveals a hyalopilitic or pilotaxitic texture.

Besides the various ingredients mentioned above, there are some xenoliths with noritic or doleritic character. They are composed of plagioclase, hypersthene, augite, magnetite and brown glass.

(5) Dacite fragments of the Itahashi-zawa agglomerate: In this agglomerate many angular or subangular fragments of hornblende-bearing two-pyroxene andesite are cemented by tuffaceous or sandy matrix. These dacite fragments, large or small, have an appearance quite similar to the Ōmori-yama lava, being characterized by the abundance of phenocrystic quartz and the presence of hornblende. They are dark grey in fresh specimens and grey or light grey in weathered ones. Moreover, some of these obtain a reddish color by reheating.

Exclusive of quartz and hornblende, the dacite fragments under consideration consist of plagioclase, hypersthene, augite, magnetite, olivine and tridymite.

Of these, the phenocrystic quartz is generally subjected to magmatic corrosion and takes a more or less rounded form, 1.5 mm, in its maximum diameter. It is traversed by many cracks, and there are some crystals with liquid inclusions. Occasionally, the crystal shows a wavy extinction and, accordingly, a biaxial character. Quartz is also an important ingredient in the groundmass which shows a microgranitic texture.

The coarse porphyritic texture of dacite fragments in the Itahashi-zawa agglomerate is due to the frequent occurrence of fairly large phenocrystic plagioclase which is 3.91 mm. × 1.95 mm. in its maximum size. Euhedral, subhedral or anhedral phenocrysts of this mineral are always well-zoned and sometimes turbid, frequently containing magnetite, augite and hypersthene. Indices of refraction measured on (010) indicate that the phenocrystic plagioclase ranges from acidic labradorite to basic labradorite with such a composition as $An_{55\sim73}$. Minute lath-shaped or granular plagioclase is a remarkable constituent in the groundmass. In the former case, it is 0.08 mm.~0.25 mm. in length and belongs to andesine.

Phenocrystic augite, subhedral or anhedral, is usually less abundant than hypersthene. The crystal generally twins on (100), and its extinction angle, $Z \wedge c$, is 41°, being 2.2 mm. × 1.7 mm. in its maximum size. Magnetite is generally found as its enclosure. Augite is also a common ingredient

in the groundmass. When it has a long prismatic form, the crystal is 0.08 mm.~0.02 mm. in length.

All specimens collected by the writer contain varying amount of hypersthene with a long primatic form. The largest phenocryst is 1.87 mm. × 0.54 mm. in size, and the prismatic crystals of this mineral in the groundmass is 0.1 mm.~0.3 mm. in length.

The composition of phenocrystic plagioclase and the optical characters of phenocrystic hypersthene and augite is as fo lows.

	(T.I. 51033107)*
Plagioclase	$An_{55\sim75}$
Augite	$\alpha = 1.682 \pm 0.002$ $\beta = 1.695 \pm 0.002$ $\gamma = 1.710 \pm 0.002$ $\gamma - \alpha = 0.028$ $(+)2V = 49°$
Hypersthene	$\alpha = 1.695 \pm 0.002$ $\beta = 1.703 \pm 0.002$ $\gamma = 1.708 \pm 0.002$ $\gamma - \alpha = 0.013$ $(-)2V = 55°$

* Dacite fragment of the Itahashi-zawa agglomerate from the upper course of the Itahashi-zawa. (Measured by F. Hori)

Hornblende is one of characteristic minerals in this rock. It has a long prismatic form, and is characterized by a strongly pleochroic scheme, viz., X=amber yellow, Y=yellowish brown, Z=reddish brown. The color probably resulted from the oxidation due to reheating. Some of it twins on (100), and the largest crystal is 1.27 mm. long. It is partly opacitized.

Octahedral or granular magnetite is always found as an enclosure in other minerals and in the groundmass, where the largest crystal is 0.56 mm. in diameter. Besides these ingredients, the rock contains basaltic xenoliths consisting of plagioclase, augite, hypersthene, magnetite and olivine.

The groundmass indicates a microgranitic texture and contains plagioclase, augite. hypersthene, magnetite and tridymite.

(6) Ōmori-yama lava: The Ōmori-yama lava is underlain by the Itahashi-zawa agglomerate, both of which seem to have been erupted successively. Therefore, the Ōmori-yama lava and dacite fragments of the Itahashi-zawa agglomerate have some similar petrographic characters, as is shown by the presence of phenocrystic quartz and hornblende.

The phenocrystic quartz with a rounded form is always abundant in all specimens. It is traversed by many cracks, and the occurrence of liquid inclusions is known in many specimens. The crystal occasionally reveals a wavy extinction, and its maximum diameter is estimated at 1.44 mm.

One of the important ingredients is the phenocrystic plagioclase with an euhedral, subhedral or anhedral form which is 2.41 mm. × 1.70 mm. in its maximum sixe. It ranges from acidic labradorite to basic labradorite with such a composition as $An_{55\sim68}$. It mostly includes augite, magnetite and apatite, partly passing into a light brown glass. The crystal is well-zoned, and it is rarely not frequently turbid along the periphery or in the inner part of crystals. When plagioclase occurs as an ingredient in the groundmass, it is mostly represented by minute lath-shaped crystals, 0.02 mm.~0.18 mm. in length. Augite and hypersthene are found in almost the same amount as those of the Itahashi-zawa agglomerate. Both minerals include magnetite grains and sometimes pass into one another, showing a parallel intergrowth in which hypersthene is always fringed by augite.

The prismatic hypersthene crystal is 1.57 mm. in its maximum length as phenocryst and 0.086 mm.~0.18 mm. long as an ingredient of the groundmass.

Augite often twins on (100) or (101), and its extinction angle, $Z \wedge c$, is 40°. It has a subhedral or anhedral form, the phenocrysts being 0.81 mm × 0.25 mm. in the maximum size, and the minute crystals in the groundmass 0.01 mm.~0.15 mm. long.

The following table shows the composition of phenocrystic plagioclase and the optical characters of augite and hypersthene.

	(T.I. 4711015)*
Plagioclase	$An_{55}\sim An_{68}$
Augite	$\alpha = 1.689 \pm 0.002$
	$\beta = 1.695 \pm 0.002$
	$\gamma = 1.710 \pm 0.002$
	$\gamma - \alpha =$?
	$(+)2V = 50°$
Hypersthene	$\alpha = 1.695 \pm 0.002$
	$\beta = 1.704 \pm 0.002$
	$\gamma = 1.709 \pm 0.002$
	$\gamma - \alpha = 0.014$
	$(-)2V = 57°$

* The Ōmori-yama lava from near the summit of Ōmori-yama.
(Measured by F. Hori)

Long prismatic hornblende is mostly of an oxidized type with a strong pleochroism changing from amber yellow (X) to yellowish brown (Y) or reddish brown (Z). In several specimens, there is also basaltic hornblende which shows the following pleochroic scheme viz., X=light yellow, Y=browish green, Z=greenish brown. The absorption is $Z > Y > X$ in both cases. These two kinds of hornblende are subhedral or anhedral, and they are sometimes opacitized entirely. The maximum size of such crystals are 1.71 mm. × 0.17 mm.

Magnetite is the commonest mineral in the groundmass. It is generally

0.01 mm.~0.08 mm. in diameter, although there are some crystals with a diameter exceeding 0.42 mm.

Tridymite fills up the interstices of the ingredient minerals in the groundmass, and olivine is only found in xenolith. The groundmass is composed of such minerals as quartz, plagioclase, augite, hypersthene, magnetite and tridymite. Of these, lath-shaped plagioclase crystals often exhibit a fluidal arrangement, but the characteristic microgranitic texture is also known. In this rock, the occurrence of xenolith is not rate. They are basaltic rocks, consisting of plagioclase, augite, hypersthene, olivine and magnetite.

History of Volcanic Activities.

The activies of the Zaō volcanoes are supposed to have repeated many times on the upheaved area composed of the Tertiary formation and such intrusives or extrusives as granite, propylite, basalt, etc. Some of these abundantly supplied lavas and ejecta to construct the Aoso volcano at the eastern end of the South Zaō.

The first eruption seems to have taken place through the Tertiary formation exposed now in the district surrounding the Aoso volcano and is supposed to have began by pouring forth the Matsu-kawa mud flow. This mud flow was first considered by Takada to be the youngest ejecta in the South Zaō, but several field evidences here suggest that it may have been the forerunner of activities which happened in the Aoso or Byōbu volcanic area. Moreover, the Matsu-kawa mud flow is believed to have been ejected in the Pleistocene, since it partly rests upon the eroded surface of nearly horizontal beds assigned to the Pliocene (?).

The next activity is indicated by the eruption of the Dō-zawa lava and agglomerate which are always associated with each other. It was, however, restricted to a small area.

The central cone of the Aoso volcano is surrounded by the Tōmori-yama lava poured out later than the Dō-zawa lava and agglomerate. Its way of distribution suggests that there was formerly a large crater at the central part of this volcano occupied now by Aoso-yama and Ōmori-yama. The lava seems to have flowed out from here or from the fissures on the flank and to have rushed down in several directions. Tōmori-yama may be a parastic cone formed in connection with this eruption. After intensely subjected to erosion, the Onashi-zawa lava was ejected from the same crater and filled up the hollow between the Tōmori-yama lava and Matsu-kawa mud flow extending northeastwards.

The final activity is represented by the eruption of the Itahashi-zawa agglomerate and Ōmori-yama lava, the latter following the former. The Ōmori-yama lava is, therefore, underlain by the Itahashi-zawa agglomerate everywhere they are exposed. Both kinds of volcanic products resulted in the formation of central cones within the crater mentioned above. They are Ōmori-yama and Aoso-yama which rise as the two main peaks of the Aoso volcano.

In these repeated activities, the remarkable feature is the occurrence of hornblende-bearing two-pyroxene dacite. This rock is the final product in the activities of the Aoso volcano and suggests that it was probably derived from the magma which had captured such acidic rocks as granite and plagioliparite.

Summary.

(i) The Aoso volcano is isolated from the main part of the Zaō volcanoes, rising at the eastern end of the South Zaō. It is a small but characteristic volcano with central cones and several explosion craters as well as a large dissected crater which is about 2500 m. across.

(ii) This volcano rests upon the eroded surface of two different Tertiary formations. They are assigned to the Miocene and Pliocene (?) respectively, the former consisting of green tuff, shale, sandstone and andesitic agglomerate, whereas the latter is represented by clay, sand and gravel. In these cases, the Miocene sediments are sometimes intruded by felstic rock, andesite and basalt.

(iii) The volcano is formed of several lavas and ejecta, viz., the Matsu-kawa mud flow, Dō-zawa lava and agglomerate, Tōmori-yama lava, Onashi-zawa lava, Itahashi-zawa agglomerate and Ōmori-yama lava.

(iv) These lava flows and ejecta are supposed to have been supplied mainly from the pre-existing crater which were largely destroyed later by repeated eruption.

(v) The volcanic activities of this area probably started with the eruption of the Matsu-kawa mud flow and were closed by the formation of central cones constructed by hornblende-bearing two-pyroxene dacite.

(vi) The first eruption here seems to have taken place in the Pleistocene. It is shown on the cliff of the Matsu-kawa near Tōgatta, where the Matsu-kawa mud flow is underlain by alternate beds of clay, sand and gravel assigned to the Pliocene (?).

Fig. 3. The Aoso volcano from near Kotsumazaka. 1=Aoso-yama, 2=Ōmori-yama (Ōmori-yama and Aoso-yama are built up of Ōmori-yama lava underlain by the Itahashi-zawa agglomerate), 3=The Matsu-kawa, 4=The Onashi-zawa, 5=The Dō-zawa, 6=The Akamatsu-zawa, 7=Itahashi-zawa agglomerate, 8=Onashi-zawa lava, 9=Tōmori-yama lava, 10=Dō-zawa lava and agglomerate, 11=Matsu-kawa mud flow, 12=Alternate beds of clay, sand and gravel assigned to the Pliocene (?). ×=Explosion crater.

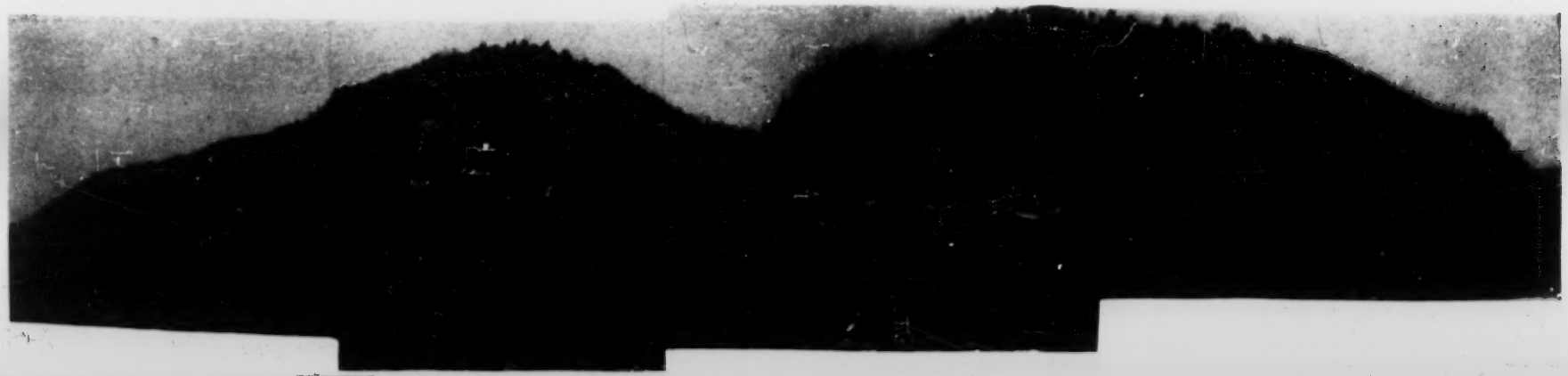

Fig. 4. The Matsu-kawa mud flow underlain by alternate beds of clay, sand and gravel assigned to the Pliocene (?). 1=The Matsu-kawa mud flow with pumice beds, 2=Alternate beds of clay, sand and gravel.

(震研彙報 第三十一号 図版 市村)

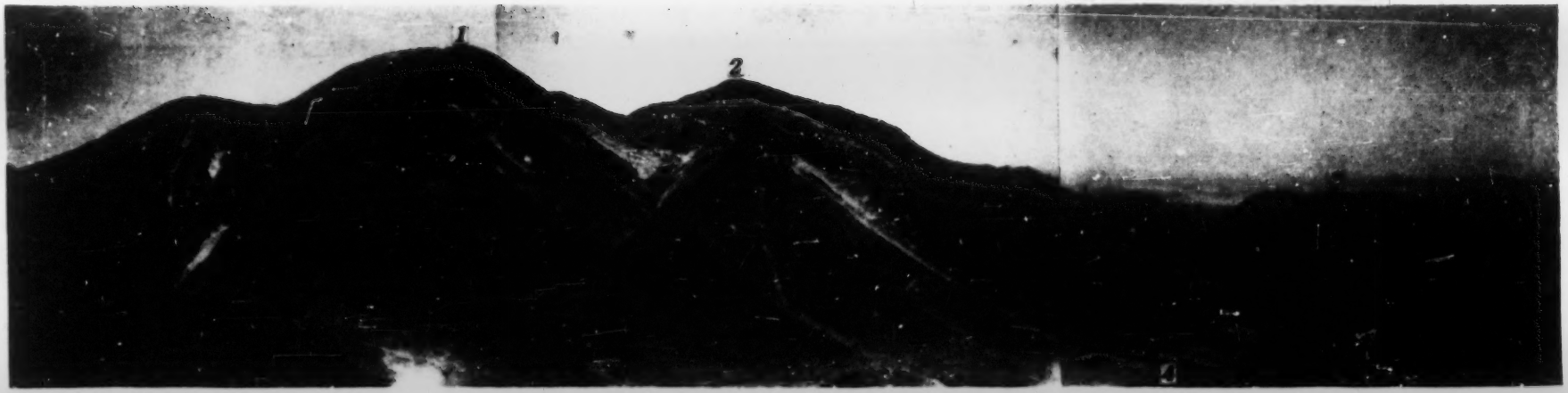

Fig. 5. Ōmori-yama and Aoso-yama, central cones of the Aoso volcano viewed from northeast.

1 = Ōmori-yama, 2 = Aoso-yama, 3 = Tōmori-yama.

Ōmori-yama and Aoso-yama are built up of hornblende-bearing two-pyroxene dacite underlain by the Itahashi-zawa agglomerate.

4 = The Itahashi-zawa.

Fig. 6. The Aoso volcano from near Yamada.
1=Aoso-yama, 2=Ōmori-yama, 3=Shinbayashi-yama, 4=Tōmori-yama, 5=Takokura-yama.

Fig. 7. Takokura-yama from near Ōmori-yama.
1=Takokura-yama (Tōmori-yama lava), 2=Ōmori-yama lava, 3=Itahashi-zawa agglomerate, 4=The Itahashi-zawa.

(震研彙報 第三十一号 図版 市村)

In conclusion, the writer wishes to offer his hearty thanks to Dr. H. Tsuya who allowed him to continue his work in the Earthquake Research Institute of Tokyo University. The writer's thanks are also due to Mr. F. Hori for his co-operation in the petrographical investigations of lavas and ejecta from this volcano.

The expense of this research was partly defrayed from the fund for the Scientific Research of the Educational Ministry.

12. 藏王火山の地質学的研究 (第二報)

地震研究所　市村　毅

東北線の白石驛又は大河原驛から遠刈田温泉へ行く途中，先づ目につくのは，道路の左側に根を張る青麻火山の姿である．此火山は，高さこそ約 800 米に過ぎないが，爆発や浸蝕作用のために変貌した外輪山とその内側に生じた中央火口丘よりなり，小さいながらも，纏つた火山の形態を見せている．然も藏王火山群の他の火山と異なり，何処からでも容易に近づけるので，その研究には極く都合の良い火山である．

青麻火山は，第三系とこれを貫く各種の火成岩を基盤として盛上り，松川泥流，ド－沢熔岩とその集塊岩，遠森山熔岩，オナシ沢熔岩，イタハシ沢集塊岩，大森山熔岩から構成されている．殊に最後に噴出した大森山熔岩とその直ぐ下位を占めるイタハシ沢集塊岩とは，他の噴出物が複輝石安山岩，含橄欖石複輝石安山岩又は橄欖石複輝石安山質なのに比べ，角閃石を含む複輝石石英安山岩なる点に特徴を有する．又最初の火山活動は，その基盤岩との関係が示す様に，第四紀に入つてから開始されたものであり，これは屏風火山の活動と相呼応して行われたものと見做される．

本文には，これ等の地質的事項と各噴出物の内容に就ての概略が纏められてある．但し熔岩や火山碎屑物に関する詳しい岩石学的研究結果の報告は化学分析が完了した後に譲ることにする．

13. *Sulphur Crystals from the Yakeyama Volcano.*

By Takeshi ICHIMURA and Hiromichi TSUYA,
Earthquake Research Institute,
and
Hideo MINATO,
Department of Earth Science.

(Read December 16, 1952.—Received March 20, 1953.)

Sulphur ores of the Yake-yama volcano were once mined near the top of the Jigokudani. The mining operation here seems to have been carried out many years ago on a very small scale, and the area is, therefore, entirely in ruins at present. In the beginning of August, 1949, some specimens of sulphur ores were obtained at this place by one of the writers (T. Ichimura) who had intended to carry out his field work together with H. Tsuya. These specimens were mineralogically investigated by the writers, and the occurrence of many crystals characterized by unusual parallel intergrowth was confirmed by H. Minato.

Sulphur ores collected at this place have generally a massive form with a characteristic yellow color and a somewhat resinous luster. When sulphur crystals occur in druses, they reveal a bellow-shaped parallel intergrowth which is repeated in the direction of *c*-axis.

The measurement of angles was carried out by using the B-type of V. Goldschmidt's two circle goniometer. The crystals selected for this purpose are generally 1–2 mm. long and 0.3–0.5 mm. across, having well reflecting faces.

(1) Simple crystals: — After the examination of several single crystals, two different kinds of form were found. Of these, two well-formed crystals were used for the measurement of angles.

(i) Type A: — It is bounded by eight $p(111)$ faces and belongs to the most simple form of sulphur crystals (Figs. 1, 4).

(ii) Type B: — The crystal is built up of two kinds of face, viz., $p(111)$ and $n(011)$ (Figs. 2, 4). In such a case, p is represented by well-grown pyramids and the edges between these faces are truncated by n. This is also a simple form common to sulphur crystals taken out from druses.

(2) Bellow-shaped crystals: — An abnormal form is frequently

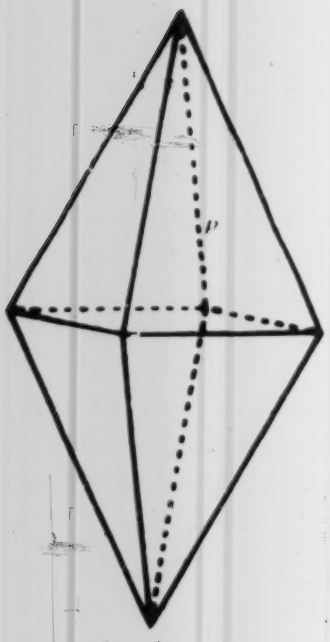

$p(111)$.
Fig. 1. Native sulphur from the Yake-yama volcano.

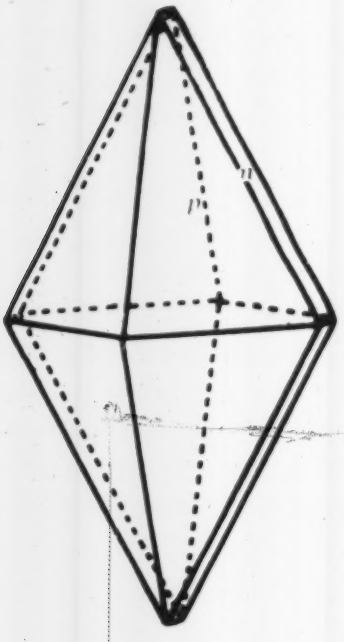

$p(111)$, $n(011)$
Fig. 2. Native sulphur from the Yake-yama volcano.

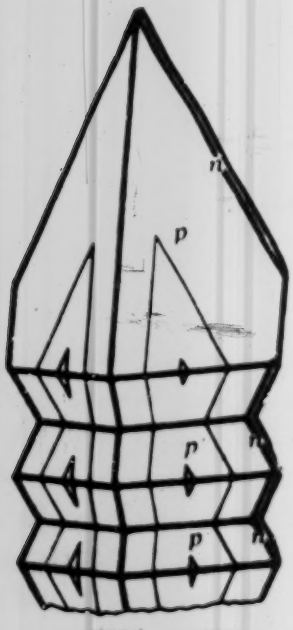

$p(111)$, $n(011)$.
Fig. 3. Native sulphur from the Yake-yama volcano.

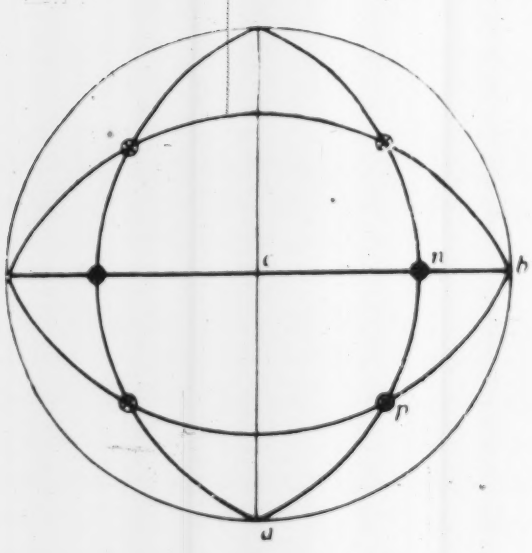

$p(111)$, $n(011)$.
Fig. 4. Native sulphur from the Yake-yama volcano.

shown by bellow-shaped crystals resulting from a parallel intergrowth. The sulphur crystals of this type is also a combination of $p(111)$ and $n(011)$, but it has a peculiar form which was generated by a bellow-shaped parallel intergrowth, exhibiting a prismatic habit and being elongated in the direction of c-axis (Figs. 3, 4). The crystal always bends to the front, because (111) and $(1\bar{1}1)$ or $(\bar{1}1\bar{1})$ and $(\bar{1}\bar{1}\bar{1})$ are highly developed at its upper or lower part respectively as compared with the imperfectness of $(\bar{1}11)$ and $(\bar{1}\bar{1}1)$ or $(11\bar{1})$ and $(1\bar{1}\bar{1})$.

The occurrence of such a type of crystal seems to be uncommon, and the presence of skeleton crystals yields remarkable striations on each face.

The result of goniometric measurement is shown in the following table.

Angle table of the native sulphur from the Yake-yama volcano.

Faces	Obs. val.		Cal. val.*		N**
	ρ	φ	ρ	φ	
$p(111)$	71°35′	50°47′	71°40′	50°51′	16
$n(011)$	62 26	0 04	62 18	0 00	4

* After the Winkeltabelen.
** Numbers of the faces of measured.

13. 燒山火山產の硫黄結晶

地震研究所 市村毅 / 津屋弘達
教養学部地学教室 湊秀雄

燒山火山產硫黄結晶の晶洞内には，小さな硫黄結晶が沢山叢生している．それ等の硫黄結晶には3通りの型があり，(i) $p(111)$ よりなるもの，(ii) $p(111)$ と $n(011)$ とよりなるもの及 (iii) 蛇腹狀の平行連晶をなすものとが認められる．(iii) の場合は最も多く，$p(111)$ と $n(011)$ との集合体であるが，(111) と $(1\bar{1}1)$ 又は $(\bar{1}1\bar{1})$ と $(\bar{1}\bar{1}1)$ とが良く発育し，その代り，$(\bar{1}11)$ と $(\bar{1}\bar{1}1)$ 又は (111) と $(11\bar{1})$ とが不完全で，此形が連晶をなし，主軸の方向に蛇腹狀をなし延びている点に著しい特徴を有する．

14. *Igneous Activities prior to the Deposition of the Chichibu System.*

By Takeshi ICHIMURA,
Earthquake Research Institute,
and
Haruko MATSUBAYASHI,
Department of Earth Science.

(Read March 17, 1953.—Received March 20, 1953.)

Introduction.

The Chichibu System has been well investigated stratigraphically, because it is widely distributed in Japan and contains abundant marine fossils in various horizons. Petrographically speaking, however, this system has been almost neglected concerning the determination of the mineral composition, although such investigation is very necessary from various geological standpoints.

In the sedimentary peterography of the Chichibu System, it would be very interesting to confirm the problem whether there were igneous activities prior to its deposition or not. With regard to such geological subjects, the Usuginu conglomerate was discussed some years ago. This conglomerate has many granite pebbles, large or small, and is supposed by T. Kobayashi[1] to have been accumulated as a delta deposit. The thin sections of these pebbles were examined by H. Yamada[2] under the microscope. According to his opinion, they are normal types of granite which are quite different from those younger than the Chichibu System, but it is still unknown from where such pebbles were supplied.

From February of 1952, one of present writers (T. Ichimura) started his peterographical work on the specimens of sandstone collected from several horizons of the Chichibu System exposed extensively in the Hannō-Agano-Shōmaru district, and another writer (H. Matsubayashi) co-operated in his laboratory work. The same area was already investigated stratigraphically by R. Morikawa[3] and Huzimoto,[4] and all specimens were

1) T. KOBAYASHI, "Nihonchihōchishitsushi" (General remarks), (1951), 89.
2) H. YAMADA, *Jour. Geol. Soc.*, **45** (1938), 688-693.
3) R. MORIKAWA and R. ENDŌ, *Jour. Geol. Soc.*, **56** (1950), 291.
,, ,, , *Jour. Geol. Soc.*, **58** (1952), 187-190.
4) H. HUZIMOTO, *Sc. Rept. T. B. D., Sect.* C, **1** (1936), No. 4, 172-178.

obtained from the beds assigned by them to the Permian. From the microscopical investigations of thin sections cut from sandstones and

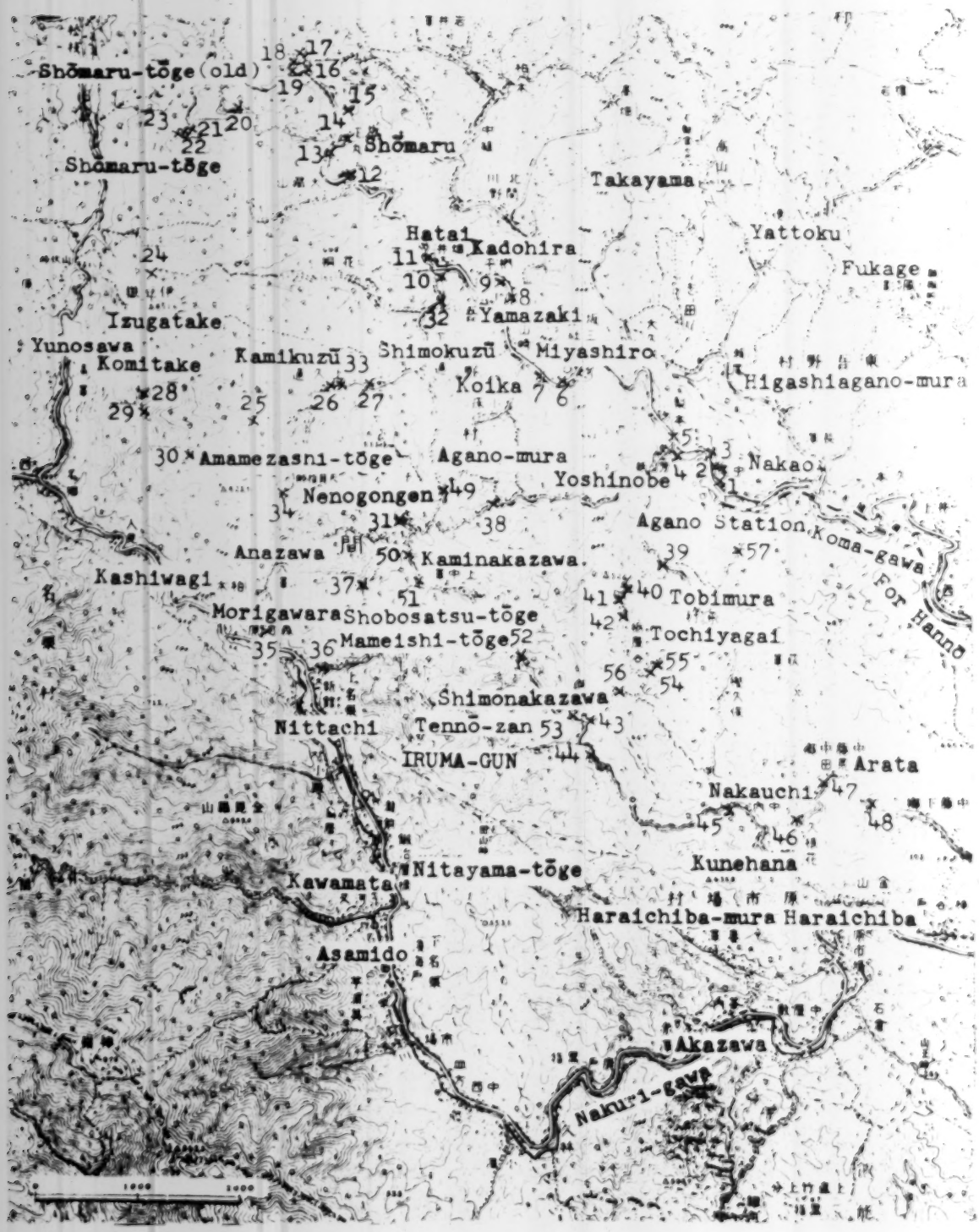

Fig. 1. Map showing the location where the specimens of sandstones were collected.

heavy minerals separated by their mechanical analyses, it was proved that igneous activities also took place before the deposition of the Chichibu System in this district. They are partly represented by granitic intrusions similar to those shown by the Usuginu conglomerate.

The writers are deeply indebted to Mr. R. Morikawa for his many useful suggestions during their field and laboratory works.

General Features.

It is necessary to give a short description of the area where sandstones were collected before the writers explain the various characters of these specimens. The district under consideration is interposed between the Koma-gawa and Nakuri-gawa and is easily accessible from Agano or Hannō of the Musashino Railway Line. It is a mountainous area extending from northwest to southeast along the backbone ridge passing through Shōmaru Pass, Izugatake, Komitake, Amamezashi Pass, Nenogongen, Mameishi Pass, etc. The highest peak here is called Izugatake, about two kilometers to the south of Shōmaru Pass, and rises up to 851.4 meters above sea-level. One of the characteristic topographical features of this area is the abundance of steep ridges due to the predominance of siliceous sediments. This is indicated clearly by Izugadake, Komitake and others (Figs. 1–2).

Fig. 2. A part of the mountainous area under consideration viewed from Takayama. 1 = Izugadake, 2 = Komitake.

The Chichibu system exposed here is composed of chert, schalstein, clayslate, shale, sandstone, limestone and conglomerate. The beds of these rocks were subjected to intense folding and faulting and show varying strikes and dips from place to place. Such a feature is commonly seen in chert beds here and there. They have, however, a general strike of N 40°–60° W and are repeatedly folded with large anticlinal or synclinal structures.

Of these sediments, chert is most extensively exposed in close associ-

ation with schalstein and limestone. They are frequently intercalated by sandstone and clayslate or shale. Sandstone seems to occur in several horizons and is occasionally found together with clayslate or shale, but the same bed has a tendency to be not traceable for a long distance. Ample exposures of this rock may be seen along the bus road between Agano and Shōmaru Pass as well as in the area including Izugadake, Amamezashi Pass, Nenogongen, Kaminakazawa, etc. In these cases, some sandstone beds are 150 meters or more in the thickest part. The occurrence of limestone is also known in many places, assuming mostly a lenticular form in alternated beds of chert and schalstein. The largest mass is now mined on the ridge behind the Agano Station for the purpose of cement industry. It is very noteworthy that the limestone of this area contains *Schwagerina*, *Neoschwagerina*, *Pseudoschwagerina* and *Yabeina*. Such *Fusulina*-bearing limestones are divided by Morikawa[5] into five zones, viz., (i) *Yebeina* zone (Kamikuzū, Yoshinobe, Tennō-zan, Nitayama Pass, etc.), (ii) *Neoschwagerina* zone (Asamido), (iii) *Schwagerina tschernyschewi* —*S. kraffti* zone (Nakao, Nenogongen, etc.), (iv) *Schwagerina vulgaris* zone (Koika, Shōmaru Pass, Shimokuzū, Tobimura, etc.) and (v) *Pseudoschwagerina* zone (Kamikuzū, Old Shōmaru Pass, etc.). From such a paleontrogical evidence, the sandstone-bearing formation of this district is assigned to the Permian.

Moreover, conglomerate is exposed on the river bed of Shimokuzū, 1 kilometer south of Hatai. It consists of abundant limestone pebbles and schalstein-like matrix. Morikawa[6] obtained many fossils from these pebbles with a greyish white or black color. They are *Pseudoschwagerina* sp., *Schwagerina vulgaris*, *S. tschernyschewi S. kraffti*, *Parafusulina japonica* var. *hayasakai*, *P. kaerimizuensis*, *Nagatoella fujimotoi*, *Mizza velebitana* and *Pleurotomaria* sp.

Distribution and Structure of Sandstone Beds.

The Chichibu System of this district is intensely folded and repeats anticline or syncline whose axis extends from northwest to southeast or west-northwest to east-southeast. The distribution of sandstone beds here depends upon such geological structure, and the same beds are repeatedly exposed.

One of these beds is traceable along the axis of anticline which seems to pass through Yunosawa, Amamezashi Pass, Kaminakazawa and

5) Personal communication by R. MORIKAWA.
6) R. MORIKAWA, *op. cit.*, 1952, 187-190.

Shimonakazawa. It appears on each wing and respectively show a steep inclination northeastwards.

By proceeding eastwards, there is also found a remarkable sandstone bed almost parallel to the exposures mentioned above. It can sporadically be followed from Kamikuzū to Tobimura and is supposed to be of a more upper horizon.

Such sandstone bed reappear along the Koma-gawa beyond the axis of syncline which stretches from Kamikuzū to Yoshinobe. This can be confirmed by the distribution of *Fusulina*-bearing limestones in this area. They are amply exposed on the bed of the Koma-gawa and the cutting of the bus road between Agano and Shōmaru Pass, forming here an anticline which again passes into a syncline in the adjacent area.

Moreover, minor exposures are observed here and there at Morigawara, Nittachi, Tochiyagai, Nakauchi, Arata, Mameishi Pass, etc.

Megascopical Characters of Sandstones.

Sandstone is one of predominant sediments of the Chichibu System in this district. It is generally represented by fine or medium-grained sandstone with a gray or black color in fresh specimens. The sandstone here is so hard and compact that it can not easily be crushed by a hammer.

Megascopically, most of the specimens are rich in quartz and feldspar, containing small fragments of black clayslate with or without regular arrangement. There are also some specimens intercalated with thin layers of clayslate and traversed by calcite veinlets. Through weathering, such sandstones obtain a yellowish brown color and is frequently stained with iron oxides.

Mineral Components and Rock-fragments in Sandstones.

Fifty seven specimens of sandstone (Fig. 1) were mechanically analysed to find out how many kinds of heavy minerals are contained in them. Moreover, each of these specimens was examined under the microscope by using thin sections. Both microscopical investigations and mechanical analyses indicate that the sandstone of the Chichibu System consists of quartz, orthoclase, microcline, plagioclase, biotite, calcite, glauconite, muscovite, sericite, allanite, anatase, augite, epidote, garnet, hornblende, hypersthene, ilmenite, limonite, magnetite, pyrite, pyrrhotite, rutile, titanite, zircon and zoisite.

Of these minerals, quartz is alway present abundantly, occurring as angular pieces, large or small, which occasionally show a wavy extinction.

They are filled up by arenaceous substances, and there are some grains penetrated by calcite veinlets.

The next predominant components are feldspars represented by orthoclase, microcline and plagioclase. So far as is known at present, orthoclase is found in almost all specimens examined by the writers, but is found with less frequency as compared with plagioclase. It is characterized by the abundance of perthite.

Microcline is partly microcline-perthite and usually occurs in a minor amount. It is absent in some specimens.

Plagioclase is, on the other hand, to be seen in all thin sections and ranges from albite to labradorite.

In these cases, feldspars have mostly a fresh appearance, although they are sometimes sericitized and invaded by calcite.

One of the important minerals is indicated by biotite whose occurrence is confirmed in all thin sections and by mechanical analyses. It is strongly pleochroic from light yellow (X) to dark brown (Y and Z) or light yellow (X) to reddish brown (Y and Z). The crystal is generally twisted and often takes an irregular form. Chlorite is an alteration product of this mineral.

Calcite is a secondary mineral derived from plagioclase or other calcareous sources. It is particularly abundant in the specimens collected at Shimonakazawa.

Glauconite is a very rare component found only in the sandstone which is exposed at Miyashiro and Kadohira. It has a bright green color and reveals an aggregate polarization.

Sericite flakes are contained in feldspars and feldspathic matrix and are more conspicuous than platey muscovite. Muscovite is commonly seen in the specimens from Shōmaru, Shōmaru Pass, Nenogongen, Nittachi, Arata, Tochiyagai, etc.

Allanite is rarely found in the sandstones exposed at Yoshinobe, Miyashiro, Kadohira, Hatai, Shōmaru, etc. It takes an irregular form and is strongly pleochroic from light brown to dark brown or dark reddish brown.

Anatase is only known in the specimens from Miyashiro, Kadohira and Hatai. The mineral has an indigo-blue color and is weakly pleochroic.

Augite is also rare and occurs in a prismatic or irregular form. It has a light green color and weak pleochroism. The crystal is noticed in the specimens from Shōmaru Pass, Amamezashi Pass, Morigawara, Kunehana, etc.

Epidote is a noteworthy mineral with a yellow or greenish yellow

color. It is weakly pleochroic and indicates a bright interference color. The crystal shows high frequency in the specimens from Nakao, Miyashiro, Hatai, Shōmaru, Morigawara, Nittachi, Nenogongen, Tochiyagai, Shimonakazawa, Nakauchi, etc.

Besides epidote, one of the important heavy minerals is garnet. The most pre-dominant is colorless or of a pink variety. There is also another kind of this mineral with a light reddish brown or a reddish brown color. Such different types of garnet are almost free of optical anomaly. In all specimens, garnet usually occurs as rounded or angular grains, but beautiful rhombic dodecahedron or combination of icositetrahedron and rhombic dodecahedron is respectively shown in the specimens from the ridge between Shōbosatsu Pass and Nenogongen as well as from Miyashiro.

Hornblende and hypersthene are unimportant components. The former is a green variety with a somewhat bluish shade, showing such a pleochroic scheme as light yellow (X), green or yellowish green (Y) and bluish green (Z), whereas the latter is pleochroic from yellow (X) to brownisn yellow (Y) or greyish green (Z). Both minerals have a prismatic or irregular form.

Magnetite and ilmenite are generally associated together, the latter being more abundant than the former. In this case, ilmenite passes into leucoxene on its surface. Hematite is very scarce, but limonite is an abundant secondary mineral.

Pyrite is present in most specimens. It is found in oolitic aggregates or single grains and is exceedingly plentiful in some specimens. This mineral is supposed to have been in close association with the deposition of sandstones. Pyrrhotite is, on the other hand, contained scantily only in two specimens.

Rutile is not widely distributed, but it is occasionaly seen in the specimens from Hatai and the ridge between Komitake and Amamezashi Pass. Mostly, the mineral occurs as rounded grains or angular fragments, although there are some prismatic crystals. Rutile has a reddish brown or yellowish brown or light yellow color and is weakly pleochroic, being characterized by the high index of refraction and adamantine luster.

Titanite is a common mineral in most specimens. It is, however, always found in low frequency, and there are some varieties different in color, ranging from nearly colorless to light brown or brownish yellow under the microscope. Of these, the brownish varieties are weakly pleochroic from colorless to light yellowish brown. The crystal generally has an irregular form. Moreover, it is very high in its index of refraction and birefringence.

The presence of tourmaline is known in many specimens. It is particularly noticeable in those collected from Shōmaru, the ridge between Komitake and Amamezashi Pass, Amamezashi Pass, Nenogongen, Kaminakazawa, Shimonakazawa, Agano, Kunehana and Arata. The crystal takes mostly a granular or fragmental form, although some of it has a stout prismatic habit. The mineral is strongly pleochroic with varying absorption color., (i) X=light brown, Z=brown: (ii) X=light blue, Z=blue: (iii) X=light bluish grey, Z=greyish blue: (iv) X=reddish brown, Z=dark brown: (v) X=yellowish brown, Z=dark brown, etc.

Zircon is an important heavy mineral with a prismatic or granular form. It is represented by the colorless or purple variety. The former is more abundant than the latter. When the crystal is well preserved, zircon has a stout or slender prismatic form, occurring usually in such

Table I. Mineral components and

	1	2	3	4	5	6	7	8	9	10	11	12	13	14	15	16	17	18	19	20	21	22	23	24
Quartz	×	×	×	×	×	×	×	×	×	×	×	×	×	×	×	×	×	×	×	×	×	×	×	×
Microcline			×			×	×	×			×	×	×	×	×	×	×	×	×	×	×		×	×
Orthoclase	×	×	×	×	×	×	×	×	×	×	×	×	×	×	×	×	×	×	×	×	×	×	×	×
Plagioclase	×	×	×	×	×	×	×	×	×	×	×	×	×	×	×	×	×	×	×	×	×	×	×	×
Biotite				×	×	×	×	×	×	×	×	×	×	×	×	×	×	×	×	×	×	×	×	×
Calcite	×	×	×	×			×		×	×														
Chlorite	×			×	×	×			×	×	×	×	×	×	×	×	×	×	×	×	×	×	×	×
Glauconite						×		?	×															
Sericite (muscovite)	×	×	×	×	×	×	×	×	×	×	×	×	×	×	×	×	×	×	×	×	×	×	×	×
Allanite				×	×	×	×	?	×		×				×						×			
Anatase						×		×			×													
Augite																					×		×	
Epidote	×	×	×	×	×	×	×	×	×		×	×	×	×	×	×	×	×	×	×	×	×	×	×
Colorless garnet	×	×	×		×	×	×	×	×	×	×	×	×	×	×	×	×	×	×	×	×	×	×	×
Light reddish brown or reddish brown garnet			×	×	×	×	×	×		×	×		×	×		×	×		×	×	×	×	×	×
Pink garnet	×	×	×	×	×	×	×	×	×	×	×	×	×	×	×	×	×		×	×	×	×	×	×
Hornblende					×																			
Hypersthene		×		×						×				×				×			×	×	×	
Limonite	×		×		×	×	×	×	×		×	×	×			×	×	×	×	×	×	×		×
Magnetite (ilmenite, hematite)	×	×	×	×	×	×	×		×	×	×	×	×	×	×	×	×	×	×	×	×		×	×
Pyrite	×	×	×	×	×		×		×	×	×			×					×	×				×
Pyrrhotite					×	×					×													
Rutile			×											×		×					×			
Titanite	×	×	×	×	×	×	×	×	×		×	×	×	×		×	×		×	×	×	×	×	×
Tourmaline				×	×	×	×		×		×			×	×	×	×	×	×		×	×		×
Colorless zircon	×	×	×	×	×	×	×	×	×	×	×	×	×	×	×	×	×	×	×	×	×	×	×	×
Purple zircon		×	×	×	×	×	×	×	×	?	×	×	×	×	×	×	×	×	×	×	×			
Zoisite		×												×										
Chert	×	×	×	×	×	×	×	×	×	×	×	×	×	×	×	×	×	×	×	×	×	×	×	×
Schalstein	×	×	×	×	×	×	×	×	×	×	×	×	×	×	×	×	×	×	×	×	×	×	×	×
Clayslate	×	×		×	×	×	×	×	×	×	×	×	×	×	×	×	×	×	×	×	×	×	×	×
Crystalline schist								×										×						×

combinations as (100), (110); (111), (110), (100); and (110), (111), (100), (311). Among these combinations, the first two are commonly observed. Purple zircon is commonly rounded except that contained in the specimen of Shōmaru. Sometimes, it encloses small prismatic or granular crystals with indistinct characters. Zoisite is a negligible component.

Besides component minerals mentioned above, the sandstones of the Chichibu System contain many angular pieces of schalstein, chert, clayslate and crystalline schist. Of these, the most abundant is black clayslate of a microscopical or megascopical size. Exclusive of such crystalline schists as graphite schist, graphite quartz schist, quartz schist, sericite schist, etc., they are found in almost all specimens investigated by the writers.

Mineral components and rock-fragments contained in sandstone under consideration are summarized in the following table.

rock-fragments in sandstones.

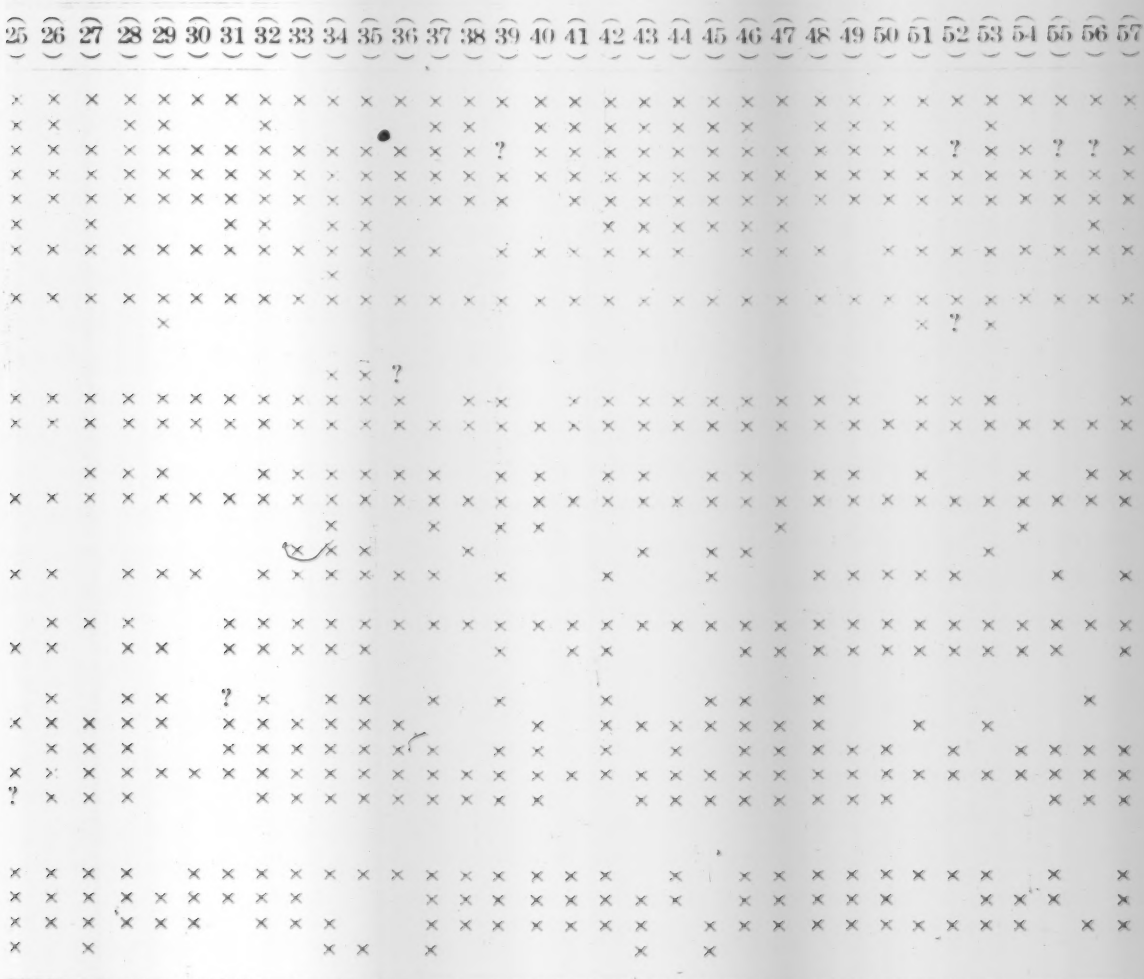

Localities of sandstones in the preceeding table.

		Village	District	Prefecture
(1)	Nakao,	Agano-mura,	Iruma-gun	Saitama
(2)	〃 ,	〃	〃	〃
(3)	〃 ,	〃	〃	〃
(4)	Yoshinobe,	〃	〃	〃
(5)	〃 ,	〃	〃	〃
(6)	Miyashiro ,	〃	〃	〃
(7)	〃 ,	〃	〃	〃
(8)	Kadohira ,	〃	〃	〃
(9)	〃 ,	〃	〃	〃
(10)	Hatai,	〃	〃	〃
(11)	〃 ,	〃	〃	〃
(12)	Shōmaru,	〃	〃	〃
(13)	〃 ,	〃	〃	〃
(14)	〃 ,	〃	〃	〃
(15)	〃 ,	〃	〃	〃
(16)	Shōmaru—Shōmaru Pass,	〃	〃	〃
(17)	〃 ,	〃	〃	〃
(18)	〃 ,	〃	〃	〃
(19)	〃 ,	〃	〃	〃
(20)	〃 ,	〃	〃	〃
(21)	〃 ,	〃	〃	〃
(22)	〃 ,	〃	〃	〃
(23)	〃 ,	〃	〃	〃
(24)	Izugatake,	Agano-mura—Nakuri-mura	〃	〃
(25)	Kamikuzū,	Agano-mura	〃	〃
(26)	〃 ,	〃	〃	〃
(27)	〃 ,	〃	〃	〃
(28)	Izugatake—Amamezashi Pass,	Agano-mura—Nakuri-mura	〃	〃
(29)	〃	〃	〃	〃
(30)	〃	〃	〃	〃
(31)	Nenogongen,	Agano-mura	〃	〃
(32)	Hatai,	〃	〃	〃
(33)	Kamikuzū,	〃	〃	〃
(34)	Amamezashi Pass,	Agano-mura—Nakuri-mura	〃	〃
(35)	Morigawara,	Nakuri-mura	〃	〃
(36)	Nittachi,	〃	〃	〃
(37)	Shōbosatsu Pass—Nenogongen,	Agano-mura	〃	〃
(38)	Nenogongen—Yoshinobe,	〃	〃	〃
(39)	Yoshinobe—Tochiyagai,	〃	〃	〃
(40)	Tochiyagai,	〃	〃	〃
(41)	〃 ,	〃	〃	〃
(42)	〃 ,	〃	〃	〃
(43)	Shimokuzū—Nakauchi,	Agano-mura—Furuichiba-mura	〃	〃
(44)	Nakauchi,	Furuichiba-mura	〃	〃
(45)	Kunehara,	〃	〃	〃
(46)	Arata,	〃	〃	〃
(47)	〃 ,	〃	〃	〃
(48)	Koika—Nenogongen,	Agano-mura	〃	〃
(49)	Nenogongen—Kaminakazawa,	〃	〃	〃
(50)	Kaminakazawa,	〃	〃	〃
(51)	Kaminakazawa—Shimonakazawa,	〃	〃	〃
(52)	Kaminakazawa—Shimonakazawa,	〃	〃	〃
(53)	Shimonakazawa,	〃	〃	〃
(54)	Tochiyagai,	〃	〃	〃
(55)	〃 ,	〃	〃	〃
(56)	Shimonakazawa,	〃	〃	〃
(57)	Agano,	〃	〃	〃

Sources of Mineral Components.

So far as is known at present, sandstones of this area have various mineral components, differing somewhat from place to place. There is, however, no characteristic mineral which is stratigraphically important to distinguish minerallogically the horizons of sandstone beds.

Of several kinds of light mineral, feldspars are found in almost the same frequency as quartz grains. On of the striking features indicated by thin sections is the abundance of perthite. This intergrowth can be seen even in microcline crystals, suggesting that they were supplied from granitic rocks together with some plagioclase and other microcline crystals. Moreover, this fact is proved by the occurrence of many fragments with a micropegmatitic or micrographic texture and biotite flakes as well as of titanite and allanite. Quartz is believed to have derived partly from such siliceous rocks as granite, granodiorite, granite porphyry and quartz porphyry. It is also noteworthy that there are rounded quartz grains subjected to magmatic corrosion. Some of the rock-fragments evidently resemble intrusive feldspathic rocks. Among various heavy minerals, anatase may have its source in quartz porphyry.

As to garnet, it is represented by several varieties with different colors and it is not clear what kinds of rock they were originally contained in. It is, however, conceivable that there are some garnets drived from the contact aureole between calcareous rocks and granites, because epidote crystals are always found together with them in almost all specimens of sandstone. Similarly, clayslate, shale and sandstone within the contact aureole may be the source of tourmaline crystals, although it is likely to occur in granite and its pegmatite as well as in granitic contamination rocks.

As to hornblende, it is uncertain whether this mineral was furnished from igneous rocks or not, but hypersthene has occasionally well-defined crystal forms and is supposed to have been an ingredient of such volcanic rocks as andesite

Rutile seems, on the other hand, to have been supplied from metamorphic rocks. On this point, the presence of garnet affords an important clue to the source of rutile.

Possibilities of Igneous Activities prior to the deposition of the Chichibu System.

The sandstones exposed here mostly indicate a high frequency of mineral components which are commonly seen in granitic rocks, suggesting

that there were some granitic intrusions before the sedimentation of the Chichibu System of this district.

The distribution of such plutonic rocks is, however, quite unknown in any part of present Japan, as has been already stated by Yamada[7] on the sources of granite pebbles contained in the Usuginu conglomerate. Moreover, all kinds of granitic rock in Japan are now believed to be younger than the Chichibu System, but it is conceivable that older granitic rocks had once been exposed somewhere in the area which disappeared later by folding and faulting. The angularity and fresh appearance of mineral components mentioned above may be an evidence that the exposures of granitic rocks were not very far from the geosyncline where the deposition of the Chichibu System took place. From such evidences, it is also inferrable that these granitic rocks subsided to the bottom of the Japan Sea. Yamada[8], however, formerly attributed their sources to granitic rocks of the continent.

The possibility of igneous activities are, furthermore, supported by the presence of corroded quartz and hypersthene as well as of augite. They are likely to have been contained in such igneous rocks as quartz porphyry, liparite, dacite and andesite. The frequent occurrence of schalstein-fragments in sandstone is also an important evidence of volcanic activities.

Summary.

1) The Chichibu System exposed in this area is composed of chert, schalstein, limestone, conglomerate, sandstone, shale and clayslate. Of these, the most predominant are chert and schalstein.

The Chichibu System here was intensely subjected to folding and faulting. It has, however, a general strike of N 40°–60° W, repeating large anticlinal or synclinal structures.

2) For the purpose of ascertaining the mineral components of sandstone, many specimens of this rock were collected from various places of the area including Hannō, Agano and Shōmaru Pass. They were determined by microscopical investigations of thin sections and heavy minerals separated by mechanical analyses.

3) So far as is known at present, these sandstones contain such minerals as quartz, orthoclase, microcline, plagioclase, biotite, calcite, glauconite, allanite, anatase, augite, epidote, garnet, hornblende, hyper-

7) H. YAMADA, *op. cit.*, 692-693.
8) ,, *op. cit.*, 693.

sthene, ilmenite, limonite, magnetite, pyrite, pyrrhotite, rutile, sericite (muscovite), titanite, zircon and zoisite.

4) Such mineral components are characterized by the frequent occurrence of orthoclase (abundant in perthite), microcline, microcline-perthite and fragments with a micropegmatitic or micrographic texture, as well as of titanite and allanite. These minerals are supposed to have been supplied from granitic rocks.

5) The sources of corroded quartz grains, hypersthene and augite may be quartz porphyry, liparite, dacite and andesite.

6) It is also noteworthy that most of the sandstones are frequently rich in angular pieces of schalstein.

7) Judging from these evidences, it is quite possible that there were granitic intrusions and other volcanic activities prior to the deposition of the Chichibu System of this district. The angularity and fresh appearance of mineral components seem, furthermore, to suggest that their sources had not been very far from the geosyncline where the sedimentation of the Chichibu System took place. It is, however, still obscure whether such sources existed really in Japan or in the area now covered by the Japan Sea or elsewhere. This is an important problem awaiting solution.

14. 秩父系堆積前の火成活動

地震研究所　市村　毅
教養学部地学教室　松林晴子

飯能から吾野及正丸峠に跨る山岳地域には，チヤート，輝緑凝灰岩，石灰岩，粘板岩，頁岩などゝ共に砂岩を伴う秩父系が広く露出している．これ等の中，各産地から採取した砂岩に就き，薄片及機械分析によって分離した重鉱物の顕微鏡的研究を行った結果，火成岩に根源を有する種々の鉱物を含むことが分った．殊にパーサイト，マイクロクラインパーサイト，微ペグマタイト状或は微文象状組織を有する破片，黒雲母，燐石，褐簾石などを屢々含むことは，砂岩の材料が花崗岩及花崗閃緑岩の如き酸性深成岩及その関係岩類から供給されたことの証據であり，又融蝕された石英の結晶，形態の整つた紫蘇輝石などの存在は，前者が石英斑岩，石英粗面岩，石英安山岩などの何れかの斑晶であったことゝ，後者が安山岩の如き火山岩の鉱物成分だったことを物語るものである．

以上の事実から判断して，此地域に露出する秩父系の堆積以前には火成活動，特に花崗岩質深成岩の貫入があったことが想像されるし，更に他方では石英斑岩，石英粗面岩，石英安山岩の様な石英斑晶を有する火成岩や安山岩などが露出していたことも，輝緑凝灰岩が示す如き火山活動も考えられる．然も各鉱物が比較的新鮮であり，且つ甚しく角立っている点は，秩父系が堆積した地向斜から余り遠くなかった処からこれ等の材料が供給された場合を暗示する様に思われる．たゞし斯る材料の根源が日本の何処にあったか，それとも今日の日本海によって占められるゝ地域にあったかに就ては，未だに不明な点が多く，それらは今後詳細な研究を要する重要な問題である．

15. *Land Deformation of the Neighbourhood of Muroto Point after the Nankaido Great Earthquake in 1946.*

By Atusi OKADA,
Earthquake Research Institute,
and
Takesi NAGATA,
Geophysical Institute.

(Read Oct. 16, 1951 and Jan. 20, 1953.—Received Mar. 20, 1953.)

Abstract.

Leveling surveys of the neighbourhood of Muroto Point, Shikoku were carried out seven times after the Nankaido great earthquake in 1946. The results of the surveys together with those before the earthquake show that the remarkable northward tilting of this locality, about 6.2″ in magnitude, accompanying the earthquake is has been gradually recovering, and the present rate of southward tilting nearly constant, being 0.035″/year, which is almost equal to that for the pre-earthquake period. The main results are graphically represented in Figs. 4 and 5.

Introduction.

In their previous paper[1], the writers dealt with a remarkably regular deformation of Muroto Point which was associated with the great earthquake on December 21, 1946. According to the results of precise leveling surveys made in 1895, 1929 and 1932, Muroto Point had been inclining in the direction of S 10° E with an almost constant velocity of 0.035″/year for more than 40 years before the earthquake, while the abrupt change accompanying the earthquake was exactly opposite in sense, namely the point inclined by about 6.2″ in the direction of N 10° W.

After the earthquake, leveling surveys were repeated four times, namely in January, February, March and July in 1947, and their results show that the Point was again inclining in about a S 10° E direction with a fairly large velocity compared with that of the pre-earthquake period. According to T. Okuda,[2] on the other hand, the land deformations occurring simultaneously with the earthquake over the whole area of Shikoku are

1) T. NAGATA and A. OKADA, *Bull. Earthq. Res. Inst.*, **25** (1947), 85.
2) T. OKUDA, *Bull. Geograph. Survey Bureau*, **2** (1951), 239.

just opposite in sense to those during the pre-earthquake period. This fact may suggest that the land deformation is closely related to the mechanism of occurrence of the earthquake. Then, Muroto Point, which showed the most remarkable and regular deformation within Shikoku, may be considered to be the most typical sample of the land deformation relating to seismicity in this district.

Under this circumstance, precise leveling surveys were repeatedly carried out in 1949, 1950 and 1952 in order to clarify the character of the after-earthquake movement.

Procedure and results of leveling surveys.

The leveling route concerned here is about 22 km from BM No. 5136 to BM No. 5147 along the seashore of Muroto Point, as will be seen in Fig. 1. The said route forms the two sides of a triangle, wherefore a tilting motion as a whole of the earth's crust in this locality can be definitely detected, and further a warping deformation with an east-west axis, if any, ought to be detected also. On the contrary, a warping deformation with a north-south axis, would not be detected so far as we rely on the leveling survey in our networks.

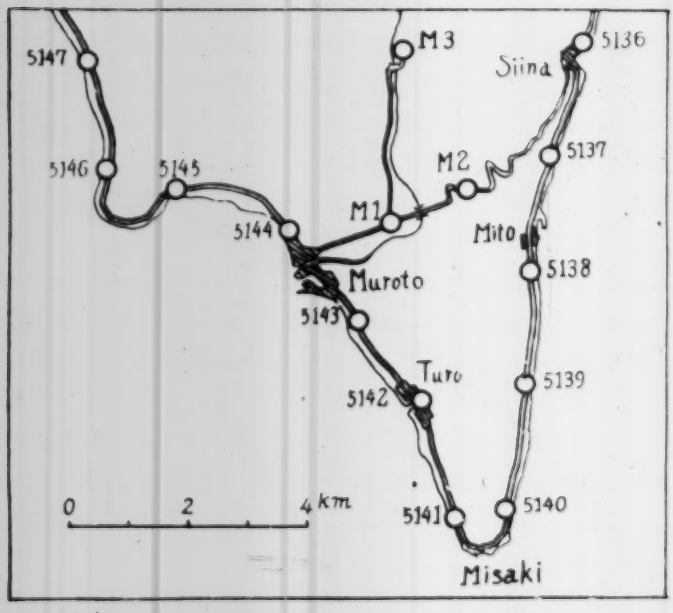

Fig. 1. Leveling route in the neighbourhood of Muroto Point.

In order to remedy the above-mentioned defect, the Geographical Survey Institute set newly three bench marks M_1, M_2 and M_3 in November, 1947 at the localities respectively shown in Fig. 1. Along all the routes including the branch routes mentioned above, the first-class precise leveling surveys (by means of a Zeiss level) were carried out in April 1949, January 1950 and December 1952. Throughout all the surveys, BM No. 5136 was always chosen as the reference point for height measurement. In Table I, the relative heights of each bench mark with respect to BM No. 5136 at respective epochs are summarized together with those obtained by the

Table I.

Relative heights of each bench mark in the neighbourhood of Muroto Point.

BM \ Date	1947 (I)	1947 (II)	1947 (III)	1947 (VII)	1949 (IV)	1950 (I)	1952 (XII)
5136	m —	m +1.4388	m —	m +1.4432	m +1.4327*	m +1.4262**	m +1.4254***
5137	−1.3874	−1.3782	−1.3784	−1.3812	−1.3845*	−1.3944**	−1.3989***
5138	−0.1831	−0.1884	−0.1870	−0.1860	−0.1894*	−0.1921**	−0.1925***
5139	+2.0786	+2.0597	+2.0556	+2.0538	+2.0561*	+2.0439**	+2.0428***
F.46	−1.3576	−1.3480	−1.3539	−1.3504	−1.3485*	−1.3488**	−1.3476***
5141	+3.7490	+3.7526	+3.7574	+3.7534	+3.7535*	+3.7636**	+3.7674***
5142	−2.2820	−2.2759	−2.2738	−2.2914	−2.2892*	−2.2861**	−2.2834***
5143	−2.1830	−2.1325	−2.1196	−2.1352	−2.1319*	−2.1239**	−2.1234***
5144	—	+4.2170	—	+4.3220	+4.2177	+4.2236	+4.2244
5145	—	−3.5878	—	−3.5835	−3.5817	−3.5810	−3.5798
5146	—	+0.0362	—	+0.0294	+0.0424	+0.0449	+0.0456
5147							

	1947 (XI)	1949 (IV)	1950 (I)	1952 (XII)
5144	m + 9.5149	m + 9.5196*	m + 9.5236**	m + 9.5235***
M_1	+27.8332	+27.8377*	+27.8416**	+27.8417***
M_2	−37.2607	−37.2561*	−37.2536**	−37.2550***
5136				
M_1	m +21.8736	m +21.8743	m +21.8865	m +21.8871
M_2				

* The closing error m −0.0070 is uniformly distributed.
** " −0.0031 "
*** " +0.0050 "

former surveys. Here, the closing errors, shown in the lowest lines of the table, are distributed uniformly along the closed leveling route.

The secular change of land deformation is represented by the difference of the height at each epoch from that in 1929 for each bench mark. The result is shown in Fig. 2 and Table II, where it is assumed that the reference point BM No. 5136 remains constant throughout the whole period. As for M_1, M_1 and M_2, the change of their height at each epoch from the value of the first survey in November 1947 is shown in Fig. 2 and Table II, while the change of height of M_3 given there is only the relative value compared with that of M_1.

It will be obvious from these results that the remarkable land

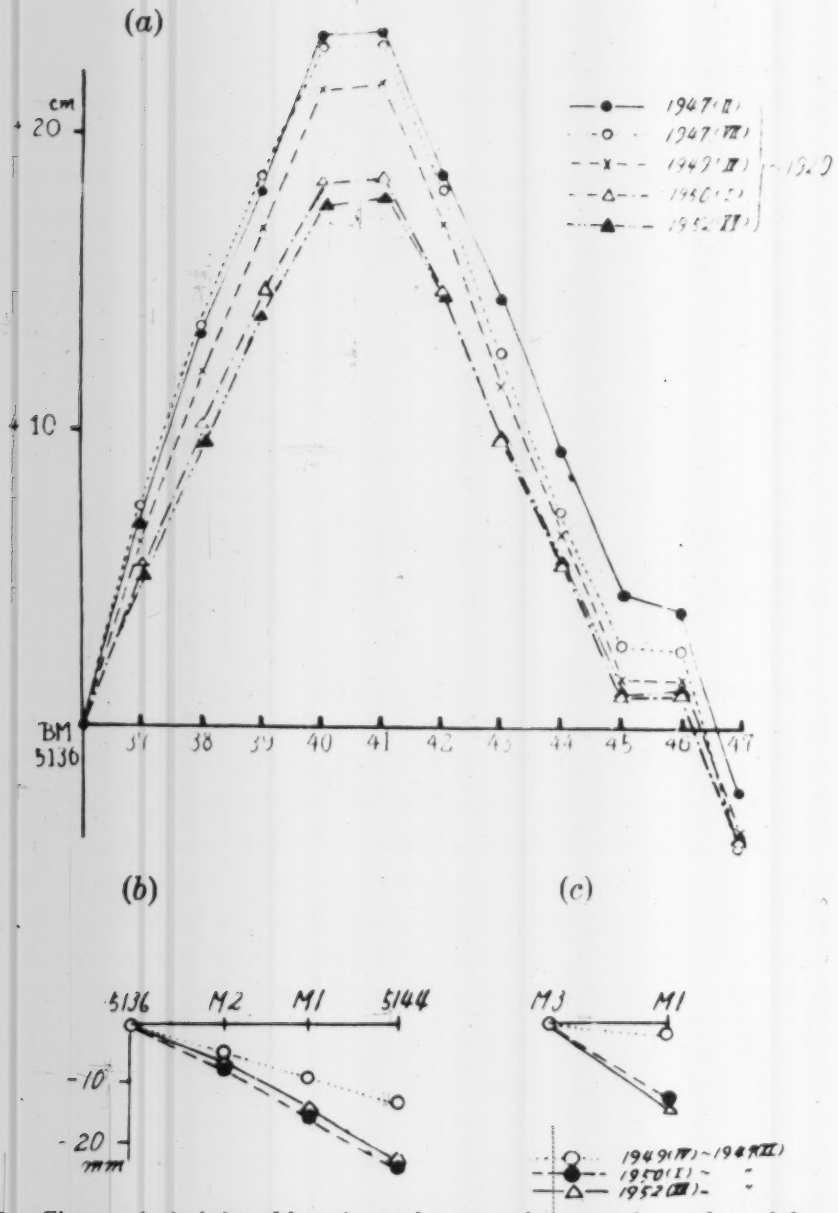

Fig. 2. Change in height of bench marks at various epochs reckoned from 1929.

deformation occurring simultaneously with the earthquake has been recovering with time. It may also be noticed, if the time interval between successive surveys is taken into consideration, that the velocity of the recovery has been gradually decreasing.

Analysis of the results.

By comparing the results given in Fig. 2 with the form of the leveling route shown in Fig. 1, one may notice that the secular change during the

Table II.

Change of height of bench marks at various epochs from that in 1929 (above) and from that in 1947 (below). (The height of BM 5136 is assumed to be zero throughout the whole period).

	(BM)	1947 (II) -1929	1947 (VII) -1929	1949 (IV) -1929	1950 (I) -1929	1952 (XII) -1929
		mm	mm	mm	mm	mm
(*a*)	5136	0.0	0.0	0.0	0.0	0.0
	5137	+ 67.8	+ 72.2	+ 61.7	+ 55.2	+ 54.4
	5138	+131.7	+133.1	+119.3	+102.9	+ 97.6
	5139	+180.3	+184.1	+166.9	+147.8	+142.1
	F 46	+231.3	+229.2	+214.3	+183.0	+176.2
	5141	+233.4	+228.9	+215.9	+184.3	+178.7
	5142	+184.8	+181.1	+168.2	+146.7	+144.9
	5143	+144.0	+124.8	+114.1	+ 95.7	+ 96.6
	5144	+ 93.8	+ 71.9	+ 64.5	+ 54.1	+ 55.5
	5145	+ 43.5	+ 26.6	+ 14.9	+ 10.4	+ 12.6
	5146	+ 37.5	+ 24.9	+ 15.0	+ 11.2	+ 12.8
	5147	− 21.6	− 41.0	− 37.9	− 39.2	− 36.9
	(BM)	1949 (IV) -1947 (XI)	1950 (I) -1947 (XI)	1952 (XII) -1947 (XI)		
		mm	mm	mm		
(*b*)	5136	0.0	0.0	0.0		
	M_2	− 4.6	− 7.1	− 5.7		
	M_1	− 9.1	−15.5	−14.2		
	5144	−13.8	−24.2	−22.8		
		mm	mm	mm		
(*c*)	M_1	0.0	0.0	0.0		
	M_2	+ 0.7	+12.9	+13.5		

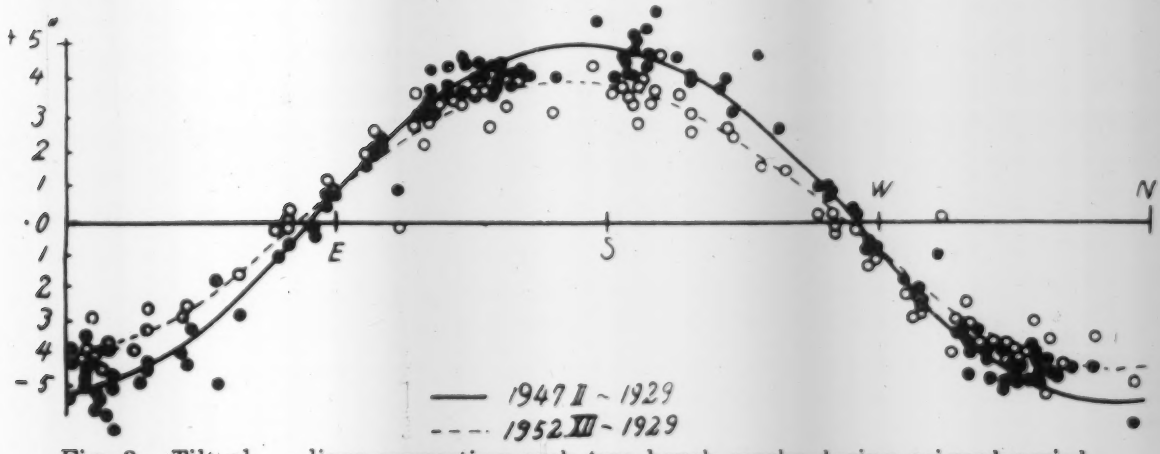

Fig. 3. Tilt a' lines connecting each two bench marks during asigned period. (After . . be's method)

Table III.
Magnitude and direction of tilt of the neighbourhood of Muroto Point, reckoned from the level of 1929.

Period	Magnitude of tilt (φ)	Direction of tilt (A)
1929-1947 (II)	4.95″	S 10°E
1929-1947 (VII)	4.42″	S 10°E
1929-1949 (IV)	4.20″	S 2°E
1929-1950 (I)	3.73″	S
1929-1952 (XII)	3.62″	S 12°E

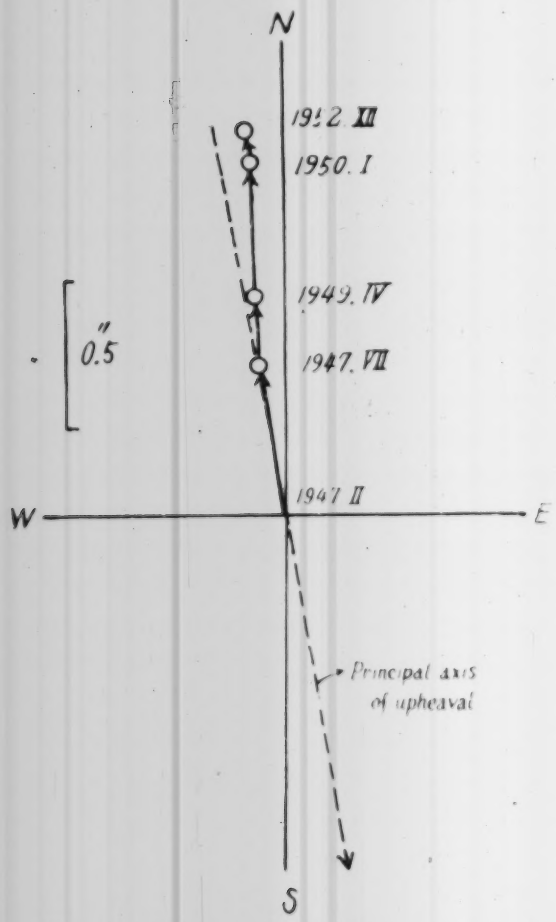

Fig. 4. Vector representation of tilting motion in the neighbourhood of Muroto Point after the earthquake.

post-earthquake period as well as the abrupt deformation simultaneous with the earthquake mainly consist of a simple tilting motion and hardly any warping deformation can be detected. This argument will be more decisively expressed by the examples shown in Fig. 3, where the change of all bench marks during 1929~1947 (full circles) and 1929~1952 (hollow circles) are represented with the aid of Miyabe's method.[3] The magnitude (φ) and direction (A) of tilting at respective epochs of the earth's crust of Muroto Point reckoned from the reference condition in 1929, thus determined from the sine curves obtained by Miyabe's method, are summarized in Table III. The tilting change of Muroto Point during the period of about six years after the earthquake is vectorially represented in Fig. 4, where the origin of coordinate corresponds to the epoch of February 1947, and the direction of a broken arrow indicates that of the tilting motion during 1929~1947 February.

As will be seen in this result, the direction of tilting change after the earthquake has been kept practically constant and it is almost opposite to that of the co-earthquake tilt. On the other hand, the rate of progress of tilting φ was fairly large for about one year after the occurrence of

3) N. MIYABE, *Bull. Earthq. Res. Inst.*, **2** (1931), 253.

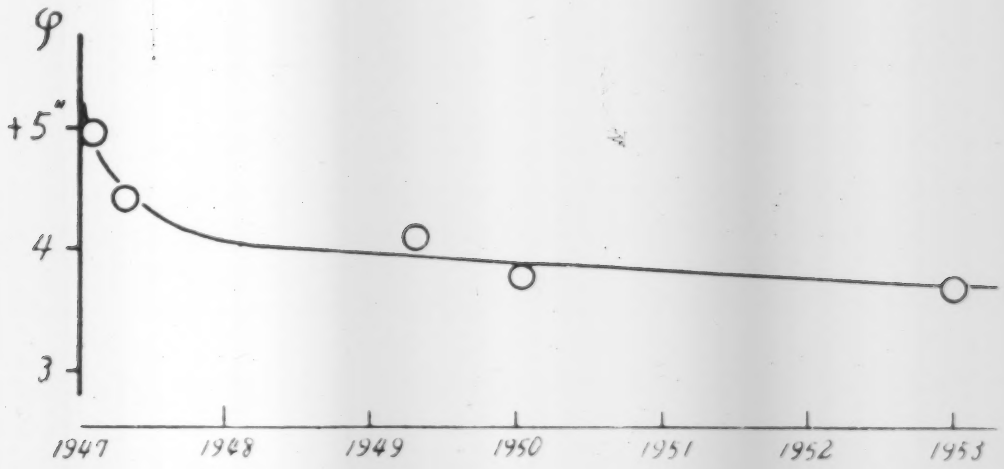

Fig. 5. Amount of tilt (into the direction of N 10° W) of the neighbourhood of Muroto Point after the earthquake.

the earthquake, but it has been diminishing gradually with time, as will be seen in Fig. 5. The empirical formula fitting the observed relation between φ and time is given by

$$\varphi = 3.90'' + 1.65'' e^{-2.232t} - 0.0348''t \ , \qquad (1)$$

where t denotes the time in unit of year reckoned from the time of occurrence of the great earthquake. It will be worthwhile to note that the third term of the above equation is practically effective for the recent years (i.e. after 1950), and it is just the same as the rate of progress of tilting motion of the same locality in the same direction during the pre-earthquake period. In other words, the rate of the after-earthquake tilting has almost recovered to the pre-earthquake steady value of about 0.035″/year, which had continued more than 40 years.

Some discussions.

The empirical formula (1) gives the amount of tilt for the after-earthquake period reckoned from the level in 1929. However, a number of observations suggest us that the pre-earthquake tilting of 0.035″/year into S 10° E direction had continued nearly uniformly until the time just before the occurrence of the earthquake. Hence, if we reckon from the level just before the earthquake in 1946, the amount of tilt for the after-earthquake period is given by

$$\varphi = 4.50'' + 1.65'' e^{-2.232t} - 0.0348''t \ . \qquad (2)$$

This means that the northward tilting of 6.15″ occuring with the earthquake

could be recovered if the present southward tilting continued for about 130 years.

The tilting motion dealt with here is not only a local phenomenon within the neighbourhood of Muroto Point, but also represents the general aspect of land deformation of a much larger area of the south-east part of Shikoku. Therefore, the northward and southward tilts result respectively in an upheaval and a subsidence of Muroto Point. Actually, the co-earthquake northward tilt there resulted in an upheaval of Muroto Point of about one meter. Since about one third of the tilt was recovered by 1953, the amount of subsidence of the Point during the period of six years after the earthquake must be about 30 cm.

According to old records the mode of land deformation accompanying both the great earthquake of 1707 and of 1854 in this district was almost the same as for the present one; namely, Muroto Point upheaved by more than one meter at the time of earthquake and gradually subsided during the interval of the earthquakes. Then, it will be seen that in this district a great earthquake accompanied by marked land deformation of a definite type has occurred periodically with a period of 100 to 150 years.

On the other hand, the old beach lines on the marine terrace along the sea coast of the neighbourhood of Muroto Point show the evidence of the periodic upheavals of this locality through a long time of many thousand years.[4] Thus, it may be assumed that a land deformation of the vicinity of Muroto Point and an occurrence of great earthquake will be directly connected to a geotechtonic motion in this district which has continued and is still going on. Consequently, it can hardly be doubted that a great earthquake will occur again in this district about 100 years from now and it will be accompanied by a land deformation quite similar to that of 1946. From this view point, studies of conceivable mechanism of the relation between earthquakes and land deformation in this district should be conducted.

Acknowledgement.

The writers are indebted to Prof. T. Hagiwara of Earthquake Research Institute and to Dr. T. Okuda of Geographical Survey Bureau for the help they afforded in the course of surveying and for their useful discussion on the present work. The present work was carried out partly by the financial support from the SHIKOKU-CHIHO-KEIZAI-KAIHATSU-IINKAI, and to the members of their staff the writers' thanks are also due.

4) G. IMAMURA, "Japan Island", p. 50, Tokyo, 1944.

15. 1946年南海道大地震後における室戸岬近傍の地殻変動

地震研究所　岡　田　悌
地球物理学教室　永　田　武

四国室戸岬近傍の精密水準測量を，1946年12月の南海道大地震以後7回繰返して施行した．これ等の測量成果と地震以前に行われた測量の結果とから次の事が言へる．

（i）地震前は40年以上の期間にわたって，S 10° E の方向へ 0.035″/年 の割合で傾動していた．

（ii）大地震に伴って，丁度反対の N 10° W の方向へ約 6.2″ 急変した．

（iii）地震後は再び S 10° E の方向へ傾動しつゝある．地震発生の時を時間 t の原点にとって，t を年単位で表わせば，地震直前に比して，任意の時 t における傾角（N 10° W 方向を正とする）φ は

$$\varphi = 4.50'' + 1.65'' e^{-2.232t} - 0.0348''t$$

で表わされる．即ち現在は，地震前におけると同じく 0.035″/年 の一定速度で S 10° E 方向への傾動が進行しつゝある．

——所　　報——

◎談話会記事

第 296 回談話会（昭和 28 年 1 月 20 日）

1. 四国高縄半島及び室戸岬附近水準測量結果　岡田　惇
   追加，秋田県焼山火山の構造と最近の爆発について　津屋弘逵

第 297 回談話会（昭和 28 年 2 月 17 日）

1. 表面波の研究 (10)
   表面波の型　ラブ波の速度を求める図表　佐藤泰夫
2. 地表層の性質と地震動振幅との関係（第 2 報）　金井清
3. 釜石の大爆破による地震動の観測　爆破地震動研究グループ
   松沢武雄
4. 中国，四国地方に於ける重力異常の分布　坪井忠二・実川順一・田島広一

第 298 回談話会（昭和 28 年 3 月 17 日）

1. 坐標変換に伴う体球函数の変換　佐藤泰夫
2. 彈性波の発生機構に関する実験（第 4 報）　笠原慶一
3. 地表を伝わる衝撃性振動の観測　・　岸上冬彦
4. 日本に於ける地磁気短周期変化の異常と地下構造（第 3 報）　横山泉・武者力・菱山よね子
5. 同上（第 4,5 報）　武者力・横山泉・菱山よね子
6. 那須鉱山の硫黄結晶　市村綏
7. 秩父系堆積前の火山活動　市村綏・松林晴子
8. 明神礁噴出の岩石について　津屋弘逵・森本良平・小坂丈予
9. 浅間火山に発生する地震の研究（続報）　水上武・佐久間修・内堀貞雄・平塚士郎・宮崎務・高橋智 外 3 名
10. 浅間山の重力測定　水上武・実川順一・田島広一
11. 近畿地方における重力異常の分布　坪井忠二・実川順一・田島広一

第 299 回談話会 (昭和 28 年 4 月 21 日)

1. 地理調査所型磁気儀の比較測定　　横山泉
2. 日立鉱山における地震動観測結果　第 4 報　　金井清・長田甲斐男・吉沢静代
3. 架構構造物における集中荷重の仮定の吟味　第 2 報　　金井清
4. 地震研究所における地震観測整備の現状 (スライド使用)　　萩原尊礼
5. 地震の場の論　その 1　地震のむれの場及びエネルギーの Menge　　松沢武雄
6. 淡路島に於ける重力測定　　坪井忠二・安芸慶一・田島広三

追加，和歌山県下の地震活動とその観測　序報　　宮村攝・堀辻実・松浦英夫

第 300 回談話会 (昭和 28 年 5 月 19 日)

1. 微小時間測定法を用いた弾性波式地下探査装置とその実際 (其の 1)　　西村源六郎・鈴木治一・古川正雄・小瀧英富・高橋浩一
2. 新型震度計の試作　　高橋龍太郎・羽鳥徳太郎
3. 表面波の研究 (11)　表面波の定義　分散性のない表面波　　佐藤泰夫
4. 地震の場の論　その 2　大地震を含む地震のむれの熱力学　　松沢武雄
5. 運研の人工地震発生装置について　　近藤正夫 (金井技官紹介)
6. 異種地盤に建つ同種建物の振動実験結果 (第 2 報)　　金井清・田中貞二・鈴木富三郎・中川恭次
7. 地震動による建物振動の観測結果 (第 2 報)　　金井清・鈴木富三郎
8. トラス橋の振動について　　岡本舜三 (那須所員紹介)
9. 三鷹における土地の脈動観測　　岸上冬彦・浅野周二
10. 関東地方における重力異常の分布　　坪井忠二・実川順一・田島広三

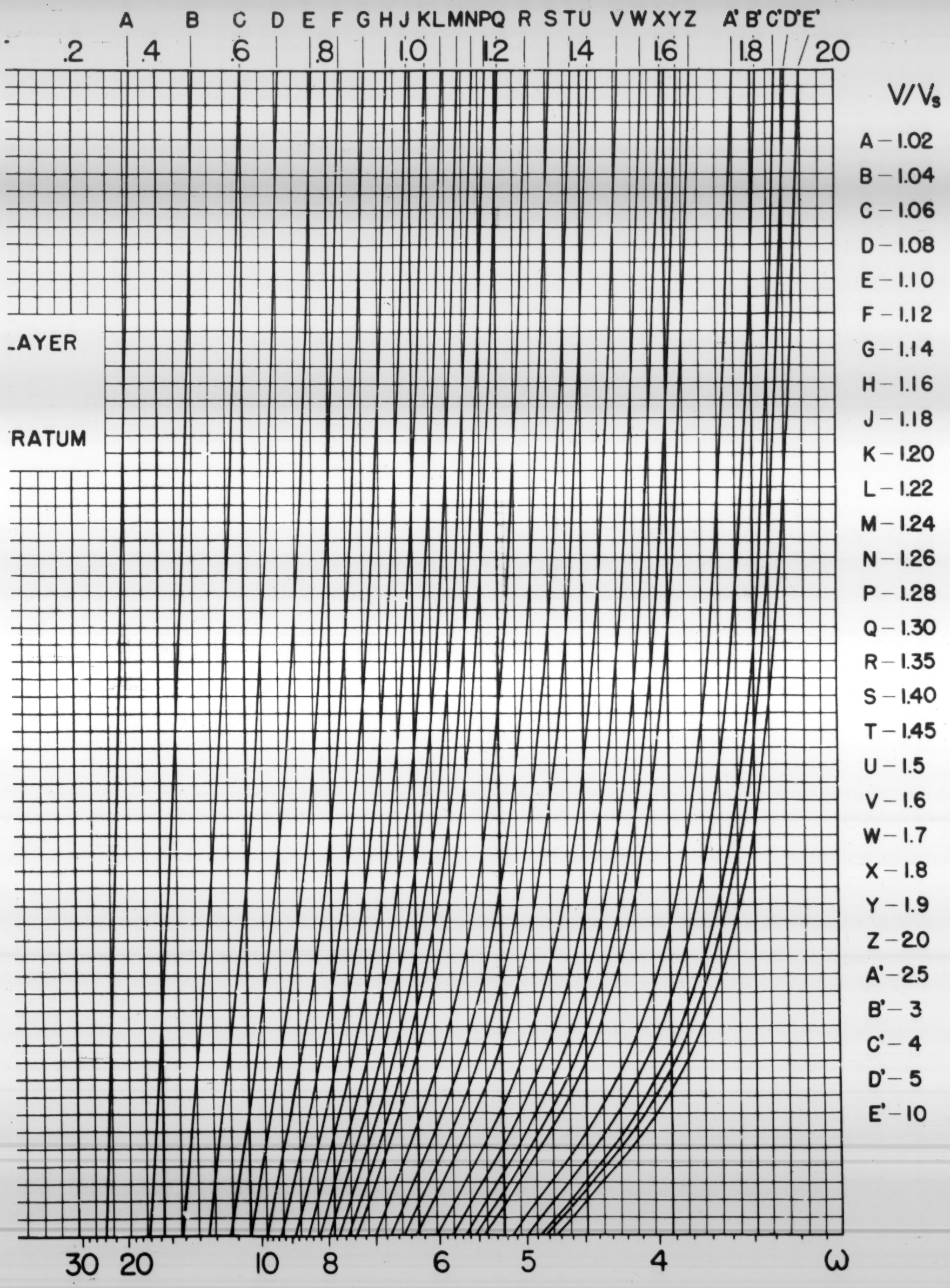
A B C D E F G H J K L M N P Q R S T U V W X Y Z A' B' C' D' E'
.2 .4 .6 .8 1.0 1.2 1.4 1.6 1.8 2.0
V/Vs
A – 1.02
B – 1.04
C – 1.06
D – 1.08
E – 1.10
F – 1.12
G – 1.14
H – 1.16
J – 1.18
K – 1.20
L – 1.22
M – 1.24
N – 1.26
P – 1.28
Q – 1.30
R – 1.35
S – 1.40
T – 1.45
U – 1.5
V – 1.6
W – 1.7
X – 1.8
Y – 1.9
Z – 20
A' – 25
B' – 3
C' – 4
D' – 5
E' – 10
LAYER
RATUM
30 20 10 8 6 5 4 ω

SE VELOCITY OF LOVE-WAVES

(WITH ONE NODE)

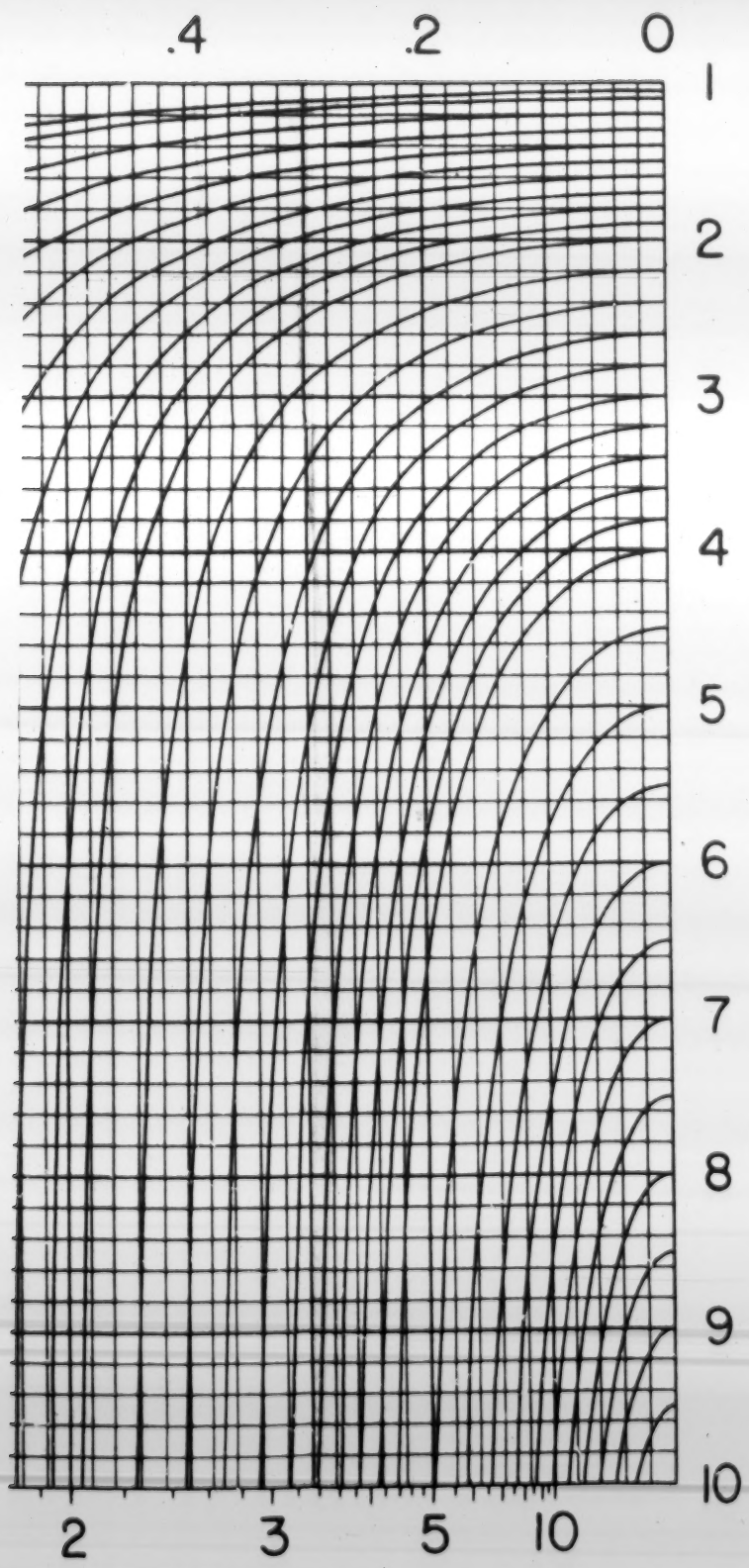

V_s : VELOCITY OF S-WAVES IN THE LAYER

V_s' : VELOCITY OF S-WAVES IN THE SUBSTRATUM

V : VELOCITY OF LOVE-WAVES

T : PERIOD

ω : FREQUENCY

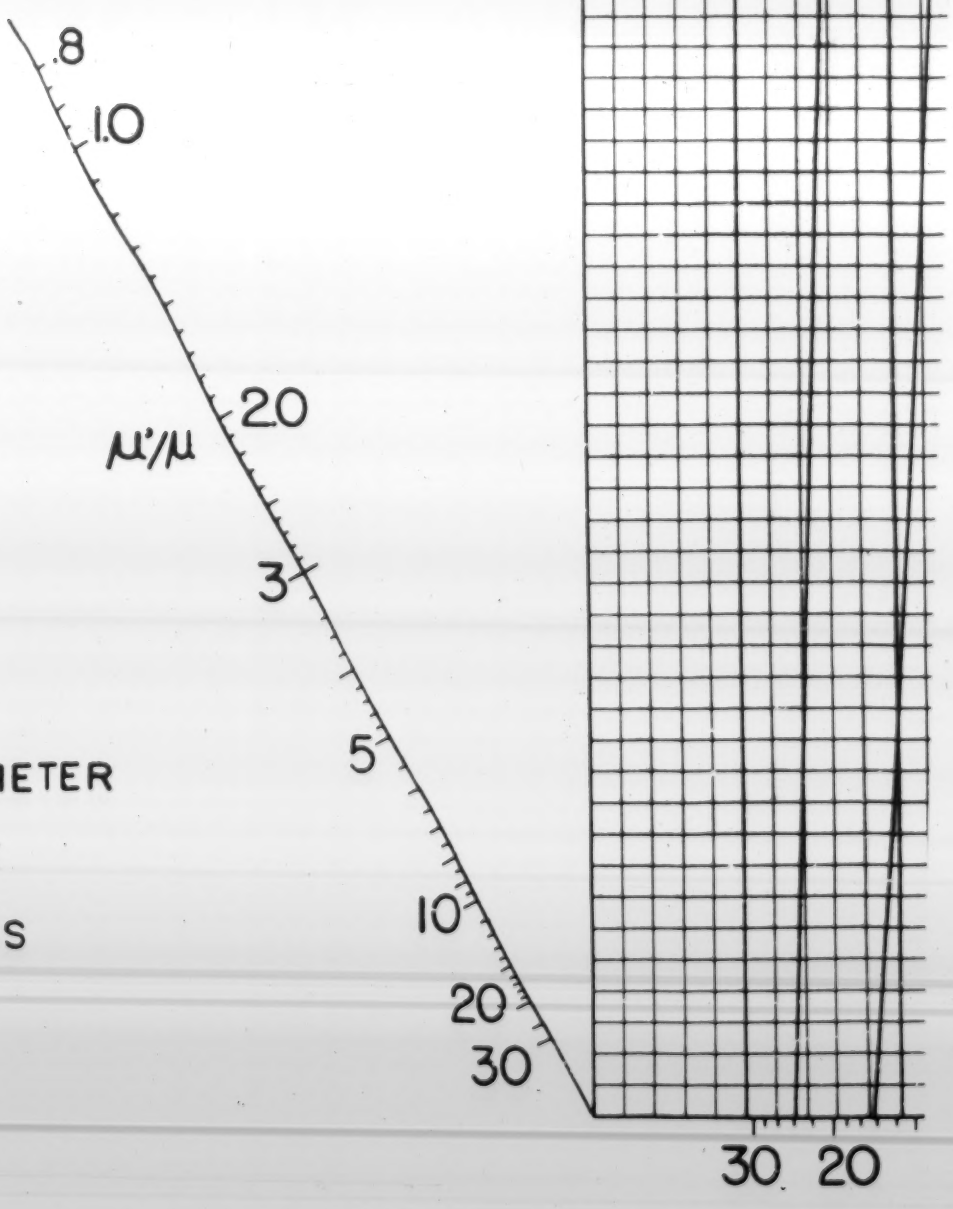

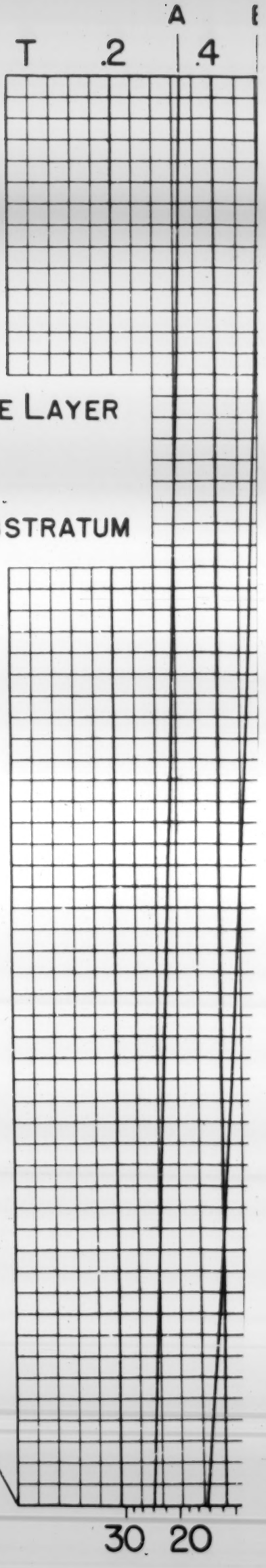

PHASE VELOCITY OF LOVE-WAVES

(With One Node)

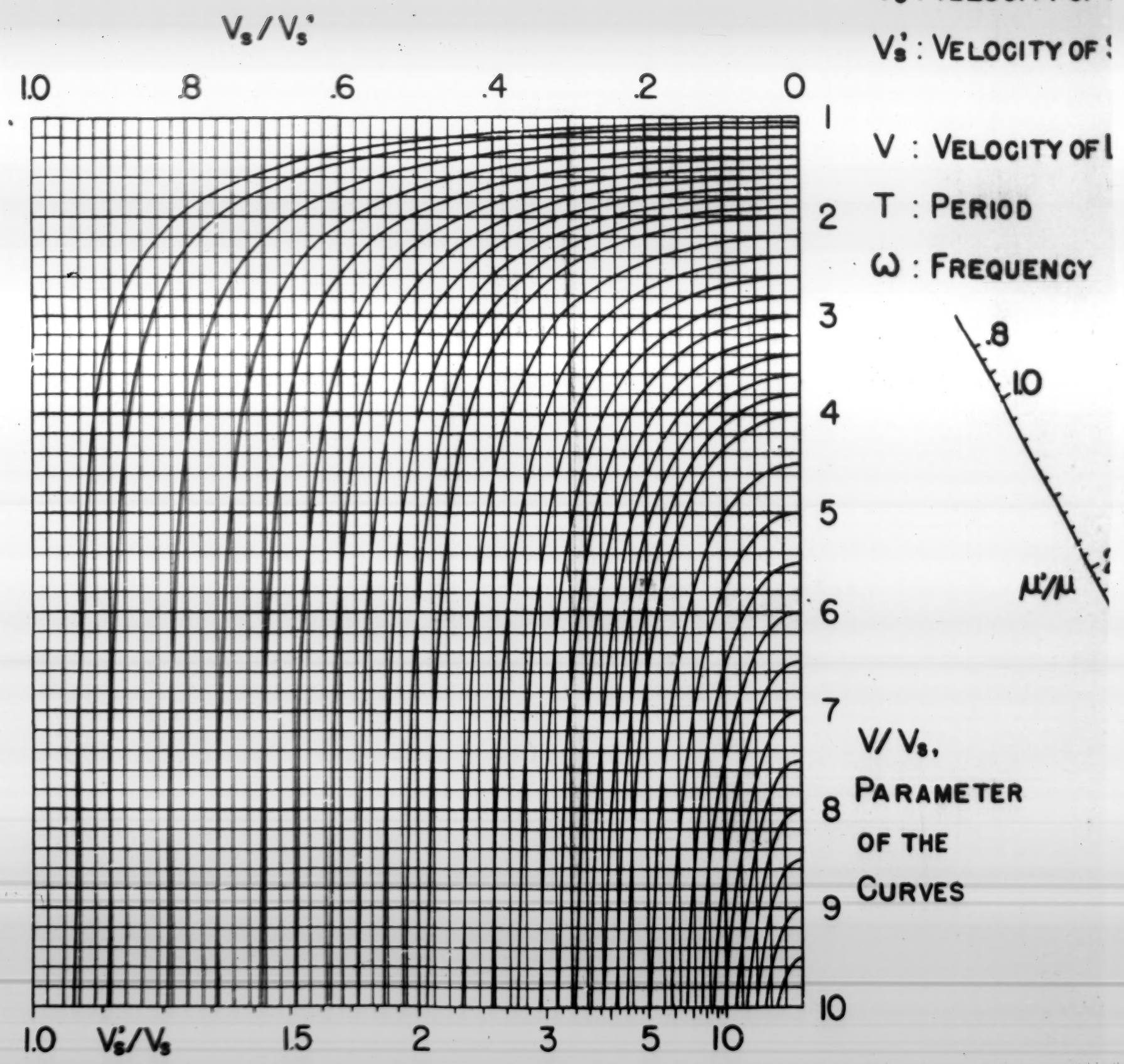

（震研彙報　第三十一号　図版　佐藤）

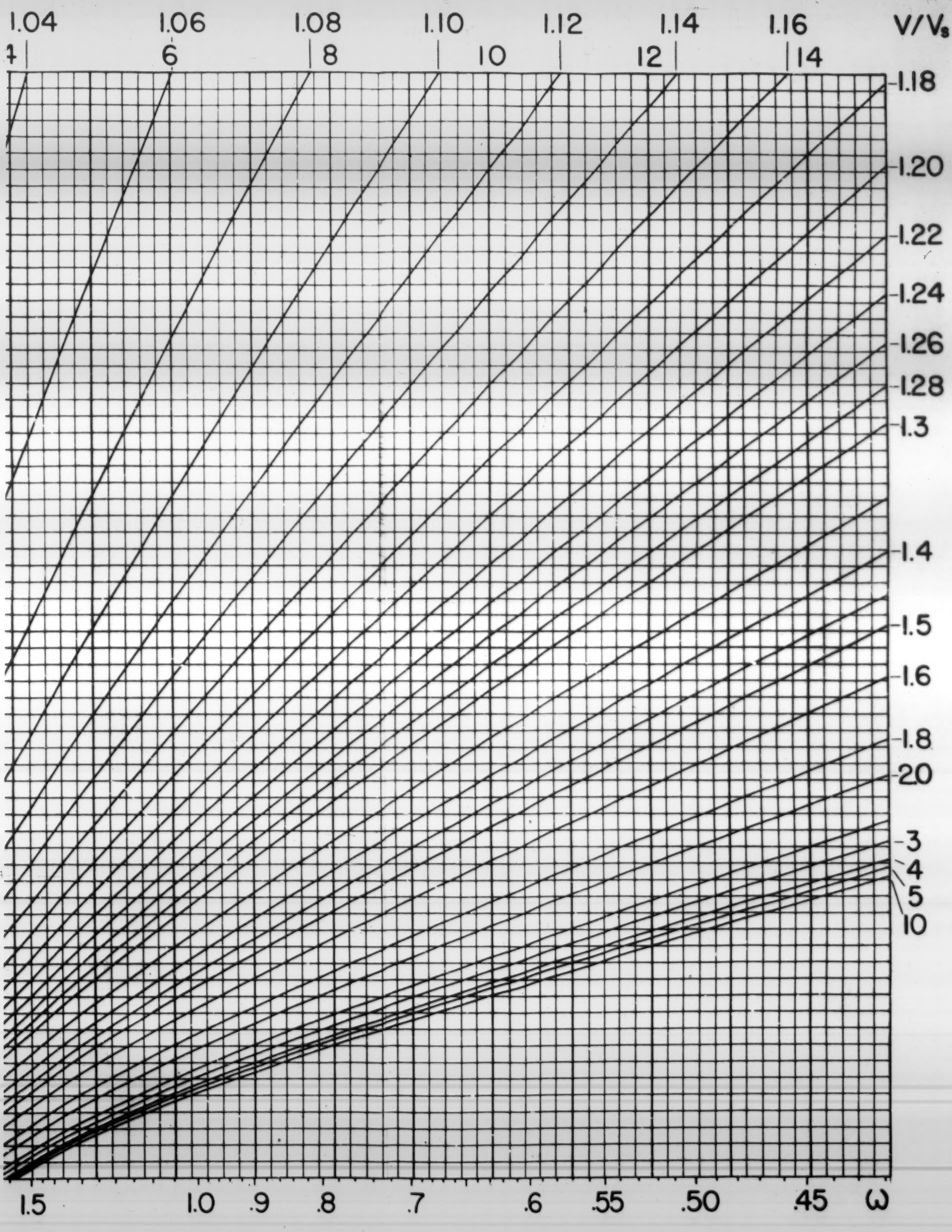
1.04
1.06
1.08
1.10
1.12
1.14
1.16
V/Vs
4
6
8
10
12
14
1.18
1.20
1.22
1.24
1.26
1.28
1.3
1.4
1.5
1.6
1.8
20
3
4
5
10
1.5
1.0
.9
.8
.7
.6
.55
.50
.45
ω

Y OF LOVE-WAVES

JT NODE)

V_s : VELOCITY OF S-WAVES IN THE LAYER

V_s' : VELOCITY OF S-WAVES IN THE SUBSTRATUM

V : VELOCITY OF LOVE-WAVES

T : PERIOD

ω : FREQUENCY

V/Vs, PARAMETER OF THE CURVES

μ'/μ

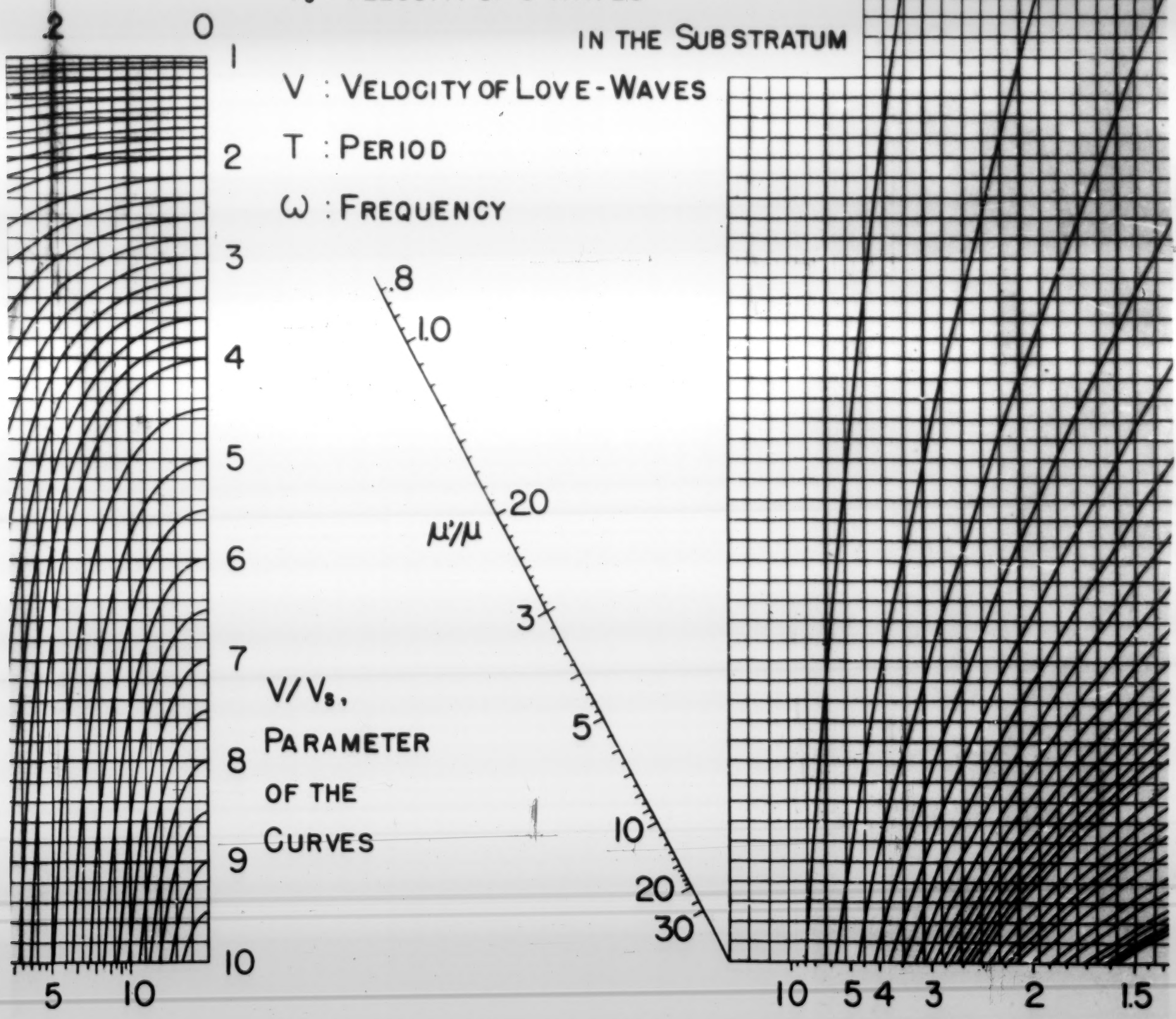

PHASE VELOCITY OF LOVE-WAVES

(WITHOUT NODE)

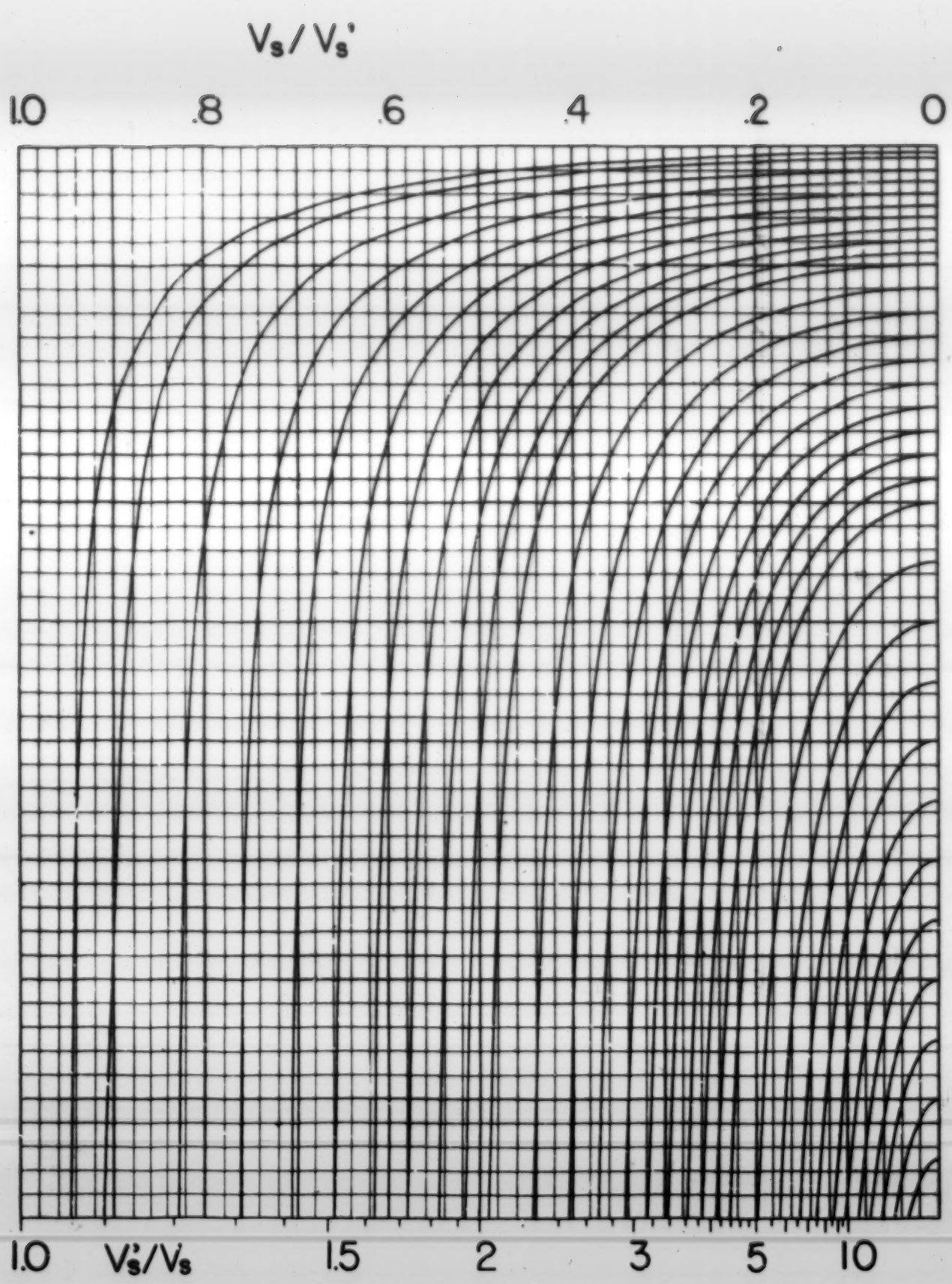

V_s : VELOCITY OF S

V_s' : VELOCITY OF S

V : VELOCITY OF L

T : PERIOD

ω : FREQUENCY

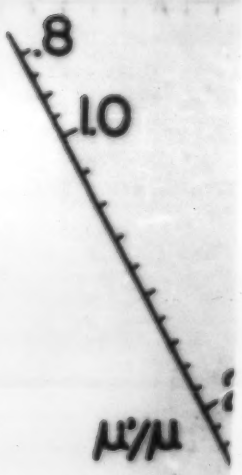

V/V_s, PARAMETER OF THE CURVES

(震研彙報 第三十一号 図版 佐藤)

BULLETIN OF THE EARTHQUAKE RESEARCH INSTITUTE.
TOKYO UNIVERSITY. Vol. XXXI, Part 3. September, 1953.

東京大學
地震研究所彙報

第 31 號　第 3 冊

昭和 28 年 9 月

目　次

論文及報告

頁

16. 地震の場の論 (独文)……松沢武雄 179

17. 坐標系の移動に伴ふ体球函数の変換 (英文)……佐藤泰夫 203

18. 電流を制御する新しい試み及びその地磁気測定への応用 (英文)……横山泉 211

19. 地震動振幅と地表層の性質との関係 (第2報) (英文)……金井清 219

20. 地下深所における地震動の観測結果 (第4報) (英文)……金井清・長田甲斐男・吉沢靜代 227

21. 彈性波の発生機構に関する実験 (第3報) (英文)……笠原慶一 235

22. 架構構造物の振動問題における集中荷重の仮定の吟味 (英文)……金井清 245

(The titles in occidental languages are given on the back cover.)

本彙報ハ年4回 (但シ第1號ヨリ第6號マデハ不定期ニ，第7號ハ3冊トシテ發行セリ)，彙報別冊ハ不定期ニ發行ス.

本彙報揭載ノ論文及ビ報告ノ內容ニ關シテハ著者ノミニ其責任アルモノトス.

本彙報ニ關スル照會通信ハ東京大學地震研究所長ヘ宛テラレタシ.

The Bulletin is published quarterly. (Vols. I–VI were published at irregular intervals and Vol. VII consisted of three parts.)
Supplementary Volume is published at irregular interval.

The authors of the papers alone are responsible for the statements and opinions contained in their respective papers.

All communications relating to this Bulletin should be addressed to the Director of the Earthquake Research Institute, Tokyo University.

16. *Feldtheorie der Erdbeben.*

Von Takeo MATUZAWA,

Institut für Erdbebenforschung.

(Vorgelegt den 19. Mai 1953.—Eingegangen den 20. Juni 1953.)

1. Idee des Erdbebenfeldes.

Wenn ein Erdbeben entsteht, dann wird eine gewisse Menge Wellenenergie durch eine gewisse Fläche ausgestrahlt, die den Bebenherd umschliesst, und zerstreut im Aussenraum. Gleich vor dem Beben ist diese Energie sicher in der Form der Spannungsenergie in einem gewissen kritisch gespannten Raum in der Erdkruste gelagert.

Dieses Spannungsfeld wird mit der Volumenmenge V repräsentiert, in der die bis zum kritischen Zustand lokalisierte Spannung gelagert ist. Es sei ein Erdbeben mit der an einer gewissen Herdentfernung z. B. 100 km beobachteten Maximum-Amplitude A repräsentiert.

Dann besteht die ein-ein Zuordnung im Sinne von der Mengenlehre zwischen einem Erdbeben A, dessen Raummenge V und der ausgestrahlten Energiemenge E, wie folgt; $A-V-E$.

2. Raummenge und Energiemenge von einigen Bebenschwärmen mit Grossbeben.

Wenn eine glockenförmige (natürlich gewisse Deformationen erlaubt) Häufigkeitskurve der Erdbeben für gewisse Zeit und Raum besteht, versteht man hier einen Bebenschwarm[1]. Die Bebengrösse wird hier vorläufig ausser Acht gelassen. Dann können die ganzen Volumenmenge V und die ganzen Energiemenge E respektiv der ganzen Bebenmenge A zugeordnet werden.

Es sei, Beben A in die Reihe der steigenden Grösse geordnet, und das i-te Beben sei A_i. Wenn A im Intervalle von ε eingeteilt wird und die Häufigkeit von A_i gleich $f(A_i)$ ist, dann

$$A_i=\varepsilon i \quad \text{und} \quad f(E_i)=f(V_i)=f(A_i).$$

Vorläufig nehme man an,

$$V_i=kA_i^q=V_n\left(\frac{i}{n}\right)^q.$$

1) Z. B., T. TERADA, *Bull Earthq. Res. Inst.*, **10** (1932), 29,

Wenn $f(A_i)=N\left(\frac{n}{i}\right)^m$ ist, wo N die Zahl der Erdbeben von der n-ten Grösse ist, dann

$$V_i f(A_i)=V_n N\left(\frac{i}{n}\right)^{q-m}.$$

Wenn $q=m$ ist, wird die Volumenmenge unter jeder Klasse Beben gleich verteilt.[2)]

In gleicher Weise ist für die Energie

$$E_i f(A_i)=E_n N\left(\frac{i}{n}\right)^{p-m},$$

wenn $$E_i=E_n\left(\frac{i}{n}\right)^p.$$

Nun gemäss der Gutenberg-Richter Formel[3)]

$$\log E=1.8M+11.3, \quad \text{und} \quad M\propto \log A,$$

bekommt man

$$E_i\propto A_i^{1.8}, \quad \text{nämlich} \quad E_i=E_n\left(\frac{i}{n}\right)^{1.8}.$$

Anderseits lautet die Ishimoto-Iida'sche Formel[4)], dass

$$f(i\varepsilon)=\frac{K}{(i\varepsilon)^m}=N\left(\frac{n}{i}\right)^m,$$

und zwar $m=1.8$.

Diese Formel ist in anderen Fällen von mehreren Autoren diskutiert und bestätigt worden[5)].

In solchen Fällen also besteht die Gleichverteilung der Energie unter jedem Klassenintervalle.

Nun $$\sum_{i=1}^{n} f(i\varepsilon)=Nn^m\sum_{i=1}^{n}\frac{1}{i^m},$$

$$\sum_{i=1}^{n} A_i f(i\varepsilon)=Nn^m\varepsilon\sum_{i=1}^{n}\frac{1}{i^{m-1}}.$$

Wenn, z. B. $m=1.8$ und $n=20$ sind,

---

2) Z. B., H. KAWASUMI, *Bull. Earthq. Res. Inst.*, **30** (1952), 327.

3) B. GUTENBERG and C. F. RICHTER, *Bull Seism Soc. Am.*, **32** (1942), 163.

4) M. ISHIMOTO and K. IIDA, *Bull. Earthq. Res. Inst.*, **17** (1939), 443.

5) T. MATUZAWA, *Bull. Earthq. Res. Inst.*, **19** (1941), 411. T. ASADA and Z. SUZUKI, *Geophys. Notes*, **2** (1949), 1; Z. SUZUKI and T. ASADA, *Geophys. Notes*, **2** (1949); T. ASADA, Z. SUZUKI and Y. TOMODA, *Bull. Earthq. Res. Inst.*, **29** (1951), 289.

$$\sum_{i=1}^{20} \frac{1}{i^{0.8}} = 4.71, \qquad \sum_{i=1}^{20} \frac{1}{i^{1.8}} = 1.762.$$

Also ist die Expektanz von A gleich 2.67ε.

Im allgemeinen haben wir sehr gute Approximation wie folgt,

$$\sum_{1}^{n} \frac{1}{i^m} \fallingdotseq \sum_{1}^{20} \frac{1}{i^m} + \int_{20}^{n} \frac{di}{i^m}.$$

Nun muss ein wichtiger Unterschied zwischen der Raummenge und der Energiemenge des Erdbebenschwarmes bemerkt werden. Nämlich ist einerseits der Durchschnitt (oder Produkt im Sinne von der Mengenlehre) der jeden Beben zugeordneten Volumenmenge nicht immer null. Anderseits aber ist derselbe von den Energiemengen sicher immer null, weil sie im Aussenraum zerstreut werden.

In anderen Worten, entstehen mehrere Beben fast in demselben Krustenteil nur in einer kurzen Zeitspanne, nämlich wird das Bebenfeld eines Bebenschwarmes in einem kleinen Raum beschränkt. Die Bebenenergie quillt aber hintereinander hervor aus fast demselben Raum.

Die folgenden Beispiele machen diese Anschauung ganz klar.

(a) *Der den Gross-Kantō-Beben vom 1. Sept. 1923 enthaltende Bebenschwarm.*

In diesem Falle entstanden sehr viele grosse Nachbeben, wie sie von A. Imamura und K. Hasegawa[6] tabelliert wurden. Mit der Tabelle kann man Grösse M und log E nach dem Gutenberg-Richter Schema schätzen, wie in Tabelle I gezeigt. In dieser Tabelle wird Grösse M ins Klassenintervall von 0.5 abgerundet, und nur Beben in Gebiet (A) von A. Imamura und K. Hasegawa Tabelle gezeigt werden.

Es sei, die ausgestrahlte Energie des Hauptbebens, $E_0 (= 10^{26}$ erg), dann ist die zusammengefasste ganze Energie ungefähr $4.8\,E_0$.

Die geographische Verteilung der Epizentren sind in Fig. 1 gezeigt.

(b) *Der Bebenschwarm, welcher die drei Grossbeben vom 7. Dez. 1944, 13. Jan. 1945 und 21. Dez. 1946 enthält.*

Tabelle II und Fig. 2 zeigen diesen Bebenschwarm.

Diese Tabelle und Figur sind mit den Daten von "The Seismological Bulletin of the Central Meteorological Observatory, Japan, for the year 1950. (1952) 173–178." hergestellt worden.

Nun wird die der ausgestrahlten Energie eines Grossbebens zugeordnete Volumenmenge geschätzt, wie folgt. Die kritische Verzerrung in

6) A. IMAMURA and K. HASEGAWA, *Bull. Imp. Earthq. Invest. Commit.*, **11** (1928), 64-92.

Tabelle I.

O	2 a m.m.	H		M	log E
		λ	φ		
Sept. 1					
11h 58m 44s	88.6	139°25′	35°07′	8.0	26
12 01 49	60	139°28′	35°10′	7.5	25
03 10	50			7.5	25
17 47	4.8	139°17′	35°02′	7.0	24
18 14	5.8			7.0	24
18 37	6.0			7.0	24
35 00	5.4			7.0	24
40 20	39.4	139°32′	35°04′	7.5	25
48 03	57.6	139°26′	35°10′	8.0	26
13 12 34	6.0			7.0	24
13 23	5.5			7.0	24
14 10	7.2			7.0	24
14 48	5.5			7.0	24
58 32	6.1	138°55′	35°23′	7.0	24
14 22 49	21.2	139°32′	35°7.5′	7.5	25
15 04 35	6.0			7.0	24
19 14	9.5			7.0	24
16 38 21	59.3	139°00′	35°20′	8.0	26
22 52 34	7.4			7.0	24
Sept. 2					
22 09 29	45.4	139°42′	35°07′	8.0	26
23 16 46	9.1	139°27.5′	35°14′	7.0	24
Sept. 26					
17 24 03	26.0	139°28′	34°41′	7.5	25
Okt. 4					
0 54 29	10.2	139°05′	35°19′	7.0	24
Nov. 5					
5 45 15	15	139°20′	35°32′	7.0	24
Nov. 23					
11 33 52	7.8	139°29′	35°15′	7.0	24
Jan. 15, 1924					
5 50 24	59.0	139°17′	35°26′	7.5	25

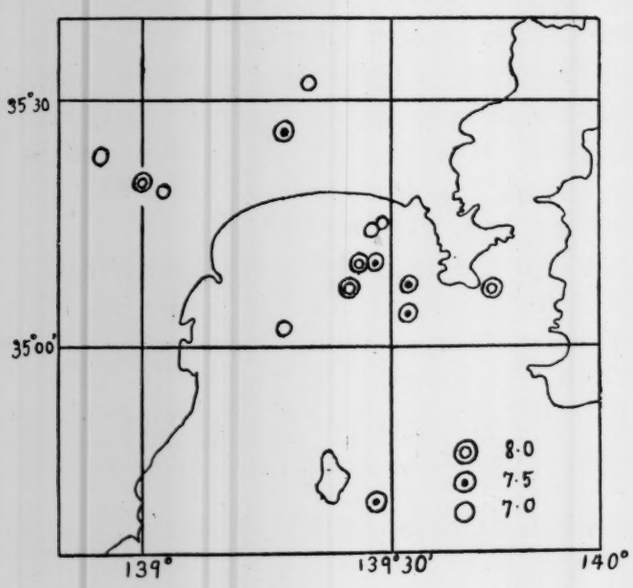

Fig. 1.

Tabelle II.

O	H		M	log E
	λ	φ		
1944 Dez. 7				
13*h* 35*m*	136.2°	33.7°	7.5	25
15 25	136.5	33.5	6.0	22
15 48	136.5	33.7	6.5	23
Dez. 12				
19 25	137.1	34.0	6.5	23
Dez. 17				
0 31	136.1	33.7	6.0	22
1945 Jan. 3				
21 15	137.9	34.7	5.5	21
Jan. 11				
10 43	137.1	34.9	6.0	22
14 57	137.2	34.7	6.5	23
Jan. 13				
3 38	137.0	34.7	7.0	24
14 36	137.1	34.8	6.0	22
19 58	137.1	34.9	5.5	21
Jan. 14				
6 00	137.0	34.9	6.0	22
21 53	137.0	34.9	6.0	22
Jan. 15				
18 49	136.9	34.9	6.0	22
Jan. 16				
16 45	137.0	35.0	5.5	21
22 36	137.1	34.9	6.5	23
1946 Juli 13.				
10 39	136.9	34.7	6.0	22
Dez. 21				
4 19	135.6	33.0	7.5	25
7 45	135.0	33.3	6.5	23
16 27	135.0	33.5	6.0	22
Dez. 22				
2 08	135.7	33.9	6.5	23
Dez. 24				
18 36	134.8	33.1	6.0	22
Dez. 26				
17 04	136.1	33.6	6.5	23
Dez. 29				
1 49	134.0	33.7	6.0	22

Fortsetzung folgt.

Tabelle II.

Fortsetzung

O	H		M	log E
	λ	φ		
1947 Jan. 16 21h 45m	134.4	34.0	5.5	21
Jan. 17 2 43	134.2	33.8	6.0	22
Jan. 25 1 48	135.3	33.2	6.5	23
Feb. 18 22 30	136.8	33.0	6.5	23
Feb. 21 15 06	138.0	34.8	6.0	22
April 11 19 31	135.7	33.5	6.0	22
Juli 17 4 19	135.7	33.4	6.0	22
Nov. 2 13 22	134.9	33.6	5.5	21
1948 April 18 1 11	135.6	33.1	6.0	22
1949 Jan. 20 20 42	137.3	34.7	5.5	21
1950 Nov. 6 2 33	134.9	33.5	7.0	24

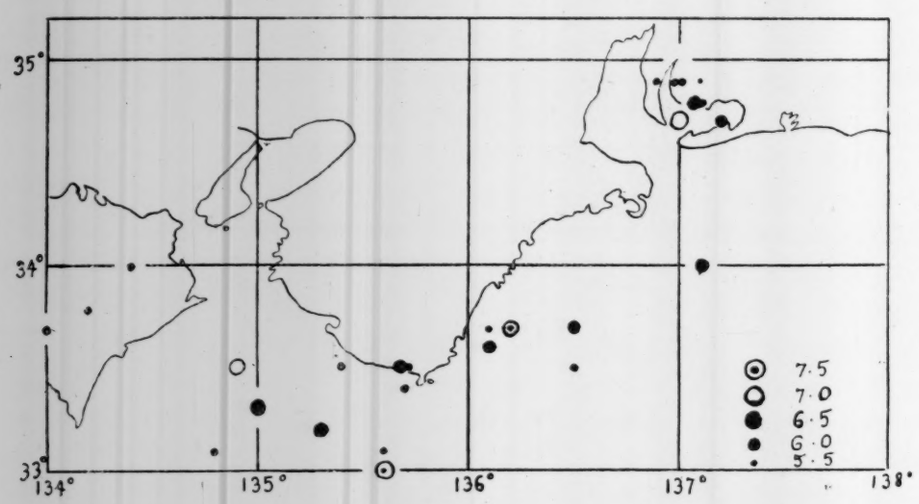

Fig. 2.

der Erdkruste wurde von T. Terada und N. Miyabe[7] oder Ch. Tsuboi[8] durch die Oberflächendeformation nach einigen Grossbeben geschätzt zu der Grössenordnung von 5×10^{-4}.

7) T. TERADA and N. MIYABE, *Proc. Imp. Acad.*, **8** (1932), 288-291.
8) Ch. TSUBOI, *Jap. Journ. Astr. Geophys.*, **10** (1933), 215-216.

In anderer Seite sind der Schubmodul oder Young'sche Modul von meisten Graniten respektiv gleich ungefähr 5×10^{11} dyne/cm^2 oder 1.3×10^{12} dyne/cm^2. Also ist der Energieinhalt pro cm^3 für die kritische Spannung ungefähr gleich

$$\frac{1}{2}\times1.3\times10^{12}\times(5\times10^{-4})^2=1.6\times10^4.$$

Darum ist der 10^{26} erg Energie enthaltende Volumeninhalt zu 6.2×10^{21} cm^3 oder 6.2×10^6 km^3 abgeschätzt.

Wir sehen also, dass das dem Hauptbeben zugeordnete Bebenfeld ungefähr das ganze Feld des ganzen Bebenschwarmes bedeckt. Es muss noch mal betont werden, dass die bis zum kritischen Spannungszustand lokalisierte grosse Energiemenge hintereinander in einer kurzen Zeitspanne von mehreren Monaten von demselben Bebenfeld ausgestrahlt wird.

Noch eine merkwürdige Tatsache in Bezug auf den Bebenschwarm mit Grossbeben ist, dass solcher Schwarm sporadisch periodisch in demselben Gebiet vorkommt mit dem Zeitintervalle von mehreren Jahrzehnten oder einigen Jahrhunderten wie schon manchmal von A. Imamura[9] erörtert wurde.

3. Thermodynamik der Grossbeben enthaltenden Bebenschwärme.

Wie man von der in vorigen Paragraphen geschilderten Tatsache leicht sehen kann, ist das Bebenfeld nichts anders als eine Maschine, die periodisch funktioniert, und zwar sie ist eine Wärmemaschine, die mit kalten und warmen Wärmereservoiren versehen ist. Das kalte Reservoir ist die Aussenwelt und das warme Reservoir ist das Erdinnere. Wenn die Wärme nur stationär vom Innern nach oben fliesst, dann besteht die periodisch funktionierende Maschine natürlich nicht. Solche Stelle ist vermutlich ein erdbebenfreies Gebiet.

Nun muss man einen konkreten Mechanismus der Maschine in der Erdkruste denken, nämlich den Mechanismus der sporadisch periodischen An- und Abspannung in der Kruste.

(i) *Schätzung der Wärmespannung in einer Platte die am Rande befestigt ist.*

Man denke nun ein Bebenfeld, d. h. einen Teil der Erdkruste durch eine am Rande befestigte Platte ersetzt.

Die x, y Koordinaten-Achsen seien an der freien Oberfläche gesetzt und die z Achse nach unten gerichtet.

9) A. Imamura, *Jap. Journ. Astr. Geophys.*, **5** (1928), 127-135.

Es sei, die Temperatur ändert sich wie $\theta=\theta_0\frac{z}{d}$ vom Nullzustand.

Die Randbedingungen an der Seite sind,

$Z_z=0, \quad X_z=Y_z=0, \quad$ für $\quad z=0,$

$Z_z=0. \quad X_z=Y_z=0, \quad$ und $\quad w=0, \quad$ für $\quad z=d.$

An der unteren Seite ist das hydrostatische Gleichgewicht in dem Nullzustand vorausgesetzt.

Wenn $u=v=0$, dann $\quad \Delta=\frac{\partial w}{\partial z} \quad$ ist.

$$X_x=\lambda\frac{\partial w}{\partial z}-\beta\theta_0\frac{z}{d}, \quad Y_y=\lambda\frac{\partial w}{\partial z}-\beta\theta_0\frac{z}{d}, \quad Z_z=(\lambda+2\mu)\frac{\partial w}{\partial z}-\beta\theta_0\frac{z}{d}, \text{ wo } \beta=E\alpha.$$

E; der Young'sche Modul,

α; der Koeffizient der linearen Wärmedehnung.

Also lautet die Gleichung des elastischen Gleichgewichtes,

$$(\lambda+2\lambda)\frac{\partial^2 w}{\partial z^2}-\beta\frac{\theta_0}{\alpha}=0.$$

Daraus bekommt man

$$w=\frac{\beta}{\lambda+2\mu}\frac{\theta_0}{d}\frac{z^2-d^2}{2}.$$

$$X_x=Y_y=-\frac{2\lambda}{\lambda+2\lambda}\beta\theta_0\frac{z}{d}, \qquad Z_z=0.$$

$$w=-\frac{\beta\theta_0}{\lambda+2\lambda}\frac{d}{2}, \qquad \text{für} \quad z=0.$$

$$X_x=Y_y=-\frac{2\mu}{\lambda+2\mu}\beta\theta_0 \qquad \text{für} \quad z=d.$$

Da $\quad \beta=E\alpha=\frac{3\lambda+2\mu}{\lambda+\mu}\mu\alpha \quad$ ist,

im Falle $\quad \lambda=\mu \quad$ ist,

$$X_x=Y_y=-\frac{5}{3}\mu\alpha\theta_0, \qquad \text{für} \quad z=d.$$

$$w=\frac{5}{6}\alpha\theta_0\frac{\mathrm{d}}{2}, \qquad \text{für} \quad z=0.$$

Also kommt die Maximum Schubspannung an der unteren Seite vor und sie ist gleich $\quad \tau=\frac{5}{6}\mu\alpha\theta_0.$

Die linearen Dehnungskoeffizienten von Gesteinen[10] sind,
z. B. Granit; $8\times10^{-6}/°C$

Basalt, Gabbro, Diabase; $5\times10^{-6}/°C$.

Also für Granit nehmen wir an, $\mu=5\times10^{11}\frac{\text{dyne}}{\text{cm}^2}$, $\alpha=8\times10^{-6}/°C$.

dann $\tau=3.3\times10^{6}$ dyne/cm² °C.

$w\fallingdotseq17$ cm/°C für $d=50$ km.

Um die kritische Spannung zu bekommen, muss die Temperaturerhöhung ungefähr 100°C sein. Es muss ziemlich schwer sein, diese Temperaturerhöhung nur durch die Wärmeleitung in der Zeitspanne von einigen Zehnten von Jahren zu bekommen.

(ii) *Phasentransformation, d. h. Solid-Liquid Transformation unter der Erdkruste.*

Es sei angenommen, die Materie gleich unter der Kruste befinde sich im thermodynamisch kritischen festen Zustand, was geophysikalisch ziemlich wahrscheinlich ist.

Wenn ein beschränkter Teil dieser Materie ein wenig erwärmt wird, dann nimmt der Druck zu, weil die elastische Kraft der oben liegenden Kruste den Widerstand zur Verflüssigung der Materie ausübt.

Nun lautet die Klausius-Clapeyron'sche Formel,

$$\Delta P=\frac{L}{T(v_1-v_2)}\Delta T,$$

wo ΔP; Zunahme des Druckes,
ΔT; „ der Schmelztemperatur,
L; Schmelzwärme pro Gramm Materie,
v_1; Volumen der Flüssigkeit pro Gramm,
v_2; „ des Kristalles pro Gramm,
T; Temperatur °K.

Mit meisten Geologen wollen wir hier basaltische Materie voraussetzen unter der Kruste.

Die Konstanten der Materie unter dem höheren Druck und Temperatur sind nicht genau bekannt. Darum nehmen wir vorläufig an die Daten unter dem normalen Druck. Die Schmelzwärme der basaltischen Materie ist mit den Daten von Roy W. Goranson[11] durch die verhältnismässige

10) E. B. Dane, Jr., Handbook of Physical Constants, *Geol. Soc. Am. Special Papers.* No. **36** (1950), Table 3-4.

11) Roy W. Goranson, Handbook of Physical Constants, *Geol. Soc. Am. Special Papers.* No. **36** (1950) Table 16-3.

Teilung der Bestandteile gerechnet worden.

Die folgende Tabelle (Tabelle III) ist aus der Tabelle von Goranson gewählt worden.

Tabelle III.

Komp.	Mineral	Phasen-Trans.	Temp. °C	L Joule/gr
$CaAl_2Si_2O_8$	Anorthit	Sol-Liq.	1550	440 440±65
$CaMg(SiO_3)_2$	Diopsid	Sol-Liq.	1391.5	445±65 430
Fe_3O_4	Magnetit	Curie-Pt.	576	Wenig
Mg_2SiO_4	Forsterit	Sol-Liq.	1274	270
$NaAlSi_3O_8$	Albit	Sol-Liq.	1105	203

Die petrographische Bestandteile der meisten Japanischen Basalte sind nach H. Kuno wie folgt,

50% von Basalt: Anorthit 60%—Albit 40%,
5% Olivine (Forsterit)
40% Diopsid
5% Magnetit.

Daraus schätzt man die Schmelzwärme des Basaltes zu 360 joule/gr oder 86 cal/gr. Betreffs der Schmelztemperatur T, wird $T=1500°K$ abgerundet genommen.

In Bezug auf die Volumenänderung beim Schmelzen von Gesteinen gibt es die Tabelle von E. B. Dane, Jr.[12]

Daraus bekommt man die folgenden Beispiele.

Tabelle IV.

Gestein	Temp. °C	Dichte		Dichte-Diff. Prozent
		Krist.	Liquid	
Diabase, Palisades	1200	2.89	2.603	9.9
„ Viriel Haven	1250	2.88	2.64	8.4

Wenn die Werte $\rho_2=2.89$ und $\rho_1=2.60$ genommen werden,

12) E. B. DANE Jr., Handbook of Phys. Const. *Geol. Soc. Am. Physical Papers* No. 36 (1950) Table 3-2.

dann $v_1=0.385$ und $v_2=0.346$.

Also $$\frac{\Delta P}{\Delta T}=\frac{3.6\times10^9}{1500\times0.039}=6.2\times10^7$$

Daher für $\Delta T=5°C$ bekommt man $\Delta P=3\times10^8$ dyne/cm².

(iii) *Spannung in einer Kreisplatte, die am Rande befestigt ist und an einer Seite konstantem Druck unterliegt.*

Wir denken nun die Kruste, die am beschränkten Teile der unteren Seite konstantem Druck unterliegt, durch die oben geschilderten Kreisplatte ersetzt. Dieses Problem wird durch die von A. E. H. Love[13] gegebenen Methode leicht gelösst.

Hier werden die x und y Achsen an der Mittelfläche der Platte und die z Achse nach unten gerichtet genommen.

Die Dicke der Platte sei $2h$, und der Radius der Platte sei a.

Die Randbedingungen sind

$$Z_z=X_z=Y_z=0, \quad \text{für} \quad z=-h,$$
$$Z_z=-p, \quad X_z=Y_z=0, \quad \text{für} \quad z=h,$$
$$u=v=w=0, \quad \frac{\partial w}{\partial z}=0, \quad \text{für} \quad z=0, \quad r=a.$$

Diesen Randbedingungen genügende Lösung lautet,

$$u'=-\frac{1+\sigma}{E}\frac{px}{8h^3}\left[(2-\sigma)z^3-3h^2z-2h^3-\frac{3}{4}(1-\sigma)z(x^2+y^2)\right],$$

$$v'=-\frac{1+\sigma}{E}\frac{py}{8h^3}\left[\quad\quad,,\quad\quad\right],$$

$$w'=\frac{1+\sigma}{E}\frac{p}{16h^3}\left[(1+\sigma)z^4-6h^2z^2-8h^3z+3(h^2-\sigma z^2)(x^2+y^2)\right.$$
$$\left.-\frac{3}{8}(1-\sigma)(x^2+y^2)^2\right],$$

$$X_x'=\frac{1}{4}p+\frac{3}{8}p\frac{z}{h^3}(x^2+y^2+h^2)-\frac{3}{32}(1-\sigma)p\frac{z}{h^3}(x^2+3y^2)-\frac{2+\sigma}{8}p\frac{z^3}{h^3},$$

$$Y_y'=\frac{1}{4}p+\frac{3}{8}p\frac{z}{h^3}(x^2+y^2+h^2)-\frac{3}{32}(1-\sigma)p\frac{z}{h^3}(3x^2+y^2)-\frac{2+\sigma}{8}p\frac{z^3}{h^3},$$

$$X_y'=\frac{3}{16}(1-\sigma)p\frac{z}{h^3}xy,$$

$$Z_z'=\frac{1}{4}h^{-3}p(z+h)^2\ (z-2h),$$

13) A. E. H. Love, Theory of Elasticity.

$$X_z' = \frac{3}{8} h^{-3} p(h^2 - z^2) x,$$

$$Y_z' = \frac{3}{8} h^{-3} p(h^2 - z^2) y.$$

$$u'' = -\frac{1+\sigma}{4} \frac{p}{E} x,$$

$$v'' = -\frac{1+\sigma}{4} \frac{p}{E} y,$$

$$w'' = \frac{1}{2} \frac{1+\sigma}{1-\sigma} \sigma \frac{p}{E} z,$$

$$X_x'' = Y_y'' = -\frac{1}{4} \frac{1+\sigma}{1-\sigma} p,$$

$$X_y'' = Z_z'' = X_z'' = Y_z'' = 0.$$

$$u''' = \frac{3}{32} \frac{(1-\sigma^2)}{h^3} \left(-a^2 + 4 \frac{h^2}{1-\sigma} \right) \frac{p}{E} zx,$$

$$v''' = \frac{3}{32} \frac{1-\sigma^2}{h^3} \left(-a^2 + 4 \frac{h^2}{1-\sigma} \right) \frac{p}{E} zy,$$

$$w''' = \frac{3}{64} \frac{1+\sigma}{h^3} \frac{p}{E} \left[-(1-\sigma) \left(a^2 + 4 \frac{h^2}{1-\sigma} \right) (x^2+y^2) - 2\sigma z^2 \left(-a^2 + 4 \frac{h^2}{1-\sigma} \right) - \frac{1-\sigma}{2} a^4 \right],$$

$$X_x''' = Y_y''' = \frac{3}{32} (1+\sigma) p \frac{z}{h^3} \left(-a^2 + 4 \frac{h^2}{1-\sigma} \right),$$

$$X_y''' = X_z''' = Y_z''' = Z_z''' = 0.$$

Lösung (′) genügt den Bedingungen an $z = \pm h$.
Lösung (′)+(″) genügt noch dazu den Bedingungen

$$u = v = 0 \quad \text{für} \quad z = 0 \quad \text{und} \quad r = a.$$

Lösung (′)+(″)+(‴) genügt den allen Bedingungen.
Im folgenden wird der Radius der Platte gleich $a = 2h$ genommen.
An der Oberfläche, d. h. $z = -h$,

$$w = \frac{1+\sigma}{16} \frac{p}{E} h \left(3 + \sigma - 14 \frac{\sigma}{1-\sigma} \right) + \frac{3}{32} \sigma (1+\sigma) \frac{p}{E} \frac{a^2}{h} - \frac{3}{128} (1-\sigma^2) \frac{p}{E} \frac{a^4}{h^3}$$
$$+ \frac{3}{16} (1-\sigma^2) \frac{p}{E} \frac{x^2+y^2}{h} \left(-\frac{\sigma}{1-\sigma} + \frac{a^2}{4h^2} \right) - \frac{3}{128} (1-\sigma^2) \frac{p}{E} \frac{(x^2+y^2)^2}{h^3},$$

$$w=\frac{1+\sigma}{16}\frac{p}{E}h\left(3+\sigma-14\frac{\sigma}{1-\sigma}\right)+\frac{3}{32}\sigma(1+\sigma)\frac{a^2}{h}\frac{p}{E}-\frac{3}{128}(1-\sigma^2)\frac{a^4}{h^3}\frac{p}{E},$$

für $r=0$. $w=-\frac{17}{4}\times\frac{5}{64}h\frac{p}{E}$, für $\sigma=\frac{1}{4}$, $a=2h$.

$w\doteqdot-200$ cm für $h=2.5\times10^3$ cm, $p=3\times10^8$ dyne/cm^2
und $E=1.25\times10^{12}$ dyne/cm^2.

$$w=\frac{1+\sigma}{16}\frac{p}{E}h\left(3+\sigma-14\frac{\sigma}{1-\sigma}\right)-\frac{3}{32}\sigma(1+\sigma)\frac{a^2}{h}\frac{p}{E},\qquad \text{für } r=a,$$

$$=-\frac{5}{64}\times\frac{33}{12}h\frac{p}{E}\qquad \text{für } \sigma=\frac{1}{4} \text{ und } a=2h,$$

$\doteqdot-160$ cm für $h=2.5\times10^3$ cm, $p=3\times10^8$ dyne/cm^2,
und $E=1.25\times10^{12}$ dyne/cm^2.

$$\widehat{rr}=\frac{p}{8}\left(1+\sigma-5\frac{1+\sigma}{1-\sigma}\right)-\frac{3}{32}p\frac{3r^2-a^2+\sigma(r^2-a^2)}{h^2}$$

$$=-\frac{5}{8}\times\frac{17}{12}p-\frac{3}{32}p\frac{3r^3-a^2+\frac{1}{4}(r^2-a^2)}{h^2},\qquad \text{für } \sigma=\frac{1}{4},$$

$$=-1\frac{61}{96}p,\qquad \text{für } r=a=2h.$$

$$\widehat{\theta\theta}=\frac{p}{8}\left(1+\sigma-5\frac{1+\sigma}{1-\sigma}\right)-\frac{3}{32}p\frac{r^2-a^2+\sigma(3r^2-a^2)}{h^2}$$

$$=-\frac{5}{8}\times\frac{17}{12}p-\frac{3}{32}p\frac{r^2-a^2+\frac{1}{4}(3r^2-a^2)}{h^2},\qquad \text{für } \sigma=\frac{1}{4},$$

$$=-1\frac{7}{96}p,\qquad \text{für } r=a=2h.$$

Am Rande der Mittelfläche *d. h.* $z=0$, $r=a=2h$,

$$\widehat{rr}=\widehat{\theta\theta}=-\frac{\sigma}{2(1-\sigma)}p,$$

$$=-\frac{1}{6}p,\qquad \text{für } \sigma=\frac{1}{4},$$

$$Z_z=-\frac{p}{2},$$

$$\widehat{rz}=\frac{3}{4}p\qquad \text{für } a=2h.$$

Die Hauptspannungen in der (r, z) Ebene sind

$$T_1=\left(-\frac{1}{3}+\frac{\sqrt{85}}{12}\right)p, \qquad T_2=\left(-\frac{1}{3}-\frac{\sqrt{85}}{12}\right)p,$$

und die Richtungskosinusse sind respektiv

$$l_1=\sqrt{\frac{1}{2}+\frac{1}{\sqrt{85}}}, \qquad m_1=\sqrt{\frac{1}{2}-\frac{1}{\sqrt{85}}},$$

$$l_2=\sqrt{\frac{1}{2}-\frac{1}{\sqrt{85}}}, \qquad m_2=-\sqrt{\frac{1}{2}+\frac{1}{\sqrt{85}}}.$$

Der Winkel mit der r-Achse ist gleich $\theta\fallingdotseq 38°40'$.
Die Maximum Schubspannung ist gleich

$$\tau=\frac{1}{2}(T_1-T_2)=\frac{\sqrt{85}}{12}p.$$

An der unteren Seite $d.h.$ $z=h$, bekommt man

$$w=\frac{1+\sigma}{16}\frac{p}{E}h\left\{\sigma\left(1+\frac{2}{1-\sigma}\right)-13\right\}+\frac{3}{32}\sigma(1+\sigma)\frac{p}{E}\frac{a^2}{h}$$
$$-\frac{3}{128}(1-\sigma^2)\frac{p}{E}\frac{a^4}{h^3}+\frac{3}{16}(1-\sigma^2)\frac{p}{E}\frac{x^2+y^2}{h}\left(-\frac{\sigma}{1-\sigma}+\frac{a^2}{4h^2}\right)$$
$$-\frac{3}{128}(1-\sigma^2)\frac{p}{E}\frac{(x^2+y^2)^2}{h^3}.$$

Für $r=0$,

$$w=\frac{1+\sigma}{16}\frac{p}{E}h\left\{\sigma\left(1+\frac{2}{1-\sigma}\right)-13\right\}+\frac{3}{32}\sigma(1+\sigma)\frac{p}{E}\frac{a^2}{h}$$
$$-\frac{3}{128}(1-\sigma^2)\frac{p}{E}\frac{a^4}{h^3},$$
$$=\frac{1+\sigma}{16}\frac{p}{E}h\left(-19+13\sigma+\frac{2\sigma}{1\sigma}\right), \quad \text{für} \quad a=2h,$$
$$=-\frac{5}{64}\times\frac{181}{12}h\frac{p}{E} \qquad \text{für} \quad \sigma=\frac{1}{4},$$
$$\fallingdotseq 710\,\text{cm} \qquad \text{für} \quad h=2.5\times10^6\,\text{cm}, \quad p=3\times10^8\,\text{dyne/cm}^2,$$
$$E=1.25\times10^{12}\,\text{dyne/cm}^2.$$

$$\widehat{rr}=\frac{p}{8}\left(3-\sigma+\frac{1+\sigma}{1-\sigma}\right)+\frac{3}{32}p\left(\frac{3r^2-a^2}{h^2}+\sigma\frac{r^2-a^2}{h^2}\right),$$
$$=\frac{p}{8}\left(4+\frac{5}{12}\right)+\frac{3}{32}p\left(\frac{2r^2-a^2}{h^2}+\frac{1}{4}\frac{r^2-a^2}{h}\right), \qquad \text{für} \quad \sigma=\frac{1}{4},$$

$$=\left(1+\frac{29}{96}\right)p, \qquad \text{für} \quad r=a=2h.$$

$$\widehat{\theta\theta}=\frac{p}{8}\left(3-\sigma+\frac{1+\sigma}{1-\sigma}\right)+\frac{3}{32}p\left(\frac{r^2-a^2}{h^2}+\sigma\frac{3r^2-a^2}{h^2}\right),$$

$$=\frac{p}{8}\left(4+\frac{5}{12}\right)+\frac{3}{32}p\left(\frac{r^2-a^2}{h^2}+\frac{1}{4}\frac{3r^2-a^2}{h^2}\right), \qquad \text{für} \quad \sigma=\frac{1}{4},$$

$$=\frac{71}{96}p \qquad \text{für} \quad r=a=2h.$$

$$Z_z=-\mathrm{p}.$$

Die Maximum Schubspannung ist gleich

$$\tau=\frac{1}{2}\left(2+\frac{29}{96}\right)p.$$

(iv) *Schätzung der Spannungsenergie in der gedruckten Kruste.* Diese Energie muß der von Druck p geleisteten Arbeit gleich sein. Diese Arbeit pro cm², E_0, ist gleich

$$E_0=-\int_0^p p\ dw=-\frac{1}{2}p[w_{z=h}].$$

Darum ist die ganze Energie gleich

$$E=2\pi\int_0^a E_0\ rdr$$

$$=-\frac{\pi}{32}\frac{p^2}{E}ha^2\left[(1+\sigma)\left\{\sigma\left(1+\frac{2}{1-\sigma}\right)-13\right\}-\frac{1}{8}(1-\sigma^2)\frac{a^4}{h^4}\right],$$

$$=-\frac{1}{64}\frac{p^2}{E}V\left[(1+\sigma)\left\{\sigma\left(1+\frac{2}{1+\sigma}\right)-13\right\}-\frac{1}{8}(1-\sigma^2)\frac{a^4}{h^4}\right],$$

wo V der Rauminhalt der gedruckten Kruste ist.

$$E=\frac{5}{4}\times\frac{1}{256}\frac{p^2}{E}V\left(\frac{145}{3}+\frac{3}{8}\frac{a^4}{h^4}\right) \qquad \text{für} \quad \sigma=\frac{1}{4},$$

$$=\frac{5}{4}\times\frac{177}{3}\times\frac{1}{256}\frac{p^2}{E}V \qquad \text{für} \quad a=2h,$$

$$\doteqdot 8.2\times10^{24}\ \text{erg} \qquad \text{für} \quad p=3\times10^8\ \text{dyne/cm}^2,$$

$$E=1.25\times10^{12}\ \text{dyne/cm}^2, \quad h=2.5\times10^6\ \text{cm}.$$

Anderseits ist $E/V\doteqdot 2.1\times10^4$ erg/cm³, was die ungefährige kritische Energie pro cm³ ist.

(v) *Schätzung der Energie zur Hebung der Kruste.*

Nach meisten Grossbeben beobachtet man Hebungen und Senkungen

der Erdoberfläche im Bebenfeld. Bei meisten bisher gut erforschten Beben hat es sicher Krustendeformation auch unter dem Meer gegeben, aber die Verteilung der Hebungen und Senkungen unter dem Meer ist leider nicht genau bekannt[14].

Wenn man voraussetzt, dass im vorliegenden Rechenbeispiele nur die Hebung stattfindet, dann schätzt man wie folgt.

Es sei, die betreffende Kruste um 4 m im Durchschnitt gehoben würde. Dann ist die gesamte Arbeit gegen die Schwere ungefähr gleich

$$E=2.6\times5\times10^{6}\times\pi\times25\times10^{12}\times9.8\times10^{2}\times4\times10^{2}=4\times10^{26}\text{ erg.}$$

Wenn ein Teil dieser Energie, etwa 9/10, durch die Senkung aufgehoben würde, dann wäre die gegen die Schwere geleistete gesamte Arbeit ungefähr gleich 4×10^{25} erg, was von der gleichen Grössenordnung der Spannungsenergie ist.

(vi) *Die Konstruktion und Funktion der Maschine.*

Im Erdbebengebiete stellt man die Form der Isothermen vor etwa wie in Fig. 3 schematisch dargestellt. Nämlich im Vergleich mit den anderen Gebieten schmiegen die Isothermen dichter in dem oberen Teile der Erdkruste und sie sind weiter gestreckt im unteren Teil.

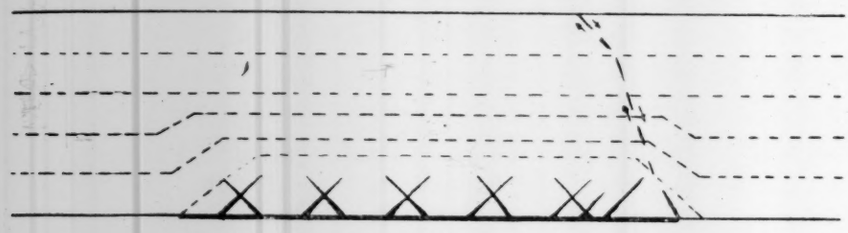

Fig. 3.

Dieser Zustand kann mit dem Anstieg der heissen flüssigen Materie d. h. Magma durch die beim Erdbeben erzeugten Risse vorkommen.

Dabei sollen die etwas gelockerten Krustenteile nach unten sinken.

Dieser Vorgang wird nachher näher beschrieben.

Dann dicht unter diesem Teile wird sicher mehr Wärme im Vorrate gehalten als unter dem neben stehenden Teile, wenn die Wärmezufuhr von unten wenigstens überall gleich ist. Noch dazu steigt die unteren heissen Materie allmählich an, obgleich die Geschwindigkeit von der Grössenordnung von einigen Metern pro 100 Jahre wäre, nämlich findet die langsame Konvektion im verallgemeinerten Sinne statt.

14) Obgleich nach dem Gross-Kantô-Beben Hebungen und Senkungen von der Ordnung von einigen Hunderten von Metern in Sagami-Bai mitgeteilt wurden, da blieben noch manche Unklarheiten.

In dieser Stufe kann der in (ii) erörterte Vorgang stattfinden. Wenn die Spannung in der oberen Kruste den kritischen Wert erreicht, wie in (iii) beispielsweise gezeigt, dann würde ein plötzlicher Bruch, d. h. Erdbeben vorkommen.

Dieser Raum direkt unter dem Bebenfeld werde nachher Quellengebiet genannt. Bei diesem Vorgang wird natürlich die teilweise plötzliche Abspannung in dem Quellengebiet stattfinden, und die Verflüssigung ziemlich schnell vorgehen. Vor dem grossen Bruch wäre der Wärmevorgang in dem Quellengebiet sehr langsam und die Materie befinde sich in dem überhitzten Zustand.

In dieser Weise kann man die ziemlich schnelle Energieausstrahlung bei hintereinander folgenden Nachbeben verstehen. Man kann die Kruste dem Kolben der Dampfmaschine und die Materie im Quellengebiet, d. i. das Arbeitsmittel dem Wasser und Dampf im Kessel vergleichen, es sei denn dass die Phasentransformation verschieden sei.

Der Kreislauf des Arbeitsmittels wird schematisch in Fig. 4 mit den gebrochenen Linien gezeigt.

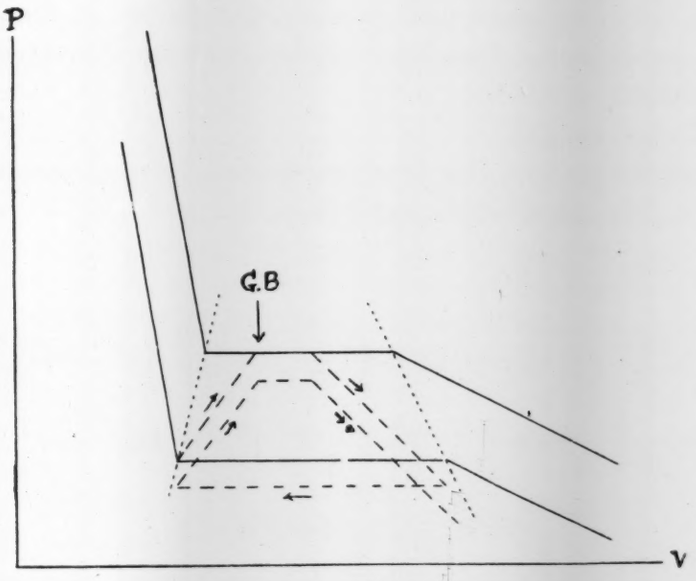

G. B. Grossbeben.

Fig. 4.

Am rechten Ende des Keislaufs flauten die Nachbebentätigkeit ab. Ein Teil Arbeitsmittel würde in die beim Beben erzeugten Risse der Kruste einzudringen gezwungen und allgemeine Hebung des Arbeitsmittles bzw. der Isothermen wird stattfinden. Daher wird die Wärmeabfuhr sicher

schneller vorgehen als in dem Nachbargebiet. Dann wird der Kreislauf nach links in Fig. 4 vorgehen und ein Kreislauf des Arbeitsmittels wird endlich geschlossen.

Weil das Arbeitsmittel bei jedem Kreislauf allmählich nach oben gehoben wird, geht der Kreislauf allmählich nach unten in Fig. 4 fort.

In dieser Weise könne die periodisch funktionierende Maschine der Grossbeben bestehen.

Es sei hier bemerkt werden, dass die Reibungskraft keinen Unterschied von der kritischen Schubspannung unter sehr hohen normalen Druck hat. Das bedeutet, dass die Erdbeben hintereinander mit kurzem Zeitintervalle in demselben Krustenteil vorkommen kann.

Wir sehen in (iii), dass die Maximum Schubspannung in der Kruste am Rande des Quellengebietes vorkommen. Darum liegt die Vermutung nahe, dass das erste Hauptbeben dort stattfinde und die meisten Nachbeben in dem Krustenteil oberhalb des Quellengebietes entstehen. Tatsächlich ist der Herd des Hauptbebens fast ausnahmslos an der extremen Stelle des Nachbebengebietes gestellt, was ich manchmal bemerkt habe[15].

Natürlich ist die Krustenstruktur nicht uniform und homogen, besonders an der Grenze der Kontinente und Ozeane, und daher ist die Quellengebiet nicht kreissymmetrisch. Folglich würden manche Variationen der Vorgänge vorkommen.

(vii) *Wärme Bilanz.*

Die Volumenzunahme des Quellengebietes beim Grossbeben wird mit w für $z=h$ in (iii) geschätzt, namlich

$$\Delta V=-2\pi\int_0^a w\, rdr$$

$$=\frac{\pi a^2 h}{16}\frac{p}{E}\left[(1+\sigma)\left\{13-\sigma\left(1+\frac{2}{1-\sigma}\right)\right\}+\frac{1}{8}(1-\sigma^2)\frac{a^4}{h^4}\right]$$

$$=\frac{5}{16\times 16}\pi a^2 h\frac{p}{E}\left(\frac{145}{3}+\frac{3}{8}\frac{a^4}{h^4}\right), \qquad \text{für} \quad \sigma=\frac{1}{4},$$

$$=\frac{5\times 163}{3\times 16\times 16}\pi a^2 h\frac{p}{E}, \qquad \text{für} \quad a=2h.$$

Für $a=2h=5\times 10^6$ cm, $p=3\times 10^8$ dyne/cm^2, und $E=1.25\times 10^{12}$ dyne/cm^2, wie früher,

15) T. MATUZAWA, *Bull. Earthq. Res. Inst.*, **14** (1936), 38-67, u. a.

Neulich habe ich kennengelernt, dass Saem. Nakamura auch in seinem Buch "Ippan Zisin-Gaku (Allgemeine Seismologie, in Japanisch) (1934) S. 32" solche Tatsache bemerkte, obgleich er etwas Unklarheiten über die Idee der Nachbeben hegte.

dann

$\Delta V = 5.1 \times 10^{16}$ cm^3.

Diese Volumenzunahme wird durch die Schmelzung vom Quellengebiet mit Volumen so gross wie $10 \times \Delta V = 5.1 \times 10^{17}$ cm^3 erzeugt.

Anderseits ist die Schmelzwärme pro cm^3 von basaltischen Materie ungefähr gleich $2.6 \times 3.6 \times 10^9 = 9.4 \times 10^9$ erg.

Also muss die gesamte Schmelzwärme ungefähr gleich 9×10^{27} erg sein. Diese Menge Wärme muss in mehreren Zehnten oder Hunderten von Jahren ins Quellengebiet zu und von demselben abgeführt werden.

In anderer Seite ist die Wärmeleitung von Gesteinen in der Nähe von der Erdoberfläche durchschnittlich gleich 5×10^{-3} cal/sec. cm. °C, und der geothermische Gradient ist gleich 1°C pro 3.5×10^3 cm ca. Also ist die Wärmemenge, die in 100 Jahren durch die Fläche mit dem Radius von 50 km durchfliesst, gleich 1.5×10^{25} erg.

Dieser Wert ist erheblich kleiner als 9×10^{27} erg. Darum kann die Wärmleitung allein nicht die Sache erklären. In anderen Worten muss die Konvektion in Acht genommen werden.

Der Anstieg der heissen Materie durch die Risse und Senkung der gelockerten Krustenteile sollen die Art und Weise der Konvektion sein. Aber man muss auch die vulkanische Tätigkeit in Acht nehmen.

In der Tat meisten Grossbebenzonen entlang laufen auch vulkanische Zonen. Die Vulkane bilden vermutlich die Ventile für den Wärmeabzug. Die Wärme im Quellengebiet wird nicht nur aufwärts sondern auch seitwärts diffundiert in der Form von Leitung und Konvektion.

Auf alle Fälle hat das Problem der Wärme Bilanz noch etwas Unklarheit.

Nebenbei, ist das Leistungsvermögen dieser Wärmemaschine von der Grössenordnung von einigen Prozent, abgesehen von der Hebung und Senkung der Kruste.

5. Erdbeben in der Zwischenzeit der Bebenschwärme mit Grossbeben.

Auch nach der Abflautung der Nachbebentätigkeit herrscht noch ein wenig Bebentätigkeit in demselben Bebenfeld. In dieser Stufe besteht meistens die Poisson'sche Verteilung der in gewisser Zeiteinheit gezählten Bebenhäufigkeit in dem Feld[16], nämlich $\frac{e^{-\nu}\nu^n}{n!}$, wo ν, durchschnittliche

16) W. INOUYE, *Bull. Earthq. Res. Inst.*, **15** (1937), 142; M. ISHIMOTO and K. IIDA, *Bull. Earthq. Res. Inst.*, **17** (1939), 443: K. IIDA, *Bull. Earthq. Res. Inst.*, **18** (1940), 575.

Bebenzahl in der Zeiteinheit ist, und n die beobachtete Bebenzahl ist.

Von dieser Tatsache vermuten wir nach R. Fürth[17], dass das betreffende Bebenfeld mit sehr vielen Keimen der Erdbeben belegt ist, und jeder Keim mit kleiner Wahrscheinlichkeit zu spriessen kommt.

Wir können diesen Keim als die Strukturirregularität im fast zum kritischen Zustand gespannten Bebenfeld ansehen. Dieser Spannungszustand wird durch die Abkühlung des eindringenden Arbeitsmittels und das Zurückstossen durch die Schwere im Stande kommen. In diesem Verfahren wird die allmähliche Änderung von ν in längerer Zeit, d. i. von der kleinen Wahrscheinlichkeit von Spriessen der Keime beobachtet[18].

Diese Änderung würde von der Geschwindigkeit der Wärmevorgänge in unserer Maschine abhangen. In unserer Maschine wird die Zahl der Keime in jedem Versuch im Sinne von Fürth in dieser Stufe als unveränderlich angesehen und zwar ohne Wahrscheinlichkeitsnachwirkung. Nämlich kann ein Beben wieder in derselben Stelle vorkommen in einem Zeitintervalle um das andere. In einem Versuch, nämlich in einer kurzer Zeiteinheit, wird jedes Beben als unabhängig voneinander angesehen. In anderen Worten hat die zu jedem Beben in dem Versuch zugeordnete Raummenge keinen gemeinsamen Teil.

In dieser Statistik der Bebenzahl wird die Grösse der Beben nicht in Betracht gezogen. Nun wollen wir die Idee der Grösse des Keimes einführen. In unserem Erdbebenproblem stellen wir irgend eine Gleitfläche als den Keim vor. Wenn ein Erdbeben von diesem Keim entsteht, wird ein gewisser Rauminhalt dazu zugeordnet. Dessen Volumen ist wahrscheinlich von der Ordnung von dem durch die Drehung der Fläche um die den Flächenschwerpunkt durchlaufende längste Achse erzeugten Raum. Dieser Raum ist, so zu sagen, ein Wirkungsbereich des Keimes. Wenn irgend ein Erdbeben von einem Keime entsteht und dessen Wirkungsbereich den anderen Keim schneidet oder ganz enthält, dann wird dieser Keim in dem Vorigen vermengt und abgespannt. Z. B. in Fig. 5 wenn ein Beben vom Keim A entsteht, wird Keim B in Keim A vermengt, aber keim A kann nicht in Keim B vermengt werden. Nämlich, auch wenn Keim B ein Beben erzeugt, hat Keim A keinen Einfluss von B.

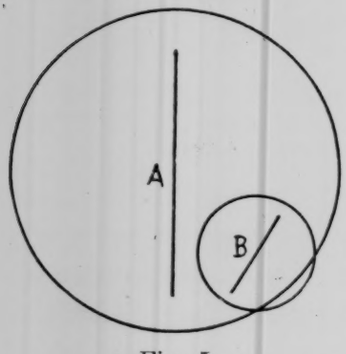

Fig. 5.

17) R. FÜRTH, Schwankungserscheinung in der Physik. (1920)

18) F. KISHINOUYE and K. KAWASUMI, *Bull. Earthq. Res. Inst.*, **4** (1928), 75.

Wenn man das betreffende Bebengebiet mit solchen Schema bedeckt, ist die Zahl der Keime N desto grösser, je kleiner die Keime sind. Daher ist die Zahl der kleineren Beben grösser als die der grösseren Beben, weil $\nu=pN$ ist.

6. Krustendeformation und der Zyklus der Wärmevorgänge.

Wie schon gut bekannt, werden beide langsame und plötzliche Krustendeformationen im Bebenfeld beobachtet. Beim Gross-Kantō-Beben vom 1. Sept. 1923 hoben sich plötzlich die Halbinseln Bōsō und Miura um einige Meter und dann sanken sie langsam nach dem Beben. Vor dem Beben herrschten dort langsame Senkungen ununterbrochen.

Eben so beim Grossbeben vom 21. Dez. 1946 befand sich die plötzliche Hebung im Südteil der Halbinseln Kii und Muroto, und dann die am Anfang ziemlich schnelle und dann langsame Senkung beobachtet wurde.

Die vorliegende thermodynamische Hypothese kann diese Erscheinung ziemlich leicht erklären. Der Krustenvorgang gleich vor dem Grossbeben ist uns etwas unklar, aber das Mareogramm[19] in Yokosuka, Miura Halbinsel, zeigte die fast plötzliche Hebung beim Grossbeben.

Die Rechnung in § 4 (iii) zeigt etwas Hebung der Oberfläche auch vor dem Beben. Anderseits aber in § 4 (i) sehen wir, dass beträchtliche Senkung vorkommen würde durch die Abkühlung der Kruste, die bei dem Beben von heissen Flüssigkeiten eingebrochen wurde. Die Differenz dieser beiden Wirkungen würde die beobachtete Senkung vor dem Grossbeben erzeugen.

Nach manchen Grossbeben, z. B. dem Tango-Beben vom 7. März 1927 und Kitaizu-Beben vom 25. Nov. 1930 gingen die Deformationen nach dem Beben in derselben Richtung fort wie beim Grossbeben. Diese Ergebnisse wurden aber direkt auf dem Verwerfungen beobachtet und zwar die relative Verschiebungen der Verwerfung wurden gegeben. Die Umstände waren also etwas anders als den vorigen Fällen.

Wenn das Magma in die Kruste eindringt, dann nimmt der Rauminhalt der betreffenden Erdkruste sicher zu und übt den Seitendruck aus. Die Geologen sprechen sehr oft vom Seitendruck, aber sehr selten vom Seiten-Zug. Die vorliegende Hypothese kann diese Umstände ziemlich gut erklären.

Wir können ein gutes Modell davon in der Verwerfung im See-Eis z. B. im Balaton-See (Platten-See) in Ungarn, Dalai-nor in Manchurei, Suwa-See in Japan u. s. w. finden. Hier spielt das Eis die Rolle der

19) T. TERADA and S. YAMAGUTI, *Rep. Imp. Earthq. Invest. Commit.*, **100B** (1925), 113.

Erdkruste und das Wasser dieselbe des Magmas. In der Verwerfung des Eises in Dalai-nor erreicht die Überschiebung etwa 15 m.

Das Kreisplattenmodell gibt grosse horizontale Verschiebung der Verwerfung nicht, aber elliptische oder rechteckige Quellenbebiete können natürlich beträchtliche horizontale Verschiebung geben.

Nun wollen wir die Wärmevorgänge im Krustenteile etwas näher betrachten. Wenn heisses Magma in die Kruste eindringt, dann werden die Geoisothermen sicher nach oben schmiegen und der Gradient an der oberen Grenze ganz steil werden. Wenn das heisses Magma z. B. um 4 km gehoben wird, mag die Temperaturdifferenz an der oberen Grenze ungefähr 100°C sein, vorausgesetzt dass der Gradient in der Nähe von der Oberfläche fortsetzt. Dort geht die Abkühlung des Magmas schneller vor und dann wird die Senkung der Isothermen wieder einsetzen. Dabei wird die allmähliche Zunahme der Wärmespannung in der Kruste erzeugt und die Entstehung der Erdbeben vorgesehen. Diese Beben sind wahrscheinlich von der kleinen Ordnung, weil das zugeordnete Spannungsfeld in ziemlich kleinen Teil lokalisiert sei.

In dieser Weise wird der Kreislauf der Erdbebenmaschine fortgehen. Wir wollen hoffentlich diesen Vorgang seismometrisch verifizieren.

7. Eine Bemerkung über die Vulkantätigkeit und die Erdbebentätigkeit.

Bei der Vulkantätigkeit, abgesehen vom Plutonismus, spielt die Liquid-Gas Phasentransformation die Hauptrolle. Dabei wird das Arbeitsmittel, d. h. das Gas oder mit Gase vermengten Lava in die Aussenwelt getrieben. In diesem Punkt ist die Vulkanmaschine fast von derselben Konstruktion wie die Dampfmaschine, abgesehen von den Verschiedenheiten der thermodynamischen Vorgängen der Vergasung im Magma, nämlich sogenannten Retrograddistillation und Verdampfung des Wassers.

Wiederholung der Ausflüsse der ungeheuren Menge Lava oder Gas aus demselben Vulkan zeigt uns, dass das Magma-Reservoir des Vulkans im allgemeinen sicher von unten Versorgt werden müsste. Dieses Versorgung könnte irgend welche Verbindung mit unserer Erdbebenmaschine haben, obgleich die Koppelung ziemlich grob sein sollte. Wenn diese Koppelung ganz ausgeschlossen würde, dann würde die Tätigkeit des betreffenden Vulkans allmählich zu Ende gehen,

Zum Schluss möchte ich Herrn Prof. H. Kuno herzlich danken für seine wichtigen Ratschläge über die petrographischen Kenntnisse.

16. Zisin no Ba no Ron.

Zisin-Kenkyûsyo, Matuzawa-Takeo.

Imamade ni wakatta Zisin no Okorikata no iroiro na taisetu na Kotogara wo tokiakasu tameni hitotu no Ba no Ron wo kangaeta. Okii Zisin no okoru Basyo no sugu Sita dewa Kotai-Ekitai no *Phase* no Uturi-kawari ga kurikaesi okori, sitagatte sone Ue no Tikaku nimo mata Dansei-hariai ga tameraretari hakidasaretari suru koto, sunawati ookii Zisin ga kurikaesi okoru to kangaeru. Tumari hitotu no Netu-Kikan wo kangaeru no de aru. Kono Baai Netu no Deiri wa Tutawarukoto dake dewa tarinai no de Tairyū no Seisitu no Mono wo kangaenaito Ma ni awanai. Kono Kikai wa Zyōki-Kikan ni nite ite, Sita no Ekitai ni naru Tokoro ga Kama no Bubun, Zisin no okoru Tikaku no Bubun ga *Piston* ni ataru node aru.

Tikyū Zentai to site mireba kono yōna Sikake no dekiyasui Tokoro ga Zisin-tai ni naru mono to omowareru.

17. *Transformation of Spherical Solid Harmonics Related to the Translation of Coordinates System.*

By Yasuo SATÔ,

Earthquake Research Institute.

(Read March 17, 1953.—Received June 20, 1953.)

1. Introduction.

For the last few years, we have studied several kinds of transformations of wave functions[1]. The study was promoted by the necessity for obtaining a wave function which is convenient to satisfy boundary conditions in the problem of generation of elastic waves. However, when we are engaged in the investigation of potential theory such as geomagnetism, electrostatics and so on, we are obliged to get a similar formula concerning spherical solid harmonics. A simple case was already solved by Lord Kelvin[2], but here we will derive a more general form of formula.

An arbitrary potential function V is, as is well known, expressed by a series of spherical solid harmonics in the form

$$\left.\begin{aligned} V &= V^+ + V^- \\ &= \sum_{n,m} R^n \bar{P}_n^m(\cos\theta)\,(A_n^{(m)} \cos m\varphi + B_n^{(m)} \sin m\varphi) \\ &+ \sum_{n,m} R^{-n-1} \bar{P}_n^m(\cos\theta)\,(C_n^{(m)} \cos m\varphi + D_n^{(m)} \sin m\varphi) \end{aligned}\right\} \qquad (1.1)$$

where R distance from the origin

θ colatitudinal angle

φ azimuthal angle

$\bar{P}_n^m(\cos\theta)$ associated Legendre function defined by Ferrers

$$\left(=\sin^m\theta\left(\frac{d}{d\cos\theta}\right)^m P_n(\cos\theta)\right)$$

and m and n are both positive integers (see Fig. 1).

Now, an arbitrary transformation of coordinates system can be analysed to rotations around its own origin and the translation of the

1) Y. SATÔ, "Transformation of Wave-functions Related to the Transformation of Coordinates Systems", First report, *Bull. Earthq. Res. Inst.*, **28** (1950), 1. Second report, *ibid.*, 175.

2) Sir W. THOMSON, *Reprint of Papers on Electrostatics and Magnatism*, § 494, London, 1872. *cf.* "A Mathematical Theory of Magnetism", *Proc. Roy Sac. Lond.* 1849. This paper was not accessible to the writer unfortunately.

origin in the z-direction[3]. Since the radial distance R remains unaltered in the case of rotation of coordinate axes, the transformation of spherical solid harmonics is quite equivalent to that of surface harmonics $\bar{P}_n^m(\cos\theta)\begin{matrix}\cos\\ \sin\end{matrix} m\varphi$, which was treated in the previous paper[4].

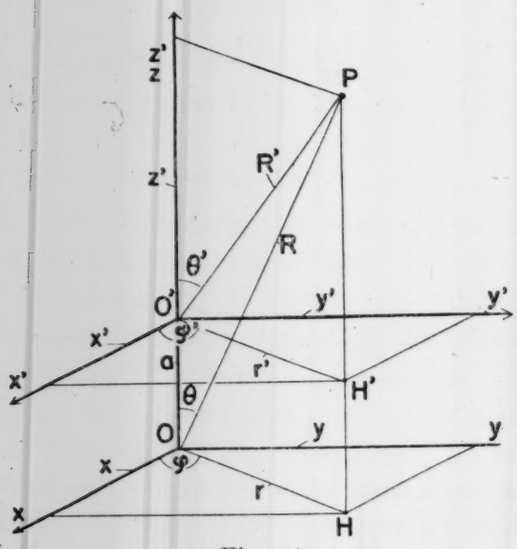

Fig. 1

Therefore, in this paper, we will treat the problem of the transformation due to the translation of the coordinates system in the z-direction. New and old coordinates are illustrated in Fig. 1, and the following relations are obtained at once.

$$\begin{aligned} x'&=x, & r'&=\sqrt{(x'^2+y'^2)}=r\\ y'&=y, & \varphi'&=\varphi\\ z'&=z-a, \end{aligned} \tag{1.2}$$

2. $R'^n\bar{P}_n^m(\cos\theta')\begin{matrix}\cos\\ \sin\end{matrix} m\varphi'$.

At first we will take up the function $R'^n\bar{P}_n^m(\cos\theta')\begin{matrix}\cos\\ \sin\end{matrix} m\varphi'$, which being a spherical solid harmonics, can be represented by a definite integral of the form[5].

$$\begin{aligned} &\int_{-\pi}^{\pi}(z'+ix'\cos u+iy'\sin u)\begin{matrix}\cos\\ \sin\end{matrix} mudu\\ &\quad=i^m2\pi\frac{n!}{(n+m)!}R'^n\bar{P}_n^m(\cos\theta')\begin{matrix}\cos\\ \sin\end{matrix} m\varphi' \end{aligned} \tag{2.1}$$

3) *loc. cit.*, 1). § 8.
4) *ibid.*
5) WHITTAKER and WATSON, *Modern Analysis*, p. 392.

Putting the relations (1.2) into this expression, we have

$$
\begin{aligned}
&R'^n \bar{P}_n^m(\cos\theta') \begin{matrix}\cos\\ \sin\end{matrix} m\varphi' \\
&= i^{-m} \frac{1}{2\pi} \cdot \frac{(n+m)!}{n!} \int_{-\pi}^{\pi} \{(z-a)+ix\cos u + iy \sin u\}^n \begin{matrix}\cos\\ \sin\end{matrix} mu\,du \\
&= i^{-m} \frac{1}{2\pi} \cdot \frac{(n+m)!}{n!} \sum_{k=0}^{n} \frac{n!}{k!\,(n-k)!} (-a)^{n-k} \int_{-\pi}^{\pi} (z+ix\cos u + iy\sin u)^k \begin{matrix}\cos\\ \sin\end{matrix} mu\,du \\
&= i^{-m} \frac{1}{2\pi} \cdot \frac{(n+m)!}{n!} \sum_{k=m}^{n} \frac{n!}{k!\,(n-k)!} (-a)^{n-k} \\
&\qquad \cdot i^m 2\pi \frac{k!}{(k+m)!} R^k \bar{P}_n^k(\cos\theta) \begin{matrix}\cos\\ \sin\end{matrix} m\varphi \\
&= \sum_{k=m}^{n} \binom{n+m}{k+m} (-a)^{n-k} R^k \bar{P}_k^m(\cos\theta) \begin{matrix}\cos\\ \sin\end{matrix} m\varphi \qquad (2.2)
\end{aligned}
$$

where $$\binom{p}{q} = \frac{p!}{q!\,(p-q)!}$$

Being a finite series the right hand member of (2.2) converges without regard to R, θ and φ. Therefore this is the formula which we aimed at in this paper.

3. $R'^{-n-1} \bar{P}_n^m(\cos\theta') \begin{matrix}\cos\\ \sin\end{matrix} m\varphi'$.

In this section we will obtain formulae concerning the spherical solid harmonics of degree n with negative power of the radial distance R'. Such a function represents a potential function that converges at infinitely distant points.

At first we will quote a formula analogous to (2.1), derived by T. Rikitake[6].

$$
\begin{aligned}
&\int_{-\pi}^{\pi} (z'+ix'\cos u + iy'\sin u)^{-n-1} \begin{matrix}\cos\\ \sin\end{matrix} mu\,du \\
&\qquad = R'^{-n-1} \cdot i^m \frac{(n-m)!}{n!} 2\pi \bar{P}_n^m(\cos\theta') \begin{matrix}\cos\\ \sin\end{matrix} m\varphi' \qquad (3.1)
\end{aligned}
$$

3.1 When $R < |a|$.

When R is smaller than $|a|$, the next treatment is possible. From (3.1)

6) T. RIKITAKE, "Magnetic Anomalies and the Corresponding Magnetic Centres. I", *Journ. Geomag. Geoelectr.*, **2** (1950), 20. Expression (2).

$$R'^{-n-1}\bar{P}_n^m(\cos\theta')\begin{matrix}\cos\\ \sin\end{matrix}m\varphi'$$
$$=i^{-m}\frac{1}{2\pi}\frac{n!}{(n-m)!}\int_{-\pi}^{\pi}(z'+ix'\cos u+iy'\sin u)^{-n-1}\begin{matrix}\cos\\ \sin\end{matrix}mudu$$
$$=i^{-m}\frac{1}{2\pi}\frac{n!}{(n-m)!}\int_{-\pi}^{\pi}\{-a+(z+ix\cos u+iy\sin u)\}^{-n-1}\begin{matrix}\cos\\ \sin\end{matrix}mudu \quad (3.2)$$

Now,

$$\left.\begin{aligned}&\max|z+ix\cos u+iy\sin u|\\ &=\max|z+ir\cos(u-\varphi)|\\ &=\sqrt{(z^2+r^2)}\\ &=R.\end{aligned}\right\} \quad (3.3)$$

Therefore, if $R<|a|$ the integrand of the expression (3.2) can be expanded by the binomial theorem, integrating term by term, we have

$$R'^{-n-1}\bar{P}_n^m(\cos\theta')\begin{matrix}\cos\\ \sin\end{matrix}m\varphi'$$
$$=i^{-m}\frac{1}{2\pi}\frac{n!}{(n-m)!}\int_{-\pi}^{\pi}(-a)^{-n-1}\{1-(z+ix\cos u+iy\sin u)/a\}^{-n-1}\cdot\begin{matrix}\cos\\ \sin\end{matrix}mudu$$
$$=i^{-m}\frac{1}{2\pi}\frac{n!}{(n-m)!}(-a)^{-n-1}$$
$$\cdot\sum_{k=m}^{n}\frac{(n+1)_k}{k!}a^{-k}\int_{-\pi}^{\pi}(z+ix\cos u+iy\sin u)^k\begin{matrix}\cos\\ \sin\end{matrix}mudu$$
$$=(-)^{n+1}\sum_{k=m}^{\infty}\binom{n+k}{m+k}a^{-n-k-1}R^k\bar{P}_k^m(\cos\theta)\begin{matrix}\cos\\ \sin\end{matrix}m\varphi \quad (3.4)$$

3.2 When $R>|a|$.

The formula (3.4) does not converge when R is greater than $|a|$, therefore we must devise another type of expression. In this case also, the expression (3.2) holds, and if $|z|>|a|$, the binomial theorem can be applied to the expansion of the integrand in the following form.

$$\{z'+ix'\cos u+iy'\sin u\}^{-n-1}$$
$$=(z+ix\cos u+iy\sin u)^{-n-1}\{1-a/(z+ix\cos u+iy\sin u)\}^{-n-1} \quad (3.5)$$

Employing this form of expression we have

$$R'^{-n-1}\bar{P}_n^m(\cos\theta')\begin{matrix}\cos\\ \sin\end{matrix}m\varphi'$$
$$=i^{-m}\frac{n!}{(n-m)!}\frac{1}{2\pi}\int_{-\pi}^{\pi}(z+ix\cos u+iy\sin u)^{-n-1}$$
$$\cdot\{1-a/(z+ix\cos u+iy\sin u)\}^{-n-1}\begin{matrix}\cos\\ \sin\end{matrix}mudu$$

$$=i^{-m}\frac{n!}{(n-m)!}\frac{1}{2\pi}\sum_{k=0}^{\infty}\frac{(n+1)_k}{k!}a^k\int_{-\pi}^{\pi}(z+ix\cos u+iy\sin u)^{-n-k-1}\begin{matrix}\cos\\ \sin\end{matrix}mudu$$

$$=\sum_{k=0}^{\infty}\binom{n-m+k}{k}a^kR^{-n-k-1}\bar{P}^m_{n+k}(\cos\theta)\begin{matrix}\cos\\ \sin\end{matrix}m\varphi \tag{3.6}$$

Now, the above expression is obtained under the condition that

$$|z|>|a|. \tag{3.7}$$

However, the same expression can be used under the wider condition

$$R>|a|. \tag{3.8}$$

For the function $V^-=R'^{-n-1}\bar{P}^m_n(\cos\theta')\begin{matrix}\cos\\ \sin\end{matrix}m\varphi'$ that satisfies Laplace's equation

$$\left(\frac{\partial^2}{\partial x'^2}+\frac{\partial^2}{\partial y'^2}+\frac{\partial^2}{\partial z'^2}\right)V^-=0 \tag{3.9}$$

also satisfies the same form of equation referring to new coordinates

$$\left(\frac{\partial^2}{\partial x^2}+\frac{\partial^2}{\partial y^2}+\frac{\partial^2}{\partial z^2}\right)V^-=0 \tag{3.10}$$

Therefore V^-which converges at infinity must be expressed as the sum of spherical solid harmonics with negative power of R. Thus we have

$$V^-=\sum_j K_j^{(m)}R^{-j-1}\bar{P}^m_j(\cos\theta)\begin{matrix}\cos\\ \sin\end{matrix}m\varphi \tag{3.11}$$

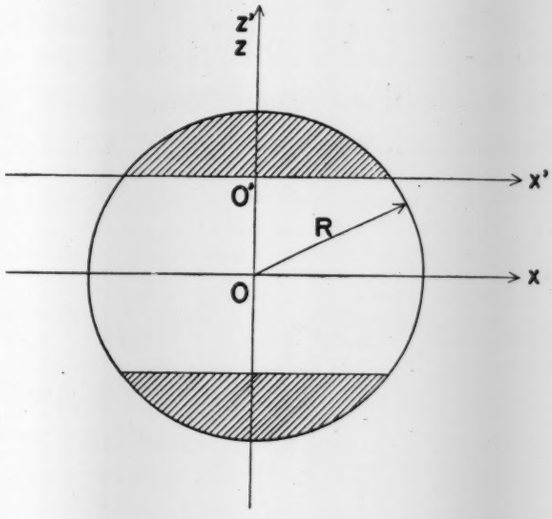

Fig. 2

When $|z|>|a|$, (shadowed part of the sphere in Fig. 2) the above expression must be identically equal to the expression (3.6), while the general theory of harmonic functions shows that the expression in such a form

is unique; therefore the same expression holds on the other part of the same spherical surface. Thus the formula (3.6) can be used under a wider condition

$$R>|a| \tag{3.8 bis}$$

4. Numerical computation of the coefficients in the formulae.

For the convenience of practical use we have calculated the coefficients in the above formulae.

1) From (2.2) we have

$$R'^{n}\bar{P}_n^m(\cos\theta')\begin{matrix}\cos\\ \sin\end{matrix}m\varphi' = (-a)^n\sum_{k=m}^{n}\binom{n+m}{k+m}(-\rho)^k\bar{P}_k^m(\cos\theta)\begin{matrix}\cos\\ \sin\end{matrix}m\varphi \tag{4.1}$$

in which $\rho=R/a$.

In Table I we show the terms $\binom{n+m}{k+m}(-\rho)^k\bar{P}_k^m(\cos\theta)$ corresponding to the cases $n=1$, 2 and 3.

Table I. $\binom{n+m}{k+m}\left(-\frac{R}{a}\right)^k\bar{P}_k^m(\cos\theta)$.

($\rho\equiv R/a$, $P_k^m\equiv\bar{P}_k^m(\cos\theta)$.)

	$n=1$		$n=2$			$n=3$			
k	$m=0$	$m=1$	$m=0$	$m=1$	$m=2$	$m=0$	$m=1$	$m=2$	$m=3$
0	1		1			1			
1	$-\rho P_1$	$-\rho P_1^1$	$-2\rho P_1$	$-3\rho P_1^1$		$-3\rho P_1$	$-6\rho P_1^1$		
2			ρ^2P_2	$\rho^2P_2^1$	$\rho^2P_2^2$	$3\rho^2P_2$	$4\rho^2P_2^1$	$5\rho^2P_2^2$	
3						$-\rho^3P_3$	$-\rho^3P_3^1$	$-\rho^3P_3^2$	$-\rho^3P_3^3$

2) From (3.4), when $R<|a|$ we have

$$R'^{-n-1}\bar{P}_n^m(\cos\theta')\begin{matrix}\cos\\ \sin\end{matrix}m\varphi' = (-a)^{-n-1}\sum_{k=m}^{\infty}\binom{n+k}{m+k}\rho^k\bar{P}_k^m(\cos\theta)\begin{matrix}\cos\\ \sin\end{matrix}m\varphi \tag{4.2}$$

In Table II, we show the terms $\binom{n+k}{m+k}\rho^k \bar{P}_k^m(\cos\theta)$ corresponding to the cases $n=1$, 2 and 3.

Table II. $\binom{n+k}{m+k}\left(\frac{R}{a}\right)^k \bar{P}_k^m(\cos\theta)$.

$(\rho \equiv R/a, \quad P_k^m \equiv \bar{P}_k^m(\cos\theta).)$

	$n=1$		$n=2$			$n=3$			
k	$m=0$	$m=1$	$m=0$	$m=1$	$m=2$	$m=0$	$m=1$	$m=2$	$m=3$
0	1		1			1			
1	$2\rho\ P_1$	$\rho\ P_1^1$	$3\rho\ P_1$	$3\rho\ P_1^1$		$4\rho\ P_1$	$6\rho\ P_1^1$		
2	$3\rho^2 P_2$	$\rho^2 P_2^1$	$6\rho^2 P_2$	$4\rho^2 P_2^1$	$\rho^2 P_2^2$	$10\rho^2 P_2$	$10\rho^2 P_2^1$	$5\rho^2 P_2^2$	
3	$4\rho^3 P_3$	$\rho^3 P_3^1$	$10\rho^3 P_3$	$5\rho^3 P_3^1$	$\rho^3 P_3^2$	$20\rho^3 P_3$	$15\rho^3 P_3^1$	$6\rho^3 P_3^2$	$\rho^3 P_3^3$
4	$5\rho^4 P_4$	$\rho^4 P_4^1$	$15\rho^4 P_4$	$6\rho^4 P_4^1$	$\rho^4 P_4^2$	$35\rho^4 P_4$	$21\rho^4 P_4^1$	$7\rho^4 P_4^2$	$\rho^4 P_4^3$
5	$6\rho^5 P_5$	$\rho^5 P_5^1$	$21\rho^5 P_5$	$7\rho^5 P_5^1$	$\rho^5 P_5^2$	$56\rho^5 P_5$	$28\rho^5 P_5^1$	$8\rho^5 P_5^2$	$\rho^5 P_5^3$
6	$7\rho^6 P_6$	$\rho^6 P_6^1$	$28\rho^6 P_6$	$8\rho^6 P_6^1$	$\rho^6 P_6^2$	$84\rho^6 P_6$	$36\rho^6 P_6^1$	$9\rho^6 P_6^2$	$\rho^6 P_6^3$
7	$8\rho^7 P_7$	$\rho^7 P_7^1$	$36\rho^7 P_7$	$9\rho^7 P_7^1$	$\rho^7 P_7^2$	$120\rho^7 P_7$	$45\rho^7 P_7^1$	$10\rho^7 P_7^2$	$\rho^7 P_7^3$
8	$9\rho^8 P_8$	$\rho^8 P_8^1$	$45\rho^8 P_8$	$10\rho^8 P_8^1$	$\rho^8 P_8^2$	$165\rho^8 P_8$	$55\rho^8 P_8^1$	$11\rho^8 P_8^2$	$\rho^8 P_8^3$
9	$10\rho^9 P_9$	$\rho^9 P_9^1$	$55\rho^9 P_9$	$11\rho^9 P_9^1$	$\rho^9 P_9^2$	$220\rho^9 P_9$	$66\rho^9 P_9^1$	$12\rho^9 P_9^2$	$\rho^9 P_9^3$
10	$11\rho^{10} P_{10}$	$\rho^{10} P_{10}^1$	$66\rho^{10} P_{10}$	$12\rho^{10} P_{10}^1$	$\rho^{10} P_{10}^2$	$286\rho^{10} P_{10}$	$78\rho^{10} P_{10}^1$	$13\rho^{10} P_{10}^2$	$\rho^{10} P_{10}^3$

3) From (3.6), when $R>|a|$ we have

$$R'^{-n-1}\bar{P}_n^m(\cos\theta')\begin{matrix}\cos\\ \sin\end{matrix} m\varphi'$$
$$=a^{-n-1}\sum_{k=0}^{\infty}\binom{n-m+k}{k}\rho^{-n-k-1}\bar{P}_{n+k}^m(\cos\theta)\begin{matrix}\cos\\ \sin\end{matrix} m\varphi \qquad (4.3)$$

In Table III, we show the terms $\binom{n-m+k}{k}\rho^{-n-k-1}\bar{P}_{n+k}^k(\cos\theta)$ corresponding to the cases $n=1$, 2 and 3.

This investigation was accomplished by Dr. T. Rikitake's advice and suggestion. The author offers hearty thanks to him.

Table III. $\binom{n-m+k}{k}\left(\frac{a}{R}\right)^{n+k+1}\bar{P}^m_{n+k}(\cos\theta)$.

$(\rho\equiv R/a,\quad P^m_j\equiv\bar{P}^m_j(\cos\theta).)$

	$n=1$		$n=2$			$n=3$			
k	$m=0$	$m=1$	$m=0$	$m=1$	$m=2$	$m=0$	$m=1$	$m=2$	$m=3$
0	$\rho^{-2}P_1$	$\rho^{-2}P_1^1$	$\rho^{-3}P_2$	$\rho^{-3}P_2^1$	$\rho^{-3}P_2^2$	$\rho^{-4}P_3$	$\rho^{-4}P_3^1$	$\rho^{-4}P_3^2$	$\rho^{-4}P_3^3$
1	$2\rho^{-3}P_2$	$\rho^{-3}P_2^1$	$3\rho^{-4}P_3$	$2\rho^{-4}P_3^1$	$\rho^{-4}P_3^2$	$4\rho^{-5}P_4$	$3\rho^{-5}P_4^1$	$2\rho^{-5}P_4^2$	$\rho^{-5}P_4^3$
2	$3\rho^{-4}P_3$	$\rho^{-4}P_3^1$	$6\rho^{-5}P_4$	$3\rho^{-5}P_4^1$	$\rho^{-5}P_4^2$	$10\rho^{-6}P_5$	$6\rho^{-6}P_5^1$	$3\rho^{-6}P_5^2$	$\rho^{-6}P_5^3$
3	$4\rho^{-5}P_4$	$\rho^{-5}P_4^1$	$10\rho^{-6}P_5$	$4\rho^{-6}P_5^1$	$\rho^{-6}P_5^2$	$20\rho^{-7}P_6$	$10\rho^{-7}P_6^1$	$4\rho^{-7}P_6^2$	$\rho^{-7}P_6^3$
4	$5\rho^{-6}P_5$	$\rho^{-6}P_5^1$	$15\rho^{-7}P_6$	$5\rho^{-7}P_6^1$	$\rho^{-7}P_6^2$	$35\rho^{-8}P_7$	$15\rho^{-8}P_7^1$	$5\rho^{-8}P_7^2$	$\rho^{-8}P_7^3$
5	$6\rho^{-7}P_6$	$\rho^{-7}P_6^1$	$21\rho^{-8}P_7$	$6\rho^{-8}P_7^1$	$\rho^{-8}P_7^2$	$56\rho^{-9}P_8$	$21\rho^{-9}P_8^1$	$6\rho^{-9}P_8^2$	$\rho^{-9}P_8^3$
6	$7\rho^{-8}P_7$	$\rho^{-8}P_7^1$	$28\rho^{-9}P_8$	$7\rho^{-9}P_8^1$	$\rho^{-9}P_8^2$	$84\rho^{-10}P_9$	$28\rho^{-10}P_9^1$	$7\rho^{-10}P_9^2$	$\rho^{-10}P_9^3$
7	$8\rho^{-9}P_8$	$\rho^{-9}P_8^1$	$36\rho^{-10}P_9$	$8\rho^{-10}P_9^1$	$\rho^{-10}P_9^2$	$120\rho^{-11}P_{10}$	$36\rho^{-11}P_{10}^1$	$8\rho^{-11}P_{10}^2$	$\rho^{-11}P_{10}^3$
8	$9\rho^{-10}P_9$	$\rho^{-10}P_9^1$	$45\rho^{-11}P_{10}$	$9\rho^{-11}P_{10}^1$	$\rho^{-11}P_{10}^2$	$165\rho^{-12}P_{11}$	$45\rho^{-12}P_{11}^1$	$9\rho^{-12}P_{11}^2$	$\rho^{-12}P_{11}^3$
9	$10\rho^{-11}P_{10}$	$\rho^{-11}P_{10}^1$	$55\rho^{-12}P_{11}$	$10\rho^{-12}P_{11}^1$	$\rho^{-12}P_{11}^2$	$220\rho^{-13}P_{12}$	$55\rho^{-13}P_{12}^1$	$10\rho^{-13}P_{12}^2$	$\rho^{-13}P_{12}^3$
10	$11\rho^{-12}P_{11}$	$\rho^{-12}P_{11}^1$	$66\rho^{-13}P_{12}$	$11\rho^{-13}P_{12}^1$	$\rho^{-13}P_{12}^2$	$286\rho^{-14}P_{13}$	$66\rho^{-14}P_{13}^1$	$11\rho^{-14}P_{13}^2$	$\rho^{-14}P_{13}^3$

17. 坐標系の移動に伴ふ体球函数の変換

地震研究所　佐　藤　泰　夫

電磁気の問題を扱ふ場合には，坐標変換に伴ふポテンシアル函数の変換を論ずる必要がおこる．筆者にさきに，坐標軸の回転に対する表面球函数の変換公式を求めたから，z-軸方向に系を移動した際の体球函数の変換を論ずれば理論的には十分である．

結果は §4 にまとめてあり，計算の便宜の爲に二三の表も加へて置いた．

18. *A New Method for Regulating Electric Currents and its Application to Measurements of Geomagnetic Field.*

By Izumi YOKOYAMA,

Earthquake Research Institute.

(Read April 21, 1953.—Received June 20, 1953.)

1. Introduction.

Among the various observations in geophysics, one of the most precise measurements is to determine the geomagnetic field with the sufficient accuracy, i. e. with the error less than 0.1 *minutes* of arc in declination and inclination and 1 *gamma* in intensity. In 1948 a portable electromagnetic magnetometer using a rotating coil as a detector for measuring the three elements of the geomagnetic field with the aforementioned preciseness was completed by I. Tsubokawa[1] of the Geographical Survey Institute and named "G. S. I. first order magnetometer".

Recently the Earthquake Research Institute has commenced to utilize the G. S. I. second order magnetometer which was also completed by Tsubokawa with the intention of simplifying the first order one at the least cost of the preciseness. For the sake of the magnetic surveys we ourselves aimed at, such as those at volcanoes and earthquake zones in case of emergencies, we devised a new method for regulating electric currents in place of the astatic galvanometer which was found to be rather inconvenient in field works.

2. A new method for regulating electric currents.

The G. S. I. type magnetometer consists of a small rotating coil as a detector and a Helmholtz-Gaugain coil to generate a constant magnetic field which are mounted on the horizontal axis of a theodolite. The axis of rotation of the detector, the central axis of the Helmholtz-Gaugain coil and the horizontal axis of the theodolite are arranged at right angles to one another. The electromotive force generated in the detector can be sensitively detected by a high gain amplifier with a magic-eye. The declination and inclination are simultaneously measured by adjusting

1) I. TSUBOKAWA, *Bull. G. S. I.*, **2** (1951), 325.

successively the horizontal and vertical directions of the axis of rotation of the detector so that the output of the amplifier becomes null, letting no current pass through the Helmholtz-Gaugain coil. The geomagnetic intensity can be measured by finding the direction of the resultant of the geomagnetic field and the constant induced field by the Helmholtz-Gaugain coil. The schematic diagram is shown in Fig. 1.

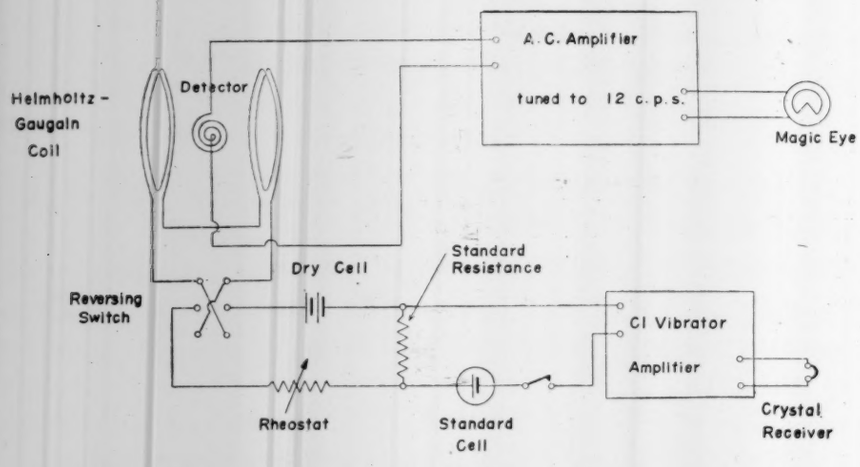

Fig. 1. Schematic diagram of the G. S. I. type magnetometer.

The electric currents passing through the Helmholtz-Gaugain coil are regulated to be constant by adjusting the rheostats so as to nullify the current in the standard-cell's circuit. Then the voltage-drop in the standard-resistance becomes strictly equal to the voltage of the standard-cell and the value of the electric current may be known exactly from the values of the standard-resistance and electromotive force of the standard-cell both being corrected by the temperature coefficients.

The balance of the standard-cell's circuit is detected by a new method in place of an astatic galvanometer of the sensitivity 10^{-6} *volt*. The circuit-diagram of the new method is shown in Fig. 2. The direct-voltage is converted into an alternating one of 1,000 c. p. s. by intermittent contact of the osmium point of the so-called "CI vibrator" which is excited by a circuit containing a small carbon-microphone, an electromagnet, and dry batteries. The voltage of the 1,000 c. p. s. alternating-current which is the same amplitude with the applied direct current, is implied in an ordinary audio-amplifier. According to the result of the experiment, the gain of the amplifier is about 40 *db* when we use 67.5 *volts* as B electric source. The output of the amplifier is connected to a high-impedance crystal receiver made of rochelle salt. The observer hears a sound of

1,000 c. p. s. modulated by the electric current in the standard-cell's circuit and no signal when the balance is completed. As our sense of hearing is most sensitive in the neighbourhood of 1,000 c. p. s., the above-mentioned method of detection is efficient and appropriate. The rheostat in Fig. 1 is able to control about one part in 100,000 and this detector is sensible of the change in this one part near the state of balancing as a result of the experiment. The magnet included in CI vibrator, whose magnetic field we had apprehension of, has been ascertained to have no appreciable influence upon the detector of the magnetometer at a distance of about 3 *meters*.

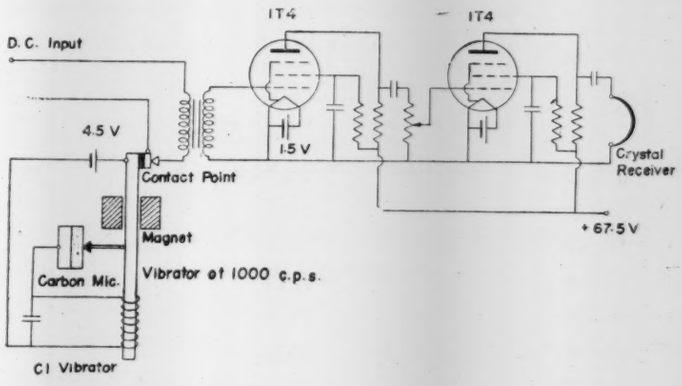

Fig. 2. Circuit-diagram of the CI vibrator-amplifier.

3. Observations of geomagnetic field using this method at the Kakioka Magnetic Observatory.

In order to determine the coil constant of the G. S. I. second order magnetometer and examine the accuracy of observations, the comparison measurement with the standard magnetometer of the Kakioka Magnetic Observatory was carried out in Oct., 1952. The above-mentioned method for regulating electric currents of the Helmholtz-Gaugain coil was applied to determining the horizontal intensity. The time required for one complete observation is less than 10 *minutes*. The results of the observation are shown in Table I and graphically represented in Fig. 3 compared with the values obtained from the magnetogram of the Observatory. The variometer-room is about 40 *meters* distant from the absolute observatory in which our observation was made. From these values, the instrumental errors and the probable errors of single observation are deduced as shown in Tables II and III, the magnetogram of the observatory being considered true. Table IV shows the other probable errors of single observation deduced from the fluctuations of the reading values independent of the magnetogram, on the assumption that the directions of the horizontal and vertical axes of the theodolite are invariable by revolving and that the respective

Table I.
Results of the comparison measurement.

Time	Declination		Inclination		Horizontal Intensity	
	Observed value	Magneto-gram	Observed value	Magneto-gram	Observed value	Magneto-gram
1952, Oct. 2nd						
09h 50m	6°24′.2w	6°24′.1w	49°23′.0	49°22′.6	30054γ	30051γ
11 46	27.6	27.8	23.2	22.4	63	66
13 28	25.4	25.6	23.3	22.5	72	69
14 40	24.1	23.4	23.3	22.7	64	65
15 59	21.5	21.9	23.9	23.1	63	61
17 01	22.5	22.5	23.9	23.1	64	62
17 37	22.5	22.4	23.9	23.2	62	60
20 39	22.4	22.6	24.1	23.4	59	58
21 16	22.4	22.7	24.5	23.5	53	55
21 51	22.6	22.6	24.8	23.8	48	50
22 32	22.0	21.9	24.8	23.8	46	50
23 08	21.2	21.2	24.2	23.5	63	64
23 48	21.4	21.4	24.4	23.6	59	59
3rd						
00 32	21.7	21.7	24.4	23.6	61	60
01 10	21.4	21.4	24.5	23.6	62	61
07 46	22.5	22.3	24.3	23.6	46	46
08 31	22.9	22.8	24.0	23.5	50	50
09 18	24.3	24.0	23.8	23.2	48	53
09 58	25.8	25.1	23.5	23.0	45	52
10 36	27.1	26.5	23.6	23.2	45	47
11 22	28.2	27.6	24.1	23.6	42	43
12 06	28.5	27.7	24.3	23.8	43	45
14 35	25.2	24.8	24.4	23.8	50	50
15 18	24.7	24.3	24.2	23.9	45	46
15 56	23.8	23.6	24.2	23.9	53	47
4th						
09 17	23.9	24.2	24.8	24.4	16	17
10 06	26.4	26.4	24.5	24.1	34	32
11 10	26.5	26.3	24.3	23.5	46	44
11 48	26.2	26.1	23.7	23.3	52	51
16 28	25.7	25.6	28.6	27.7	29966	29965
17 04	24.3	24.1	28.5	27.8	977	971
17 32	23.7	23.8	28.3	27.8	989	982

Table II.
Instrumental error.

Westerly Declination	Inclination	Horizontal Intensity
-0′.13	-0′.65	*

* Coil constant was determined by the least square method.

Table III.
Probable error of a single observation deduced from the comparison with the magnetogram.

Declination	Inclination	Horizontal Intensity
0′.20	0′.13	1.5γ

Table IV.
Probable error of a single observation deduced from the fluctuations of reading values.

Declination	Inclination	Horizontal Intensity
0′.22	0′.16	1.6γ

components of geomagnetic field are constant during the time of observation.[2)]

As shown in Table II, the instrumental error in inclination is of not negligible quantity. This may be attributed to the following origins:

1) The systematic errors of the magnetometer due to errors in graduations of circles or some magnetic deposits.
2) The difference of the main field between the variometer-room and the absolute observatory.
3) The systematic errors of the standard magnetometer — the values of inclination corresponding to magnetogram in Table I are computed from the magnetograms of horizontal and vertical components.

Referring to Tables III and IV, it may be said that the probable errors of single observation are respectively less than 0′.20 in declination, 0′.15 in inclination and 1.5 γ in intensity.

2) *loc. cit.*, 1), 357.

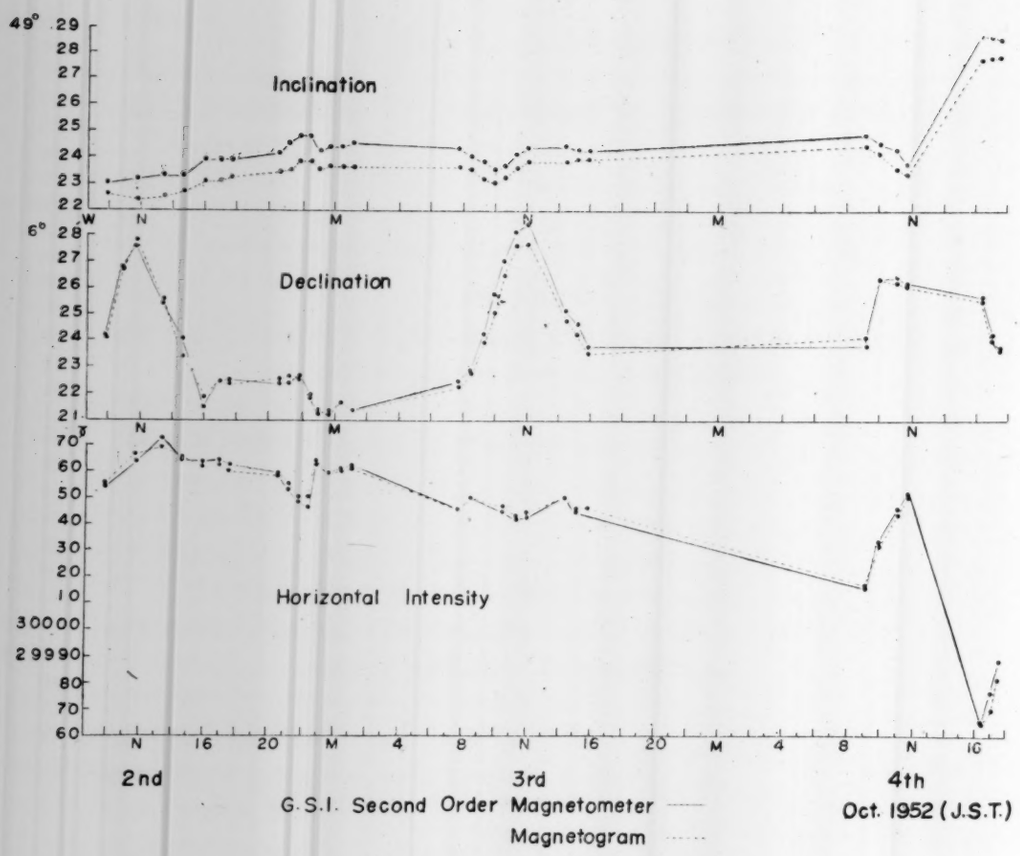

Fig. 3. Results of the comparison measurement.

4. Conclusion.

As a result of the comparison measurement with the standard magnetometer, it was found that the new method for regulating the electric currents applied to measurements of geomagnetic field is almost as highly sensitive as the astatic galvanometer and furthermore that it lightens the observer's burden in field works. The G. S. I. second order magnetometer was also found to be very excellent in its simplicity and rapidity of operation and in its high accuracy.

In conclusion, the writer wishes to express his hearty thanks to Dr. T. Rikitake for his helpful support. The writer also wishes to record his indebtedness to Mr. I. Tsubokawa of the Geographical Survey Institute. The writer's hearty thanks are also due to Mr. T. Oguchi who assisted the writer in the comparison measurement.

18. 電流を制御する新しい試み及びその地磁気測定への応用

地震研究所　横山　泉

今迄，地磁気を電磁的に測定する場合，ヘルムホルツ・コイルに通ずる電流をポテンシオメーター的に制御するに際して，無定位電流計が用いられた．これは野外観測においては種々の煩わしさを伴うものであった．今回，この無定位電流計の代りに CI 発振器を利用した直流増幅器を用いた．柿岡における比較観測の結果から，この新しい方法は十分な精度を有するものであり，又，観測者の負担を大いに減ずるものであることが判った．

19. *Relation between the Nature of Surface Layer and the Amplitude of Earthquake Motions. II.*

By Kiyoshi KANAI,

Earthquake Research Institute.

(Read Feb. 17, 1953.—Received June 20, 1953.)

1. Introduction

Many observational studies show how the property of earthquake motion at ground surface depends upon the nature of ground. For instance, Ishimoto[1] who made the observations at ten and several places such as Tokyo, Yokohama etc. by means of acceleration seismograph, found each place to have a predominant period of earthquake motion peculiar to it.

The observation of aftershocks made by Minakami and others[2] reveals that there was little difference of amplitude of acceleration according to the nature of ground, though the difference of the amplitude of displacement was remarkable. Recently in U.S.A.[3] the changes of the property of earthquake motion according to ground nature have become a distinguished subject of discussion.

As to the relation between earthquake damage and ground nature, the statistical studies as well as the observational ones have been made from various standpoints. Saita[4], viewing from the standpoint of predominant period, explained that the relations of ground nature both to the damage of 3-storied wooden houses and to that of godowns at the time of the Kwanto Earthquake of 1923, are entirely opposite to each other, while the author[5] intended to prove it from the idea of the dissipation of the vibration energy of building to ground.

There are also the researches[6] making it clear that the damage done

1) M. ISHIMOTO, *Bull. Earthq. Res. Inst.*, **10** (1932), 171; **12** (1934), 234; **13** (1935), 592.

2) T. MINAKAMI and S. SAKUMA, *Bull. Earthq. Res. Inst.*, **26** (1949), 61; T. MINAKAMI, *Report, Fukui Earthq.*, 1950, Tokyo, 77.

3) F. NEUMANN, *Proc. Synpos. Earthq. and.....*, Los Angeles, 1952, p. 8.

4) T. SAITA, *Bosai-Kagaku*, Vol. 2, 298, Iwanami-shoten, 1935 (in Japanese).

5) K. KANAI and S. YOSHIZAWA, *Bull. Earthq. Res. Inst.*, **27** (1949), 91; **29** (1951), 209.

6) S. OMOTE, *Bull. Earthq. Res. Inst.*, **27** (1949), 57; S. OMOTE and S. MIYAMURA, *Bull. Earthq. Res. Inst.*, **29** (1951), 183; H. KAWASUMI, *Journ. Architect. Inst. Japan*, Vol. 66, No. 773 (1951), 8 (in Japanese); H. KAWASUMI and others, *Monthly Colloq. Earthq. Res. Inst.*, Sept. 16, 1952.

to wooden houses old Japanese style is closely connected with the thickness of alluvium and reclaimed mud. Also, the relations between earthquake damage and the velocity of surface wave and between the damage and the damping of ground vibration have been studied[7].

As to the mathematical studies, there are the papers written by Sezawa and others[8] dealing with the possibility of free oscillation of surface layer. Takahasi and Hirano[9] calculated the vibration of the surface of the ground where the bed rocks are disclosed from the seismogram of the surface of a ground with weak surface layer. The author[10] investigated the problem of the oscillations of doubly stratified visco-elastic layers as well as a stratified visco-elastic layer excited by seismic waves.

Generally the upper part of ground consists of several layers. As it is necessary to study the cases in which there are at least two layers near the ground surface in this paper, the author will show the results of calculation with numerical values of close approximation to actual cases.

2. Results of mathematical studies

In order to make the calculation easier, the damping of the third layer is neglected and dampings of both the first and the second layers

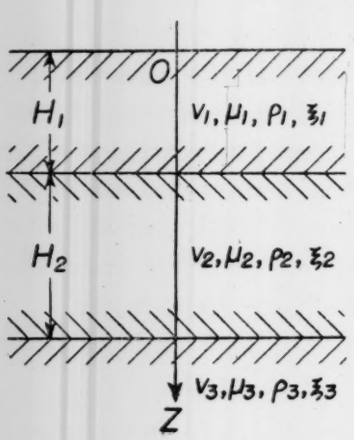

Fig. 1.

7) *Bull. Disast. Prevent. Res. Inst., Kyoto Univ.*, **2** (1949), 6, 17; **3** (1950), 1, 3, 7 (in Japanese).

8) K. SEZAWA, *Bull. Earthq. Res. Inst.*, **8** (1930), 1; K. SEZAWA and K. KANAI, *Bull. Earthq. Res. Inst.*, **10** (1932), 273.

9) R. TAKAHASI and K. HIRANO, *Bull, Earthq. Res. Inst.*, **19** (1941), 534.

10) K. KANAI, *Bull. Earthq. Res. Inst.*, **28** (1950), 31; **30** (1952), 31.

are assumed to be very small. That is to put the conditions $\xi_3 p/\mu_3=0$, $\xi_2 p/\mu_2 \ll 1$, and $\xi_1 p/\mu_1 \ll 1$ into equations (11) and (12) given in the previous paper[11]. Then we obtain

$$\frac{|u_{1z=0}|}{2|u_0|}=\frac{2}{\sqrt{\Phi_1^2+\Phi_2^2}}, \tag{1}$$

$$\begin{aligned}\Phi_1=&2(1+\gamma Q_2+\beta Q_1)\cos P_2\cos P_1-2(\alpha+\beta Q_2+\gamma Q_1)\sin P_2\sin P_1\\&-(\beta N_1+\gamma N_2)(\cos P_2\sin P_1+\sin P_2\cos P_1),\\ \Phi_2=&(-\beta N_1+\gamma N_2)\cos P_2\cos P_1+\{-\beta N_1+\gamma N_2+2\alpha(N_2-N_1)\}\sin P_2\sin P_1\\&+2(\beta+\alpha Q_2+Q_1)\cos P_2\sin P_1+2(\gamma+Q_2+\alpha Q_1)\sin P_2\cos P_1,\end{aligned} \tag{2}$$

$$\begin{aligned}&\alpha=\frac{\rho_1 v_1}{\rho_2 v_2},\quad \beta=\frac{\rho_1 v_1}{\rho_3 v_3},\quad \gamma=\frac{\rho_2 v_2}{\rho_3 v_3},\quad P_1=\frac{v_2}{v_1}\cdot\frac{H_1}{H_2}\cdot\frac{pH_2}{v_2}\left(=\frac{pH_1}{v_1}\right),\\&P_2=\frac{pH_2}{v_2},\quad Q_1=\frac{1}{2}\cdot\frac{H_1}{H_2}\cdot\frac{v_2^2}{H_2}\cdot\frac{\xi_1}{\mu_1 v_1}\left(\frac{pH_2}{v_2}\right)^2\left(\equiv\frac{pH_1}{v_1}N_1\right),\\&Q_2=\frac{1}{2}\cdot\frac{v_2^2}{H_2}\frac{\xi_2}{\mu_2 v_2}\left(\frac{pH_2}{v_2}\right)^2\left(\equiv\frac{pH_2}{v_2}N_2\right),\\&N_1=\frac{1}{2}\cdot\frac{v_1}{v_2}\cdot\frac{v_2^2}{H_2}\cdot\frac{\xi_1}{\mu_1 v_1}\frac{pH_2}{v_2}\left(\equiv\frac{1}{2}\frac{\xi_1 p}{\mu_1}\right),\quad N_2=\frac{1}{2}\cdot\frac{v_2^2}{H_2}\cdot\frac{\xi_2}{\mu_2 v_2}\cdot\frac{pH_2}{v_2}\left(=\frac{1}{2}\frac{\xi_2 p}{\mu_2}\right)\end{aligned} \tag{3}$$

In equation (3), H= thickness of the layer, μ= rigidity, ρ= density, ξ= coefficient of solid viscosity, $p=2\pi/T$, T= period. Suffix 1, 2 and 3 represent respectively the first layer, the second layer and the lowest medium.

In equation (1) $u_{1z=0}$ represents the amplitude at ground surface and u_0 the amplitude of incident wave in the lowest medium. In equation (3), if μ is replaced by $\lambda+2\mu$, it shows the case when dilatational wave come from right below.

As an example of numerical calculation, the relations between period and amplitude in such four cases as $H_1/H_2=1/15$, 1/6, 1/3 and 1 are given by assuming $\rho_1 v_1 : \rho_2 v_2 : \rho_3 v_3=1:3:6$, $\xi_2/\mu_2 v_2=\xi_1/\mu_1 v_1=5\times 10^{-8}$ *C.G.S.*, $v_1/v_2=1/3$, $v_2^2/H_2=4\times 10^5$ *C.G.S.*

The numerical values used here are commonly observed near the ground surface. According to the results of former researches[12] regard-

11) *loc. cit.*, 10), p. 33.

12) K. KANAI and K. OSADA, *Bull. Earthq. Res. Inst.*, **29** (1951), p. 514, Table II. A. KUBOTERA, *Journ. Seism. Soc. Japan*, **5** (1952), 9 (in Japanese). Though the physical meaning of this fact cannot be made clear, it is known that the values of ξ/E concerning various kinds of building are of the same order. E represents effective Young's modulus.

ing damping coefficient, it is acknowledged that the coefficient is always about of equal order in any of the cases of superficial soil, the depth of crust, P-waves and S-waves, when it is expressed in the form of $\xi/\mu v$. $v_2^2/H_2=4\times10^5 C.G.S.$ corresponds to the cases where $v_2=400\,\mathrm{m/s}$ and $H_2=40\,\mathrm{m}$.

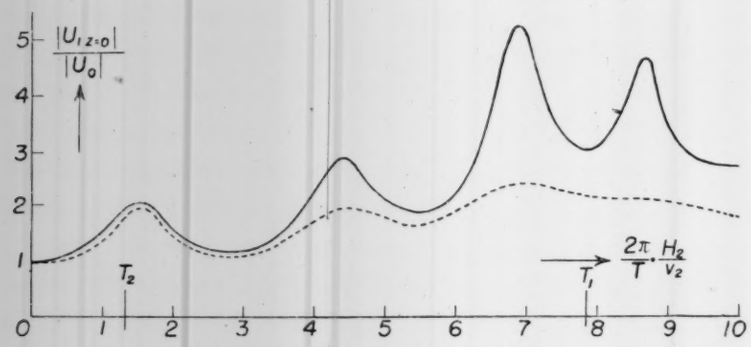

Fig. 2. $H_1/H_2=1/15$.

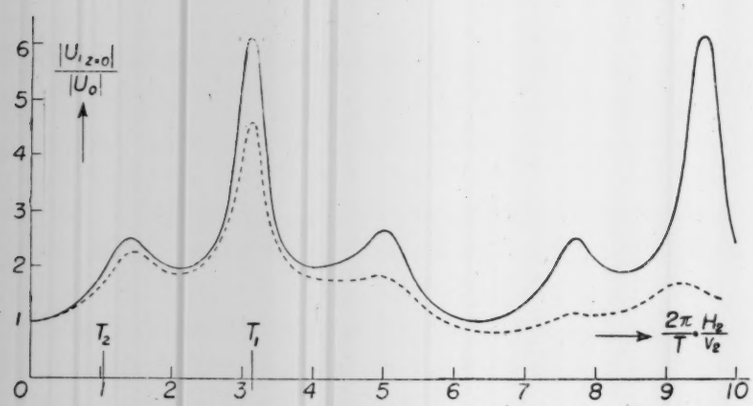

Fig. 3. $H_1/H_2=1/6$.

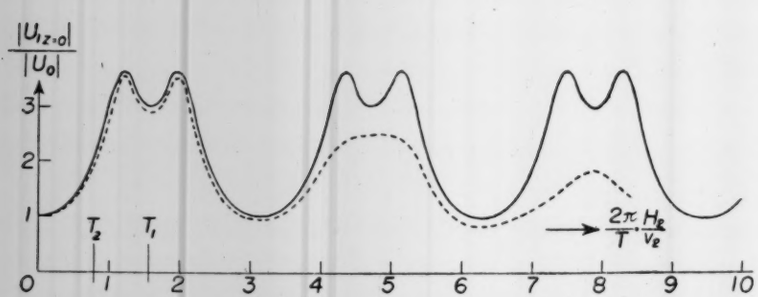

Fig. 4. $H_1/H_2=1/3$.

The results of numerical calculation are shown in Figs. 2–5. The full line represents the case where damping is zero. In these figures the strips perpendicular to abscissa correspond to the natural period of the first layer and to the natural period of the strata between ground surface and the bottom of the second layer, Naturally, these strips in this case do not always mean the maxima of amplitude, because there are two reflecting surface of waves in the ground.

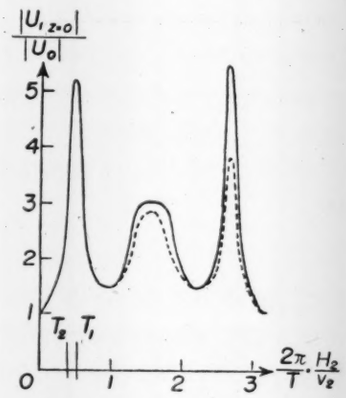

Fig. 5. $H_1/H_2=1$.

From these figures it can be seen that the amplitude becomes maximum about the natural period of the first layer, that is about $T_1=4H_1/V_1$, while the amplitude is not so large about the natural period of the strata between the bottom of the second layer and ground surface, that is about $T_2=4(H_1/V_1+H_2/V_2)$.

But there is damping and the first layer is rather thin, the amplitude, influenced by damping, cannot become so large even about the period which synchronizes in the first layer. In other words, when there is a very soft layer near ground surface, the amplitude at the surface, in general, becomes large, but if the layer is very thin, the effect of this layer, considered as an actual problem, will be rather small.

The facts mentioned above are the results of the study concerning the amplitude at ground surface with the assumption that the amplitudes of incident wave of earthquake are equal regardless of period. If the law of equipartition of energy holds for incident wave, i. e. if the amplitude of incident wave is proportional to the period, the ratio between the amplitude at ground surface and that of incident wave regarding any period is not different from the ratio in the above-mentioned case of equal amplitude. But as a matter of course it does not mean that the amplitudes at ground surface with regard to respective periods are equal to those of the above-mentioned case regarding the corresponding periods. In this case, comparing the amplitude at ground surface of the wave which synchronizes between the surface and the bottom of the second layer with that of the one synchronizing in the first layer, the former is found to be larger than the latter.

3. Application to the actual ground

Table I shows the results of the ground survey operated by S. Omote

and others[13] by means of the seismic prospecting at Sumida Park, Taito-ku, Tokyo.

Table I.

Thickness (m)		Velocity of *P*-waves (m/sec)		
1st layer	2nd layer	1st layer	2nd layer	3rd layer
10	40	750	1100	1800

Suppose density, coefficient of solid viscosity and velocity of *S*-wave as follows: (1) the density of every layer is definite, (2) regarding the coefficient of solid viscosity $\xi/\mu v$ is taken for $5\times10^{-8}C.G.S.$ (3) the velocity of *S*-waves in the first layer: the velocity of *P*-waves in the first layer $=1:5$, in the second layer $=1:3$, and in the third layer $=1:2$. Using these values for equations (1)−(3), we have the results illustrated

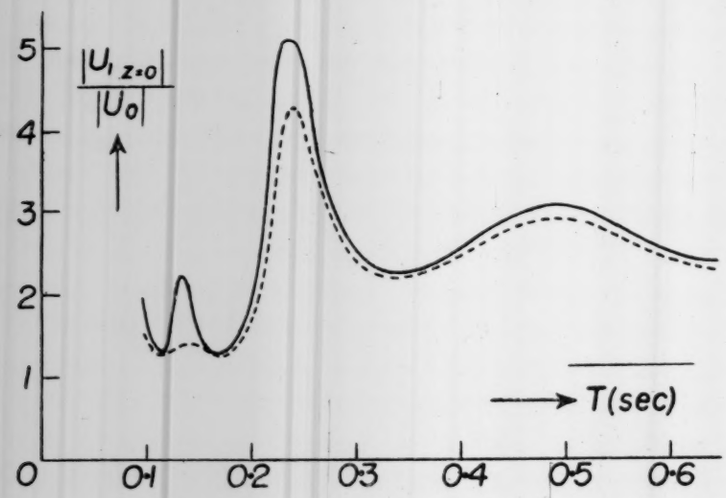

Fig. 6. Mathematical result using the values at Sumida Park.

in Fig. 6 after a numerical calculation. Then from the observation of ground noise we made at midnight in the same place we have the frequency of the number of wave concerning period as illustrated in Fig. 7.

In comparing Fig. 6 with Fig. 7, it is found that the amplitude obtained from the calculation is maximum and the frequency of ground noise is

13) *Monthly Colloq. Earthq. Res. Inst.*, Sept. 16, 1952.

most predominant at about 0.25 sec, the period synchronizing in the first layer. Also, it can be seen that there are peaks of frequency in ground noise at other periods which correspond to maxima of amplitude obtained from calculation.

In other words, it is acknowledged as to the ground noise that the wave which corresponds to about the period synchronizing with the layer appears more frequently. Besides, the amplitude grows greater in case the period of the wave synchronizes with the layer, according as the frequency of the wave in ground noise becomes greater.

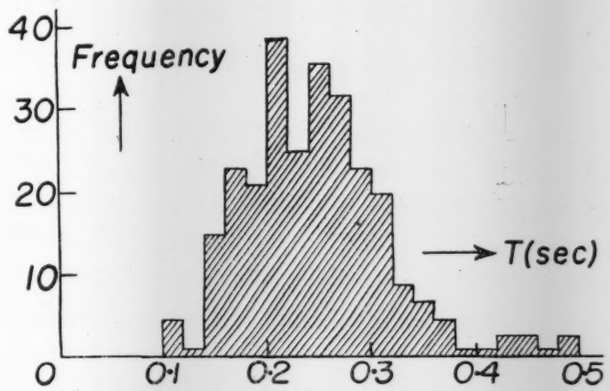

Fig. 7. Period frequency of ground noise at Sumida Park.

4. Conclusion

We studied the vibration of ground surface which consists of two layers in the case when earthquake waves come from right below, taking the solid viscosity into consideration, and revealed the followings. The amplitude at ground surface in general becomes maximum when the waves of the period synchronize with the first layer. But if the first layer is too thin to give effects, such a case will be exceptional.

We are expecting that a correlation exists between the results of mathematical researches concerning the relation of the amplitude at ground surface to the period and the observational results regarding the relation of the frequency of the number of wave to the period of ground noise. This problem will be the subject of future research.

In conclusion, my cordial thanks are due to Mr. T. Tanaka who operated the observation of ground noise, and to Miss S. Yoshizawa who assisted me in preparing this paper.

19. 地震動振幅と地表層の性質との関係 (第2報)

地震研究所 金 井 清

地表附近の構造は多くの場合に数層からなっている．筆者は，地表近くに少くとも 2 層ある場合の地震動の性質をしらべておく必要を感じ，前論文の数理的研究では，固体粘性を考慮に入れた解式を求めておいた．

本論文では，前論文の解式に，実際問題に近い数値を入れた計算結果を報告する．

一般に地表の振幅は第 1 層に同期する周期の波が来たときに最も大きくなる．しかし，第1層が極端に薄い場合には，固体粘性の作用をうけて，この層の影響は余りあらわれない．

地表面の振幅と周期との関係についての数理的研究結果と，自然微動の観測から求めた周期頻度との間には，相関性がありそうである．この問題については，今後研究を進めるつもりである．

20. *Observational Study of Earthquake Motion in the Depth of the Ground. IV. (Relation between the Amplitude at Ground Surface and the Period.)*

By Kiyoshi KANAI, Kaio OSADA and Sizuyo YOSHIZAWA,

Earthquake Research Institute.

(Read Apr. 21, 1953; June 16, 1953.—Received June 20, 1953.)

1. Introduction.

Since the problem of comparing the earthquake motions in the depth with the motions on the surface of ground has attracted the attention of many researchers, many mathematical studies[1] as well as observational ones[2] have been made till now.

Recently this problem has been given so much importance even in the fields of architecture and civil engineering, that the ground survey is under way at various places in Japan.

This paper, in comparing the earthquake-motions in the depth with the motions at two points on the ground which are of different ground property and very adjacent to each other, concerns the vibration at surface layer.

2. Observational results.

Observations were made at the following three places: 300 m in depth under the ground of Hitachi Mine (paleozoic system) in Ibaraki Prefecture; the ground surface of the same mine; Hitachi First High School (on alluvium) about 6 km east-south of Hitachi Mine.

These places and the epicentres treated in this paper are shown in Fig. 1. The representative seismograms of the earthquakes used in this investigation are illustrated in Figs. 2–5. And Table I shows the maxi-

1) K. SEZAWA, *Bull. Earthq. Res. Inst.*, **8** (1930), 1;
R. TAKAHASI and K. HIRANO, *Bull. Earthq. Res. Inst.*, **19** (1941), 534;
K. KANAI, *Bull. Earthq. Res. Inst.*, **28** (1950), 31; **30** (1952), 31.

2) N. NASU, *Bull. Earthq. Res. Inst.*, **9** (1931), 454;
U. INOUYE, *Bull. Earthq. Res. Inst.*, **12** (1934), 712;
T. SAITA and M. SUZUKI, *Bull. Earthq. Res. Inst.*, **12** (1934), 517;
K. KANAI and T. TANAKA, *Bull. Earthq. Res. Inst.*, **29** (1951), 107.

mum amplitude of *S*-waves and the average period of those waves of 14 earthquakes treated in this paper. This average period was struck with 10–20 waves in the vicinity of the maximum amplitude (the waves within the range, containing the wave of maximum amplitude, limited by the waves of a half amplitude of the maximum). The amplitude shown in Table I is the average of 3 waves in the vicinity of the maximum.

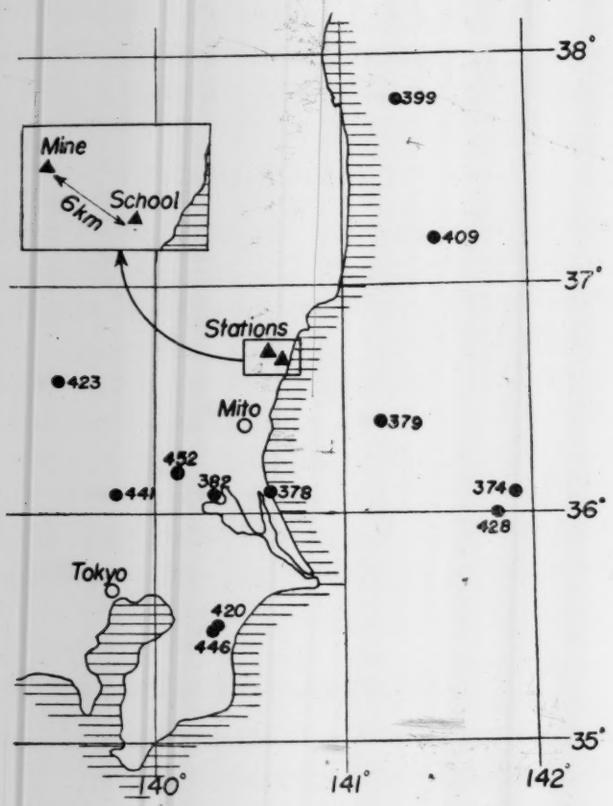

Fig. 1.

From Table I, we get the ratios of the amplitudes at the surfaces of paleozoic system (Mine) and alluvium (School) to the amplitude at the point of 300 m underground. The relation between the ratios thus obtained and the period of earthquake-motions at 300 m depth is represented in Table II and Figs. 6 and 7.

Then, from the seismograms of the surfaces of paleozoic system (Mine) and alluvium (School), the frequency of the number of waves concerned with the period of earthquake-motions is plotted in Figs. 8–11.

Table I.

No.	Date	Hypocenter			Average Period (sec)			Amplitude (μ)		
		φ	λ	H (km)	300 m Depth	Surface		300 m Depth	Surface	
						Mine	School		Mine	School
374	1952 XI 16	36.1	141.9	40	0.68	0.38	0.38	10	17	53
378	1952 XI 18	36.1	140.6	60	0.29	0.15	0.31	4.4	16	16
379	1952 XI 19	36.4	141.2	40	0.25	0.12	0.19	2.2	10	12
382	1952 XI 19	36.1	140.3	40	0.37	0.15	0.24	5.0	10	15
390	1952 XI 22	31.0	137.0	300	0.29	0.25	0.32	2.9	7.5	13
399	1952 XI 27	37.8	141.3	60	0.30	0.12	0.17	1.9	4.6	7.4
409	1952 XII 11	37.2	141.5	30	0.22	0.14	0.21	4.5	15	40
414	1952 XII 16	36.1	139.9	40	0.13	0.10	0.16	1.0	6.0	3.4
420	1952 XII 25	35.5	140.3	50	0.30	0.21	0.24	4.0	12	18
423	1953 I 12	36.6	139.5	10	0.21	0.13	0.24	1.2	4.7	10
428	1953 I 14	36.0	141.8	60	0.41	0.31	0.48	1.7	27	70
441	1953 I 26	36.1	139.8	40	0.28	0.14	0.21	6.5	16	50
446	1953 II 3	35.5	140.3	50	0.26	0.19	0.28	8.5	19	70
452	1953 II 14	36.2	140.1	50	0.22	0.11	0.24	2.5	6.0	11

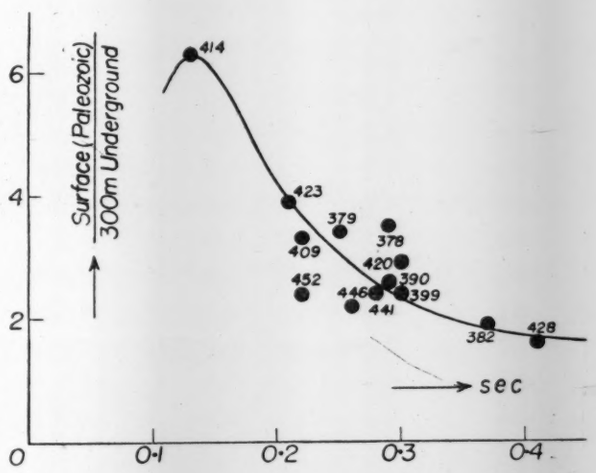

Fig. 6. Relation between the amplitude ratio of Mine to 300 m depth and the period at 300 m depth.

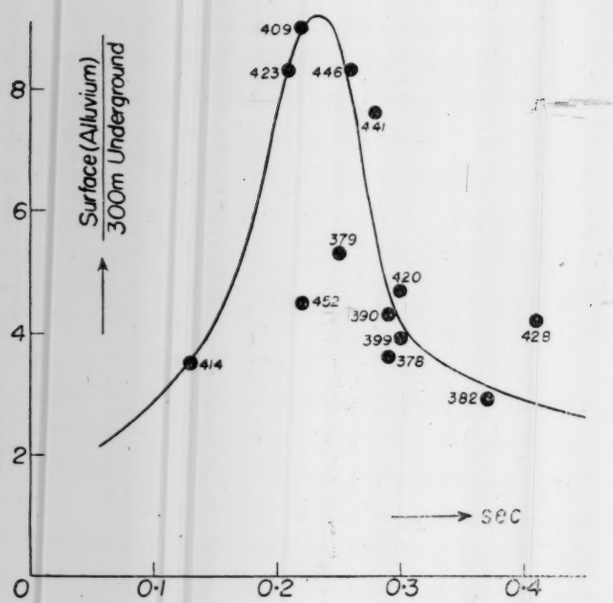

Fig. 7. Relation between the amplitude ratio of School to 300 m depth and the period at 300 m depth.

Table II.

No.	Average period at 300 m depth (sec)	Amplitude ratio	
		Mine/300 m	School/300 m
374	0.68	1.7	5.3
378	0.29	3.5	3.6
379	0.25	3.4	5.3
382	0.37	1.9	2.9
390	0.29	2.6	4.3
399	0.30	2.4	3.9
409	0.22	3.3	9.0
414	0.13	6.3	3.5
420	0.30	2.9	4.7
423	0.21	3.9	8.3
428	0.41	1.6	4.2
441	0.28	2.4	7.6
446	0.26	2.2	8.3
452	0.22	2.4	4.5

Figs. 6, 7 and Figs. 8–11 make it clear that the amplitude at ground surface becomes maximum when the period of earthquake-motions in the depth of 300 m coincides with the period which corresponds to the peak of period frequency. Supposing that the period corresponding to the peak

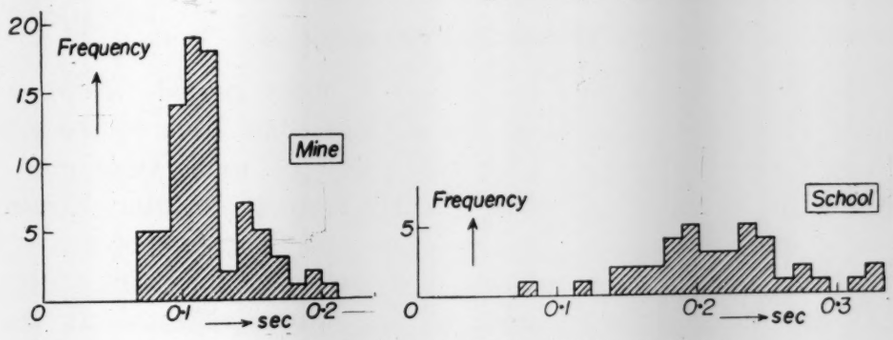

Fig. 8. Period frequency of No. 378 earthquake.

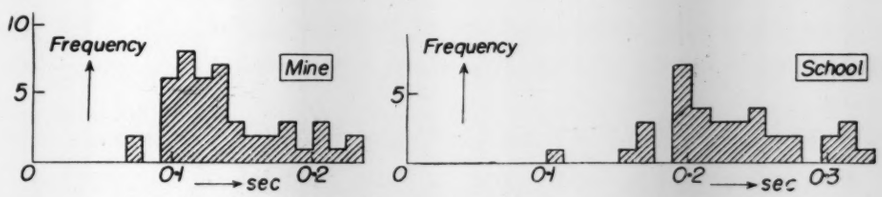

Fig. 9. Period frequency of No. 382 earthquake.

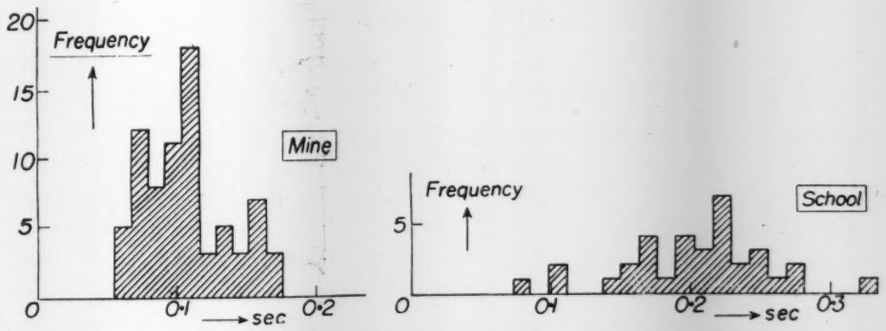

Fig. 10. Period frequency of No. 409 earthquake.

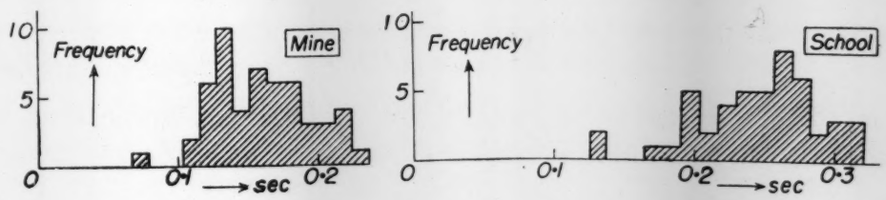

Fig. 11. Period frequency of No. 446 earthquake.

frequency of the period at the ground surface indicates the natural period of the ground, the relation between the amplitude at the surface and the period of earthquake-motions shown in Figs. 6 and 7 coincides very well with the results of mathematical study.

3. Theoretical examination.

As this paper treats only the waves of short period, about 0.1–0.3 sec, waves which are reflected at the surface come back to the point of 300 m deep under the ground with the delay of more than one period compared with waves which come directly from the origin. Consequently it can be considered that the amplitude and the period of waves in the vicinity of the maximum amplitude of *S*-waves at the point of 300 m in the depth are under little influence of the waves reflected at the free surface.

In other words, even if the waves in the depth of 300 m are the ones incident upon the under surface of surface layer, the error may be small as far as it concerns few waves in the vicinity of the maximum of *S*-waves.

When the periodical waves continue infinitely, advance vertically upward and synchronize with the natural period of the surface layer, the ratio between the amplitude at the free surface and that of primary waves, that is A_s/A_0, will be

$$A_s/A_0=2V_2\rho_2/V_1\rho_1\,, \qquad (1)$$

in which V_1, ρ_1 and V_2, ρ_2 represent the velocities and the densities of surface layer and subjacent medium respectively. In that case the damping due to the solid viscosity of media is neglected.

From the maximum value in Figs. 6, 7 and equation (1), we obtain the value of $V_2\rho_2/V_1\rho_1$. At Mine $V_2\rho_2/V_1\rho_1=3$, while at School $V_2\rho_2/V_1\rho_1=4.5$.

Then, in case the waves of finite train which synchronize with the natural period of the surface layer come, the ratio between the maximum amplitude at the free surface and amplitude of incident waves, A_s/A_0, becomes

$$\frac{A_s}{A_0}=\frac{2}{\alpha}\left\{1-\left(\frac{1-\alpha}{1+\alpha}\right)^n\right\}^{3)}. \qquad (2)$$

Where $\alpha=V_1\rho_1/V_2\rho_2$ and n represents the number of successive waves (See Fig. 12). From equation (2) the relation between the amplitude

3) K. SEZAWA, *loc. cit.*, 1).

ratio and wave number in the case of $\alpha=1/3$ (Mine) and $\alpha=1/4.5$ (School) is plotted in Fig. 12.

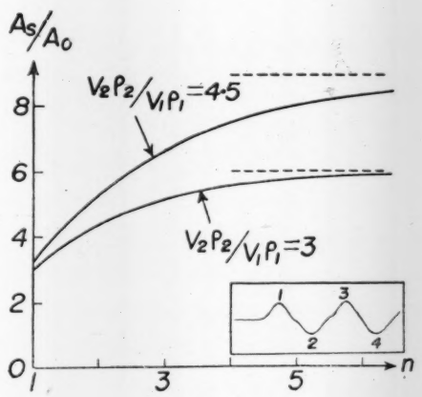

Fig. 12.

Fig. 12 makes it known that, in the case of observation at such places as treated here, if 3 or 5 waves of which the periods are nearly equal to the natural period of the surface layer appear in succession, the amplitude at free surface may become approximate to the amplitude in the case of perfect synchronization.

From equation (2) and Fig. 12, it is also seen that with the surface layer of soft substance the amplitude at the free surface becomes very large if there come such a seismic-waves as will cause synchronization in the surface layer. But even if the period of primary waves is very approximate to the natural period of surface layer, the amplitude at the free surface may be almost constant, regardless of hardness of the substance of layer, unless the number of primary waves appearing in succession is satisfactory.

In brief, such a property is the same with the forced vibration of pendulum in consideration of damping.

4. Conclusion.

The results of the comparative observations made at Hitachi Mine, both on the surface and in the depth of 300 m under the ground, and at Hitachi First High School (on alluvium) about 6 km from Hitachi Mine, proved the followings more evidently.

(1) In case where the period of the earthquake-motions in the depth of 300 m coincides with the period which corresponds to the peak of period frequency at the surface, the amplitude at the ground surface becomes maximum. Suppose such period as corresponds to the peak of period frequency to be the natural period of surface layer. Then it is possible to admit the above-mentioned fact to be a synchronization (resonance) of surface layer.

(2) If the surface layer is of soft substance, the amplitude at the surface becomes very large if there come seismic-waves which may cause a synchronization (resonance) at surface layer. But if the waves which appear in succession are few, the difference of ground property have

little influence upon the amplitude at the surface, even if the period of primary waves may be approximate to the natural period of surface layer.

In conclusion, we wish to express our hearty thanks to the members of Motoyama Office, Hitachi Mine and the authorities of Hitachi First High School for their contributions to this investigation. We also wish to express our thanks to Messrs. T. Tanaka and T. Suzuki who took part in the observation.

---

20. 地下深所における地震動の観測結果 (第4報)

地震研究所 { 金井 清 / 長田甲斐男 / 吉沢 静代 }

地盤の差違によって，地震動の性質が異る問題は，古くから多くの地震学者の注意をひき，数多くの験震学的並びに数理的な研究が行われて来た．

この問題は，耐震構造上大切な事柄なので，近年になって，日本の各都市でいろんな方法による地盤調査が行われようとしている．

この研究は，日立鉱山の地下 300 m と地表面及び日立鉱山から約 6 km 離れた沖積層上とで地震動の比較観測を行い，地表附近の振動的性質の究明を試みたものである．

研究の結果，地下 300m の地震動の周期が，地表面の地震動の周期瀕度の山にあたる周期に一致する場合に，地表面の振幅が最も大きくなる．しかして，S 波の最大振幅附近では，地下 300m の地震動は，一応，地表層と下層との境界面に入射する波と考えてよさそうである．従って，周期瀕度の山にあたる周期を，表面層の固有周期と考えれば，地表面の振幅と周期との関係は表面層の同期現象に関係するものと解釈される．

次に，表面層に同期現象を起すような地震波が来た場合には，表面層の物質が軟い程，地表面の振幅の大きさは増す．しかし，たとえ入射波の周期が表面層の固有周期に近いものであっても，入射波の連続する波数がごく少い場合には，地盤の硬軟の差違は地表面の振巾にあまり影響を与えないことも明かになった．

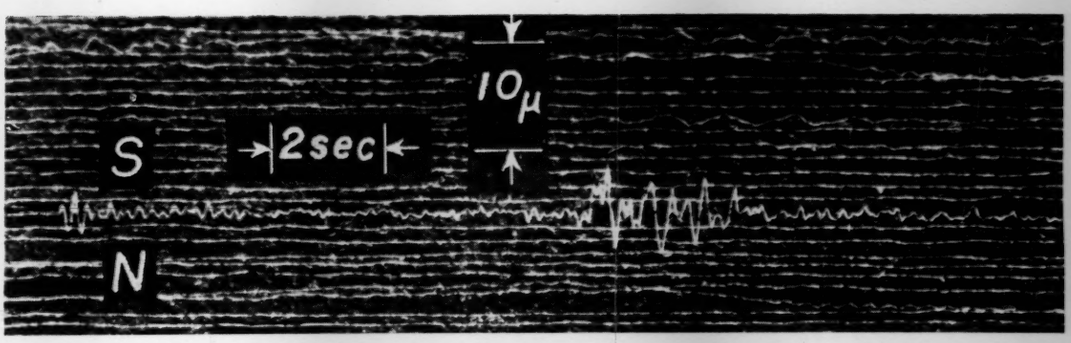

Fig. 2-a. Earthquake No. 378. 300 m depth.

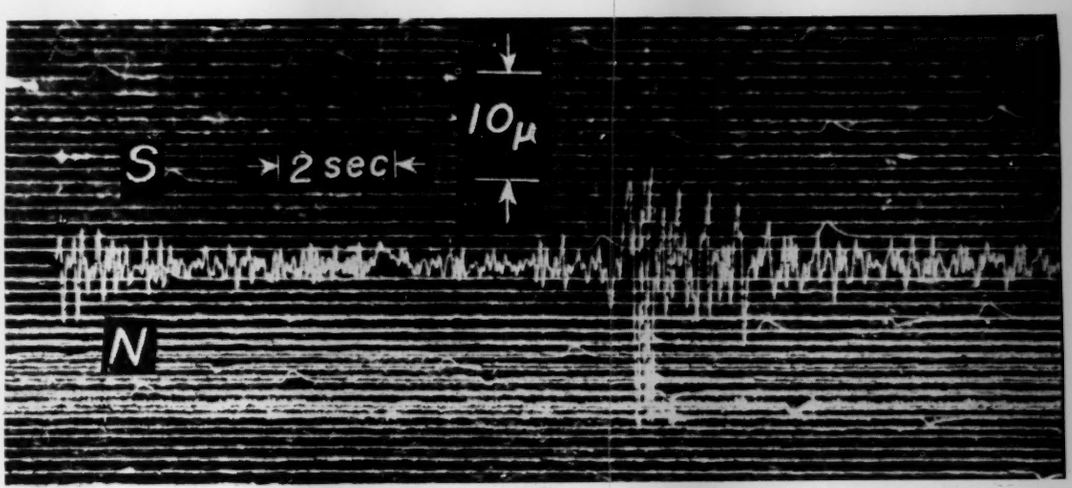

Fig. 2-b. Earthquake No. 378. Mine.

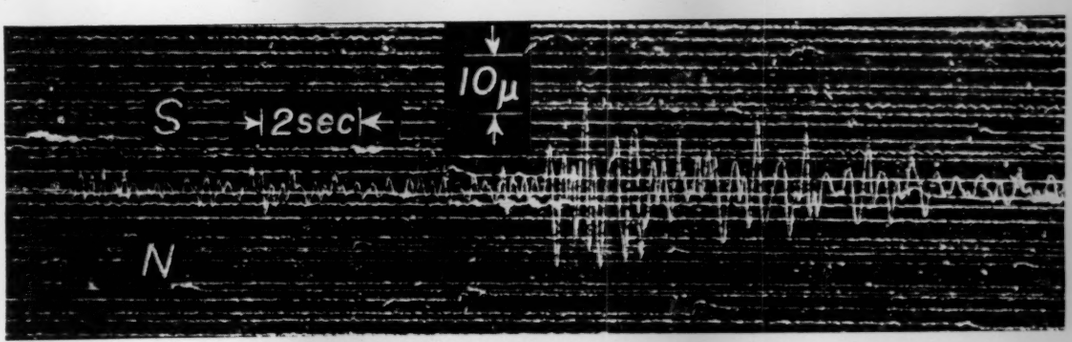

Fig. 2-c. Earthquake No. 378. School.

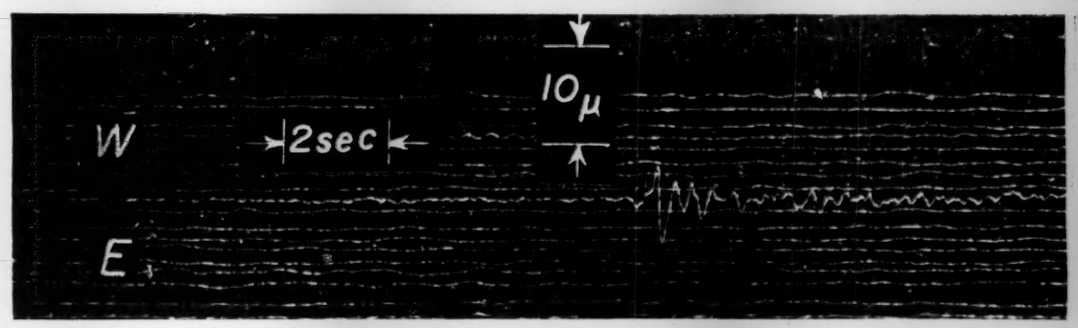

Fig. 3-a. Earthquake No. 382. 200 m depth.

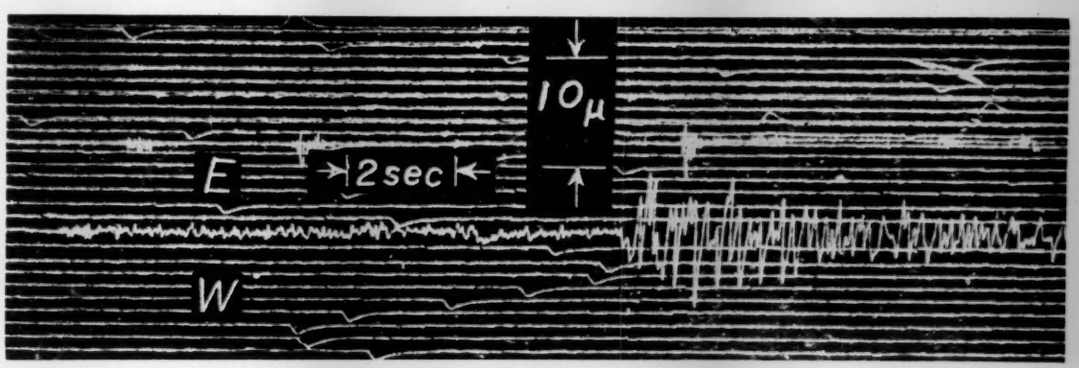

Fig. 3-b. Earthquake No. 382. Mine.

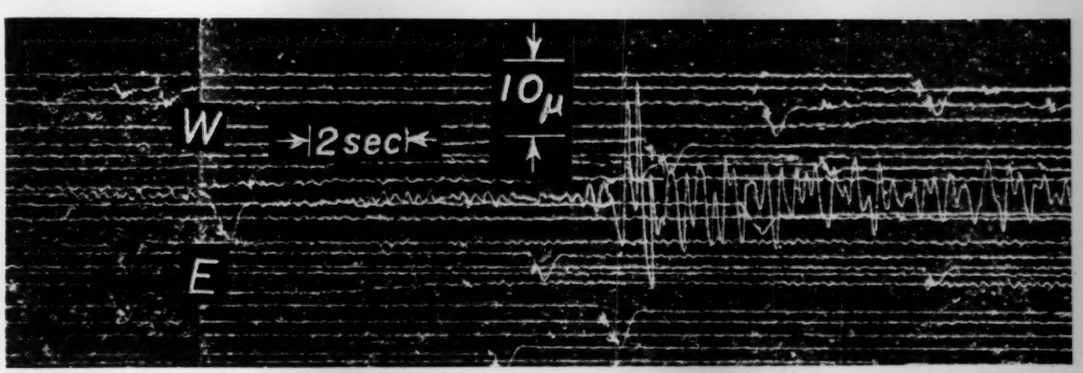

Fig. 3-c. Earthquake No. 382. School.

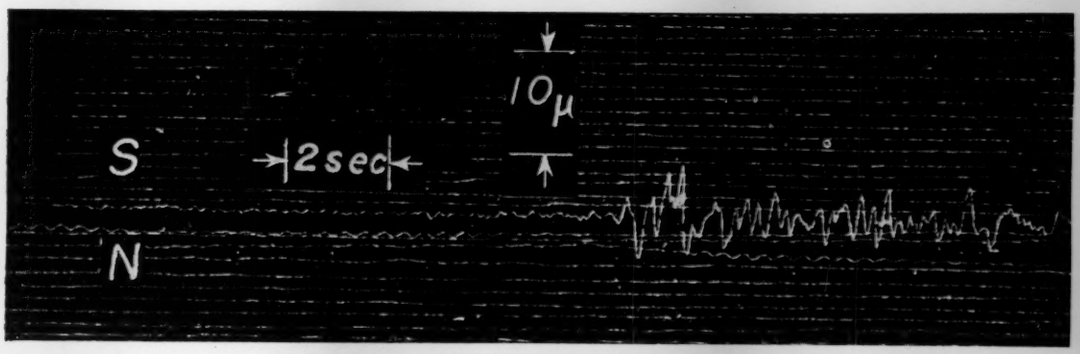

Fig. 4-a. Earthquake No. 409. 300 m. depth.

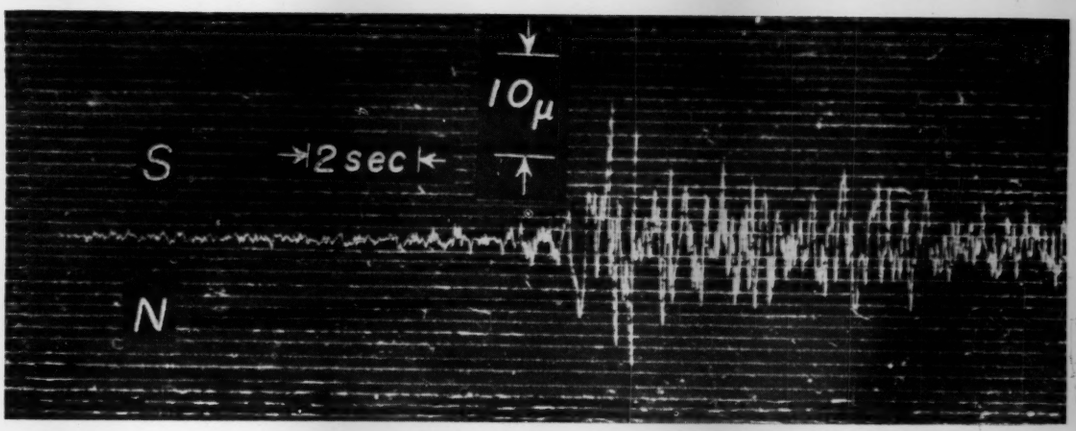

Fig. 4-b. Earthquake No. 409. Mine.

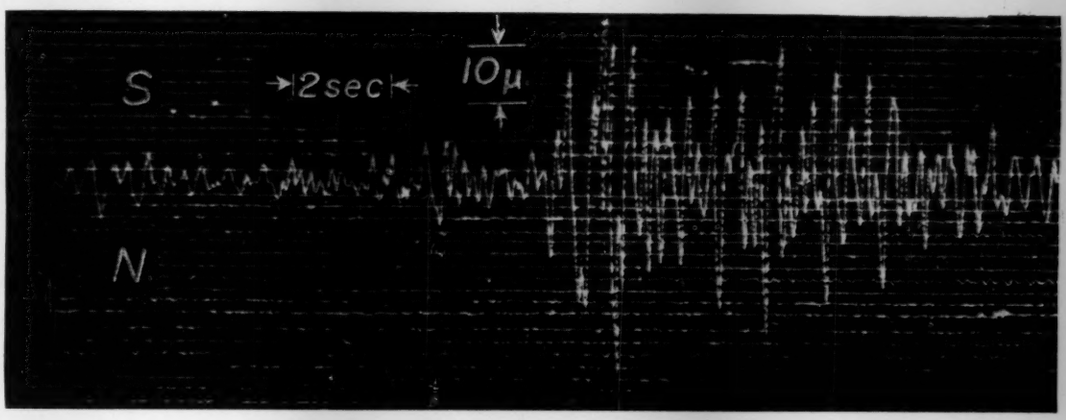

Fig. 4-c. Earthquake No. 409. School.

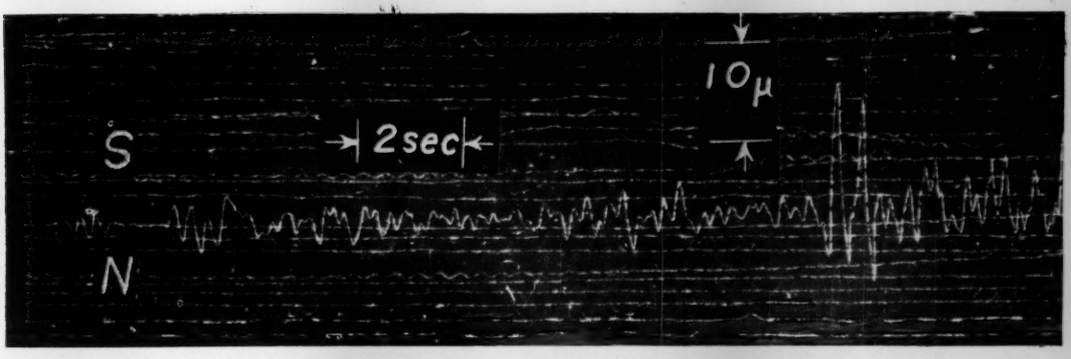

Fig. 5-a. Earthquake No. 446. 300 m depth.

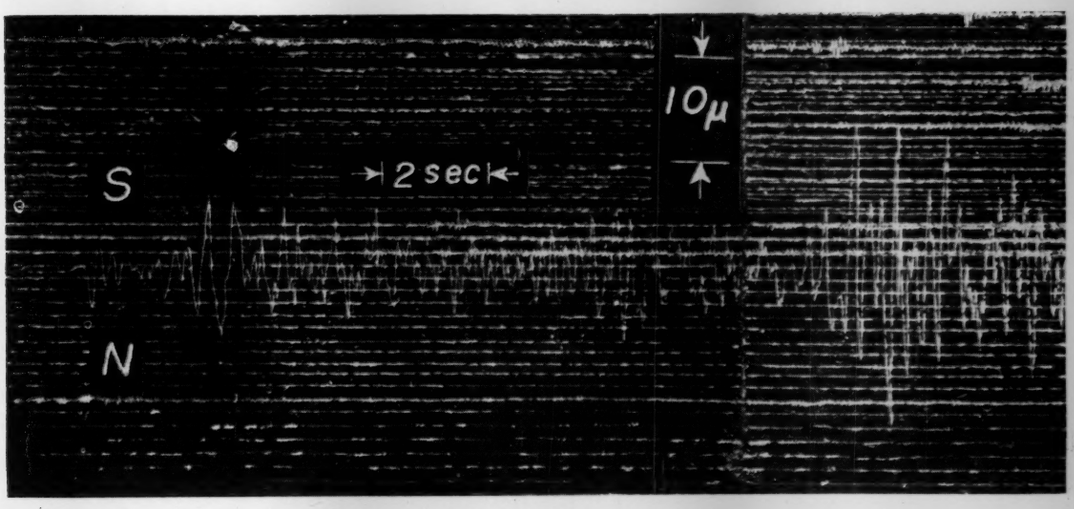

Fig. 5-b. Earthquake No. 446. Mine.

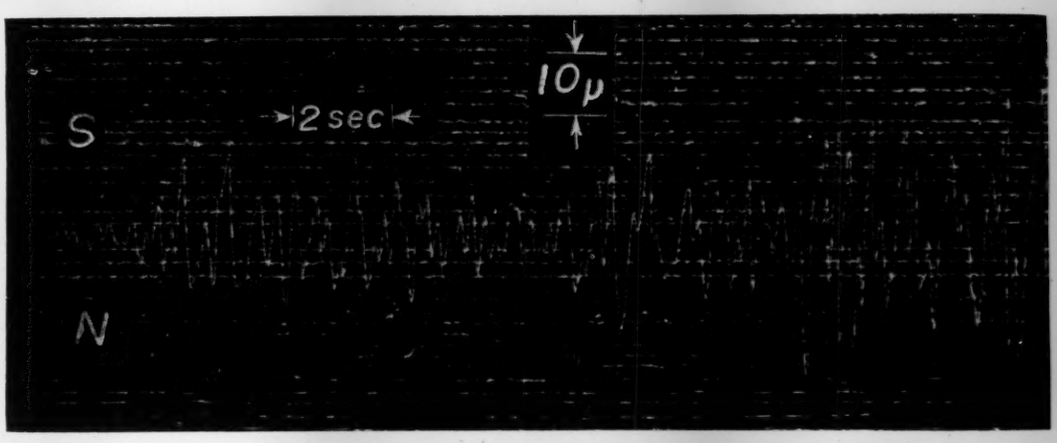

Fig. 5-c. Earthquake No. 446. School.

21. *Experimental Studies on the Mechanism of Generation of Elastic Waves III.*

By Keichi KASAHARA,

Earthquake Research Institute.

(Read March 17, 1953.—Received June 23, 1953.)

1. Introduction.

In the previous papers[1], we found peculiar disturbances on the surface of a semi-infinite elastic body; that is, when the surface is subjected to an impulsive vertical force, characteristic deformation occurs in the vicinity of the origin, and then propagates away forming finally the complete type of the free Rayleigh wave. It is considered to be one of the fundamental projects in the studies of elastic waves to explain how surface waves can be generated and propagated. Of course, efforts made by Rayleigh, Lamb, Sezawa, Nakano and others[2], have enriched our knowledge on the characters of surface waves, but these efforts usually made on the matter observed at distant points from the origin, and concerning the problem how the energy of shocks can be transformed to that of surface waves, we are not yet given enough explanation by physicists either theoretically or experimentally.

It is not easy to describe the processes of generation of surface waves in different case *en bloc*, but from the results of previous experiments, we may conceive in imagination three stages in the generation of surface waves, that is,

1) Initial deformation of the surface in the vicinity of the origin.
2) Propagation of the strain energy to more distant places. Initial deformation of the medium, whose characters are improper to free surface waves, changes its form to more proper one.
3) Deformation, which arranged the complete form of surface waves in this way, propagates with their own velocities.

The main object of the present paper is to make some considerations on the second stage, which seems to involve the most essential mechanism. As the first step, exciting the origin on the surface in different mode,

1) K. KASAHARA, *Bull. Earthq. Res. Inst.*, **30** (1952), 259-268: *ibid*, **31** (1953), 71-79.
2) See for example, Y. SATÔ, *Kagaku*, **19** (1949), 311-319 (in Japanese).

formation of free surface waves are investigated experimentally; and then some mathematical considerations have been made on the strain energy accompanying the surface waves.

Throughout these studies, all the phenomena have been regarded as two-dimensional under the consideration that it will bring into the results no essential discrepancies.

2. Experiments.

A block of agar-agar is used as the elastic medium, whose dimensions and elastic characters are listed in Table I. To pick-up the elastic disturbances on the surface, a variable capacity type transducer is employed and an electromagnetic type oscillograph is used in recording. Details of these instruments were reported in the previous paper[3].

Table I.

Dimensions of the medium	length 70 cm, width 35 cm, depth 15 cm.	
Elastic constants of the medium	Young's modulus	9.11×10^4 c.g.s.
	Rigidity	3.24×10^4 c.g.s.
	Poisson's ratio	0.41
	Density	1.0

To cause elastic disturbances in the medium, a special wave-generater is constructed. As shown in Fig. 1 and 2, a pair of eccentric wheels W_1 and W_2 are mounted on the same shaft S, which is driven by a synchronous motor M transiently or continuously. To W_1 and W_2 are connected rods R_1 and R_2, as well as strings S_1 and S_2, respectively, which transmit the back and forth motions of W_1 and W_2. A vibrator made of an aluminum bar (20 cm long) lies beneath the surface of the medium, being supported in its neutral position with holders H and rubber packings P. When the elastic properties of S_1, S_2, and P are chosen properly the vibrator can displace in moderate amplitudes proportionally to the motion of R_1 and R_2. As can be seen in Fig. 1, and 3 the vibrator is excited with W_1 and W_2 in two directions (perpendicular to each other) at the same time, and these circumstances allow us to obtain different modes of excitations of the origin by changing the combination of eccentricities and phase angles of two wheels.

3) *loc cit.*

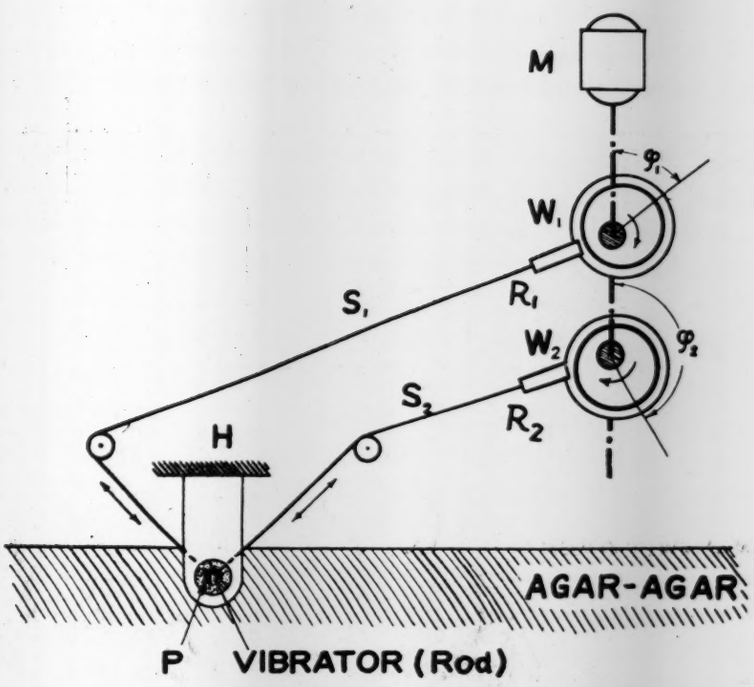

Fig. 1. H: holders: M: synchronous motor; P: rubber packing; R_1, R_2: connecting rods; S_1, S_2: strings; W_1, W_2: eccentric wheels; φ_1, φ_2; phase angles of W_1, W_2, respectively.

In the course of experiments, transient excitations are employed under the consideration that the continuous method will bring into the results undesirable effects of the walls of the medium. Experiments are made employing the phase angle $\varphi_1-\varphi_2$ as the indicator of the mode of excitation, while other conditions including amplitudes of excitation are kept unchanged. As is well known, the condition of particle motions which correspond to the excitation of stationary free surface waves is decided uniquely and we can imagine innumerable sets of conditions which do not satisfy the characters of free surface waves. The phase angle seems most convenient to indicate these differences, because a slight change in the phase angle between two components of excitation will cause easily a remarkable difference in the character

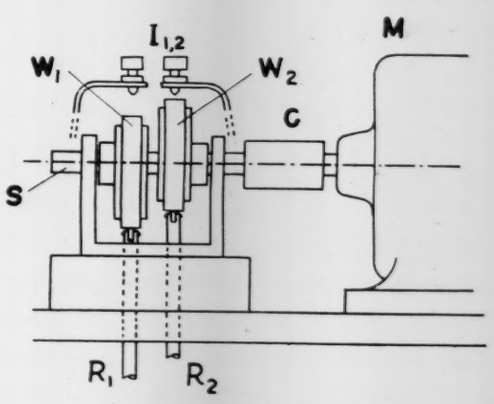

Fig. 2.

of origin. And therefore, we can see the outline of the phenomena in this way, without making other series of experiments changing other factors, such as amplitude ratios, decay of amplitudes with depth *etc.*

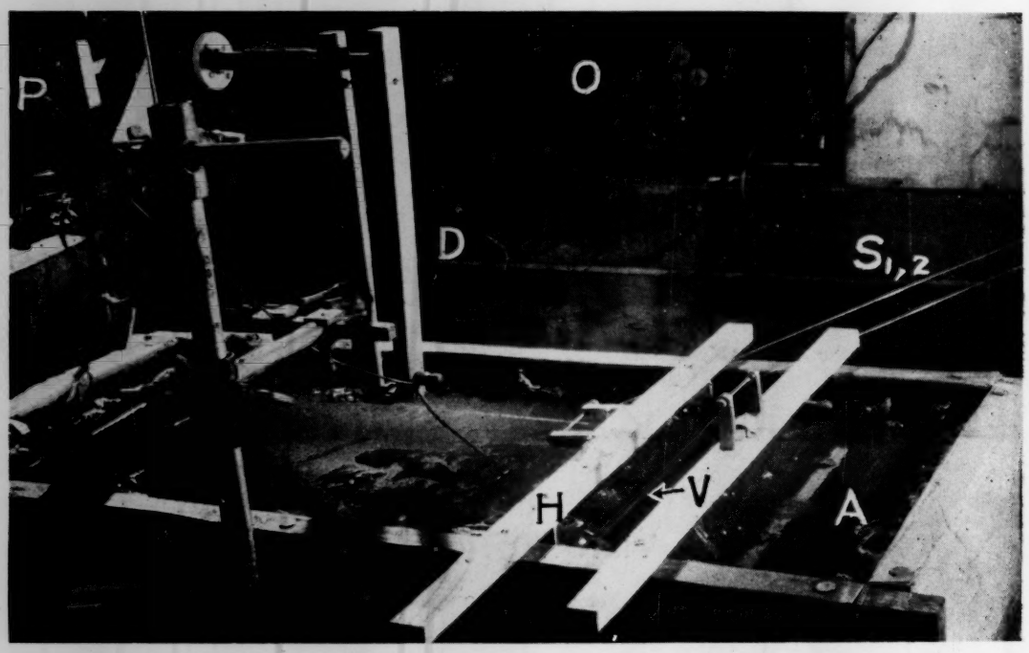

Fig. 3 A: agar-agar; D: detector; H: holder; O: oscillograph; P: Pierce's circuit; $S_{1,2}$: strings; V: vibrator.

Fig. 4 illustrates loci of particle motions observed at different points on the surface. Eccentric wheels are driven suddenly by three or four rotations, and taking the beginning of drive as the origin of time, we traced particle motions about x/V_R time after, where V_R and x represents the velocity of the surface wave and the distance of the point from the origin, respectively. The motion thus obtained coincides actually with the first main shock.

Four values of the phase angle are picked out, that is,

a) 0, b) $\pi/2$, c) π, d) $3\pi/2$.

Actual motion of the origin corresponding to these phase angles are drawn in Fig. 4 in the column of origin. As can be seen in the figure, case b) is the most similar to the particle motion under the free surface wave, while case d) is the most different one among them. Cases a) and c) are between both extreme cases.

At those points distant enough from the origin, particles on the surface move according to the conditions of the free surface wave in any

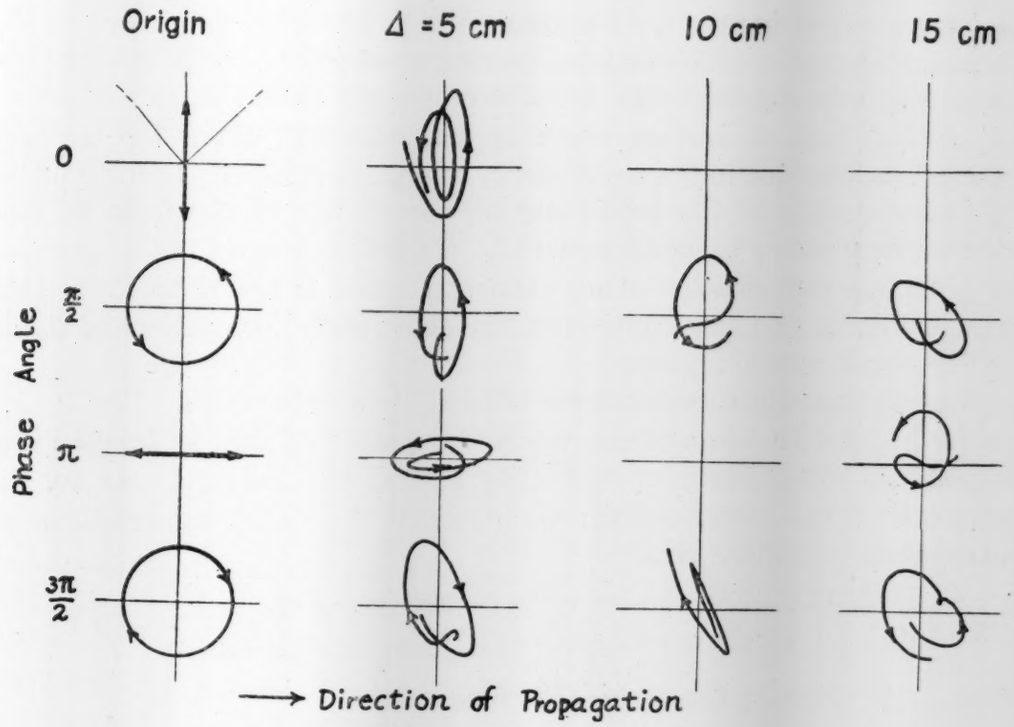

Fig. 4 Loci of particle motions, observed.

case of the phase angle. Loci at points more than 15 cm distant are considered to belong to this group. On the other hand, at nearer points about several centimetres distant, particle motions are affected severely by the condition of excitation, that is by the phase angle. When the origin is excited in the similar mode of the surface wave as in the case of b), particles on the surface show normal motions as stationary surface waves, while in the case of d), the abnormal motion of the origin affects the particle motions remarkably. In other two cases, the phenomena show intermediate characters.

Change of forms of loci in the case of d) is considered to contain valuable suggestions on the present problem, but further considerations will have to be given in the future, when the stress distribution in the medium becomes measurable with more improved instruments.

3. Mathematical Considerations.

Corresponding to the present experiment, simple mathematical considerations will be made in the following, that is, strain energies accompanying the free surface wave and other modes of surface deformations

will be compared together. Needless to say, the Rayleigh wave is the unique surface wave which satisfies boundary conditions of the free surface of a semi-infinite elastic body, and therefore, we cannot expect in actual case another kind of surface wave to be travelling along the surface. However, as clarified in the experiment, complicated forms of deformations exist in the vicinity of the origin and so, the change of the form to that of the surface wave becomes essential. To find an answer to the question why a surface deformation of an abnormal mode is transformed to that corresponding to the Rayleigh wave, the above-stated comparison of strain energies seems worth trying.

We will consider a semi-infinite body of two dimensions. The x axis is taken parallel to the surface, while the positive z axis is directed into the medium. The origin of the axes lies on the surface. As to the expressions of the deformations we consider the following relations of displacements u and v, viz.,

$$\left.\begin{aligned} u &= K\{(2K^2-k^2)e^{-\alpha z}-2\alpha\beta e^{-\beta z}\}\ C_0 \sin(pt-Kx), \\ v &= -\alpha\{(2K^2-k^2)e^{-\alpha z}-2K^2 e^{-\beta z}\}\ C_0 \sin(pt-Kx-\theta), \end{aligned}\right\} \qquad (1)$$

where, $\alpha=\sqrt{(K^2-h^2)}$, $\beta=\sqrt{(K^2-k^2)}$,

$$h^2=\frac{p^2\rho}{\mu}, \qquad k^2=\frac{p^2\rho}{\lambda+2\mu},$$

and K is the real root of the equation, $(2q^2-k^2)^2-4q^2\alpha\beta=0$.

As (1) coincides with the expressions of the free surface wave in the case of $\theta=\frac{\pi}{2}$, (Fig. 5 and 6) the equations are adoptable for the present purpose, when we consider θ as a variable.

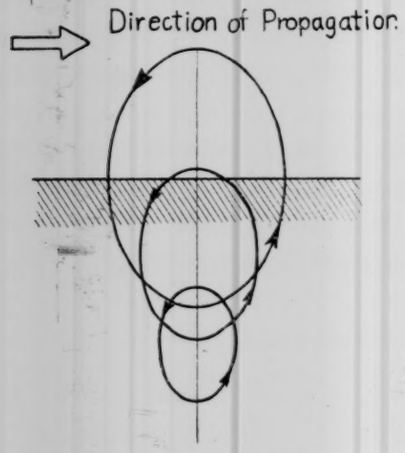

Fig. 5

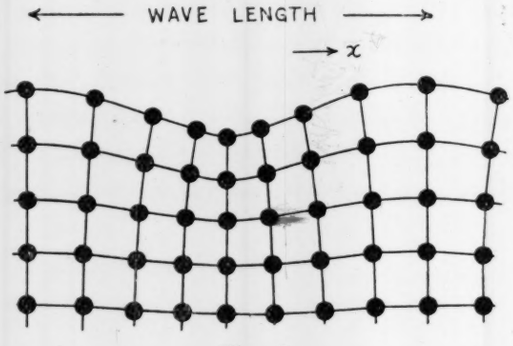

Fig. 6

The strain energy of a unit volume of a deformed elastic body is expressed, in general, as follows,

$$V_0=\frac{1}{2}\lambda e^2+\frac{1}{2}G\left\{\left(\frac{\partial u}{\partial x}\right)^2+\left(\frac{\partial w}{\partial z}\right)^2\right\}+\frac{1}{2}G\left(\frac{\partial u}{\partial z}+\frac{\partial w}{\partial x}\right)^2 \qquad (2)$$

where λ, G, and e represents one of the Lamé's constants, rigidity, and volume dilatation, respectively. Corresponding to the deformation (1), each term of (2) becomes,

$$\left.\begin{aligned}
&\frac{1}{2}\lambda e^2=\frac{1}{2}\lambda\Big[A^2\cos^2(pt-Kx)+2AD\cos(pt-Kx)\\
&\qquad\times\sin(pt-Kx+\theta)+D^2\sin^2(pt-Kx+\theta)\Big],\\
&\frac{1}{2}G\left\{\left(\frac{\partial u}{\partial x}\right)^2+\left(\frac{\partial v}{\partial z}\right)^2\right\}=\frac{1}{2}G\Big[A^2\cos^2(pt-Kx)\\
&\qquad+D^2\sin^2(pt-Kx+\theta)\Big],\\
&\frac{1}{2}G\left\{\frac{\partial u}{\partial z}+\frac{\partial w}{\partial x}\right\}^2=\frac{1}{2}G\Big[C^2\sin^2(pt-Kx)+2BC\sin(pt-Kx)\\
&\qquad\times\cos(pt-Kx+\theta)+B^2\cos^2(pt-Kx+\theta)\Big],
\end{aligned}\right\} \qquad (3)$$

where

$$\left.\begin{aligned}
&\mathrm{A}=-K^2C_0\{(2K^2-k^2)e^{-\alpha z}-2\alpha\beta e^{-\beta z}\},\\
&\mathrm{B}=-K\alpha C_0\{(2K^2-k^2)e^{-\alpha z}-2K^2e^{-\beta z}\},\\
&\mathrm{C}=-K\alpha C_0\{(2K^2-k^2)e^{-\alpha z}-2\beta^2e^{-\beta z}\},\\
&\mathrm{D}=-\alpha C_0\{\alpha(2K^2-k^2)e^{-\alpha z}-2\beta K^2e^{-\beta z}\}.
\end{aligned}\right\} \qquad (4)$$

The total strain energy accompanying the deformation (1) at a given time can be obtained by integrating the sum of the righthand side of (3) from 0 to ∞ with regard to z and from $-\frac{pt}{K}$ to $\frac{2\pi-pt}{K}$ with regard to x, viz.,

$$\left.\begin{aligned}
&\int V_0\,dx\,dz=\frac{\pi}{2}\Big[(\lambda+2G)(A'^2+D'^2)+G(B'^2+C'^2)\\
&\qquad+2(\lambda\cdot A'D'-G\cdot B'C')\sin\theta\Big],
\end{aligned}\right\} \qquad (5)$$

(per every unit wave-length).

where, for brevity,

$$
\left.\begin{aligned}
A' &= -\frac{K^2}{\alpha} C\left\{(2K^2-k^2)-2\alpha^2\right\}, \\
B' &= -\frac{KC}{\beta}\left\{(2K^2-k^2)\beta-2K^2\alpha\right\}, \\
C' &= -KC\{(2K^2-k^2)-2\alpha\beta\}, \\
D' &= -\alpha C\{(2K^2-k^2)-2K^2\}.
\end{aligned}\right\} \qquad (6)
$$

As all quantities in (5) except θ can be regarded as constant in the present case, total strain energy depends only on the third term of the equation. Taking into consideration the relations $K>\alpha>\beta$ and $\lambda \geqq G$, we can see that $\lambda \cdot A'D' - G \cdot B'C'$ in the third term is always positive. (5) depends, therefore, only on the value of $\sin\theta$, and reaches to its minimum value when $\theta = \frac{\pi}{2}$ (Fig. 7). This case coincides with the Rayleigh wave,

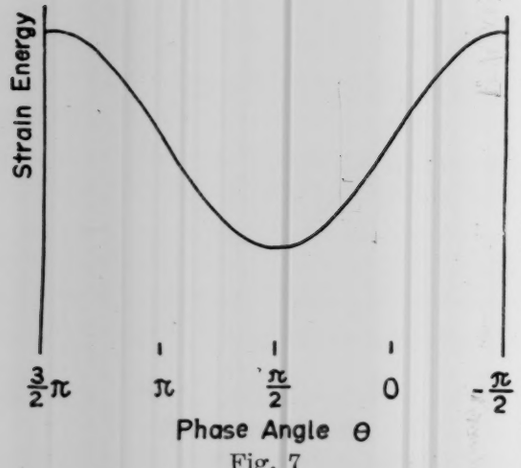

Fig. 7

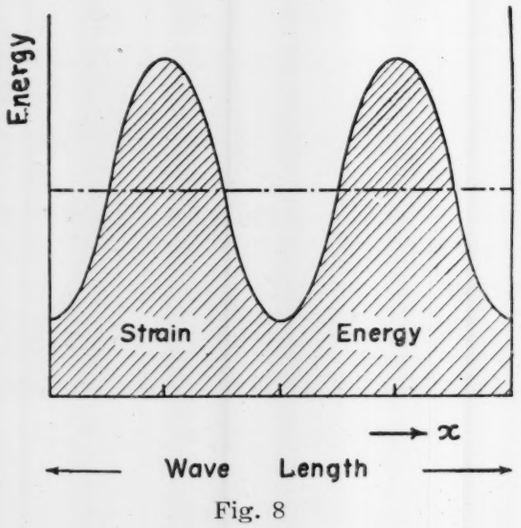

Fig. 8

leading to the conclusion: among the surface deformations of (1), one showing the phase angle equal to that of the Rayleigh wave is accompanied by the minimum strain energy, while the maximum corresponds to the phase angle of $\frac{3\pi}{2}$. Of course, this conclusion is to be expected from the standpoint that the Rayleigh wave is the unique solution that satisfies the condition of the surface free from stresses. However, the discussion here described is not without significance because it make us possible to treat the problem quantitatively.

The strain energy involved in the elementary column of the medium can also be calculated from (3). Fig. 8 is the numerical example for the medium deformed according to the conditions of the free surface wave.

4. Concluding Remarks.

In the present paper we have treated model experiments and some mathematical considerations on the problem how the complete type of the free surface wave can be produced from the initial deformation of the surface. The experiments, carried out by exciting the origin in two directions with constant amplitudes and variable phase angles, showed that even complicated modes of deformations are changeable to normal form of the surface wave and the more proper become the conditions of excitation, the more easily forms the surface wave.

Mathematical considerations made in correspondence to the experiments proved that the total strain energy accompanying the Rayleigh wave is less than that of any other deformation of which phase angle does not satisfy the given condition.

The results discussed in this paper is believed to be suggestive in the problem of generation of the surface wave. However, the present study is not yet complete enough to discuss the matter in more detail, and further discussions will have to be postponed.

Finally, the writer wishes to express his hearty thanks to Prof. Hagiwara, who has shown interest in this series of studies and encouraged him. The writer's thanks are also due to Mr. Saito for his kind assistance in the course of experiments. The present work has been supported by the Grant in Aid for the Miscelleraneous Scientific Researches of the Department of Education.

---

21. 彈性波の発生機構に関する実験 (第3報)

地震研究所 笠 原 慶 一

源点に起された表面変形が遠方へ伝播しながら次第に Rayleigh 波を形づくって行くことは，前からの実験で確かめられている．Rayleigh 波に対応しない変形状態が，正規の表面波に移って行く機構を研究する目的で簡単な実験と考察を試みた．

媒質中の源点を，互に直交する二方向の力で運動を起させる．その振巾を一定に保ったまゝ，両成分の位相関係を変化させ，源点から発射される彈性変形の伝播を考察した．位相角をどんな組合わせにしても十分遠方では完全な表面波が形成されるが位相角が正規 Rayleigh 波に近づく程，表面波の形成は源点近くから認められる．

之に対応する彈性論的考察として Rayleigh 波に相当する変位状況のうちで，水平，垂直両成分の位相差を変数として，全歪エネルギーを計算して見ると，Rayleigh 波の條件が充されるとき，最小値をとり，それと 180° 位相が異なるとき最大値をとる．

---

22. *Examination of the Assumption of the Concentrated Mass in the Vibration of Framed Structure (Rahmen).*

By Kiyoshi KANAI,

Earthquake Research Institute.

(Read June 15, 1943; April 21, 1953.—Received June 20, 1953.)

Since the exact solution for the vibration problem of framed structure (Rahmen) is a very complicated work, we often adopt a simplified method using various assumptions.

In this paper, we studied, for the purpose of deciding the limitation of approximation made under such an assumption, in what cases the value of the natural period of Rahmen obtained from the exact solution is in agreement with the value obtained under the assumption of concentrated mass.

The vibration problem of Rahmen is treated exactly if the equation of motion (1) regarding each member of the structure is solved by giving the boundary conditions met with each structure mode.

$$EI\frac{\partial^4 y}{\partial x^4}+\rho a\frac{\partial^2 y}{\partial t^2}=0. \tag{1}$$

In equation (1), x is coordinate, y deflection, E Young's modulus and I, a and ρ represent moment of inertia of cross-section, sectional area and density respectively.

As to single-storied Rahmen of infinite span in the case of clamped conditions at the floors and the base, viz., the boundary conditions of usual Rahmen, frequency equation becomes as follow:

$$\begin{aligned}&2(\zeta^3\nu)^{1/4}\{(\cos\alpha\,\mathrm{sh}\alpha+\sin\alpha\,\mathrm{ch}\,\alpha)+\alpha\nu\phi(\cos\alpha\,\mathrm{ch}\,\alpha-1)\}\\&\quad\times\{\sin\beta(\mathrm{ch}\,\beta-1)+\mathrm{sh}\,\beta(1-\cos\beta)\}\\&\quad-\{(\cos\alpha\,\mathrm{ch}\,\alpha+1)+\alpha\nu\phi(\cos\alpha\,\mathrm{sh}\,\alpha-\sin\alpha\,\mathrm{ch}\,\alpha)\}(\cos\beta\,\mathrm{ch}\,\beta-1)=0^{1)}.\end{aligned} \tag{2}$$

where α and β are the functions of frequency p;

$$\alpha^4=\frac{\rho_1 a_1 l_1^4}{E_1 I_1}p^2,\qquad \beta=\alpha\phi\left(\frac{\nu}{\zeta}\right)^{1/4}. \tag{3}$$

1) K. SEZAWA and K. KANAI, "Vibration of a Singled-storyed Framed Structure", *Bull. Earthq. Res. Inst.*, **10** (1932), p. 770, Eq. (26).

Also

$$\phi=\frac{l_2}{l_1}, \quad \zeta=\frac{E_2I_2}{E_1I_1}, \quad \nu=\frac{\rho_2 a_2}{\rho_1 a_1} \tag{4}$$

where suffix 1 indicates being a vertical member and suffix 2 a horizontal one.

In order to derive the frequency from equation (2), it is necessary to carry out a very complicated calculation using the trial and error method. Therefore, by assuming each member of Rahmen to be massless, the method of concentrating the whole mass on the panel points is often adopted. Then the equation of motion of each member can be written as follows:

$$\partial^4 y/\partial x^4=0. \tag{5}$$

The frequency equation under the boundary clamped conditions at the floors and the base is

$$\frac{mp^2l_1^3}{E_1I_1}=\frac{3(\phi+12\zeta)}{\phi+3\zeta}\ ^{2)}. \tag{6}$$

Suppose that the mass which acts as an inertia force concentrating at the panel point is the sum of the masses of horizontal members and the upper part of vertical ones. Then the concentrated mass, m, by using the notation in Fig. 1, is expressed as follows:

$$m=\rho_2 a_2 l_2+\rho_1 a_1 l_0, \tag{7}$$

Introducing equation (7) into equation (6)

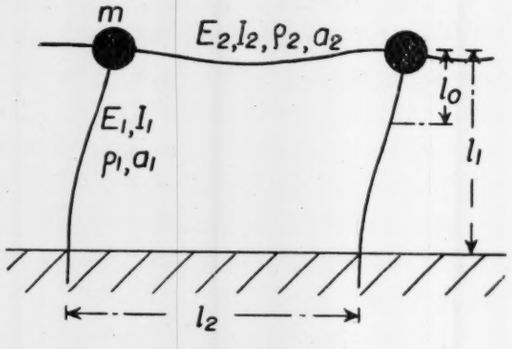

Fig. 1.

$$\frac{\rho_1 a_1 l_1^4}{E_1I_1}p^2(\equiv\alpha^4)=\frac{3(\phi+12\zeta)}{(\nu\phi+\kappa)(\phi+3\zeta)} \tag{6'}$$

where $\kappa=l_0/l_1$.

By applying various quantities of the material for horizontal and vertical members, the natural period of Rahmen will be exactly obtained from equation 2) in a form of α in equation (3). Then, introducing the value of α obtained in equation (2) into equation (6′) we can obtain the value of $\kappa(=l_0/l_1)$. In other words we can tell how much mass of

2) K. SEZAWA and K. KANAI, "Theory of the Aseismic Properties of the Brace Struts .....", *Bull. Earthq. Res. Inst.*, **16** (1938), p. 710, Eq. (40′).

the upper part of vertical member must be added to the mass of horizontal member as a concentrated mass used in approximate calculation, in order to get the natural period equal to the one given by an exact calculation.

Under such considerations, the values of $\kappa(\equiv l_0/l_1)$ in regard to various cases are determined from equations (2) and (6′), and are shown in Tables I and II.

Table I. The values of $(\rho_1 a_1/E_1 I_1)^{1/2} l_1^2 p$.

$\frac{l_2}{l_1}$	$\frac{\rho_2 a_2}{\rho_1 a_1}$	1			2		5
	$\frac{E_2 I_2}{E_1 I_1}$	1	2	10	2	5	5
0.2		4.482	4.515	4.545	3.893	3.917	2.941
0.5		3.542	3.616	3.683	2.880	2.924	2.019
1		2.699	2.816	2.924	2.135	2.200	1.457
2		1.899	2.044	2.199	1.498	1.584	1.028
5		1.032	1.184	1.411	0.848	0.963	0.615

Table II. The values of l_0/l_1.

$\frac{l_2}{l_1}$	$\frac{\rho_2 a_2}{\rho_1 a_1}$	1			2		5
	$\frac{E_2 I_2}{E_1 I_1}$	1	2	10	2	5	5
0.2		0.37	0.37	0.38	0.37	0.37	0.38
0.5		0.35	0.37	0.38	0.36	0.37	0.38
1		0.34	0.35	0.37	0.36	0.37	0.38
2		0.33	0.35	0.37	0.36	0.37	0.36
5		0.99	0.65	0.37	0.99	0.51	0.82

If horizontal member is heavy or weak beyond a certain extent, the effect of its vertical motion increases as the span grows larger, and it makes the summary method unsuitable. And also this is the reason why the values in the bottom line in Table I are somewhat peculiar.

To summarize, if the span of Rahmen is within the double of the height, the sum of the mass of horizontal members and 33–38 percent of

the mass of vertical members is to be thought of as a concentrated mass regardless of the material of horizontal and vertical members. Consequently this study permits us to express the practical equation which will determine the natural period regarding a one-storied framed structure as follows:

$$T=\frac{2\pi}{3}\sqrt{\frac{\frac{\rho_1 a_1 l_1^4}{E_1 I_1}\left(1.1+3\frac{\rho_2 a_2 l_2}{\rho_1 a_1 l_1}\right)\left(1+3\frac{E_2 I_2 l_1}{E_1 I_1 l_2}\right)}{1+12\frac{E_2 I_2 l_1}{E_1 I_1 l_2}}}\,. \qquad (8)$$

---

22. 架構構造物の振動問題における集中荷重の仮定の吟味

地震研究所　金　井　　清

架構構造物の振動問題を正確に解くことは，非常に繁雑なため，しばしば種々の仮定のもとに，簡易化した解法がとられている．

この研究では，1 層無限張間の架構構造物の固有周期を，集中荷重の仮定で求めた値と，正確な解法で求めた値とが，どのような場合に，どの程度に合うかをしらべた．

その結果，かなり安心して使える実用計算式として (8) 式が得られた．

昭和28年9月10日印刷
昭和28年9月15日發行

東京都文京區本富士町一番地
東京大學構内
編纂發行者 東京大學地震研究所

東京都千代田區富士見町一丁目十番地
印刷者 笠井康賴

東京都千代田區富士見町一丁目十番地
印刷所 株式會社 國際文献印刷社

賣捌所 東京都千代田區神田一ツ橋通
岩波書店

東京都中央區日本橋通二丁目六番地
丸善株式會社

Sold by
Iwanami Shoten,
Hitotsubashi dôri, Chiyoda-ku, Tôkyô,
and
Maruzen Co., Ltd.,
Nihonbashi dôri, Chûô-ku, Tôkyô.
Price of this copy: 270 Yen. (Postage exclusive.)

BULLETIN OF

THE EARTHQUAKE RESEARCH INSTITUTE

TOKYO UNIVERSITY

Vol. XXXI, Part 3. September, 1953.

Contents.

Papers and Reports.

Page

16. T. MATUZAWA, Feldtheorie der Erdbeben. (im Deutschen) 179
17. Y. SATÔ, Transformation of Spherical Solid Harmonics Related to the Translation of Coordinates System. (in English) 203
18. I. YOKOYAMA, A New Method for Regulating Electric Currents and its Application to Measurements of Geomagnetic Field. (in English) 211
19. K. KANAI, Relation between the Nature of Surface Layer and the Amplitude of Earthquake Motions. II. (in English) 219
20. K. KANAI, K. OSADA and S. YOSHIZAWA, Observational Study of Earthquake Motion in the Depth of the Ground. IV. (Relation between the Amplitude at Ground Surface and the Period.). (in English) 227
21. K. KASAHARA, Experimental Studies on the Mechanism of Generation of Elastic Waves III. (in English) 235
22. K. KANAI, Examination of the Assumption of the Concentrated Mass in the Vibration of Framed Structure (Rahmen). (in English) 245

(For the papers written in Japanese or in occidental languages, the abstracts are given in occidental languages or in Japanese respectively.)

BULLETIN OF THE EARTHQUAKE RESEARCH INSTITUTE,
TOKYO UNIVERSITY. Vol. XXXI, Part 4. December, 1953.

東京大學
地震研究所彙報

第 31 號　第 4 冊

昭和 28 年 12 月

目　次

論文及報告

			頁
23.	地震の場の論　1946 年 12 月 21 日の大地震と 1948 年 4 月 18 日の余震との比較 (独文)	松沢武雄	249
24.	表面波の研究　IX　ラブ波の群速度を求める図表 (英文)	佐藤泰夫	255
25.	いくつかの平行な不連続面による地震波の反射及び透過 (英文)	松本利松	261
26.	地震動振幅と地表層の性質との関係　第4報 (英文)	金井清・吉沢静代	275
27.	東北日本における第3回爆破地震動観測 (英文)	爆破地震動研究グループ	281
28.	高温に於ける火山岩の粘性及び弾性　第3報　大島熔岩 (英文)	佐久間修三	291
29.	建物の振動的性質と地盤の性質との関係 (実在建物における地震動観測) (英文)	金井清・鈴木富三郎	305
30.	簡易弾性波式地下探査装置の研究 (英文)	西村源六郎・鈴木正治・古川英一・小滝富雄・高橋浩一	317
31.	東京都南東部の地盤沈下測量 (邦文)	那須信治・岸上冬彦・岡田惇	335

所　報

索　引

(The titles in occidental languages are given on the back cover.)

本彙報ハ年4回（但シ第1號ヨリ第6號マデハ不定期ニ，第7號ハ3冊トシテ發行セリ），彙報別冊ハ不定期ニ發行ス．

本彙報掲載ノ論文及ビ報告ノ内容ニ關シテハ著者ノミニ其責任アルモノトス．

本彙報ニ關スル照會通信ハ東京大學地震研究所長ヘ宛テラレタシ．

The Bulletin is published quarterly. (Vols. I–VI were published at irregular intervals and Vol. VII consisted of three parts.)
Supplementary Volume is published at irregular interval.

The authors of the papers alone are responsible for the statements and opinions contained in their respective papers.

All communications relating to this Bulletin should be addressed to the Director of the Earthquake Research Institute, Tokyo University.

23. *Feldtheorie der Erdbeben: Vergleichung vom Grossbeben vom 21. Dez. 1946 mit dem Nachbeben vom 18. April 1948.*

Von Takeo MATUZAWA,

Institut für Erdbebenforschung.

(Vorgelegt den 27. Okt. 1953.—Eingegangen den 29. Okt. 1953.)

1. R. Yoshiyama'sche Forschung der beiden Erdbeben.

R. Yoshiyama[1] hat diese zwei Erdbeben eingehend untersucht. Sein wichtiges Resultat lautet wie folgt.

Die beiden Erdbeben, wenigstens insofern die erste Phase der P-Wellen betrifft, entstanden in fast derselben Stelle. Die P-Wellen der beiden Beben, die an den Erdbebenstationen in Hukuoka, Saga, Kagosima, Miyazaki, und Simonoseki beobachtet wurden, bestanden aus drei Stufen. Die Amplituden der ersten Stufe waren ungefähr gleich miteinander. Dagegen waren die folgenden Phasen, besonders die dritte Phase, des ersten Bebens entscheidend grösser als die des zweiten Bebens. Die ausgestrahlte Energie des ersten Bebens wurde geschätzt zu 10^{25} erg, im Gegensatz zu 10^{23} erg des zweiten. Es scheint mir, dass R. Yoshiyama dort einige Probleme über die Erdbeben überhaupt stellte, aber nicht die Erklärung davon gäbe.

2. Seismogramme in Simonoseki der beiden Erdbeben.

R. Yoshiyama hat mir freundlicherweise photographische Kontaktkopien der Seismogramme der beiden Erdbeben geschenkt, die an der Station in Simonoseki beobachtet wurden. Das Original des ersten Bebens war ziemlich verletzt durch Schrammen aber doch lesbar.

Fig. 1 ist die Abbildung nach der Kontaktkopien der Seismogramme.

In dieser Abbildung werden kleine superponierte Zacken der Wellen vernachlässigt, aber sie zeigt sicher die Hauptzüge der Wellen. In ihr können wir drei Phasen der Wellen ziemlich klar unterscheiden, wie P, P* und $\overline{P}$ markiert. Die Herdentfernungen dieser beiden Beben sind je ungefähr 470 km. Die P–P* und P*–$\overline{P}$ Zeiten sind andererseits respektiv ungefähr 9 sek. und 14 sek. Darum können wir sehr wahrscheinlich

1) R. YOSHIYAMA, *Zisin* (*Jour. Seism. Soc. Japan*), [ii] **3** (1950), 22–26.

diese Phasen als die P, P* und $\bar{P}$ im gewöhnlichen Sinne ansehen gemäss der Laufzeiten dieser Wellen, die ich schon in 1928 veröffentlichte.[2)]

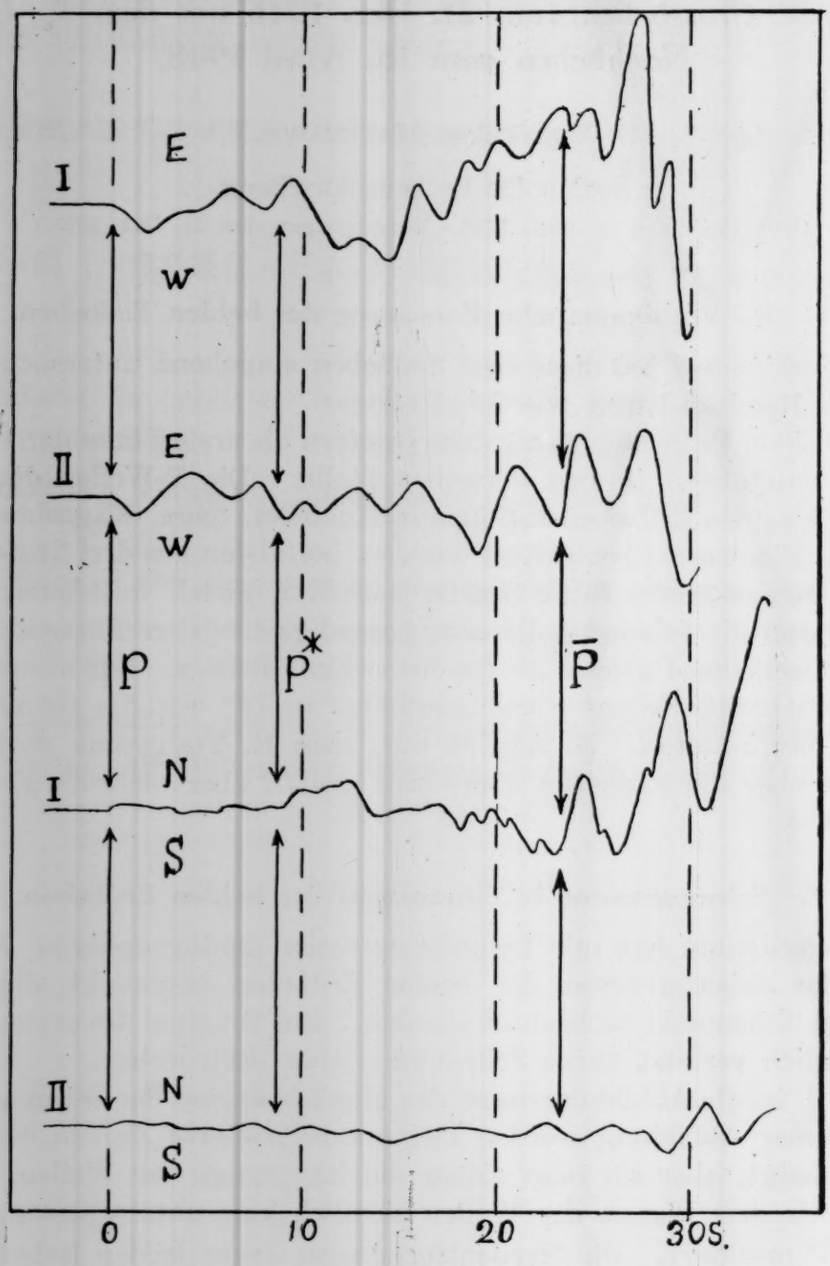

Δ=470 km. V=57

Fig. 1.

2) T. MATUZAWA, *Bull. Earthq. Res. Inst.*, **5** (1928), 1–28.

3. Relative Grösse jeder Phase.

Wie schon R. Yoshiyama bemerkt hat, sehen wir in der Figur deutlich, dass die späteren Phasen des ersten Bebens erheblich grösser als die des zweiten Bebens, während die erste Phase ungefähr gleich miteinander bei jedem Beben ist. Obendrein sind sehr langperiodische Wellen besonders in der EW-Komponente des ersten Bebens deutlich bemerkbar, wie gewöhnlich beim Grossbeben der Fall ist[3].

Wenn man einen punktförmigen Herd für jedes Beben annimmt, dann ist es ziemlich schwer, diese oben gezeigten Eigentümlichkeiten der Seismogramme genug zu erklären.

Ein Versuch zur Erklärung nach meiner Feldtheorie[4] der Erdbeben ist wie folgt.

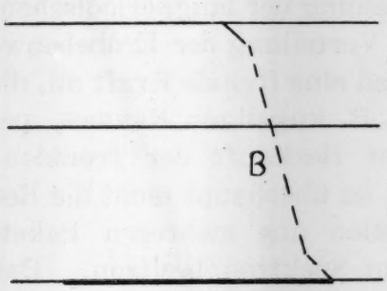

Fig. 2a

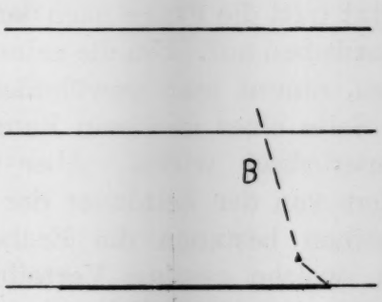

Fig. 2b

Beim Hauptbeben wäre eine Kette von Brüchen etwa wie B in Fig. 2a erzeugt worden, und beim zweiten wie B in Fig. 2b. Nämlich, beim Hauptbeben hätte die Kette der Brüche vom Quellengebiet bis zur Erdoberfläche sich erstreckt, was man von der Hebungen und Senkungen der Erdoberfläche und der Entstehung der grossen Tunami sehr wahrscheinlich vermuten kann.

Beim zweiten Beben aber wegen der Verminderung des Energievorrates im Quellengebiet und der Erniedrigung des Druckes hätte die Kette der Brüche nur in den unteren Teil der obersten Schicht eindringen können.

Nun bei dieser Annahme muss der erste Einsatz der P-Wellen an Stationen mit Herdentfernungen von einigen Hunderten von Kilometern vom unteren Teil der Bruchkette stammen. Dann wird die Grösse der ersten Phase jedes Bebens wahrscheinlich ungefähr gleich sein, weil der

3) T. MATUZAWA, und K. SATÔ, *Bull. Earthq. Res. Inst.*, **17** (1939), 624.
4) T. MATUZAWA, *Bull. Earthq. Res. Inst.*, **31** (1953), 179–201.

Spannungszustand gleich vor der Entstehung jedes Bebens fast gleich sein mag, insofern die erste Phase anbetrifft.

Nun was die $\overline{P}$-Phase betrifft, kommt natürlich der Bruch in der oberen Schicht in Frage. Gemäss des vorigen Modells in Fig. 2a und 2b muss sicher die $\overline{P}$-Welle des Hauptbebens grösser sein als die des zweiten, weil die im grösseren Herdgebiet gelagerte Spannungsenergie, nämlich grössere Menge Energie, befreit werden kann.

Nun vor etwa 25 Jahren setzte ich beinahe solches Modell[5] für die Grossbeben wie das vorigen voraus, um den frühzeitigen Eintritt der P-Welle in herdnahen Stationen zu erklären. Diese Annahme wird durch die jetzigen Überlegungen vorteilhaft gestützt.

4. Die langperiodische Wellen im Grossbeben.

Jetzt tritt die Frage nach der Entstehung der langperiodischen Wellen bei Grossbeben auf. Um die azimuthale Verteilung der Erdbebenwellen zu erklären, nimmt man gewöhnlich irgend eine fremde Kraft an, die an die innere Seite eines gewissen Raumes, z. B. kugeligen Raumes, periodisch oder aperiodisch wirkt. Aber von der Herkunft der fremden Kraft, besonders von der Zeitdauer der Kraft, ist überhaupt nicht die Rede. Im allgemeinen bestehen die Erdbebenwellen aus mehreren Paketen von Wellen, welche gewisse Verteilung von Spektren besitzen. Das Paket der langperiodischen Wellen beim Grossbeben ist auch der Fall. Unser Modell des Erdbebenfeldes kann ein Schwingungssystem mit Quasi-eigenwert bilden, weil die elastische Eigenschaft des Quellengebietes beträchtlich verschieden im Vergleich mit der Umgebung ist.

Nun beim Hauptbeben, bei dem die Kette der Brüche vom Quellengebiet bis zur Erdoberfläche erzeugt wird, kann die Quasi-eigenschwingung des Bebenfeldes sehr wahrscheinlich erregt werden.

In dieser Beziehung ist die Forschung der langperiodischen Wellen an herdnahen Stationen bei Grossbeben sehr wichtig. Dazu ist der langperiodige Seismograph für starke Beben[6] unbedingt nötig.

---

5) T. MATUZAWA, *Bull. Earthq. Res. Inst.*, **5** (1928), 1–28.

6) T. MATUZAWA, *Jour. Fac. Sci. Imp. Univ. Tokyo*, [II], **5** (1938), 59.

23. Zisin no Ba no Ron; 1946 nen 12 gatu 21 niti no Oozisin to 1948 nen 4 gatu 18 niti no Yosin tono Hikaku.

Zisin-Kenkyûsyo, Matuzawa-Takeo.

R. Yoshiyama ni yoreba kono hutatu no Zisin ni tuiteno omona Kotogara wa tugi no tôri de aru.

1. Hotondo onazi Basyo ni okotte iru.
2. P-Nami no Bubun wa 3-dan ni natte iru.
3. Dai-iti no Nami wa Ryôhô tomo hotondo hitosii.
4. Dai-san no Nami de Ookisa ga taihen tigau.
5. Hazime no Zisin niwa Syûki no nagai Nami ga kasanatte iru.
6. Energie wa mae no Zisin de 10^{25} erg, noti no Zisin dewa 10^{23} erg no Teido de aru.

Korera no Kotogara wo Zisin no Ba no Ron no Kangae kara Setumei suru.

24. *Study on Surface Waves* IX. *Nomogram for the Group Velocity of Love-Waves.*

By Yasuo SATÔ,

Earthquake Research Institute.

(Read Sept. 15, 1953.—Received Sept. 26, 1953.)

1. Introduction.

In a former paper[1] we have published a nomogram which is convenient for the computation of the phase velocity of Love-waves. As a natural sequel of this work, we tried to make a nomogram useful for obtaining the group velocity of Love-waves.

For the practical investigation of dispersive seismic surface waves, group velocity is rather more important that the phase velocity, and if we intend to get the former from the previously published nomogram, we must numerically differentiate the computed values. This procedure, however, necessarily includes some error, and besides it takes time and labour to arrive at the result. Consequently it becomes a natural desire for everyone who is engaged in the study of surface waves to have a nomogram directly affording the group velocity.

2. Formula.

We start from the following two formulae.[2]

$$\omega = \sec\theta \cdot \operatorname{Arctan}\{\chi \sec\theta \sqrt{(\sin^2\theta - \sin^2\theta_0)}\} \tag{2.1}$$

$$\mathfrak{V} = \frac{d\omega}{d\xi} \tag{2.2}$$

in which

ω	Circular frequency of Love-waves (time unit is H/V_s, where H is the thickness of the layer).
$\chi \equiv \mu'/\mu$	Ratio of the rigidity of lower and upper media.
$\operatorname{cosec}\theta_0 \equiv V_s'/V_s$	V_s' and V_s are the velocity of S-waves in the lower and upper media respectively.

1) Y. SATÔ, "Study on Surface Waves VIII. Nomogram for the Phase Velocity of Love-Waves...," *Bull. Earthq. Res. Inst.*, **31** (1953), 81.

2) Y. SATÔ, "Study on Surface Waves I. Velocity of Love-Waves," *ibid.*, **29** (1951), 1.

$\operatorname{cosec}\theta \equiv V/V_s$	Phase velocity of Love-waves measured by the unit V_s.
V, U	Phase and group velocity of Love-waves respectively.
v, $\mathfrak{V}$	Phase and group velocity of Love-waves measured by the unit V_s respectively.
$\xi = \omega/v$	

The first expression (2.1) is a well-known formula representing the relation of the period and the phase velocity of Love-waves, while the second expression (2.2) is the formula of group velocity.

From (2.1) we have

$$\omega = \sec\theta \cdot \operatorname{Arctan} Z$$

$$Z = \chi \sec\theta \cdot \sqrt{(\sin^2\theta - \sin^2\theta_0)}\,, \tag{2.3}$$

$$\frac{d\omega}{d\theta} = \sec\theta \cdot \tan\theta \cdot \operatorname{Arctan} Z + \sec\theta \cdot \frac{1}{1+Z^2}\frac{dZ}{d\theta}\,, \tag{2.4}$$

$$\begin{aligned}\frac{dZ}{d\theta} &= \chi\left[\sec\theta \cdot \tan\theta \cdot \sqrt{(\sin^2\theta - \sin^2\theta_0)} + \sec\theta \cdot \sin\theta\cos\theta/\sqrt{(\sin^2\theta - \sin^2\theta_0)}\right] \\ &= Z\tan\theta\left(1 + \frac{\cos^2\theta}{\sin^2\theta - \sin^2\theta_0}\right).\end{aligned} \tag{2.5}$$

Therefore

$$\frac{d\omega}{d\theta} = \sec\theta \cdot \tan\theta \cdot \left[\operatorname{Arctan} Z + \frac{Z}{1+Z^2}\left(1 + \frac{\cos^2\theta}{\sin^2\theta - \sin^2\theta_0}\right)\right]. \tag{2.6}$$

While from (2.2)

$$\begin{aligned}\mathfrak{V} &= \frac{d\omega}{d\xi} = \frac{d\omega}{d\theta}\Big/\frac{d\xi}{d\theta}\,, \\ \xi &= \omega\sin\theta\,, \\ \frac{d\xi}{d\theta} &= \frac{d\omega}{d\theta}\sin\theta + \omega\cos\theta\,, \\ \frac{1}{\mathfrak{V}} &= \sin\theta + \omega\cos\theta\Big/\frac{d\omega}{d\theta}\,.\end{aligned} \tag{2.7}$$

Introducing (2.6) we have

$$\frac{\mathfrak{v}}{\mathfrak{V}}=1+\sec\theta\cdot\operatorname{Arctan}Z\cdot\cot\theta$$
$$+\left\{\sec\theta\cdot\tan\theta\left[\operatorname{Arctan}Z+\frac{Z}{1+Z^2}\left(1+\frac{\cos^2\theta}{\sin^2\theta-\sin^2\theta_0}\right)\right]\right\}$$
$$=1+\cot^2\theta\Big/\left[1+\frac{Z}{\operatorname{Arctan}\theta\cdot(1+Z^2)}\left(1+\frac{\cos^2\theta}{\sin^2\theta-\sin^2\theta_0}\right)\right]. \tag{2.8}$$

Modifying the above expression we have at once

$$\frac{\mathfrak{V}}{\mathfrak{v}}=1\Big/\left(1+\frac{\cot^2\theta}{1+\dfrac{1}{\operatorname{Arctan}\theta\cdot\left(Z+\dfrac{1}{Z}\right)}\left(1+\dfrac{\cos^2\theta}{\sin^2\theta-\sin^2\theta_0}\right)}\right). \tag{2.9}$$

If we put

$$Y\equiv Z/\chi=\sec\theta\sqrt{(\sin^2\theta-\sin^2\theta_0)}\,, \tag{2.10}$$

$$F(Z)\equiv 1\Big/\operatorname{Arctan}Z\cdot\left(Z+\frac{1}{Z}\right), \tag{2.11}$$

$$S^2(\chi,Y)\equiv F(\chi Y)\cdot\left(1+\frac{1}{Y^2}\right), \tag{2.12}$$

we have from (2.9), (2.10), (2.11) and (2.12)

$$\frac{\mathfrak{V}}{\mathfrak{v}}=1\Big/\left[1+\frac{\mathfrak{v}^2-1}{1+S^2}\right]$$
$$=\frac{\mathfrak{v}^2+S^2}{1+S^2}\,. \tag{2.13}$$

Using this formula we can obtain $\mathfrak{V}/\mathfrak{v}$ and $\mathfrak{V}$.

3. Constitution of the nomogram and directions for use.

First we calculate $1/Y$.

In Fig. 1, the nomogram at the lower left gives the value of $1/Y$. First we take A on [1]-axis so that $\overline{OA}$ is equal to assigned value of V_s/V_s'.

Now, α is the curve of

$$\frac{1}{Y}=\frac{\cos\theta}{\sqrt{(\sin^2\theta-\sin^2\theta_0)}} \tag{3.1}$$

therefore, if we choose some value of $\mathfrak{v}=V/V_s$ and pick out a curve whose parameter is equal to this chosen value of $\mathfrak{v}$, then the point C on [2]-axis expresses $1/Y$, or

$$\overline{OC}=\frac{1}{Y}=\sqrt{\frac{V^2}{V_s^2}-1}\Big/\sqrt{1-\frac{V^2}{V_s'^2}} \tag{3.2}$$

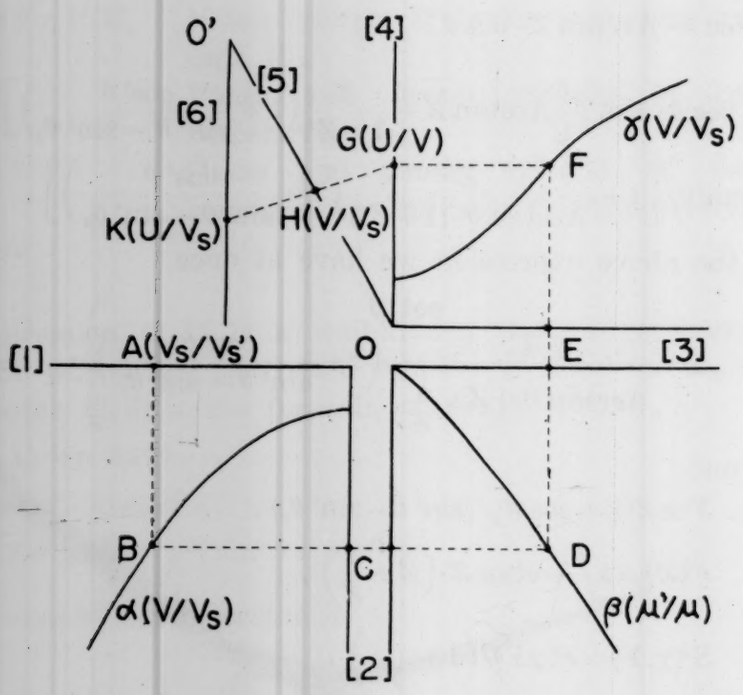

Fig. 1.

Next, [3] is the axis of S (cf. expression (2.12)). Since the parameter of the curve β in the second nomogram is $\chi=\mu'/\mu$, we can obtain the value of

$$S(\chi,Y)=\sqrt{\left\{F(\chi Y)\cdot\left(1+\frac{1}{Y^2}\right)\right\}} \tag{3.3}$$

combining $1/Y$ and χ which is naturally determined when the distribution of matter is given, viz.,

$$\overline{OE}=S(\chi,Y)\,. \tag{3.4}$$

At the third step we obtain $U/V=\mathfrak{V}/\mathfrak{v}$. In the third nomogrom, curve γ gives

$$\frac{U}{V}=\frac{\mathfrak{V}}{\mathfrak{v}}=\frac{\mathfrak{v}^2+S^2}{1+S^2}\,. \tag{3.5}$$

The parameter of γ is $\mathfrak{v}=V/V_s$, which must of course be equal to that employed in the first step of this calculation. Thus we obtain the point G on [4]-axis. $\overline{OG}$ gives the value expressed in (3.5).

If we aim at the ratio of the group and phase velocity of Love-waves, the computation is finished by the above procedure. But if we aim at the group velocity $\mathfrak{V}=U/V_s$, we must multiply $\mathfrak{v}$ to the above obtained

value by the next nomogram and get the final result. This procedure is very simple and requires no explanation. H is the point representing $v=V/V_s$, and $O'K$ on [6]-axis gives $\mathfrak{V}=U/V_s$.

By the above explanation, the way of using this nomogram will be understood.

4. Example.

We will give some numerical examples in this section.

We have employed some numerical assumptions and calculated the relation of phase velocity and period in the former paper.[3] Using again the same example we will obtain the corresponding values of group velocity.

Now the former example employed was

$$\begin{cases} \chi \equiv \mu'/\mu = 5.0 \\ \rho'/\rho = 1.25 \\ \sin\theta_0 \equiv V_s/V_s' = 0.50 \end{cases} \tag{4.1}$$

and the phase velocity was assumed to be

$$\begin{aligned} v &= V/V_s = \operatorname{cosec}\theta \\ &= 1.00,\ 1.05,\ 1.10,\ 1.15,\ldots.1.85,\ 1.90,\ 1.95,\ 2.00. \end{aligned} \tag{4.2}$$

Now we will calculate the group velocity by means of the nomogram presented here. The results are also obtained by applying Stirling's formula of numerical differentiation to the strictly calculated values of phase velocity. Namely,

$$\mathfrak{V} = v + \xi \Big/ \frac{d\xi}{dv} \tag{4.3}$$

and

$$\begin{aligned} \frac{d}{dx}y(x+p\Delta x) = \frac{1}{\Delta x}\Big\{ & \frac{\Delta y_{-1}+\Delta y_0}{2} + p\Delta^2 y_{-1} \\ & + \frac{3p^2-1}{6}\,\frac{\Delta^3 y_{-2}+\Delta^3 y_{-1}}{2} + \frac{2p^3-p}{6}\Delta^4 y_{-2} + \ldots.\Big\}^{4)}. \end{aligned} \tag{4.4}$$

Both values are shown in the following table. The coincidence seems to be satisfactory.

The nomogram is included in the pocket of back cover.

3) *loc. cit.*, 1). §4.

4) We put p=0 in this expression.

Table I.

$\mathfrak{v}=\frac{V}{V_S}$	$\xi=\frac{\omega}{\mathfrak{v}}$	$\mathfrak{B}/\mathfrak{v}=U/V$	
		Numerical differentiation	Nomograph
1.00	∞		1.000
1.05	4.671		0.910
1.10	3.189		0.839
1.15	2.523		0.780
1.20	2.121		0.731
1.25	1.842	0.690	0.691
1.30	1.632	0.660	0.660
1.35	1.4664	0.636	0.639
1.40	1.3298	0.620	0.621
1.45	1.2142	0.608	0.610
1.50	1.1134	0.608	0.607
1.55	1.0236	0.613	0.614
1.60	0.9419	0.626	0.623
1.65	0.8655	0.648	0.648
1.70	0.7924	0.676	0.674
1.75	0.7209	0.714	0.714
1.80	0.6475	0.761	0.762
1.85	0.5683	0.817	0.815
1.90	0.4755		0.883
1.95	0.3500		
2.00	0		1.000

24. 表面波の研究 IX
ラブ波の群速度を求める図表

地震研究所 佐 藤 泰 夫

ラブ波の群速度を求める計算図表を作つた．§2 に基本公式を，§3 に使用法を，§4 に計算例を示す．

25. *Transmission and Reflection of Seismic Waves through Multilayered Elastic Medium.*

By Tosimatu MATUMOTO,

Earthquake Research Institute.

(Read Sept. 16, 1952.—Received Sept. 28, 1953.)

1. Introduction.

The problem of reflection and refraction of elastic wave has been studied by many authorities[1)2)3)4)5)6)7)], but owing to the complicated nature of elastic wave which produces four secondary waves when primary wave meets a discontinuous plane (with the exeception of SH type wave), their studies had to be limited only to the case of one or two boundary planes.

When there exist n parallel discontinuities in elastic medium and the incident wave is the dilatational one, the calculation of the amplitude of transmitted waves as well as reflected waves is reduced to the problem of the simultaneous linear equation of $4n$-th order, and though it is a simple problem in principle, it is extremely subtle in actual treatment. However, in spite of this difficulty which has prevented further study of the problem, we must, in view of the importance of the problem, investigate how the multilayered medium affects the transmission and reflection of elastic wave.

Recently useful studies have been perfomed by Thomson[8)] and Torikai[9)]

---

1) C. G. KNOTT, "Reflexion and Refraction of Elastic Waves, with Seismological Applications", *Phil. Mag.*, **48** (1899), 64.

2) G. W. WALKER, "Surface Reflection of Earthquake Waves", *Phil. Trans.*, *A* **218** (1819), 373.

3) H. JEFFREYS, "The Reflexion and Refraction of Elastic Waves", *M. N. R. A. S. Geophys. Suppl.*, **1** (1926), 321–334.

4) K. SEZAWA, "Possibility of the Free-oscillations of the Surface-layer Excited by the Seismic Waves", *Bull. Earthq. Res. Inst.*, **8** (1930), 1

5) T. MATUZAWA, "An Example of Surface Reflection of Elastic Plane Waves", *Zisin*, **4** (1932), 7. (in Japanese)

6) K. KAWASUMI and T. SUZUKI, "Reflexion and Refraction of Seismic Waves at Plane Interface of the Earth's Surface Crust", Zisin **4** (1932), 277. (in Japanese)

7) K. SEZAWA and K. KANAI, "Possibility of Free-oscillations of Strata Excited by Seismic Waves (Part 4)", *Bull. Earthq. Res. Inst.*, **10** (1932), 273.

8) W. T. THOMSON, "Transmission of Elastic Waves through a Stratified Solid", *J. Appl. Phys.*, **21** (1950), 89.

9) Y. TORIKAI, "Transmission of Acoustic Waves through a Stratified Solid Medium", *J. Acoust. Soc. Japan.*, **8** (1952), 21.

concerning the transmission of super-sonic wave through the multilayered elastic plate. They both utilize the matrix calculation and express the solution of that problem in a very compact form.

Following their mothod in this paper, we employ the boundary conditions applicable to the seismic wave, and obtain the amplitude of transmitted and reflected waves in the case of the incidence of the dilatational and distortional wave. Using this result, we calculated numerically the amplitudes for the case $n=2$. The results of these calculations may show some light on the discussion of wave amplitude transmitted through a layer.

2. Expression of Stress and Displacement Components.

In this paper, we will confine our problem to the two-dimensional waves for the sake of simplicity, and each elastic medium is assumed to be isotropic and homogeneous. We take a Cartesian coordinate system and assume that the incident waves as well as refracted and reflected waves are included in xy-plane.

Putting the density and Lamé's elastic constants as ρ and λ, μ respectively, the equations of motion in that medium are

$$\left.\begin{aligned} \rho\frac{\partial^2\Delta}{\partial t^2} &= (\lambda+2\mu)\left(\frac{\partial^2\Delta}{\partial x^2}+\frac{\partial^2\Delta}{\partial y^2}\right) \\ \rho\frac{\partial^2\tilde{\omega}}{\partial t^2} &= \mu\left(\frac{\partial^2\tilde{\omega}}{\partial x^2}+\frac{\partial^2\tilde{\omega}}{\partial y^2}\right) \end{aligned}\right\} \quad (2.1)$$

where Δ is the dilatation, $\tilde{\omega}$ is the rotation, and they are both expressed by means of the displacement components u and v as follows;

$$\left.\begin{aligned} \Delta &= \frac{\partial u}{\partial x}+\frac{\partial v}{\partial y} \\ 2\tilde{\omega} &= \frac{\partial v}{\partial x}-\frac{\partial u}{\partial y} \end{aligned}\right\} \quad (2.2)$$

The fundamental solution of equation (2.1) which represents the progressive waves towards the positive side of x-axis is

$$\left.\begin{aligned} \Delta &= \left\{\begin{matrix} A \\ C \end{matrix}\right\} \exp\{ih(V_p t - x\sin\theta \mp y\cos\theta)\} \\ 2\tilde{\omega} &= \left\{\begin{matrix} B \\ D \end{matrix}\right\} \exp\{ik(V_s t - x\sin\omega \mp y\cos\omega)\} \end{aligned}\right\} \quad (2.3)$$

where

$$\left.\begin{aligned} h^2&=\rho p^2/(\lambda+2\mu)=(p/V_p)^2 \\ k^2&=\rho p^2/\quad \mu \quad =(p/V_s)^2 \end{aligned}\right\} \qquad (2.4)$$

and θ and ω are the angles measured from y-axis to the normal of wave front of the dilatational and equivoluminal wave respectively. From Snell's law the next relation is easily found:

$$h\sin\theta=k\sin\omega \qquad (\equiv\xi;\ \text{constant}) \qquad (2.5)$$

If the elastic medium is bounded by two planes of separation perpendicular to the y-axis, the waves in the layered medium, are wholly expressed by the two upward-going waves and the two downward-going waves. (Here the consideration of the z component of displacement is not necessary.) In the following calculations, we will denote the amplitudes of upward-going P- and S-wave as A and B, and downward-going P- and S-wave as C and D. The displacement components due to the above waves A and B are denoted as u_A, v_A and u_B, v_B respectively. Then the displacement components are calculated from (2.3) and (2.2) as follows:

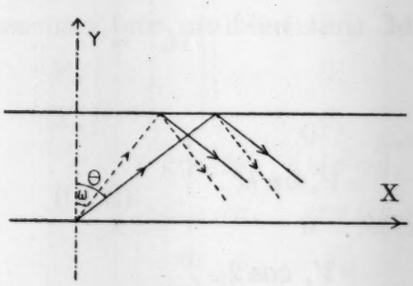

Fig. 1.

$$\left.\begin{aligned} u_A&=\ ip^{-1}V_pA\sin\theta\cdot\exp\{ih(V_pt-x\sin\theta-y\cos\theta)\} \\ v_A&=\ ip^{-1}V_pA\cos\theta\cdot\exp\{ih(V_pt-x\sin\theta-y\cos\theta)\} \\ u_B&=-ip^{-1}V_sB\cos\omega\cdot\exp\{ik(V_st-x\sin\omega-y\cos\omega)\} \\ v_B&=\ ip^{-1}V_sB\sin\omega\cdot\exp\{ik(V_st-x\sin\omega-y\cos\omega)\} \\ u_C&=\ ip^{-1}V_pC\sin\theta\cdot\exp\{ih(V_pt-x\sin\theta+y\cos\theta)\} \\ v_C&=-ip^{-1}V_pC\cos\theta\cdot\exp\{ih(V_pt-x\sin\theta+y\cos\theta)\} \\ u_D&=\ ip^{-1}V_sD\cos\omega\cdot\exp\{ik(V_st-x\sin\omega+y\cos\omega)\} \\ v_D&=\ ip^{-1}V_sD\sin\omega\cdot\exp\{ik(V_st-x\sin\omega+y\cos\omega)\} \end{aligned}\right\} \qquad (2.6)$$

The displacement at an arbitrary point in that medium is expressed as the sum of each displacement component in (2.6).

From these expressions we can easily calculate the velocity components of a particle $\dot{u}$ and $\dot{v}$ and stress components X_y and Y_y. Using the matrix expression and omitting the factor $\exp\{i(pt-\xi x)\}$ for convenience, we get

$$\begin{pmatrix} \dot{u} \\ \dot{v} \\ Y_y \\ X_y \end{pmatrix} = \begin{pmatrix} -V_p \sin\theta, & 0, & V_s \cos\omega, & 0, \\ 0, & -V_p \cos\theta, & 0, & -V_s \sin\omega \\ \rho V_p^2 \cos 2\omega, & 0, & \rho V_s^2 \sin 2\omega, & 0, \\ 0, & \rho V_s^2 \sin 2\theta, & 0, & -\rho V_s^2 \cos 2\omega \end{pmatrix} \begin{pmatrix} Ae^{-i\alpha y} + Ce^{i\alpha y} \\ Ae^{-i\alpha y} - Ce^{i\alpha y} \\ Be^{-i\beta y} - De^{i\beta y} \\ Be^{-i\beta y} + De^{i\beta y} \end{pmatrix} \tag{2.7}$$

in which

$$h \cos\theta = \alpha \qquad k \cos\omega = \beta \tag{2.8}$$

In the right side of (2.7), we can find that the first matrix involves only the material constants and the angles of incidence, and is dependent neither on the period nor the amplitude of waves. Therefore we will call this matrix the characteristic matrix of that medium and express it by $[\boldsymbol{M}]$, then

$$\begin{pmatrix} \\ \boldsymbol{M} \\ \\ \end{pmatrix} = \begin{pmatrix} -V_p \sin\theta, & 0, & V_s \cos\omega, & 0 \\ 0, & -V_p \cos\theta, & 0, & -V_s \sin\omega \\ \rho V_{p1}^3 \cos 2\omega, & 0, & \rho V_s^2 \sin 2\omega, & 0 \\ 0, & \rho V_s^2 \sin 2\theta, & 0, & -\rho V_s^2 \cos 2\omega \end{pmatrix} \tag{2.10}$$

Modifying the equation (2.7), we have

$$\begin{pmatrix} \dot{u} \\ \dot{v} \\ Y_y \\ X_y \end{pmatrix} = \begin{pmatrix} \\ \boldsymbol{M} \\ \\ \end{pmatrix} \begin{pmatrix} \cos\alpha y, & -i\sin\alpha y, & 0, & 0 \\ -i\sin\alpha y, & \cos\alpha y, & 0, & 0 \\ 0, & 0, & \cos\beta y, & -i\sin\beta y \\ 0, & 0, & -i\sin\beta y, & \cos\beta y \end{pmatrix} \begin{pmatrix} A+C \\ A-C \\ B-D \\ B+D \end{pmatrix} \tag{2.10}$$

Further, solving this equation with respect to A, B, C, and D

$$\begin{pmatrix} A+C \\ A-C \\ B-D \\ B+D \end{pmatrix} = \begin{pmatrix} \cos\alpha y, & i\sin\alpha y, & 0, & 0 \\ i\sin\alpha y, & \cos\alpha y, & 0, & 0 \\ 0, & 0, & \cos\beta y, & i\sin\beta y \\ 0, & 0, & i\sin\beta y, & \cos\beta y \end{pmatrix} \begin{pmatrix} \\ \boldsymbol{M} \\ \\ \end{pmatrix}^{-1} \begin{pmatrix} \dot{u} \\ \dot{v} \\ Y_y \\ X_y \end{pmatrix} \tag{2.11}$$

where $[\boldsymbol{M}]^{-1}$ is the reciprocal matrix of the characteristic matrix $[\boldsymbol{M}]$, and its elements all take finite value except on the occasion when the determinant $|\boldsymbol{M}|$ vanishes.

Calculating this reciprocal matrix actually, we get

$$\left(\begin{array}{c} \\ \boldsymbol{M} \\ \\ \end{array}\right)^{-1} = \begin{pmatrix} -\dfrac{V_s \sin 2\omega}{V_p^2 \cos\omega}, & 0, & \dfrac{1}{\rho V_p^2}, & 0 \\ 0, & -\dfrac{\cos 2\omega}{V_p \cos\theta}, & 0, & \dfrac{\sin\theta}{\rho V_p^2 \cos\theta} \\ \dfrac{\cos 2\omega}{V_s \cos\omega}, & 0, & \dfrac{\sin\omega}{\rho V_s^2 \cos\omega}, & 0 \\ 0, & -\dfrac{\sin 2\theta}{V_p \cos\theta}, & 0, & -\dfrac{1}{\rho V_s^2} \end{pmatrix} \tag{2.12}$$

Now, if we substitute $y+d$ for y in the equation (2.10), and put the equation (2.11) into the relation just obtained

$$\begin{aligned} \begin{pmatrix} \dot{u} \\ \dot{v} \\ Y_y \\ X_y \end{pmatrix}_{y+d} &= \left(\begin{array}{c} \\ \boldsymbol{M} \\ \\ \end{array}\right) \begin{pmatrix} \cos\alpha(y+d), & -i\sin\alpha(y+d), & 0, & 0 \\ -i\sin\alpha(y+d), & \cos\alpha(y+d), & 0, & 0 \\ 0, & 0, & \cos\beta(y+d), & -i\sin\beta(y+d) \\ 0, & 0, & -i\sin\beta(y+d), & \cos\beta(y+d) \end{pmatrix} \\ &\quad \times \begin{pmatrix} \cos\alpha y, & i\sin\alpha y, & 0, & 0 \\ i\sin\alpha y, & \cos\alpha y, & 0, & 0 \\ 0, & 0, & \cos\beta y, & i\sin\beta y \\ 0, & 0, & i\sin\beta y, & \cos\beta y \end{pmatrix} \left(\begin{array}{c} \\ \boldsymbol{M} \\ \\ \end{array}\right)^{-1} \begin{pmatrix} \dot{u} \\ \dot{v} \\ Y_y \\ X_y \end{pmatrix}_y \\ &= \left(\begin{array}{c} \\ \boldsymbol{M} \\ \\ \end{array}\right) \begin{pmatrix} \cos\alpha d, & -i\sin\alpha d, & 0, & 0 \\ -i\sin\alpha d, & \cos\alpha d, & 0, & 0 \\ 0, & 0, & \cos\beta d, & -i\sin\beta d \\ 0, & 0, & -i\sin\beta d, & \cos\beta d \end{pmatrix} \left(\begin{array}{c} \\ \boldsymbol{M} \\ \\ \end{array}\right)^{-1} \begin{pmatrix} \dot{u} \\ \dot{v} \\ Y_y \\ X_y \end{pmatrix}_y \end{aligned} \tag{2.13}$$

This is the very relation connecting the elements on the plane $y=y$ and that on $y=y+d$, which is invariable even if the conditions of the outer part of the plenes $y=y$ and $y=y+d$ are replaced by different ones.

Now we assume that there exist n discontinuous boundary planes perpendicular to y-axis and lying at $y=y_1, y_2, y_3, \ldots . y_n$. Expressing the elements on the boundary plane $y=y_k$ by the suffix k, we get the relation generally

$$\begin{pmatrix} \dot{u} \\ \dot{v} \\ Y_y \\ X_y \end{pmatrix}_{y_k} = \left(\begin{array}{c} \\ \boldsymbol{K}_{k-1} \\ \\ \end{array}\right) \begin{pmatrix} \dot{u} \\ \dot{v} \\ Y_y \\ X_y \end{pmatrix}_{y_{k-1}} \tag{2.14}$$

where

$$\begin{pmatrix} \\ \boldsymbol{K}_{k-1} \\ \\ \end{pmatrix} = \begin{pmatrix} \\ \boldsymbol{M}_{k-1} \\ \\ \end{pmatrix} \begin{pmatrix} \cos\alpha_{k-1}(y_k-y_{k-1}), & -i\sin\alpha_{k-1}(y_k-y_{k-1}), \\ -i\sin\alpha_{k-1}(y_k-y_{k-1}), & \cos\alpha_{k-1}(y_k-y_{k-1}), \\ 0, & 0, \\ 0, & 0, \end{pmatrix}$$

$$\begin{pmatrix} 0, & 0 \\ 0, & 0 \\ \cos\beta_{k-1}(y_k-y_{k-1}), & -i\sin\beta_{k-1}(y_k-y_{k-1}) \\ -i\sin\beta_{k-1}(y_k-y_{k-1}), & \cos\beta_{k-1}(y_k-y_{k-1}) \end{pmatrix} \begin{pmatrix} \\ \boldsymbol{M}_{k-1} \\ \\ \end{pmatrix}^{-1} \tag{2.15}$$

The matrix $[\boldsymbol{M}_{k-1}]$ is the characteristic matrix defined by the medium between $y=y_{k-1}$ and $y=y_k$.

If we connect the boundary conditions by the relation (2.14) from y_1-plane to y_n-plane, in the order of $k=2, 3, 4, \ldots . n$, we reach the following result;

$$\begin{pmatrix} \dot{u} \\ \dot{v} \\ Y_y \\ X_y \end{pmatrix}_{y_n} = \begin{pmatrix} \\ \boldsymbol{K}_{n-1} \\ \\ \end{pmatrix} \begin{pmatrix} \\ \boldsymbol{K}_{n-2} \\ \\ \end{pmatrix} \cdots \begin{pmatrix} \\ \boldsymbol{K}_1 \\ \\ \end{pmatrix} \begin{pmatrix} \dot{u} \\ \dot{v} \\ Y_y \\ X_y \end{pmatrix}_{y_1} = \begin{pmatrix} \\ \boldsymbol{L} \\ \\ \end{pmatrix} \begin{pmatrix} \dot{u} \\ \dot{v} \\ Y_y \\ X_y \end{pmatrix}_{y_1} \tag{2.16}$$

where

$$\begin{pmatrix} \\ \boldsymbol{L} \\ \\ \end{pmatrix} = \begin{pmatrix} l_{11} & l_{12} & l_{13} & l_{14} \\ l_{21} & l_{22} & l_{23} & l_{24} \\ l_{31} & l_{32} & l_{34} & l_{35} \\ l_{41} & l_{42} & l_{43} & l_{44} \end{pmatrix} = \begin{pmatrix} \\ \boldsymbol{K}_{n-1} \\ \\ \end{pmatrix} \begin{pmatrix} \\ \boldsymbol{K}_{n-2} \\ \\ \end{pmatrix} \cdots \begin{pmatrix} \\ \boldsymbol{K}_1 \\ \\ \end{pmatrix} \tag{2-17}$$

Equation (2.16) is the relation connecting the elements on the plane of discontinuity $y=y_n$ and that on $y=y_1$. Here $[\boldsymbol{L}]$ is the product of $3(n-1)$ matrices shown in (2.17) and (2.15). The equation (2.16) indicates that the velocity and stress component at y_n-plane can be calculated by operating $3n$ matrices to the velocity and stress components at y_1-plane.

3. The Solution when the Multilayered Medium Exists between Two Semi-Infinite Elastic Media.

First we assume that n discontinuities exist at $y=y_1, y_2, y_3, \ldots, y_n$ and dilatational wave is incident upon y_1 plane as shown in Fig. 2. Further, we denote the amplitudes of waves as follows;

Incident P-wave: $\mathfrak{A}$
Transmitted P-wave: A^*
Transmitted S-wave: B^*

Reflected P-wave: C^*
Reflected S-wave: D^*

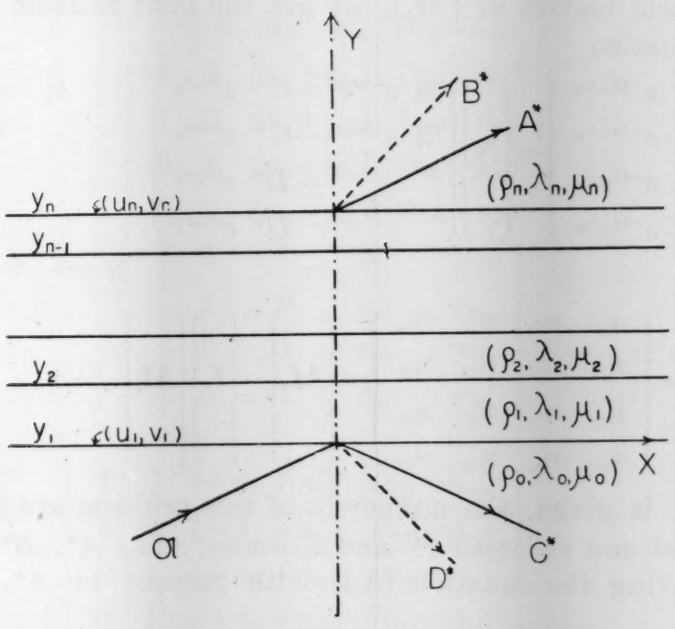

Fig. 2.

From the equation (2.7), the velocity and stress components which are produced on y_1 plane by the waves $\mathfrak{A}$, C^* and D^* are expressed as

$$\begin{pmatrix} \dot{u} \\ \dot{v} \\ Y_y \\ X_y \end{pmatrix}_{y_1} = \begin{pmatrix} \\ \boldsymbol{M}_0 \\ \\ \end{pmatrix} \begin{pmatrix} \mathfrak{A}\ e^{-i\alpha_0 y_1} + C^*\ e^{i\alpha_0 y_1} \\ \mathfrak{A}\ e^{-i\alpha_0 y_1} - C^*\ e^{i\alpha_0 y_1} \\ -D^*\ e^{i\beta_0 y_1} \\ D^*\ e^{i\beta_0 y_1} \end{pmatrix} \tag{3.1}$$

$$\begin{pmatrix} \dot{u} \\ \dot{v} \\ Y_y \\ X_y \end{pmatrix}_{y_n} = \begin{pmatrix} \\ \boldsymbol{M}_n \\ \\ \end{pmatrix} \begin{pmatrix} A^*\ e^{-i\alpha_n y_n} \\ A^*\ e^{-i\alpha_n y_n} \\ B^*\ e^{-i\beta_n y_n} \\ B^*\ e^{-i\beta_n y_n} \end{pmatrix} \tag{3.2}$$

Put these equations into (2.16), and we have

$$\begin{pmatrix} \\ \boldsymbol{M}_n \\ \\ \end{pmatrix} \begin{pmatrix} A^*\ e^{-i\alpha_n y_n} \\ A^*\ e^{-i\alpha_n y_n} \\ B^*\ e^{-i\beta_n y_n} \\ B^*\ e^{-i\beta_n y_n} \end{pmatrix} = \begin{pmatrix} \\ \boldsymbol{L} \\ \\ \end{pmatrix} \begin{pmatrix} \\ \boldsymbol{M}_0 \\ \\ \end{pmatrix} \begin{pmatrix} \mathfrak{A}\ e^{-i\alpha_0 y_1} + C^*\ e^{i\alpha_0 y_1} \\ \mathfrak{A}\ e^{-i\alpha_0 y_1} - C^*\ e^{i\alpha_0 y_1} \\ -D^*\ e^{i\beta_0 y_1} \\ D^*\ e^{i\beta_0 y_1} \end{pmatrix} \tag{3.3}$$

where $[M_n]$ and $[M_0]$ are the characteristic matrices which are determined by the medium $y>y_n$ and the medium $y<y_1$ respectively. When there exists reciprocal matrix of $[M_n]$, we get the next relation by modifying the above equation

$$\begin{pmatrix} A^* e^{-i\alpha_n y_n} \\ A^* e^{-i\alpha_n y_n} \\ B^* e^{-i\beta_n y_n} \\ B^* e^{-i\beta_n y_n} \end{pmatrix} = \begin{pmatrix} \\ N \\ \\ \end{pmatrix} \begin{pmatrix} \mathfrak{A} e^{-i\alpha_0 y_1} + C^* e^{i\alpha_0 y_1} \\ \mathfrak{A} e^{-i\alpha_0 y_1} - C^* e^{i\alpha_0 y_1} \\ -D^* e^{i\beta_0 y_1} \\ D^* e^{i\beta_0 y_1} \end{pmatrix} \tag{3.4}$$

where

$$\begin{pmatrix} \\ N \\ \\ \end{pmatrix} = \begin{pmatrix} n_{11} & n_{12} & n_{13} & n_{14} \\ n_{21} & n_{22} & n_{23} & n_{24} \\ n_{31} & n_{32} & n_{33} & n_{34} \\ n_{41} & n_{42} & n_{43} & n_{44} \end{pmatrix} = \begin{pmatrix} \\ M_n \\ \\ \end{pmatrix}^{-1} \begin{pmatrix} \\ L \\ \\ \end{pmatrix} \begin{pmatrix} \\ M_0 \\ \\ \end{pmatrix} \tag{3.5}$$

When $\mathfrak{A}$ is given, the unknowns of this problem are the amplitudes of transmitted and reflected P- and S-waves; viz., A^*, B^*, C^*, and D^*. Therefore solving the equation (3.4) with respect to A^*, B^*, C^* and D^*, we get

$$\begin{pmatrix} A^* \\ B^* \\ C^* \\ D^* \end{pmatrix} = \begin{pmatrix} e^{-i\alpha_n y_n} & 0 & (-n_{11}+n_{12})e^{i\alpha_0 y_1} & (n_{13}-n_{14})e^{i\beta_0 y_1} \\ e^{-i\alpha_n y_n} & 0 & (-n_{21}+n_{22})e^{i\alpha_0 y_1} & (n_{23}-n_{24})e^{i\beta_0 y_1} \\ 0 & e^{-i\beta_n y_n} & (-n_{31}+n_{32})e^{i\alpha_0 y_1} & (n_{33}-n_{34})e^{i\beta_0 y_1} \\ 0 & e^{-i\beta_n y_n} & (-n_{41}+n_{42})e^{i\alpha_0 y_1} & (n_{43}-n_{44})e^{i\beta_0 y_1} \end{pmatrix}^{-1}$$

$$\times \begin{pmatrix} n_{11}+n_{12} \\ n_{21}+n_{22} \\ n_{31}+n_{32} \\ n_{41}+n_{42} \end{pmatrix} \mathfrak{A} e^{-i\alpha_0 y_1} \tag{3.6}$$

This is the solution we seek for, and it gives the amplitudes of reflected and transmitted waves. Here, $[N]$ is the product of $(3n-1)$ matrices of the 4th order shown in the equations (3.5), (2.17) and (2.1). In actual treatment, the next formula is more convenient for numerical calculation. That is,

$$A^* = -\frac{2\, e^{-i(\alpha_0 y_1 - \alpha_n y_n)}\, \mathfrak{A}}{\Gamma} \begin{vmatrix} 0 & n_{11} & n_{12} & (n_{13}-n_{14}) \\ 0 & n_{21} & n_{22} & (n_{23}-n_{24}) \\ 1 & n_{31} & n_{32} & (n_{32}-u_{34}) \\ 1 & n_{41} & n_{42} & (n_{43}-n_{44}) \end{vmatrix}$$

$$
\left.\begin{aligned}
B^* &= \frac{2\,e^{-i(\alpha_0 y_1-\beta_n y_n)}\,\mathfrak{A}}{\Gamma}\begin{vmatrix} 1 & n_{11} & n_{21} & (n_{13}-n_{14}) \\ 1 & n_{21} & n_{22} & (n_{23}-n_{24}) \\ 0 & n_{31} & n_{32} & (n_{33}-n_{34}) \\ 0 & n_{41} & n_{42} & (n_{43}-n_{44}) \end{vmatrix} \\
C^* &= \frac{e^{-2i\alpha_0 y_1}\,\mathfrak{A}}{\Gamma}\begin{vmatrix} 1 & 0 & (n_{11}+n_{12}) & (n_{13}-n_{14}) \\ 1 & 0 & (n_{21}+n_{22}) & (n_{23}-n_{21}) \\ 0 & 1 & (n_{31}+n_{32}) & (n_{33}-n_{34}) \\ 0 & 1 & (n_{41}+n_{42}) & (n_{43}-n_{44}) \end{vmatrix} \\
D^* &= \frac{2\,e^{-i(\alpha_0-\beta_0)y_1}\,\mathfrak{A}}{\Gamma}\begin{vmatrix} 1 & 0 & n_{11} & n_{12} \\ 1 & 0 & n_{21} & n_{22} \\ 0 & 1 & n_{31} & n_{32} \\ 0 & 1 & n_{41} & n_{42} \end{vmatrix}
\end{aligned}\right\} \quad (3.7)
$$

where

$$
\Gamma = \begin{vmatrix} 1 & 0 & (-n_{11}+n_{12}) & (n_{13}-n_{14}) \\ 1 & 0 & (-n_{21}+n_{22}) & (n_{23}-n_{24}) \\ 0 & 1 & (-n_{31}+n_{32}) & (n_{33}-n_{34}) \\ 0 & 1 & (-n_{41}+n_{42}) & (n_{43}-n_{44}) \end{vmatrix}
$$

4. The Reflection at the Surface of the Layered Crust.

In the foregoing paragraph, we have treated the case in which the multilayered medium is placed between two semi-infinite elastic media. But in actual cases, our observation of seismic wave is performed at the free surface of the earth crust which are known to have layered structure. Therefore the problem must be treated in which one boundary plane is free from any traction.

In order to solve this problem in this section, first we assume the boundary plane at $y=y_n$ to be free, and denote the amplitudes of incident P-, reflected P- and reflected S-wave as $\mathfrak{A}$, C^* and D^* respectively.

From (2.16) and (3.1), we get

$$
\begin{pmatrix} \dot{u} \\ \dot{v} \\ Y_y \\ X_y \end{pmatrix}_{y_n} = \begin{pmatrix} \\ \boldsymbol{L} \\ \\ \end{pmatrix} \begin{pmatrix} \\ \boldsymbol{M}_0 \\ \\ \end{pmatrix} \begin{pmatrix} \mathfrak{A}\,e^{-i\alpha_0 y_1}+C^*\,e^{i\alpha_0 y_1} \\ \mathfrak{A}\,e^{-i\alpha_0 y_1}-C^*\,e^{i\alpha_0 y_1} \\ -D^*\,e^{i\beta_0 y_1} \\ D^*\,e^{i\beta_0 y_1} \end{pmatrix} = \begin{pmatrix} \\ \boldsymbol{F} \\ \\ \end{pmatrix} \begin{pmatrix} \mathfrak{A}\,e^{-i\alpha_0 y_1}+C^*\,e^{i\alpha_0 y_1} \\ \mathfrak{A}\,e^{-i\alpha_0 y_1}-C^*\,e^{i\alpha_0 y_1} \\ -D^*\,e^{i\beta_0 y_1} \\ D^*\,e^{i\beta_0 y_1} \end{pmatrix} \quad (4.1)
$$

where

$$\begin{pmatrix} \\ \boldsymbol{F} \\ \\ \end{pmatrix} = \begin{pmatrix} f_{11} & f_{12} & f_{13} & f_{14} \\ f_{21} & f_{22} & f_{23} & f_{24} \\ f_{31} & f_{32} & f_{33} & f_{34} \\ f_{41} & f_{42} & f_{43} & f_{44} \end{pmatrix} = \begin{pmatrix} \\ \boldsymbol{L} \\ \\ \end{pmatrix} \begin{pmatrix} \\ \boldsymbol{M}_0 \\ \\ \end{pmatrix} \tag{4.2}$$

From the condition of free surface, normal stress Y_y and tangential stress X_y vanish at $y=y_n$. Putting this condition into (4.1), we get

$$\begin{pmatrix} C^* \\ D^* \end{pmatrix} = \begin{pmatrix} (-f_{31}+f_{32})e^{i\alpha_0 y_1} & (f_{33}-f_{34})e^{i\beta_0 y_1} \\ (-f_{41}+f_{42})e^{i\alpha_0 y_1} & (f_{43}-f_{44})e^{i\beta_0 y_1} \end{pmatrix}^{-1} \begin{pmatrix} f_{31}+f_{32} \\ f_{41}+f_{42} \end{pmatrix} \mathfrak{A} e^{-i\alpha_0 y_1} \tag{4.3}$$

or employing the expression of another form

$$\left.\begin{aligned} C^* &= \frac{e^{-2i\alpha_0 y_1}\ \mathfrak{A}}{\Gamma} \begin{vmatrix} (f_{31}+f_{32}) & (f_{33}-f_{34}) \\ (f_{41}+f_{42}) & (f_{43}-f_{44}) \end{vmatrix} \\ D^* &= \frac{-2\, e^{-i(\alpha_0+\beta_0)y_1}\ \mathfrak{A}}{\Gamma} \begin{vmatrix} f_{31} & f_{32} \\ f_{41} & f_{42} \end{vmatrix} \end{aligned}\right\} \tag{4.4}$$

where

$$\Gamma = \begin{vmatrix} (-f_{31}+f_{32}) & (f_{33}-f_{34}) \\ (-f_{41}+f_{42}) & (f_{43}-f_{44}) \end{vmatrix}$$

5. When the Incident Wave is Distortional.

In the foregoing problems, we have treated chiefly the case in which the incident wave is dilatational. Here we start under the condition that the incident wave is distortional and the displacement is involved in xy-plane (SV type wave). If we put the amplitudes of distortional wave as $\mathfrak{B}$, we get the expression corresponding to (3.1),

$$\begin{pmatrix} \dot{u} \\ \dot{v} \\ Y_y \\ X_y \end{pmatrix}_{y_1} = \begin{pmatrix} \\ \boldsymbol{M}_0 \\ \\ \end{pmatrix} \begin{pmatrix} C^*\ e^{i\alpha_0 y_1} \\ -C^*\ e^{i\alpha_0 y_1} \\ \mathfrak{B}\, e^{-i\beta_0 y_1} - D^*\ e^{i\beta_0 y_1} \\ \mathfrak{B}\, e^{-i\beta_0 y_1} + D^*\ e^{i\beta_0 y_1} \end{pmatrix} \tag{5.1}$$

Further calculation is quite similar to the foregoing one. Resulting equation corresponding to (3.6) is as follows:

$$\begin{pmatrix} A^* \\ B^* \\ C^* \\ D^* \end{pmatrix} = \begin{pmatrix} e^{-i\alpha_n y_n} & 0 & (-n_{11}+n_{12})e^{i\alpha_0 y_1} & (n_{13}-n_{14})e^{i\beta_0 y_1} \\ e^{-i\alpha_n y_n} & 0 & (-n_{21}+n_{22})e^{i\alpha_0 y_1} & (n_{23}-n_{24})e^{i\beta_0 y_1} \\ 0 & e^{-i\beta_n y_n} & (-n_{31}+n_{32})e^{i\alpha_0 y_1} & (n_{33}-n_{34})e^{i\beta_0 y_1} \\ 0 & e^{-i\beta_n y_n} & (-n_{41}+n_{42})e^{i\alpha_0 y_1} & (n_{43}-n_{44})e^{i\beta_0 y_1} \end{pmatrix}^{-1} \begin{pmatrix} n_{13}+n_{14} \\ n_{23}+n_{24} \\ n_{33}+n_{34} \\ n_{43}+n_{44} \end{pmatrix} \mathfrak{B}\, e^{-i\beta_0 y_1} \tag{5.2}$$

6. Numerical Examples.

We treat here the case $n=2$, that is, the case of a single layer existing. In this circumstance, the matrix $[\boldsymbol{N}]$ in (3.5) becomes $[\boldsymbol{M}_2]^{-1} \times [\boldsymbol{K}_1]\,[\boldsymbol{M}_0]$.

We assume that Poisson's ratio σ is 1/4 in each medium and the incident angle of P-wave θ_0 is $\pi/6$. We take two models of the layered medium, one containing the low velocity layer among the high velocity media, and the other containing the high velocity layer.

In the former case, we assume that the ratio of the P-wave velocity and that of the density in each medium are as follows:

$$V_{p0} : V_{p1} : V_{p2} = 1 : 1/2 : 1$$
$$\rho_0 : \rho_1 : \rho_2 = 1 : 3/4 : 1$$

The results of numerical calculation are shown in Table I and Fig. 3.

In the latter case, the ratio of the P-wave velocity and that of the density in each medium are as follows:

$$V_{p0} : V_{p1} : V_{p2} = 1 : \sqrt{2} : 1$$
$$\rho_0 : \rho_1 : \rho_2 = 1 : 4/3 : 1$$

The results of numerical calculation are shown in Table II and Fig. 4.

In both figures, we take the ordinate as the ratio of the absolute value of the amplitude of transmitted and reflected P-wave A^* and C^* to that of incident wave $\mathfrak{A}$, and the abscissa as the ratio of thickness of the layer d to the wave length L of P-wave in that layer.

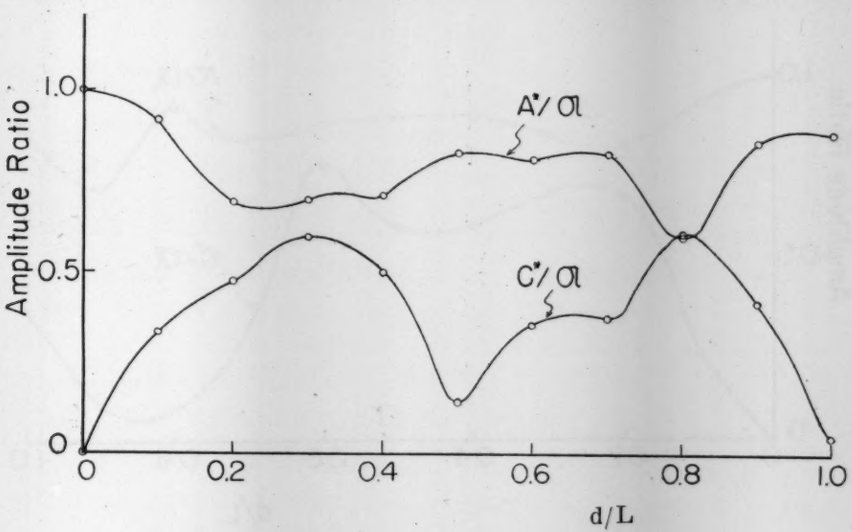

Fig. 3. Amplitude Ratio (low velocity layer)
($\theta_0 = \frac{\pi}{6}$, $V_{p0} : V_{p1} : V_{p2} = 1 : 1/2 : 1$, $\rho_0 : \rho_1 : \rho_2 = 1 : 3/4 : 1$)

Table I. Amplitude Ratio (low velocity layer).

d/L	0	0.1	0.2	0.3	0.4	0.5	0.6	0.7	0.8	0.9	1.0
Transmitted *P*-wave	1.0000	0.9180	0.6893	0.6928	0.7053	0.8251	0.8071	0.8206	0.5932	0.8533	0.8753
Transmitted *S*-wave	0.0000	0.1520	0.1807	0.7192	0.8556	0.6251	0.6944	0.9196	0.8648	0.4805	0.5023
Reflected *P*-wave	0.0000	0.3373	0.4748	0.5929	0.4992	0.1407	0.3568	0.3774	0.6001	0.4165	0.0459
Reflected *S*-wave	0.0000	1.0250	1.1660	0.6052	0.6425	0.6608	0.7354	0.6191	0.7988	0.4638	0.8632

Table II. Amplitude Ratio (high velocity layer).

d/L	0	0.1	0.2	0.3	0.4	0.5	0.6	0.7	0.8	0.9	1.0
Transmitted *P*-wave	1.0000	0.9248	0.8048	0.8345	0.8878	0.8865	0.8671	0.8268	0.9147	0.6932	0.8668
Transmitted *S*-wave	0.0000	0.2519	0.4693	0.5866	0.6389	0.8508	0.8993	0.7699	0.6772	0.6336	0.8837
Reflected *P*-wave	0.0000	0.2380	0.6662	0.6785	0.5861	0.5812	0.7529	0.3176	0.0855	0.0977	0.3607
Reflected *S*-wave	0.0000	0.5895	0.6804	0.7372	0.4192	0.4738	0.9521	0.8977	0.5280	0.4107	1.4150

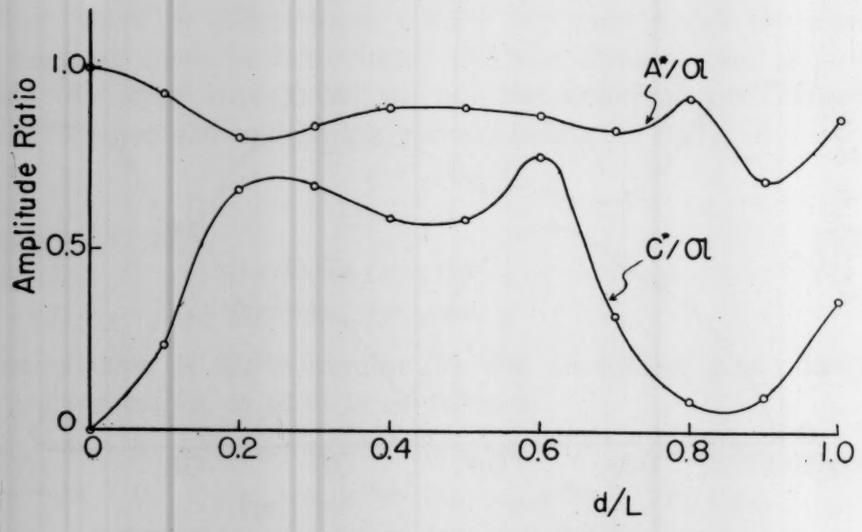

Fig. 4. Amplitude Ratio (high velocity layer)
($\theta_0=\frac{\pi}{6}$, $V_{p0}:V_{p1}:V_{p2}=1:\sqrt{2}:1$, $\rho_0:\rho_1:\rho_2=1:{}^4/_3:1$)

7. Acknowledgement.

At the end of this paper, I would like to express my thanks to Prof. T. Matuzawa and Prof. T. Hagiwara for the instructions they have kindly given me. My hearty thanks are also due to Assist. Prof. Y. Satô who afforded me useful advices and facilities for this calculation and revised this paper with goodwill.

---

25. いくつかの平行な不連続面による地震波の反射及び透過

地震研究所　松　本　利　松

平行な不連続面が一般に n 個ある場合に弾性波の反射・屈折の問題を解くことは原理的には簡単であるが，実際の取扱では非常に繁雑になる．ここではマトリツクスによる表現を用いて P 波及び SV 波入射に対する反射波及び透過波の振幅を求めた．

単一層の介在する場合についての数値計算の結果は，波長に対してかなりに薄い層でも相当に大きな反射波の振幅を与えることがわかつた．

---

26. *Relation between the Amplitude of Earthquake Motions and the Nature of Surface Layer. III.*

By Kiyoshi KANAI and Shizuyo YOSHIZAWA,

Earthquake Research Institute.

(Read Sept. 22, 1953.—Received Oct. 1, 1953.)

The present paper is the continuation of our research work on the problem of earthquake movement of superficial stratum and deals with the case where the primary seismic waves are incident upwards normally to trebly stratified layers residing on the surface of a semi-infinite body.

Let, ρ_1, μ_1, V_1, H_1; ρ_2, μ_2, V_2, H_2; ρ_3, μ_3, V_3, H_3 be the density, rigidity, velocity and the thickness of the first layer, the second layer and the third layer respectively, and ρ_4, μ_4, V_4, be the density, rigidity, velocity of the bottom medium. Again, let U_1, U_2, U_3, U_4, be the respective displacements in the first layer, the second layer, the third layer and the bottom medium. And, H represents the thickness between the free surface and the bottom medium, that is, $H=H_1+H_2+H_3$.

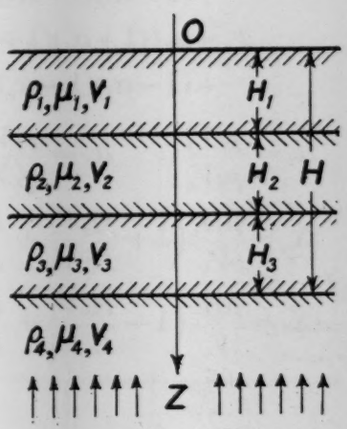

Fig. 1.

Then the equation of motion of each medium is written as follows;

$$\mu_n \frac{\partial^2 U_n}{\partial z^2} = \rho_n \frac{\partial^2 U_n}{\partial t^2}. \qquad [n=1,2,3,4] \tag{1}$$

The typical solutions of this equation are expressed by

$$\left.\begin{aligned} U_4 &= \mathfrak{A} e^{i(pt+f_4 z)} + B_4 e^{i(pt-f_4 z)}, \\ U_n &= A_n e^{i(pt+f_n z)} + B_n e^{i(pt-f_n z)}, \quad [n=1,2,3] \end{aligned}\right\} \tag{2}$$

where $\mathfrak{A}$ is the amplitude of the incident waves and B_4, B_3, B_2, B_1; A_3, A_2, A_1 are arbitrary constants to be determined from the boundary conditions. $2\pi/p$ and $2\pi/f$ mean the period and the wave length.

The boundary condition at the plane $z=0$ is

$$\frac{\partial U_1}{\partial z} = 0, \tag{3}$$

and the boundary conditions at the planes $z=H_1$, $z=H_1+H_2$, $z=H_1+H_2+H_3$ ($\equiv H$) are as follows;

$$U_n=U_{n+1}, \tag{4}$$

$$\mu_n\frac{\partial U_n}{\partial z}=\mu_{n+1}\frac{\partial U_{n+1}}{\partial z}. \qquad [n=1,2,3] \tag{5}$$

In the case of dilatational waves, it is necessary to replace μ by $\lambda+2\mu$. Putting equation (2) into equations (3)–(5), we find finally

$$\frac{|U_{1_{H_1=0}}|}{2|U_0|}=\frac{4}{\sqrt{\Phi_1^2+\Phi_2^2}}, \tag{6}$$

in which

$$\left.\begin{aligned}\Phi_1&=(1+\alpha_1)(1+\alpha_2)\cos X_1+(1+\alpha_1)(1-\alpha_2)\cos X_2\\&\quad+(1-\alpha_1)(1-\alpha_2)\cos X_3+(1-\alpha_1)(1+\alpha_2)\cos X_4,\\\Phi_2&=\alpha_3\{(1+\alpha_1)(1+\alpha_2)\sin X_1-(1+\alpha_1)(1-\alpha_2)\sin X_2\\&\quad+(1-\alpha_1)(1-\alpha_2)\sin X_3-(1-\alpha_1)(1+\alpha_2)\sin X_4\},\end{aligned}\right\} \tag{7}$$

$$\left.\begin{aligned}&\alpha_1=\frac{\rho_1V_1}{\rho_2V_2}, \quad \alpha_2=\frac{\rho_2V_2}{\rho_3V_3}, \quad \alpha_3=\frac{\rho_3V_3}{\rho_4V_4},\\&X_1=\frac{pH_1}{V_1}\left(1+\frac{H_2V_1}{H_1V_2}+\frac{H_3V_1}{H_1V_3}\right), \quad X_2=\frac{pH_1}{V_1}\left(1+\frac{H_2V_1}{H_1V_2}-\frac{H_3V_1}{H_1V_3}\right),\\&X_3=\frac{pH_1}{V_1}\left(1-\frac{H_2V_1}{H_1V_2}+\frac{H_3V_1}{H_1V_3}\right), \quad X_4=\frac{pH_1}{V_1}\left(1-\frac{H_2V_1}{H_1V_2}-\frac{H_3V_1}{H_1V_3}\right).\end{aligned}\right\} \tag{8}$$

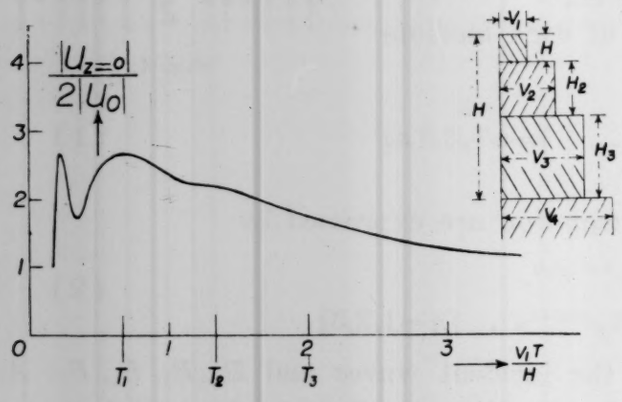

Fig. 2. $H_1:H_2:H_3=1:2:3$, $V_1:V_2:V_3:V_4=1:2:3:4$, $\rho_1=\rho_2=\rho_3=\rho_4$.

Some special cases are calculated using equations (6), (7) and (8), and are plotted in the following drawings. Figs. 2, 3 and 4 are the cases of (i) $H_1:H_2:H_3:=1:2:3$, $V_1:V_2:V_3:V_4=1:2:3:4$, (ii) $H_1:H_2:H_3=1:2:6$, $V_1:V_2:V_3:V_4=1:2:3:4$ and (iii) $H_1:H_2:H_3=1:3:6$, $V_1:V_2:V_3:V_4=1:2:4:8$ respectively, besides the conditions $\rho_1=\rho_2=\rho_3=\rho_4$ are in common. In these figures, T_1, T_2, and T_3 represent the period of free oscillations of the first layer, the upper two layers and the whole layers respectively, that is, $T_1=4H_1/V_1$, $T_2=4(H_1/V_1+H_2/V_2)$ and $T_3=4(H_1/V_1+$

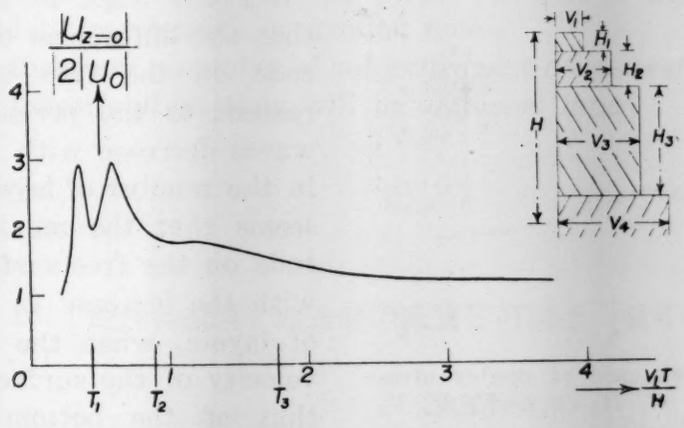

Fig. 3. $H_1:H_2:H_3=1:2:6$, $V_1:V_2:V_3:V_4=1:2:3:4$, $\rho_1=\rho_2=\rho_3=\rho_4$.

$H_2/V_2+H_3/V_3$). Figs. 2, 3 and 4 show that, even when the period of seismic waves synchronize with T_2 or T_3, the amplitude on the free surface becomes slightly larger than the cases of other periods. In other words, Figs. 2, 3 and 4 tell us that, neither in the upper two layers nor in the whole layers, resonance-like phenomena appear clearly.

On the other hand, the resonance-like phenomenon of the first layer appeared clearly, and the maximum amplitude on the free surface is somewhat small compared with that of a superficial layer.

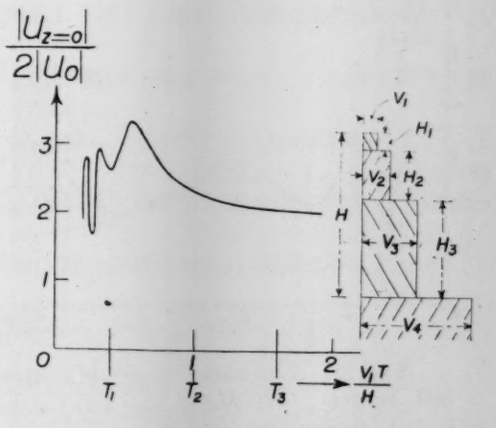

Fig. 4. $H_1:H_2:H_3=1:3:6$, $V_1:V_2:V_3:V_4=1:2:4:8$, $\rho_1=\rho_2=\rho_3=\rho_4$.

The cause of the phenomena mentioned above is the coherent effect which exists among the waves reflected at different boundary planes.

In order to ascertain the coherent effect of the seismic waves in the surface stratum, we illustrate the results of the numerical calculations of such cases as doubly stratified layers,[1] a stratified layer[2] and a surface layer of varying elasticity,[3] which were studied previously, in Figs. 5–8.

1) K. KANAI, "Relation between the Nature of Surface Layer and the Amplitude of Earthquake Motions. II", *Bull. Earthq. Res. Inst.*, **31** (1953), 219.

2) K. SEZAWA and K. KANAI, "Decay Constants of Seismic Vibrations of a Surface Layer", *Bull. Earthq. Res. Inst.*, **13** (1935), 251.

3) K. SEZAWA and K. KANAI, "The Rate of Damping in Seismic Vibrations of a Surface Layer of Varying Density or Elasticity", *Bull. Earthq. Res. Inst.*, **13** (1935), 484.

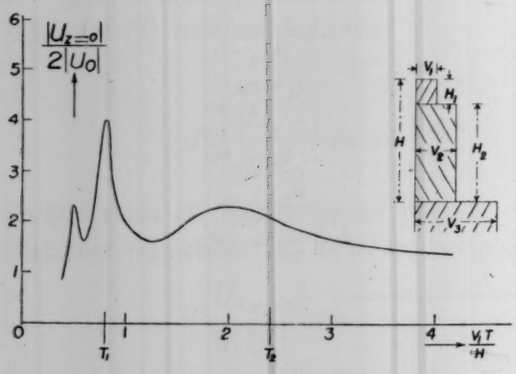

Fig. 5. The case of doubly stratified layers. $H_1:H_2=1:4$, $V_1:V_2:V_3=1:2:4$, $\rho_1=\rho_2=\rho_3$.

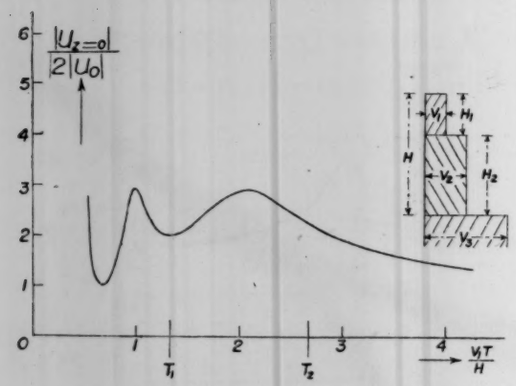

Fig. 6. The case of doubly stratified layers. $H_1:H_2=1:2$, $V_1:V_2:V_3=1:2:4$, $\rho_1=\rho_2=\rho_3$.

From Figs. 2–8, it appears that the differences of the amplitude on the free surface with respect to the period of incident waves decrease with the increase in the number of layers. And, it seems that the maximum amplitude on the free surface decreases with the increase in the number of layers, when the ratio of the velocity of the surface medium to that of the bottom medium is constant.

The results of the observational studies show that, when the superficial stratum consists of more than two layers as in the down-town of Tokyo, the relation of frequency to period of the ground movements which are caused by earthquake or ground noise is represented by a flat curve. On the other hand, when the superficial stratum is a layer such as in the up-town of Tokyo, the relation of frequency to period of the ground movements is described by a predominant sharp peak.

Now, it is noteworthy that the diagrammatical features of the results of the present theoretical investigations closely resembles the

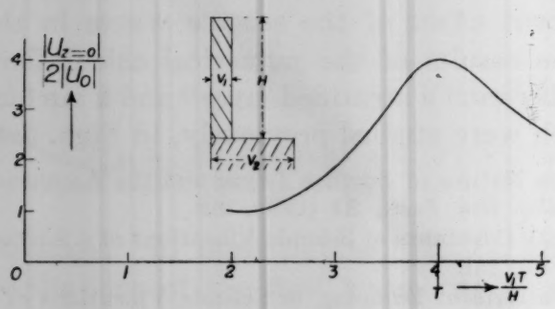

Fig. 7. The case of a stratified layer. $V_1:V_2=1:4$, $\rho_1=\rho_2$.

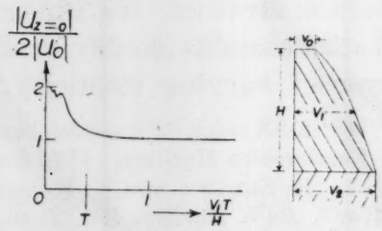

Fig. 8. The case of a surface layer of varying elasticity. $V_0:V_2=1:4$, $V_1\propto\sqrt{z}$, $\rho_1=\rho_0$.

diagramms regarding the frequency-period relation of the ground movements caused by earthquake or ground noise.

Though there are a number of subjects under consideration concerning the present investigation, they will be discussed later.

---

26. 地震動振幅と地表層の性質との関係　第4報

地震研究所 {金井　清
吉沢静代

弾性波地下探査の結果によると，冲積層が相当厚い土地では，弾性波速度の不連続面が，3つある場合が少くない．それで今回は，地表面近くに1層或は2層ある場合の前回の研究につづいて，3層ある場合の数理的研究を行つた．

地震波が2以上の不連続面で反射屈折をすると，それらの波が干渉し合つて，いわゆる重複反射によつて地表面の振幅が増大する度合は減らされることになる．

その結果，地表と第2層の下面の間，又は，地表と第3層の下面の間の自己振動周期にあたる周期の波が来た場合でも，地表面振幅の特別な増大はおこらず，それらの周期よりも，少し短い周期の波が来た場合に，振幅の多少の増大がある．しかし，地表第1層の自己振動周期にあたる周期の波の場合，地表面振幅は相当に増大する．

従つて，地表層の層数が増すほど，地表面振幅と震動周期との関係を示す曲線は平らになることになる．

厚い冲積層上の地震或は自然微動記録から，頻度周期曲線，振幅周期曲線を求めると，一般に，0.6秒とか1秒とかいう比較的に長い周期のところに，山ができる場合と，山がほとんどみとられない場合とがある．しかし，0.2秒とか0.4秒とかの比較的短い周期のところには，大抵の場合に，はつきりした山がみとめられる．地盤震動記録に対する，以上の解析結果は，今回の研究で，一応，理論的な説明がつく．

---

27. *The Third Explosion Seismic Observations in North-Eastern Japan.*

By The Research Group for Explosion Seismology.*

(Read Oct. 21, 1953.—Received Oct. 31, 1953.)

1. Introduction.

The third explosion seismic observations in North Eastern Japan were made on July 25th, 1952 when five tons of explosives were fired at the construction site of Isibuti dam. The place of explosion was adjacent to the site of the last two explosions utilized for the same experiments. Their results had already been published.[1)]

Nineteen temporary field stations were established along two profiles, as shown in Fig. 1. To the south from the shot point along the island arc of Japan, the seismological profile was extended for more than 300 kms as far as Tukuba, where a branch observatory of E. R. I. is located. Another profile, transverse to the island, was extended westward from the shot point, in the opposite direction to that in the last experiment.

Some necessary improvements had been made on the instruments, especially on those in distant stations. Special care was also taken to increase the ratio of signal to noise in picking up the weak initial motions. Consequently, in order to minimize the ground noise, the

---

* Members of the group, who participated in the project are as follows (in alphabetic order);

AKIMA T., ASANO S., HAGIWARA Terukazu, HORI M., KASAHARA K., KOBAYASI Naoyosi, MATUMOTO H., MATUMOTO T., MIYAMURA S., OMOTE S., OSADA K., SAITO S., SIBANO M., SIMA E., TANAKA T., TUZIURA M., WATANABE M., YAMAZAKI Y., YANAGISAWA M., (E. R. I.) ASADA T., CHUJO S., DEN N., KOBAYASI Naota, MOGI K., SATO R., (Geophys. Inst., Tokyo Univ.) UTSU T., (C. M. O.) FURUYA S., KOJIMA S., MORI K., UZIIE A., (Geol. Surv.) MINE N., NORITOMI K., SUZUKI Z., TAKAGI A., (Geophys. Inst., Tohoku Univ.) TAZIME K., (Akita Univ.), ASANUMA S., HONDA T., MURAUCHI S., (Nat. Sci. Mus.) KOZUKI A., TAMAKI H., (Geophys. Inst., Kyoto Univ.) KOONO K., NISIOKA K., YOSHIYAMA R., (Phys. Inst., Kyusyu Univ.)

1) La Groupe pour Recherches de Séismologie par Explosion, Tokio, "Observation Sismique par Explosion d'Isibuti"., *Zisin* Ser. [ii], **3** (1951), 77–82. **6** (1953), 7–12. **6** (1953), 84–90.

The Research Group for Explosion Seismology, Tokyo, "Explosion Seismic Observations in North-eastern Japan", *Bull. Earthq. Res. Inst.*, **29** (1951), 97–106, **30** (1952), 279–292.

seismometers of distant stations were set up in caves or galleries, selected after the mail investigation and field inspections. However, no essential change was seen in the observational method.

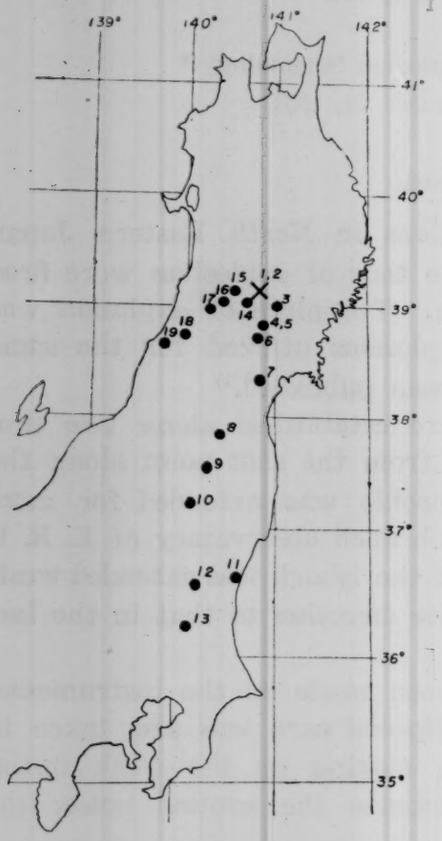

Fig. 1. Seismic observation stations for the third Isibuti explosion.

In Table I, the locations of stations and the names of observers are shown, together with some descriptions of the equipments in each station.

The communication from the shot point to each station was made available by the short wave radio network of the Tohoku District Construction Bureau and also by the civil telegram and telephone network. In addition, Nippon Hoso Kyokai (Radio Broadcasting Corporation) cooperated with the experiment in broadcasting some information about an expected time of explosion in several times before and on the very day.

The explosives were carlit as before, and the amount was 5.546 tons. They were charged in 12 chambers; three of them were inserted electric circuits fed with weak current, so that the exact time of explosion could be marked on the oscillogram by the interruption of the current. The exact time, thus registered, was 12h 04m 59.42s (Japan Standard Time). At all stations, the time marks were placed directly by the JJY short wave time signals of every second which were kept by the Tokyo Astronomical Observatory. At some stations chronometers with second contact were also employed, and some of them covered successfully the bad condition of short wave receiving.

2. Results of Observations.

In Table II, the arrival times of phases and epicentral distances are shown. The arrival times are, also, plotted in Fig. 2 and grouped in several straight lines. Travel times in the southern profile are given by

Table I. The third Isibuti explosion-seismic observations.
(1952-VII-25, 12h 04m 59.42s, φ=39° 06′ 22″ N, λ=140° 53′ 39″ E, h=300 m)

		Observation point	Location		Distance from shot	Seismographs	Amplifier	Observers
Southern profile	1	Shot point	Near the shot point		0~2km	Haeno type-5 (12c/s)	None	Kozima, Furuya
	2	South point from shot			2~4	Haeno type-4	D-2	Mori, Uziie
	3	Hondera	140°58′.5 E	38°58′.4 N	15.3	3V-1, 3H-1 10V-1	D-3	Hori, Tuziura
	4	Hosokura (I)	140 54.6	38 38.2	32.2	H-1	Kyoto Univ.-H	Kozuki
	5	Hosokura (II)			32.2	3V-1	None	Yosiyama, Nisioka, Kawano
	6	Kawatabi	140 45.5	38 44.6	41.9	3V-2, 3H-1	D-3	Matumoto, Kobayasi, Asano,
	7	Neno-siraisi	140 48.9	38 19.0	87.8	3V-1, 3H-1	D-2	Noritomi, Takagi
	8	Daiyama	140 24.7	37 49.2	148.8	3V-1, 3H-1	H-3	Kobayasi, Hagiwara
	9	Takatama	140 17.6	37 30.6	185.0	3V-2, 3H-1 1H-1 (K)	H-3	Yamazaki, Saito, Hiraoka
	10	Hatori	140 05.5	37 15.7	216.4	3V-1, 3H-1 1H-1 (A)	H-3	Suzuki, Mine
	11	Hitati	140 36.8	36 35.5	280.2	3V-1, 1H-1 (K)	D-1	Tanaka, Nagata
	12	Motegi	140 11.3	36 32.9	290.7	3V-2, 1H-1 (A)	H-1, H-2	Den, Chujo, Sato
	13	Tukuba	140 06.7	36 12.6	327.1	3V-1, 3H-1 1H-1 (A)	H-1, H-3	Kasahara, Watanabe, Mogi
Western profile	14	Katurazawa	140 40.6	38 59.8	22.2	3V-1 3H-1	D-1, H-1	Akima, Matumoto
	15	Yuzawa	140 30.5	39 09.6	33.8	H-1	Kyoto Univ.-H	Tamaki
	16	Innai	140 21.9	39 02.8	46.0	3V-2	D-2	Sima, Sibano, Yanagisawa
	17	Mamurogawa	140 17.2	38 52.0	58.7	3V-1 1/3H-1	D-2	Utu
	18	Sinasawa	140 00.5	38 41.0	90.0	3V-1 3H-1	H-3	Honda, Asanuma
	19	Tagawa	139 41.0	38 30.0	116.1	3V-1 3H-1	D-2	Tazime

three straight lines, and their equations given by the least squares method are as follows:

$$t_3' = 12^h05^m + (-0.06 \pm 0.06)^{sec} + (0.1673 \pm 0.0003)^{sec}\Delta,$$
$$t_4' = 12^h05^m + (3.7 \pm 0.3)^{sec} + (0.139 \pm 0.002)^{sec}\Delta,$$
and $$t_5' = 12^h05^m + (1.9 \pm 0.3)^{sec} + (0.279 \pm 0.001)^{sec}\Delta.$$

The velocities corresponding to the above travel times are

$$V_3' = 5.98 \pm 0.01 \text{ km/sec},$$
$$V_4' = 7.17 \pm 0.07 \text{ km/sec},$$
and $$V_5' = 3.58 \pm 0.002 \text{ km/sec}, \quad \text{respectively.}$$

Table II. Arrival times of the third Isibuti explosion tremors observed at the temporary stations of the group.

		Observation point	Distance from shot	Elevation	Time of phase commencement (12^h05^m+)		
					t_4	t_3	t_5
			km	m			
Southern profile	1	Shot point	0.22; 0.31	340		0.63; 0.67	
	2	South point from shot	1.50; 1.73	340		1.18; 1.27	
	3	Hondera	15.3	200		2.44	
	5	Hosokura	32.2	140		5.25	10.40
	6	Kawatabi	41.9	220		7.01	—
	7	Neno-siraisi	87.8	230		14.66	26.88
	8	Daiyama	148.8	450	24.49	—	43.70
	9	Takatama	185.0	560	—	—	—
	10	Hatori	216.4	700	34.0	36.2	—
	11	Hitati	280.2	400	—	—	80.00
	12	Motegi	290.7	150	34.92	48.5	83.39
	13	Tukuba	327.1	280	49.6	—	93.0
Western profile	14	Katurazawa	22.2	540		3.83	
	15	Yuzawa	33.8	120		5.73	10.61
	16	Innai	46.0	280		7.98	14.41
	17	Mamurogawa	58.7	100		10.16	17.77
	18	Sinasawa	90.0	200		15.46	
	19	Tagawa	116.1	560			

Suffixes indicate the order of horizontal layering from the surface, which is supposed in the region from the previous experiments, and V_i represents the characteristic longitudinal wave velocity in the layer. "′" indicates the quantities in the southern profile as in the previous publi-

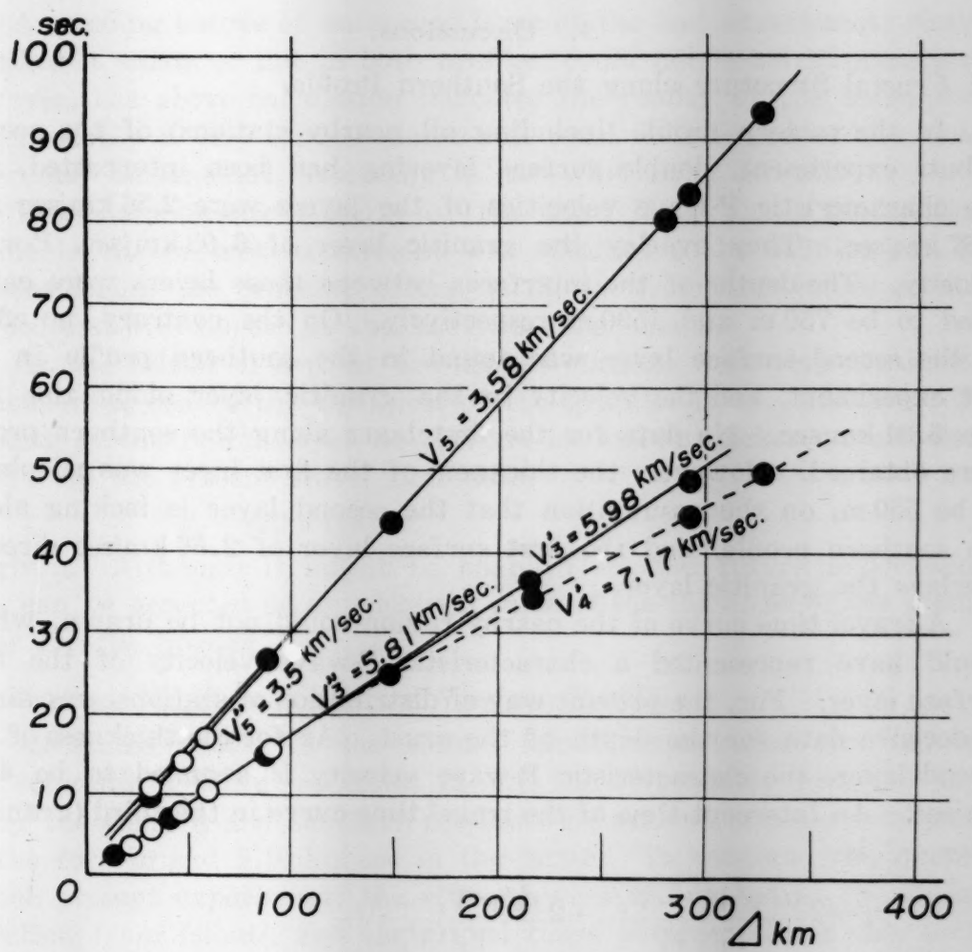

Fig. 2. Travel time curves from the third Isibuti explosion. V' represent velocities from the southern profile and V'' represent velocities from the western profile.

cation, and " $''$ ", those in the western profile, while letters with no mark represent the quantities in the eastern profile in the last experiment.

The travel time equations in the western profile are calculated as follows:

$$t_3'' = 12^h05^m + (0.00 \pm 0.05)^{sec} + (0.172 \pm 0.001)^{sec}\Delta,$$
$$t_5'' = 12^h05^m + (1.03 \pm 0.4)^{sec} + (0.287 \pm 0.009)^{sec}\Delta.$$

The corresponding velocities are

$$V_3'' = 5.81 \pm 0.03 \text{ km/sec},$$

and $$V_5'' = 3.5 \pm 0.2 \text{ km/sec}, \quad \text{respectively.}$$

3. Discussions.

3-1 Crustal Structure along the Southern Profile.

In the eastern profile (including all nearby stations) of the second Isibuti experiment, double surface layering had been interpreted, and the characteristic P-wave velocities of the layers were 2.56 km/sec and 4.67 km/sec. They overlay the granitic layer of 6.08 km/sec, P-wave velocity. The depths of the interfaces between those layers were calculated to be 750 m and 1590 m respectively. On the contrary, no effect of the second surface layer was found in the southern profile in the last experiment, and the velocity in the granitic layer along this line was 5.91 km/sec. No data for the first layer along the southern profile were obtained. However, the thickness of the first layer was calculated to be 550 m, on the assumption that the second layer is lacking along the southern profile, and the first surface layer of 2.56 km/sec directly overlays the granitic layer.

A travel time curve of the nearby region could not be drawn, which would have represented a characteristic P-wave velocity of the first surface layer. For, the present way of distribution of stations was aimed at decisive data for the depth of the crust. As for the thickness of the second layer, the characteristic P-wave velocity is assumed to be 4.67 km/sec. An intercept time of the travel time curve in the third (granitic) layer, τ_3' is

$$\tau_3'=2\frac{d_1'\sqrt{V_3'^2-V_1'^2}}{V_1'\ V_3'}+2\frac{d_2'\sqrt{V_3'^2-V_2'^2}}{V_2'\ V_3'}$$

In this equation V_3' and τ_3' are given by the hodograph obtained in the present experiment; d_1', V_1' and V_2' are assumed to be 750 m, 2.56 km/sec and 4.67 km/sec respectively. Thus, the thickness of the second layer, d_2' is

$$d_2'=\frac{V_2'\ V_3'}{2\sqrt{V_3'^2-V_2'^2}}\left\{\tau_3-\frac{2d_1'\sqrt{V_3'^2-V_1'^2}}{V'_1\ V_3'}\right\}=0.04\,\text{km}$$

and this value seems to be almost negligible as a thickness of the layer. In neglecting d_2' and assuming d_1' be unknown, the relation

$$\tau_3'=\frac{2d_1'\sqrt{V_3'^2-V_1'^2}}{V_1'\ V_3'}$$

is given. From this equation, the thickness of the first layer, d_1', which directly overlays the granitic layer, is 0.74 ± 0.01 km. This value is very close to that of $d_1=750$ m in the eastern profile in the last experiment.

A puzzling nature of the second layer of the last experiment, namely whether it exists or not in both profiles, could not be solved completely; however, the above calculation indicates the reality of the assumption, and probably a very narrow horizontal zonal distribution of the second layer may be assumed, extending in east-west under Isibuti.

The characteristic velocity of the third layer along the southern profile in the present experiment was obtained to be 5.98 km/sec, and in considering the probable errors, it differs from the values of 6.13 km/sec and 5.91 km/sec in the last two experiments.

As the initial on-sets at the distant stations were very weak, it is premature to deduce the thickness of the granitic layer. However, if a velocity of the fourth layer be 7.17 km/sec and its thickness is calculated only from the present travel time data,

$$d_3' = (20 \pm 4)\,\text{km}$$

is given. Although it might be changed by the future experiments, this can be accepted as an adequate value of the thickness of the granitic layer for the present.

3-2 Crustal Structure along the Western Profile.

As stated above, in the second Isibuti experiment two different characteristic P-wave velocities in the third (probably granitic) layer along the eastern and southern profiles were derived, namely 6.08 km/sec in the former and 5.91 km/sec in the latter. To conclude this problem in the present experiment, the stations were distributed in the western direction from Isibuti, and the travel times obtained along this profile gave 5.81 km/sec as a characteristic velocity of the third layer. It will be a consistent interpretation for the above result, that the thickness of the surface layer or layers overlaying the granitic layer is thinner in the eastern profile than in the western profile. If the structure shown in Fig. 3 is assumed, which lacks the second layer of 4.67 km/sec velocity,

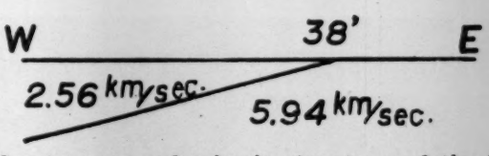

Fig. 3. An assumed seismic structure of the E-W profile in the N-E Japan.

the slope of the interface between the surface and granitic layers becomes 38′, and the true velocity in the granitic layer becomes 5.94 km/sec, which is very close to the value of 5.98 km/sec for the southern profile

obtained in the present experiment. If a value, 740m as a thickness of the surface layer at Isibuti is employed, this sloping interface comes up to the surface of the ground about 70 km to the east of Isibuti.

Geologic map of the district in large scale shows that from about 20–30 km to the east of Isibuti, extends the palaeozoic mass of Kitakami mountains which are intruded by granite mass at places, and no low-velocity surface layer is seen in that region. Western part of the island arc in N–E Japan are deposited by thick tertiary formations, and in the central part volcanic rocks of newer stages are found. Base of these canozoic rocks is the so-called green-tuff which is found widely over the N–E Japan.

The geologic fact stated above is very illustrative to explain the results obtained. Nevertheless, discussion on the problem will rather be postponed to the future.

4. Acknowledgements.

Many thanks go to the agencies and persons under whose helpful cooperation and patronage this experiment was successfully made. They were Tohoku District Construction Bureau of Ministry of Construction, Nisimatu-Construction Co., Tohoku Electric Co., Tokyo Electric Co., Sendai Broadcasting Station of NHK, Broadcasting Station of Standard Wave JJY, Mizusawa Forestry Bureau, Prefectural Authorities and Police Authorities of Iwate, Miyagi, Hukusima, Akita, Yamagata, Ibaraki and Totigi. Much help was also given by the Geophysical Committee of the National Council, Central Meteorological Observatory, Earthquake Research Institute and all other organizations to which the members of the group belong.

The present study received encouragement and guidance from Prof. T. Matuzawa.

---

27. 東北日本における第3回爆破地震動観測

爆破地震動研究グループ

岩手県胆沢郡若柳村石淵における石塊堰堤工事採石の大爆破はすでに1950年10月，1951年12月の2回にわたり爆破地震学の目的のために利用された．1952年7月25日この工事としては最後の大爆破が行われ，われわれもふたたびその地震動観測を実施した．

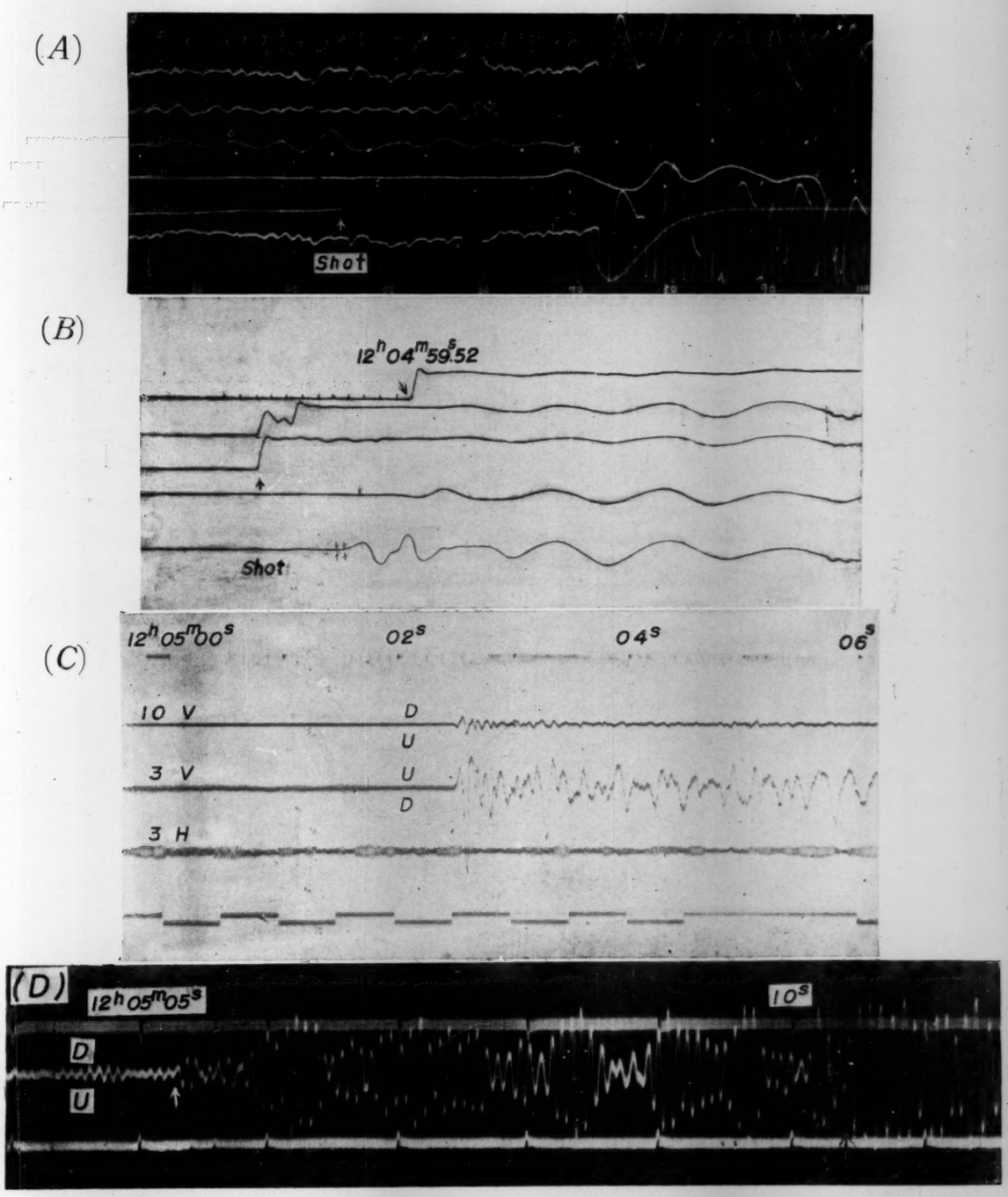

Fig. 4. Seismograms obtained at the third Isibuti explosion of 1952 on the southern profile at Isibuti (*A* and *B*), Hondera (*C*) and Hosokura (*D*).

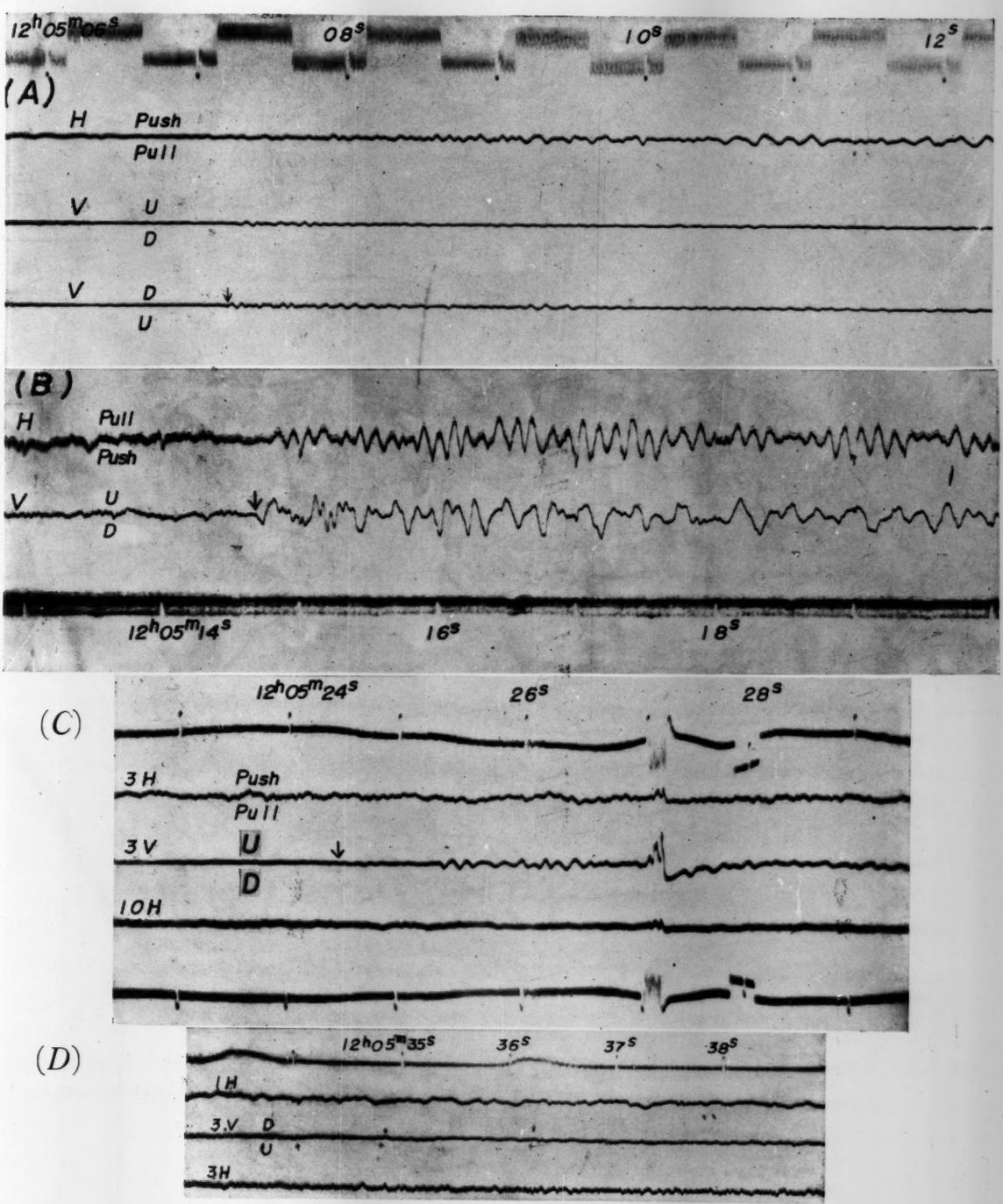

Fig. 5. Seismograms obtained at the third Isibuti explosion of 1952 on the southern profile at Kawatabi (*A*), Nenosiraisi (*B*), Daiyama (*C*) and Hatori (*D*).

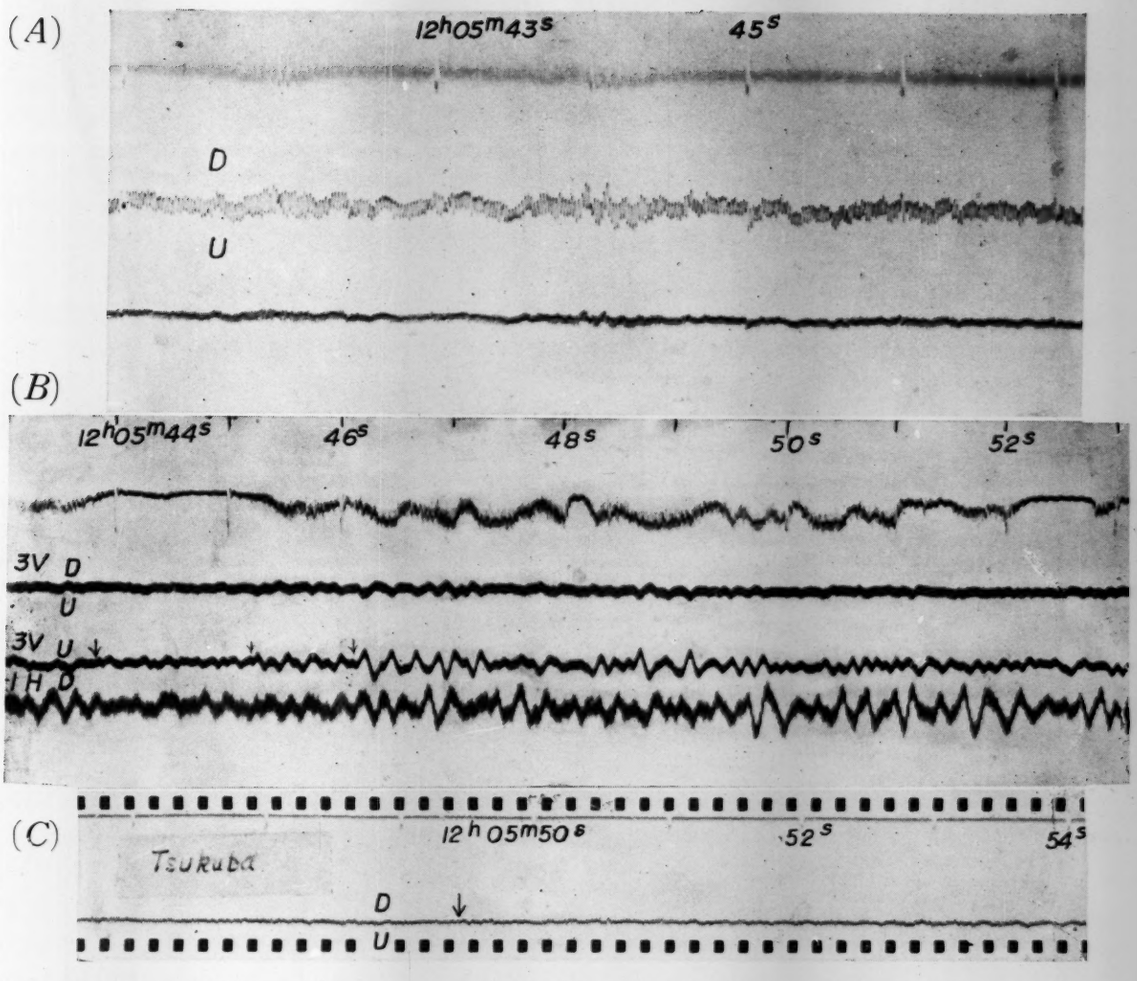

Fig. 6. Seismograms obtained at the third Isibuti explosion of 1952 on the southern profile at Hitati (*A*), Motegi (*B*) and Tukuba (*C*).

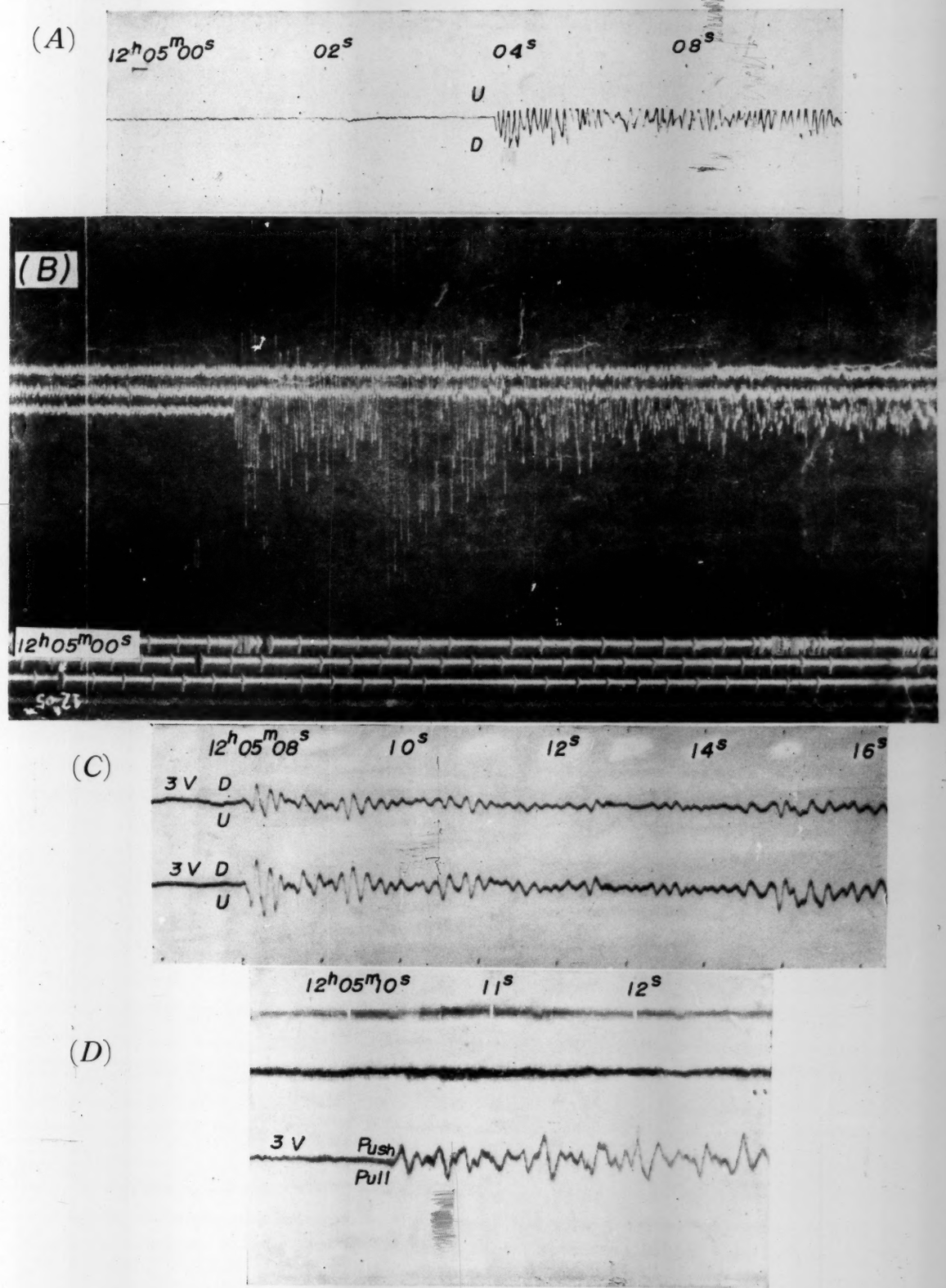

Fig. 7. Seismograms obtained at the third Isibuti explosion of 1952 on the western profile at Katurazawa (*A*), Yuzawa (*B*), Innai (*C*) and Mamurogawa (*D*).

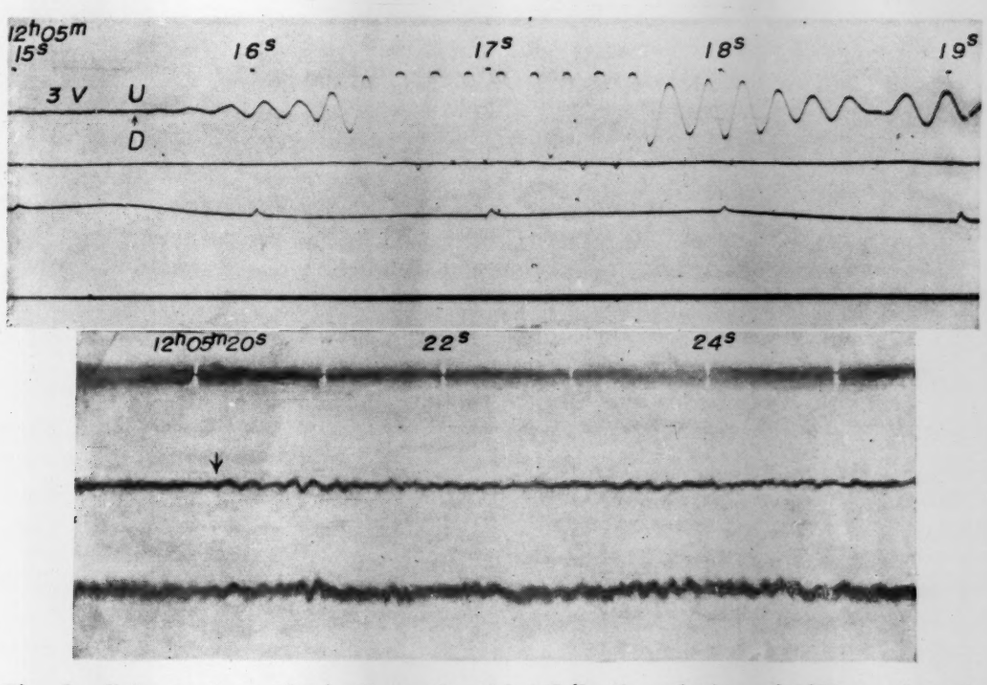

Fig 8. Seismograms obtained at the third Isibuti explosion of 1952 on the western profile at Sinazawa (*A*) and Tagawa (*B*).

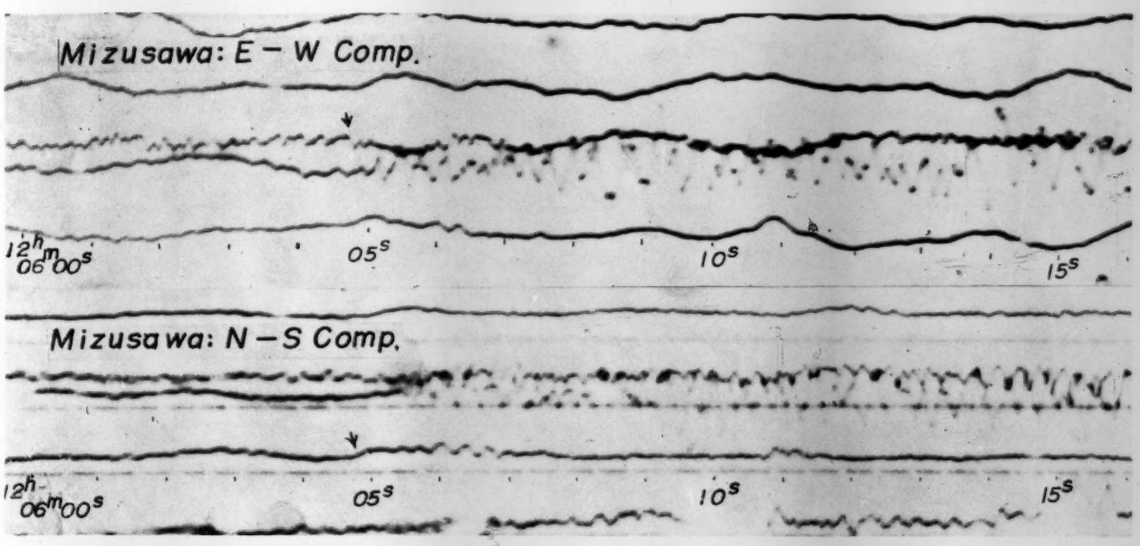

Fig. 9. Seismograms obtained in the case of the *second* Isibuti explosion of *1951* at Mizusawa stations, which were to be placed in our preceding paper. (Bull. E. R. I. **30**, 1952, 279-292).

装薬はカーリット 5.546 トンで 12 個の薬室にわけられ，前回までと同様の方法で爆破された．爆破点は前回より約 20 m 南，爆破時刻は薬室に挿入した導線切断のオツシログラムを標準電波 *JJY* の分秒報時と比較して $12h04m59.42s$ ともとめられた．

地震動観測班は南方，西方計 19 点で，使用計器は前回と大体おなじである．(第 I 表，第 1 図)

えられたおもな位相のよみは第 II 表に示すとおりで，これを震源距離に対してとつたのが第 2 図にしめす走時図である．これらの走時を直線として南方，西方各測線別に最小自乗法によりきめた走時式およびその対応する速度はつぎのとおりである．

南方測線：
$$t_3'=12h05m+(-0.06\pm0.06)s+(0.1673\pm0.0003)\Delta.s,$$
$$t_4'=12h05m+(3.7\pm0.3)s+(0.139\pm0.002)\Delta.s,$$
$$t_5'=12h05m+(1.9\pm0.3)s+(0.279\pm0.001)\Delta.s,$$
$$V_3'=5.98\pm0.01\,km/s,\quad V_4'=7.17\pm0.07\,km/s,\quad V_5'=3.58\pm0.002\,km/s.$$

西方測線：
$$t_3''=12h05m+(0.00\pm0.05)s+(0.172\pm0.001)\Delta.s,$$
$$t_5''=12h05m+(1.03\pm0.4)s+(0.287\pm0.009)\Delta.s,$$
$$V_3''=5.81\pm0.03\,km/s,\quad V_5''=3.5\pm0.2\,km/s.$$

地殻構造の推定については，南方測線では今回は震源近くに観測点がすくないため，地表層 (前回の第 1，第 2 層) の走時はえられてないので，前回の結果を用い第 1 層第 2 層の速度を 2.56 km/s，4.67 km/s とし第 1 層のあつさ $d_1=750\,m$ ととり，今回の第 3 層の走時をつかつて，第 2 層のあつさを出すと $d_2'=0.04\,km$ となり，無視できる．そこで第 1 層の下に直接第 3 層がくるとして計算すると $d_1=0.74\pm0.01\,km$ となる．第 3 層の速度は第 1 回 6.13 km/s，第 2 回 5.91 km/s，今回が 5.98 km/s で誤差範囲をこえて相違しているが，測線がちがうので確かなことはいえない．第 4 層の走時はなお決定的とはいえないが，これをもちい第 3 層のあつさを出すと $d_3'=20\pm4\,km$ となる．

西方測線では第 3 層の速度が 5.81 km/s となつて，前回東方測線の第 3 層の 6.08 km/s と大変ちがう．しかしこれは第 3 図のような構造を考えると一応了解できることがわかつた．しかし，この傾きの値などの数値については確定的なものとは考えられない．ただ傾向としては，地質学的事実とも矛盾しないように思われるので，一応このよに考えられるというだけである．

今回の実験についても前回同様建設省，西松建設，東北電力，東京電力，電波庁，水沢営林署，NHK，県庁，警察其他各方面関係者の甚大なる後援をえた．あつく御礼申し上げたい．

なお本研究経費の一部は文部省科学研究費によるものである．記して謝意を表する．

28. *Elastic and Viscous Properties of Volcanic Rocks at High Temperatures. Part 3. Oosima lava.*

By Shūzō SAKUMA,

Earthquake Research Institute.

(Read Oct. 27, 1953.—Received Oct. 31, 1953.)

Introduction.

Enormous volume of hot lava was given out during the recent activities of Volcano Oosima in 1950–51. Most of the ejected materials were in the form of lava-flows which were belched out of the pit crater, filled up the inner somma, overflowed it, then ran down the flank as streams of several metres' width, and at last spread over the wide area of the atrio. Incandescent lava, above 1100°C at the time of ejection, was so fluidal that phenomena like lava-fountains and lava-pools could be seen. The lava started as incandescent fluidal streams, and became more and more viscous at downstreams with stiff skins on them, by loss of heat through radiation as well as through liberating gases. Many vesicles of a little distorted form, the diametre of which ranges from several centimetres to about a millimeter, scatter in the solidified rock especially densely near its clinkery surface. Most of the solidified lava-flows may be classified into the aa type because of their clinkery, jagged or fragmental surface[1]. But there were seen in places ropy flows which may be classified more properly as the pahoehoe type although the surface was not so smooth. Beneath the fragmental surface of the aa type flow, we can often see a continuous layer of non-fragmental rock. Investigations on viscosity and temperature of flowing lava were carried out by T. Minakami and others[2]. The mode of flowing was also described by T. Minakami. It appears very interesting as well as useful to study the relations existing among such volcanic phenomena as fountain and flow, physical and petrographical properties of the lava. The present writer has been interested in the laboratory experiments of rocks at high temperatures, and intended to investigate the lava from Oosima too.

---

1) G. A. MACDONALD, *Am. J. Sci.*, **251** (1953), 169.
2) T. MINAKAMI, *Bull. Earthq. Res. Inst.*, **29** (1951), 427.
Jour. Geography, Tokyo, **60** (1951) (in Japanese).

Method.

As stated in the previous papers[3], the bending or sagging method of experiment was adopted. A thin plate of lava-specimen (ca. 0.3 cm × 8 cm × 1 cm) is supported between two knife-edges of fused silica and is loaded at the centre through another knife-edge or sags due to its own weight. The whole contrivance, chiefly made of special porcelain, is inserted in an electric furnace. The electric furnace of platinum wire was used only for the experiments above 1100°C and most of the experiments were carried out in the electric furnace of nichrome wire. The uniformity of temperature in the furnace was satisfactory. The temperature was indicated by a Pt-PtRh thermocouple inserted closely to the specimen, and the temperature was raised and lowered through manual regulation of electric supply always slowly enough to render the difference of temperature less than ±5°C between the surface and inside of the specimen. The specimen was heated and cooled nearly quasi-stationarily, and in addition, it was kept in a constant temperature from at least ten minutes before to the end of one series of measurements. Thus the experiments were done under nearly constant and uniform temperatures. Various constant load, less than 600 gr, were applied to the specimens. When a load is applied, the specimens show more or less visco-elastic behaviours as shown on Fig. 1. That is, after a sudden elastic deformation, there takes place anelatic relaxation with decreasing velocity which tends to be constant as time goes on, representing the viscous flow of material.

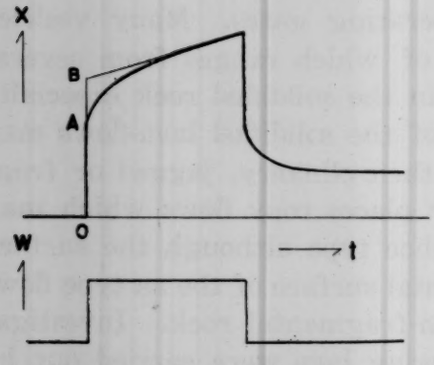

Fig. 1. Deformation (X) of a viscoelastic body under constant load (W).

Amount of deformation is measured by doubly reflected light through two prisms on both ends of the specimen. As mentioned in the previous report, the observed subsidence at the centre (x) is expressed as follows,

$$x=\left(\frac{Wl^3g}{4bd^3}+\frac{5wl^4g}{32bd^3}\right)\left\{\frac{1}{E_U}\left(1+\frac{t}{\tau}\right)+\left(\frac{1}{E_R}-\frac{1}{E_U}\right)\left(1-e^{-\frac{t}{\tau'}}\right)\right\},$$

where W: applied weight,

3) S. SAKUMA, *Bull. Earthq. Res. Inst.*, **30** (1952), 269; **31** (1953), 63.

w : weight of specimen of unit length,
b & d : width and thickness of specimen,
l : distance between knife-edges,
E_U : unrelaxed Young's modulus,
E_R : relaxed Young's modulus,
τ & τ' : relaxation times.

Viscosity is derived from the following equation which is based on the assumption of incompressible viscous liquid.

$$\eta = \frac{\tau E_U}{3} .$$

τ can be calculated on the basis of the terminal velocity of deformation under constant load.

As a dimensionless measure of anelasticity, another quantity $\Delta_E = \frac{E_U - E_R}{E_R}$ is introduced after Zener[4]. This quantity may be correlated to other physical constants such as thermal expansion coefficient, as has been done in the field of metallurgy.

Specimens.

The following three kinds of lava specimens were examined. (Fig. 9. a–c.)

(1) Glassy lava. (G). Collected on the top of the inner somma. The lava was one of the most fluidal flows in the 1951 activity. The detailed descriptions of this flow which went through the windows of Kakô-Jaya was given by H. Foster[5]. The specimen was taken from a side of the flow near the Kakô-Jaya. Beneath the clinkery surface, there was a comparatively uniform layer with many vesicles. The largest of the vesicles was about one centimeter and most of them were smooth but a little distorted. Colour of the rock is dark black. Glass in the groundmass is the richest among the tested three kinds. Three specimens of this kind were tested in the laboratory.

(2) Lava of high crystallinity (H). Collected from a crack in the typical massive phase of aa. There are many deep cracks in the 1951 lava-flows which buried the inner somma, especially around the former pit crater. The present specimens were collected from the bottom of one of those cracks which were several metres deep. The surface of

4) C. M. Zener, "*Elasticity and Anelasticity of Metals*", 1952, Chicago.
5) H. L. Foster & A. C. Mason, *Am. J. Sci.*, **251** (1953), 249.

the flow is not so clinkery. The rock is of light black colour and contains fine vesicles only scarcely. Glass can be seen in the groundmass very rarely. Plagioclase as phenocryst is more equigranular than G. Two specimens of this kind were tested in the laboratory.

(3) Intermediate lava (I). It was collected and described by R. Morimoto and others, and was afforded to the writer. Quantity of glass is intermediate between the two described above. To be more precise, however, the glass is slightly less than the *G* and far more than the *H*. Three specimens of this kind were treated in the laboratory. These kind of specimens were formerly[6] tested under various conditions such as repeated heat-treatments.

Generally speaking, though the three kinds of specimens differ in their quantity of glass and regularity of microlites in the groundmass, the difference is rather little. All of the lava-flows where the specimens were taken may be classified at the aa type, in spite of the above-mentioned difference in appearance. The area of crystalline part distinguishable on the respective photomicrographs (Fig. 9) was measured. It gave the results of 50%～60% glass for *G*, 40%～50% glass for *I*, and about 10% glass for *H*. These numbers are not so exact, because extremely small crystallites and some crystallites in extinction-angle were omitted. But difference of crystallinity is fairly reflected.

Petrographical features of the 1950–51 lava were studied by H. Tsuya, R. Morimoto and J. Ossaka[7]. According to them, fixed constituents of the lavas and fragmental ejecta are the same during the changing phase of the activities, and they are identified as an uniform augite-hypersthene-bytownite basalt. This basalt contains anorthite, bytownite, hypersthene and augite as porphyritic minerals scattered in the groundmass composed of bytownite, pigeonite, iron ores and glass. Porphyritic structure is not so remarkable; phenocrysts occupy 5–10% of the rock in volume, they are seriate to the groundmass minerals in size in the higher crystalline portion of the rock.

The specimens which were heated up to 1150°C and cooled slowly or quenched into water suffered no remarkable petrographical changes, but glass in the groundmass became black owing to oxidation of iron. Further development of crystallization by heating was not ascertained microscopically. But more minute studies should be done in this connection.

---

6) S. SAKUMA, *loc. cit.*, 3).

7) H. TSUYA & others, *Bull. Earthq. Res. Inst.*, **29** (1951), 563: **30** (1952), 231.

The necessitated size for the present method of experiment restricted the available kind of specimen. Specimens of different petrographic properties and of different type of flow, as various as possible, were to be tested. But we could not examine the specimen from the most glassy part of the flows because of its smallness in dimension. Some specimens were abandoned because of their fragileness due to rapid cooling and to too much included gas bubbles. Thus the available sort of specimen was restricted to some extent.

Results of Experiments.

A part of this series of experiments has been made public in which the intermediate lava in the temperature range of 0°–1100°C was treated. The points which were stressed in the paper were as follows.

(1) Young's modulus increases with temperature up to a certain critical temperature (T_c) at the first heating, and it decreases abruptly at a higher temperature. (Fig. 2)

(2) Young's modulus in cooling differs from that in heating. It also varies with the highest temperature (T_M) which the specimen was treated with in the laboratory.

(3) Repeated heating and cooling of one specimen result in elevation of T_c.

(4) Viscosity coefficient decreases with the rise of temperature, but its value is exceedingly higher than that observed in the field in its natural molten state.

(5) Viscosity increases as heat-treatment is repeated.

Concerning the unrelaxed Young's modulus, the tendency of increasing elasticity in heating was found to be common to all of the present three types. However, the critical temperature T_c at which the modulus shows a decrease differs from one another (Fig. 2–5). The following fact should also be noticed. The T_c of the glassy specimen is nearly the same as that of the intermediate one in the initial heating stage, and the T_c of the intermediate one in the second and third heating falls close to the T_c of the lava of high crystallinity. The temperature at which E_U is maximum is adopted as T_c in the Table I. Another temperature of the same curve is listed for reference, where $\left|\frac{\partial^2 E_U}{\partial T^2}\right|$ is maximum. The relaxed Young's modulus changes in the similar way as the unrelaxed modulus, though the value of E_R is less accurate.

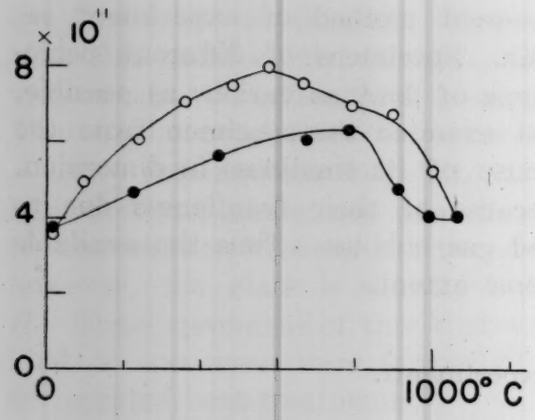

Fig. 2.

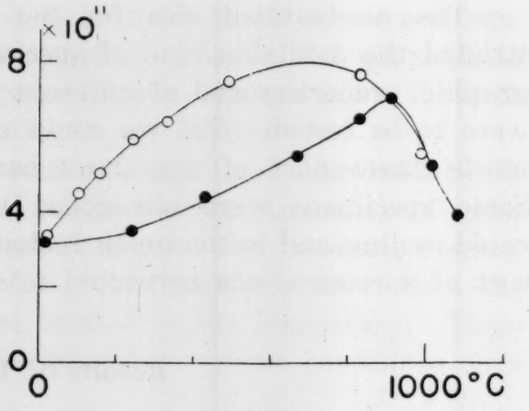

Fig. 3.

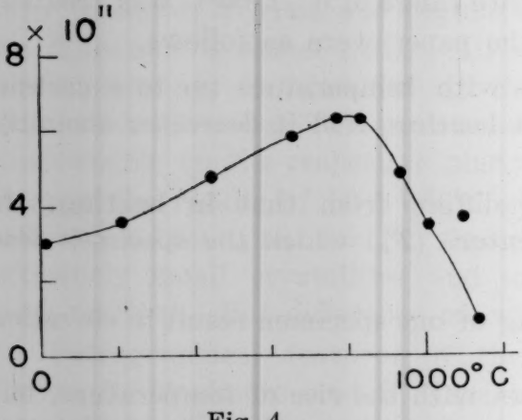

Fig. 4.

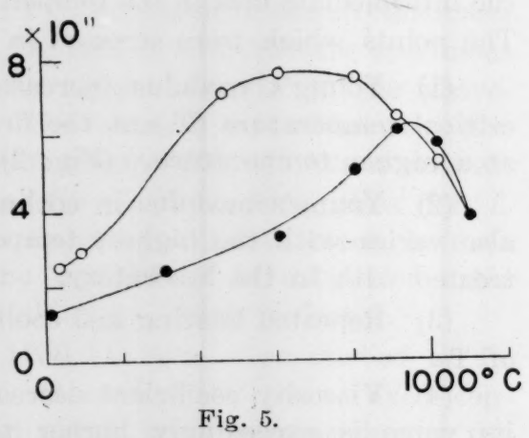

Fig. 5.

Fig. 2. Unrelaxed Young's modulus (in dyne/cm²) of intermediate lava at the first run. filled circles: heating, open circles: cooling.
Fig. 3. Unrelaxed Young's modulus of intermediate lava at the second run. filled circles: heating, open circles: cooling.
Fig. 4. Unrelaxed Young's modulus of glassy lava.
Fig. 5. Unrelaxed Young's modulus of the highly crystalline lava. filled circles: heating, open circles: cooling.

Table I. Critical Temperature for Elasticity of Oosima-lava.

Specimen		$\frac{\partial E_U}{\partial T}=0$	$\frac{\partial E_R}{\partial T}=0$	$\left\|\frac{\partial^2 E_U}{\partial T^2}\right\|$ =max.
Glassy		790°C	760°C	800°C
Intermediate	1st heat	800	680 (?)	830
	2nd 〃	910	950	940
	3rd 〃	930	820	950
High crystallinity		950	920	950

Difference in the critical temperature of elasticity among various kind of lavas is also reflected in Δ_E. Glassy lava is distinctly more anelastic than the crystalline lava. Δ_E of the intermediate one is intermediate, but it is omitted on the Fig. 6 for simplicity's sake. Concerning the relaxation time τ' of strain under constant stress, there is found little decisive difference among the various specimens. (Fig. 7)

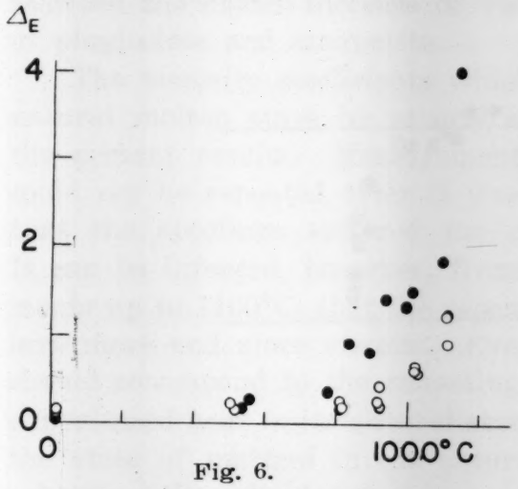

Fig. 6.

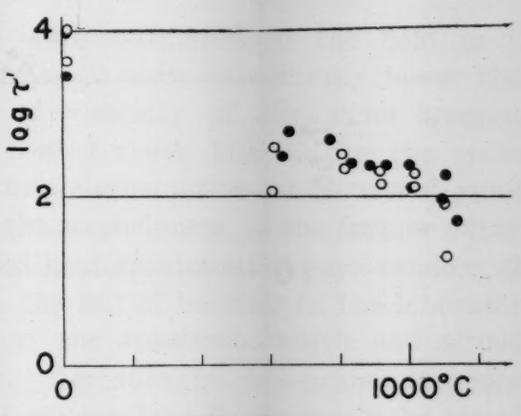

Fig. 7.

Fig. 6. Variation of Δ_E with rising temperature.
filled circles: glassy lava, open circles: crystalline lava.
Fig. 7. Variation of relaxation time (τ') with temperature (in seconds).
filled circles: glassy lava, open circles: crystalline lava.

Table II. Chemical Composition of Specimens.

Specimen	1950 lava[8] (Intermediate)	Somma lava
Experimenter	Sakuma	Kani
SiO_2	52.02	51.80
Al_2O_3	15.83	15.00
Fe_2O_3	2.28	3.68
FeO	10.80	10.14
MgO	4.47	5.36
CaO	9.48	9.77
Na_2O	1.58	1.76
K_2O	0.29	0.32
H_2O_+	0.99	0.62
H_2O_-	0.24	
TiO_2	1.52	0.60
P_2O_5	n.d.	0.31
MnO	0.09	0.20
Total	99.59	100.56

8) H. TSUYA & others, *loc. cit.*, 7).

Remarkable difference could not be found among the viscosity coefficients of various specimens. The coefficient η of the *H*-lava looks only a little greater than that of *G*-lava. One very significant fact was found concerning viscosity, however. (Fig. 8) That is the abrupt decrease

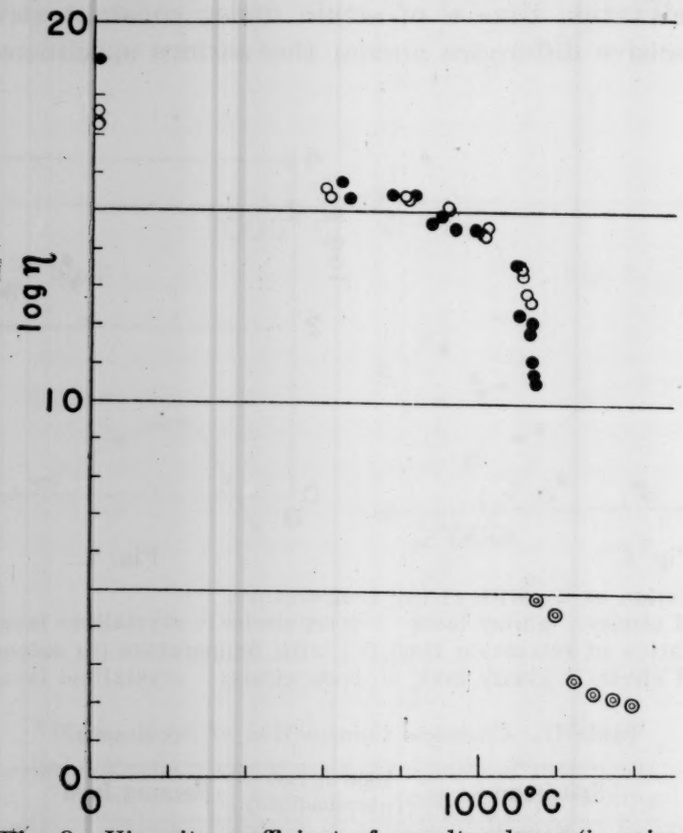

Fig. 8. Viscosity coefficient of remolten lavas (in poises).
filled circles: glassy lava,
open circles: crystalline lava,
double circles: somma lava (from K. Kani's experiment).

of viscosity, or increase of fluidity, within the narrow limits of 30~70 degrees above 1100°C. The present bending or sagging method failed above the temperature where η became less than 10^{10} poises. Fortunately, the results of K. Kani's experiments can be cited.[9] He had remolten the lava of the outer somma of Oosima between two concentric cylinders and had measured its viscosity from 1400°C down to 1150°C. Its chemical composition is not so much different from those used in the present experiments. His results are also illustrated on Fig. 8. A glance at this

9) K. KANI, *Proc. Imp. Acad. Japan*, **10** (1934), 79.

figure will be sufficient to convince us of the existence not of the discrepancy between the two different experiment but of some discontinuity in physical properties caused by some phase change. T.Nagata[10] also found out a discontinuity in the electric conductivity of remolten Oosima lava at about 1130°C. Accordingly, it leaves no doubt that the Oosima lava "melts" at about 1130°C when it is reheated in laboratory. Kani ascribed the sudden increase of viscosity below 1250°C to crystallization of plagioclase and magnetite.

The viscosity coefficients which were estimated in the field in its natural molten state by several authors[11] were exceedingly lower than the present results. Measurement of viscosity of the same specimen could not be repeated after it was heated above 1130°C, for the reason that the specimen suffered too much deformation to be tested again. It can be inferred, however, from the experiences in the former experiments up to 1100°C, that the repeated heat-treatment always renders the lava more and more viscous. Even the initial heating in the laboratory should correspond to the reheating of the specimen which had already experienced heat in its natural state. Accordingly, one cannot reproduce the state of matters in the natural molten lava-flow exactly by simply reheating the solidified lava.

Discussions.

The writer would like to refer to the following three problems on the basis of the experiments. They are: (1) Can we infer the dynamical properties of the natural molten lava from the result of the laboratory experiments?, (2) What part of the mentioned physical properties of the specimens can be correlated with their petrographical features?, (3) Can we explain the origin of various forms of lavas, such as aa or pahoehoe, on the basis of their respective dynamical properties?

Major characteristics of the dynamical properties were found to be common to all of the tested specimens. They were the increase of elasticity with rising temperature, the decrease of elasticity above T_c and the decrease of viscosity with temperature especially abrupt above 1100°C. Difference among the three kinds were rather small, but none the less important. Difference itself, if any, even it be small, is a precious key. The difference was comparatively remarkable in T_c and Δ_E.

10) T. NAGATA, *Bull. Earthq. Res. Inst.*, **15** (1937), 663.

11) T. MINAKAMI, *loc. cit.*, 2).
R. TAKAHASI & T. NAGATA, *Bull. Earthq. Res. Inst.*, **15** (1937), 1047.

The difference in T_c should have been caused by the quantity as well as quality of glass in the groundmass, because all of the specimens are similar in their phenocrysts and microlites. When the glassy rock is reheated and recooled in the laboratory, the dissolved gases may probably escape and incipient crystallization may be hastened. Such phenomena like devitrification are frequently met in glass techniques. If we assume that the mentioned process of crystallization can take place submicroscopically as well, it will be naturally accepted that the G-specimen behaves like the crystalline one in the second heating run.

Another consideration should be taken before inferring how the elasticity of the natural molten lava varies with cooling. The "cooling" experiment in the laboratory has one essential defect. All cooling experiments must inevitably be conducted after the cooling in the nature and the first heating in the laboratory. And in consequence, the experimental values of elasticity in cooling are very much affected by the highest temperature T_M. Subsequently the present writer cannot help hesitating in applying the result of cooling experiment directly to the lava in the natural state. It seems more reasonable to suppose that the essential feature of change of elasticity in nature would be better reflected in its change in the first "heating" in the laboratory, especially as regards the glassy specimens. There is no doubt that the cooling lava in the field contains much more gases in its liquor and is of lower crystallinity than the tested glassy specimen at the same temperature. Accordingly we may well infer the most probable change of elasticity in the cooling natural lava by extrapolating the character and its change of the glassy specimen. We come to imagine naturally that the T_c must have been lower in the natural lava than that observed in the laboratory.

After all, elasticity of the Oosima lava in its natural state would have varied as follows. Elasticity is very faint above 1250°C, with scattered phenocrysts in fluidal liquor. The lava becomes slightly elastic below 1150°C with abrupt development of crystallization. A part of the separated gases is dissolved in the liquid phase and lessens the viscosity as well as the elasticity of it. Other part of the gases forms vesicles and decreases the apparent viscosity and elasticity of the flow, until it is liberated at last in the air. The liberation of gases has a threefold effect. It increases apparent elasticity and viscosity, develops crystallization and deprives heat. The temperature thus decreasing, elasticity increases down to around 700°–800°C, where the elastic modulus is at least nearly same as the value at the room-temperature. Elasticity

may probably increase a little further at lower temperature, because the internal stress increases due to the forced crystallization in highly viscous liquid which has long relaxation times for stress. The modulus tends to decrease, however, near the room-temperature because of release of stress due to thermal contraction of constituent minerals. The solidified lava is not under perfect thermodynamical equilibrium, but remains as the aeolotropic mixture of crystals and highly viscous quenched liquid with gases. When the specimen is heated again in the laboratory, its elasticity increases at first because of stress by expansion of crystals, and then decreases at the temperature where the thermal stress relaxes rapidly and some part of material comes to melt. Heat-treatment in the laboratory always develops crystallization and liberates dissolved gases and results in the approach of its elasticity to that of the highly crystalline lava.

τ', the time of anelastic relaxation, is a result of various diffusions within the specimen. Δ_E has a similar character. It is related to the change of entropy in specimen. But increase of Δ_E may possibly have more intimate relations to randomness of arrangement of crystallites than to that of atomic scale. Both τ' and Δ_E are undoubtfully connected also to the liquid viscosity η implicitly, but they do not always vary in parallel, as shown in the previous report of the writer. Judging from the distinct higher value of Δ_E of G than H, we can expect more higher Δ_E for the natural molten lava, which means poorer relaxed elastic modulus in the natural state.

We will next discuss the most important part, that is, the viscosity of the lava. The abrupt change of viscosity at about 1130°C is remarkable in itself and distinguishes the Oosima lava from the other formerly tested rocks such as obsidian. But the viscosity of the natural molten lava is believed to be less than the value obtained in the laboratory. Similar state of matters, as mentioned above under the item of natural elasticity, should have occurred concerning viscosity as well. The irreversible physico-chemical processes, such as liberation of gases and resulting crystallization, is not reproduced perfectly in the experiment. The temperature of 1130°C must be a kind of eutectic point, but it is the eutectic point under a certain definite circumstance. If the circumstance, the quantity of gases dissolved in the liquor phase for instance, changes the temperature will shift inevitably. Although the observed difference in viscosity between the glassy and crystalline specimens was rather small, it seems more proper to think that the critical temperature

for viscosity also would be somewhat lower than 1130°C in the natural molten lava. Besides the just mentioned physico-chemical condition, the apparent viscosity of lava as a mass is expected to be reduced much more, if more vesicles are included.

Other factors like the cooling velocity or quantity of remnant gas also affect the physical properties of rocks considerably. The crystallinity, or the quantity of glass, was adopted here as a parameter including these factors. The relations of crystallinity itself to the physical properties should be discussed after more detailed studies subsequently.

The writer wishes to make some remarks on the possible cause of formation of aa and pahoehoe, though the specimen of typical pahoehoe was not treated in the present experiments. The main differences of pahoehoe from aa are its smoothness of the surface, smooth spheroidal vesicles inside and the lower crystallinity at least near its surface. The cause of such differences has been ascribed to the circumstance when the lava is solifying. The undistorted vesicles in pahoehoe might possibly imply also the existence of part or all of the following factors, i. e. high internal pressure of gas, more fluidity just before consolidation and greater gradient of increase of viscosity with cooling. The present experiment, however, could reveal any distinct difference between glassy and crystalline specimens neither in their absolute value nor in the critical temperature of change of viscosity. Consequently, possibility of existence of original difference in viscous properties between the aa-making lava and pahoehoe-making lava seems to be rather small, and the rôle of mechanical disturbance around the critical temperature was proved as a result to be of more importance, as already pointed out by many authors[12]. Turbulent motion inside the lava-flow, due to topography for instance, causes liberation of more gases, develops crystallization and increases viscosity in parallel. The jagged surface and distorted vesicles which are the feature of aa, are considered to have resulted from further movement such highly viscous lava. Another experimental fact, i. e. the fact that the elasticity of glassy lava is less at some range of temperature than that of crystalline lava, should be recollected too. It means that glassy surface is much more extensible at around 800°–900°C than the surface of the crystalline lava. Even though the skin must be broken by the stress greater than the tensile strength of the material, the higher extensibility of glassy skin may also contribute to the for-

12) G. A. MACDONALD, *loc. cit.*, 1).
O. H. EMERSON, *Am. J. Sci., Ser.* **5**, **12** (1926), 109.

(a) Glassy lava (×36)

(b) Intermediate lava (×36)

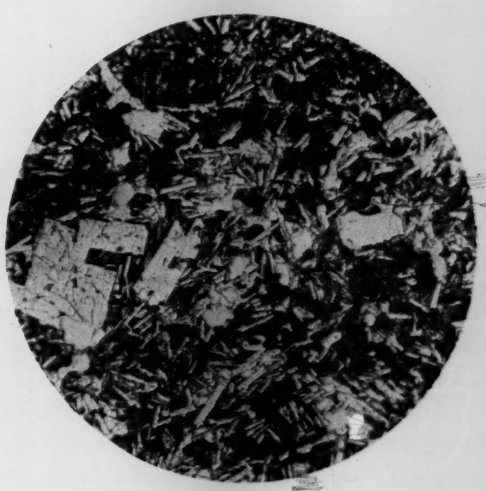

(c) Crystalline lava (×34)

Fig. 9 a.–c. Photomicrographs of lava-specimens.

(震研彙報 第三十一号 図版 佐久間)

mation of pahoehoe lava to some extent.

We have here tried to infer the characters of the natural fresh lava from the results of experiments in the laboratory. The results of experiments are useful in the study of volcanic phenomena, though we should be careful enough in applying the results to the natural phenomena.

In concluding, the writer wishes to express his cordial thanks to Dr. T. Minakami, Dr. R. Morimoto and Mr. J. Ossaka for their kind advices and criticisms as well as for the facilities given to the writer.

---

28. 高温に於ける火山岩の粘性及び彈性
第3報 大島熔岩

地震研究所 佐久間修三

前と同じ撓み法で，室温から約 1150°C 迄の領域で下記3種の大島熔岩を徐々に加熱した場合の力学的性質の変化をしらべた．

その一 (*G*) は流動的であつた熔岩流の表面近くにあり，石基にガラス分をやや多くふくみ，その二 (*H*) は熔岩池深部で固結し，石基の結晶度が高い．その三 (*I*) は第1報にものべてある試料で，前二者の中間にあたる．

加熱するとヤング率は徐に増し，或温度 (T_c) 以上では急に減少する．T_c の値は *G* が最も低く約 790°C，*H* では約 950°C であるが，*I* では第1回加熱では *G* にちかく第2回以後は *H* にちかい値となる．即ち加熱によつて T_c は上昇する．

Anelasticity の程度をあらわす量 $\Delta_E=(E_U-E_R)/E_R$ については *G* が *H* より明かに大い．歪緩和時間 τ' については大差がない．粘性係数 η についても各種熔岩の間の差異は著しくないが，1130°C 附近に於て融解と考えられる粘性の急変が見出された．

自然の熔岩流は，結晶度や，液相に溶解し或は分離して気相となつている gas 量の点で実験試料と全く同じではないであろう．しかし実験室で得られた上述の力学的性質を，よりガラス質且より気体の多い状態に外挿することにより，自然の熔岩流の力学的性質を想像し得るであろう．

尙，800°～900°C 附近に於てガラス質熔岩の彈性が結晶質熔岩のそれより小さい，即ち伸び易いことは，pahoehoe 型，aa 型など熔岩流の型の成生に若干の関係があると思われる．

---

29. *Relation between the Property of Building Vibration and the Nature of Ground.* (*Observation of Earthquake Motion at Actual Buildings.*)

By Kiyoshi KANAI and Tomisaburo SUZUKI,

Earthquake Research Institute.

(Read June 17, 1952; May 19; Oct. 27, 1953.—Received Oct. 31, 1953.)

1. Introduction.

The property of building vibration has a variety according to the ground property even if the same vibrational force acts on the buildings of same structure, and the property of earthquake motion depends on the ground nature. Therefore it can be said that the buildings under earthquake are doubly influenced by the ground property.

On one hand the influence of the ground property on building vibration is made clear by giving forced vibration artificially to the building through a vibrator or other means, and on the other hand the property of earthquake motion itself is observed on the ground of various properties. Then these results may be combined so as to make it possible to presume the vibration of actual buildings caused by earthquake. Not a few studies from these two standpoints have been made and the relation between them is getting clearer.

Besides such an indirect method of study which can be applied generally, a direct method, that is the observation of earthquake motion in the buildings on various kinds of ground has been adopted. In Japan earthquake motions were observed in various wooden houses and a few reinforced concrete buildings by installing acceleration seismographs temporarily. In U. S. A., observations are made by means of strong motion seismographs installed at both the upper and lower parts of some buildings of reinforced concrete.

The present paper is intended to show systematically the relation of the property of building vibration in the course of earthquake to the ground property, which is obtained from the simultaneous observation made at the ground-floor and the roof-floor of the buildings of same structure standing on the ground of different properties.

2. Method of examination.

Two combinations of buildings of same structure with the ground of different properties are represented by A and B. In both A and B combinations, the buildings are four-storied apartments of bearing wall reinforced concrete construction. The building in A is called "49B of the Construction Ministry", the observation was made at two places: halfway up a mountain in Hyōgo Prefecture (the surface; piled up clay, bearing power; 6.5 t/m^2) and on the alluvium in the same prefecture (the surface; reclaimed land of a pond, bearing power; 7 t/m^2). In B, the type of building is called "Tokyo-to Residential Association 46" and observations were made on the diluvium and the thick alluvium in Tokyo.

The data concerning each building and place and the seismograph constants are shown in Table I. In Table I, the natural period of building is obtained from the results of vibration experiments made by using a vibrator[1].

Table I. (a; Earthquake No. B1–B3, b; B4–B8)

	Building			Seismograph				
	Type	Period (sec)	Position	Position	Period (sec)	Damp. ratio	Magnif.	
A	49 B	0.20	Takaha-Takemaru, Nada-ku, Kōbe-city	Roof	1.0	13:1	160	
				Ground	〃	〃	208	
		0.27	Kita-Nagato-chō, Nishinomiya-city	Roof	〃	〃	186	
				Ground	〃	〃	246	
B	46	0.32	Komagome-chō, Toshima-ku, Tokyo	Roof	〃	〃	138	102
				Ground	〃	〃	174	98
		0.28	Senju-hashido-chō, Adachi-ku, Tokyo	Roof	〃	〃	198	117
				Ground	〃	〃	233	146
							a	b

Figs. 1 and 2 illustrate the sketches of the buildings of type 49B and type 46, and Figs. 3 and 4 are the photographs of these buildings.

3. Results of observations.

The earthquakes in A and B are indicated in Tables II and III, and the epicenters are shown in Figs. 5 and 6.

The frequency-period relation of main shocks obtained from the seismograms of the earthquakes in A and B are shown in Figs. 7–16

1) K. KANAI, T. HISADA, K. NAKAGAWA and T. SUZUKI, *Res. Report, Architect. Inst., Japan*, No. **24** (1953), 185 (in Japanese).

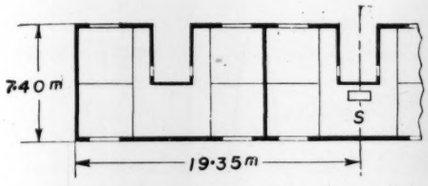

Fig. 1a. Plan view of type 49B.

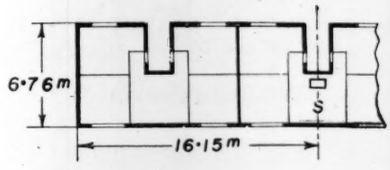

Fig. 2a. Plan view of type 46.

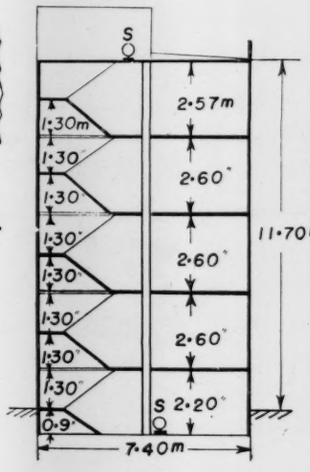

Fig. 1b. Side view of type 49B.

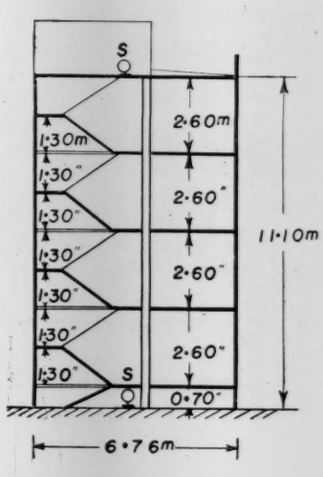

Fig. 2b. Side view of type 46.

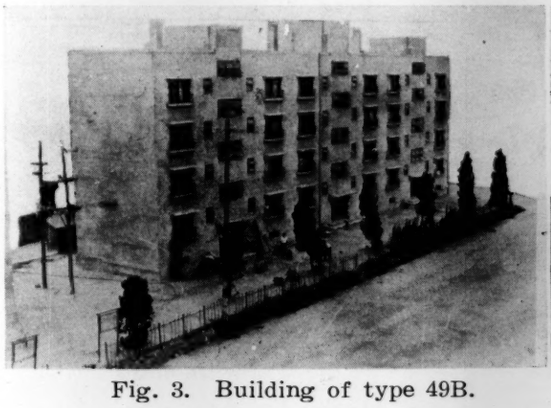

Fig. 3. Building of type 49B.

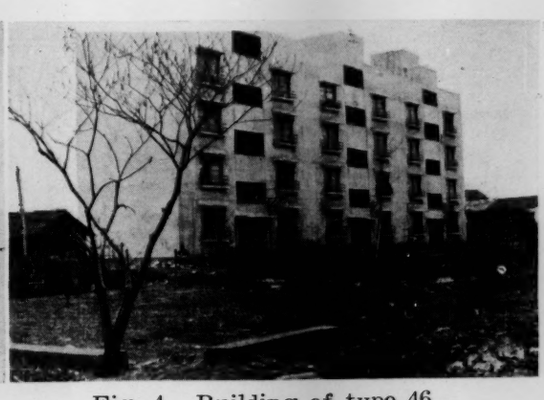

Fig. 4. Building of type 46.

Table II.

Earthq. No.	Date	Origin		
		Depth (km)	φ	λ
A 1	1951 IX 23	40	34.3	136.2
A 2	〃 〃 27	20~30	33.9	135.1
A 3	〃 〃 30	0~10	34.3	134.1
A 4	〃 〃 31	0~10	34.3	134.1
A 5	〃 X 9	20	34.7	135.0
A 6	〃 〃 11	40	33.7	134.4
A 7	〃 〃 14	80	32.5	137.2
A 8	〃 〃 16	40~50	32.8	134.3
A 9	〃 〃 23	20	34.6	135.0
A10	〃 〃 27	10	34.5	135.9

Table III.

Earthq. No.	Date	Origin		
		Depth (km)	φ	λ
B 1	1953 I 20	40	36.9	141.4
B 2	〃 〃 22	60	36.2	141.3
B 3	〃 〃 26	40	36.1	139.8
B 4	〃 II 11	10	36.4	140.6
B 5	〃 〃 13	—	Chiba-Prefect?	
B 6	〃 〃 18	40	36.5	141.0
B 7	〃 〃 〃	60	35.3/4	140.1/2
B 8	〃 〃 22	—	Tochigi-Prefect.	

Fig. 5.

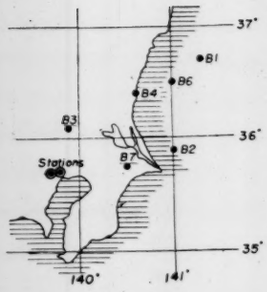

Fig. 6.

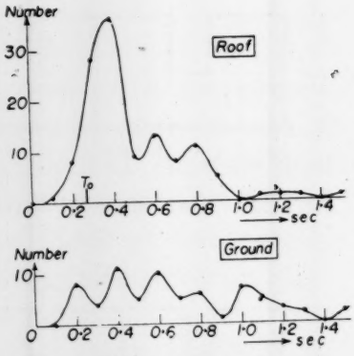

Nishinomiya

Fig. 7. Earthquake No. A1.

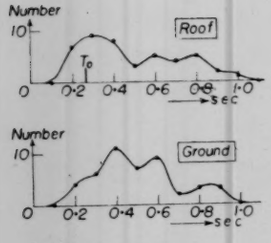

Nishinomiya

Fig. 8. Earthquake No. A2.

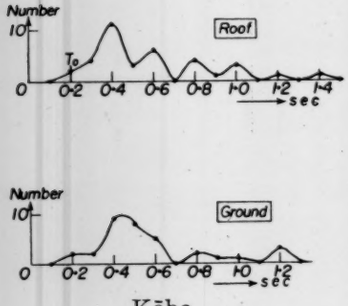

Kōbe

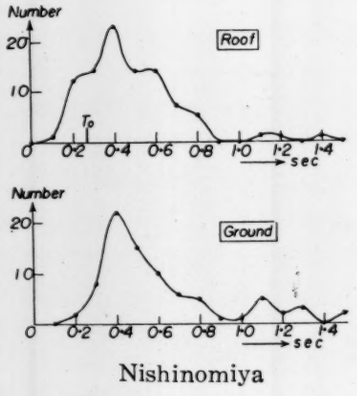

Nishinomiya

Fig. 9. Earthquake No. A3.

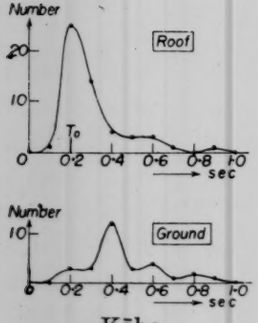

Kōbe

Fig. 10. Earthquake No. A4.

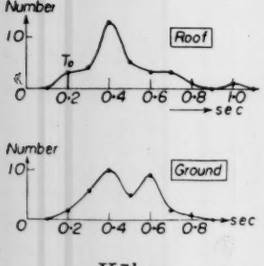

Kōbe

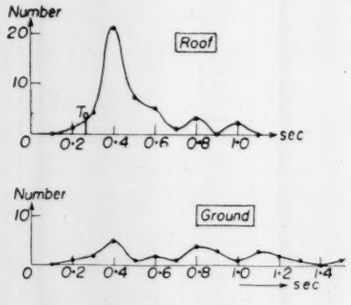

Nishinomiya

Fig. 11. Earthquake No. A5.

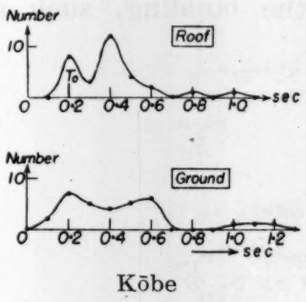

Fig. 12. Earthquake No. A6.

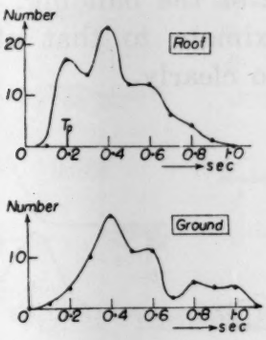

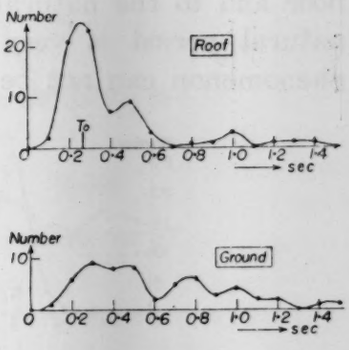

Fig. 13. Earthquake No. 7.

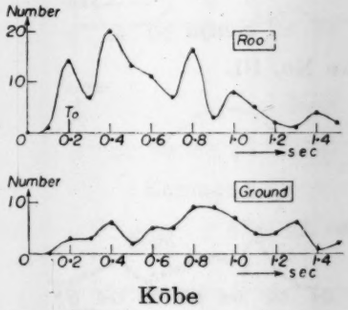

Fig. 14. Earthquake No. A8.

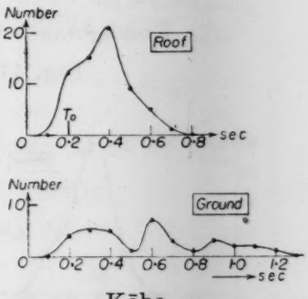

Fig. 15. Earthquake No. A9.

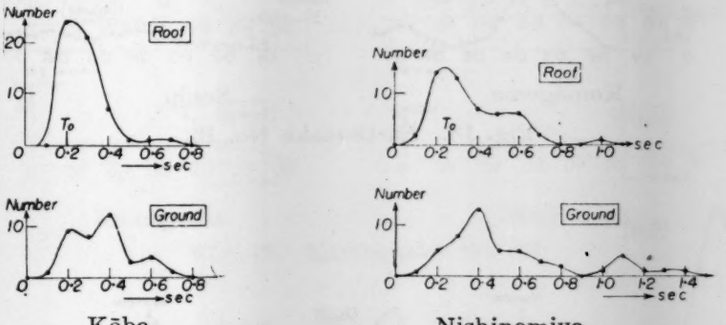

Fig. 16. Earthquake No. A10.

and Figs. 17–24 respectively. Among these earthquakes, the representative seismograms concerning A and B are shown in Figs. 25 and 26 respectively.

As for the frequency-period curves of Kōbe, Nishinomiya and Senju, it can be seen that generally the frequency at roof-floor has peaks at both periods corresponding to the maximum of frequency at the ground-

floor and to the natural period of the building. At Komagome, as the natural period is very approximate to that of the building, such a phenomenon can not be seen so clearly.

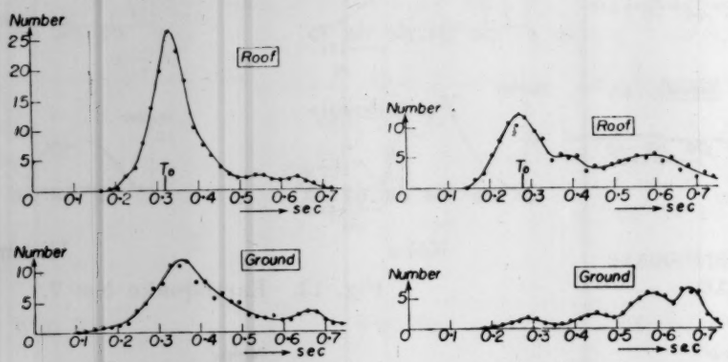

Fig. 17. Earthquake No. B1.

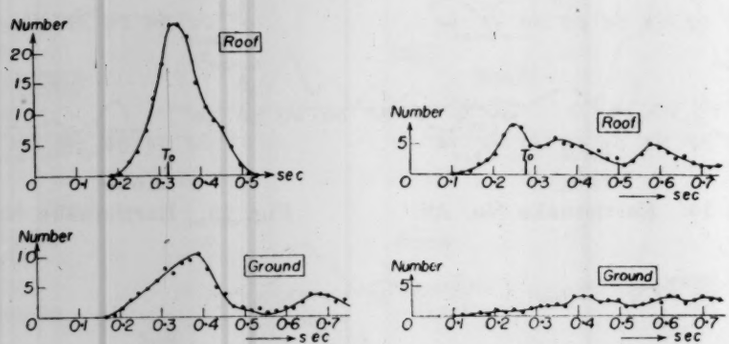

Fig. 18. Earthquake No. B2.

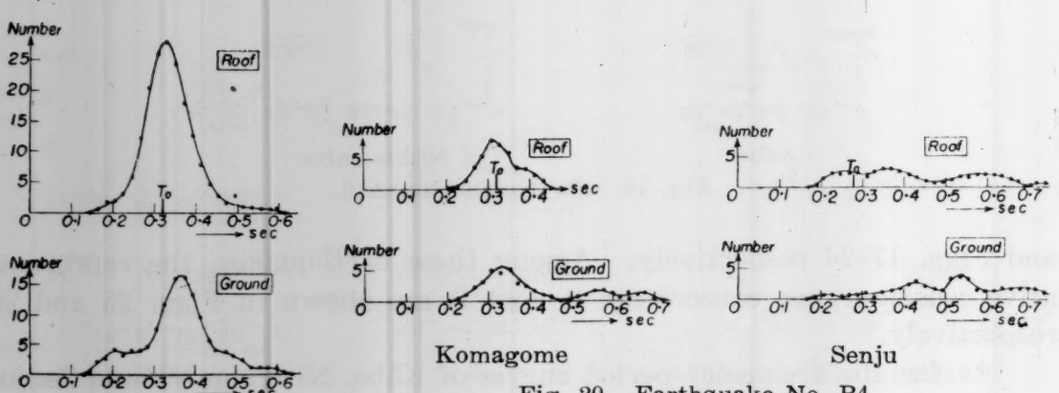

Fig. 19. Earthquake No. B3.

Fig. 20. Earthquake No. B4.

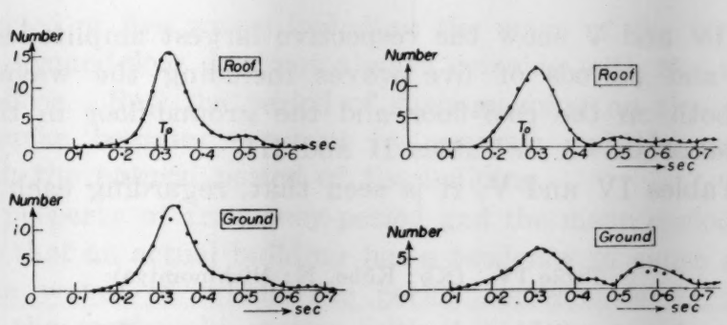

Fig. 21. Earthquake No. B5.

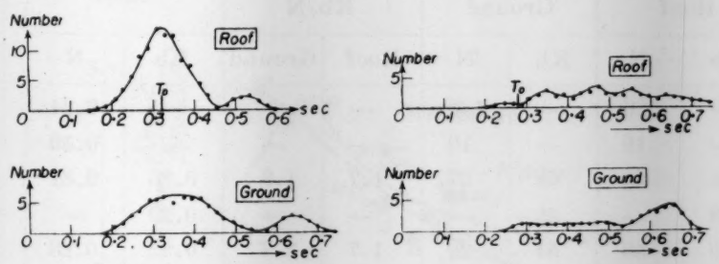

Fig. 22. Earthquake No. B6.

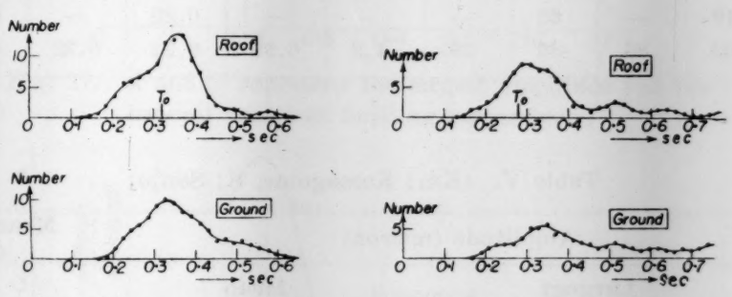

Fig. 23. Earthquake No. B7.

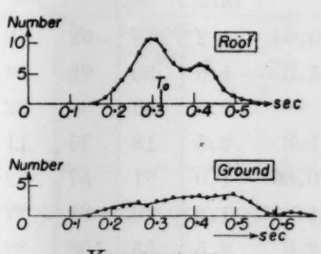

Fig. 24. Earthquake No. B8.

Tables IV and V show the respective largest amplitudes, the mean amplitudes and periods of five waves including the wave of largest amplitude both on the roof-floor and the ground-floor in the course of the earthquakes shown in Tables II and III.

From Tables IV and V, it is seen that, regarding each earthquake,

Table IV. (Kb; Kōbe, N; Nishinomiya)

Earthq. No.	Amplitude (micron)						Mean Period (sec)			
	Largest									
	Roof		Ground		Kb/N		Roof		Ground	
	Kb	N	Kb	N	Roof	Ground	Kb	N	Kb	N
A 1	—	236	—	146	—	—	—	0.24	—	0.60
A 2	—	19	—	10	—	—	—	0.30	—	0.36
A 3	104	63	69	37	1.7	1.9	0.36	0.31	0.44	0.40
A 4	58	—	25	—	—	—	0.29	—	0.40	—
A 5	90	53	54	20	1.7	2.7	0.22	0.28	0.46	0.26
A 6	31	—	17	—	—	—	0.29	—	0.40	—
A 7	30	30	16	11	1.0	1.5	0.31	0.27	0.50	0.30
A 8	159	—	180	—	—	—	0.44	—	0.70	—
A 9	116	—	62	—	—	—	0.25	—	0.50	—
A10	100	86	36	39	1.2	0.92	0.22	0.32	0.22	0.40

Table V. (Km; Komagome, S; Senju)

Earthq. No.	Amplitude (micron)										Mean Period (sec)			
	Largegt						Mean							
	Roof		Ground		S/Km		Roof		Ground		Roof		Ground	
	Km	S	Km	S	Roof	Ground	Km	S	Km	S	Km	S	Km	S
B 1	135	86	65	81	0.64	1.2	113	63	48	60	0.32	0.49	0.46	0.60
B 2	69	101	43	70	1.5	1.6	53	73	34	58	0.33	0.46	0.45	0.87
B 3	127	—	34	34	—	1.0	90	—	32	27	0.34	—	0.37	0.41
B 4	28	49	17	42	1.8	2.5	18	35	11	31	0.35	0.47	0.45	0.56
B 5	83	74	42	42	0.89	1.0	71	57	32	29	0.34	0.28	0.41	0.31
B 6	76	104	40	73	1.4	1.8	49	81	27	53	0.33	0.31	0.44	0.46
B 7	67	133	41	102	2.0	2.5	55	103	32	79	0.43	0.57	0.49	0.63
B 8	91	—	51	—	—	—	64	—	32	—	0.31	—	0.47	—

the mean period of five waves including the wave of the largest amplitude on the ground-floor does not always coincide with the mean period on the roof-floor. But, the period of such meaning on the roof-floor of each earthquake becomes constant in general, and the value agrees roughly with the natural period of the building.

Such a property of frequency-period and the mean period as relation here implies that an actual building has a tendency to cause a resonance selecting the waves of which the period corresponds to its natural period from the earthquake motion with irregular wave-form.

Fig. 27 and 28 show the ratio of largest amplitude obtained both on the ground-floor and the roof-floor to the mean period of five waves

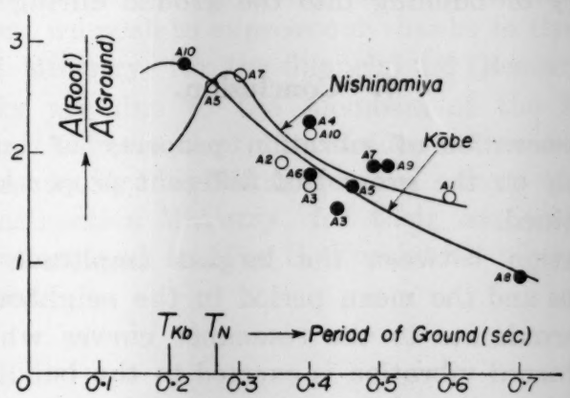

Fig. 27. A and T represent the largest amplitude and the natural period of building respectively.

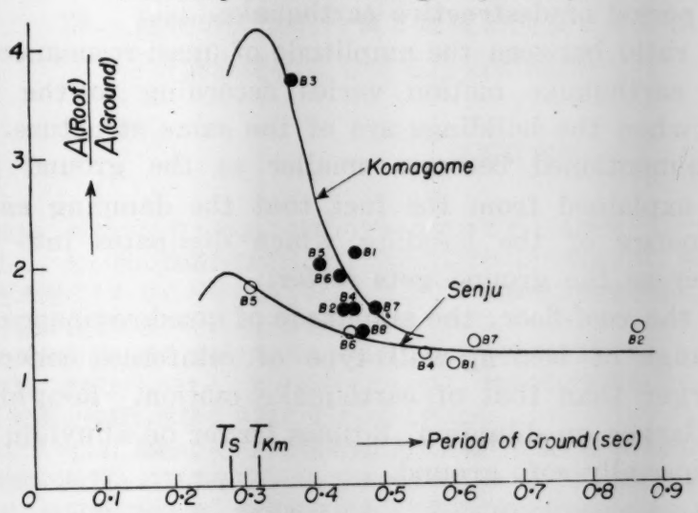

Fig. 28. A and T represent the largest amplitude and the natural period of building respectively.

including the largest amplitude on the ground-floor. (This relation is unchanged in the case of the mean amplitude of five waves including the wave of the largest amplitude observed both of the ground and roof floors). These figures indicate that the relation between the amplitude of building vibration and the period of earthquake motion strongly resembles that of the amplitude to the period of the building to which the forced vibration is exerted sinusoidally.

From the results related above it is found that the quasi-resonance amplitude obtained on the roof-floor becomes 2–4 time larger than that of the ground motion and the value gets smaller as the ground increases its softness. This is easily explained qualitatively from the nature of vibrational energy of building into the ground during earthquake[2].

4. Conclusion.

From the observation of vibration property of buildings of same structure standing on the ground of different properties, the following results were obtained.

(i) The relation between the largest amplitude of buildings in actual earthquakes and the mean period in the neighbour of the largest amplitude is approximate to the resonance curves which are obtained when sinusoidal forced vibration is exerted to the buildings. Therefore, from the point of earthquake-proof construction, it is needed that the resonance amplitude of the building is considered before it is possible to presume the period of destructive earthquake.

(ii) The ratio between the amplitude of quasi-resonance of building and that of earthquake motion varies according to the property of ground even when the buildings are of the same structure. The value of the above-mentioned becomes smaller as the ground gets softer. This can be explained from the fact that the damping caused by the vibrational energy of the building which dissipates into the ground becomes larger as the ground gets softer.

(iii) On the roof-floor, the amplitude of quasi-resonance of the four-storied buildings of bearing-wall type of reinforced concrete becomes 2–4 times larger than that of earthquake motion. Roughly speaking, it is 4-times larger on diluvium, 3-times larger on alluvium and 2-times larger on a specially soft ground.

---

2) K. SEZAWA and K. KANAI, "Improved Theory of Energy Dissipation in Seismic Vibrations of a Structure", *Bull. Earthq. Res. Inst.*, **14** (1936), 168.

(iv) The extent of the amplitude of ground vibration depends on the property of ground in case of earthquake is related to the period of seismic waves which reach the boundary surface between base rock and surface layer. Moreover, as seen from Tables IV and V, the ratio between the respective largest amplitudes obtained on the ground-floor of the buildings of same structure which stand on different kind of ground depends on the property of earthquake, but, generally speaking, on softer ground the value gets larger.

Therefore, at the time of earthquake, the effect of the amplitude of ground vibration on buildings counteracts the effect of damping of building vibration, and the difference among the largest amplitudes of buildings due to the ground property is not so great.

In conclusion, we wish to express our thanks to the Science Section of the Educational Ministry, for the financial aid (Research Funds) granted us. Also thanks are due to the members of the Building Section of Hyōgo Prefectural Office and of the Residential Association of Tokyo-to for their help and to Mr. K. Nakagawa and others of the Architectural Institute of Construction Ministry, for their cooperation in the course of these observations and to Miss S. Yoshizawa who assisted us in preparing this paper.

---

29. 建物の振動的性質と地盤の性質との関係
(実在建物における地震動観測)

地震研究所 {金井清 / 鈴木富三郎}

地震による建物の振動の性質が地盤の性質の影響を受けることは概念としては既によく知られているところである．わが国の建築方面では，既に建物の設計に使う地震力に，構造の種類と，地盤の性質の差違とを考慮に入れることになつている．しかし，地震時の建物の振動と地盤の性質との量的な関係は，今後の研究にまつところが非常に多い．

同種の構造の建物に同じ形の強制力を与えた場合でも，地盤の性質がちがうと，建物の振動性状は異る．又，地盤の性質がちがうと，同じ地震についても，地表面の震動が異る．従つて，地震時の建物の振動は，地盤の性質の影響を2重に受けることになる．

前者の研究については，建物に人工的な強制力，例えば偏心荷重の廻転による力を与えて，建物の振動的性質と地盤の性質との関係をしらべる方法がとられている．又，後者については，このことを直接の目的とする地震動の理論的，験震的研究並びに震害の統計的研究があるほかに，地震動の性質をしらべるためのいろいろな立場からの研究の中に自然に数多くふくまれている．しかし，現在までのところ，両者をむすびつけて，量的な結果を得るための研究はあまり試みられていない．

本研究は，耐震設計上の地盤係数を求めるために，性質の異る地盤の上に建つ同種構造の建物の地階と屋上とで地震動の比較観測を行つたものである．

あらゆる地盤について，地震時の建物の振動は，地階と屋上では波形が異る．最も手軽な地震記録の解析方法として，いわゆる頻度一周期曲線を作つて見ると，屋上の頻度一周期曲線には，地階の頻度一周期曲線の山のできるところと建物の固有周期にあたるところとの，少くとも2つの山ができる．又，屋上の最大動附近の数波の平均周期は，多くの地震について建物の固有周期に近い．この2つのことは，地震時に建物は自己振動を起し安い性質のあることを示すものである．

次に，最大動について，地階の振動周期に対する，屋上変位と地階変位との比の関係を求めてみると，その形は，あたかも，建物に正弦波形の強制力を加えた場合に得られる共振曲線によく似ている．このことは，起振機のようなものを使つて求めた建物の振動特性は，地震時の建物の振動特性として，工学的には採用できることを意味する．

今回の研究結果によると，地動変位に対するこの種の建物の屋上の変位の比は2～4倍となり，地盤が堅い程大きい値をとる．その原因は，地震時に建物の振動勢力が地中に逸散するための振動減衰性によると考えられる．他方において，地震動振幅は一般に地盤が軟いほど大きくなる．

従つて，地震時における建物の振動に対する地盤の影響としては，建物の振動減衰性と地盤の性質との関係と，基礎の振動振幅と地盤の性質との関係が互に消し合う傾向になる．

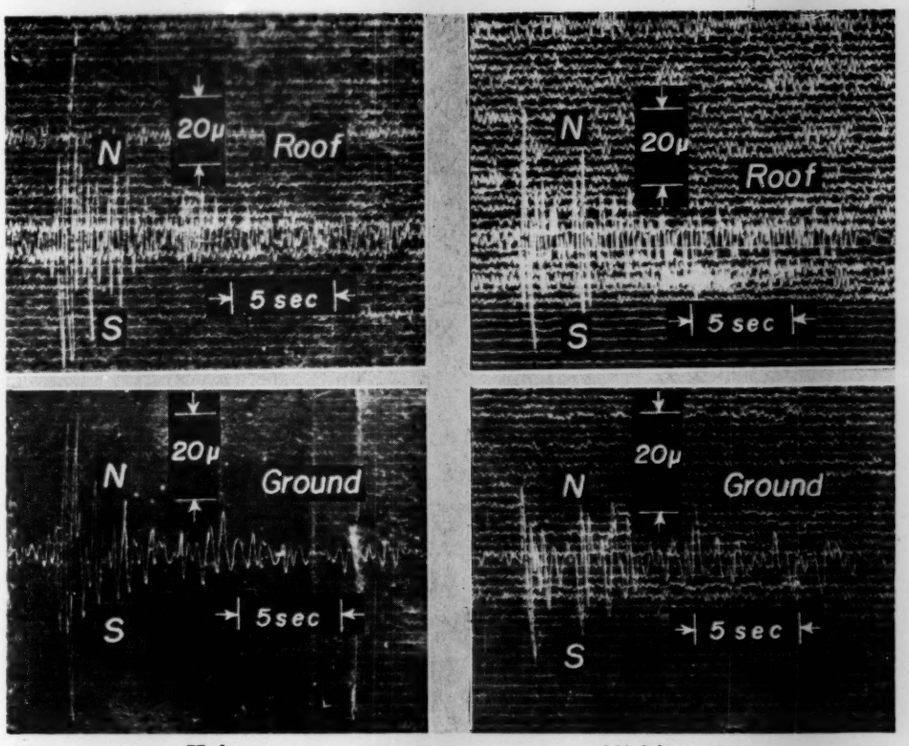

Kōbe Nishinomiya

Fig. 25. Earthquake No. A3.

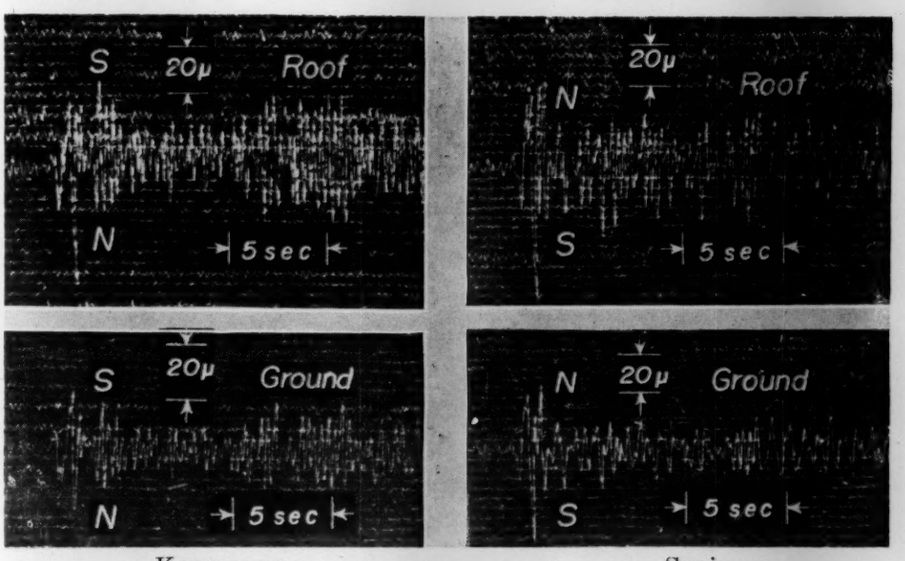

Komagome Senju

Fig. 26. Earthquake No. B6.

30. A *New-Designed Prospecting Apparatus.*

By Genrokuro NISHIMURA, Masazi SUZUKI,
Earthquake Research Institute,
and Eiichi FURUKAWA, Tomio KOTAKI,
and Koichi TAKAHASHI,
Faculty of Engineering,
Chuo University, Tokyo.

(Read June 16, 1953.—Received Oct. 31, 1953.)

1. Introduction.

It is well known that, as a prospecting method for determining the construction of the earth's layers, there is a device which makes use of artificial seismic waves. In this method, the waves are of course generated by a shock applied to the earth's surface by dropping a suitable weight or by exploding a effective dynamite. In measuring the travel times of the waves in the earth, generally at least two seismometers of moving coil type are used for detecting weak seismic waves, which are usually set at two different localities, i.e. A and B on the ground respectively, the locality A being near the shock origin. The output voltages of the transducers of these two seismometers induced by the travelling seismic waves are amplified and then recorded on an oscillograph paper by using an electro-magnetic oscillograph. The travel time of the shock between the two localities A and B is obtained by measuring the distance between the two thresholds of initial motions of the respective wave-phases taken on the paper. Varying the distance between the two localities A and B on the ground by moving the locality B, we obtain the travel time of the shock for respective varied distances, and hence we are able to obtain the "time-distance curve" which is necessary in determining the properties of the stratified layers of the earth. Fig. 1 shows schematically the paths of propagated waves which are excited by a shock. In Fig. 1, if the transducer B is set near the transducer A which is set near the position of the shock origin, the wave propagated directly through the surface of the earth arrives first at the seismometer B. But, if the distance between the two localities of seismometers becomes rather long,

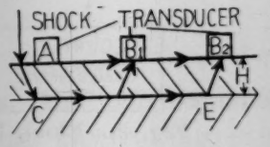

Fig. 1.

the wave which propagates through the second layer arrives at the locality B faster than the direct one, because the velocity in the second layer becomes larger than that in the first, or in other words, the wave propagated through the path$ACEB_2$ becomes faster than that propagated through the path AB_2. Now, the surface of the earth consists generally of a number of layers in which the seismic waves have different velocities respectively, and therefore we can see, on the "time-distance curve", many lines with different tangents in accordance with the layers under the ground. Assuming the boundaries of the stratified layers to be parallel to the surface of the earth, we are able to obtain the depth of the first layer H with the aid of the "time-distance curve", which is determined by the following formula:

$$H=\frac{Z}{2}\sqrt{\frac{v_2+v_1}{v_2-v_1}}\ ,$$

in which Z shows the horizontal distance between the origin and the point which corresponds to the first intersection point of the "time-distance curve", and both v_1, v_2 are velocities corresponding to the first and the second layers respectively, they being directly read off from the tangents of the "time-distance curve".

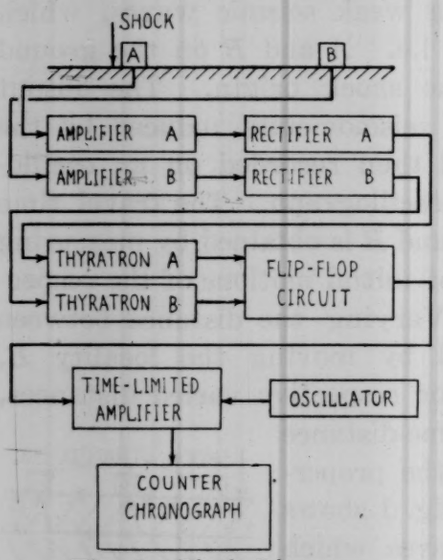

Fig. 2. Block Diagram of the Apparatus.

Now, in the usual method, to obtain the "time-distance curve", we must measure the time interval between the two initial motions recorded on the oscillograph paper, as already explained. In the present prospecting apparatus, however, the procedures of measuring the time interval on the oscillograph paper and using an electro-magnetic oscillograph, are dispensed with and the measuring procedure of the time interval is done automatically by electronic circuits. The principles of the present new-designed apparatus will be explained by both diagramatic and schematic methods as follows. In the block diagram Fig. 2, the output voltages gained from two transducers A and B are fed to the amplifiers A and B respectively. The output of the amplifiers is rectified in the next circuit. The respective output voltages gained from the rectifying circuits appear always in the

positive no matter whether the sign of the input voltage given to the rectifying circuit becomes positive or negative, owing to the mechanism of the circuit. The respective output voltages are fed to the following thyratron grids respectively. When the shock waves arrive at the seismometer, the thyratron ignites instantaneously, and then the differentiated pulse appears at the output of it. Next, the two pulses produced at *A* and *B* thyratron outputs are fed successively to the grids of flip-flop circuit. Then the variation of the plate voltages at the flip-flop circuit becomes rectangular as shown in Fig. 3. On the other hand, a local oscillator of 8000 c/s is involved in this instrument and the output voltages of this oscillator are amplified by an amplifier which is controlled by the plate voltage of the above-mentioned flip-flop circuit and is capable of amplifying the 8000 c/s waves during only the time interval in which voltage of rectangular form as shown Fig. 3 is excited. In short, the 8000 c/s waves are amplified during the time interval between the two thresholds of output voltages gained from the two seismometers *A* and *B*. Hence, these waves excited only for finite time interval are fed to the counter chronograph which is constructed to indicate the number of the fed pulse by the neon lamp ignition device. From the above explanation, we can see that when we use the present electronic instrument, we are able to read quickly and easily in direct manner the time interval which is necessary to obtain the "time-distance curve".

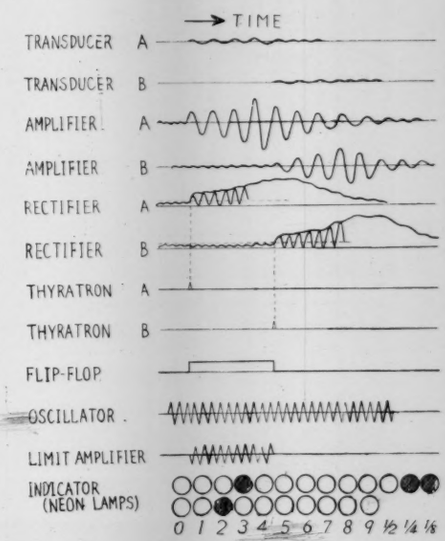

Fig. 3. Schematic Show of the Principle of the Apparatus.

2. Apparatus I. Transducer.

As in the usual seismic prospecting apparatus, the seismometer used for the present apparatus is also composed of an electromagnetic transducer of the moving coil type. The sensitivity of it, however, becomes pretty higher than that of the transducers of the same type used heretofore, because for its mechanical construction we adopt a new design wherein the motion of its moving coil is magnified with

Eden's twin strips[1], one end of which is connected to the moving pendulum weight of the seismometer. Figs. 4a, 4b and 5 show the diagram and the photograph of the seismometer for the present study. The present seismometer consists mainly of the following seven parts: (1) the outer case *A*, (2) the pendulum weight *B*, (3) supporting spring plates C of the weight, (4) a moving coil *E*, (5) supporting lever *F* of the moving coil, (6) the Eden twin strips *D*, and (7) the clamps *G* of

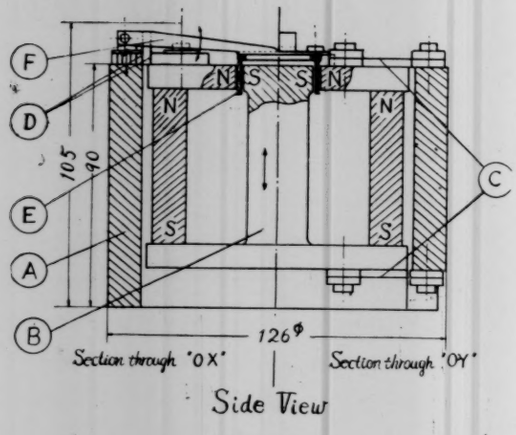

Fig. 4a. Seismometer with Eden's Twin Strips.

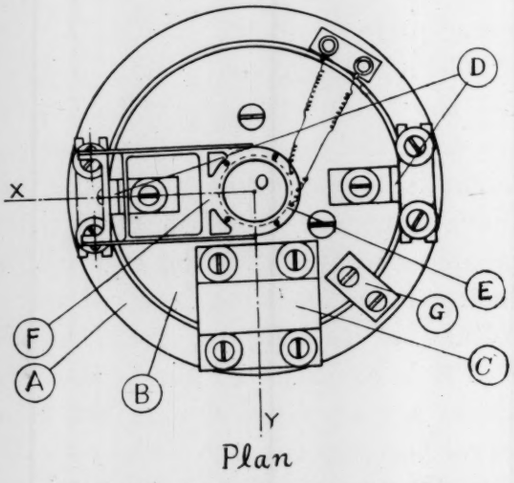

Fig. 4b. Seismometer with Eden's Twin Strips.

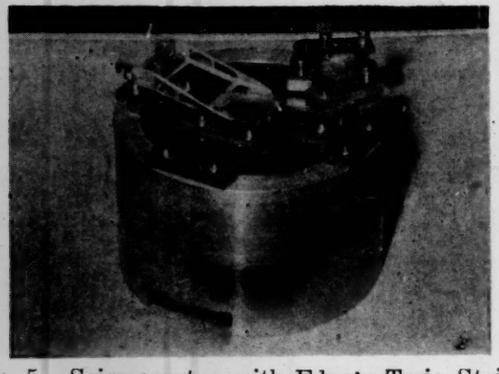

Fig. 5. Seismometer with Eden's Twin Strips.

the weight. The case *A* is made of an Aluminium cylinder of which the inner and outer diameters are 150 mm and 190 mm respectively and the height 150 mm. The pendulum weight *B* of 3 Kg is fixed to and

1) Eden's twin strips is generally used for statical magnifying device as for precise comparator. Both the statical and dynamical properties have been theoretically and experimentally studied by us in a minute manner, and be fully reported in the next occasion.

supported by the ends of the two parallel spring plates C of phosphorous bronze at its top and bottom surfaces respectively and the other ends of these spring plates C are fixed to the case A. Therefore, through the total restitutive forces of the two spring plates, the weight B can only do vertical motions in its small vibration amplitudes. The weight B is composed of two parts: (1) MK permanent magnet of hollow cylinder and (2) mild steel block which is so shaped that the annular gap is prepared for the motion of the moving coil E which moves up and down through the gap where the magnetic flux is concentrated. The coil E is attached to one end of the lever F, the other end of which is fixed to the point of Eden's twin strips D as shown Figs. 4 and 5. The end of one of Eden's twin strips is fixed to the pendulum weight B, and the end of the other strip to the top surface of the case A. The longitudinal axis of Eden's twin strips becomes of course parallel to the vertical axis of the pendulum weight of cylinder. We are able, therefore, to understand, concerning the motion of the moving coil E connected to the weight B with Eden's twin strips, that if the pendulum moves upwards or downwards a little, the movement of the coil becomes also upwards or downwards respectively. But, as a matter of fact, in spite of the infinitesimal movement of the pendulum weight, the coil's movement becomes factually large, because it comes to be magnified greatly by means of both the magnification mechanisms of Eden's twin strips and also the lever system F. Hence, the moving coil with those magnification mechanisms can move through the gap of concentrated magnetic flux with fast speed which becomes larger than that of the pendulum weight. It is characteristic of the present transducer that the sensitivity becomes larger than that of the ordinary transducers of moving coil type. The moving coil is made of 7000 turns of No. 48 enamel covered copper wire and has an electric resistance of 2000 ohms, its mass being 16 grams weight. When the shock waves arrive at the seismometer, it begins to vibrate and the output voltage induced in the transducer becomes of course proportional to the relative velocity between the coil E and the pendulum weight B.

Considering the mass of the coil, we can easily derive, from the fundamental equation of vibration, the relation between dynamical magnification V and geometrical magnification V_G of the seismometer as follows:

$$V = V_G/(1 + V_G^2/\mu),$$

where $\mu = M/m$, and M and m are the masses of the pendulum and the coil respectively. From the expression of V, we can obtain Fig. 6

which shows the characteristics of the seismometer. From Fig. 6, we can see that there is a maximum value of V and this value becomes large when the value μ becomes large. It is actually difficult, from

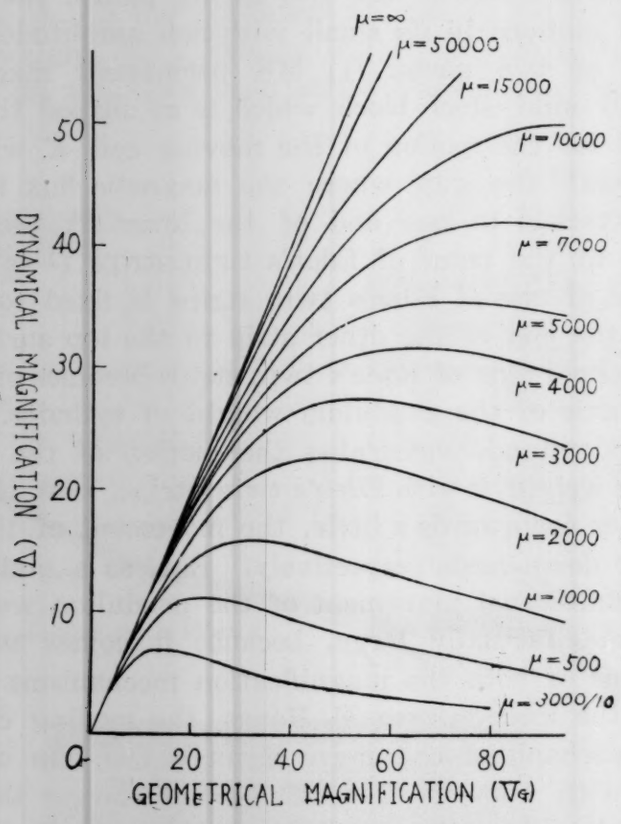

Fig. 6. Characteristic Curve of Seismometer.

the technical point of view, to make the value μ large, and in the present case μ becomes as follows:

$$\mu=(3\text{ kg})/(16\text{ gr})=(3000)/(16).$$

Therefore the maximum point of V for the present seismometer has the value $V=6.7$ when $V_G=13.6$.

The natural frequency of the present seismometer becomes about 20 c/s and the sensitivity of it becomes 5 Volt/cm/sec which is almost ten times as large as the ordinary one.

Generally, we know that there are two kinds of magnetic type transducer: (1) the reluctance type and (2) the moving-coil type. From the viewpoint of our request, the moving-coil type is more convenient than the reluctance type, because the reluctance type cannot easily

obtain suitable damping of the seismometer in spite of its high gains. The damping h of the present seismometer is expressed by the following formula which is also derived from the basic consideration of both the electro-magnetic transducer and the equation of vibration:

$$h=\varepsilon/n=R/(2nM)\cdot V_G^2/(1+V_G^2/\mu),$$

in which R becomes a constant concerning the electro-magnetic effects and the construction of both the coil and the lever and also h, n and ε are indicated in the following equation which is reduced from equations concerning electro-magnetic transducer:

$$d^2x/dt^2+2\varepsilon dx/dt+n^2x=f,$$

where n is free angular frequency and ε damping coefficient. Here, we can see that the damping becomes proportional to V_G^2 in the range of small value of V_G. In our case, the existence of damping is rather convenient for preventing the noise effect of the ground.

3. Apparatus II. Gate Circuit.

The gate circuit operates between two successive pulses and is composed of the following six parts: (1) two amplifiers, (2) two rectifiers,

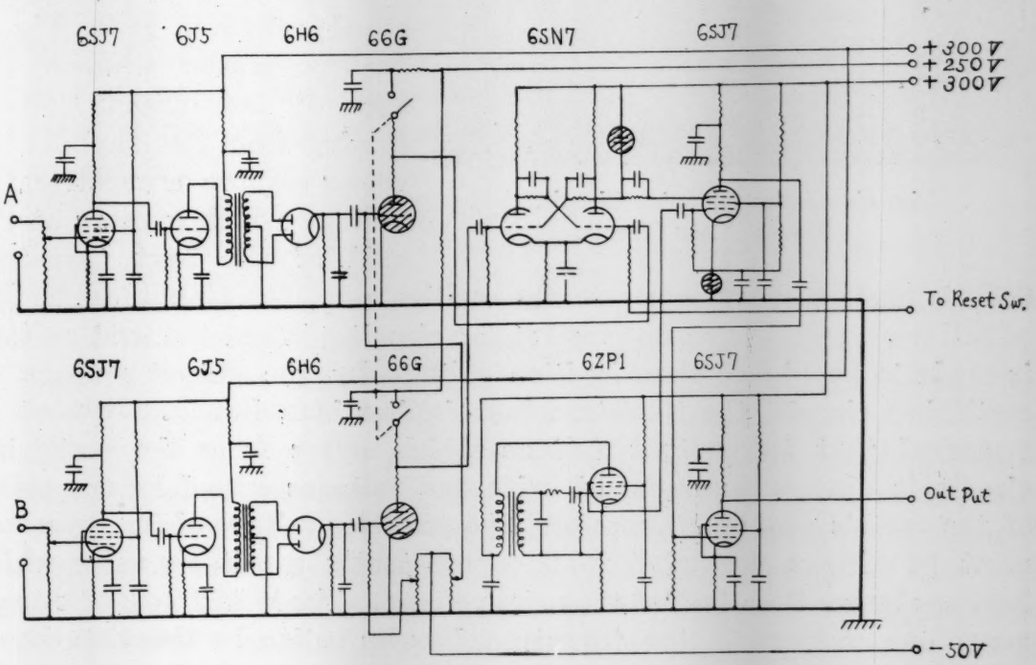

Fig. 7. Gate Circuit.

(3) two thyratron circuits, (4) a flip-flop circuit, (5) a local oscillator and (6) a time-limited amplifier. Fig. 7 is the diagram of this circuit, and its apparatus is shown in Figs. 8a and 8b.

The two amplifiers consist of the two bulbs 6SJ7 and 6J5 respectively, and they amplify the respective voltages gained from the two seismometers. The gains of these amplifiers are regulated by the variable resistances at the inputs and the maximum gains becomes about 50 db. Of course, these two amplifiers are specially designed to obtain their respective voltage supply independently for the purpose of avoiding any coupled relation which shall be excited between these two amplifiers.

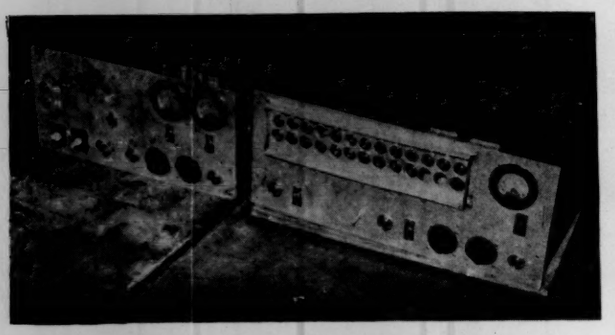

Fig. 8a. Left: Gate Circuit.
Right: Counter Circuit.

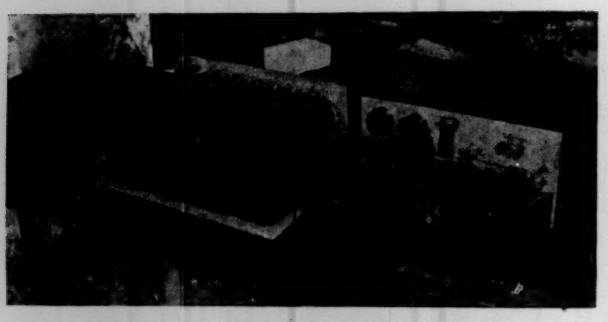

Fig. 8b. Left: Counter Circuit.
Right: Gate Circuit.

Next, the output voltage which comes from the amplifier is fed through the audio transformer to the rectifying circuit of 6H6. We can understand moreover from Fig. 7 that no matter whether the sign of the output voltage coming from the amplifier becomes positive or negative, the voltage which appears at the grid of the next thyratron 66G, is made to show a constantly positive sign, the circuit connection of full wave rectifying being used in the circuit. When the grid voltage is made to be higher than ignition voltage by the output voltage of rectifying circuit, the thyratron bulb ignites immediately. It must be remarked that the output voltage which comes from the rectifying circuit is always accompanied with the voltages caused by the noises of the earth's ground. Therefore, the grid bias voltage of the thyratron must be always regulated to have constantly a suitable value which becomes larger than that of the noise voltage. For it will not, of course, serve our purpose if the thyratron does its action by the disturbance voltages due to noises in the earth. The magnitude of the noises varies always with time and place, and therefore, in respective cases of the prospecting procedure, we must regulate the action level of the thyratron appropriately so that it will not be influenced by the noise voltages.

After the two thyratrons do their actions of ignition for respective signal voltages, respective plate voltages in the parallel circuits are differentiated by passing the circuit with a condenser and a resistor respectively. These two differentiated voltages are successively fed to each grid of the flip-flop circuit of 6SN7 as shown in Fig. 7. By reset switching, the flip-flop circuit is previously set in the state in which the plate in one side of 6SN7 becomes conducting and that in the other side becomes not conducting. Then the voltage of the suppressor grid of the next amplifying bulb 6SJ7 becomes lower, and therefore the amplifying action of it is lost. When the first pulse comes in the flip-flop circuit, a change occurs in the state of the flip-flop circuit and the suppressor grid voltage of the next bulb becomes high and the bulb recovers its function of amplifying. Next, when the second pulse comes in, the state of it returns again to the original one. On the other hand, the sinusoidal waves of 8000 c/s produced by the local oscillator of 6ZP1 are fed constantly to the control grid of 6SJ7. Therefore, the waves of 8000 c/s appear at the plate of this bulb during the time when the suppressor grid attains high voltage.

In order to know the duration time in which the shock makes the action on the first seismometer *A* and next on the second seismometer *B* on the ground, we must count the numbers of the waves which appeared at the output of the bulb 6SJ7 by the next counter chronograph circuit.

4. Apparatus III. Counter Chronograph Circuit.

The diagram shown in Fig. 9 is the circuit of the counter chronograph for the present apparatus, and its practical apparatus is shown in Figs. 8a and 8b. The first bulb of the circuit has an important rôle in making the operations of the next flip-flop circuits smooth and changing the sine wave form of the waves which come from the preceding circuit into square form. Because, in the case of sinusoidal waves of 8000 c/s, the circuits cannot operate owing to their low frequency. The squared voltages are then fed to the series of many flip-flop circuits as shown in Fig. 9. Now, the flip-flop circuit used for the present apparatus becomes Higinbotham's[2] "scale of two" circuit. The action of the series of the first three steps of these is to reduce the 8000 c/s scaling down to 1000 c/s. Beside these series, there are two groups which are constructed by four "scale of two" circuits. These are "scale of ten" circuits modified

2) W. A. Higinbotham, *R.S.I.*, **18** (1947), 706.

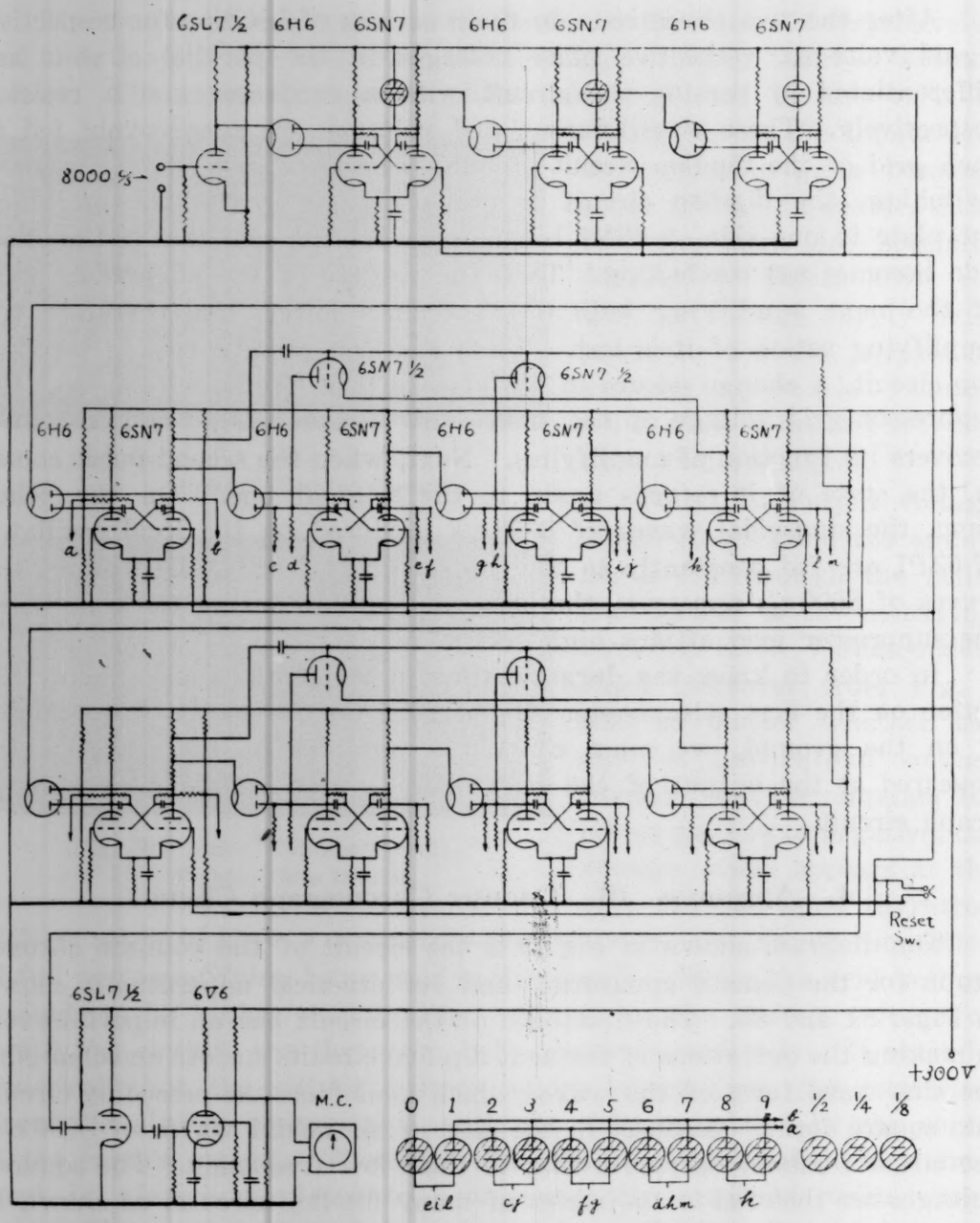

Fig. 9. Counter Chronograph Circuit.

by the "scale of sixteen" by the leap phenomena, in counting, produced by the two triods as shown in Fig. 9. By the two "scale of ten" circuits above mentioned, the square waves of 1000 c/s is reduced to those of 10 c/s.

By these procedures, the states of all flip-flop circuits are varied

favourably in accordance with the numbers of fed pulses of square waves, and henceforth the numbers which show the time duration, are instantly indicated by the twenty-three neon tubes connected suitably to the present circuit. These neon tubes are schematically shown in the last line in Fig. 3. In the circuits connected as shown in Fig. 9, three neon-tubes indicate 1/8, 1/4 and 1/2 milli-seconds, and ten neon-tubes indicate respectively the numbers of 1 milli-second order, and also another ten the numbers of 10 milli-second order respectively. By these procedures with this counter chronograph circuit, we can actually and easily read the numbers of the fed pulses which come from the gate circuit. For instance, in the last line in Fig. 3, if we assume that the shaded four neon tubes are lightened by the fed pulses, we can immediately read that the time interval of the fed two pulses becomes 32 and 3/8 milli-seconds.

For the time intervals which becomes longer than 100 milli-seconds, this circuit repeats the operation of the same procedures as already discussed, so that the mechanical counter is able to indicate the repeated numbers. The circuits composed of the bulbs of 6SL7 and 6V6 are made to drive the mechanical counter.

For this counter chronograph, the time is measured at an accuracy of 1/8000 seconds, because the frequency of the local oscillator becomes 8000 c/s for the present case. Therefore, if we want to change the accuracy of the counter, it may be done by changing the frequency of the local oscillator. In the actual case of the prospecting of detecting the rather shallow layers, we think that it is suitable to use the frequency of 8000~1000 c/s as the time scale.

5. Experiment.

The experiment with the present new-designed prospecting apparatus was carried out at the ground in front of the Department of Geophysics, Faculty of Science, Univ. of Tokyo. At this ground, the seismic prospecting by ordinary method with electro-magnetic oscillograph has already been done by some investigators, and therefore the structure of the earth's surface under this ground is somewhat clear.

The two new-designed seismometers were also set on the ground, and one of them was set of course very near the place where the artificial shocks were given. Before the commencement of the measurement proceeding, both the gains of the amplifier and the grid bias of the thyratron were regulated to secure the state in which the thyratron

grid voltage becomes a little higher than the noise level of the ground under prospecting. We then closed the "reset switch". Then, the state of the flip-flop circuit in the gate circuit became normal and the twenty three neon lamps indicated zero. Hereby, we made the complete preparation for the measurement procedure. At a signal to produce a shock on the ground surface, a steel ball filled with lead weighing the 40 kg, was dropped from a suitable height as shown in Fig. 10. Then the set of the neon-tubes of the counter chronograph instantly showed the time interval needed for the shock travel between the two seismometers on the ground. By this procedure, varying the distance between the two seismometers, we were able to obtain the data in Table I quickly and easily. Therefore the "time-distance curve" were obtained from Table I as shown in Figs. 11 and 12, in which the unit of ordinate becomes 10^{-2} sec., and that

Fig. 10. Shock Generation Device With Ball.

Table I. Indication of neon lamp.
(Data A & B show in Figs. 11 and 12 respectively.)

Distance (m)	Data A (milli-sec.)	Data B (milli-sec).	Distance (m)	Data B (milli-sec.)
3	21, 22, 23, 25 30. 32	20, 22	22	84, 86
4	29, 30, 31	26, 27, 27, 29	24	87, 87
5	36, 36, 37	28, 30, 31, 33	26	89, 92
6	39, 40	32, 35, 37, 37	28	85, 86, 90, 94, 96,101
7	43, 43, 44, 52, 53		30	95, 97, 104, 106
8	48, 48, 49, 56	39, 43, 44, 47	32	92, 93, 104, 109, 114
9	50, 51, 51, 52	41, 47, 48, 49		
10	54, 55			
11	57, 57, 58	49, 51, 54		
12	62, 63, 63			
13	65, 67	63, 63		
14	68, 69, 70, 75			
16		72, 73		
17		78, 79		
18		80, 81		
19		82, 82		

of abscissa is shown in meter. Of course, these two Figures are taken from two respective measuring lines on different days. As Fig. 12 shows, at the distances far from the shock origin, the points showing the

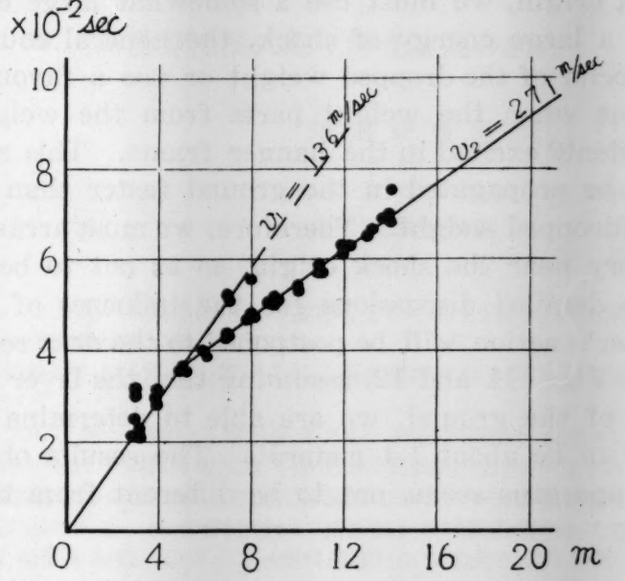

Fig. 11. Time-Distance Curve.

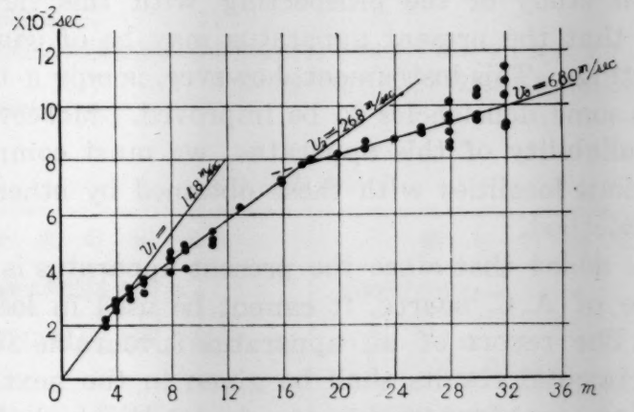

Fig. 12. Time-Distance Curve.

measured time tends to scatter and it becomes somewhat difficult to determine exactly the "time-distance curves" for these points. The reason for the occurrence of this phenomenon, perhaps, is as follows: The magnitude of the noise voltage at this ground becomes comparable with that of the threshold voltage due to the shock wave at the locality distant from the shock origin, and also at times the thyratron *B* in

Fig. 7 does its action for another shock of unknown origin different from the shock wave excited by the experimented shock origin. From these facts, therefore, it must be remarked that in case of distances far from the shock origin, we must use a somewhat large energy of shock. For obtaining a large energy of shock, the general course is to increase the falling velocity of the dropped weight or use a favourable dynamite. At the moment when the weight parts from the weight hanger, the reaction is suddenly excited in the hanger frame. This reaction through the frame will be propagated in the ground faster than the shock wave excited by the dropped weight. Therefore, we must arrange seismometer, which is set very near the shock origin, so as not to be excited by this reaction. The detailed discussions for the influence of this reaction on the seismometer's action will be postponed to the next report. From the data shown in Figs. 11 and 12, assuming that the layer becomes parallel to the surface of the ground, we are able to determine the depth H of the first layer to be about 1.4 meters[3]. The results obtained so far by this present apparatus seems not to be different from those obtained by other methods.

6. Conclusion and Acknowledgement.

The present study of the prospecting with this new-designed apparatus shows that the present apparatus may be of some use in actual seismic prospecting. This instrument, however, is only a trial and therefore it contains some deficiencies to be improved. Moreover, in order to develop the availability of this apparatus, we must compare the results obtained at various localities with those obtained by other methods such as the boring method.

It must be added that since the present apparatus is combined with eliminater type of A. C. source, it cannot be used in localities with no A. C. source. The report of an apparatus favourable for D. C. source with the experimental results shall be given in the next occasion.

In conclusion, we must express our sincere thanks to Mr. Shigematsu Ito and Mr. Yoshiro Komatsu of the Ministry of Agriculture and Forestry who suggested the necessity of the present study to one of the present writers and made every exertion in obtaining some expenses for the present study. The authors also express hearty thanks to Mr. Torawo Yamazaki of the Shimada Rika Industry Company, Ltd., who also

3) From Fig. 12, we obtained the following results: The thickness of the first layer=1.3 m, and that of the second layer=2.7 m.

suggested the necessity of the present study and encouraged the writers during the course of the present investigation.

30. 簡易彈性波式地下探査装置の研究

地震研究所 西村源六郎 鈴木正治
中央大学工学部 古川英一 小滝富雄 高橋浩一

電源開発，農耕用水，上水道，工業等の用水の調節など，水の合理的な利用開発のため，今全国各地で，ダムやトンネルの建設が盛に行われている．

そこで，其等の工事の基礎となる地盤の様子を知る事が重要になるのであるが，此の目的には色々な方法が用いられている．

直接的には，ボーリングを行つて調べる事が出来るが，経済的理由から種々の，間接的方法で推定する事が行われている．玆に所謂彈性波式地下探査法は間接的方法の一種である．

之は二つの換振器（地震計の一種）をある距離だけ隔てておき，一方の換振器の近くで地面に衝撃を与えて，彈性波を起すのである．此の彈性波が，換振器から換振器迄伝わるに要する時間を距離の函数として，測定し，時間と距離とのグラフ（走時曲線）から地表下にある幾つかの地層の位置や状態を理論的に推定するのである．

従来は，此の場合の時間測定の方法として，電磁オスシロを用いて感光紙上に現れた記録のうち，一方の初動から他の初動迄の時間差を読みとつたのであるが，実際は可成り手数が，かかる上に，初動以外の記録は不必要である．

本装置では此の操作を，両換振器からの初動だけを捉えてエレクトロニツクスを応用した真空管回路が，自動的に働いて，呉れるので，非常に簡単化された．玆に本探査法の特徴を従来のものと比較して列挙して見ると次の如くなる．

表 1

従来の装置	新しい装置
1 回の実験に時間を要する．	短時間ですむ．
1 回の実験に要する経費が割合に多い．	経費が要らぬ．従つて回数を増し誤差を少くする事が出来る．
実験にかなりの人数を要する．	最小限二人で済む．
初動を写真現像で読む装置に非常な経費を要する．	此の操作がない．装置の経費は従来のものの $1/10$ 以下．
全装置は可成りの容積になる．	割合に小型である．

彈性波が通過するに応じて，近い方から A，B なる二つの換振器が動かされて，それぞれの端子に相次いで第 3 図に表わされたような形の電圧を生ずる．之等の電圧は別々に次の増幅器 A 及び B に入つて増幅され，更に整流回路に入る．玆で整流された電圧が次のサイラトロン回路に入ると，急に放電電流が流れてパルスを生ずる．

之等のパルスが第3図に表わされているが，此のパルス間隔が波の通過時間を表わしているのである．

此の二つのパルスが次のフリツプフロツプ回路に相次いで入ると，初めのパルスで電圧が上り，次のパルスで元に戻つて，第3図に表わされるような矩形電圧が出来る．

一方，発振器から 8000 サイクルの電流が常時，時限増幅器に入つているのであるが，此の増幅器は，矩形電圧の間だけしか，増幅作用が無いようになつているので，此の矩形の枠に入るだけの波数が増幅されて出て来る．

8000 サイクルの交流は丁度，二つのパルス間隔を測る物指しになるわけで，増幅されて出て来た波数を数えれば時間が判る事になる．

次のカウンター，クロノグラフは，此の波数を数えて，指示する装置である．

指示は第3図に示したように，10 桁を示すネオン管が 10 個，1 桁のが 10 個，$1/2$ を示すものが 3 個總計 23 個のネオン管があつて，例えば，第3図のネオン管に於て斜線をしたものが点いている時には $32\,3/8$ ミリ-セコンド，と容易に時間々隔がわかる．

次に各ブロツクの働きを稍詳細に述べる事にする．

(イ) 換 振 器

弾性波が来ると換振器は第3図で表わされるような揺れ方をするのが普通であるが，此の場合必要なのは，最初の波の立上りだけである．

而も初動の立上りが，急激である方が時間測定の誤差が少くなるので，玆で用いた換振器は第4図及び第5図でみるように，斯様な点を考慮し，且感度が大になるように設計された．

之は従来の電磁型換振器が普通，磁石が固定していて，可動線輪が振子に直結していただけであるのに較べて，磁石自身が振子の質量 (3 kg) になつて居り，此の振子の振動はエデンバネ機構で拡大されて，可動線輪の動きとなるので，感度は一般の電磁型換振器の 10 倍程度になつている．

尙此の場合可動線輪の質量は 16gr であつて，エデンバネは幅 0.35mm，厚み 0.1mm，長さ 12mm の燐青銅の板を用いた．線輪は B.S. 48″ のエナメル銅線を 7000 回巻き，其の直流抵抗は約 2000Ω である．振子と可動線輪の質量比 μ は此の場合 $3000/16$ となるので，基本倍率 V と幾何倍率 V_G との関係式

$$V=\frac{V_G}{1+\frac{V_G^2}{\mu}}$$

から V と V_G との関係を求めると第6図の曲線が得られる．

此の曲線から基本倍率が最大になるように幾何倍率を定めると $V_G=13.6$，$V=6.9$ を得た．斯様にして，設計，製作したものは，写真に示されていて，固有振動数，毎秒 37 サイクルで速度振幅 1 糎毎秒 5 Volt の電圧を生ずる．

(ロ) 増幅器回路

6SJ7 及び 6J5 を用いた二段増幅である．

2 個の可変抵抗を用いて，調節が出来るようになつている．

(ハ) 整 流 回 路

6H6 を用いた両波整流方式である．初動が ＋ で来ても － でも正の電圧が起るようになつている．

(ニ) サイラトロン回路

予めサイラトロンのグリツドは直流の低い電圧に保つておくが，整流された正の電圧が入つて来て此の電圧を放電電圧以上に上げると，プレート電流が流れる．

最初の直流電圧の定め方は，測定地によつて条件が異るので，第7図の可変抵抗器を調節して，サイラトロンが放電しない最大限の値に其の都度定める事が出来る．

サイラトロンが放電して，生じた電圧は小容量のコンデンサーを通ると微分されてパルスになり次のフリツプ-フロツプ (Flip-Flop) 回路に入る．

(ホ) フリツプ-フロツプ回路

双三極管 6SN7 を用いた．此の回路はトリツガー，アムプリフアイヤーとも云われ，お互いのプレートとグリツド同志が結合されているので両方に等量の電流が流れると云う事は不安定のため起り得ない．安定に存在するのは一方が流れて，他方は流れないと云う状態で，流れている方のグリツトに負のパルスを入れてやると，状態が反転する．

始め，リセツトスイツチを押して第7図の右側真空管が流れている状態にしておく．

従つて，プレート電圧は低い値になつている．此のグリツドに負のパルスが入ると状態が反転するので，プレートの電圧は上るが，次のパルスが反対のグリツトに入るに及んで，状態は元に戻るので，電圧も下り第3図に示めしたような，矩形電圧を生ずる事になる．

(ヘ) 時限増幅器

前のフリツプ-フロツプ矩形電圧が此の増幅管 6SJ7 のサプレツサー，グリツドに入ると，高い電圧の場合にだけしか増幅作用がないので，常時コントロールグリツドに入つている発振器からの 8000 サイクル交流は第3図の矩形枠の時間だけ増幅されて，次にもう一度，6SJ7 で増幅された後，カウンター，クロノグラフ回路に入る．

(ト) カウンタークロノグラフ回路

第7図に示されているように，カウンタークロノグラフ回路はフリツプフロツプ回路が単位になつていて，何段にも重なつている．前に述べたように，フリツプフロツプ回路は 2 個のパルスに対して 1 個の矩形波を生ずるので，最初の双二極管 6SN7 三段で 8000 サイクルは 1000 サイクルになる．

奇数のパルスはネオン管に指示される．

次に一双づつ，4 個並んだ 6SN7 は 10 進法回路である．

元来フリツプ，フロツプを 4 個使うと 2 の三乗即ち 16 分の 1 に周波数が落ちるのであるが図の上の方にある双二極管 6SN7 が状態を 6 個だけ跳ばす役目をして，丁度 10 個に 1 個の割合で周波数が落ちるようになつている．之等の真空管の各プレートを第9図の右下に示すように 10 個のネオン管に結合すると，例えば 6 個のパルスが来た時には 6 を示すネオン管が点いて，他は全部消えるようになるので，読取りが極めて簡便，容易である．

10 進法の回路はもう一つ重ねられている．

之等の回路によつて，8000 サイクルの交流は始め3個のネオン管で $1/8\times10^{-3}$, $1/4\times10^{-3}$, $1/2\times10^{-3}$ 秒を読み次の 10 進法で 10 milli-second 迄，もう一つの 10 進法で 100 milli-second 迄読みとられるわけである．

それ以上に長い時間は，指示が繰返しになるので繰返しの数はメカニカル，カウンター (M.C.) が指示して呉れる．

6SL7 及び 6V6 の回路はメカニカルカウンターのドライバー回路である．

操 作

実際に使用する場合には先づサイラトロンのグリツド電圧をノイズ状態に応じて適当に調節しておき，SW を入れてサイラトロンプレートに電圧を与える．

次にリセツトスイツチを押すとフリツプフロツプ回路が正規の状態をとると同時にカウンタークロノグラフは零を指示する．

此のようにして，地面に衝撃を与えると直ぐに時間がネオン管の点滅から読みとれる．

実 験

東京大学地震研究所 2 号館前のテニスコート附近でテストを行つたがその際に得られた実験結果を第11図及び第12図に示した．

換振器 B を A に近いところから或る間隔おきに遠ざけて行つて，各々の距離について 4～5 回時間測定を繰返した．

図に示されているように近い距離では測点が割合いにかたまつて出るのに反して，遠方になると，稍，散らばる傾向がある．

遠方では初動が小さくなるため，時間が短かく指示される事もあるし，或は初動が小さくて，ノイズと同程度以下であると，時間が長く指示される事もあり得るのである．

然し乍ら斯様な難点は衝撃の与え方を大きくする事によつて楽に解決出来るのであつて，此の実験では一応或る距離迄繰返し測点がとれて割合確からしい走時を決定する事が出来ると云う事を強調したい．

之等の纏つた点を結ぶと数本の直線の上に載つて居る事が明瞭にわかる．

各直線の傾斜は，各層の速度を表わすのでは，層が存在している事が明かである．

之等の直線群から各層の深さが計算出来る．例えば第 11 図で上層の速度から順次 v_1，v_2 とし，v_1，v_2 を表わす直線の交点の距離座標を Z とすると上層の厚み H は次式

$$H=\frac{Z}{2}\sqrt{\frac{v_2+v_1}{v_2-v_1}}$$

によつて算出される．

この場合 $H=1.4$ m である．

第 12 図の場合は表層の厚みが 1.3 m 第二層の厚みは 2.7 m となる．

此の実験で行つた衝撃の与え方は第 10 図に示されているように，櫓を組んで，40 kg 程度の鉄球を懸垂装置で吊り上げ，落下させるには電気的にスイツチを働かせて遠隔操作が出来るように，なつている．

鉄球が地面を打つ前に，懸垂装置を離れる時，生ずる衝撃が櫓を伝わつて先に地面に走るので，際の衝撃波の前に換振器が揺れてしまう場合がある．

之を防ぐには櫓の柱をバネの上に浮かせて，鉄球が離れる時に生ずる衝撃を，小さくするようにして，実験した．

猶近い点を測定する場合には櫓を用いずに手で持ち上げて落す程度で充分である．

結　言

此の実験によつて，地下 10 m 程度迄は簡単に而も費用も要せず測定出来る事がわかつた．

例えば第 11 図に表わされた測点をとるのに約 30 分内外で完了するのである．

一つの測点を定めるのに此の方法によると十数秒で済むのであるが従来の方法では写真現像や色々な操作を含めて一時間程度は必要である．

茲で用いた電気装置はエリミネーター式であつて，交流電源のない山の中などでの探査実験には適さないので電池式電源に改良すれば其の他に増幅感度もより以上に増大出来よう．

猶，装置をポータブルにして，搬送に便利な設計を試たみいと思つている．

31. 東京都南東部の地盤沈下測量

地震研究所 那須信治・岸上冬彦・岡田悖

(昭和26年3月20日発表—昭和28年9月20日受理)

東京都の南東部が地盤沈下することは，本彙報に度々書かれたことである．この沈下地域の西側は山の手といわれるローム質の高地で限界をつくられているが，東側の限界は明らかでなかつた．他方では沈下の著しい所が，前には隅田川の東岸に近かつたが次第に東に移り最近は荒川放水路に近ずいている．この沈下の最大地域が更に東に移るか否かを知るためにも東部の沈下状況を一層詳しく調べる必要がある．そこで第1図に示す様

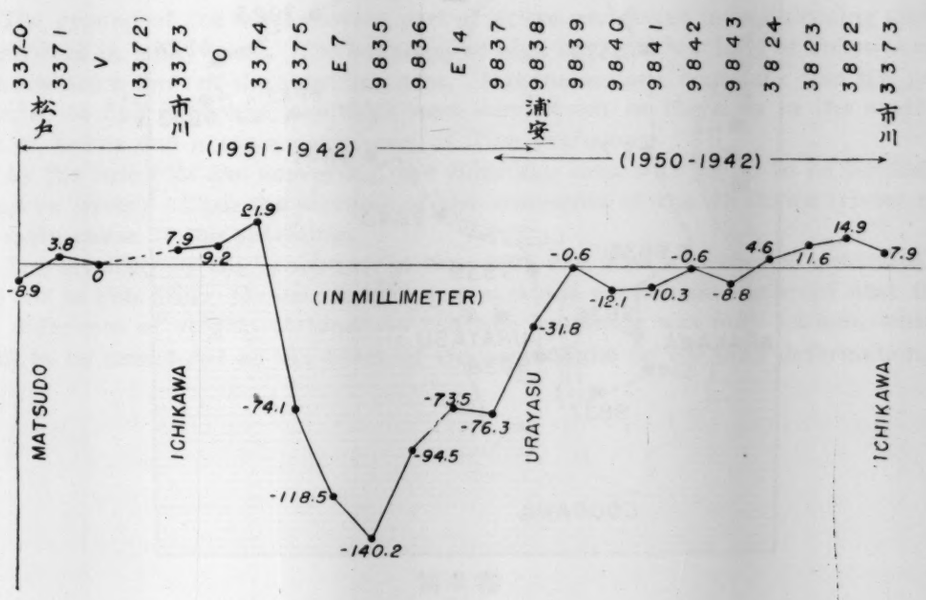

第1図

に東京都の東部から千葉県の西部にかけて地理調査所の水準点及び東京都で設けた水準点をツアイスの一等水準儀で測量した，行政区劃としては東京都江東区及び江戸川区，千葉県市川市及び船橋市にわたる範囲である．水準点の数は21個で環状になるようにし，片道観測であるが，環状閉塞をして誤差を明らかにして且少くするようにした．その制限誤差は $1.5\,\mathrm{mm}\sqrt{S(\mathrm{km})}$ としたが，長い橋を渡るときは必ず異なる方法を使つて往復測量を行い，その観測の精度と閉塞差を明らかにした．前の測量が1942年であつたので第2回はそれからの変動量を示したものである．此時の変動量の基準点としては地盤沈下が

ないと考えられる松戸市の南の台地にある水準点をとつた．これを見ると千葉では変動が少なくて，東京都の地盤沈下は東側は江戸川で境され，結局，荒川の下流域の冲積層が沈下すると考えられる．

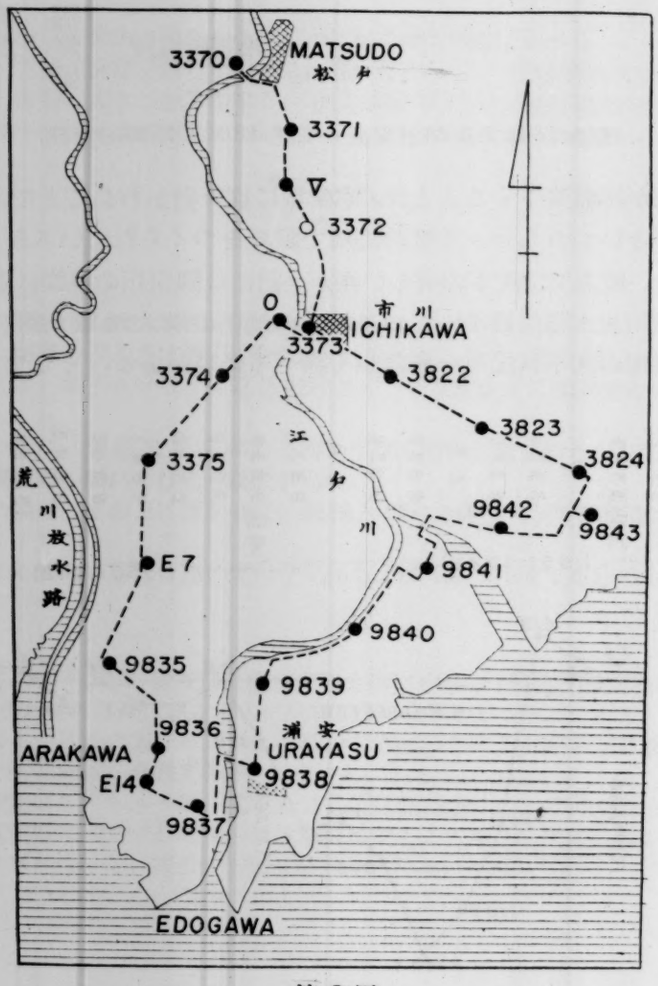

第 2 図

この測量は 1950 年の 12 月東の千葉県内を測かり，1951 年 2 月に西の東京都内を観測した，そして水準点 9837 (葛西町 1 丁目) と 9838 (浦安町) とは測量線路をつなぐ為に上にのべた様に 3 個月目に測量したことになつた．勿論，川を渡たる測量であるから多少誤差が大きい恐れはあるが，その 2 回の測量の差は次の通りであつた

1951. II +1,2504 (B.M. 9837–9839)
1950. XII −1,2492 (B.M. 9838–9837)

この様に 9837 の方が +1.2 mm 高くなつたことを示した，この 2 回の測量の間，即ち 1 月 9 日 3 時 32 分頃 (J.S.T.) に千葉県北西部に顕著な地震があり，関東地方から

中部地方及び東北地方の一部でも有感の顕著な地震があつた，測量地域に震源の近い地震であつたので，その前後に行つた水準測量によつて変動が現われるかと考えたが，1.2 mm の差では測定誤差の範囲内と見做されるから，この程度の地震では地殻変動は起つたとは云えなかつた.

---

31. *Levelling of the Subsiding Area in the South-eastern Part of Tokyo.*

By Nobuji NASU, Fuyuhiko KISHINOUYE
and Atusi OKADA,

Earthquake Research Institute.

The ground of the south-eastern part of Tokyo was found to be subsiding moderately as reported in many cases. The boundary of high land and low land of Tokyo is regarded as the western limit of the subsiding area. But the eastern boundary was not yet made clear, so to find it precise levellings were carried out in the area in the southeastern part of Tokyo and north-western part of Tiba prefecture.

As the result of the surveying, the subsiding area was found to be limited by the Edogawa (river). Then the settling of the sediments of the Arakawa (river) must be the main cause of the subsiding.

The levelling of the bench marks Nos. 9837 and 9838 was carried out twice, in Dec. 1950 and in Feb. 1951. On Jan. 9. 1951 a remarkable earthquake occurred near the area. But difference of heights obtained by the two levellings was only 1.2 mm, which is too small to be considered as the effect of the earthquake on the land deformation.

——所　　報——

◎談話會記事

第 301 回談話会 (昭和 28 年 6 月 16 日)

1. 三原山の地球磁気学的研究
   第 4 報　最近二ケ年間の地磁気変化　　横山泉
2. 日立鉱山における地震観測結果
   第 4 報　補遺　　金井清
3. エデンばねの静及び動特性とその応用 (第 2 報)　　西村源六郎・鈴木正治・古川英一
4. 「三鷹に於ける土地の脈動観測」の訂正　　岸上多彦・浅野周三
5. 地震の場の論　その 3　余震の分布　地震発生のポアソン分布　石本・飯田の式　　松沢武雄

第 302 回談話会 (昭和 28 年 7 月 21 日)

1. 一般化されたブシネスク問題について　　谷本勉之助 (西村所員紹介)
2. 地震記象における刻時の精度について　　萩原尊礼・松本利松
3. 震害と地盤の性質との関係 第 3 報　　金井清
4. 基盤の振動測定 第 1 報　　河角広・嶋悦三郎・佐川睦・柴野馬都住・柳沢住

第 303 回談話会 (昭和 28 年 9 月 22 日)

1. 表面波の研究 (12) ラブ波の群速度を求める図表　　佐藤泰夫
2. 地震動振幅と地表層の性質との関係 (第 3 報)　　金井清・吉沢静代
3. 衝撃性地動に対する防振の一例　　岸上多彦
4. 微小時間測定法を用いた弾性波式地下探査装置とその実際 (其の 2)　　西村源六郎・小滝富雄・高橋浩一

第 304 回談話会 (昭和 28 年 10 月 27 日)

1. 浅間山湯の平における地電位差観測　　横山泉
2. 三原山の地球磁気学的研究　第 4 報の補遺　　横山泉・岡田悼夫・斎藤貞
3. 高温における岩石の粘性と弾性について
   続報　大島熔岩　　佐久間修三
4. 地震に伴う土地歪の観測　序報　　萩原尊礼・笠原慶一・斎藤貞夫

5. 線歪計方式による振動測定装置　笠原慶一
6. 地震動による建物振動の観測結果　補遺　金井清
7. 東京都内地盤調査結果　第2報　地震研究所地盤調査班
8. 地震の場の論　1946年12月21日の大地震と1948年4月18日の地震との比較　松沢武雄
9. 東北地方に於ける重力異常の分布　坪井忠二・実川顕一・田島広一

第305回談話会（昭和28年11月24日）

1. 三原山の小活動と三宅島の異変の報告　小坂丈予
2. 1953年7月26日箱根早雲山山津浪調査　岸上多彦・小坂丈予
3. 第2回釜石大爆破による地震動の観測　爆破地震動研究グループ
4. レスポンス計算器の試作　高橋竜太郎・相田勇

第306回談話会（昭和28年12月22日）

1. 弾性波の発生機構に関する実験（第5報）　笠原慶一・斎藤貞夫
2. 分散した地震波の解析の試み　佐藤泰夫
3. 液体，固体の界の面のSH波　松沢武雄
4. 但馬玄武洞の玄武岩の帯磁と地磁気異常　横山泉
5. 油壺に於ける潮位変化　山口生知（那須所員紹介）
6. 台風13号による三河湾沿岸の高潮調査報告　高橋竜太郎・平能金太郎・秋葉芳雄
7. 中部地方に於ける重力異常の分布　坪井忠二・実川顕一・田島広一
8. 浅間火山の活動と微小地震（続報）　水上武・佐久間修三・内堀貞雄・外
9. 浅間火山の微小地震と地形変動　水上武・岡田惇

Index to Vol. XXXI.

Page

FURUKAWA, E. and OTHERS, (30) A New-Designed Prospecting Apparatus. (in English) 317

HISHIYAMA, Y. and OTHERS, (2) The Anomalous Behavior of Geomagnetic Variations of Short Period in Japan and Its Relation to the Subterranean Structure. The 2nd report. (in English).. 19

HISHIYAMA, Y. and OTHERS, (9) The Anomalous Behavior of Geomagnetic Variations of Short Period in Japan and Its Relation to the Subterranean Structure. The 3rd report. (in English).. 89

HISHIYAMA, Y. and OTHERS, (10) The Anomalous Behavior of Geomagnetic Variations of Short Period in Japan and Its Relation to the Subterranean Structure. The 4th report. (in English).. 101

HISHIYAMA, Y. and OTHERS, (11) The Anomalous Behavior of Geomagnetic Variations of Short Period in Japan and Its Relation to the Subterranean Structure. The 5th report. (in English).. 119

ICHIMURA, T., (12) Geological Investigations on the Zaō Volcanoes. II. Aoso Volcano. (in English) 129

ICHIMURA, T. and OTHERS, (13) Sulphur Crystals from the Yakeyama Volcano. (in English) 151

ICHIMURA, T. and MATSUBAYASHI, H., (14) Igneous Activities prior to the Deposition of the Chichibu System. (in English) 155

KANAI, K., (19) Relation between the Nature of Surface Layer and the Amplitude of Earthquake Motions. II. (in English) 219

KANAI, K., (22) Examination of the Assumption of the Concentrated Mass in the Vibration of Framed Structure (Rahmen). (in English) 245

KANAI, K. and OTHERS, (4) The Relation between the Amplitude and the Period of Earthquake Motion. (in English) 45

KANAI, K. and OTHERS, (5) Relation between the Earthquake Damage and the Nature of the Ground. (Case of Wooden Houses and Peat Bed.) (in English) 57

KANAI, K. and OTHERS, (20) Observational Study of Earthquake Motion in the Depth of the Ground. IV. (Relation between the Amplitude at Ground Surface and the Period.) (in English). 227

KANAI, K. and YOSHIZAWA, S., (26) Relation between the Amplitude of Earthquake Motions and the Nature of Surface Layer. III. (in English) 275

KANAI, K. and SUZUKI, T., (29) Relation between the Property of Building Vibration and the Nature of Ground. (Observation of

Earthquake Motion at Actual Buildings.) (in English)..... 305
KASAHARA, K., (7) Experimental Studies on the Mechanism of Generation of Elastic Waves II. (in English)..... 71
KASAHARA, K., (21) Experimental Studies on the Mechanism of Generation of Elastic Waves III. (in English) 235
KISHINOUYE, F. and OTHERS, (31) Levellings of the Subsiding Area in the South-eastern Part of Tokyo. (in Japanese)..... 335
KOTAKI, T. and OTHERS, (30) A New-Designed Prospecting Apparatus. (in English)..... 317
MATSUBAYASHI, H. and ICHIMURA, T., (14) Igneous Activities prior to the Deposition of the Chichibu System. (in English) 155
MATUMOTO, T., (25) Transmission and Reflection of Seismic Waves through Multilayered Elastic Medium. (in English) 261
MATUZAWA, T., (16) Feldtheorie der Erdbeben. (im Deutschen) 179
MATUZAWA, T., (23) Feldtheorie der Erdbeben: Vergleichung Grossbeben vom 21. Dez. 1946 mit dem Nachbeben vom 18. April 1948. (im Deutschen)..... 249
MINATO, H. and OTHERS, (13) Sulphur Crystals from the Yakeyama Volcano. (in English)..... 151
NAGATA, T. and OKADA, A., (15) Land Deformation of the Neighbourhood of Muroto Point after the Nankaido Great Earthquake in 1946. (in English) 169
NASU, N. and OTHERS, (31) Levellings of the Subsiding Area in the South-eastern Part of Tokyo. (in Japanese)..... 335
NISHIMURA, G. and OTHERS, (30) A New-Designed Prospecting Apparatus. (in English) 317
OKADA, A. and NAGATA, T., (15) Land Deformation of the Neighbourhood of Muroto Point after the Nankaido Great Earthquake in 1946. (in English) 169
OKADA, A. and OTHERS, (31) Levellings of the Subsiding Area in the South-eastern Part of Tokyo. (in Japanese)..... 335
OSADA, K. and OTHERS, (4) The Relation between the Amplitude and the Period of Earthquake Motion. (in English)..... 45
OSADA, K. and OTHERS, (20) Observational Study of Earthquake Motion in the Depth of the Ground. IV. (Relation between the Amplitude at Ground Surface and the Period.). (in English) .. 227
RIKITAKE, T. and OTHERS, (2) The Anomalous Behavior of Geomagnetic Variations of Short Period in Japan and Its Relation to the Subterranean Structure. The 2nd report. (in English).. 19

RIKITAKE, T. and OTHERS, (9) The Anomalous Behavior of Geomagnetic Variations of Short Period in Japan and Its Relation to the Subterranean Structure. The 3rd report. (in English).. 89
RIKITAKE, T. and OTHERS, (10) The Anomalous Behavior of Geomagnetic Variations of Short Period in Japan and Its Relation to the Subterranean Structure. The 4th report. (in English).. 101
RIKITAKE, T. and OTHERS, (11) The Anomalous Behavior of Geomagnetic Variations of Short Period in Japan and Its Relation to the Subterranean Structure The 5th report. (in English).. 119
SAKUMA, S., (6) Elastic and Viscous Properties of Volcanic Rocks at Elevated Temperatures. Part 2. (in English)..... 63
SAKUMA, S., (28) Elastic and Viscous Properties of Volcanic Rocks at High Temperatures. Part 3. Oosima lava. (in English).... 291
SATÔ, Y., (1) Velocity of Elastic Waves Propagated in Media with Small Obstacles. (in English) 1
SATÔ, Y., (8) Study on Surface Waves VIII. Nomogram for the Phase Velocity of Love-Waves and Maximum Thickness of the Surface Layer. (in English)..... 81
SATÔ, Y., (17) Transformation of Spherical Solid Harmonics Related to the Translation of Coordinates System. (in English)..... 203
SATÔ, Y., (24) Study on Surface Waves IX. Nomogram for the Group Velocity of Love-Waves. (in English)..... 255
SUZUKI, M. and OTHERS, (30) A New-Designed Prospecting Apparatus. (in English)..... 317
SUZUKI, T. and OTHERS, (5) Relation between the Earthquake Damage and the Nature of the Ground. (Case of Wooden Houses and Peat Bed). (in English)..... 57
SUZUKI, T. and KANAI, K., (29) Relation between the Property of Building Vibration and the Nature of Ground. (Observation of Earthquake Motion at Actual Buildings). (in English)..... 305
TAKAHASHI, K. and OTHERS, (30) A New-Designed Prospecting Apparatus. (in English) 317
TANAKA, T. and OTHERS, (5) Relation between the Earthquake Damage and the Nature of the Ground. (Case of Wooden Houses and Peat Bed). (in English) 57
TSUYA, H. and OTHERS, (13) Sulphur Crystals from the Yakeyama Volcano. (in English) 151
YOKOYAMA, I., (3) Geomagnetic Anomaly on Mt. Haruna and Its Relation to the Reverse Thermo-Remanent Magnetism of the Pumice Covering the Place. (in English)..... 33

YOKOYAMA, I., (18) A New Method for Regulating Electric Currents and its Application to Measurements of Geomagnetic Field. (in English) 211
YOKOYAMA, I. and OTHERS, (2) The Anomalous Behavior of Geomagnetic Variations of Short Period in Japan and Its Relation to the Subterranean Structure. The 2nd report. (in English).. 19
YOKOYAMA, I. and OTHERS, (9) The Anomalous Behavior of Geomagnetic Variations of Short Period in Japan and Its Relation to the Subterranean Structure. The 3rd report. (in English).. 89
YOKOYAMA, I. and OTHERS, (10) The Anomalous Behavior of Geomagnetic Variations of Short Period in Japan and Its Relation to the Subterranean Structure. The 4th report. (in English).. 101
YOKOYAMA, I. and OTHERS, (11) The Anomalous Behavior of Geomagnetic Variations of Short Period in Japan and Its Relation to the Subterranean Structure. The 5th report. (in English).. 119
YOSHIZAWA, S. and OTHERS, (4) The Relation between the Amplitude and the Period of Earthquake Motion. (in English)..... 45
YOSHIZAWA, S. and OTHERS, (20) Observational Study of Earthquake Motion in the Depth of the Ground. IV. (Relation between the Amplitude at Ground Surface and the Period.). (in English). 227
YOSHIZAWA, S. and KANAI, K., (26) Relation between the Amplitude of Earthquake Motion and the Nature of Surface Layer. III. (in English) 275
The Research Group for Explosion Seismology, (27) The Third Explosion Seismic Observations in North-Eastern Japan. (in English) 281

索 引 第31号

頁

古川英一·他 (30) 簡易弾性波式地下探査装置の研究 (英文) 317
菱山よね子·他 (2) 日本に於ける地磁気短周期変化の異常と地下構造 (第2報) (英文) 19
菱山よね子·他 (9) 日本における地磁気短周期変化の異常と地下構造 第3報 (英文) 99
菱山よね子·他 (10) 日本に於ける地磁気短周期変化の異常と地下構造 第4報 (英文) 101
菱山よね子·他 (11) 日本に於ける地磁気短周期変化の異常と地下構造 第5報 (英文) 119
市村 毅 (12) 蔵王火山の地質学的研究 (第二報) (英文) 129
市村 毅·他 (13) 焼山火山産の硫黄結晶 (英文) 151
市村 毅·松林晴子 (14) 秩父系堆積前の火成活動 (英文) 155
金井 清 (19) 地震動振幅と地表層の性質との関係 第2報 (英文) 219
金井 清 (22) 架構構造物の振動問題における集中荷重の仮定の吟味 (英文) ... 245
金井 清·他 (4) 地震動の振幅と周期との関係 (英文) 45
金井 清·他 (5) 震害と地盤の性質との関係 (泥炭地にある木造家屋の場合) (英文) 57
金井 清·他 (20) 地下探所における地震動の観測結果 (第4報) (英文) 227
金井 清·吉沢静代 (26) 地震動振幅と地表層の性質との関係 第4報 (英文) .. 275
金井 清·鈴木富三郎 (29) 建物の振動的性質と地盤の性質との関係 (実在建物における地震動観測) (英文) 305
笠原慶一 (7) 弾性波の発生機構に関する実験 (第2報) (英文) 71
笠原慶一 (21) 弾性波の発生機構に関する実験 (第3報) (英文) 235
岸上冬彦·他 (31) 東京都南東部の地盤沈下測量 (邦文) 335
小滝富雄·他 (30) 簡易弾性波式地下探査装置の研究 (英文) 317
松林晴子·市村 毅 (14) 秩父系堆積前の火成活動 (英文) 155
松本利松 (25) いくつかの平行な不連続面による地震波の反射及び透過 (英文) .. 261
松沢武雄 (16) 地震の場の論 (独文) 179
松沢武雄 (23) 地震の場の論 1946年12月21日の大地震と1948年4月18日の余震との比較 (独文) 249
湊 秀雄·他 (13) 焼山火山産の硫黄結晶 (英文) 151
永田 武·岡田 惇 (15) 1946年南海道大地震後における室戸岬近傍の地殻変動 (英文) 169
那須信治·他 (31) 東京都南東部の地盤沈下測量 (邦文) 335

西村源六郎·他 (30) 簡易弾性波式地下探査装置の研究 (英文) 317
岡田 惇·永田 武 (15) 1946年南海道大地震後における室戸岬近傍の地殻変動 (英文) 169
岡田 惇·他 (31) 東京都南東部の地盤沈下測量 (邦文) 335
長田甲斐男·他 (4) 地震動の振幅と周期との関係 (英文) 45
長田甲斐男·他 (20) 地下深所における地震動の観測結果 (第4報) (英文) 227
力武常次·他 (2) 日本に於ける地磁気短周期変化の異常と地下構造 (第2報) (英文) 19
力武常次·他 (9) 日本における地磁気短周期変化の異常と地下構造 第3報 (英文) 89
力武常次·他 (10) 日本に於ける地磁気短周期変化の異常と地下構造 第4報 (英文) 101
力武常次·他 (11) 日本に於ける地磁気短周期変化の異常と地下構造 第5報 (英文) 119
佐久間修三 (6) 高温に於ける火山岩の粘性及び弾性 第2報 (英文) 63
佐久間修三 (28) 高温に於ける火山岩の粘性及び弾性 第3報 大島熔岩 (英文). 291
佐藤泰夫 (1) 小さな異物を含む媒質内を伝はる弾性波の速さ (英文) 1
佐藤泰夫 (8) 表面波の研究 VIII ラブ波の位相速度を求める図表と表面層の厚さの極大値 (英文) 81
佐藤泰夫 (17) 坐標系の移動に伴ふ体球函数の変換 (英文) 203
佐藤泰夫 (24) 表面波の研究 IX ラブ波の群速度を求める図表 (英文) 255
鈴木正治·他 (30) 簡易弾性波式地下探査装置の研究 (英文) 317
鈴木富三郎·他 (5) 震害と地盤の性質との関係 (泥炭地にある木造家屋の場合) (英文) 57
鈴木富三郎·金井 清 (29) 建物の振動的性質と地盤の性質との関係 (実在建物における地震動観測) (英文) 305
高橋浩一·他 (30) 簡易弾性波式地下探査装置の研究 (英文) 317
田中貞二·他 (5) 震害と地盤の性質との関係 (泥炭地にある木造家屋の場合) (英文) 57
津屋弘逵·他 (13) 焼山火山産の硫黄結晶 (英文) 151
横山 泉 (3) 榛名山の地磁気異常とその浮石の逆熱残留磁気との関係 (英文) .. 33
横山 泉 (18) 電流を制御する新しい試み及びその地磁気測定への応用 (英文) . 211
横山 泉·他 (2) 日本に於ける地磁気短周期変化の異常と地下構造 (第2報) (英文) 19
横山 泉·他 (9) 日本における地磁気短周期変化の異常と地下構造 第3報 (英文) 89

横山　泉·他　(10)　日本に於ける地磁気短周期変化の異常と地下構造　第4報
(英文) 101
横山　泉·他　(11)　日本に於ける地磁気短周期変化の異常と地下構造　第5報
(英文) 119
吉沢静代·他　(4)　地震動の振幅と周期との関係 (英文) 45
吉沢静代·他　(20)　地下深所における地震動の観測結果 (第4報) (英文) 227
吉沢静代·金井　清　(26)　地震動振幅と地表層の性質との関係　第4報 (英文) . 275
爆破地震動研究グループ　(27)　東北日本における第3回爆破地震動観測 (英文) . 281

BULLETIN

OF THE

EARTHQUAKE RESEARCH INSTITUTE

TOKYO UNIVERSITY

VOL. XXXI

1953

東京大學

地震研究所彙報

第 31 号

昭 和 28 年

CONTENTS.

Vol. XXXI.

Part 1. March, 1953.

Papers and Reports.

Page

1. Y. SATÔ, Velocity of Elastic Waves Propagated in Media with Small Obstacles. (in English) 1
2. T. RIKITAKE, I. YOKOYAMA and Y. HISHIYAMA, The Anomalous Behavior of Geomagnetic Variations of Short Period in Japan and Its Relation to the Subterranean Structure. The 2nd report. (in English) 19
3. I. YOKOYAMA, Geomagnetic Anomaly on Mt. Haruna and Its Relation to the Reverse Thermo-Remanent Magnetism of the Pumice Covering the Place. (in English) 33
4. K. KANAI, K. OSADA and S. YOSHIZAWA, The Relation between the Amplitude and the Period of Earthquake Motion. (in English) 45
5. K. KANAI, T. TANAKA and T. SUZUKI, Relation between the Earthquake Damage and the Nature of the Ground. (Case of Wooden Houses and Peat Bed.) (in English) 57
6. S. SAKUMA, Elastic and Viscous Properties of Volcanic Rocks at Elevated Temperatures. Part 2. (in English)..... 63
7. K. KASAHARA, Experimental Studies on the Mechanism of Generation of Elastic Waves II. (in English) 71

Part 2. June, 1953.

8. Y. SATÔ, Study on Surface Waves VIII. Nomogram for the Phase Velocity of Love-Waves and Maximum Thickness of the Surface Layer. (in English)..... 81
9. T. RIKITAKE, I. YOKOYAMA and Y. HISHIYAMA, The Anomalous Behavior of Geomagnetic Variations of Short Period in Japan and Its Relation to the Subterranean Structure. The 3rd report. (in English) 89
10. T. RIKITAKE, I. YOKOYAMA and Y. HISHIYAMA, The Anomalous Behavior of Geomagnetic Variations of Short Period in Japan

and Its Relation to the Subterranean Structure. The 4th report. (in English) 101
11. T. RIKITAKE, I. YOKOYAMA and Y. HISHIYAMA, The Anomalous Behavior of Geomagnetic Variations of Short Period in Japan and Its Relation to the Subterranean Structure. The 5th report. (in English) 119
12. T. ICHIMURA, Geological Investigations on the Zaō Volcanoes. II. Aoso Volcano. (in English)..... 129
13. T. ICHIMURA, H. TSUYA and H. MINATO, Sulphur Crystals from the Yakeyama Volcano. (in English)..... 151
14. T. ICHIMURA and H. MATSUBAYASHI, Igneous Activities prior to the Deposition of the Chichibu System. (in English) 155
15. A. OKADA and T. NAGATA, Land Deformation of the Neighbourhood of Muroto Point after the Nankaido Great Earthquake in 1946. (in English) 169

Part 3. September, 1953.

16. T. MATUZAWA, Feldtheorie der Erdbeben. (im Deutschen)..... 179
17. Y. SATÔ, Transformation of Spherical Solid Harmonics Related to the Translation of Coordinates System. (in English)..... 203
18. I. YOKOYAMA, A New Method for Regulating Electric Currents and its Application to Measurements of Geomagnetic Field. (in English)..... 211
19. K. KANAI, Relation between the Nature of Surface Layer and the Amplitude of Earthquake Motions. II. (in English) ... 219
20. K. KANAI, K. OSADA and S. YOSHIZAWA, Observational Study of Earthquake Motion in the Depth of the Ground. IV. (Relation between the Amplitude at Ground Surface and the Period.) (in English)..... 227
21. K. KASAHARA, Experimental Studies on the Mechanism of Generation of Elastic Waves III. (in English) 235
22. K. KANAI, Examination of the Assumption of the Concentrated Mass in the Vibration of Framed Structure (Rahmen). (in English) 245

Part 4. December, 1953.

23. T. MATUZAWA, Feldtheorie der Erdbeben: Vergleichung Grossbeben vom 21. Dez. 1946 mit dem Nachbeben vom 18. April

1948. (im Deutschen) 249
24. Y. SATÔ, Study on Surface Waves IX. Nomogram for the Group Velocity of Love-Waves. (in English) 255
25. T. MATUMOTO, Transmission and Reflection of Seismic Waves through Multilayered Elastic Medium. (in English) 261
26. K. KANAI and S. YOSHIZAWA, Relation between the Amplitude of Earthquake Motions and the Nature of Surface Layer. III. (in English) 275
27. The Research Group for Explosion Seismology, The Third Explosion Seismic Observations in North-Eastern Japan. (in English) 281
28. S. SAKUMA, Elastic and Viscous Properties of Volcanic Rocks at High Temperatures. Part 3. Oosima lava. (in English). 291
29. K. KANAI and T. SUZUKI, Relation between the Property of Building Vibration and the Nature of Ground. (Observation of Earthquake Motion at Actual Buildings.) (in English)... 305
30. G. NISHIMURA, M. SUZUKI, E. FURUKAWA, T. KOTAKI and K. TAKAHASHI, A New-Designed Prospecting Apparatus. (in English) 317
31. N. NASU, F. KISHINOUYE and A. OKADA, Levellings of the Subsiding Area in the South-eastern Part of Tokyo. (in Japanese) 335

目　次

第 31 号

第 1 冊　昭和 28 年 3 月

論文及報告　　頁

1. 小さな異物を含む媒質内を伝はる弾性波の速さ（英文）..... 佐藤泰夫 1
2. 日本に於ける地磁気短周期変化の異常と地下構造（第2報）（英文）..... 力武常次・横山泉・菱山よね子 19
3. 榛名山の地磁気異常とその浮石の逆熱残留磁気との関係（英文）..... 横山泉 33
4. 地震動の振幅と周期との関係（英文）..... 金井清・長田甲斐男・吉沢静代 45
5. 震害と地盤の性質との関係（泥炭地にある木造家屋の場合）（英文）..... 金井清・田中貞二・鈴木富三郎 57
6. 高温に於ける火山岩の粘性及び弾性 第2報（英文）..... 佐久間修三 63
7. 弾性波の発生機構に関する実験（第2報）（英文）..... 笠原慶一 71

第 2 冊　昭和 28 年 6 月

8. 表面波の研究 VIII ラブ波の位相速度を求める図表と表面層の厚さの極大値（英文）..... 佐藤泰夫 81
9. 日本における地磁気短周期変化の異常と地下構造 第3報（英文）..... 力武常次・横山泉・菱山よね子 89
10. 日本に於ける地磁気短周期変化の異常と地下構造 第4報（英文）..... 力武常次・横山泉・菱山よね子 101
11. 日本に於ける地磁気短周期変化の異常と地下構造 第5報（英文）..... 力武常次・横山泉・菱山よね子 119
12. 蔵王火山の地質学的研究（第二報）（英文）..... 市村毅 129
13. 焼山火山産の硫黄結晶（英文）..... 市村毅・津屋弘逵・湊秀雄 151
14. 秩父系堆積前の火成活動（英文）..... 市村毅・松林晴子 155
15. 1946 年南海道大地震後における室戸岬近傍の地殻変動（英文）..... 岡田惇・永田武 169

第 3 冊　昭和 28 年 9 月

16. 地震の場の論 (独文) ..... 松沢武雄 179
17. 坐標系の移動に伴ふ体球函数の変換 (英文) ..... 佐藤泰夫 203
18. 電流を制御する新しい試み及びその地磁気測定への応用 (英文) ..... 横山泉 211
19. 地震動振幅と地表層の性質との関係　第2報 (英文) ..... 金井清 219
20. 地下深所における地震動の観測結果　第4報 (英文) ..... 金井清・長田甲斐男・吉沢静代 227
21. 弾性波の発生機構に関する実験　第3報 (英文) ..... 笠原慶一 235
22. 架構構造物の振動問題における集中荷重の仮定の吟味 (英文) 金井清 245

第 4 冊　昭和 28 年 12 月

23. 地震の場の論, 1946 年 12 月 21 日の大地震と 1948 年 4 月 18 日の余震との比較 (独文) ..... 松沢武雄 249
24. 表面波の研究 IX ラブ波の群速度を求める図表 (英文) .... 佐藤泰夫 255
25. いくつかの平行な不連続面による地震波の反射及び透過 (英文) ..... 松本利松 261
26. 地震動振幅と地表層の性質との関係　第4報 (英文) ..... 金井清・吉沢静代 275
27. 東北日本における第3回爆破地震動観測 (英文) ..... 爆破地震動研究グループ 281
28. 高温に於ける火山岩の粘性及び弾性　第3報　大島熔岩 (英文) ..... 佐久間修三 291
29. 建物の振動的性質と地盤の性質との関係 (実在建物における地震動観測) (英文)..... 金井清・鈴木富三郎 305
30. 簡易弾性波式地下探査装置の研究 (英文) ..... 西村源六郎・鈴木正治・古川英一・小滝富雄・高橋浩一 317
31. 東京都南東部の地盤沈下測量 (邦文) ..... 那須信治・岸上冬彦・岡田悖 335

V/Vs	V/Vs	μ'/μ
A'-1.02	A-2.0	a-100
B'-1.06	B-2.2	b-80
C'-1.10	C-2.4	c-60
D'-1.15	D-2.6	d-50
E'-1.20	E-2.8	e-40
F'-1.25	F-3.0	f-30
G'-1.3	G-3.2	g-25
H'-1.4	H-3.4	h-20
J'-1.5	J-3.5	j-15
K'-1.6	K-3.6	k-12
L'-1.7	L-3.8	l-10
M'-1.8	M-4.0	m-8
N'-1.9	N-4.5	n-6
	P-5.0	p-5
	Q-5.5	q-4
	R-6.0	r-3
	S-6.5	s-2.5
	T-7.0	t-2.0
	U-7.5	u-1.5
	V-8.0	v-1.0
	W-8.5	w-0.5
	X-9.0	
	Y-9.5	
	Z-10.0	

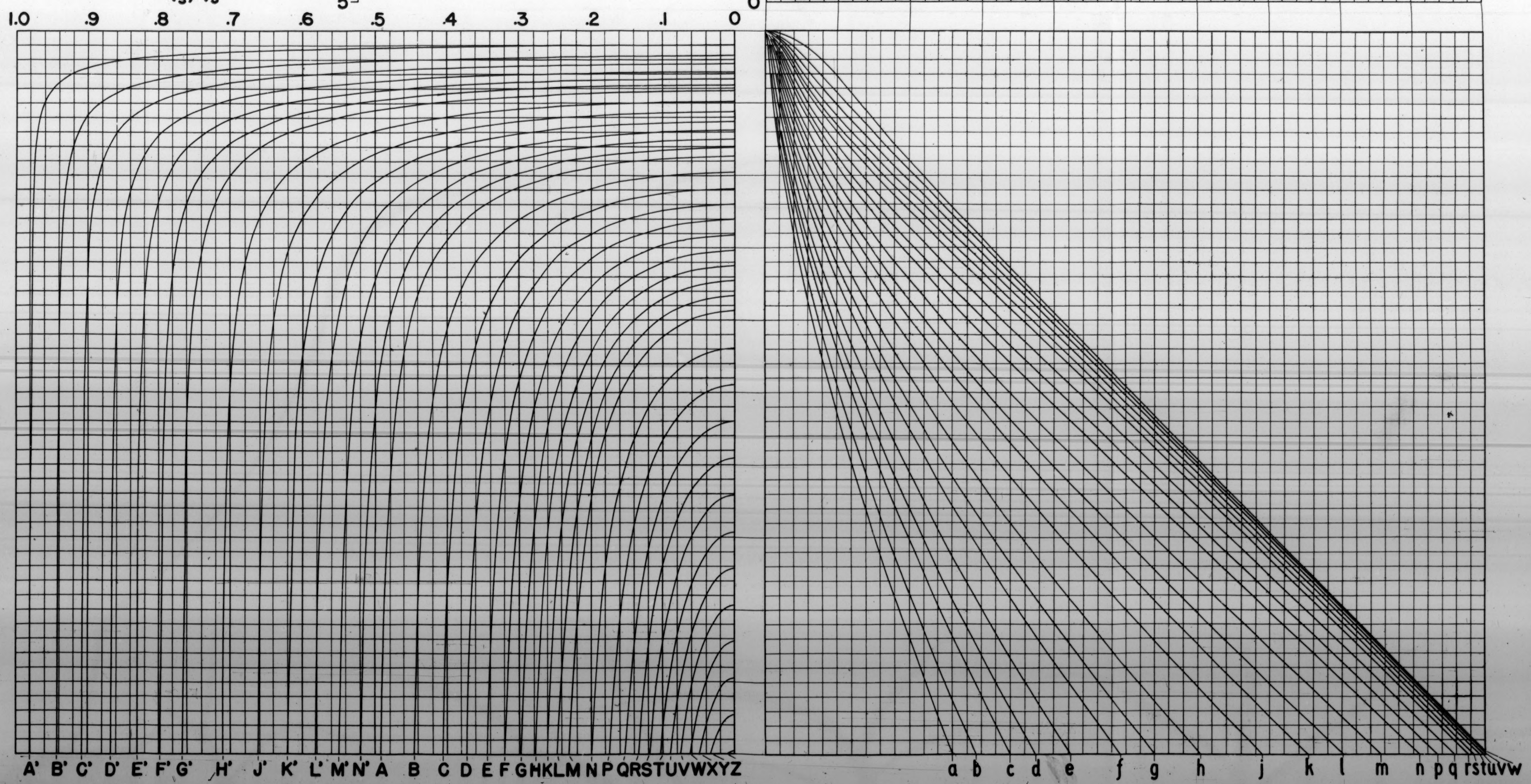

(震研彙報 第三十一号 図版 佐藤)

GROUP VELOCITY OF LOVE-WAVES

U - GROUP VELOCITY OF LOVE-WAVES

V - PHASE VELOCITY OF LOVE-WAVES

V_S - VELOCITY OF S-WAVES IN THE LAYER

V_S' - VELOCITY OF S-WAVES IN THE SUBSTRATUM

μ - RIGIDITY OF THE LAYER

μ' - RIGIDITY OF THE SUBSTRATUM

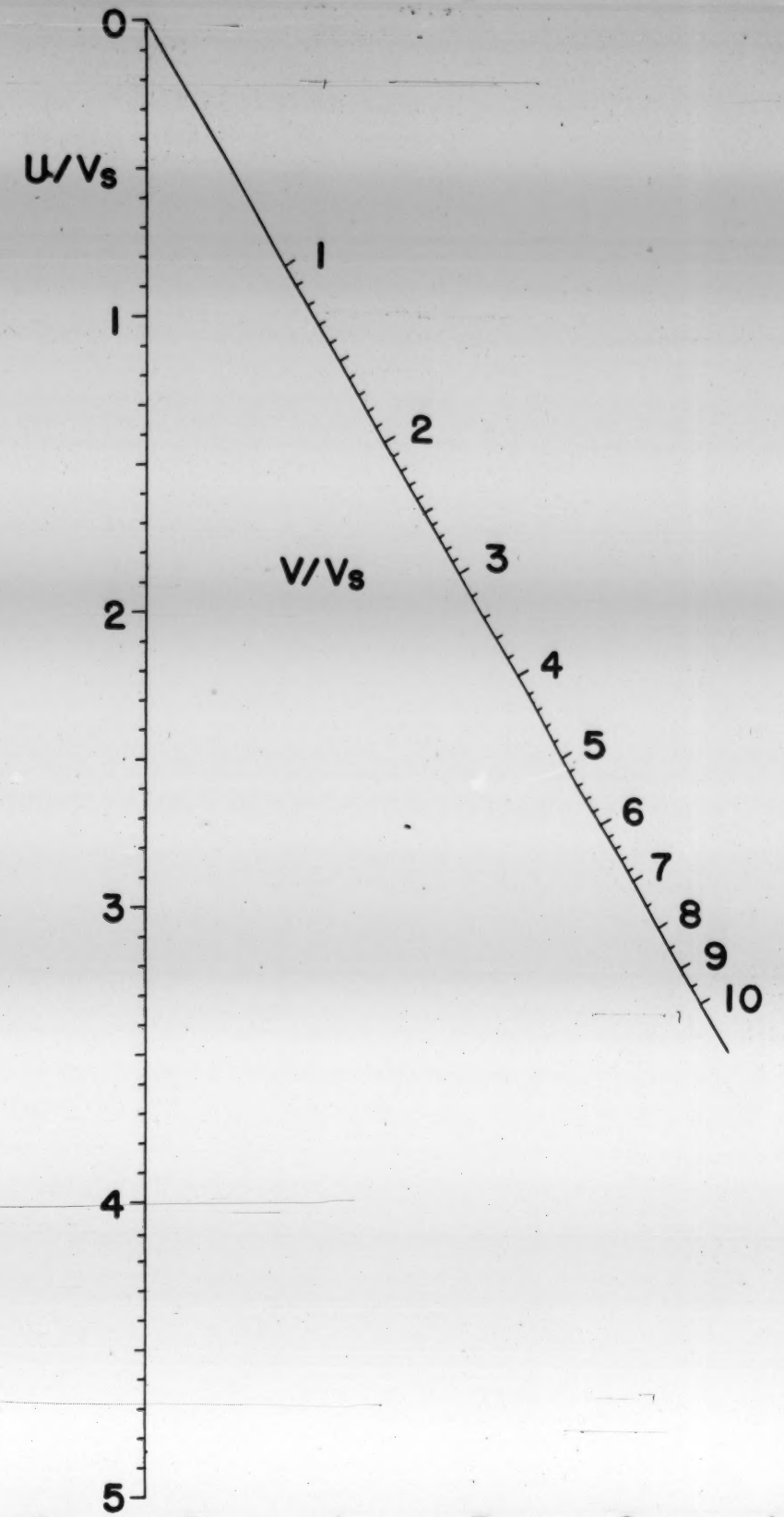

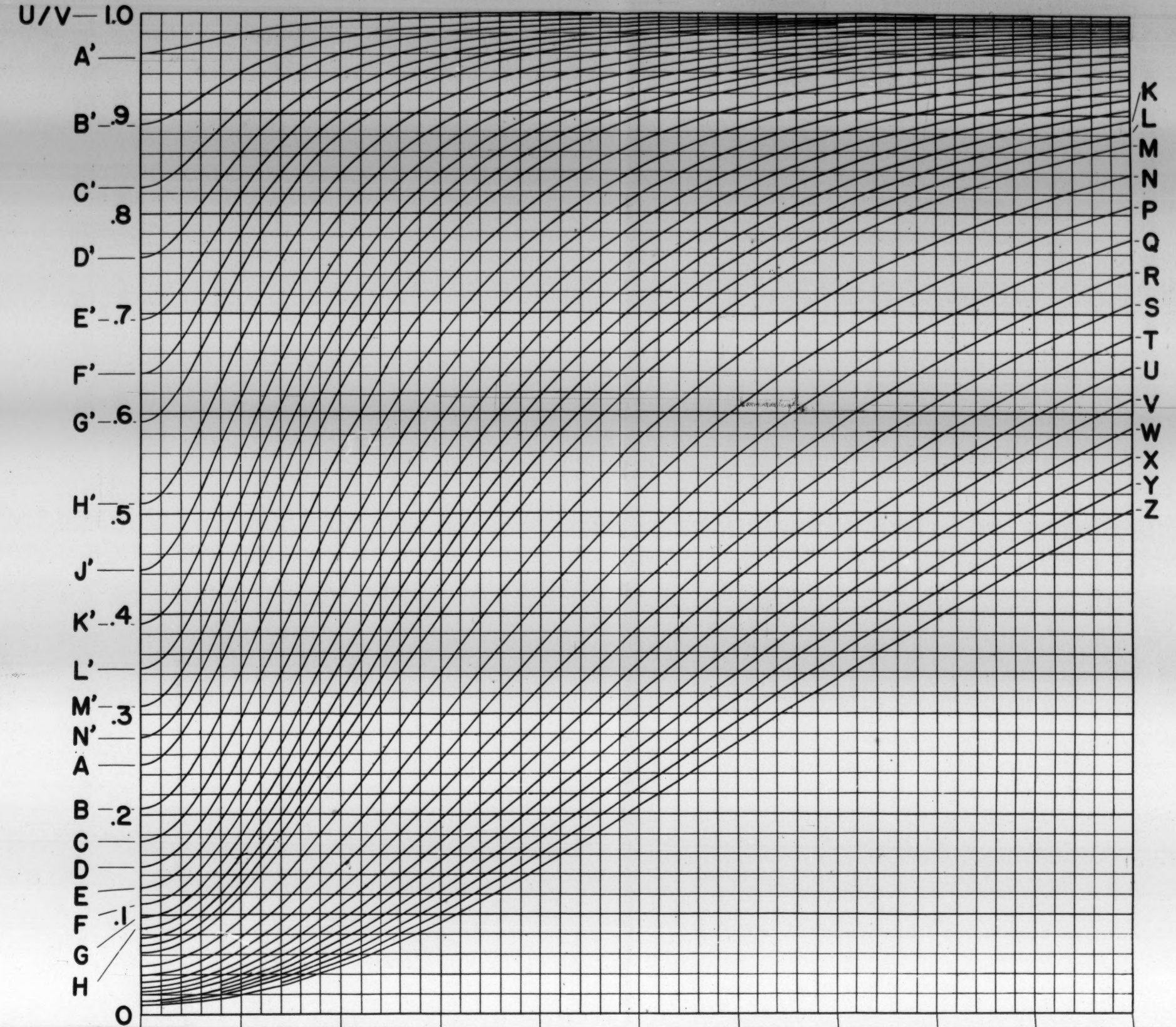

昭和29年2月15日印刷
昭和29年2月20日發行

東京都文京區本富士町一番地
東京大學構内
編纂兼發行者 東京大學地震研究所

東京都千代田區富士見町一丁目十番地
印刷者 笠井康賴

東京都千代田區富士見町一丁目十番地
印刷所 株式會社 國際文献印刷社

賣捌所 東京都千代田區神田一ツ橋通
岩波書店

東京都中央區日本橋通二丁目六番地
丸善株式會社

Sold by
Iwanami Shoten,
Hitotsubashi dôri, Chiyoda-ku, Tôkyô,
and
Maruzen Co., Ltd.,
Nihonbashi dôri, Chûô-ku, Tôkyô.
Price of this copy: 453 Yen. (Postage exclusive.)

BULLETIN OF

THE EARTHQUAKE RESEARCH INSTITUTE

TOKYO UNIVERSITY

Vol. XXXI, Part 4. December, 1953.

Contents.

Papers and Reports.

Page

23. T. MATUZAWA, Feldtheorie der Erdbeben: Vergleichung vom Grossbeben vom 21. Dez. 1946 mit dem Nachbeben vom 18. April 1948. (im Deutschen).. 249
24. Y. SATÔ, Study on Surface Waves IX. Nomogram for the Group Velocity of Love-Waves. (in English)..... 255
25. T. MATUMOTO, Transmission and Reflection of Seismic Waves through Multilayered Elastic Medium. (in English) 261
26. K. KANAI and S. YOSHIZAWA, Relation between the Amplitude of Earthquake Motions and the Nature of Surface Layer. III. (in English)..... 275
27. The Research Group for Explosion Seismology, The Third Explosion Seismic Observations in the North-Eastern Japan. (in English)..... 281
28. S. SAKUMA, Elastic and Viscous Properties of Volcanic Rocks at High Temperatures. Part 3. Oosima lava. (in English)..... 291
29. K. KANAI and T. SUZUKI, Relation between the Property of Building Vibration and the Nature of Ground. (Observation of Earthquake Motion at Actual Buildings.) (in English) 305
30. G. NISHIMURA, M. SUZUKI, E. FURUKAWA, T. KOTAKI and K. TAKAHASHI, A New-Designed Prospecting Apparatus. (in English)..... 317
31. N. NASU, F. KISHINOUYE and A. OKADA, Levelling of the Subsiding Area in the South-eastern Part of Tokyo. (in Japanese) 335

Institute Notes.

Index.

(For the papers written in Japanese or in occidental languages, the abstracts are given in occidental languages or in Japanese respectively.)